frontiers | Research Topics

XVII SOLANACEAE2022 meets the 2020 decade challenges

Edited by
Angelos K. Kanellis, Ifigeneia Mellidou, Mondher Bouzayen, Hiroshi Ezura, Alain Goossens, Antonio Granell, Panagiotis Kalaitzis, Nathalie Gonzalez and Julien Pirrello

Published in
Frontiers in Plant Science

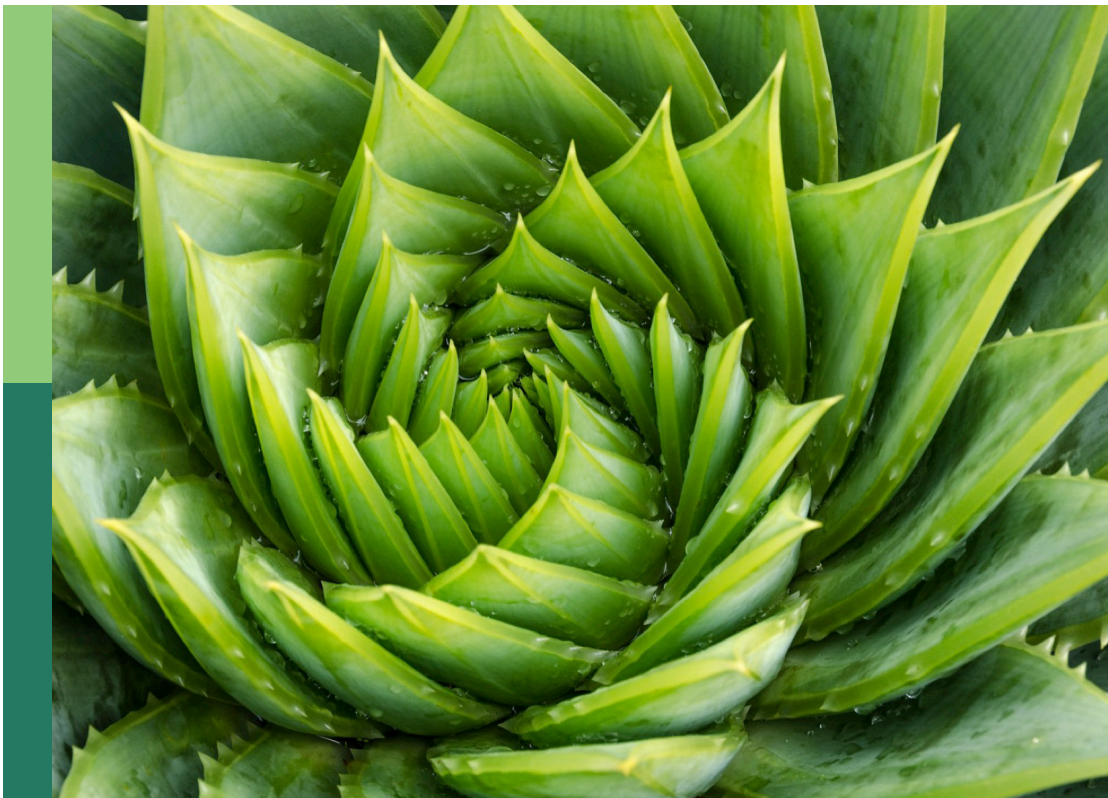

ISSN 1664-8714
ISBN 978-2-8325-6154-6
DOI 10.3389/978-2-8325-6154-6

About Frontiers

Frontiers is more than just an open access publisher of scholarly articles: it is a pioneering approach to the world of academia, radically improving the way scholarly research is managed. The grand vision of Frontiers is a world where all people have an equal opportunity to seek, share and generate knowledge. Frontiers provides immediate and permanent online open access to all its publications, but this alone is not enough to realize our grand goals.

Frontiers journal series

The Frontiers journal series is a multi-tier and interdisciplinary set of open-access, online journals, promising a paradigm shift from the current review, selection and dissemination processes in academic publishing. All Frontiers journals are driven by researchers for researchers; therefore, they constitute a service to the scholarly community. At the same time, the *Frontiers journal series* operates on a revolutionary invention, the tiered publishing system, initially addressing specific communities of scholars, and gradually climbing up to broader public understanding, thus serving the interests of the lay society, too.

Dedication to quality

Each Frontiers article is a landmark of the highest quality, thanks to genuinely collaborative interactions between authors and review editors, who include some of the world's best academicians. Research must be certified by peers before entering a stream of knowledge that may eventually reach the public - and shape society; therefore, Frontiers only applies the most rigorous and unbiased reviews. Frontiers revolutionizes research publishing by freely delivering the most outstanding research, evaluated with no bias from both the academic and social point of view. By applying the most advanced information technologies, Frontiers is catapulting scholarly publishing into a new generation.

What are Frontiers Research Topics?

Frontiers Research Topics are very popular trademarks of the *Frontiers journals series*: they are collections of at least ten articles, all centered on a particular subject. With their unique mix of varied contributions from Original Research to Review Articles, Frontiers Research Topics unify the most influential researchers, the latest key findings and historical advances in a hot research area.

Find out more on how to host your own Frontiers Research Topic or contribute to one as an author by contacting the Frontiers editorial office: frontiersin.org/about/contact

XVII SOLANACEAE2022 meets the 2020 decade challenges

Topic editors

Angelos K. Kanellis — Aristotle University of Thessaloniki, Greece
Ifigeneia Mellidou — Hellenic Agricultural Organization – ELGO, Greece
Mondher Bouzayen — Institut National Polytechnique de Toulouse, France
Hiroshi Ezura — University of Tsukuba, Japan
Alain Goossens — Ghent University, Belgium
Antonio Granell — Spanish National Research Council (CSIC), Spain
Panagiotis Kalaitzis — Mediterranean Agronomic Institute of Chania, Greece
Nathalie Gonzalez — VIB-UGent Center for Plant Systems Biology, Belgium
Julien Pirrello — École Nationale Supérieure Agronomique de Toulouse, France

Citation

Kanellis, A. K., Mellidou, I., Bouzayen, M., Ezura, H., Goossens, A., Granell, A., Kalaitzis, P., Gonzalez, N., Pirrello, J., eds. (2025). *XVII SOLANACEAE2022 meets the 2020 decade challenges*. Lausanne: Frontiers Media SA.
doi: 10.3389/978-2-8325-6154-6

Table of contents

frontiers | Frontiers in Plant Science

TYPE Editorial
PUBLISHED 10 March 2025
DOI 10.3389/fpls.2025.1570346

OPEN ACCESS

EDITED AND REVIEWED BY
Laigeng Li,
Chinese Academy of Sciences (CAS), China

*CORRESPONDENCE
Angelos K. Kanellis
kanellis@pharm.auth.gr
Ifigeneia Mellidou
imellidou@elgo.gr

RECEIVED 03 February 2025
ACCEPTED 21 February 2025
PUBLISHED 10 March 2025

CITATION
Mellidou I, Granell A, Ezura H, Kalaitzis P, Gonzalez N, Goossens A, Bouzayen M and Kanellis AK (2025) Editorial: XVII SOLANACEAE2022 meets the 2020 decade challenges.
Front. Plant Sci. 16:1570346.
doi: 10.3389/fpls.2025.1570346

Editorial: XVII SOLANACEAE2022 meets the 2020 decade challenges

Ifigeneia Mellidou[1*], Antonio Granell[2], Hiroshi Ezura[3], Panagiotis Kalaitzis[4], Nathalie Gonzalez[5], Alain Goossens[6,7], Mondher Bouzayen[8] and Angelos K. Kanellis[9*]

[1]Institute of Plant Breeding and Genetic Resources, Hellenic Agricultural Organization – DEMETER, Thessaloniki, Greece, [2]Instituto de Biología Molecular y Celular de Plantas (IBMCP), Consejo Superior de Investigaciones Científicas (CSIC), Universitat Politècnica de València, València, Spain, [3]Institute of Life and Environmental Sciences, University of Tsukuba, Tsukuba, Japan, [4]Department of Horticultural Genetics and Biotechnology, Mediterranean Agronomic Institute of Chania, Chania, Greece, [5]National Research Institute for Agriculture, Food and Environment (INRAE), UMR1332 Biologie du Fruit et Pathologie, Université Bordeaux, Villenave d'Ornon, France, [6]Department of Plant Biotechnology and Bioinformatics, Ghent University, Ghent, Belgium, [7]VIB Centre for Plant Systems Biology, Ghent, Belgium, [8]Laboratoire de Recherche en Sciences Végétales, Equipe Génomique et Biotechnologie des Fruits, UMR 5546, Centre national de la recherche scientifique (CNRS), Paul Sabatier (UPS), Toulouse Institut National Polytechnique (INP), Université de Toulouse, Toulouse, France, [9]Group of Biotechnology of Pharmaceutical Plants, Laboratory of Pharmacognosy, Department of Pharmaceutical Sciences, Aristotle University of Thessaloniki, Thessaloniki, Greece

KEYWORDS

***Solanaceae*, cultivation, postharvest physiology, fruit quality, fruit ripening**

Editorial on the Research Topic
XVII SOLANACEAE2022 meets the 2020 decade challenges

Given the ever-increasing world population and the striking losses of plant productivity due to global warming, new breeding strategies are necessary to fortify stress resilience of crops (He et al., 2018). The International Conference XVII SOLANACEAE2022 on the Plant Family of *Solanaceae* took place in Thessaloniki, GREECE, on November 1-5, 2022, and attracted more than 200 distinguished researchers and academics from more than 20 countries. The present Research Topic hosts a series of current research studies that are relevant for *Solanaceae* species, on the mechanisms underlying different phases of fruit development, ripening, postharvest potential, and stress-responses.

Fruit development is a critical process for plants that usually starts with fertilization (Quinet et al., 2019). Parthenocarpic fruits, however, can be produced independently of fertilization, and parthenocarpy is considered a highly desirable agronomic trait. The study of Tran et al. on pollination, pollen tube growth and fertilization highlighted the intricate signaling pathways and cellular mechanisms that regulate tomato fruit set and development. By using different types of pollen, the authors reveal that full penetration of pollen tubes can trigger fruit set and early development without need for fertilization, as evidenced by parthenocarpic fruit formation, most likely by activating the transcriptomic reprogramming that leads to initiation and progress of fruit development.

Fruit set is an essential transition process from opening flower to developing fruit, triggered by sophisticated interactions between multiple hormonal signals and diverse transcriptional alterations (Ezura et al., 2023). By combining genome-wide transcriptomic

profiling and ChIP-seq analysis, Li et al. (2025) demonstrated that both pollination-dependent and -independent (induced by auxin treatment) fruit set triggered the expression of a large set of genes, that are mainly expressed in maternal tissues and related to auxin, gibberellin, brassinosteroid and ethylene signaling. This transcriptional reprogramming correlates with the dynamic changes in H3K9ac and H3K4me3 histone marks regardless of the type of fruit set.

Fruit ripening is a complex process inducing alterations in fruit texture and color involving cell-wall metabolic processes. During ripening, cell wall assembly can be modified by changes in the structure and distribution of arabinogalactan proteins (AGPs), that are present in the extracellular matrix (Kutyrieva-Nowak et al., 2023). Using transgenic tomato lines with modified prolyl-4-hydroxylase (*P4H3*) gene expression, Kutyrieva-Nowak et al. demonstrated that changes in P4H3 activity significantly affected AGP content and structure during fruit ripening, resulting in altered cell-wall composition and stability. Silencing *P4H3* reduced AGP content and delayed fruit ripening, while overexpression enhanced AGP levels and accelerated ripening, highlighting the critical role of AGPs and *P4H3* in regulating cell-wall dynamics and fruit softening.

Cold storage is a common method employed to prolong the postharvest life of tomatoes, but this practice can also trigger undesirable chilling injury symptoms, which contribute to extensive fruit losses (Albornoz et al., 2022). Mitalo et al. conducted a comprehensive transcriptome analysis of the effect of an inhibitor of ethylene perception 1-methylcyclopropene (1-MCP), on fruit ripening and chilling injury during tomato storage. Their study revealed that cold stress can trigger a large-scale and unique transcriptome adjustment, associated with active ethylene biosynthesis and signaling, ribosome biogenesis, DNA methylation, chromatin remodeling, and alternative splicing events.

Genetic factors have a major impact on tomato postharvest potential. Notwithstanding the large genetic erosion in the gene pool among modern cultivars, some landraces exhibiting excellent nutritional and organoleptic properties and post-harvest behavior can be still found in local markets (Blanca et al., 2022; Pons et al., 2022). Mellidou et al. investigated the postharvest life and nutritional quality of 130 Greek tomato accessions, using metabolomics and transcriptomics. Distinct differences in flavor and nutritional compounds between short shelf-life (SSL) and long shelf-life (LSL) cultivars were emphasized and correlated with the up-regulation of key genes involved in cell wall synthesis, polyamine synthesis, and ABA catabolism in LSL cultivars, while those related to ethylene biosynthesis and cell-wall degradation were stimulated in SSL cultivars.

Apart from traditional varieties, unravelling the reproductive bottlenecks present in the *Lycopersicon* clade caused by tomato domestication would facilitate the use of wild relative germplasm in plant breeding (Muñoz-Sanz et al., 2020). The reproductive barriers within the tomato clade were examined by Moreels et al., focusing on self-incompatibility (SI) and unilateral incompatibility (UI). The review described the *modus operandi* of gametophytic and sporophytic SI and explored the genetic regulation involving S-RNases and F-box proteins. The paper also discussed the SI-to-self-compatible transition in different tomato species and the role of UI in preventing interspecific crosses.

In the context of global warming, breeding for heat stress tolerance is becoming of utmost importance (Han et al., 2021). The utilization of wild crops may provide the means to introduce heat tolerance traits into modern varieties, as highlighted in Bollier et al. Transcriptome profiling of floral buds in a large set of tomato cultivars identified specific genes that contribute to heat tolerance, such as those encoding heat shock proteins, reactive oxygen species scavengers and transporters that maintain cellular integrity under stress.

Among tomato wild species, *S. pimpinellifolium* is considered as an attractive source for breeding, with several accessions being characterized as salt-tolerant (Rao et al., 2013). Bashary et al. explored the development of heat stress-tolerant tomato cultivars obtained by backcrossing inbred lines derived from a cross between *S. pimpinellifolium* and *S. lycopersicum*. The study identified a 0.8 Mb region on chromosome 9 common to the thermotolerant lines, containing several candidate genes linked to heat stress response, including genes related to chaperonin 60 and ABC transporters, providing a valuable genetic reservoir for the breeding of more heat-resilient tomato varieties.

In nature, plants typically encounter a combination of stresses such as concomitant heat and salinity (Nadeem et al., 2022). David-Rogeat et al. investigated the effect of these combined stresses on African eggplant (*Solanum aethiopicum* L.) cultivars. Combination of stresses can have synergistic, antagonistic, or additive effects, making it complicated to establish an adequate plant response. High temperatures reduced leaf biomass while cell membrane stability was reduced by salinity. Although heat stress alone affected pollen viability and fruit set, the combination with salinity exacerbated these effects, leading to a greater drop in yield. Understanding these interactions is crucial for breeders to determine if a tolerant crop can withstand a combination of stresses.

Modern genomic tools have revolutionized plant stress research, providing detailed insights into the genetic and molecular basis of stress responses. Zagorščak et al. developed a unified potato genome model (Hoopes et al., 2022; Bozan et al., 2023), UniTato, by combining annotations from all the existing gene models, offering a useful platform, accessible via an Apollo web interface, to explore genetic variations and identify candidate genes associated with stress tolerance. Such resources are invaluable for breeding programs, enabling the selection of desirable traits with greater precision and efficiency.

Author contributions

IM: Writing – original draft. AGr: Writing – review & editing. HE: Writing – review & editing. PK: Writing – review & editing. NG: Writing – review & editing. AGo: Writing – review & editing. MB: Writing – review & editing. AK: Writing – original draft, Writing – review & editing.

Conflict of interest

The authors declare that the research was conducted in the absence of any commercial or financial relationships that could be construed as a potential conflict of interest.

The author(s) declared that they were an editorial board member of Frontiers, at the time of submission. This had no impact on the peer review process and the final decision.

Generative AI statement

The author(s) declare that no Generative AI was used in the creation of this manuscript.

Publisher's note

References

Albornoz, K., Zhou, J., Yu, J., and Beckles, D. M. (2022). Dissecting postharvest chilling injury through biotechnology. *Curr. Opin. Biotechnol.* 78, 102790. doi: 10.1016/j.copbio.2022.102790

Blanca, J., Pons, C., Montero-Pau, J., Sanchez-Matarredona, D., Ziarsolo, P., Fontanet, L., et al. (2022). European traditional tomatoes galore: a result of farmers' selection of a few diversity-rich loci. *J. Exp. Bot.* 73, 3431–3445. doi: 10.1093/jxb/erac072

Bozan, I., Achakkagari, S. R., Anglin, N. L., Ellis, D., Tai, H. H., and Strömvik, M. V. (2023). Pangenome analyses reveal impact of transposable elements and ploidy on the evolution of potato species. *Proc. Natl. Acad. Sci. United States America* 120, e22111171205. doi: 10.1073/pnas.2211117120

Ezura, K., Nomura, Y., and Ariizumi, T. (2023). Molecular, hormonal, and metabolic mechanisms of fruit set, the ovary-to-fruit transition, in horticultural crops. *J. Exp. Bot.* 74, 6254–6268. doi: 10.1093/jxb/erad214

Han, S.-H., Kim, J. Y., Lee, J.-H., and Park, C.-M. (2021). Safeguarding genome integrity under heat stress in plants. *J. Exp. Bot.* 72, 7421–7435. doi: 10.1093/jxb/erab355

He, M., He, C. Q., and Ding, N. Z. (2018). Abiotic stresses: general defenses of land plants and chances for engineering multistress tolerance. *Front. Plant Sci.* 1. doi: 10.3389/fpls.2018.01771

Hoopes, G., Meng, X., Hamilton, J. P., Achakkagari, S. R., Guesdes, F.d. A.F., Bolger, M. E., et al. (2022). Phased, chromosome-scale genome assemblies of tetraploid potato reveal a complex genome, transcriptome, and predicted proteome landscape underpinning genetic diversity. *Mol. Plant* 15, 520–536. doi: 10.1016/j.molp.2022.01.003

Kutyrieva-Nowak, N., Leszczuk, A., Zając, A., Kalaitzis, P., and Zdunek, A. (2023). Arabinogalactan protein is a molecular and cytological marker of particular stages of the tomato fruit ripening process. *Sci. Hortic.* 310, 1–10. doi: 10.1016/j.scienta.2022.111718

Muñoz-Sanz, J. V., Zuriaga, E., Cruz-García, F., McClure, B., and Romero, C. (2020). Self-(In)compatibility systems: target traits for crop-production, plant breeding, and biotechnology. *Front. Plant Sci.* 11. doi: 10.3389/fpls.2020.00195

Nadeem, H., Khan, A., Gupta, R., Hashem, M., Alamri, S., Siddiqui, M. A., et al. (2022). Stress combination—when two negatives may become antagonistic, synergistic, or additive for plants: A review. *Pedosphere* 33, 287–300. doi: 10.1016/j.pedsph.2022.06.031

Pons, C., Casals, J., Palombieri, S., Fontanet, L., Riccini, A., Rambla, J. L., et al. (2022). Atlas of phenotypic, genotypic and geographical. *Hortic. Res.* 9, uhac112. doi: 10.1093/hr/uhac112

Quinet, M., Angosto, T., Yuste-Lisbona, F. J., Blanchard-Gros, R., Bigot, S., Martinez, J.-P., et al. (2019). Tomato fruit development and metabolism. *Front. Plant Sci.* 10. doi: 10.3389/fpls.2019.01554

Rao, E. S., Kadirvel, P., Symonds, R. C., and Ebert, A. W. (2013). Relationship between survival and yield related traits in *Solanum pimpinellifolium* under salt stress. *Euphytica* 190, 215–228. doi: 10.1007/s10681-012-0801-2

frontiers | Frontiers in Plant Science

TYPE Original Research
PUBLISHED 20 June 2023
DOI 10.3389/fpls.2023.1205816

OPEN ACCESS

EDITED BY
Md Asaduzzaman,
NSW Government, Australia

REVIEWED BY
Prakash Babu Adhikari,
Huazhong Agricultural University, China
Ruud A. de Maagd,
Wageningen University & Research, Netherlands

*CORRESPONDENCE
Hiroshi Ezura
ezura.hiroshi.fa@u.tsukuba.ac.jp

RECEIVED 14 April 2023
ACCEPTED 30 May 2023
PUBLISHED 20 June 2023

CITATION
Tran LT, Sugimoto K, Kasozi M, Mitalo OW and Ezura H (2023) Pollination, pollen tube growth, and fertilization independently contribute to fruit set and development in tomato.
Front. Plant Sci. 14:1205816.
doi: 10.3389/fpls.2023.1205816

Pollination, pollen tube growth, and fertilization independently contribute to fruit set and development in tomato

Long T. Tran[1], Koichi Sugimoto[2,3], Michael Kasozi[1], Oscar W. Mitalo[1] and Hiroshi Ezura[2,3]*

[1]Graduate School of Science and Technology, University of Tsukuba, Tsukuba, Japan, [2]Faculty of Life and Environmental Sciences, University of Tsukuba, Tsukuba, Japan, [3]Tsukuba-Plant Innovation Research Centre, University of Tsukuba, Tsukuba, Japan

In flowering plants, pollination, pollen tube growth, and fertilization are regarded as the first hierarchical processes of producing offspring. However, their independent contributions to fruit set and development remain unclear. In this study, we examined the effect of three different types of pollen, intact pollen (IP), soft X-ray-treated pollen (XP) and dead pollen (DP), on pollen tube growth, fruit development and gene expression in "Micro-Tom" tomato. Normal germination and pollen tube growth were observed in flowers pollinated with IP; pollen tubes started to penetrate the ovary at 9 h after pollination, and full penetration was achieved after 24 h (IP24h), resulting in ~94% fruit set. At earlier time points (3 and 6 h after pollination; IP3h and IP6h, respectively), pollen tubes were still in the style, and no fruit set was observed. Flowers pollinated with XP followed by style removal after 24 h (XP24h) also demonstrated regular pollen tubes and produced parthenocarpic fruits with ~78% fruit set. As expected, DP could not germinate and failed to activate fruit formation. Histological analysis of the ovary at 2 days after anthesis (DAA) revealed that IP and XP comparably increased cell layers and cell size; however, mature fruits derived from XP were significantly smaller than those derived from IP. Furthermore, there was a high correlation between seed number and fruit size in fruit derived from IP, illustrating the crucial role of fertilization in the latter stages of fruit development. RNA-Seq analysis was carried out in ovaries derived from IP6h, IP24h, XP24h and DP24h in comparison with emasculated and unpollinated ovaries (E) at 2 DAA. The results revealed that 65 genes were differentially expressed (DE) in IP6h ovaries; these genes were closely associated with cell cycle dormancy release pathways. Conversely, 5062 and 4383 DE genes were obtained in IP24h and XP24h ovaries, respectively; top enriched terms were mostly associated with cell division and expansion in addition to the 'plant hormone signal transduction' pathway. These findings indicate that full penetration of pollen tubes can initiate fruit set and development independently of fertilization, most likely by activating the expression of genes regulating cell division and expansion.

KEYWORDS

x-ray irradiated pollen, pollen tube growth, parthenocarpy, tomato fruit set, tomato fruit development

1 Introduction

Tomato (*Solanum lycopersicum* L.) is both an economically important crop in the world and a model plant for fruit science and production (Ezura, 2009). Fruit initiation and development from tomato flowers can be divided into four distinct phases (Ariizumi et al., 2013; Quinet et al., 2019), viz. fruit set (phase I), cell division (phase II), cell expansion (phase III), and fruit ripening (phase IV), all of which require the coregulation of genetic and hormonal elements *via* complicated pathways (Molesini et al., 2020; Fenn and Giovannoni, 2021). Both pollination and fertilization are believed to be prerequisites for fruit set and development (Quinet et al., 2019), but seedless fruits can be produced independently of fertilization, as is the case with the parthenocarpy phenomenon which can be achieved either by exogenous hormone treatments or genetic mutation approaches. Parthenocarpy is a highly desirable agronomic trait, as fruit formation is less affected by environmental factors (Molesini et al., 2020). Thus far, several parthenocarpic mutations, such as *pat-2*, *iaa9-3*, and *pad-1*, display high seedless fruit set ratios, and hence, they are considered potential genetic materials for the breeding of seedless tomato fruit cultivars (Takisawa et al., 2019; Matsuo et al., 2020; Takisawa et al., 2020; Tran et al., 2021).

Like in other flowering plants, pollination in tomato occurs on the stigma surface as the first step in the reproduction process. Pollination is then followed by germination of pollen grains to form unique structures known as pollen tubes. The pollen tubes provide a link between pollination and fertilization, as they act as vehicles to deliver sperm cells in pollen grains to egg cells in the ovules which are located in the ovary. Interestingly, soft X-ray-irradiated pollen containing inactivated sperm cells produced standard pollen tubes which penetrated ovules and eventually resulted in parthenocarpic fruit development in watermelons (Hu et al., 2019). The soft X-ray-irradiated pollen induced both auxin signalling and the accumulation of various hormones including gibberellins, cytokinins, and auxins, and the resultant parthenocarpic watermelons were comparable in size to normal seeded fruits (Hu et al., 2019). Other reports have also demonstrated that there is a swift activation of ethylene biosynthesis and perception during pollen tube growth in multiple plant species (Holden et al., 2003; Jia et al., 2018; Althiab-Almasaud et al., 2021). These data suggest the potential roles of pollen tubes in the regulation of hormonal synthesis and signalling to induce fruit set and development even in the absence of fertilization. In tomato, however, soft X-ray irradiation applied directly to dried pollen strongly impaired pollen germination and led to production of tiny parthenocarpic fruits (Nishiyama and Tsukuda, 1961; Uematsu and Nishiyama, 1967). In this sense, no further research on this topic has been conducted since then, and hence the potential use of X-ray-irradiated pollen to produce parthenocarpic fruits in tomato remains unexplored. Furthermore, the role of pollen tubes in fruit initiation and development at the molecular level in tomato is still unknown.

In this study, we used dead, intact, and soft X-ray-treated pollen to explore the independent effects of pollination, pollen tube growth, and fertilization on fruit initiation and development in tomato. Partial pollen tube growth in the styles triggered the expression of various genes which are associated with the release of cell cycle dormancy, but these changes did not adequately initiate fruit set. However, full penetration of the pollen tubes into the ovary activated genes associated with cell expansion and division most likely through many hormonal pathways independently of fertilization and eventually initiated fruit set and development. In addition, we show that fertilization could contribute to the latter stages of fruit development by activating the expression of a distinct set of cell expansion genes. Altogether, these findings suggest that pollen tube penetration into the ovary can sufficiently trigger normal fruit set and development regardless of fertilization, a physiological function of pollen tubes that has not been established previously in tomato.

2 Materials and methods

2.1 Plant material and growth conditions

Seeds of *S. lycopersicum* cultivar "Micro-Tom", both wild type (ID: TOMJPF00001) and an EMS parthenocarpic mutant *iaa9-3* (ID: TOMJPE2811-1), were supplied by the National Bioresource Project archived at the TOMATOMA database[1]. The plants were grown in rockwool blocks in a growth room set at 25°C under photosynthetically active light (75-110 mmol/m^2/s) for 16 h and 20° C in the dark for 8 h.

2.2 Pollen preparation

Fresh anther cones were collected at the anthesis stage and then used to prepare three types of pollen, that is, dead pollen (DP), soft X-ray-treated pollen (XP), and intact/normal pollen (IP). To prepare DP, the anther cones were dried at 100°C for 2 h. IP were prepared by drying the anther cones at 35°C for 6 h. Finally, to make XP, fresh anther cones were first subjected to a soft X-ray irradiation (Model: OM-303M, OMIC Corporation, Japan) of 1000 Gy for 72.15 minutes followed by drying at 35°C for 6 h. The protocol for soft X-ray irradiation was derived from our work (unpublished data) at the University of Tsukuba.

2.3 Pollination and treatments

Flowers were emasculated one day before anthesis (-1 DAA) to avoid self-pollination. The emasculated flowers were then pollinated on the next day (0 DAA) using the pollen types described in section 2.2. Styles were removed from IP-pollinated flowers 3 h, 6 h, 9 h, 12 h, and 24 h after pollination (denoted as IP3h, IP6h, IP9h, IP12h, and IP24h, respectively). For XP- and DP-pollinated flowers, styles were removed 24 h after pollination

[1] http://tomatoma.nbrp.jp

(denoted as XP24h and DP24h, respectively). In all cases (IP3h, IP6h, IP9h, IP12h, IP24h, XP24h and DP24h), ovaries that remained after style removal were left to stand on the plants (10 plants per each treatment) for further histological and RNA-Seq analyses as well as assessment of fruit set ratios. The ovaries were collected at 2 DAA (for RNA-Seq analysis) and from 2–10 DAA (for histological analysis). Ovaries from emasculated but unpollinated flowers (denoted as E) with style removal 24 h after anthesis were also collected at the same timepoints to represent control treatments.

2.4 *In vivo* pollen tube growth assays and aniline blue staining

Pistils were collected 3 h, 6 h, 9 h, 12 h, and 24 h after pollination with IP pollen, and 24 h after pollination with XP and DP. The pistils were then fixed in 3:1 ethanol (100%): acetic acid (100%) solution for 12 h, washed in 70% ethanol and finally softened in 5 N NaOH for 12 h. Softened pistils were washed five times in distilled water and stained overnight in the dark with 0.01% aniline blue solution in K_3PO_4 buffer. The stained pistils were then mounted in 100% glycerol on a slide and observed under a UV microscope (Olympus BX50, Olympus-Life Science Company, Japan). At least three pistils were observed for each of the seven treatments.

2.5 Determination of fruit set ratios

Fruit set ratios were evaluated using five different plants and a total of 21-30 flowers for each style removal (IP3h, IP6h, IP9h, IP12h, IP24h, XP24h and DP24h) treatment. The ratios were expressed as the percentage of ovaries which remained on the flowers and showed an increase in size at 10 DAA.

2.6 Histological analysis and fruit growth measurements

Histological analyses were carried out using Technovit 7100 (Kulzer Technik, Germany) according to the protocol of Yeung and Chan (2015) with slight modifications. Briefly, ovaries collected at 0, 2, 4, and 10 DAA were fixed as described in Section 2.4 and then dehydrated by passing them sequentially through graded ethanol (70%/2 h → 80%/2 h → 90%/2 h → 100%/overnight). This was followed by three infiltration steps in ethanol:Technovit solutions at different concentrations (2:1/2 h → 1:1/2 h → 1:2/2 h), and overnight immersion in pure Technovit. The ovaries were then embedded in a mixture of Technovit and Hardener II (15:1 v/v) and allowed to polymerize at room temperature for 12 h before sectioning at a thickness of 5 µm using a rotary microtome machine (Leica RM2235, Leica Biosystem Ltd., China). Finally, the sections were mounted in water on a glass slide, dried at 40°C, and stained with toluidine blue (Sigma-Aldrich T3260, Merck, USA). A drop of Entellan New (Sigma-Aldrich 107961, Merck, USA) was added to the slide before observation under a light microscope (Olympus BX50). At least three ovaries were observed for each style removal treatment. To estimate fruit growth, cell layer and cell volume measurements were conducted on the microscope images using ImageJ software.

2.7 RNA extraction, library construction and RNA sequencing

Samples for RNA-Seq analysis included emasculated but unpollinated ovaries (E) as a control (absence of pollination, pollen tube growth and fertilization), and ovaries from IP6h, IP24h, DP24h, and XP24h style removal treatments. These samples were selected based on pollen tube growth observations; IP6h represented partial pollen tube growth (no penetration into the ovaries and hence no fertilization), IP24h represented full pollen penetration into the ovaries with fertilization, XP24h represented full pollen tube penetration without fertilization, while DP24h represented pollination only (no pollen tube growth and no fertilization). All samples were collected 48 h after pollination (2 DAA), and each sample contained 5 ovaries with three replications. Total RNA was extracted from the ovary samples using the RNeasy® Plant Mini Kit (Qiagen, Hilden, Germany) according to the manufacturer's instructions. Treatment with DNase I (Nippon Gene, Tokyo, Japan) was carried out to remove genomic DNA contamination. mRNA was then purified from the total RNA using a poly(A) mRNA magnetic isolation module kit (New England BioLabs). The pure mRNA was used to construct paired-end libraries for Illumina using the Ultra™ II directional RNA library prep kit (New England BioLabs), and sequencing was performed on an Illumina NovaSeq 6000 platform (Illumina, Inc.).

2.8 RNA-seq data analysis

RNA-Seq data were analysed on the Galaxy main server[2]. The raw RNA sequence reads were qualified using the FastQC tool and then trimmed by the Trimmomatic tool (Bolger et al., 2014). The resultant high-quality sequences were then mapped to tomato reference genomes (v. SL4.0) using the Hisat2 tool with default parameters (Kim et al., 2019). Mapped reads were counted using the featureCounts tool (Liao et al., 2014). The read counts obtained were normalized to the gene expression level as transcripts per kilobase million (TPM) reads. Gene Ontology (GO) enrichment and Kyoto Encyclopedia of Genes and Genomes (KEGG) analyses were conducted on the web application iDEP (v. 0.93)[3] and ShinyGO (v. 0.77)[4] (Ge et al., 2018).

[2] http://usegalaxy.org

[3] http://bioinformatics.sdstate.edu/idep93

[4] http://bioinformatics.sdstate.edu/go

2.9 Statistical analysis

Data obtained in this study are presented as average values ± SE. Mean comparisons were tested by Tukey's HSD (honestly significant difference) test at $P < 0.05$. All statistical analyses were performed using Statistical Tool for Agricultural Research (STAR), version 2.0.1 (Gulles et al., 2014).

3 Results

3.1 Effect of pollen tube growth on fruit setting in tomato

In vivo pollen tube growth assays, following pollination of tomato flowers with IP, XP and DP, were crucial in this study to determine the independent effects of pollination, pollen tubes, and fertilization on fruit setting. For IP-pollinated flowers, pollen tubes elongated to approximately one-third and three-quarters of the styles after 3 h and 6 h (Figure 1A), respectively and the earliest penetration of the pollen tubes into the ovaries, indicated by a limited signal below the style baseline, was observed 9 h after pollination. Full penetration of IP-generated pollen tubes into the ovaries occurred 12 h and 24 h after pollination, as the signal strengths inside the ovaries were comparable. Likewise, pollen tubes in XP-pollinated flowers elongated and fully penetrated the ovaries 24 h after pollination (Figure 1A). As expected, DP failed to germinate and hence pollen tubes could not be observed in the styles of DP-pollinated flowers even after 24 h. Therefore, at the specified times of style removal, pollen tubes were still in the styles for IP3h and IP6h, but there was partial penetration into the ovaries for IP9h. For IP12h, IP24h and XP24h, full penetration of the pollen tubes into the ovaries had already taken place.

Ovaries that were left on the plants after style removal treatments were then assessed at 10 DAA for their ability to develop into fruits. Results indicated that IP3h and IP6h ovaries

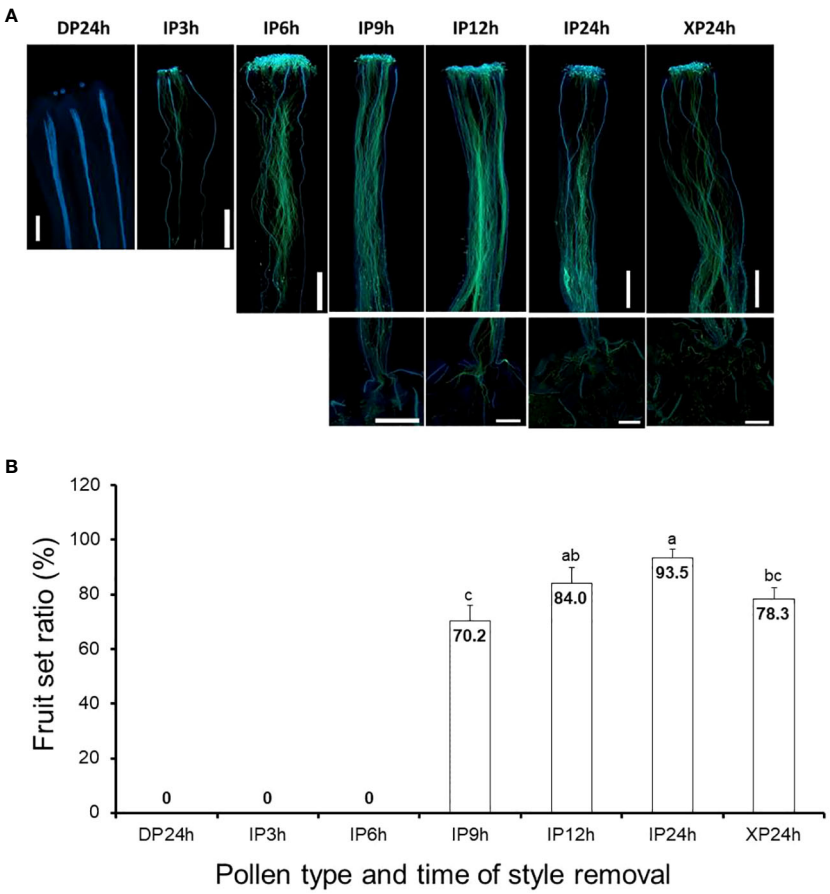

FIGURE 1
Pollen tube growth and its effect on fruit setting in tomato. **(A)** Images showing pollen tubes in the pistils. Pollen tubes were stained by aniline blue and appear green under UV microscopy at a magnification of 40X (n = 6). Lower panels in IP9h, IP12h, IP24h and XP24h columns indicate pollen tube signals inside the ovary. **(B)** Fruit set ratios of ovaries of the specified pollen type and style removal treatments. Values are percentages of fruit numbers on the examined flowers (21–30 flowers per treatment) at 10 DAA. Different letters indicate statistical difference using Tukey's HSD (honestly significant difference) test at $P < 0.05$. White bars in **(A)** images = 50 µm. IP3h – pollinated with intact pollen and styles removed 3 h later; IP6h – pollinated with intact pollen and styles removed 6 h later; IP9h – pollinated with intact pollen and styles removed 9 h later; IP12h – pollinated with intact pollen and styles removed 12 h later; IP24h – pollinated with intact pollen and styles removed 24 h later; XP24h – pollinated with x-ray-irradiated pollen and styles removed 24 h later; DP24h – pollinated with dead pollen and styles removed 24 h later.

failed to initiate fruit set, similar to DP24h (Figure 1B). On the other hand, IP9h ovaries displayed a considerable fruit set ratio (70.2%), although it was significantly lower than IP12h (84.4%) and IP24h (93.5%) ovaries. Interestingly, XP24h ovaries also showed a noticeably high fruit set ratio (78.3%), albeit significantly lower than that of IP24h ovaries. Together, these findings indicate that pollination alone (represented by DP24h) or partial pollen tube growth (represented by IP3h, IP6h and to some extent, IP9h) were not sufficient to initiate fruit setting. Contrarily, full penetration of pollen tubes into the ovaries even in the absence of fertilization (as shown in XP24h) can sufficiently trigger fruit set.

3.2 Full penetration pollen tubes results in normal fruit development

After fruit set assessments, we asked whether full penetration of pollen tubes into the ovaries minus fertilization can also lead to normal cell division and expansion. Histological analyses showed that both the number of cell layers and cell sizes of pericarp tissues of XP24h ovaries were higher at 2 DAA compared to the initial 0 DAA ovaries (Figures 2A–C). It is worth noting that both the number of cell layers and area of pericarp cells in XP24h ovaries at 2 DAA were not statistically different from those of IP12h and IP24h ovaries at the same timepoint (Figures 2B, C). By contrast, IP9h ovaries, which had only partial pollen tube penetration (Figure 1A), only showed larger cells at 2 DAA with no significant increase in cell layer numbers. Ovaries of IP6h, DP24h and the control E showed insignificant changes in both the cell area and number of cell layers, and the cell sizes were similar to those of ovaries at 0 DAA.

Pericarp cell measurements were also conducted on the young fruits (at 4 and 10 DAA) that developed from XP24h and IP24h ovaries. As shown in Figure 2D, young fruits of XP24h and IP24h showed a comparable number of cell layers both at 4 and 10 DAA. However, IP24h fruits showed a consistently larger pericarp cell area than XP24h fruits at the evaluated timepoints. It is worth noting that from 0 DAA to 2 DAA, there were no significant differences between IP24h and XP24h with regards to the increase in both cell layer numbers (26%) and cell area (30%) (Figures 2A–C). At 4 DAA, however, the increase in cell area relative to control E ovaries at 2 DAA was remarkably higher (210%) than that of the number of cell layers (46%). Furthermore, there was only a slight increase in cell layer numbers between 4 DAA and 10 DAA (11%), but a remarkably sharp increase in cell area (830%) was recorded. Altogether, these findings suggested that during early stages of fruit development (0–4 DAA), cell division (indicated by cell layer numbers) has a greater contribution than cell expansion (indicated by cell area). By contrast, cell expansion has a greater contribution than cell division during later fruit developmental stages (from 4 DAA).

To examine the impact of fertilization on late fruit developmental stages, fruit size and seed numbers in ripe fruits derived from style removal treatments that successfully set fruits (IP9h, IP12h, IP24h and XP24h) were also determined (Figure 3). The largest fruit weight was registered in ripe fruits obtained from IP12h and IP24h (3.69 g and 3.61 g, respectively) (Figure 3A). Fruits that developed from IP9h ovaries displayed the smallest average weight (1.77 g), but XP24h fruits had a slightly higher average weight (2.38 g), albeit significantly smaller than IP12h and IP24h fruits. Both the diameter and height of IP12h and IP24 h fruits were bigger than those of XP24h (Figure 3D), which correlated well with fruit weight data. These results suggested that the degree of fertilization might have a positive impact on the final size of fruits at maturity. Specifically, IP12h and IP24h ovaries underwent full penetration of pollen tubes (and hence presumably, complete fertilization) which likely led to the development of normal-sized fruits. However, IP9h ovaries underwent only partial pollen tube penetration, and hence partial fertilization, which might account for the small fruit sizes. Indeed, there was no significant difference in the number of seeds per fruit for IP12h and IP24h, but IP9h fruits had noticeably a smaller number of seeds (Figure 3B). Likewise, XP24h ovaries did not undergo fertilization even though full penetration of pollen tubes from the sterile X-ray-irradiated occurred, likely contributing to smaller fruit sizes than IP12h and IP24h. It is also worth noting that XP24h fruits did not produce regular seeds; instead, they produced many tiny seed-like structures (Figure 3D), which failed to germinate (data not shown). This finding therefore confirmed that the X-ray-treated pollen used in the present study indeed lost their fertilization function. Finally, combination of fruit weight and seed number data revealed a strong positive correlation (R^2 = 0.85) between these two phenotypes (Figure 3C).

3.3 Transcriptome sequencing analysis

After phenotypical analyses, RNA-Seq was performed to identify transcriptomic changes in ovaries at 2 DAA triggered by the different pollen types and style removal times. A total of 500 most variable genes were used to construct a heatmap showing the overall expression patterns based on the $\log_{10}$ transformed TPM values. As shown in Figure 4A, the expression patterns in DP24h and IP6h ovaries were similar to those in the control (E) ovaries, while XP24h and IP24h ovaries showed highly similar patterns. Indeed, Pearson's correlation coefficient analysis, based on 75% of the top variable genes, confirmed that there were highly positive correlations between XP24h and IP24h samples (r = 0.99), while there were high correlations (r=0.98~0.99) among E, DP24h, and IP6h samples (Figure 4B). In addition, principal component analysis (PCA) was conducted to explain 78% of the variation in the datasets (PC1 = 74%, and PC2 = 4%), in which XP24h and IP24h samples were also grouped together, but clearly separated from E, DP24h, and IP6h (Figure 4C).

3.4 Differential gene expression analysis

The DEGs with a minimal fold change of 2 and FDR < 0.01 were

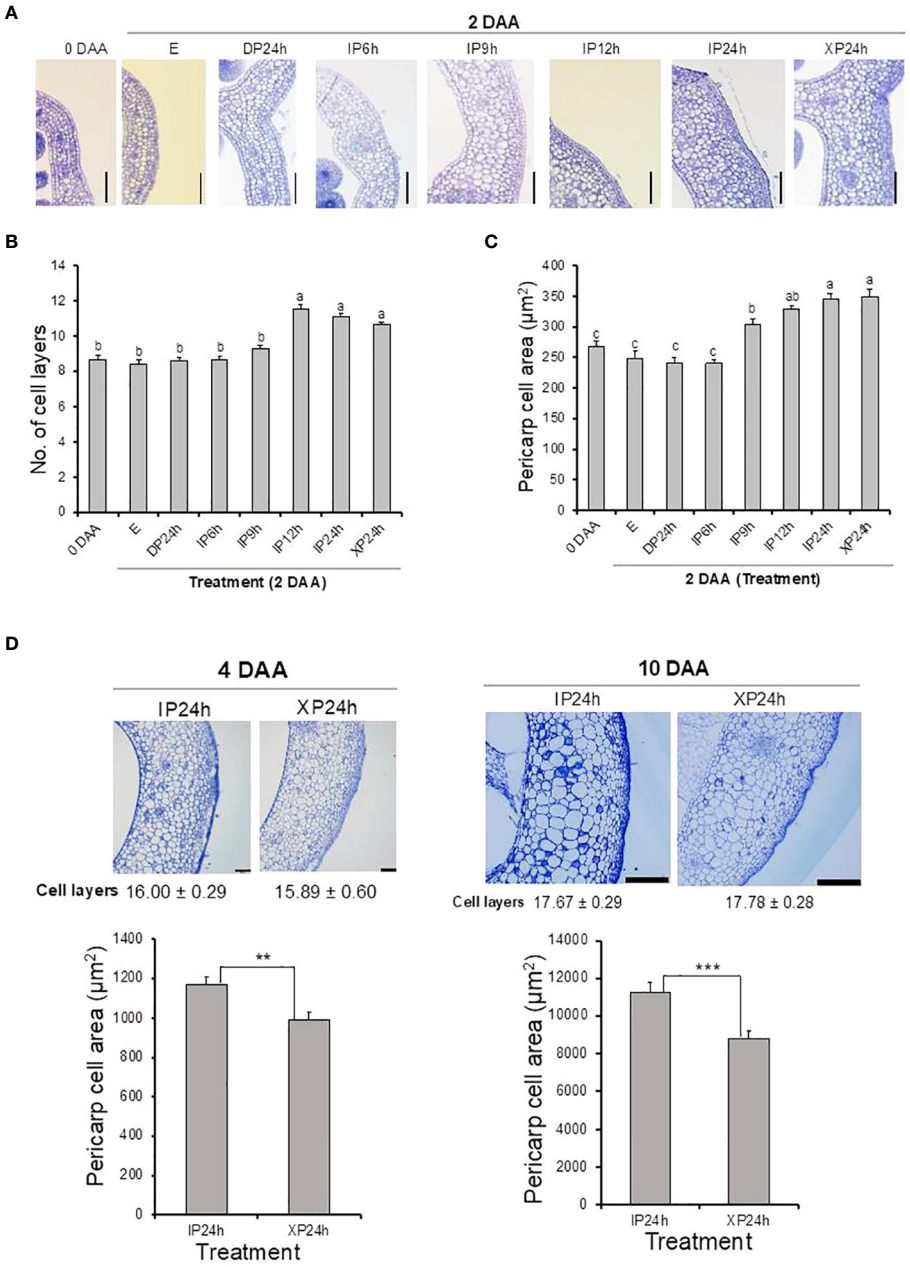

FIGURE 2
Histological analysis of ovary pericarp tissues after pollination with three different pollen types and style removal treatments. Ovaries were collected at 0 DAA and 2 DAA **(A–C)**, and at 4 DAA and 10 DAA **(D)**. Samples were stained with toluidine blue after carrying out the Technovit 7100 (Kulzer Technik, Germany) procedure, and observed under a light microscope at a magnification of 100X. Data in **(B, D)** are means ± SE. Different letters in **(B, C)** indicate statistical difference using Tukey's HSD test at $P < 0.05$. Significant differences in **(D)** bar charts were analysed using Student's t-test assessment (**P < 0.01; ***P < 0.001). White bars = 100 µm in **(A, D)** (4 DAA) and 500 µm in **(D)** (10 DAA). IP6h – pollinated with intact pollen and styles removed 6 h later; IP9h – pollinated with intact pollen and styles removed 9 h later; IP12h – pollinated with intact pollen and styles removed 12 h later; IP24h – pollinated with intact pollen and styles removed 24 h later; XP24h – pollinated with x-ray-irradiated pollen and styles removed 24 h later; DP24h – pollinated with dead pollen and styles removed 24 h later; (E) – emasculated but unpollinated control.

considered significant and selected for enrichment analysis. As illustrated in Figures 5A, D, 65 DEGs were detected in IP6h ovaries, of which 11were upregulated while 54 were downregulated compared to the control (E). The numbers of DEGs in XP24h ovaries were 4383 (1401 up-regulated and 2982 down-regulated) (Figures 5C, D), while in IP24h ovaries, 5062 DEGs (1514 up-regulated and 3548 down-regulated) were detected (Figures 5B, D). By contrast, there were no DEGs between DP24h vs E samples or between XP24h vs IP24h (Figure 5D).

Venn diagrams were also constructed to visualize the commonly or uniquely up- or down-regulated DEGs under different pollen treatments. This analysis revealed that XP24h and

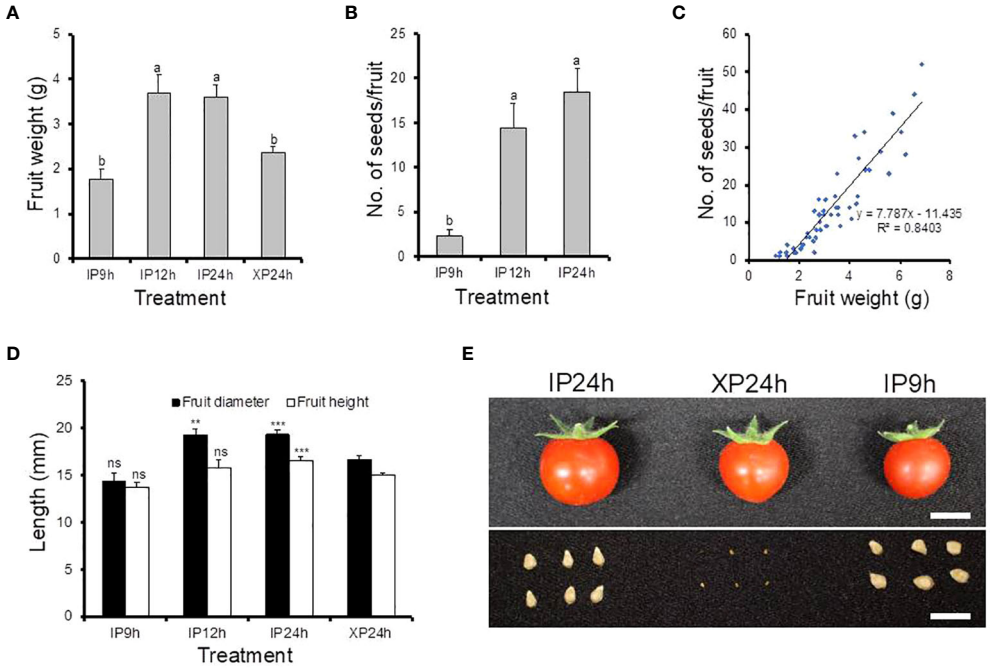

FIGURE 3
Morphological characteristics and seed production of fruits derived from IP9h, IP12h, IP24h and XP24h ovaries. **(A)** Average fruit weight. **(B)** Number of seeds per fruit. **(C)** The correlation between fruit weight and seed number. **(D)** Fruit diameter and height. Values in **(A, B, D)** are means ± SE of 10 fruits. Different letters in **(A, B)** indicate statistical difference, using Tukey's HSD test at $P < 0.05$. Student's T-test analysis was conducted to compare fruit indexes between XP24h and other treatments; *** = $P < 0.001$, **= $P < 0.01$, and ns = not significant. **(E)** Images showing the appearance of fruits and their respective seeds. White bars = 1 cm. IP9h – pollinated with intact pollen and styles removed 9 h later; IP12h – pollinated with intact pollen and styles removed 12 h later; IP24h – pollinated with intact pollen and styles removed 24 h later; XP24h – pollinated with x-ray-irradiated pollen and styles removed 24 h later.

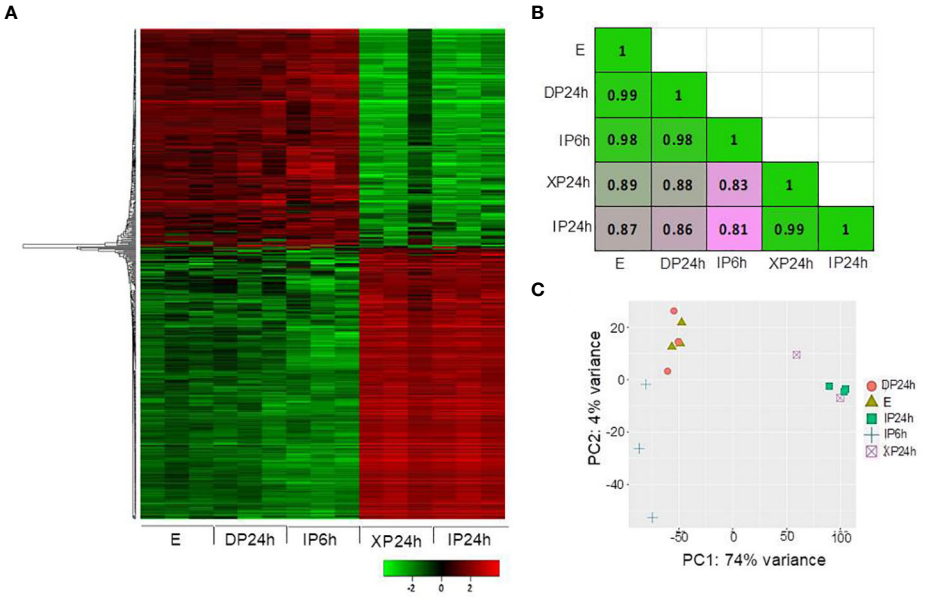

FIGURE 4
Overall expression patterns of the top variable genes. **(A)** Heatmap based on the $\log_{10}$ transformed TPM values of the top 500 variable genes. **(B)** Pearson's correlation coefficient analysis using 75% of the top variable genes. **(C)** Principal component analysis (PCA) results showing PC1 and PC2. The ovary samples were collected 48 h after pollination (2 DAA), and each sample contained 5 ovaries with three replications. IP6h – pollinated with intact pollen and styles removed 6 h later; IP24h – pollinated with intact pollen and styles removed 24 h later; XP24h – pollinated with x-ray-irradiated pollen and styles removed 24 h later; DP24h – pollinated with dead pollen and styles removed 24 h later; E – emasculated but unpollinated control.

10.3389/fpls.2023.1205816

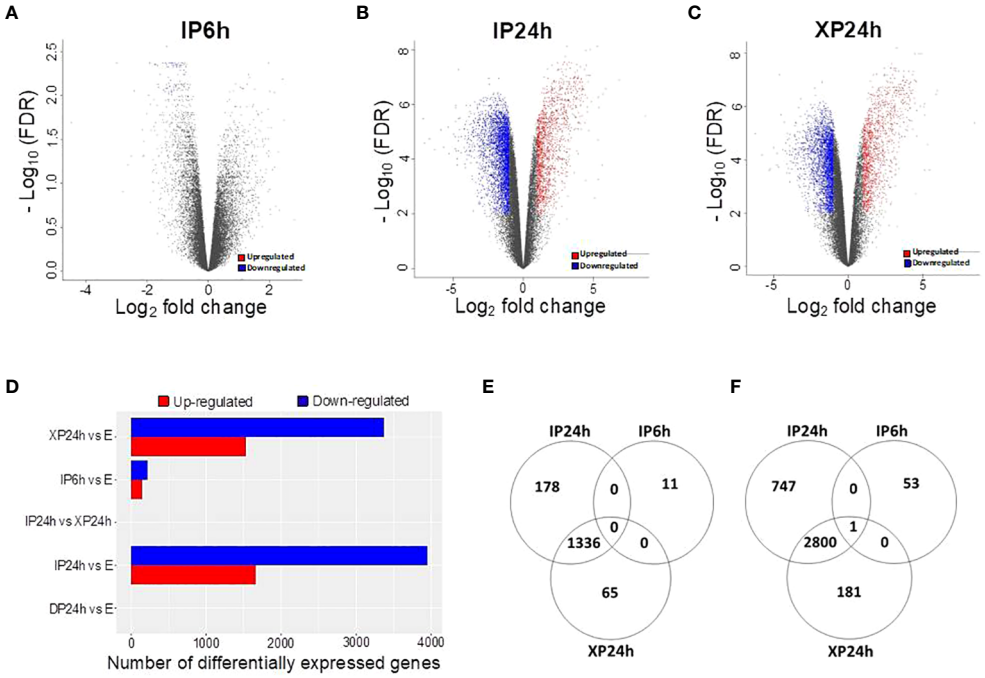

FIGURE 5
Identification of differentially expressed genes (DEGs) and the effect of pollen type and timing of style removal on their expression. **(A–C)** Volcano plots of all significant DEGs ($log_2FC \geq 1$ and $- log_{10}FDR \geq 2$) for IP6h, IP24h, and XP24h ovaries. Grey dots represent genes with insignificant expression changes; blue and red dots represent down-regulated and up-regulated genes, respectively. **(D)** Number of DEGs for the indicated treatment comparisons. Venn diagrams showing common or unique up-regulated **(E)** and down-regulated **(F)** genes relative to the control **(E)** samples. IP6h – pollinated with intact pollen and styles removed 6 h later; IP24h – pollinated with intact pollen and styles removed 24 h later; XP24h – pollinated with x-ray-irradiated pollen and styles removed 24 h later; DP24h – pollinated with dead pollen and styles removed 24 h later; E – emasculated but unpollinated control.

IP24h samples shared the majority of up-regulated DEGs (1336 genes), while there were 11, 65, and 178 uniquely up-regulated genes in IP6h, XP24h, and IP24h samples, respectively (Figure 5E). Among the downregulated DEGs, 2800 genes were common between XP24h and IP24h samples (Figure 5F). We found that 53, 181, and 747 genes were uniquely downregulated in IP6h, XP24h and IP24h samples, but only 1 gene was commonly downregulated in all three samples (Figure 5F).

3.5 DEG enrichment analysis

Term enrichment analysis of the identified DEGs was then performed in an attempt to zoom in on the molecular changes triggered in XP24h ovaries relative to E ovaries (Figure 6). We found that the 1,401 up-regulated genes were classified into 40 GO terms and 15 KEGG pathways (Table S1). The top biological processes were 'regulation of cell cycle process' (30 genes), 'mitotic cell cycle' (44 genes), 'cell cycle process' (52 genes), and 'cell cycle' (61 genes) (Figure 6A). Additionally, the tope enriched cellular components were 'DNA packing complex' (28 genes), 'nucleosome' (27 genes), and 'protein–DNA complex' (32 genes), while molecular functions that stood out were 'cyclin-dependent protein serine/threonine kinase regulator activity' (13 genes), 'protein kinase regulator activity' (14 genes), 'kinase regulator activity' (15 genes), and 'protein kinase binding' (15 genes). For the KEGG pathways, 15 terms were found among the upregulated genes and these were related to many critical pathways such as 'photosynthesis' (13 genes), 'biosynthesis of cofactor' (15 genes), 'plant hormone signal transduction' (13 genes), and 'biosynthesis of secondary metabolites' (57 genes) (Figure 6B; Table S1).

The 2,982 downregulated DEGs belonged to 32 GO terms and 10 KEGG pathways (Table S1). Notable GO terms included 'response to hormone' (63 genes), 'response to endogenous stimulus' (63 genes), 'response to organic substance' (72 genes), 'response to chemical' (86 genes), 'SCF ubiquitin ligase complex' (9 genes), 'plasma membrane' (86 genes), 'cell periphery' (99 genes), 'ubiquitin conjugating enzyme activity' (9 genes), 'DNA-binding transcription factor activity' (86 genes), and 'transcription regulator activity' (91 genes) (Figure 6A). Furthermore, the main enriched KEGG pathways were 'plant hormone signal transduction' (34 genes), 'plant–pathogen interaction' (14 genes), and 'biosynthesis of secondary metabolites' (72 genes) (Figure 6B; Table S1).

Interestingly, the term enrichment analysis results for IP24h ovaries were highly similar to those of the XP24h ovaries (Figure S1B; Table S1). In contrast, the GO terms and KEGG pathways for the 65 DEGs (11 up-regulated and 54 downregulated) identified in IP6h ovaries were different. Notable GO terms and KEGG pathways in IP6h ovaries were 'deoxyribonucleotide biosynthesis process' 'nucleosome assembly', 'chromatin remodelling', 'nucleosome', 'DNA packing complex', 'asparagine synthase (glutamine-hydrolysing) activity', 'purine metabolism' and 'pyrimidine

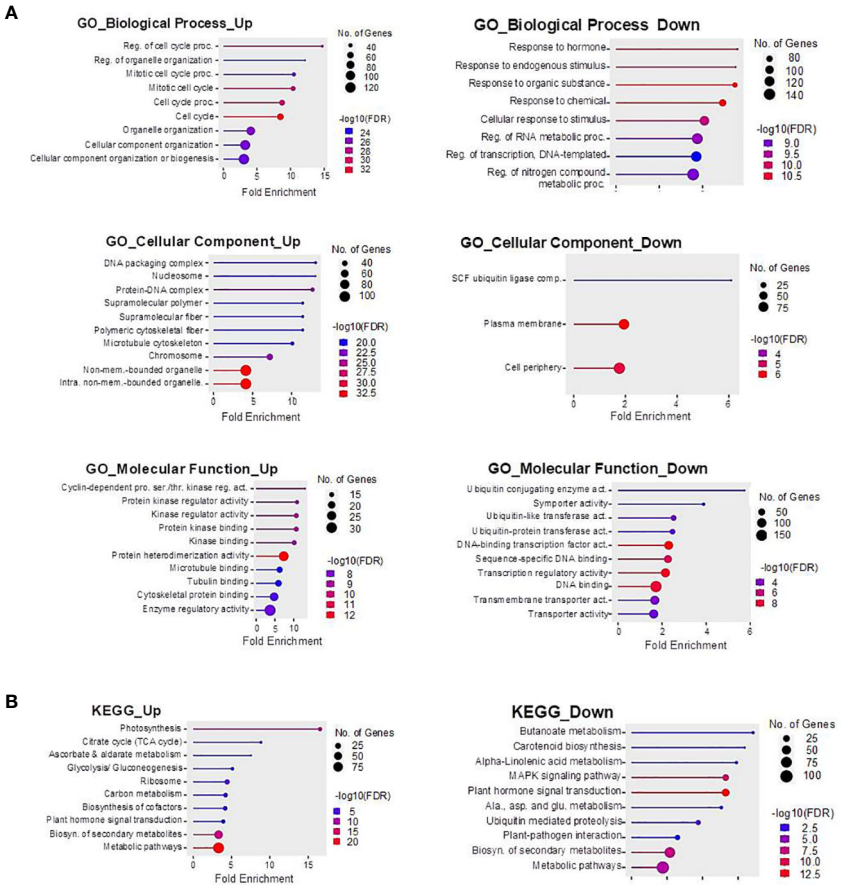

FIGURE 6
Gene Ontology **(A)** and KEGG pathways **(B)** enriched among up-regulated and down-regulated DEGs in XP24h ovaries. The GO terms and KEGG pathways were selected based on FDR values and sorted by fold enrichment values. The size of the dots represents the number of genes, and different colours indicate -$\log_{10}$(FDR) values.

metabolism' (Figure S1A; Table S1). These findings further supported the notion that partial pollen tube might have limited effects on the remodelling of genetic materials. The changes induced might be essential preparations for cell division, but they are likely not sufficient to initiate fruit set in tomato.

3.6 Identification of potential genes/gene families responding to fully elongated pollen tubes

To explain the histological results that XP24h led to increased cell layer numbers and cell size at 2 DAA, we examined the expression patterns of some genes which are well-known for regulating cell division and expansion at the early stage of tomato fruit development. As illustrated in Figure 7A, thirteen members belonging to three subclasses (A, B, and D) of the cyclin family were significantly upregulated in XP24h and IP24h ovaries; highly expressed genes were *cyclin B1_2* (Solyc10g080950) and *cyclin B2_7* (Solyc03go32190). Likewise, five members of the expansin gene family and one gene encoding an expansin precursor (Soly02g088100) showed up to 3.6-fold higher expression in XP24h and IP24h ovaries (Figure 7B), than in IP6h and DP24h ovaries.

The vital role of phytohormones in regulating tomato fruit initiation and development was illustrated consistently through previous reports (Fenn and Giovannoni, 2021). In the present study, the KEGG enrichment analysis results also revealed that many DEGs were involved in the 'plant hormone signal transduction' pathway (Figure 6B). We therefore examined the expression pattern of genes involved in the synthesis, transportation, and signalling of various hormones (Figure 7C; Table S2). As indicated in Figure 7C, ethylene and auxin seemed to be the most active hormones in XP24h and IP24h ovaries. The expression of 8 genes related to ethylene (3 encoding ethylene receptors and 5 encoding ethylene biosynthesis enzymes) and 12 genes related to auxin (10 involved in auxin response and signalling, and 2 involved in auxin transport) were changed significantly. Specifically, there was significant downregulation ($\log_2$FC = -2) of *ARF7* and *ARF5*, which are key transcription factors that regulate

10.3389/fpls.2023.1205816

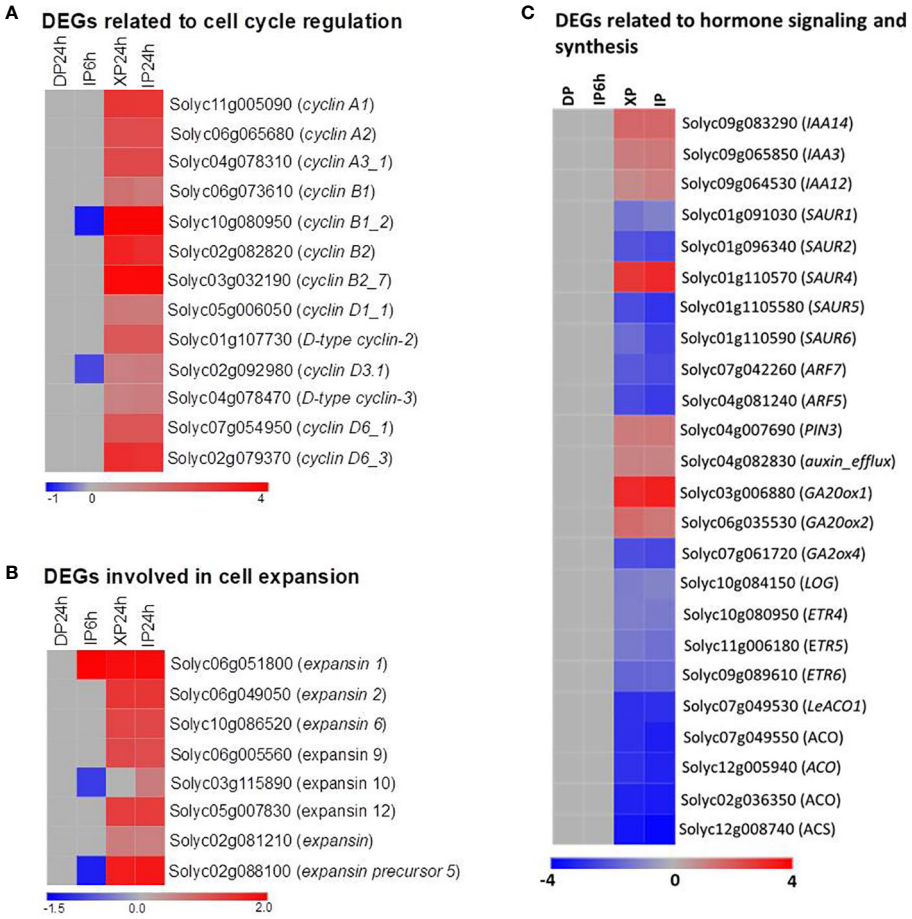

FIGURE 7
Expression patterns of genes involved in cell division and expansion, and phytohormones. **(A)** DEGs belonging to the cyclin family. **(B)** DEGs belonging to the expansin family. **(C)** DEGs related to phytohormone signalling, synthesis, and transportation. IP6h – pollinated with intact pollen and styles removed 6 h later; IP24h – pollinated with intact pollen and styles removed 24 h later; XP24h – pollinated with x-ray-irradiated pollen and styles removed 24 h later; DP24h – pollinated with dead pollen and styles removed 24 h later.

fruit set and early fruit development. In addition, XP24h and IP24h ovaries displayed increased expression of two genes that positively regulate gibberellin synthesis (*GA20ox1* and *GA20ox2*), and repression of *GA2ox4*, a negative controller of gibberellin catabolism (Figure 7C). Altogether, these results illustrated that complete penetration of pollen tubes (as in XP24h) might broadly affect hormonal responses to activate both cell division and cell expansion events by increasing the expression of cyclin and expansin genes.

3.7 The effect of fully elongated pollen tubes on the expression of genes associated with parthenocarpy

In this study, pollination by X-ray-irradiated pollen resulted in a considerably high fruit set ratio (78.3%) of parthenocarpic fruits (Figure 1B), with an average weight approximately 65% that of seeded fruits on the same plant (Figure 3A). These effects are comparable to many previously reported parthenocarpy mutations in tomato (Sharif et al., 2022). We therefore examined the expression patterns of 23 well-known parthenocarpic genes in XP24h ovaries, compared to IP6h, IP24h, and DP24h. As a result, we found that 10 of these genes were differentially expressed ($\log_2$FC ≥ 2), particularly in XP24h and IP24h ovaries (Figure 8A). The top variable genes were *GA20ox1* ($\log_2$FC = 3.09), *NCED1* ($\log_2$FC = -2.75), *GA2ox2* ($\log_2$FC = -2.26), *AGL6* (*pat-k*) ($\log_2$FC = -2.17), and *ARF7* ($\log_2$FC = -2.02).

Although many genes related to auxin signalling and transport were differentially expressed in XP24h ovaries, *IAA9* which is an early auxin-responsive gene remained unchanged (Figure 8A). To further examine whether IAA9 is involved in parthenocarpic fruit development from XP24h ovaries, we pollinated the flowers of *iaa9-3*, a well-known parthenocarpic mutant (Saito et al., 2011), with X-ray-irradiated pollen. Compared to the control (E), X-ray-irradiated pollen slightly increased fruit set by approximately 14% (Figure 8B), but had little effect on cell layer formation (Figure 8C). In addition, the average weight of XP24h fruits (3.82 g) was similar to that of E

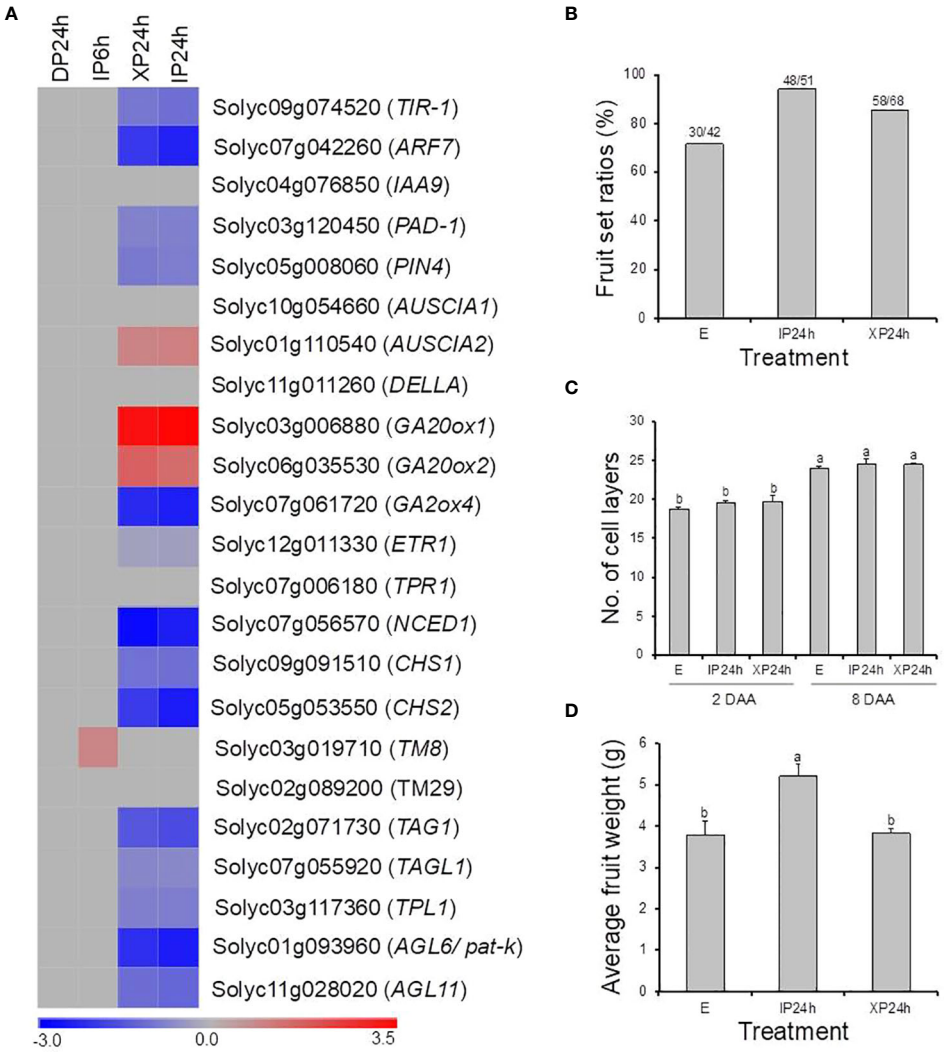

FIGURE 8
The potential involvement of well-known parthenocarpic genes in seedless fruit formation in flowers pollinated with X-ray irradiated pollen. **(A)** The expression patterns of 21 genes (previously associated with parthenocarpy in tomato) as affected by the different pollen types and style removal timing. **(B–D)** The effect of pollination with IP or XP and varying style removal timings on fruit initiation and development in *iaa9-3*, a well-established parthenocarpic "Micro-Tom" mutant line. Different letters in C and D indicate statistical difference, using Tukey's HSD test at $P < 0.05$. IP24h – pollinated with intact pollen and styles removed 24 h later; XP24h – pollinated with x-ray-irradiated pollen and styles removed 24 h later; E – emasculated but unpollinated control.

fruits (Figure 8D), both of which were nearly 75% of the weight of IP24h fruits. These results suggested that full pollen tube penetration might regulate auxin signalling *via* altering the interaction between ARF7 and IAA9 proteins.

4 Discussion

The role of pollen tubes in both the production of seedless fruits and study of parthenocarpic mechanisms has been well established in watermelons, through pollination tests with soft X-ray-irradiated pollen (Sugiyama and Morishita, 2002; Qu et al., 2016; Hu et al., 2019), or foreign (bottle gourd) pollen (Sugiyama et al., 2014). In either case, penetration of watermelon ovaries by pollen tubes led to reasonably high fruit set and the resultant parthenocarpic fruits had virtually the same size as control seeded fruits, most likely due to accumulation of various phytohormones including auxins, gibberellins, and cytokinins (Hu et al., 2019). Attempts to replicate these findings in tomato (both *S. lycopersicum* and *S. pimpinellifolium*) have been unsuccessful to date, as irradiation with X-ray or gamma-ray on dried pollen severely affected pollen germination, reduced fruit set, and resulted in very tiny parthenocarpic fruits (Nishiyama and Tsukuda, 1961; Uematsu and Nishiyama, 1967). In the present study, X-ray irradiation was applied on fresh anther cones before drying, as opposed to previous studies where it was applied directly on dried pollen. As a result, we

found that pollen germination was unaffected and pollen tubes from XP elongated in a similar manner as those from IP, fully penetrating the ovaries 24 h after pollination (Figure 1A). This observation allowed us to further study the distinct function of pollen tubes in tomato fruit formation.

It is intriguing that full penetration of the ovaries by pollen tubes emanating from XP triggered comparably high fruit set (Figure 1B), unlike partial pollen tube growth (as in IP6h) which resulted in failed fruit set. Although the parthenocarpic fruit which developed after XP pollination were slightly smaller than seeded fruit obtained by IP pollination (Figure 3), their average weight was within acceptable limits of most previously reported parthenocarpic tomato fruits. A possible explanation for the relatively small-sized XP-derived fruits is the lack of fertilization, evidenced by production of empty seeds (Figure 3E). In strawberry, successful fertilization was recently shown to induce auxin biosynthesis, resulting in normal fruit growth and development (Guo et al., 2022). Increased expression of auxin biosynthetic genes coupled with accumulation of auxins was also reported in watermelon ovaries at 2 DAA following pollination with X-ray-irradiated pollen (Hu et al., 2019), which most likely accounted for comparable sizes between parthenocarpic and seeded fruits (Sugiyama and Morishita, 2000; Sugiyama and Morishita, 2002). In the present study, auxins were not quantified but transcriptome analysis revealed that only auxin signalling and transportation genes were differentially expressed while auxin biosynthetic genes remained unchanged in XP-pollinated ovaries at 2 DAA (Figure 7C). Given that the genes associated with cell expansion were upregulated in XP-pollinated ovaries to a similar degree as IP-pollinated ones (Figure 3E), it is plausible that lack of fertilization (and hence no auxin accumulation) hinders normal fruit growth and development. The auxin effect most likely targets cell expansion rather than cell division (Figure 2D), ultimately affecting fruit size at maturity. This hypothesis is further supported by recent findings that the auxin content in ovaries of a new parthenocarpic tomato line "R35-P" was twice as much as that of the normal line "R35-N" (Zhang et al., 2021), resulting in similar-sized seeded and seedless fruits. Future studies should explore possible strategies to increase auxin content at early developmental stages for production of normal-sized parthenocarpic tomatoes.

In the present study, many previously reported parthenocarpic genes were differentially expressed in response to ovary penetration by pollen tubes (Figure 8A), which was consistent with their respective mutants (Schijlen et al., 2007; De Jong et al., 2009; García-Hurtado et al., 2012; Martínez-Bello et al., 2015; Liu et al., 2018; Takisawa et al., 2018). This finding suggests that the regulatory mechanisms by which full pollen tube penetration into the ovary induces seedless fruit development in tomato involves the coordinated action of diverse parthenocarpic genes. However, it was puzzling that the expression of *IAA9* did not change (Figure 8A), yet its loss-of-function mutant *iaa9-3* was shown to induce parthenocarpy (Saito et al., 2011). Pollination of *iaa9-3* flowers with XP slightly increased fruit set but failed to impact fruit development (Figures 8B–D). A possible explanation lies in the downregulation of *ARF7* following pollination of wild type "Micro-Tom" flowers with XP (Figure 8A). Previously, the ARF7/IAA9 complex was shown to regulate fruit initiation in tomato by acting as a transcriptional repressor of auxin and gibberellin biosynthetic genes (Hu et al., 2018). Therefore, a decrease in *ARF7* transcript levels points towards a weakening ARF7/IAA9 complex, which would then result in increased expression of gibberellin biosynthetic genes (Figure 7C), as well as *expansins* and *cyclins* (Figures 7A, B), eventually leading to fruit initiation and development.

Both ethylene production and signalling were also reported to change significantly during pollen tube growth in tomato (Althiab-Almasaud et al., 2021), and increased ethylene content in young tomato ovaries inhibit fruit set, either by promoting pedicel abscission (Roberts et al., 1984), or inhibiting cell division (Vandenbussche et al., 2007). In the present study, ethylene biosynthetic genes were down-regulated in ovaries at 2 DAA following full penetration by pollen tubes from XP (Figure 7C), a change that, in all likelihood, would avert pedicel abscission and promote cell division culminating in successful fruit formation.

Based on the results of this study, we propose a revised schematic model illustrating the distinct contributions of pollination, pollen tubes and fertilization to fruit formation in tomato (Figure 9). According to this model, the effect of pollination alone is non-significant. Partial pollen tube growth (or growing pollen tubes) significantly alters several pathways related with 'nucleosome assembly', 'chromatin assembly', 'DNA packaging complex', and 'protein-DNA complex', to release cell cycle dormancy. However, these changes are limited and cannot sufficiently activate cell division and expansion processes, resulting in failed fruit set. On the other hand, full pollen tube penetration sufficiently initiates fruit set and contributes to the early stages of fruit development (at least up to 4 DAA) by regulating different hormonal pathways likely through diverse parthenocarpic genes, such as *ARF7*, *ARF5*, *CHS1*, *CHS2*, *AGL6*, and *GA20ox1*. Finally, fertilization contributes to fruit development primarily by upregulating auxin synthesis, which then stimulates gibberellin synthesis and accelerates the expression of late-responding cell expansion genes. The effect of fertilization is evident towards later stages (beyond 4 DAA) of fruit development. In addition, our results suggest that the contribution of cell expansion to fruit development is greater than that of cell division from 4 DAA onwards, which is a much earlier timepoint than previous models (Ariizumi et al., 2013; Quinet et al., 2019).

5 Conclusion

Overall, we reported that the complete penetration of pollen tubes into ovaries regulates the expression of essential genes involved in diverse pathways to accelerate both cell division and cell expansion events in tomato ovary tissue. These effects are

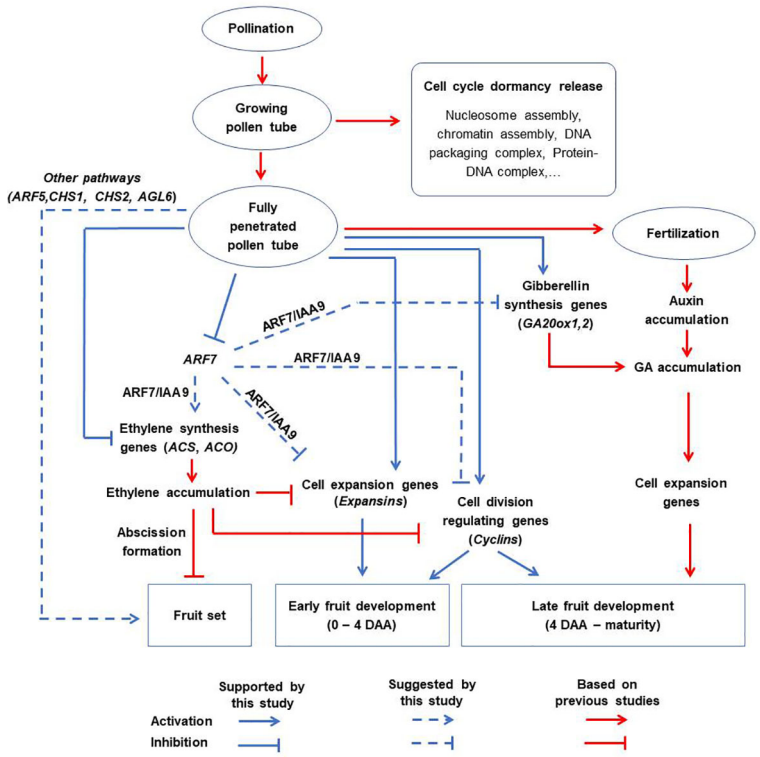

FIGURE 9
A proposed schematic model for tomato fruit initiation and development. Pollination alone has no significant effect. Partial pollen tube growth alters the expression of genes related to cell cycle dormancy release but this is not sufficient to initiate fruit set. Full penetration of pollen tubes into ovaries initiates fruit set and contributes to the early stages of fruit development (up to 4 DAA) *via* diverse pathways which might include inhibition of ethylene biosynthetic genes, stimulation of genes associated with gibberellin biosynthesis (*GA20ox1*), cell expansion (*expansins*), and division (*cyclins*). This might involve diverse parthenocarpic genes (particularly *ARF7*) as intermediate regulators. Finally, fertilization is responsible for auxin accumulation, which enhances the expression of cell expansion genes and hence contributes to late fruit development.

independent of fertilization, resulting in a high fruit set ratio and parthenocarpic fruit development. These findings contribute to a better understanding of the mechanism by which tomato fruits are set and developed.

Data availability statement

The datasets presented in this study can be found in online repositories. The names of the repository/repositories and accession number(s) can be found below: DNA Data Bank of Japan (DDBJ) database (DRR461225-DRR461239).

Author contributions

All authors contributed to the article and approved the submitted version. Conceptualization: LT, HE, KS. Experimental design: LT, HE, KS. Data curation: LT, MK. Data analysis and visualization: LT, KS, OM. Writing-original draft preparation: LT, KS. Writing-review and editing: LT, HE, KS, OM, MK. Supervision: HE, KS. Resources: HE.

Funding

This work was supported by a grant-in-aid for scientific research, category A (no. 25252008) to HE from the Ministry of Education, Culture, Sports, Science and Technology of Japan.

Acknowledgments

LT acknowledges the Ministry of Education, Culture, Sports, Science and Technology (MEXT) of Japan for providing the scholarship to conduct the current research under the MEXT Special Scholarship Program on Trans-world Professional Human Resources Development Program on Food Security & Natural Resources Management (TPHRD) for Doctoral Course. We thank Mr Shunsuke Oka (M.A., Centre Research Institute, Nippn Co., Ltd., Kanagawa Prefecture, Japan) for technical help with X-ray treatment.

Conflict of interest

The authors declare that the research was conducted in the absence of any commercial or financial relationships that could be construed as a potential conflict of interest.

Publisher's note

All claims expressed in this article are solely those of the authors and do not necessarily represent those of their affiliated organizations, or those of the publisher, the editors and the reviewers. Any product that may be evaluated in this article, or claim that may be made by its manufacturer, is not guaranteed or endorsed by the publisher.

Supplementary material

The Supplementary Material for this article can be found online at: https://www.frontiersin.org/articles/10.3389/fpls.2023.1205816/full#supplementary-material

References

Althiab-Almasaud, R., Chen, Y., Maza, E., Djari, A., Frasse, P., Mollet, J. C., et al. (2021). Ethylene signaling modulates tomato pollen tube growth through modifications of cell wall remodeling and calcium gradient. *Plant J.* 107 (3), 893–908. doi: 10.1111/tpj.15353

Ariizumi, T., Shinozaki, Y., and Ezura, H. (2013). Genes that influence yield in tomato. *Breed. Sci.* 63 (1), 3–13. doi: 10.1270/jsbbs.63.3

Bolger, A. M., Lohse, M., and Usadel, B. (2014). Trimmomatic: a flexible trimmer for illumina sequence data. *Bioinformatics* 30 (15), 2114–2120. doi: 10.1093/bioinformatics/btu170

De Jong, M., Wolters-Arts, M., Feron, R., Mariani, C., and Vriezen, W. H. (2009). The solanum lycopersicum auxin response factor 7 (*SlARF7*) regulates auxin signaling during tomato fruit set and development. *Plant J.* 57 (1), 160–170. doi: 10.1111/j.1365-313X.2008.03671.x

Ezura, H. (2009). Tomato is a next-generation model plant for research and development. *J. Jpn. Soc Hortic. Sci.* 78 (1), 1–2. doi: 10.2503/jjshs1.78.1

Fenn, M. A., and Giovannoni, J. J. (2021). Phytohormones in fruit development and maturation. *Plant J.* 105 (2), 446–458. doi: 10.1111/tpj.15112

García-Hurtado, N., Carrera, E., Ruiz-Rivero, O., López-Gresa, M. P., Hedden, P., Gong, F., et al. (2012). The characterization of transgenic tomato overexpressing gibberellin 20-oxidase reveals induction of parthenocarpic fruit growth, higher yield, and alteration of the gibberellin biosynthetic pathway. *J. Exp. Bot.* 63 (16), 5803–5813. doi: 10.1093/jxb/ers229

Ge, S. X., Son, E. W., and Yao, R. (2018). iDEP: an integrated web application for differential expression and pathway analysis of RNA-seq data. *BMC Bioinf.* 19 (1), 1–24. doi: 10.1186/s12859-018-2486-6

Gulles, A., Bartolome, V., Morantte, R., Nora, L., Relente, C., Talay, D., et al. (2014). Randomization and analysis of data using STAR [Statistical tool for agricultural research]. *Philipp. J. Crop Sci.* 39, 137.

Guo, L., Luo, X., Li, M., Joldersma, D., Plunkert, M., and Liu, Z. (2022). Mechanism of fertilization-induced auxin synthesis in the endosperm for seed and fruit development. *Nat. Commun.* 13 (1), 3985. doi: 10.1038/s41467-022-31656-y

Holden, M. J., Marty, J. A., and Singh-Cundy, A. (2003). Pollination-induced ethylene promotes the early phase of pollen tube growth in *Petunia inflata*. *J. Plant Physiol.* 160 (3), 261–269. doi: 10.1078/0176-1617-00929

Hu, J., Israeli, A., Ori, N., and Sun, T.-P. (2018). The interaction between DELLA and ARF/IAA mediates crosstalk between gibberellin and auxin signaling to control fruit initiation in tomato. *Plant Cell* 30 (8), 1710–1728. doi: 10.1105/tpc.18.00363

Hu, Z., Lan, S., Zhao, N., Su, N., Xue, Q., Liu, J., et al. (2019). Soft-x-irradiated pollens induce parthenocarpy in watermelon *via* rapid changes of hormone-signalings and hormonal regulation. *Sci. Hortic.* 250, 317–328. doi: 10.1016/j.scienta.2019.02.036

Jia, H., Yang, J., Liesche, J., Liu, X., Hu, Y., Si, W., et al. (2018). Ethylene promotes pollen tube growth by affecting actin filament organization *via* the cGMP-dependent pathway in *Arabidopsis thaliana*. *Protoplasma* 255, 273–284. doi: 10.1007/s00709-017-1158-0

Kim, D., Paggi, J. M., Park, C., Bennett, C., and Salzberg, S. L. (2019). Graph-based genome alignment and genotyping with HISAT2 and HISAT-genotype. *Nat. Biotechnol.* 37 (8), 907–915. doi: 10.1038/s41587-019-0201-4

Liao, Y., Smyth, G. K., and Shi, W. (2014). featureCounts: an efficient general purpose program for assigning sequence reads to genomic features. *Bioinformatics* 30 (7), 923–930. doi: 10.1093/bioinformatics/btt656

Liu, S., Zhang, Y., Feng, Q., Qin, L., Pan, C., Lamin-Samu, A. T., et al. (2018). Tomato AUXIN RESPONSE FACTOR 5 regulates fruit set and development *via* the mediation of auxin and gibberellin signaling. *Sci. Rep.* 8 (1), 1–16. doi: 10.1038/s41598-018-21315-y

Martínez-Bello, L., Moritz, T., and López-Díaz, I. (2015). Silencing C19-GA 2-oxidases induces parthenocarpic development and inhibits lateral branching in tomato plants. *J. Exp. Bot.* 66 (19), 5897–5910. doi: 10.1093/jxb/erv300

Matsuo, S., Miyatake, K., Endo, M., Urashimo, S., Kawanishi, T., Negoro, S., et al. (2020). Loss of function of the *Pad-1* aminotransferase gene, which is involved in auxin homeostasis, induces parthenocarpy in solanaceae plants. *Proc. Natl. Acad. Sci. U. S. A.* 117 (23), 12784–12790. doi: 10.1073/pnas.2001211117

Molesini, B., Dusi, V., Pennisi, F., and Pandolfini, T. (2020). How hormones and mads-box transcription factors are involved in controlling fruit set and parthenocarpy in tomato. *Genes* 11 (12), 1441. doi: 10.3390/genes11121441

Nishiyama, I., and Tsukuda, S. (1961). Radiobiological studies in plants, V effects of X-and gamma-irradiations on pollen fertility of *Lycopersicum pimpinellifolium*. *Jpn. J. Genet.* 36 (11-12), 423–427. doi: 10.1266/jjg.36.423

Qu, H.-Y., Zhang, C., and Sun, Y. (2016). The mechanism of seedlessness in watermelon generated using soft-X-ray irradiated pollen. *Afr. J. Agric. Res.* 11 (25), 2200–2204. doi: 10.5897/AJAR2015.9890

Quinet, M., Angosto, T., Yuste-Lisbona, F. J., Blanchard-Gros, R., Bigot, S., Martinez, J.-P., et al. (2019). Tomato fruit development and metabolism. *Front. Plant Sci.* 10, 1554. doi: 10.3389/fpls.2019.01554

Roberts, J. A., Schindler, C. B., and Tucker, G. A. (1984). Ethylene-promoted tomato flower abscission and the possible involvement of an inhibitor. *Planta* 160, 159–163. doi: 10.1007/BF00392864

Saito, T., Ariizumi, T., Okabe, Y., Asamizu, E., Hiwasa-Tanase, K., Fukuda, N., et al. (2011). TOMATOMA: a novel tomato mutant database distributing micro-tom mutant collections. *Plant Cell Physiol.* 52 (2), 283–296. doi: 10.1093/pcp/pcr004

Schijlen, E. G., de Vos, C. R., Martens, S., Jonker, H. H., Rosin, F. M., Molthoff, J. W., et al. (2007). RNA Interference silencing of chalcone synthase, the first step in the flavonoid biosynthesis pathway, leads to parthenocarpic tomato fruits. *Plant Physiol.* 144 (3), 1520–1530. doi: 10.1104/pp.107.100305

Sharif, R., Su, L., Chen, X., and Qi, X. (2022). Hormonal interactions underlying parthenocarpic fruit formation in horticultural crops. *Horticulture Res.* 9. doi: 10.1093/hr/uhab024

Sugiyama, K., Kami, D., and Muro, T. (2014). Induction of parthenocarpic fruit set in watermelon by pollination with bottle gourd (*Lagenaria siceraria* (Molina) *Standl.*) pollen. *Sci. Hortic.* 171, 1–5. doi: 10.1016/j.scienta.2014.03.008

Sugiyama, K., and Morishita, M. (2000). Fruit and seed characteristics of diploid seedless watermelon (*Citrullus lanatas*) cultivars produced by soft-x-irradiated pollen. *J. Jpn. Soc Hortic. Sci.* 69 (6), 684–689. doi: 10.2503/jjshs.69.684

Sugiyama, K., and Morishita, M. (2002). New method of producing diploid seedless watermelon fruit. *Jpn. Agric. Res. Q.* 36 (3), 177–182. doi: 10.6090/jarq.36.177

Takisawa, R., Koeda, S., and Nakazaki, T. (2019). Effects of the *pat-2* gene and auxin biosynthesis inhibitor on seed production in parthenocarpic tomatoes (*Solanum lycopersicum* l.). *Hortic. J.* 88 (4), 481–487. doi: 10.2503/hortj.UTD-085

Takisawa, R., Maai, E., Nakano, R., and Nakazaki, T. (2020). Effect of parthenocarpic genes *pat-2* and *pat-k* on vegetative and fruit traits in tomato (*Solanum lycopersicum* 'Micro-tom'). *Hortic. J.* 89 (3), 261–267. doi: 10.2503/hortj.UTD-127

Takisawa, R., Nakazaki, T., Nunome, T., Fukuoka, H., Kataoka, K., Saito, H., et al. (2018). The parthenocarpic gene *Pat-k* is generated by a natural mutation of *SlAGL6* affecting fruit development in tomato (*Solanum lycopersicum* l.). *BMC Plant Biol.* 18, 1–12. doi: 10.1186/s12870-018-1285-6

Tran, L. T., Nguyen, A. T., Nguyen, M. H., Nguyen, L. T., Nguyen, M. T., Trinh, L. T., et al. (2021). Developing new parthenocarpic tomato breeding lines carrying *iaa9-3* mutation. *Euphytica* 217 (7), 1–13. doi: 10.1007/s10681-021-02853-5

Uematsu, S., and Nishiyama, I. (1967). Radiobiological studies in plants. XII. further studies on effects of X-rays on pollen functions. *Radiat. Bot.* 7, 477–480.

Vandenbussche, F., Vancompernolle, B., Rieu, I., Ahmad, M., Phillips, A., Moritz, T., et al. (2007). Ethylene-induced arabidopsis hypocotyl elongation is dependent on but not mediated by gibberellins. *J. Exp. Bot.* 58 (15-16), 4269–4281. doi: 10.1093/jxb/erm288

Yeung, E. C., and Chan, C. K. (2015). *The glycol methacrylate embedding resins—technovit 7100 and 8100.* (Germany: Springer Cham). doi: 10.1007/978-3-319-19944-3_4

Zhang, S., Gu, X., Shao, J., Hu, Z., Yang, W., Wang, L., et al. (2021). Auxin metabolism is involved in fruit set and early fruit development in the parthenocarpic tomato "R35-p". *Front. Plant Sci.* 12. doi: 10.3389/fpls.2021.671713

frontiers | Frontiers in Plant Science

TYPE Original Research
PUBLISHED 28 July 2023
DOI 10.3389/fpls.2023.1227349

OPEN ACCESS

EDITED BY
Luciano Freschi,
University of São Paulo, Brazil

REVIEWED BY
Diane Maria Beckles,
University of California, Davis, United States
Ann Louise Thomas Powell,
University of California, Davis, United States

*CORRESPONDENCE
Hiroshi Ezura
ezura.hiroshi.fa@u.tsukuba.ac.jp

RECEIVED 23 May 2023
ACCEPTED 10 July 2023
PUBLISHED 28 July 2023

CITATION
Mitalo OW, Kang SW, Tran LT, Kubo Y, Ariizumi T and Ezura H (2023) Transcriptomic analysis in tomato fruit reveals divergences in genes involved in cold stress response and fruit ripening. *Front. Plant Sci.* 14:1227349. doi: 10.3389/fpls.2023.1227349

Transcriptomic analysis in tomato fruit reveals divergences in genes involved in cold stress response and fruit ripening

Oscar W. Mitalo[1], Seung Won Kang[1,2], Long T. Tran[1], Yasutaka Kubo[3], Tohru Ariizumi[1,2] and Hiroshi Ezura[1,2]*

[1]Graduate School of Life and Environmental Sciences, University of Tsukuba, Tsukuba, Japan, [2]Tsukuba-Plant Innovation Research Center, University of Tsukuba, Tsukuba, Japan, [3]Graduate School of Environmental and Life Science, Okayama University, Okayama, Japan

Cold storage is widely used to extend the postharvest life of most horticultural crops, including tomatoes, but this practice triggers cold stress and leads to the development of undesirable chilling injury (CI) symptoms. The underlying mechanisms of cold stress response and CI development in fruits remain unclear as they are often intermingled with fruit ripening changes. To gain insight into cold responses in fruits, we examined the effect of the potent ethylene signaling inhibitor 1-methylcyclopropene (1-MCP) on fruit ripening, CI occurrence and gene expression in mature green tomatoes during storage at 20°C and 5°C. 1-MCP treatments effectively inhibited ethylene production and peel color changes during storage at 20°C. Storage at 5°C also inhibited both ethylene production and peel color change; during rewarming at 20°C, 1-MCP treatments inhibited peel color change but failed to inhibit ethylene production. Furthermore, fruits stored at 5°C for 14 d developed CI symptoms (surface pitting and decay) during the rewarming period at 20°C regardless of 1-MCP treatment. Subsequent RNA-Seq analysis revealed that cold stress triggers a large-scale transcriptomic adjustment, as noticeably more genes were differentially expressed at 5°C (8,406) than at 20°C (4,814). More importantly, we have found some important divergences among genes involved in fruit ripening (up- or down-regulated at 20°C; inhibited by 1-MCP treatment) and those involved in cold stress (up- or down-regulated at 5°C; unaffected by 1-MCP treatment). Transcriptomic adjustments unique to cold stress response were associated with ribosome biogenesis, NcRNA metabolism, DNA methylation, chromatin formation/remodeling, and alternative splicing events. These data should foster further research into cold stress response mechanisms in fruits with the ultimate aim of improving tolerance to low temperature and reduction of CI symptoms during cold storage.

KEYWORDS

cold stress, chilling injury, "Micro-Tom", "Moneymaker", RNA-Seq, ripening

1 Introduction

Cold storage is an inevitable technique during postharvest handling of horticultural produce, mainly because of the broad spectrum inhibitory effects of low temperature on quality deterioration and postharvest loss. Low temperature is generally thought to slow most cell metabolic processes (Chinnusamy et al., 2007; Rao, 2015), including those which contribute to reduced postharvest life such as fruit ripening, respiration and senescence. Storage at low temperatures also inhibits growth of most postharvest pathogens which are popularly associated with reduced quality (Vico et al., 2010; Manning et al., 2016). However, certain crops particularly tropical and subtropical types are sensitive to low temperatures, and hence suboptimal cold storage triggers a multitude of physiological disorders collectively referred to as chilling injury (CI) (Sevillano et al., 2009). CI symptoms are complex in nature and vary depending on species, cultivar, tissue and organ, and maturity stage (Wang, 1994; Sevillano et al., 2009). As CI symptoms are deleterious and contribute greatly to horticultural crop loss and heavy economic losses, there is an ongoing effort to understand the regulatory mechanisms involved in order to develop resilient crops.

Relevant progress in understanding cold stress responses and CI development has been made in vegetative plant and organs, particularly leaves. In tolerant plants such as Arabidopsis, wheat and barley, cold stress triggers an adaptive response called cold acclimation, which refers to a suite of physiological and biochemical changes that are primarily regulated by three C-repeat binding factor/drought response element binding factor 1B (CBF/DREB1) genes (Jiang et al., 2017). Low temperature rapidly triggers the expression of *CBFs*, and the cold-induced CBF proteins activate the expression of numerous cold-regulated genes, thus enhancing tolerance to cold stress (Kidokoro et al., 2022). While cold sensitive plants generally lack the capacity to cold acclimate, a limited but relevant ability to adapt to chilling stress was reported in three-week old tomato seedlings (Barrero-Gil et al., 2016), as well as in the seedlings of maize (Anderson et al., 1994), rice (Kuk et al., 2003), and sweet pepper (Liu et al., 2001).

Unlike in the vegetative stages, cold stress responses and the mechanisms regulating CI development in the fruit remain unclear. This is partly because the adjustments that occur in response to cold stress at the vegetative stage are not necessarily similar to those taking place in the fruits of the same plant. For instance, cold stress activated the expression of *SlCBF1* in the leaves of "Micro-Tom" tomato plants but not in the fruits (Weiss and Egea-Cortines, 2009), while citrus *COR15*–which encodes a dehydrin–was swiftly induced by cold stress in leaves but expressed constitutively in fruits (Sanchez-Ballesta et al., 2004). Secondly, cold stress responses in fruits are often intermingled with fruit ripening and senescence (Biswas et al., 2016; Shipman et al., 2021), and hence it is hard to ascribe the resultant physio-molecular adjustments and symptoms to CI.

Tomato is an important horticultural crop and an established model for the study of fleshy fruit species (Ezura, 2009; Menda et al., 2013). Tomato fruits are very sensitive to cold stress and storage at temperatures below 10°C triggers several CI symptoms such as flavor loss, impaired ripening, surface pitting, poor texture, increased susceptibility to postharvest decay and discoloration (Biswas et al., 2016). As a typical climacteric fruit, the ripening process in tomato is largely controlled by the phytohormone ethylene (Li et al., 2019), through up- or down-regulation of various ripening-associated genes. Mutations in ethylene receptors have been shown to significantly inhibit fruit ripening in tomatoes (Lanahan et al., 1994; Okabe et al., 2011), but partial retention of ethylene sensitivity in these mutants likely due to functional redundancy among several receptors was also reported (Tieman et al., 2000; Gratão et al., 2012; Chen et al., 2019). 1-Methylcyclopropene (1-MCP) is a synthetic compound that irreversibly binds to ethylene receptors (Serek et al., 2006; Watkins, 2006), at a higher affinity than ethylene (Blankenship and Dole, 2003), thus preventing the hormone from binding to the receptors and blocking ethylene activation of downstream events. A major advantage of using 1-MCP to block ethylene signaling over other approaches is that 1-MCP indiscriminately binds to all ethylene receptors in addition to providing precision and high efficiency (Schotsmans et al., 2009; Kamiyoshihara et al., 2012), which allows researchers to study both ethylene-dependent and -independent processes in a relatively short period of time.

Here, RNA-Seq analysis was used to identify transcriptional adjustments which occur during normal ripening at 20°C or in response to cold stress (5°C, 14 d) in "Micro-Tom" tomatoes. In an attempt to differentiate cold stress-induced *versus* ethylene-induced (to a large extent, fruit ripening) changes, we also monitored gene expression changes in both "Micro-Tom" and "Moneymaker" tomatoes that had been repeatedly treated with 1-MCP during storage at 20°C and 5°C. This analysis revealed that genes associated with epigenetic modifications, ribosome biogenesis, proteasome and non-coding RNA metabolism, alternative splicing events and several transcription factors could be involved in the series of events unique to cold stress and CI development in fruits.

2 Materials and methods

2.1 Plant material and treatments

Solanum lycopersicum "Micro-Tom" (TOMJPF00001) and "Moneymaker" cultivars were obtained from the National Bioresource Project (MEXT, Japan) through the TOMATOMA database (Saito et al., 2011). Fruits were harvested at the mature green stage (before onset of autocatalytic ethylene production), washed in commercial bleach (1:10 dilution of sodium hypochlorite) and sorted to ensure uniform size, color and absence of defects or damage. This timing of harvest was well thought out to avoid the effect of large amounts of ethylene, which are produced at later maturity stages, during cold stress tests. For each cultivar, two groups of 50 fruits were used to characterize the ripening behavior at 20°C; the first group were treated (2–3 times a week) with 2 μLL^{-1} 1-MCP for 12 h, while the second group were a non-treated control. For cold stress tests, two groups of 50 fruits were also used; the first group was treated with 1-MCP as described above while the other group was a non-treated control. "Micro-

Tom" fruits were stored at 5°C for 14 d before being transferred to 20°C for up to 21 d. Three separate storage trials were carried out on "Micro-Tom" fruits. "Moneymaker" fruits were also stored at 5°C but for 21 d; after every 7 d, 10 fruits were transferred to 20°C to observe CI symptoms. 1-MCP treatments were carried out to keep the fruits insensitive to ethylene. To release 1-MCP gas, SmartFresh™ powder (AgroFresh, PA, USA) was dissolved in water and soda lime was added in the sealed treatment containers to reduce CO_2 accumulation. For DNA methylation inhibitor treatment, "Moneymaker" fruits at the mature green stage were used. The fruits were injected with 100 µL of 50 mM 5-azacytidine aqueous solution into the columella at harvest and every 7 d during storage at 5°C. The negative controls were injected with the same amount of distilled water. In all treatments, pericarp samples of three replicate fruits were collected, frozen in liquid nitrogen and stored at -80°C for future analysis.

2.2 Determination of peel color

Peel color measurements were carried out on four evenly distributed equatorial sites using a Konica Minolta Color Reader CR-10 (Konica Minolta, Tokyo, Japan). The Hunter lab parameter a*, which is a measure of greenness or redness, was recorded and then expressed as the mean of six replicate fruits.

2.3 Ethylene measurements

Individual fruits were incubated at the respective storage temperatures for 1 h. Headspace gas (1 mL) was then withdrawn and injected into a Shimadzu 5890 series gas chromatograph (Shimadzu, Kyoto, Japan) equipped with a flame ionization detector (200°C) and an activated alumina column (80°C). Ethylene production rates were expressed as the mean of 10 replicate fruits.

2.4 Determination of CI index

Fruits were assessed visually for severity of CI symptoms based on a five-point scale (0 = no injury; 1 = < 10%; 2 = 11 to 25%; 3 = 26–40%, and 4 = > 40%) consisting of three parameters: surface pitting, uneven ripening, and decay (Vega-García et al., 2010; Albornoz et al., 2019). The CI index was then calculated by determining the average of the injury levels of surface pitting, uneven ripening, and decay. For each time point, 10 fruits were evaluated individually, and the CI indexes were averaged.

2.5 Library construction and RNA sequencing

Pericarp samples of "Micro-Tom" fruits collected at harvest (0 d), after 14 d storage at either 5°C or 20°C, and after 21 d at 20°C or 14 d at 5°C followed by 7 d at 20°C (three fruit per treatment) were used for RNA-Seq analysis. Total RNA was extracted from 100 mg samples using the RNeasy® Plant Mini Kit (Qiagen, Hilden, Germany), treated with DNase I (Nippon Gene, Tokyo, Japan) to remove genomic DNA contamination and further purified with FavorPrep after Tri-Reagent RNA Clean-up Kit (Favorgen Biotech. Co., Ping-Tung, Taiwan). Paired-end libraries were then constructed using NEBNext® Ultra™ II Directional RNA Library Prep Kit (New England Biolabs), and sequencing was performed on an Illumina Novaseq 6000 platform (Illumina, Inc.).

2.6 Differential gene expression analysis

The sequenced reads were analyzed primarily on the Galaxy online platform[1]. Trimming was first carried out to exclude both low quality sequences and adapter sequences. The trimmed reads were then mapped to the reference *S. lycopersicum* genome (SL4.0), and mapped reads were counted using the featureCounts tool. Gene expression levels were then normalized as transcripts per kilobase million (TPM) reads. Differentially expressed genes (DEGs) were obtained by comparing the expression levels in samples after 14 d of storage at either 5°C or 20°C with those of at-harvest (0 d) samples on the iDEP (v. 0.96) web-based toolkit (Ge et al., 2018). Three criteria were used to detect DEGs: (i) TPM ≥ 1.0 in either of the three replicate samples, (ii) false discovery rate ≤ 0.01, and (iii) two-fold increase or increase in expression levels. Weighted gene co-expression network analysis (WGCNA) method (Langfelder and Horvath, 2008) was then employed to generate clusters of highly correlated genes with 8 and 0.15 as thresholding power and tree-cut parameters, respectively. Significantly enriched gene ontology (GO) terms and KEGG pathways were established using the ShinyGO (v. 0.77) web-based toolkit (Ge et al., 2020). The cut-off for significantly enriched terms was $P < 0.05$.

2.7 Quantitative real-time PCR (qPCR) analysis

cDNA was synthesized from 1 µg of clean DNase I-treated RNA (same samples as those used for library construction) using the SuperScript® III First-Strand Synthesis SuperMix for qRT-PCR kit (Invitrogen). Gene-specific primers (Supplementary Table 1) were designed using the Primer3 online software (version 0.4.0[2]). Gene expression of three biological replicates was examined on a Stratagene Mx3005P Real-Time QPCR System (Agilent Technologies, Santa Clara, CA, USA) using KOD SYBR® qPCR Mix (Toyobo, Osaka, Japan). *SlActin* (*Solyc03g078400*) was used as the housekeeping gene after examining its constitutive expression pattern from the RNA-Seq data. Relative expression values were calculated using the $2^{-\Delta\Delta Ct}$ method with at-harvest (0 d) samples calibrated as 1.

1 https://usegalaxy.org/

2 http://bioinfo.ut.ee/primer3-0.4.0/

2.8 McrBC-qPCR analysis

Genomic DNA was extracted from the pericarp of "Moneymaker" fruits (three replicates for each time point) using the Nucleospin® Plant II kit (Takara, Shiga, Japan).The genomic DNA (1 µg) was then digested at 37°C overnight with McrBC (Takara), before performing qPCR analysis as described in section 2.7 with 20 ng digested DNA as a template. Undigested gDNA samples were used as controls. Relative methylation was then calculated as $2^{Ct(digested) - Ct(undigested)}$, such that higher relative McrBC-qPCR signals correspond to higher methylation levels.

2.9 Gene expression analysis in tomato leaves

Three-week old "Moneymaker" seedlings were transferred to 5°C or 20°C for up to 7 d. Leaves were collected at 0, 3, 5, and 7 d for RNA extraction and qPCR analysis as described in section 2.7.

2.10 Statistical analysis

Data obtained in this study were subjected to statistical analysis using R v.3.4.0[3]. Differences in ethylene production rates, peel color, CI index, methylation levels and gene expression levels were determined using ANOVA followed by Tukey's *post hoc* tests.

3 Results

3.1 Characterization of fruit ripening, chilling injury and the effect of 1-MCP

Non-treated tomato fruits started to lose their green peel color after 7 d at 20°C, attaining a uniform red color after 21 d (Figure 1A; Supplementary Figure 1). This was evidenced by an increase in parameter a* from negative values to positive values (Figure 1C; Supplementary Figure 1). The changes in peel color were consistent with ethylene production rates (Figure 1D), which increased from 7 d in fruits during storage at 20°C and peaked at 14 d in a typical climacteric pattern. For the 1-MCP-treated fruits, both peel color changes and ethylene production rates did not change significantly in the first 14 d at 20°C; although ethylene production rates increased later on, the peak was 58% lower than that of non-treated fruits, and the fruits never attained a red color throughout the 35 d storage period.

During storage at 5°C, both non-treated and 1-MCP-treated fruits did not show any noticeable change in peel color (Figures 1B, C), and the ethylene production rates also did not change significantly (Figure 1D). On rewarming at 20°C, ethylene production rates increased, with a lag of about 6 d in 1-MCP-treated fruits (Figure 1D). The rewarmed fruits, however, failed to ripen normally, developed pitted surfaces and showed decay symptoms as evidenced by the high CI index values (Figures 1B, E, F; Supplementary Figure 1).

3.2 Transcriptomic responses in the pericarp: cold response *versus* fruit ripening

RNA-Seq analysis was then performed to identify gene expression changes during normal fruit ripening (at 20°C) and in response to cold stress (triggered by storage at 5°C for 14 d) in "Micro-Tom" fruits. By comparing samples collected after 14 d storage at 20°C and 5°C with at-harvest (0 d) samples, we identified 10,042 DEGs. Interestingly, we found more upregulated and downregulated genes at 5°C (8,406) than at 20°C (4,814) (Figure 2A). Subsequent hierarchical clustering of the DEGs against temporal expression patterns in at-harvest, stored and rewarmed samples outlined 9 major modules (Figure 2B; Supplementary Tables 2-10). Among them, modules I, II, III, IV, VII and VIII comprised genes which were differentially expressed both at 20°C and 5°C, and 1-MCP treatment affected their expression levels at both temperatures; this indicated that they are regulated by either ethylene or low temperature. Genes in modules V and VI were up- or down-regulated during storage at 20°C, a change that was reversed by 1-MCP treatment; these expression changes were suppressed during storage at 5°C, but they recovered (at least to some extent) upon rewarming. Interestingly, module IX genes displayed insignificant expression changes during storage at 20°C, but they were up- or down-regulated at 5°C in both 1-MCP-treated and non-treated samples with a reversion to original levels upon rewarming at 20°C.

To further understand the molecular changes that are induced during cold response *versus* fruit ripening, we performed GO term and KEGG pathway-based enrichment analyses of the DEGs in each of the modules identified above. GO analysis confirmed that genes in module VI were associated with 'fruit ripening' (Figure 2C), especially the 'carotenoid biosynthesis pathway' (Figure 2D). On the other hand, module IX genes were dominated by functions such as 'gene expression', 'translation', 'ribosome biogenesis', 'proteasome' and 'NcRNA metabolism' (Figures 2C, D). Other functions that were uniquely enriched in module IX genes included 'spliceosome', 'organonitrogen biosynthesis', and 'linolenic acid metabolism'.

All in all, our results indicated that there was a divergence in the molecular adjustments triggered by cold response and those involved in fruit ripening in tomatoes. Module VI genes, in particular, were mostly involved in changes that lead to fruit ripening and they were under the influence of ethylene signaling (i.e., affected by 1-MCP treatment). Conversely, module IX genes were regulated by low temperature while ethylene signaling had little or no significant influence on their expression levels (i.e., unchanged by ethylene at 20°C and unaffected by 1-MCP at 5°C.

3 www.r-project.org

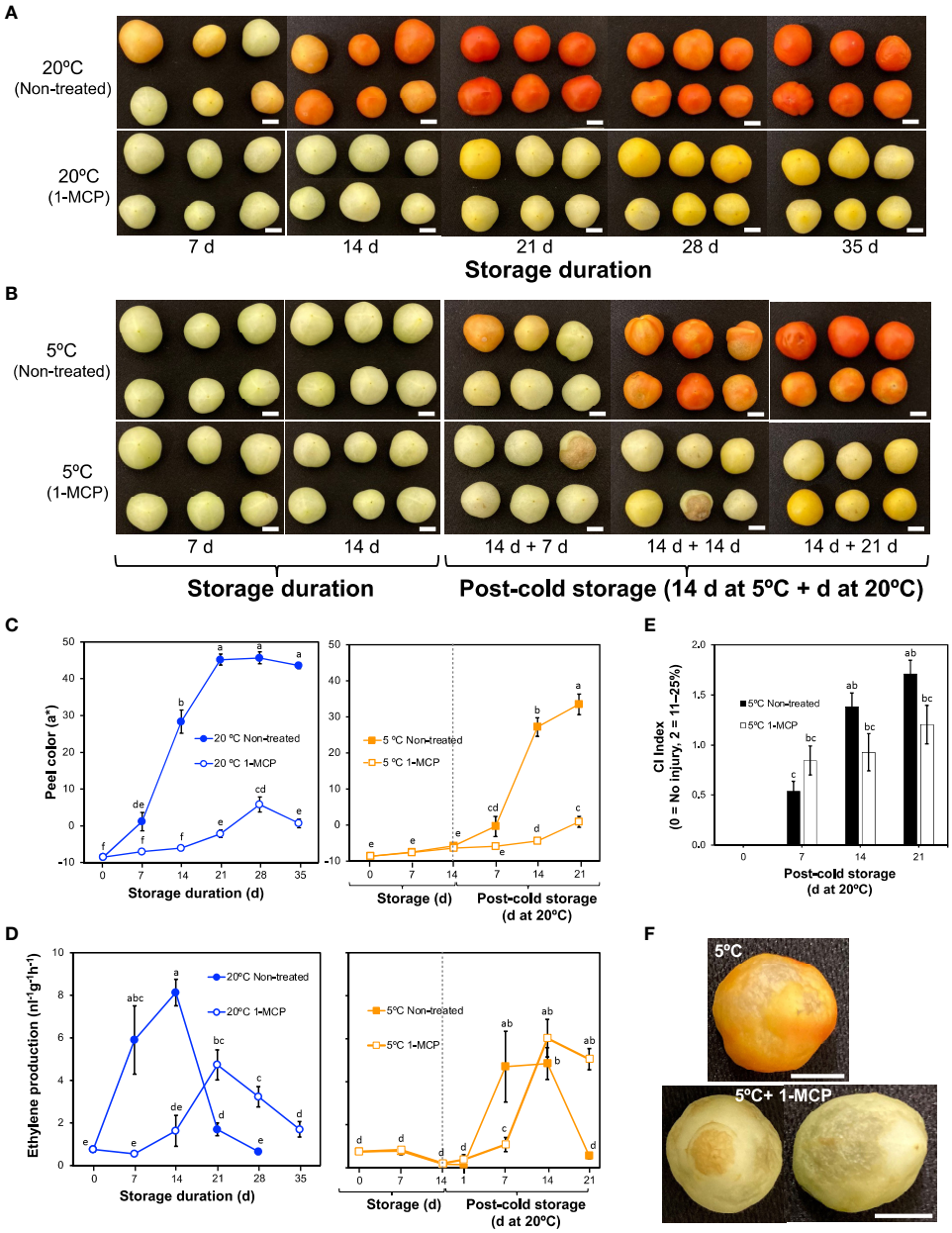

FIGURE 1
External changes and ethylene production rates in mature green "Micro-Tom" tomato fruits during storage at 20 and 5°C with or without 1-methylcyclopropene (1-MCP) treatment. **(A)** Effect of 1-MCP on external appearance during storage at 20°C. **(B)** Effect of 1-MCP on external changes during storage at 5°C and post-cold storage at 20°C. **(C)** Changes in CIELAB color parameter a* during storage at 20°C (left panel) and 5°C (right panel) with or without 1-MCP treatment. Each datapoint represents the average (± SE) of 6 fruits. **(D)** Ethylene production rates. Each datapoint represents the average (± SE) of 10 fruits. **(E)** Chilling injury index in fruits during storage at 20°C following 14 d at 5°C. Each column represents the average (± SE) of 10 fruits. **(F)** Images of fruits showing uneven ripening and surface pitting after storage at 5°C, and decay with surface pitting in 1-MCP treated fruits. Fruits were stored at 5°C for 14 d followed by post-cold shelf life at 20°C for 7 d. Different letters in **(C, D, E)** indicate significant differences in ANOVA (Tukey's test, $P < 0.05$). White horizontal bars in **(A, B, F)** indicate 1 cm.

3.3 Transcripts associated with fruit ripening

Genes that have been commonly associated with fruit ripening were selected from among the DEGs for further examination and to assert the inhibitory effect of 1-MCP. Most of these genes belonged to module VI; they were upregulated at 20°C in accordance with ethylene production rates and 1-MCP treatment inhibited this change (Figure 3A). However, one gene (*SlSGR*, *Solyc12g056480*), which encodes magnesium dechelatase that is involved in chlorophyll degradation (Shimoda et al., 2016), was upregulated only at 5°C and 1-MCP treatment did not inhibit this expression change, indicating that it responded only to low temperature and was independent of ethylene signaling.

Six of the genes in Figure 3A were then selected for validation by qPCR analysis. These included *ripening inhibitor* (*SlRIN*) and *non-ripening* (*SlNOR*) which encode established molecular regulators of fruit ripening, *1-aminocyclopropane-1-carboxylic acid synthase 2*

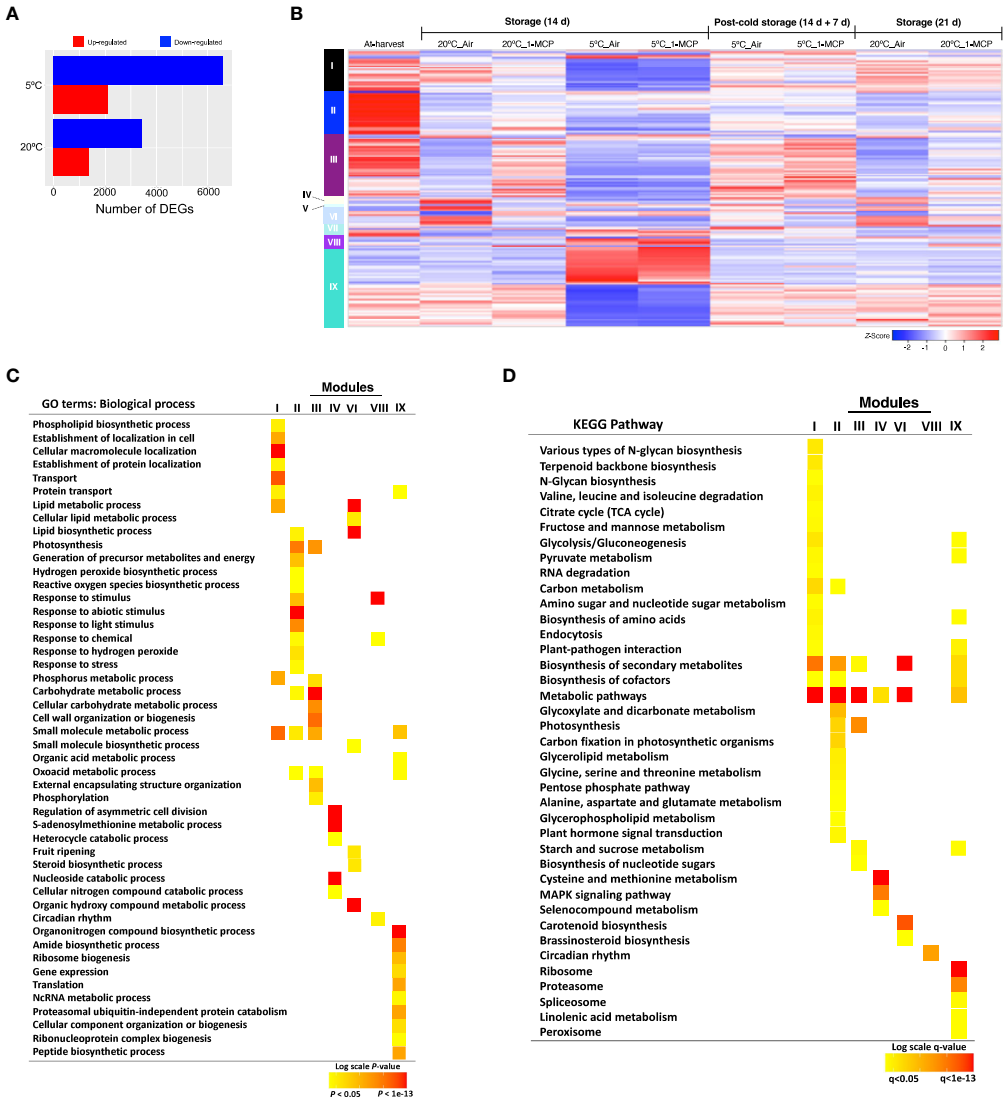

FIGURE 2
Gene expression changes in mature green "Micro-Tom" tomato fruits during storage at 20 and 5°C, and the effect of 1-MCP treatment. **(A)** Numbers of up- and down-regulated genes during storage at 20 and 5°C. Samples after 14 d of storage were compared to those collected at-harvest (0 d). **(B)** Heatmap visualization of the highly co-expressed gene clusters. **(C)** GO terms enriched among the differentially expressed genes in each cluster. Color panels indicate the *P*-value of GO enrichment. **(D)** KEGG pathway enrichment analysis among the differentially expressed genes in each cluster. Color panels indicate the significance level of enrichment.

(*SlACS2*) which encodes an ethylene biosynthetic enzyme, *polygalacturonase 2a* (*SlPG2a*) which is involved in fruit softening, *phytoene synthase 1* (*SlPSY1*) which is involved in carotenoid metabolism and the aroma volatile production-associated *alcohol acyl transferase* (*SlAAT*). As expected, the expression levels of these six genes increased markedly in non-treated fruits during storage at 20°C (Figure 3B), which corresponded with the ethylene production patterns observed earlier (Figure 1D). In 1-MCP-treated fruits at 20°C, little or insignificant changes in expression levels were registered during the first 14 d; increases however occurred at 21 d as ethylene production levels rose. The expression levels of these ripening-associated genes (except for *SlSGR*) remained mostly unchanged during storage at 5°C and even after 1 d of rewarming at 20°C; significant transcript accumulation occurred after post-cold storage for 7 d at 20°C. Together, these results reaffirmed that ethylene signaling regulates the ripening process in tomatoes and 1-MCP treatment effectively blocks ethylene-mediated regulation of the genes involved.

3.4 Transcripts associated with oxidative damage

Cold stress results in increased levels of reactive oxygen species which cause oxidative damage in fruits and vegetables (Sevillano et al., 2009; Valenzuela et al., 2017). To avoid or tolerate this oxidative damage, several enzymatic reactions catalyzed by lipoxygenases (LOX), peroxidases (POX), alternative oxidases (AOX), catalases (CAT), and superoxide dismutases (SOD) are generated in the affected plants. We therefore examined further the

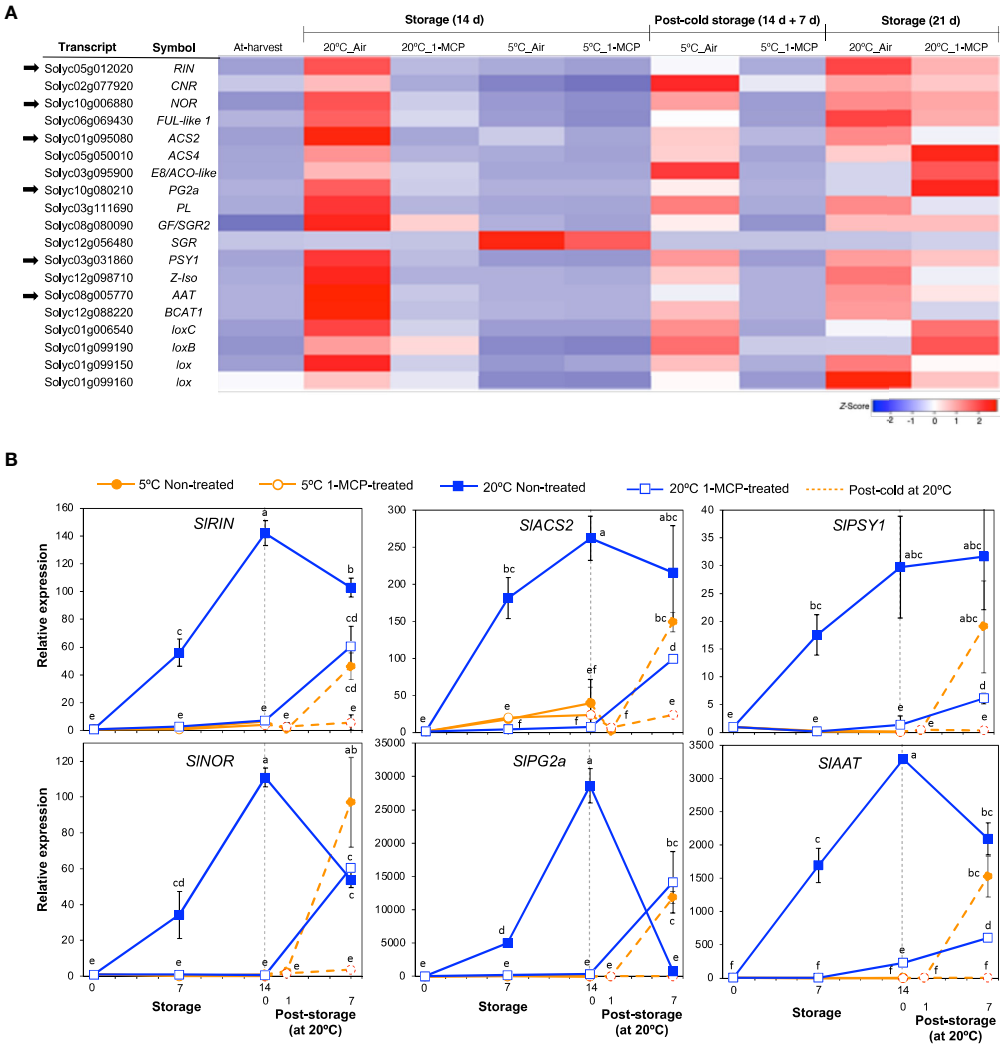

FIGURE 3
Expression patterns of selected genes commonly associated with fruit ripening and the effect of 1-MCP. **(A)**. Heatmap of DEGs encoding transcription factors and enzymes in mature green "Micro-Tom" tomato fruits at the indicated storage temperatures and duration. **(B)** RT-qPCR analysis of selected genes from **(A)** in mature green "Micro-Tom" tomato fruits at the indicated times. Expression values are relative to the value at harvest (0 d) and the housekeeping gene was *SlActin*. Datapoints indicate means (± SE) of three replicate fruits. Different letters indicate significant differences in ANOVA (Tukey's test, $P < 0.05$).

expression patterns of genes encoding these antioxidant defense enzymes from among the DEGs. Interestingly, out of the 18 genes that we found (Figure 4A), a majority (13 genes, 72%) belonged to module IX as they showed insignificant changes in expression levels during storage at 20°C, but they were differentially expressed at 5°C with or without 1-MCP treatment. Furthermore, only 2 out of these 13 genes were downregulated while the rest (11 genes) were upregulated in fruits stored at 5°C.

We then studied the expression of *SlAOX1a* (*Solyc08g075540*) and *SlPOX65* (*Solyc08g007150*) in both "Micro-Tom" and "Moneymaker" fruits during storage at 5°C and 20°C via qPCR analysis. As indicated in Supplementary Figure 1, "Moneymaker" fruits also exhibited CI symptoms during rewarming at 20°C following storage at 5°C for 7, 14, and 21 d. *SlAOX1a* and *SlPOX65* transcript levels notably increased in both "Micro-Tom" and "Moneymaker" fruits during storage at 5°C with or without 1-MCP treatment, and decreased immediately after the fruits were rewarmed to 20°C (Figures 4B, C). During storage at 20°C, the expression levels remained mostly unchanged except for a relatively slight but relevant increase in *SlAOX1a* transcript levels in "Moneymaker" fruits. Therefore, it appears that the adaptive responses to cold stress-triggered ROS accumulation in tomato fruits are typically not influenced by ethylene signaling.

3.5 Transcripts associated with ribosome biogenesis

Term enrichment analysis of our RNA-Seq data (Figures 2C, D) indicated that one of the molecular responses to low temperature alone (with respect to fruit ripening) was adjustments among ribosomal proteins and the ribosome biogenesis pathway in

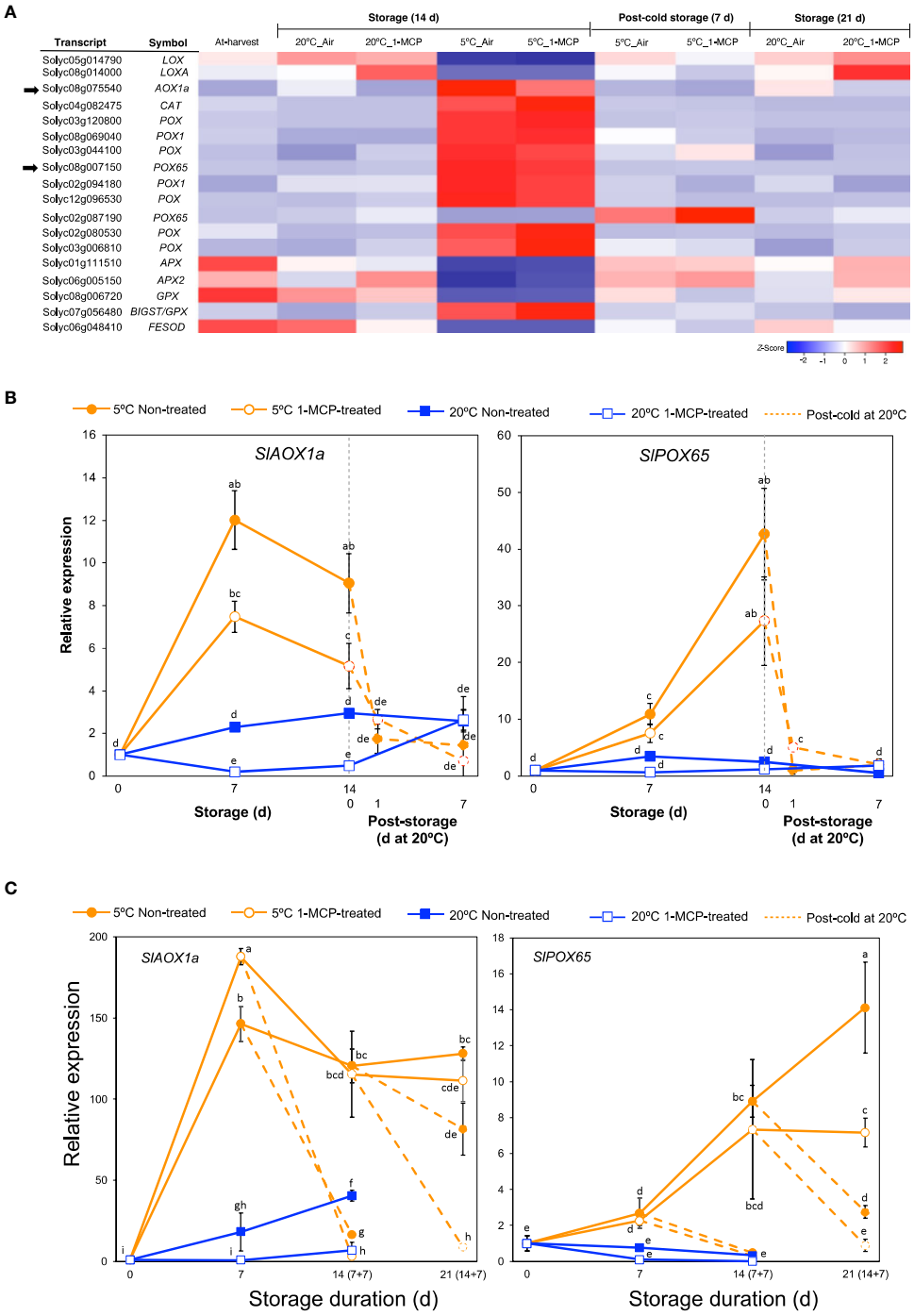

FIGURE 4
Expression patterns of genes associated with oxidative damage. **(A)** Heatmap of DEGs responding to low temperature alone in mature green "Micro-Tom" tomato fruits at the indicated storage temperatures and duration. **(B)** RT-qPCR analysis of selected genes from **(A)** in mature green "Micro-Tom" tomato fruits at the indicated times. **(C)** RT-qPCR analysis of selected genes from **(A)** in mature green "Moneymaker" tomato fruits at the indicated times. Values in brackets on the horizontal axis indicate number of days at 5°C + 7 days of rewarming at 20°C. Expression values are relative to the value at harvest (0 d) and the housekeeping gene was *SlActin*. Datapoints in **(B, C)** indicate means (± SE) of three replicate fruits. Different letters indicate significant differences in ANOVA (Tukey's test, $P < 0.05$).

addition to 'NcRNA metabolism'. Visualization of enriched pathways suggested that low temperature triggers comprehensive changes in both large and small ribosomal subunits as well as ribosomal biogenesis factors (Figure 5A). After a closer look at the DEGs, we found 30 genes belonging to module IX (Figure 5B). Their expression levels did not change significantly during storage at 20°C, but 18 of them were upregulated while the remaining 12 were downregulated during storage at 5°C both in 1-MCP-treated and non-treated fruits. qPCR analysis further confirmed the upregulation of *SlZFP622/REIL1* (*Solyc08g006470*), encoding a ribosome biogenesis factor, during storage at 5°C with transcript levels peaking at 7 d in both "Micro-Tom" and "Moneymaker" tomatoes (Figure 5C).

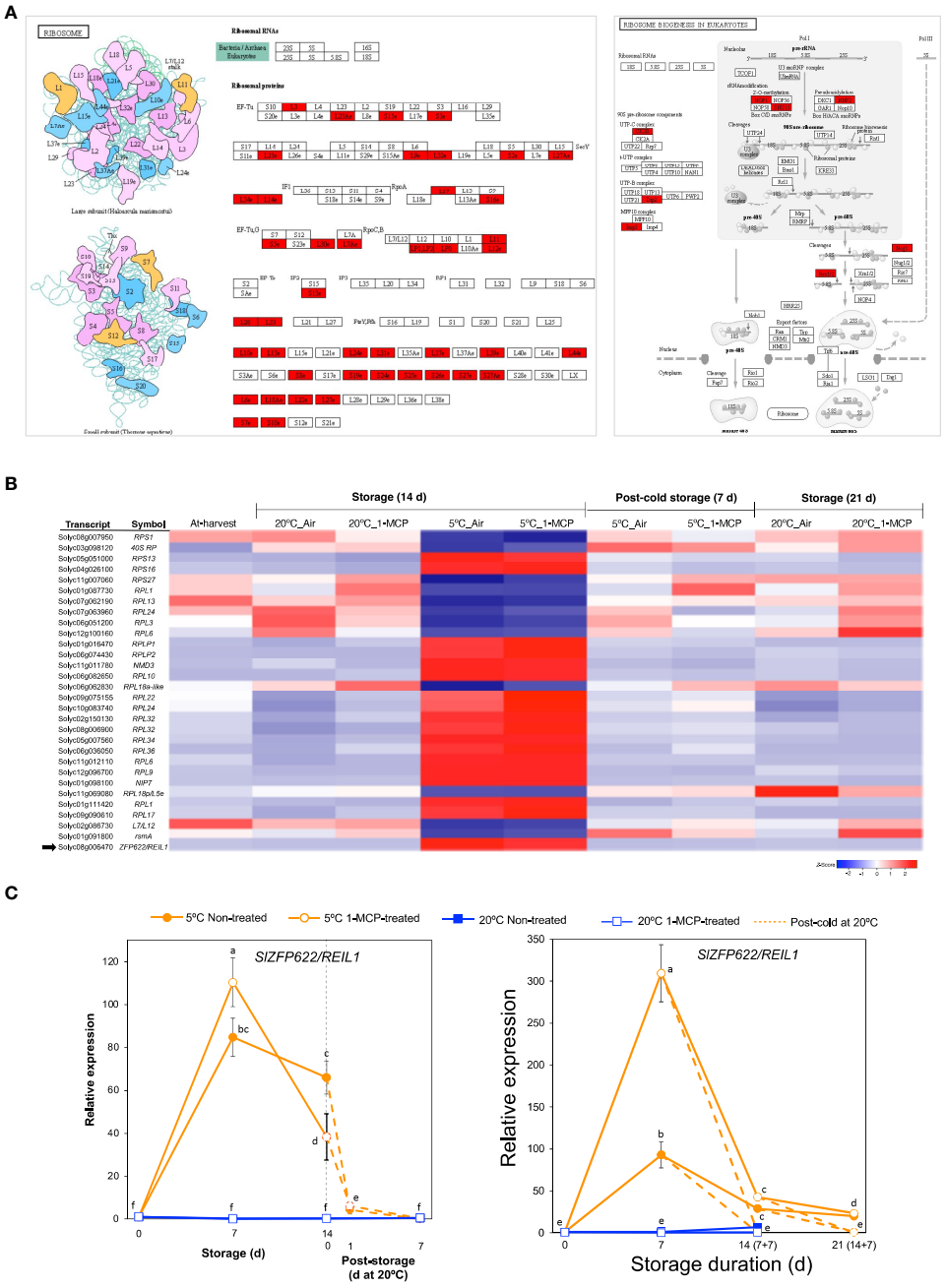

FIGURE 5
Transcriptional changes associated with ribosome biogenesis. **(A)**. Enrichment of pathways related with ribosomal proteins and their biogenesis. **(B)** Heatmap of DEGs responding to low temperature alone in mature green "Micro-Tom" tomato fruits at the indicated storage temperatures and duration. **(C)** RT-qPCR analysis of *ZFP622/REIL2* (indicated by a black arrow in **B**) in mature green "Micro-Tom" tomato fruits (left panel) and mature green "Moneymaker" tomato fruits (right panel) at the indicated times. Expression values are relative to the value at harvest (0 d) and the housekeeping gene was *SlActin*. Values in brackets on the horizontal axis indicate number of days at 5°C + 7 days of rewarming at 20°C. Datapoints indicate means (± SE) of three replicate fruits. Different letters indicate significant differences in ANOVA (Tukey's test, $P < 0.05$).

3.6 Transcripts associated with the spliceosome

Another category that stood out among the DEGs responding to low temperature alone (module IX) was 'spliceosome' (Figure 2D), a protein complex in which introns are removed from immature mRNAs to generate uninterrupted open reading frames for translation or to produce different splicing variants of the same gene and hence potentially increase the total number of proteins in the cell (Reddy et al., 2013; Wang et al., 2022). Further visualization of the spliceosome pathway confirmed that several components were highly enriched among the module IX DEGs (Figure 6A). Twelve genes associated with the spliceosome were then isolated from the total DEGs (Figure 6B), of which 11 were upregulated only in fruits stored at 5°C for 14 d with or without 1-MCP treatment while 1 gene was downregulated. This

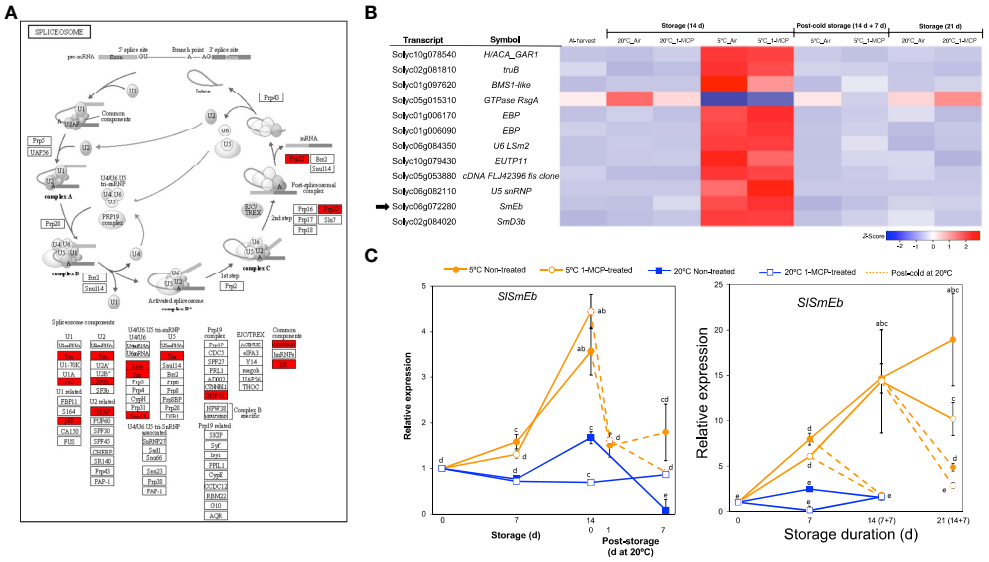

FIGURE 6
Transcriptional changes associated with the spliceosome. **(A)**. Enrichment of spliceosome-associated components among DEGs responding to low temperature alone. **(B)** Heatmap of DEGs associated with the spliceosome in mature green "Micro-Tom" tomato fruits at the indicated storage temperatures and duration. **(C)** RT-qPCR analysis of the spliceosome component *SlSmEb* (indicated by black arrow in **B**) in mature green "Micro-Tom" tomato fruits (left panel) and mature green "Moneymaker" tomato fruits (right panel) at the indicated times. Expression values are relative to the value at harvest (0 d) and the housekeeping gene was *SlActin*. Values in brackets on the horizontal axis indicate number of days at 5°C + 7 days of rewarming at 20°C. Datapoints indicate means (± SE) of three replicate fruits. Different letters indicate significant differences in ANOVA (Tukey's test, $P < 0.05$).

included *SlSmEb* (*Solyc06g072280*) whose ortholog in Arabidopsis has been associated with proper alternative splicing events during chilling stress responses (Wang et al., 2022). By qPCR analysis, we confirmed that *SlSmEb* transcripts accumulate in both "Micro-Tom" and "Moneymaker" tomatoes during storage at 5°C irrespective of 1-MCP treatments, but little or insignificant changes in expression occur at 20°C (Figure 6C). The cold-specific upregulation of *SlSmEb* is further supported by the swift drop in expression levels (within 1 d in "Micro-Tom" tomatoes) when fruits were transferred from 5°C to 20°C.

3.7 Transcripts associated with transcription factors, chaperones and signaling peptides

As is the case with other biotic and abiotic stresses, the physiological and biochemical alterations which occur in plants under cold stress are controlled by several regulatory hubs that include various transcription factors, hormones, chaperones and signaling peptides (Kosová et al., 2018; Mehrotra et al., 2020). We therefore scrutinized our DEGs particularly in module IX to see how genes associated with these regulatory hubs are affected by cold stress. This led to the identification of 99 DEGs of which 60 encoded various transcription factor families, 14 were associated with jasmonate and auxin signaling, 10 encoded heat shock proteins, 13 were related with calcium signaling and 2 encoded clavata3/embryo surrounding region-related (CLE) signaling peptides (Supplementary Table 11). qPCR analyses were then performed on a selected nine genes to validate the RNA-Seq data and to evaluate their expression patterns in response to cold stress in "Micro-Tom" and "Moneymaker" tomatoes. In both cultivars, transcripts of *SlERF13*, *SlNAC22*, *SlHSP*, *SlMADS43*, *SlJAZ2*, *SlBEL3* and *SlCLE2* increased dramatically, while those of *SlPIF3* decreased during storage at 5°C regardless of 1-MCP treatment; changes at 20°C were insignificant (Figure 7). Transcript levels in fruits at 5°C also dropped following transfer to 20°C. However, while *SlCBF2* transcripts increased during storage at both 5 and 20°C in "Micro-Tom" fruits (Figure 7A), increased expression levels were registered only at 5°C in "Moneymaker" fruits especially after 14 d (Figure 7B).

3.8 Transcripts associated with epigenetic modifications

The finding that 'NcRNA metabolism' was one of the highly enriched GO terms among module IX DEGs (Figure 2C) prompted us to also look into the expression patterns of genes associated with epigenetic modifications. Out of the 20 genes that we identified, 12 were associated with DNA methylation while 8 were associated with chromatin formation/remodeling (Figure 8A). Among the DNA methylation-related genes, 6 encoded short interfering RNA-producing dicer-like enzymes of which 4 were upregulated while 2 were downregulated only during storage at 5°C for 14 d regardless of 1-MCP treatments. Interestingly, we also found 2 genes that encode RNA-directed DNA methylation 1 (RDM1) protein; *SlRDM1-like 1* (*Solyc10g045190*) was slightly downregulated while *SlRDM1-like 2* (*Solyc09g082480*) was highly upregulated in both 1-MCP-treated and non-treated fruits after 14 d at 5°C. For the genes

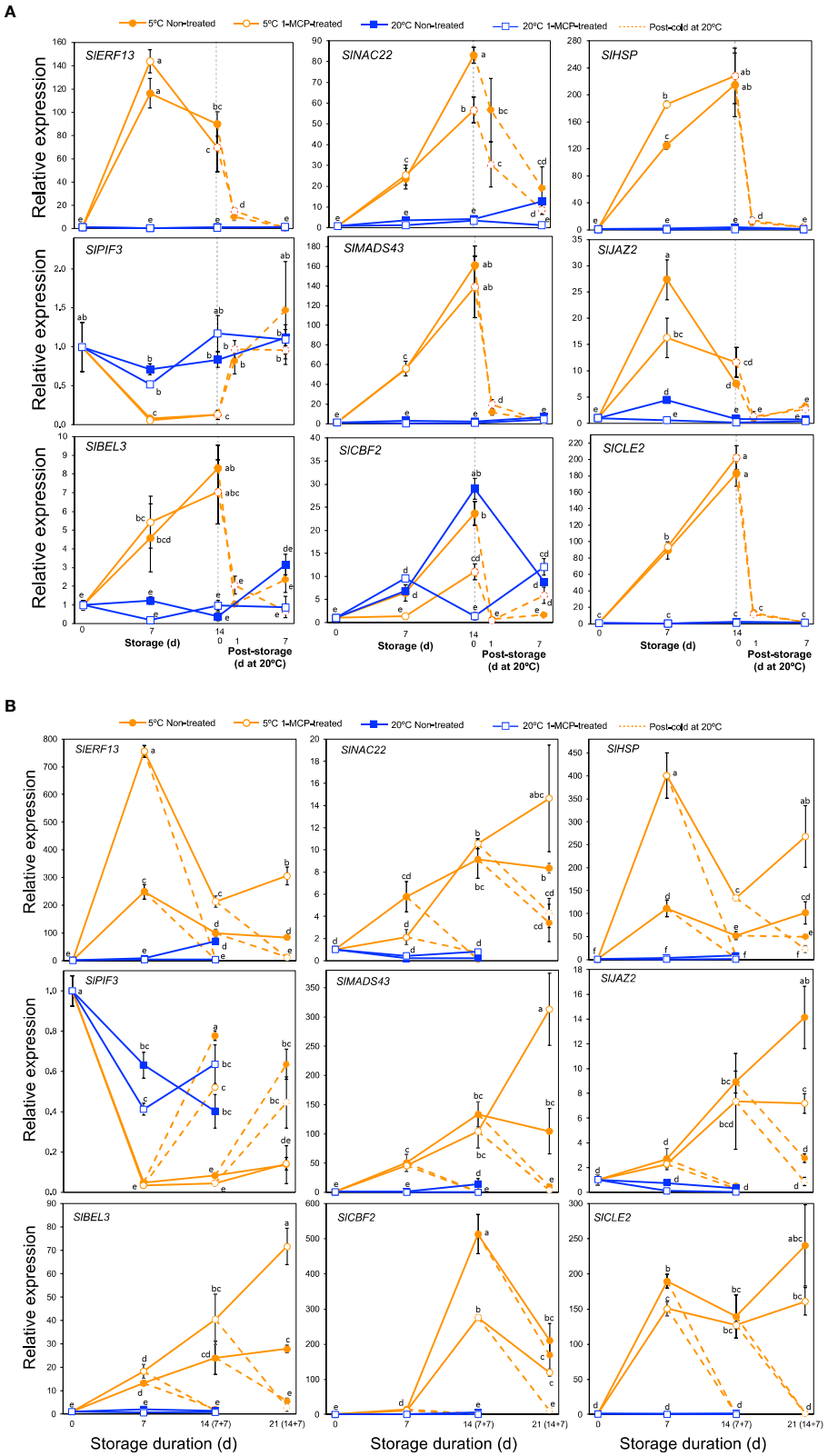

FIGURE 7
Expression patterns of genes encoding various transcription factors, chaperones and signaling peptides. **(A)**. RT-qPCR analysis in mature green "Micro-Tom" tomato fruits. **(B)** RT-qPCR analysis in mature green "Moneymaker" tomato fruits. Expression values are relative to the value at harvest (0 d) and the housekeeping gene was *SlActin*. Values in brackets on the horizontal axis in B indicate number of days at 5°C + 7 days of rewarming at 20°C. Datapoints indicate means (± SE) of three replicate fruits. Different letters indicate significant differences in ANOVA (Tukey's test, $P < 0.05$) *SlERF13* (*Solyc10g076370*), *SlNAC22* (*Solyc09g025310*), *SlHSP* (*Solyc06g054150*), *SlPIF3* (*Solyc01g102300*), *SlMADS43* (*Solyc05g013370*), *SlJAZ2* (*Solyc12g009220*), *SlBEL3* (*Solyc04g080790*), *SlCBF2* (*Solyc03g124110*) and *SlCLE2* (*Solyc01g098890*).

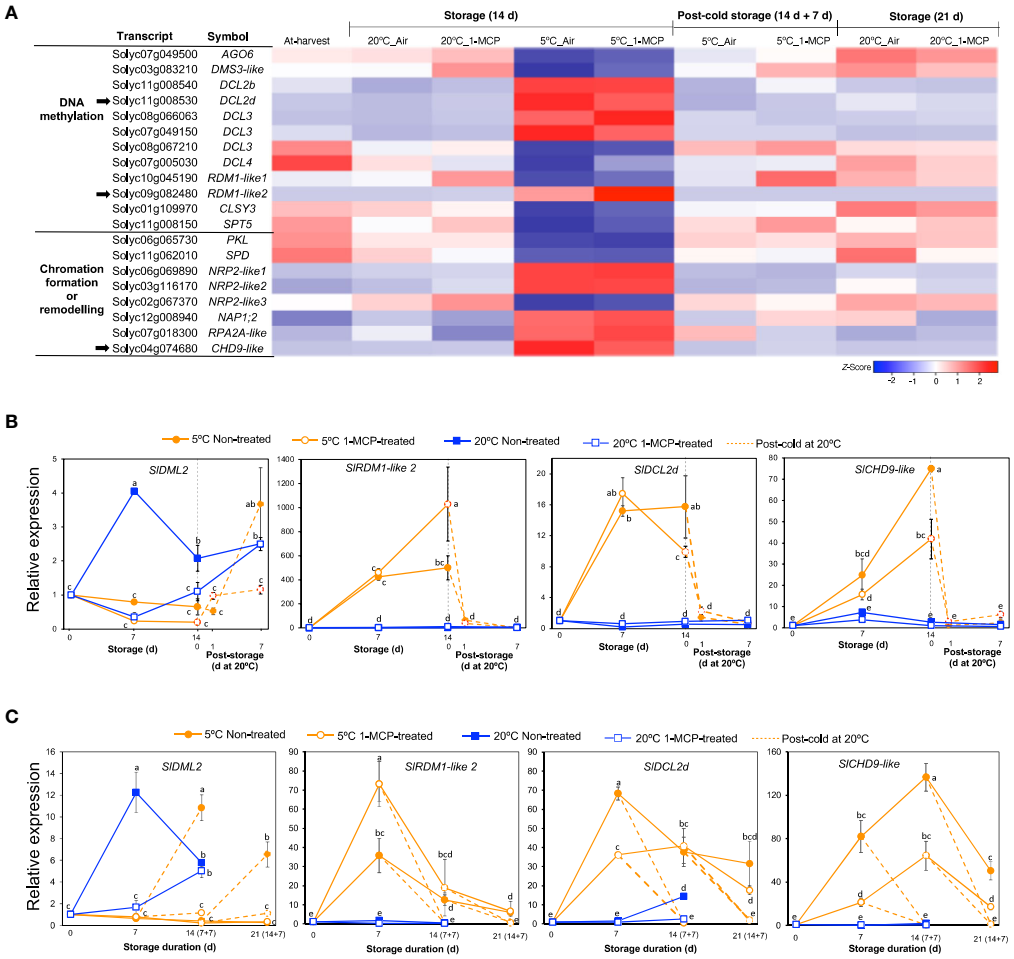

FIGURE 8
Expression patterns of genes associated with epigenetic modifications. **(A)** Heatmap of DEGs associated with DNA methylation and chromatin formation/remodelling in mature green "Micro-Tom" tomato fruits at the indicated storage temperatures and duration. **(B)** RT-qPCR analysis of selected genes (indicated by black arrow in **A**) in mature green "Micro-Tom" tomato fruits. **(C)** RT-qPCR analysis in mature green "Moneymaker" tomato fruits. Expression values are relative to the value at harvest (0 d) and the housekeeping gene was *SlActin*. Values in brackets on the horizontal axis in **(C)** indicate number of days at 5°C + 7 days of rewarming at 20°C. Datapoints indicate means (± SE) of three replicate fruits. Different letters indicate significant differences in ANOVA (Tukey's test, $P < 0.05$).

associated with chromatin formation/remodeling, 5 were upregulated while only 3 were downregulated in both 1-MCP-treated and non-treated fruits after 14 d at 5°C. All of these genes (both DNA methylation- and chromatin formation/remodeling-associated) showed insignificant expression changes during storage at 20°C and the expression changes induced at 5°C were reversed when fruit were rewarmed to 20°C.

We then selected three genes which showed high and clear expression changes based on their TPM values, that is *SlRDM1-like 2*, *dicer-like 2d* (*SlDCL2d*, *Solyc11g008530*) and *chromodomain helicase 9 (CHD9)-like* (*SlCHD9-like*, *Solyc04g074680*), for further analysis by qPCR. In addition, we also examined the expression of *Demeter-like 2* (*SlDML2*, *Solyc10g083630*) which is associated with active DNA demethylation in tomatoes (Lang et al., 2017). In both "Micro-Tom" and "Moneymaker" tomatoes, *SlDML2* transcripts increased significantly during storage at 20°C and peaked after 7 d, but this increase was inhibited in 1-MCP-treated fruits (Figures 8B, C). However, the expression of *SlDML2* did not change significantly during storage at 5°C, but increases were observed only after rewarming at 20°C. Transcripts of *SlRDM1-like 2*, *SlDCL2d*, and *SlCHD9-like* showed little or no significant changes during storage at 20°C, but they accumulated highly during storage at 5°C irrespective of 1-MCP treatments (Figures 8B, C). The increased expression registered at 5°C was reversed within 1 d (in "Micro-Tom" fruits) and after 7 d (in "Moneymaker" fruits) of rewarming at 20°C.

After examining gene expression patterns, we determined the involvement of DNA methylation in cold response and CI development in "Moneymaker" fruits using 5-azacytidine, an inhibitor of DNA methylation (Huang et al., 2019; Zhu et al., 2020) and McrBC, a restriction enzyme that cuts methylated DNA. Fruits injected with 5-azacytidine developed relatively severe symptoms

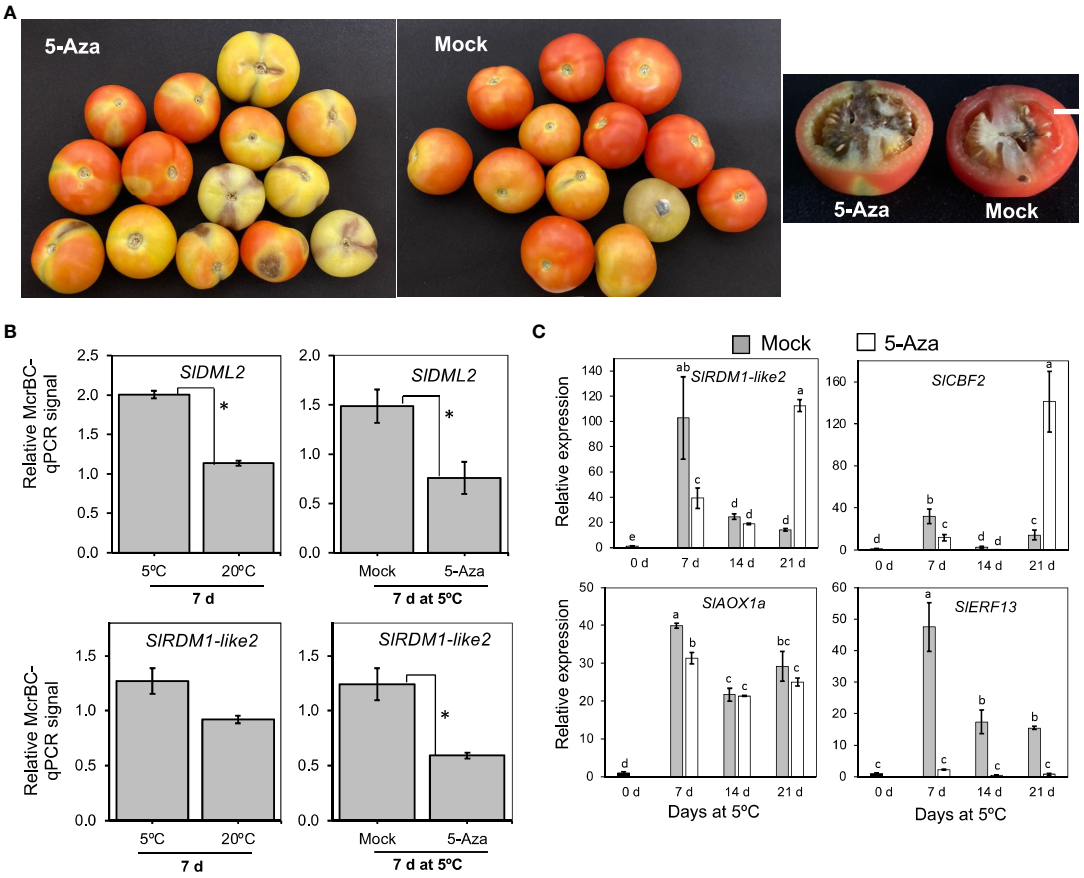

FIGURE 9
The importance of DNA methylation in cold response and chilling injury development in tomato fruit. **(A)** Images of "Moneymaker" tomato fruits that were treated with the DNA methylation inhibitor, 5-Azacytidine (5-Aza) or mock (distilled water) during storage at 5°C for 21 d followed by 7 d holding at 20°C. White horizontal bars indicate 1cm. **(B)** DNA methylation levels of *SlDML2* and *SlRDM1-like 2*. McrBC-qPCR analysis was carried out in fruits stored at 5°C or 20°C for 7 d, as well as in mock or 5-Aza-treated samples after 7 d at 5°C. McrBC digests methylated DNA, thus higher McrBC-qPCR signals indicate higher Ct values and hence higher methylation levels. Asterisks indicate significant differences ($P < 0.05$) **(C)** RT-qPCR analysis of selected low temperature-upregulated genes in mock and 5-Aza-treated samples during storage at 5°C for the indicated times. Expression values are relative to the value at harvest (0 d) and the housekeeping gene was *SlActin*. Datapoints indicate means (± SE) of three replicate fruit. Different letters indicate significant differences in ANOVA (Tukey's test, $P < 0.05$).

(dark spots on the skin and darkening of columella) compared to those injected with distilled water (mock) (Figure 9A). Furthermore, fruits injected with 5-azacytidine were generally firmer at the end of cold storage than mock fruits (Supplementary Figure 2). We then assayed the DNA methylation levels of *SlDML2* and *SlRDM1-like 2* using McrBC-qPCR analysis. Genomic DNA was first extracted from the pericarp of fruits stored at either 5°C or 20°C for 7 d and then digested with McrBC before performing qPCR using both digested and undigested DNA as templates. Results revealed that methylation levels of both *SlDML2* and *SlRDM1-like 2* were higher in samples at 5°C than at 20°C, and treatment with 5-azacytidine significantly lowered the methylation levels at 5°C with respect to mock samples (Figure 9B). To further investigate the influence of 5-azacytidine treatment on gene expression, we examined the transcript levels of 4 genes induced by low temperature alone which we previously identified by RNA-Seq analysis. As shown in Figure 9C, 5-azacytidine treatment decreased the expression of *SlRDM1-like 2*, *SlCBF2*, and *SlAOX1a* only after 7 d. However, it is intriguing that the inhibitor completely decreased the expression of *SlERF13* throughout the 21 d of storage at 5°C (Figure 9C). These results show that DNA methylation has an important role in cold responses and CI development in tomato fruits.

4 Discussion

Cold stress responses and the underlying mechanisms have been well deliberated in the vegetative plant organs (Kidokoro et al., 2022), but conclusions from these studies cannot be directly extrapolated to fruits partly because ripening responses cloud our view. In this work, cold stress studies were performed in tomato fruits at the mature green stage to avoid the effects of autocatalytic ethylene (system II ethylene), which is produced at later maturity stages and largely controls fruit ripening. Additionally, treatments

with 1-MCP were done regularly during cold storage to inhibit any probable effects of system I ethylene. Ultimately, we show by RNA-Seq analysis that low temperature triggers defined transcriptional adjustments, including those associated with epigenetic modifications, NcRNA metabolism, ribosome biogenesis, proteosome, alternative splicing and a certain set of transcription factors, which are clearly distinct from fruit ripening-related changes.

Tomatoes are typical climacteric fruits and thus ripening-associated are largely regulated by the phytohormone ethylene (Li et al., 2019). Ethylene-controlled ripening responses are completely inhibited by 1-MCP (Watkins, 2006), a synthetic chemical that boasts a competitive edge over ethylene for receptor binding sites (Blankenship and Dole, 2003). In agreement with these previous findings, our results show that peel color changes from green to red, which occurred in non-treated tomato fruits during storage at 20°C (Figures 1A, C), were accompanied by a sharp increase in ethylene production rates (Figure 1D; Supplementary Figure 1). These changes were strongly inhibited in the 1-MCP-treated fruits. Recovery of ethylene sensitivity and fruit ripening following 1-MCP treatment, likely due to ethylene receptor turnover, has been reported previously (Watkins, 2006). The recovery periods vary depending on fruit species but in tomatoes, Opiyo and Ying (2005) demonstrated that it occurs 2 d after treatment with 1-MCP. In the present study, 1-MCP treatments were carried out 2–3 times per week to overcome possible recovery and hence keep the fruits insensitive to ethylene throughout the experimental duration. As a result, fruit ripening was completely inhibited during the first 14 d (Figure 1A), and even though ethylene production rates increased afterwards, the fruits remained yellow and failed to attain the red ripe stage throughout the 35-d storage period. The role of ethylene in fruit ripening and the inhibitory effect of 1-MCP are further confirmed by the identification of module VI genes by RNA-Seq analysis. Precisely, module VI genes were up- or down-regulated at 20°C (Figure 2B) in the presence of large ethylene amounts (Figure 1D), showed insignificant changes at 5°C, and comprised well-known fruit ripening regulators such as *SlRIN*, *SlNOR*, and *SlCNR* (Figure 3). 1-MCP treatments also abolished these expression changes at 20°C, confirming that the genes were under ethylene regulation. Interestingly, *SlSGR* (*Solyc12g056480*) failed to respond to ethylene (at 20°C), but its transcript levels increased appreciably at 5°C (Figure 3A), indicating that it is regulated by low temperature most likely in an ethylene-independent manner. This finding agrees with our previous findings in lemons (Mitalo et al., 2020), Satsuma mandarins (Mitalo et al., 2022), and kiwifruits (Mitalo et al., 2019a), where we demonstrated that the expression of certain fruit ripening-associated genes is modulated by low temperature independently of ethylene.

Like other cold sensitive crops, tomatoes develop CI symptoms when stored at sub-optimum low temperatures (< 10°C). Common CI symptoms, including impaired or blotchy ripening, surface pitting and decay, often occur during rewarming after cold storage (Biswas et al., 2016). In the present study, both "Micro-Tom" and "Moneymaker" fruits also showed CI symptoms during rewarming at 20°C following storage at 5°C (Figures 1B, E, F; Supplementary Figure 1), regardless of whether ethylene signaling was inhibited (by 1-MCP treatment) or not. RNA-Seq analysis revealed that cold stress causes a greater transcriptome response than fruit ripening, as the expression of more genes was altered after 14 d at 5°C (8,406) than at 20°C (4,814) (Figure 2A). It is however intriguing that 3,244 genes (in module IX) showed insignificant expression changes at 20°C, but they were differentially expressed at 5°C (Figure 2B), which implied that they responded to a low temperature stimulus. Furthermore, the observation that repeated 1-MCP treatments failed to inhibit their expression at 5°C, indicated that their regulation by low temperature is independent of ethylene signaling. It is noteworthy that the expression of a considerable number of genes which are associated with oxidative damage, an indirect outcome of cold stress and abiotic stress in general, was also triggered uniquely by low temperature (Figure 4). Transcripts of *SlAOX1a* and several *SlPOXs* were also previously shown to accumulate in tomato fruits during cold storage (Cruz-Mendívil et al., 2015; Albornoz et al., 2019). However, the present study is the first time we are demonstrating that several of these redox genes respond uniquely to cold stress. Furthermore, the existence of low temperature-induced and ethylene-independent gene expression has been previously reported in kiwifruits (Mitalo et al., 2019a), "Passe Crassane" pears (Mitalo et al., 2019b), and some citrus fruit species (Mitalo et al., 2020; Mitalo et al., 2022), but to the best of our knowledge, this study is the first report of such a phenomenon in tomato fruits.

We then used GO and KEGG pathway enrichment analysis to identify molecular processes that are uniquely triggered by cold stress in tomato fruits. The results pointed out that ribosome biogenesis, proteasome, spliceosome and regulation of gene expression are relevant processes (Figures 2C, D, 5, 6). A notable member of the ribosome biogenesis group was *SlZFP622/REIL1* (Figure 5C), while *SlSmEb* stood out among the spliceosome genes (Figure 6C). In Arabidopsis, *AtREIL2* encodes a cytosolic ribosomal 60S-biogenesis factor which was shown to activate the biosynthesis of specialized ribosomes during cold acclimation (Schmidt et al., 2013; Cheong et al., 2021), whereas AtSmEb was recently shown to control the splicing of pre-mRNAs during chilling stress (Wang et al., 2022). An understanding of why these genes are activated in tomato fruits under cold stress, yet the fruits still develop CI symptoms requires further research. The global transcriptome analysis revealed, moreover, that several genes encoding transcription factors, chaperones, hormone signaling, and small signaling peptides are induced uniquely by cold stress in tomato fruits (Supplementary Table 11). Furthermore, qPCR analysis confirmed their low temperature-specific responsiveness (Figure 7), as their induction was swiftly and consistently reversed upon rewarming of the fruits. Orthologs of some of these genes, including *SlPIF3*, *SlJAZ2* and *SlERF13*, have been linked with cold tolerance in leaves of other plant species (Jiang et al., 2017; Li et al., 2017; Lv et al., 2020). However, the others have not been reported previously even though several CLE peptides have been linked with various abiotic stresses in plants (Kim et al., 2021). It is also worth

mentioning that *SlCBF2* showed a clearly cold-specific expression pattern in "Moneymaker" fruits (Figure 7B), but in "Micro-Tom" fruits, it was induced by both ethylene and cold stress (Figure 7A). The reason for this discrepancy cannot be expounded in this study, as both cultivars displayed CI symptoms at almost the same degree. However, it could be an indicator of minor cultivar differences in terms of the regulation of cold responsive genes.

Epigenetic regulation has been associated with plant responses to a broad range of stresses, including cold stress (Kim et al., 2015). In this respect, Zhang et al. (2016) demonstrated that cold stress triggers an increase in DNA methylation in red ripe tomatoes, which significantly affects the expression patterns of various ripening-related genes. In the present study, RNA-Seq analysis underscored the relevance of epigenetic modifications in cold-specific responses in tomato fruits. A considerable number of genes involved in *de novo* DNA methylation and chromatin formation/remodeling were up- or down-regulated at 5°C with ethylene signaling having little or no significant effect on their expression (Figure 8), while expression changes at 20°C were also minimal. Notable among these genes was *SlRDM1-like 2*, whose loss-of-function mutations in Arabidopsis showed reduced DNA methylation together with impaired accumulation of 24-nt short-interfering RNAs (Gao et al., 2010). Another major change was the exclusive accumulation of transcripts related with dicer-like enzymes, particularly *SlDCL2d*, during storage at 5°C (Figure 8). *SlDCL2s* have been widely studied in terms of plant defense against viral pathogens (Wang et al., 2018; Suzuki et al., 2019; Alcaide et al., 2022). Hunter et al. (2021) also demonstrated that transcripts of both *SlDCL2b* and *SlDCL2d* accumulated to a great degree in ripe cherry tomato fruits during cold storage, but our present study is the first to show that this accumulation is unique to cold stress and is independent of ethylene signaling. Treatment of mature green tomato fruit with the DNA methylation inhibitor, 5-azacytidine, confirmed the existence of cold stress-induced methylation dynamics and its influence on gene expression (Figure 9). While 5-azacytidine effects are more pronounced in actively dividing cells (Jones and Taylor, 1980), recent reports have demonstrated the effectiveness of the chemical in studying methylation dynamics even in mature fruits having non-dividing cells (Huang et al., 2019; Zhu et al., 2020). Nevertheless, one of the major limitations of using 5-azacytidine is that it induces cytotoxicity. In the present study, we did not detect toxicity symptoms in 5-azacytidine-treated fruits at 20°C for up to 14 d (data not shown), but at 5°C treated fruits appeared to exhibit severe ripening inhibition symptoms than mock fruits. It is therefore possible that a complex interaction between cold stress and 5-azacytidine and this needs to be studied further. All in all, further research is required to understand the role and involvement of the cold-specific *SlRDM1-like 2* as well as *SlDCLs* in *de novo* DNA methylation (as shown in Figure 9) and RNA silencing mechanisms during cold responses and CI development in tomato fruits.

A diverse number of genes have been shown to be likely involved in cold tolerance in tomato plants. However, although it was demonstrated that *LeGPA1* and *LeCOR413PM2* are induced by cold stress in tomato leaves (Guo et al., 2020; Zhang et al., 2021), both genes were downregulated with no cold-specific expression in the fruit pericarp samples analyzed in the present study. A possible explanation is that cold stress-induced gene expression can differ due to variations in tissue-specific physiological and developmental responses, as previously reported in tomato (Weiss and Egea-Cortines, 2009), as well as other plant species (Sanchez-Ballesta et al., 2004; Xin et al., 2019). In the present study, most of the cold-specific genes identified in the fruits showed similar expression patterns in the leaves (Supplementary Figure 3), suggesting their involvement in cold responses in both tissues.

In conclusion, we have utilized RNA-Seq analysis to pinpoint the transcriptional dynamics triggered by cold stress in tomato fruits, particularly those which are clearly distinct from ethylene signaling (and by extension, fruit ripening)-mediated ones. We have further demonstrated the likely involvement of *de novo* DNA methylation in the regulation of these cold-specific transcriptional changes. Other cold-specific transcriptional adjustments like the spliceosome, ribosome biogenesis, peptide biosynthesis and proteasomal catabolism point towards a strong re-alignment to alter the protein composition of tomato fruit cells in response to cold stress. These changes present potential regulators and players in the regulatory network for cold stress sensing and signaling pathways in fruits. Furthermore, considering that these changes do not occur during normal fruit ripening (at 20°C), the genes identified in the present study will encourage further research on genetic improvement of cold tolerance and CI reduction, without having to worry about undesirable effects on fruit ripening.

Data availability statement

The data presented in the study are deposited in the DNA Data Bank of Japan (DDBJ) repository, accession numbers DRR461198-DRR461224.

Author contributions

OM, HE, and YK conceived and designed the study. OM did most of the experiments with close supervision from HE, TA, and SK. LT provided technical assistance especially with growing of plants and data analysis. OM wrote the first draft of the manuscript which was substantially improved by all authors. All authors contributed to the article and approved the submitted version.

Funding

This study was supported by a Grant-in-Aid for JSPS Fellows (grant no. 21F21400) to OM by the Japan Society for the Promotion of Science, Japan (JSPS).

Conflict of interest

The authors declare that the research was conducted in the absence of any commercial or financial relationships that could be construed as a potential conflict of interest.

Publisher's note

All claims expressed in this article are solely those of the authors and do not necessarily represent those of their affiliated organizations, or those of the publisher, the editors and the reviewers. Any product that may be evaluated in this article, or claim that may be made by its manufacturer, is not guaranteed or endorsed by the publisher.

Supplementary material

The Supplementary Material for this article can be found online at: https://www.frontiersin.org/articles/10.3389/fpls.2023.1227349/full#supplementary-material

References

Albornoz, K., Cantwell, M. I., Zhang, L., and Beckles, D. M. (2019). Integrative analysis of postharvest chilling injury in cherry tomato fruit reveals contrapuntal spatio-temporal responses to ripening and cold stress. *Sci. Rep.* 9, 2795. doi: 10.1038/s41598-019-38877-0

Alcaide, C., Donaire, L., and Aranda, M. A. (2022). Transcriptome analyses unveiled differential regulation of AGO and DCL genes by pepino mosaic virus strains. *Mol. Plant Pathol.* 23, 1592–1607. doi: 10.1111/mpp.13249

Anderson, M. D., Prasad, T. K., Martin, B. A., and Stewart, C. R. (1994). Differential gene expression in chilling-acclimated maize seedlings and evidence for the involvement of abscisic acid in chilling tolerance. *Plant Physiol.* 105, 331–339. doi: 10.1104/pp.105.1.331

Barrero-Gil, J., Huertas, R., Rambla, J. L., Granell, A., and Salinas, J. (2016). Tomato plants increase their tolerance to low temperature in a chilling acclimation process entailing comprehensive transcriptional and metabolic adjustments. *Plant Cell Environ.* 39, 2303–2318. doi: 10.1111/pce.12799

Biswas, P., East, A. R., Hewett, E. W., and Heyes, J. A. (2016). Chilling injury in tomato fruit. *Hortic Rev.* 44, 229–278. doi: 10.1002/9781119281269.ch5

Blankenship, S. M., and Dole, J. M. (2003). 1-methylcyclopropene: a review. *Postharvest Biol. Technol.* 28, 1–25. doi: 10.1016/S0925-5214(02)00246-6

Chen, Y., Rofidal, V., Hem, S., Gil, J., Nosarzewska, J., Berger, N., et al. (2019). Targeted proteomics allows quantification of ethylene receptors and reveals SlETR3 accumulation in never-ripe tomatoes. *Front. Plant Sci.* 10. doi: 10.3389/fpls.2019.01054

Cheong, B. E., Beine-Golovchuk, O., Gorka, M., Ho, W. W. H., Martinez-Seidel, F., Firmino, A. A. P., et al. (2021). Arabidopsis REI-LIKE proteins activate ribosome biogenesis during cold acclimation. *Sci. Rep.* 11, 1–25. doi: 10.1038/s41598-021-81610-z

Chinnusamy, V., Zhu, J., and Zhu, J. K. (2007). Cold stress regulation of gene expression in plants. *Trends Plant Sci.* 12, 444–451. doi: 10.1016/j.tplants.2007.07.002

Cruz-Mendívil, A., López-Valenzuela, J. A., Calderón-Vázquez, C. L., Vega-García, M. O., Reyes-Moreno, C., and Valdez-Ortiz, A. (2015). Transcriptional changes associated with chilling tolerance and susceptibility in 'Micro-Tom' tomato fruit using RNA-Seq. *Postharvest Biol. Technol.* 99, 141–151. doi: 10.1016/j.postharvbio.2014.08.009

Ezura, H. (2009). Tomato is a next-generation model plant for research and development. *J. Jpn Soc Hortic. Sci.* 78, 1–2. doi: 10.2503/jjshs1.78.1

Gao, Z., Liu, H. L., Daxinger, L., Pontes, O., He, X., Qian, W., et al. (2010). An RNA polymerase II-and AGO4-associated protein acts in RNA-directed DNA methylation. *Nature* 465, 106–109. doi: 10.1038/nature09025

Ge, S. X., Jung, D., and Yao, R. (2020). ShinyGO: a graphical gene-set enrichment tool for animals and plants. *Bioinform.* 36, 2628–2629. doi: 10.1093/bioinformatics/btz931

Ge, S. X., Son, E. W., and Yao, R. (2018). iDEP: an integrated web application for differential expression and pathway analysis of RNA-Seq data. *BMC Bioinform.* 19, 534. doi: 10.1186/s12859-018-2486-6

Gratão, P. L., Monteiro, C. C., Carvalho, R. F., Tezotto, T., Piotto, F. A., Peres, L. E., et al. (2012). Biochemical dissection of diageotropica and never ripe tomato mutants to Cd-stressful conditions. *Plant Physiol. Biochem.* 56, 79–96. doi: 10.1016/j.plaphy.2012.04.009

Guo, X., Li, J., Zhang, L., Zhang, Z., He, P., Wang, W., et al. (2020). Heterotrimeric G-protein α subunit (LeGPA1) confers cold stress tolerance to processing tomato plants (*Lycopersicon esculentum* Mill). *BMC Plant Biol.* 20, 394. doi: 10.1186/s12870-020-02615-w

Huang, H., Liu, R., Niu, Q., Tang, K., Zhang, B., Zhang, H., et al. (2019). Global increase in DNA methylation during orange fruit development and ripening. *Proc. Natl. Acad. Sci.* 116, 1430–1436. doi: 10.1073/pnas.1815441116

Hunter, D. A., Napier, N. J., Erridge, Z. A., Saei, A., Chen, R. K., McKenzie, M. J., et al. (2021). Transcriptome responses of ripe cherry tomato fruit exposed to chilling and rewarming identify reversible and irreversible gene expression changes. *Front. Plant Sci.* 12. doi: 10.3389/fpls.2021.685416

Jiang, B., Shi, Y., Zhang, X., Xin, X., Qi, L., Guo, H., et al. (2017). PIF3 is a negative regulator of the CBF pathway and freezing tolerance in Arabidopsis. *Proc. Natl. Acad. Sci.* 114, E6695–E6702. doi: 10.1073/pnas.1706226114

Jones, P. A., and Taylor, S. M. (1980). Cellular differentiation, cytidine analogs and DNA methylation. *Cell* 20, 85–93. doi: 10.1016/0092-8674(80)90237-8

Kamiyoshihara, Y., Tieman, D. M., Huber, D. J., and Klee, H. J. (2012). Ligand-induced alterations in the phosphorylation state of ethylene receptors in tomato fruit. *Plant Physiol.* 160, 488–497. doi: 10.1104/pp.112.202820

Kidokoro, S., Shinozaki, K., and Yamaguchi-Shinozaki, K. (2022). Transcriptional regulatory network of plant cold-stress responses. *Trends Plant Sci.* 27, 922–935. doi: 10.1016/j.tplants.2022.01.008

Kim, J. S., Jeon, B. W., and Kim, J. (2021). Signaling peptides regulating abiotic stress responses in plants. *Front. Plant Sci.* 12. doi: 10.3389/fpls.2021.704490

Kim, J. M., Sasaki, T., Ueda, M., Sako, K., and Seki, M. (2015). Chromatin changes in response to drought, salinity, heat, and cold stresses in plants. *Front. Plant Sci.* 6. doi: 10.3389/fpls.2015.00114

Kosová, K., Vítámvás, P., Urban, M. O., Prášil, I. T., and Renaut, J. (2018). Plant abiotic stress proteomics: the major factors determining alterations in cellular proteome. *Front. Plant Sci.* 9. doi: 10.3389/fpls.2018.00122

Kuk, Y. I., Shin, J. S., Burgos, N. R., Hwang, T. E., Han, O., Cho, B. H., et al. (2003). Antioxidative enzymes offer protection from chilling damage in rice plants. *Crop Sci.* 43, 2109–2117. doi: 10.2135/cropsci2003.2109

Lanahan, M. B., Yen, H. C., Giovannoni, J. J., and Klee, H. J. (1994). The never ripe mutation blocks ethylene perception in tomato. *Plant Cell.* 6, 521–530. doi: 10.1105/tpc.6.4.521

Lang, Z., Wang, Y., Tang, K., Tang, D., Datsenka, T., Cheng, J., et al. (2017). Critical roles of DNA demethylation in the activation of ripening-induced genes and inhibition of ripening-repressed genes in tomato fruit. *Proc. Natl. Acad. Sci.* 114, E4511–E4519. doi: 10.1073/pnas.1705233114

Langfelder, P., and Horvath, S. (2008). WGCNA: an R package for weighted correlation network analysis. *BMC Bioinform.* 9, 559. doi: 10.1186/1471-2105-9-559

Li, S., Chen, K., and Grierson, D. (2019). A critical evaluation of the role of ethylene and MADS transcription factors in the network controlling fleshy fruit ripening. *New Phytol.* 221, 1724–1741. doi: 10.1111/nph.15545

Li, S., Yu, X., Cheng, Z., Yu, X., Ruan, M., Li, W., et al. (2017). Global gene expression analysis reveals crosstalk between response mechanisms to cold and drought stresses in cassava seedlings. *Front. Plant Sci.* 8. doi: 10.3389/fpls.2017.01259

Liu, P., Meng, Q. W., Zou, Q., Zhao, S. J., and Liu, Q. Z. (2001). Effects of cold-hardening on chilling-induced photoinhibition of photosynthesis and on xanthophyll cycle pigments in sweet pepper. *Photosynthetica.* 39, 467–472. doi: 10.1023/A:1015155032135

Lv, K., Li, J., Zhao, K., Chen, S., Nie, J., Zhang, W., et al. (2020). Overexpression of an AP2/ERF family gene, *BpERF13*, in birch enhances cold tolerance through upregulating CBF genes and mitigating reactive oxygen species. *Plant Sci.* 292, 110375. doi: 10.1016/j.plantsci.2019.110375

Manning, M., Burdon, J., De Silva, N., Meier, X., Pidakala, P., Punter, M., et al. (2016). Maturity and postharvest temperature management affect rot expression in 'Hort16A' kiwifruit. *Postharvest Biol. Technol.* 113, 40–47. doi: 10.1016/j.postharvbio.2015.10.012

Mehrotra, S., Verma, S., Kumar, S., Kumari, S., and Mishra, B. N. (2020). Transcriptional regulation and signalling of cold stress response in plants: An

overview of current understanding. *Environ. Exp. Bot.* 180, 104243. doi: 10.1016/j.envexpbot.2020.104243

Menda, N., Strickler, S. R., and Mueller, L. A. (2013). Advances in tomato research in the post-genome era. *Plant Biotechnol.* 30, 243–256. doi: 10.5511/plantbiotechnology.13.0904a

Mitalo, O. W., Asiche, W. O., Kang, S. W., Ezura, H., Akagi, T., Kubo, Y., et al. (2022). Examining the role of low temperature in Satsuma mandarin fruit peel degreening via comparative physiological and transcriptomic analysis. *Front. Plant Sci.* 13. doi: 10.3389/fpls.2022.918226

Mitalo, O. W., Otsuki, T., Okada, R., Obitsu, S., Masuda, K., Hojo, Y., et al. (2020). Low temperature modulates natural peel degreening in lemon fruit independently of endogenous ethylene. *J. Exp. Bot.* 71, 4778–4796. doi: 10.1093/jxb/eraa206

Mitalo, O. W., Tokiwa, S., Kondo, Y., Otsuki, T., Galis, I., Suezawa, K., et al. (2019a). Low temperature storage stimulates fruit softening and sugar accumulation without ethylene and aroma volatile production in kiwifruit. *Front. Plant Sci.* 10. doi: 10.3389/fpls.2019.00888

Mitalo, O. W., Tosa, Y., Tokiwa, S., Kondo, Y., Azimi, A., Hojo, Y., et al. (2019b). 'Passe Crassane' pear fruit (*Pyrus communis* L.) ripening: revisiting the role of low temperature via integrated physiological and transcriptome analysis. *Postharvest Biol. Technol.* 158, 110949. doi: 10.1016/j.postharvbio.2019.110949

Okabe, Y., Asamizu, E., Saito, T., Matsukura, C., Ariizumi, T., Bres, C., et al. (2011). Tomato TILLING technology: development of a reverse genetics tool for the efficient isolation of mutants from Micro-Tom mutant libraries. *Plant Cell Physiol.* 52, 1994–2005. doi: 10.1093/pcp/pcr134

Opiyo, A. M., and Ying, T. J. (2005). The effects of 1-methylcyclopropene treatment on the shelf life and quality of cherry tomato (*Lycopersicon esculentum* var. cerasiforme) fruit. *Int. J. Food Sci. Technol.* 40, 665–673. doi: 10.1111/j.1365-2621.2005.00977.x

Rao, C. G. (2015). *Engineering for storage of fruits and vegetables: cold storage, controlled atmosphere storage, modified atmosphere storage* (London: Academic Press).

Reddy, A. S., Marquez, Y., Kalyna, M., and Barta, A. (2013). Complexity of the alternative splicing landscape in plants. *Plant Cell* 25, 3657–3683. doi: 10.1105/tpc.113.117523

Saito, T., Ariizumi, T., Okabe, Y., Asamizu, E., Hiwasa-Tanase, K., Fukuda, N., et al. (2011). TOMATOMA: a novel tomato mutant database distributing Micro-Tom mutant collections. *Plant Cell Physiol.* 52, 283–296. doi: 10.1093/pcp/pcr004

Sanchez-Ballesta, M. T., Rodrigo, M. J., Lafuente, M. T., Granell, A., and Zacarias, L. (2004). Dehydrin from citrus, which confers in *vitro* dehydration and freezing protection activity, is constitutive and highly expressed in the flavedo of fruit but responsive to cold and water stress in leaves. *J. Agric. Food Chem.* 52, 1950–1957. doi: 10.1021/jf035216+

Schmidt, S., Dethloff, F., Beine-Golovchuk, O., and Kopka, J. (2013). The REIL1 and REIL2 proteins of Arabidopsis thaliana are required for leaf growth in the cold. *Plant Physiol.* 163, 1623–1639. doi: 10.1104/pp.113.223925

Schotsmans, W. C., Prange, R. K., and Binder, B. M. (2009). 1-Methylcyclopropene: mode of action and relevance in postharvest horticulture research. *Hortic. Rev.* 35, 263–313. doi: 10.1002/9780470593776.ch5

Serek, M., Woltering, E. J., Sisler, E. C., Frello, S., and Sriskandarajah, S. (2006). Controlling ethylene responses in flowers at the receptor level. *Biotechnol. Adv.* 24, 368–381. doi: 10.1016/j.biotechadv.2006.01.007

Sevillano, L., Sanchez-Ballesta, M. T., Romojaro, F., and Flores, F. B. (2009). Physiological, hormonal and molecular mechanisms regulating chilling injury in horticultural species. Postharvest technologies applied to reduce its impact. *J. Sci. Food Agric.* 89, 555–573. doi: 10.1002/jsfa.3468

Shimoda, Y., Ito, H., and Tanaka, A. (2016). Arabidopsis STAY-GREEN, Mendel's green cotyledon gene, encodes magnesium-dechelatase. *Plant Cell* 28, 2147–2160. doi: 10.1105/tpc.16.00428

Shipman, E. N., Yu, J., Zhou, J., Albornoz, K., and Beckles, D. M. (2021). Can gene editing reduce postharvest waste and loss of fruit, vegetables, and ornamentals? *Hortic. Res.* 8, 1. doi: 10.1038/s41438-020-00428-4

Suzuki, T., Ikeda, S., Kasai, A., Taneda, A., Fujibayashi, M., Sugawara, K., et al. (2019). RNAi-mediated down-regulation of Dicer-like 2 and 4 changes the response of 'Moneymaker' tomato to potato spindle tuber viroid infection from tolerance to lethal systemic necrosis, accompanied by up-regulation of miR398, 398a-3p and production of excessive amount of reactive oxygen species. *Viruses* 11, 344. doi: 10.3390/v11040344

Tieman, D. M., Taylor, M. G., Ciardi, J. A., and Klee, H. J. (2000). The tomato ethylene receptors NR and LeETR4 are negative regulators of ethylene response and exhibit functional compensation within a multigene family. *Proc. Natl. Acad. Sci.* 97, 5663–5668. doi: 10.1073/pnas.090550597

Valenzuela, J. L., Manzano, S., Palma, F., Carvajal, F., Garrido, D., and Jamilena, M. (2017). Oxidative stress associated with chilling injury in immature fruit: postharvest technological and biotechnological solutions. *Int. J. Mol. Sci.* 18, 1467. doi: 10.3390/ijms18071467

Vega-García, M. O., López-Espinoza, G., Ontiveros, J. C., Caro-Corrales, J. J., Vargas, F. D., and López-Valenzuela, J. A. (2010). Changes in protein expression associated with chilling injury in tomato fruit. *J. Am. Soc Hortic. Sci.* 135, 83–89. doi: 10.21273/JASHS.135.1.83

Vico, I., Jurick, W. M., Camp, M. J., Janisiewicz, W. J., and Conway, W. S. (2010). Temperature suppresses decay on apple fruit by affecting *Penicillium solitum* conidial germination, mycelial growth and polygalacturonase activity. *Plant Pathol. J.* 3, 144–148. doi: 10.3923/ppj.2010.144.148

Wang, C. Y. (1994). Chilling injury of tropical horticultural commodities. *HortScience* 29, 986–987. doi: 10.21273/HORTSCI.29.9.986

Wang, T., Deng, Z., Zhang, X., Wang, H., Wang, Y., Liu, X., et al. (2018). Tomato DCL2b is required for the biosynthesis of 22-nt small RNAs, the resulting secondary siRNAs, and the host defense against ToMV. *Hortic. Res.* 5, 62. doi: 10.1038/s41438-018-0073-7

Wang, Z., Hong, Y., Yao, J., Huang, H., Qian, B., Liu, X., et al. (2022). Modulation of plant development and chilling stress responses by alternative splicing events under control of the spliceosome protein SmEb in Arabidopsis. *Plant Cell Environ.* 45, 2762–2779. doi: 10.1111/pce.14386

Watkins, C. B. (2006). The use of 1-methylcyclopropene (1-MCP) on fruits and vegetables. *Biotechnol. Adv.* 24, 389–409. doi: 10.1016/j.biotechadv.2006.01.005

Weiss, J., and Egea-Cortines, M. (2009). Transcriptomic analysis of cold response in tomato fruits identifies dehydrin as a marker of cold stress. *J. Appl. Genet.* 50, 311–319. doi: 10.1007/BF03195689

Xin, H., Xianchao, N., Pan, X., Wei, L., Min, Y., Yu, K., et al. (2019). Comparative transcriptome analyses revealed conserved and novel responses to cold and freezing stress in *Brassica napus* L. *G3: Genes Genom. Genet.* 9, 2723–2737. doi: 10.1534/g3.119.400229

Zhang, L., Guo, X., Zhang, Z., Wang, A., and Zhu, J. (2021). Cold-regulated gene *LeCOR413PM2* confers cold stress tolerance in tomato plants. *Gene* 764, 145097. doi: 10.1016/j.gene.2020.145097

Zhang, B., Tieman, D. M., Jiao, C., Xu, Y., Chen, K., Fei, Z., et al. (2016). Chilling-induced tomato flavor loss is associated with altered volatile synthesis and transient changes in DNA methylation. *Proc. Natl. Acad. Sci.* 113, 12580–12585. doi: 10.1073/pnas.1613910113

Zhu, Y. C., Zhang, B., Allan, A. C., Lin-Wang, K., Zhao, Y., Wang, K., et al. (2020). DNA demethylation is involved in the regulation of temperature-dependent anthocyanin accumulation in peach. *Plant J.* 102, 965–976. doi: 10.1111/tpj.14680

frontiers | Frontiers in Plant Science

TYPE Original Research
PUBLISHED 25 September 2023
DOI 10.3389/fpls.2023.1267340

OPEN ACCESS

EDITED BY
Rakesh Kumar,
Central University of Karnataka, India

REVIEWED BY
Prateek Gupta,
SRM University, India
Oscar Witere Mitalo,
University of Tsukuba, Japan

*CORRESPONDENCE
Angelos K. Kanellis
kanellis@pharm.auth.gr
Ifigeneia Mellidou
ifimellidou@gmail.com

†These authors have contributed equally to this work

RECEIVED 26 July 2023
ACCEPTED 05 September 2023
PUBLISHED 25 September 2023

CITATION
Mellidou I, Koukounaras A, Frusciante S, Rambla JL, Patelou E, Ntoanidou S, Pons C, Kostas S, Nikoloudis K, Granell A, Diretto G and Kanellis AK (2023) A metabolome and transcriptome survey to tap the dynamics of fruit prolonged shelf-life and improved quality within Greek tomato germplasm. *Front. Plant Sci.* 14:1267340. doi: 10.3389/fpls.2023.1267340

A metabolome and transcriptome survey to tap the dynamics of fruit prolonged shelf-life and improved quality within Greek tomato germplasm

Ifigeneia Mellidou[1,2*†], Athanasios Koukounaras[2,3†], Sarah Frusciante[4], José L. Rambla[5,6], Efstathia Patelou[2], Symela Ntoanidou[2], Clara Pons[5,7], Stefanos Kostas[2,3], Konstantinos Nikoloudis[8], Antonio Granell[5], Gianfranco Diretto[4] and Angelos K. Kanellis[2*]

[1]Institute of Plant Breeding and Genetic Resources, Hellenic Agricultural Organization – DEMETER, Thessaloniki, Greece, [2]Group of Biotechnology of Pharmaceutical Plants, Laboratory of Pharmacognosy, Department of Pharmaceutical Sciences, Aristotle University of Thessaloniki, Thessaloniki, Greece, [3]Department of Horticulture, Aristotle University of Thessaloniki, Thessaloniki, Greece, [4]Italian National Agency for New Technologies, Energy, and Sustainable Development (ENEA), Biotechnology Laboratory, Casaccia Research Center, Rome, Italy, [5]Instituto de Biología Molecular y Celular de Plantas (IBMCP), Consejo Superior de Investigaciones Científicas (CSIC), Universitat Politècnica de València, València, Spain, [6]Department of Biology, Biochemistry and Natural Sciences, Universitat Jaume I, Castellón de la Plana, Spain, [7]Instituto de Conservación y Mejora de la Agrodiversidad Valenciana (COMAV), Universitat Politècnica de València, València, Spain, [8]Agroindustrial Cooperative of Tympaki, Tympaki, Greece

Introduction: Tomato is a high economic value crop worldwide with recognized nutritional properties and diverse postharvest potential. Nowadays, there is an emerging awareness about the exploitation and utilization of underutilized traditional germplasm in modern breeding programs. In this context, the existing diversity among Greek accessions in terms of their postharvest life and nutritional value remains largely unexplored.

Methods: Herein, a detailed evaluation of 130 tomato Greek accessions for postharvest and nutritional characteristics was performed, using metabolomics and transcriptomics, leading to the selection of accessions with these interesting traits.

Results: The results showed remarkable differences among tomato Greek accessions for overall ripening parameters (color, firmness) and weight loss. On the basis of their postharvest performance, a balance between short shelf life (SSL) and long shelf life (LSL) accessions was revealed. Metabolome analysis performed on 14 selected accessions with contrasting shelf-life potential identified a total of 206 phytonutrients and volatile compounds. In turn, transcriptome analysis in fruits from the best SSL and the best LSL accessions

revealed remarkable differences in the expression profiles of transcripts involved in key metabolic pathways related to fruit quality and postharvest potential.

Discussion: The pathways towards cell wall synthesis, polyamine synthesis, ABA catabolism, and steroidal alkaloids synthesis were mostly induced in the LSL accession, whereas those related to ethylene biosynthesis, cell wall degradation, isoprenoids, phenylpropanoids, ascorbic acid and aroma (*TomloxC*) were stimulated in the SSL accession. Overall, these data would provide valuable insights into the molecular mechanism towards enhancing shelf-life and improving flavor and aroma of modern tomato cultivars.

KEYWORDS

landraces, metabolomics, nutritional quality, ripening, shelf-life, storage, transcriptomics

1 Introduction

Based on FAOSTAT database for 2020, tomato (*Solanum lycopersicum* L.) has an extremely high economic value importance worldwide, cultivated in over five million hectares with a production of over 186 million tons. The existing biodiversity within tomato genetic resources during its cultivation history is mainly the result of the progressive anthropogenic selection pressure (Pons et al., 2022). Through the long-term domestication process, farmer- and breeder-driven choices had narrowed down tomato genetic diversity, limiting their improvement potential. Nowadays, growers almost exclusively use tomato hybrids, focusing on yield performance and disease resilience, that comes usually at the expense of fruit taste, aroma, and phytonutrients. In Europe, and especially in Mediterranean countries, a remarkable phenotypic diversity related to fruit quality, aroma and taste attributes, as well as postharvest potential is evident, mostly because of the long cultivation history in the area, which therefore can be regarded as a secondary diversity hotspot (Mazzucato et al., 2008; Blanca et al., 2022). In the past few years, there were numerous genetic studies aiming to depict diversifications among the existing genetic pools in different South European countries (Cortés-Olmos et al., 2015; Sacco et al., 2015; Parisi et al., 2016; Blanca et al., 2022; Pons et al., 2022), some of them including Greek Gene Bank accessions.

Tomato is a typical climacteric fruit, that can be harvested either in early mature or full ripe stage depending on the market requirements, the distance until the retail market, or the season of the year. On the basis on their end-use, tomatoes can be classified as processing, fresh market, cherry, or traditional tomatoes, with the first three groups corresponding to breeding material characterized by the introgression of genes for disease resistance (Blanca et al., 2022). On the contrary, traditional varieties, including heirlooms, landrace and "vintage" germplasm, have not been widely incorporated into advanced breeding programs, presumably due to the lack of comprehensive genomic information within this traditional group. Thus, although several pre- and postharvest factors including cultivation practices, climate, or storage conditions have been widely studied (Conesa et al., 2014), it was only recently that the genomic effect has gained attention (Blanca et al., 2022; Pons et al., 2022), in order to unravel the history and domestication of the European traditional varieties. Notwithstanding the large genetic erosion with the gene pool present within modern varieties that has led to a significant drop-off in tomato aroma, some traditional varieties, with excellent taste and aroma properties, can be still found in local markets (Pons et al., 2022). Among them, some Greek varieties like "Tomataki Santorinis" are highly appreciated by consumers, being important for the local market (Koutsika-Sotiriou et al., 2016). However, the majority of this Greek traditional germplasm has been exploited for morphological diversity, heterogeneity and yield (Gonias et al, 2019; Mellidou et al., 2020), without any available information about their nutritional value and postharvest life performance. In this frame, the characterization of this traditional germplasm for its future exploitation can provide a valuable reservoir of genes not only to restore tomato taste and aroma in the commercial varieties, but also due to its great adaptability to local environmental and farming conditions.

Despite these genetic studies aiming to unveil the diversification history of the European traditional tomato varieties, a comprehensive study on its fruit composition, nutritional value and flavor attributes is still lacking. Globally, tomato is among the main consumed crops essential for the human diet, containing many healthy and beneficial biologically active compounds, including lycopene, vitamin C and E, and flavonoids (Klee, 2010; Ilahy et al., 2019). The majority of these metabolic routes have been well-characterized in tomato fruit, with a plethora of transgenic lines enriched in these compounds (Verhoeyen et al., 2002; Bulley et al., 2012; Koukounaras et al., 2022). At the same time, tomato fruit contains high amounts of steroidal alkaloids and glycoalkaloids, such as α-tomatine, that are toxic for humans, thus considered as antinutritional factors (Zhao et al., 2023). A wide group of genes related to glycoalkaloid metabolism (*GAME*) has been previously demonstrated to participate in glycoalkaloid

synthesis, whereas through the process of ripening and a series of hydroxylation and glycosylation reactions, these genes convert tomatine to the non-toxic and non-bitter esculeoside A (Cárdenas et al., 2016) that also possess some health benefits (Nohara et al., 2010).

Along with these important phytonutrients that are appreciated by consumers, tomato flavor greatly affects consumer acceptance and preferences, re-directing breeders' goal from yield-oriented towards nutritional- and flavor-oriented strategies, regenerating the necessity of exploring the genetics underlying tomato flavor (Wang et al., 2023). Tomato's unique flavor arises from the balance between sugars (glucose and fructose), acids (citrate, malate, ascorbate and glutamate) and volatile organic compounds (VOCs), constituting of a huge heterogeneous group of diverse molecules (Colantonio et al., 2022; Kaur et al., 2023). The loss of positive contributors to fruit aroma has been previously associated to linkage drag with other commercial traits such as fruit weight and disease resistance (Li et al., 2022a). Among the nearly 400 volatile compounds identified in tomato fruit and derived from essential phytonutrients, such as apocarotenoids, and derivatives of branched amino-acids, lipids/fatty acids, sulfur, phenylalanine and phenylpropanoid, only a small fraction of them are regarded as important contributors to the typical aroma of fresh tomato (Tieman et al., 2017). These include (*Z*)-3-hexenal, β-ionone, hexanal, β-damascenone, 1-penten-3-one, 3-methylbutanal, (*E*)-2-hexenal, (*Z*)-3-hexenol, 6-methyl-5-hepten-2-one, methyl salicylate and 2-isobutylthiazole, with the rest contributing as background notes (Ilahy et al., 2019). The interaction of these compounds released sensorial odors described as "sweet", "smoky", or "fruity" (Martina et al., 2021). The dissatisfaction of consumers concerning the loss of tomato flavor in modern fresh market tomatoes is well-documented (Tieman et al., 2017), but breeding for enriched tomato flavor has proven to be a difficult task due to complex interacting metabolic networks as well as the strong environmental effect. However, the progression of fast-evolving analytical techniques and data mining tools for the accurate determination of "flavor-omics" (Bineau et al., 2022), along with the functional characterization of hub genes involved in these pathways, may open new avenues for plant breeding towards the biofortification of tomatoes (Alseekh et al., 2021). Nonetheless, there is still a long way towards the development of the "perfect" tomato, as well as an emerging need to exploit all the available germplasm collections to shed light into these multifaceted interactions.

In this study, a total of 130 accessions of tomato from the Greek Gene Bank (ELGO-Demeter) were initially characterized for fruit traits and postharvest performance. In turn, fruit metabolome of a selection of seven long shelf-life (LSL) and seven short shelf-life (SSL) varieties was exploited to identify differentially accumulated metabolites (DAMs) related to fruit quality, taste and flavor, between groups. As a further step, fruit transcriptomes of the best LSL and the best SSL genotypes, substantially differing in ethylene production, were investigated to expand our understanding on the relationships between the transcriptome and the postharvest shelf-life attributes. The knowledge produced herein can be valuable for future functional studies, and can assist breeders to improve decision-making towards the development of the "perfect" tomato.

2 Materials and methods

2.1 Plant material and growth conditions

The experiment was conducted in Tympaki, Crete Island, Greece, in a non-heated plastic greenhouse. The establishment of the crop was done according to the usual cultural practices. At the time that fruit were at the required maturity stage (see below), they were harvested and transferred within 24h to the facilities of Aristotle University of Thessaloniki for evaluation. During the 1st year of the experiment, 130 accessions from the Greek Gene Bank (ELGO-Demeter) with five plants per accession were cultivated and evaluated (Supplementary Figure 1), as described below. In the 2nd year of the experiment, 14 accessions selected based on the results of the previous year with 10 plants per accession were cultivated and evaluated.

2.2 Postharvest evaluation

During the 1st year of the experiments, due to the absence of prior knowledge about the postharvest behavior of the accessions, both SSL and LSL protocols were employed in order to properly classify accessions based on their postharvest characteristics. These two protocols were commonly applied in all postharvest experiments performed by the EU-TRADITOM partners. In particular, for the SSL protocol (Protocol A), fruits at the breaker stage were harvested and stored at 12 °C for 10 days, and then transferred to 20 °C for 3 days. Fruit weight, fruit color with the use of a digital colorimeter (CR-400 Chroma Meter, Konica Minolta Inc., Tokyo, Japan), as well as firmness with durometer (Turoni, Italy), were recorded in all fruits during the cold storage period (CS), and during shelf life (SL), as well as both periods (total). In particular, firmness loss (FL) was expressed as the average of the % of firmness loss (FL) and is calculated as $FL=100-(F_t*100/F_0)$. Where F_t is the measured firmness at each time and F_0, the measured firmness at the reference time. Color Index change (ΔCa/b or CI) was expressed as the average of ratio a/b increment in relation to the reference time. Weight loss was expressed as % of the initial value. On the other hand, for the LSL protocol (Protocol B), fruits at the red stage were harvested and stored at 20 °C (Protocol B). Once per week, red fruits were evaluated for weight loss, firmness, color, as described above, as well as for decay. As a result of the 1st year experimentation, the accessions were classified as short self life (SSL: shelf life < 1 week), as medium shelf life (MSL: shelf life < 2 weeks) or as long shelf life (LSL: shelf life > 2 weeks). During the 2nd year of experimentation, the evaluation protocol A was applied for SSL accessions, while protocol B for the LSL accessions.

The ethylene production rate was measured during the 2nd year by injecting a gas sample, 1 mL each, which was taken from the exit tube of a jar with fruit inside, into a gas chromatograph (model Varian 3300, Varian Instruments, Walnut Creek, CA) equipped with a flame ionization detector, essentially as previously described (Koukounaras et al., 2022). To identify significant differences in ethylene production between SSL and LSL genotypes, Tukey's test

with significant level $P \leq 0.05$ was performed using SPSS 27 (IBM, USA).

2.3 Non-volatile metabolomic profiling

Non-polar (NP) and semi polar (SP) metabolites were extracted from, respectively, 3 and 10 mg of freeze-dried tomatoes, harvested at the red stage, for a total of three replicates for each of the seven SSL and the seven LSL genotypes. Liquid chromatography coupled to high-resolution mass spectrometry (HPLC-APCI/ESI-HRMS) conditions were as previously reported for NP (Teixeira et al., 2023) and SP (Dono et al., 2022) metabolome, respectively. Metabolites were identified through the comparison with authentic standards or MS/MS spectra when available and on the basis of the accurate masses obtained from the Pubchem database (http://pubchem.ncbi.nlm.nih.gov/) for native compounds or from the Metabolomics Fiehn Lab Mass Spectrometry Adduct Calculator (http://fiehnlab.ucdavis.edu/staff/kind/Metabolomics/MS-Adduct-Calculator/) for adducts. Data were quantified as fold internal standard levels: alfa-tocopherol acetate (Cat. N. 47786, Sigma Aldrich) has been used in case of NP metabolites and daidzein (Cat. N.16587-10MG, Supelco) for SP metabolites.

2.4 Determination of volatile compounds

Headspace solid phase microextraction (HS-SPME) was used for the capture of volatile compounds, which were then separated and detected by means of gas chromatography coupled to mass spectrometry (GC/MS), similarly as described in Rambla et al. (2017). The pericarp of red ripe tomato fruits from seven SSL and seven LSL genotypes, was excised, immediately frozen in liquid nitrogen, milled to a fine powder under cryogenic conditions and stored at -80°C until analysis. Three biological replicates were analyzed, each consisting a mixture of two or three fruits.

Five hundred milligrams of the tomato samples were placed in a 15 mL glass vial and incubated in a water bath for 10 min at 37°C. Five hundred mL of an EDTA 100 mM, pH 7.5 solution and 1.1 g of $CaCl_2.2H_2O$ were added, gently mixed and sonicated for 5 min. One mL of the resulting paste was transferred to a 10 mL screw cap headspace vial with silicon/PTFE septum and analyzed within 10 hours. Volatile compounds in the headspace were extracted by a 65 µm PDMS/DVB SPME fiber (Supelco). Volatile extraction was performed automatically with a CombiPAL autosampler (CTC Analytics). Vials were first incubated at 50°C for 10 min with 500 rpm agitation. The fiber was then exposed for 20 min to the vial headspace under the same agitation and temperature conditions. Desorption was performed at 250°C during 1 min in a 6890N gas chromatograph (Agilent) in splitless mode. After desorption, the fiber was cleaned in an SPME fiber conditioning station (CTC Analytics) at 250°C for 5 min under a helium flow to prevent cross contamination. Chromatography was performed on a DB-5ms (60 m, 0.25 mm, 1 µm) capillary column (J&W) with 1.2 mL/min constant helium flow. Temperatures of the GC interface and MS source were 260°C and 230°C, respectively. Oven programming conditions were 40°C for 2 min, 5°C/min ramp until 250°C, and a final hold at 250°C for 5 min. Data was recorded in a 5975B mass spectrometer (Agilent) in the 35-250 m/z range at 6.2 scans/s, with 70 eV electronic impact ionization. Chromatograms were processed by means of MassHunter version 10.1 (Agilent). Identification of compounds was based on comparison of both retention time and mass spectrum with those of pure standards (Merck). For quantitation, the extracted ion chromatogram for one specific ion was integrated for each compound. The criteria for ion selection were specificity and high signal-to-noise ratio. An admixture reference sample was prepared for each season by thoroughly mixing equal amounts of each sample. A 500 mg aliquot of the admixture was analyzed regularly (one admixture for every ten samples) and processed as any sample as part of the injection series. This admixture was used as a reference to normalize for temporal variation and fiber aging. The normalized results for a sample are expressed as the ratio of the abundance of each compound in that particular sample to those in the reference admixture.

Finally, the identified metabolites were subjected to Principal Component Analysis. Heatmaps and hierarchical clustering of the identified metabolites were constructed using Clustvis online tool (Metsalu and Vilo, 2015). The software package "corrplot" in R was used to calculate the Pearson correlation coefficient of metabolites of the 14 genotypes (Wei and Simko, 2017). To identify significant differences within the metabolomic data between the best SSL and the best LSL genotypes, Student's T-test at 0.05 level was performed using SPSS 27 (IBM, USA).

2.5 RNA isolation and sequencing

Fruits of the best LSL (TRTH1620) and the best SSL (TRTH2510) genotypes at the red stage of ripening were used for total RNA extraction using Spectrum Plant Total RNA kit (Sigma-Aldrich, St. Louis, MO, USA). Three biological replicates were used per genotype. Quantification and qualification of the extracted RNA was checked using Nanodrop 2000 (NanoDrop Technologies, Wilmington, DE, USA) and 1% agarose gel electrophoresis, or Agilent 4200 TapeStation System (Agilent, CA, USA), respectively. Six RNA samples were sent to the Beijing Genome Institute (BGI, Shenzhen, China) for sequencing (BGI, Shenzhen, China). Raw data were deposited in the National Centre for Biotechnology Information (NCBI) Sequence Read Archive (SRA) under BioProject accession number: PRJNA991925.

2.6 Transcriptome data analysis

As a first step, BBDuk (Decontamination Using Kmers) was employed to trim and filter the raw sequences, in Geneious Prime v2021.1.1. Adapters were trimmed on paired read overhangs, with minimum overlap of 20, while short reads with minimum length of 20 were discarded. The high quality paired-end reads were then aligned to the tomato reference genome (Hosmani et al., 2019) using Geneious Prime Mapper with high sensitivity, essentially as previously described. Afterwards, the mapped reads for each

transcript were generated using the Calculate Expression Levels feature in Geneious Prime, to calculate fragments per kilobase for exon model per million mapped reads (FPKM). Differentially Expressed Genes (DEGs) between TRTH1620 and TRTH2510 were calculated using DESeq2 package in R (Love et al., 2014). Transcripts were screened based on adjusted $p \leq 0.01$ and $|Log2(\text{fold-change, FC})| \geq 2$, to identify the most significant DEGs. Finally, Gene Ontology (GO) and KEGG enrichment analysis of DEGs was investigated using clusterProfiler in R studio (Yu et al., 2012), to elucidate the functional representation of genotypic differences.

2.7 RT-qPCR verification

Quantitative real-time PCR (qPCR) analysis was performed to verify the RNAseq results, using the same total RNA per sample. Based on transcriptomic data, the expression levels of eleven (11) genes from key metabolic pathways during tomato ripening were investigated. The cDNA was synthesized with the Superscript® III Reverse Transcriptase kit (Invitrogen), according to manufacturer's instructions. Primers were developed using the genomic data of the two genotypes (Pons et al., 2022). The internal standard used in the qPCR analysis was the endogenous tomato gene CAC (clathrin adaptor complexes medium subunit) (Mellidou et al., 2012). Each sample was represented by three biological replicates and all qPCR analyses were performed in duplicates. The qPCR reactions were performed in a 20 µl reaction volume containing 0.2 ng cDNA, 0.1 pmol each primer, 1 × KAPA SYBR FAST Master Mix (KAPABIOSYSTEMS, Boston, U.S.A.) and sterile, nuclease free H2O. The amplification was conducted at 95 °C for 4 min, followed by 6 cycles of 95 °C for 35 s, T annealing, 57 °C for 30 s and 72 °C for 20 s, and in turn by 44 cycles of 95 °C for 25 s, T annealing, 57 °C for 20 s, 72 °C for 15 s, and plate read at 80 °C. To identify the PCR products a melting curve was performed from 65 °C to 95 °C with readings every 0.1 °C and a 10-s hold between observations. Relative quantification and statistical analyses were done using the comparative CT (ΔΔCT) method (Schmittgen and Livak, 2008), with the DataAssist™ v3.0 data analysis tool. Relative quantification of gene expression was carried out in respect to differences observed between TRTH1620 and TRTH2510. The primers used for RT-qPCR are listed in Supplementary Table 1.

3 Results

3.1 Post-harvest dynamics of the tomato accessions

Among the 130 tomato Greek accessions, there were highly significant differences ($P < 0.01$ or <0.001) for overall ripening parameters, weight loss as well as fruit weight (Supplementary Table 2). The average firmness loss rate during the whole storage period was found to be 3.66%, ranging widely from 1.49 to 6.45%. Similarly, for color index change the mean value was 0.093, the lowest and the maxim value were 0.014 and 0.144, respectively. Classification of accessions based on the postharvest performance

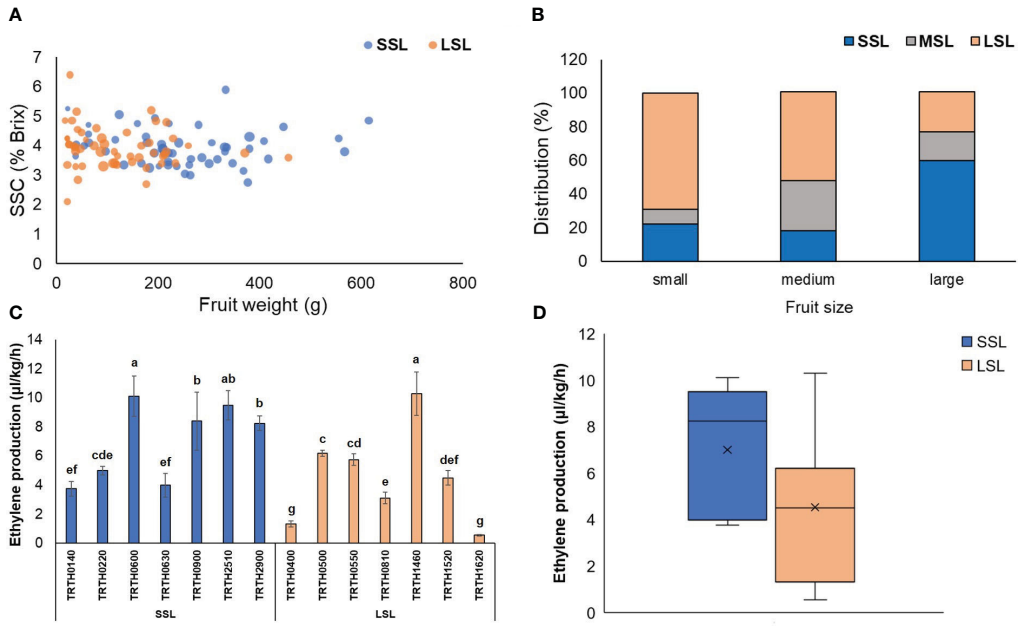

FIGURE 1
(A) 4-D bubble plot analysis displaying the relationship between fruit weight, SSC (°Brix), fruit firmness (%) and postharvest characterization. The x-axis represents fruit weight (g), the y-axis represents °Brix, the bubble size represents firmness, and the bubble color the postharvest characterization. **(B)** Distribution (%) of the 130 tomato accessions classified as SSL, MSL and LSL, based on their fruit size. **(C)** Ethylene production rate (µl kg^{-1} h^{-1}) of seven (7) SSL and seven (7) LSL accessions, determined at the red stage of ripening. Different letters indicate statistically significant differences based on Tukey's test ($P < 0.05$). **(D)** Boxplots of the average ethylene production (µl kg^{-1} h^{-1}) determined in the seven (7) SSL and the seven (7) LSL accessions. SSL, short shelf-life; MSL, medium shelf-life; LSL, long shelf-life.

10.3389/fpls.2023.1267340

showed a balance between SSL and LSL (Figure 1A), with a portion of 42.3 and 40.8%, respectively. Fruit size had a significant effect over the classification of the accessions to a shelf-life category. In particular, for small-fruited accessions, the postharvest performance was relatively good (69% of the accessions characterized as LSL, and only about 22% as SSL). Large-fruited accessions had the opposite behavior (60% of the accessions characterized as SSL and only about 24% as SSL). Accessions with medium fruit size showed an intermediate performance and classification as MSL (Figure 1B).

Out of the 130 accessions, seven LSL and seven SSL varieties were selected based on the results of the 1st year in order to repeat post-harvest phenotyping during the 2nd year. Heatmaps for SSL accessions showed that TRTH0140 and TRTH0220 had the best postharvest performance, exhibiting extremely slow color change, softening and low weight loss for the whole storage period, followed by TRTH2510 and TRTH0900 that also performed well (Supplementary Figure 2A). By contrast, TRTH0630 exhibited the worst postharvest performance. Accordingly, the best performing accession from the LSL group was TRTH1520, followed by TRTH1620, with decay rates after 4 weeks storage of 5% and 11%, respectively, whereas a number of accessions showed extremely low storability (Supplementary Figure 2B). All the above findings were generally in line with the ethylene production rate of the fruits, with SSL accessions exhibiting in average the highest rates (Figures 1C, D), and those classified as LSL (especially TRTH1620 and TRTH0400) low ethylene production. Nonetheless, there were some LSL accessions (TRTH1460, TRTH0500, TRTH0550) that exerted high ethylene production, at similar levels to SSL accessions. In future studies, this observation might be of interest in understanding how i.e. TRTH1460 exhibits high ethylene production rates, yet being LSL.

3.2 Metabolomic analysis of the differences in phytonutrients and volatiles within the collection

To explore the differences in flavor and taste compounds among the 14 selected Greek tomato accessions, a metabolomic comparison including NP and SP metabolites, as well as volatiles, of seven LSL and seven SSL cultivars was performed. A total of 206 metabolic compounds were identified, among them, 17 amino acids, 13 organic acids, 17 carotenoids, 36 polyphenolic compounds, and 77 volatiles (Supplementary Table 3). Cluster analysis of metabolite concentration indicated that all biological replicates for the same accession were grouped together, indicating a high reliability and reproducibility of the resulting metabolome data (Supplementary Figure 3).

Principal component analysis (PCA) was performed, PC1 and PC2 explaining 36.3% and 17.3% of total variance, respectively (Supplementary Figure 4). Accessions in the first component were separated mainly by total firmness loss after postharvest, being those with the highest firmness loss. The second component, mostly separated the LSL accession TRTH1620 from the rest of accessions (Figure 2; Supplementary Figure 3). The genotype TRTH1620 had a distinguished metabolome profile, being particularly rich in the majority of flavonoid compounds, as well as in esculeoside A, a steroidal alkaloid glycoside, possessing potential health benefits for humans (Huang et al., 2021), as will be discussed below.

Within metabolome data according to our experimental conditions, the most abundant sugar was glucose, whereas pyruvic and lactic acids were the top organic acids (Supplementary Table 3). Among the amino acids, tomato fruits were rich in glutamate, representing the umami perception, and phenylalanine, followed by leucine/isoleucine and tryptophan. With

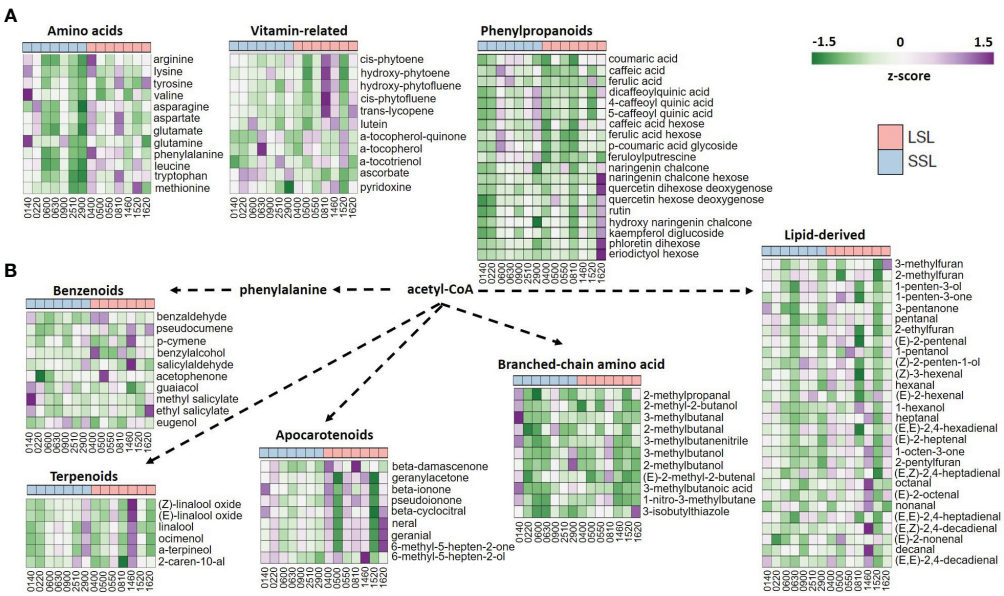

FIGURE 2
Heatmaps of the metabolomic profiles of the seven SSL and the seven LSL genotypes, with regard to amino acids, vitamins and phenylpropanoid abundance **(A)**, as well as to volatiles **(B)**. Mean values represent the average of three biological replicated, and are normalized based on z-score.

regard to postharvest potential, it was evident that LSL genotypes accumulated more amino acids than SSL genotypes, except for TRTH0140, which belongs to the SSL group (Figure 2). Similarly, the most abundant carotenoids were 15-cis-phytoene, all-trans-lycopene and 9,15-cis-phytofluene, whereas vitamin E (α-tocopherol), vitamin C (ascorbic acid), and vitamin B6 (pyridoxine) were also abundant, yet with remarkable differences between the different varieties. In particular, LSL genotypes seemed to accumulate more carotenoids than SSL ones, whereas SSL genotypes had more tocopherols and ascorbic acid than LSL ones. Notably, the highest pyridoxine levels were measured in TRTH0220 (SSL) and TRTH1460 (LSL). Among the phenylpropanoids, 4-caffeoyl-quinic acid, caffeic acid hexose and naringenin chalcone were the most represented compounds, with LSL genotypes being richer in flavonoids, and the SSL genotypes in hydroxycinnamic acids, with only a few exceptions.

The 77 volatile compounds were grouped as apocarotenoids, benzenoids, branched-chain amino acid related, phenylalanine-derived, sulfur compounds, terpenoids, esters and lipid-derived, that contained nearly half of the identified VOCs (Supplementary Table 3). PCA analysis and heatmap depicted a remarkable variability in volatile compounds among the 14 accessions, however they also indicated that VOC did not seem to correlate with postharvest properties (Supplementary Figure 5). For example, TRTH0140 (SSL) was rich in VOCs derived from the benzenoid and branched-chain amino acid pathways, but so did the LSL varieties TRTH1460 and TRTH0810, respectively. Furthermore, apocarotenoids such as geranial, neral, and 6-methyl-5-hepten-2-one were highly abundant in TRTH1620, and to a lesser extent in TRTH1460, TRTH0550 and TRTH0810, all from the LSL group, but not in other LSL varieties such as TRTH0500 and TRTH1520, suggesting the complexity of the routes involved in tomato aroma, flavor and postharvest attributes. The LSL variety TRTH1460 also contained the highest amounts of terpenoids and lipid-derived VOCs, which also correlated with the highest ethylene accumulation determined within the collection (Figure 1C). In this LSL genotype, an interesting correlation between apocarotenoid VOCs that are related to precursors localized in plastids and increased during ripening, and lipid-derived VOCs that are linked to precursors of membrane fatty acids, was evident, in line with previous reports (Colantonio et al., 2022). Additionally, TRTH0500 and TRTH0550, both from the LSL group, were rich in 1-penten-3-one, an important compound for tomato flavor. The LSL variety TRTH0400 contained high amounts of the umami-related influencers, 2-phenylethanol and 1-nitro-2-phenylethane, from the phenylalanine-derived pathway. The lipid-derived VOC (*E*)-2-pentenal, previously identified as important contributor to flavor enhancement and umami, was highly accumulated in the LSL varieties, TRTH0400, TRTH0500 and TRTH0550.

By comparing the average values of SSL and LSL varieties, a total of 15 metabolites (amino acids, organic acids, carotenoids, hydroxycinnamic acids and VOCs) were significantly differentially accumulated in the fruits with the contrasting postharvest properties (Table 1; Supplementary Table 4). Among them, the amino acids phenylalanine, leucine and tryptophan, the organic acids, adipate, glutarate and itaconate, as well as 1-octen-3-one (lipid-derived VOC), were up-regulated in the LSL varieties. By contrast, ascorbic acid (AsA), hydroxyproline, 9-cis-violaxanthin,

TABLE 1 Differentially accumulated metabolites between SSL and LSL based on Student's t-test.

		Average content			
Group	Metabolite	SSL	LSL	log2FC (LSL/SSL)	sig.
amino acids	phenylalanine	104.2 ± 22.0	193.8 ± 30.8	0.27	*
	leucine/isoleucine	46.77 ± 8.65	73.18 ± 7.37	0.19	*
	tryptophan	15.38 ± 2.48	26.82 ± 2.93	0.24	*
	hydroxyproline	0.10 ± 0.01	0.08 ± 0.01	-0.09	*
organic acids and derivatives	ascorbic acid	2.67 ± 0.55	1.59 ± 0.26	-0.22	**
	adipic acid	0.48 ± 0.08	0.73 ± 0.07	0.18	*
	glutaric acid	1.09 ± 0.02	1.30 ± 0.05	0.07	**
	itaconic acid	0.56 ± 0.03	0.73 ± 0.03	0.11	**
carotenoids	9-cis-violaxanthin	0.014 ± 0.001	0.008 ± 0.002	-0.27	*
hydroxycinnamic acids and derivatives	Ferulic acid hexose	7.66 ± 1.19	4.31 ± 0.84	-0.25	*
	N-Feruloylputrescine	5.51 ± 0.76	2.24 ± 0.49	-0.39	**
VOCs - esters	2-methylpropyl acetate	1.20 ± 0.14	0.80 ± 0.11	-0.18	*
	3-methylbutyl acetate	1.25 ± 0.16	0.75 ± 0.11	-0.22	*
	2-methylbutyl acetate	1.47 ± 0.27	0.53 ± 0.10	-0.44	*
VOCs - lipids	1-octen-3-one	0.87 ± 0.03	1.13 ± 0.08	0.11	*

Values represent mean values ± SE.

two hydroxycinnamic acids (ferulic acid hexose), N-feruloylputrescine, and three ester-related VOCs (2-methylpropyl acetate, 3-methylbutyl acetate and 2-methylbutyl acetate) were up-regulated in the SSL varieties. The small number of significant correlations found between the 206 compounds and postharvest potential within this germplasm collection, clearly suggest that promising germplasm with excellent flavor and taste can also be detected among varieties with prolonged storability.

Pearson correlation coefficient for all the abundant metabolites (36 compounds and 60 VOCs) was calculated (Supplementary Table 5), with those having R^2> 0.8 being illustrated in Supplementary Figure 6. The most significant correlations in our sample set were identified between rutin and kaempferol diglucoside (R^2 = 0.99), aspartate and glutamate (R^2 = 0.95), as well as glutamate and pyruvate (R^2 = 0.97). Other important correlations included various amino acids with each other (positive correlations), or amino acids with phenolic compounds (negative correlations). Similarly, regarding VOCs, neral and geranial (R^2 = 0.99) or 6-methyl-5-hepten-2-one (R^2 = 0.99), 2-phenylethanol and 1-nitro-2-phyenylethane (R^2 = 0.97), α-terpineol and methional (R^2 = 0.98) or linalool (R^2 = 0.96), (*E*)-2-heptenal and hexanal (R^2 = 0.97), as well as octenal and heptanal (R^2 = 0.96) were significantly correlated.

As a further step, the metabolomic data of the best LSL (TRTH1620) and the best SSL genotype (TRTH2510) were utilized to identify the differentially accumulated metabolites (DAMs), with p<0.05 (Figure 3; Supplementary Table 6). Among the 93 compounds, there were a total of 13 VOCs from different pathways, 16 flavonoids, nine amino acids, and 12 carotenoids, of which 66 were up-regulated in the LSL and only 27 in the SSL genotype. Overall, individual amino acids were more abundant in the LSL genotype. Similarly, the shikimate pathway proceeding towards flavonoids was enhanced in TRTH1620, whereas the pathway from glyceraldehyde 3-phosphate towards the production of fatty acids was increased in TRTH2510. Regarding isoprenoid biosynthetic pathways, carotenoids and quinones were more abundant in the LSL genotype, while tocopherols in the SSL genotype. Other metabolites that were over-accumulated in the LSL genotype included esculeoside A and hydroxytomatine I (approximately 4-fold higher). The greatest differences were observed for all-trans-lycopene (carotenoids), naringenin chalcone hexose II and eriodictyol hexose (flavonoids and glycosides), as well as esculeoside B. With regard to VOCs that were differentially accumulated in the two genotypes, it was evident that one apocarotenoid (β-damascenone), one terpenoid (2-caren-10-al), one branched amino acid related (2-methyl-2-butenal), and one benzenoid related (salicylaldehyde) were significantly higher in the SSL genotype (Figure 3). By contrast, a phenylalanine-derived, three benzenoid-related, and two branched amino acid related, were more abundant in the LSL genotype. Among the VOCs, salicylaldehyde was the top differentially accumulated VOC in TRTH2510 (2-fold), whereas 2-isobutylthiazole and 1-nitro-2-phenylethane were the top differentially accumulated metabolites in TRTH1620 (6- and 10-fold, respectively).

3.3 Transcriptome sequencing, clustering and enrichment

As a further step towards exploring pathways contributing to fruit quality and postharvest potential, transcriptome analysis was performed in fruits from the best SSL, TRTH2510 and the best LSL, TRTH1620) accessions, producing high and low ethylene levels, respectively. A total of 524.7 M with an average of 87.4 M clean

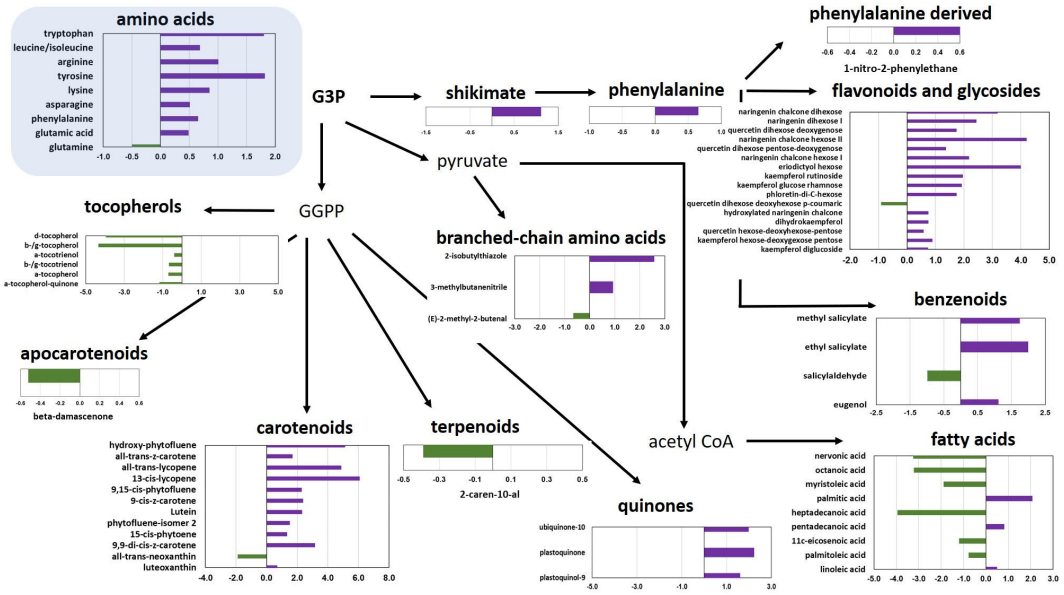

FIGURE 3
Significantly differentially accumulated metabolites over-accumulated in LSL (TRTH1620; purple) or in SSL (TRTH2510; green), with p< 0.05. Values represent log2 fold change in the LSL/SSL genotype.

reads were generated for the six cDNA libraries (Supplementary Table 7). The clean reads had an average total mapping ratio of 95.6%. Total transcripts with FPKM>1, averaged from the three biological replicates, varied from 14105 in TRTH1620 to 14588 in TRTH2510 fruits (Supplementary Table 8). The abscisic stress-ripening protein 1 (ID543574) had the highest FPKM values in both genotypes. However, in LSL, it was followed by dehydrin (ID101253585), whereas in the SSL, by the metallocarboxypeptidase inhibitor TCMP-2 (ID543980) and a polygalacturonase (*PG*) precursor (ID544051). Commonly expressed transcripts accounted for 91% of the total expressed genes with FPKM >1, whereas the uniquely expressed transcripts ranged from 437 in LSL (2.9%) to 920 in SSL (6.1%) (Figure 4A).

DEGs were defined using $|\log2(FC) > 2|$ and corrected (p values ≤ 0.01). In total, 379 and 315 DEGs were up- or down-regulated, respectively, in fruits obtained from TRTH1620 compared to TRTH2510 (Figure 4B; Supplementary Table 9), highlighting a series of changes in their gene expression profiles that could be associated with short- or long-shelf-life regulatory points. The list of DEGs is also depicted in a volcano plot based on log2 transformed FPKM values (Figure 4C), underlying the fact that the majority of DEGs were up-regulated in fruits of the LSL line. Among the top up-regulated transcripts in the LSL genotype, there were two homologs of glutathione-S-transferases (LOC101253021, LOC101257702, LOC101244300), whereas in the SSL genotype, there were a carbonyl reductase [NADPH] (LOC101244566), related to folate biosynthesis, and *PG* (LOC101246713) (Supplementary Table 9).

Enrichment analysis of GO annotations of DEGs between TRTH1620 and TRTH2510 returned 204 GO terms, classified into the three GO classes (BP: Biological Process; MF: Molecular Function; CC: Cellular Component). Among them, 99 and 105 GO annotations were enriched in the LSL and the SSL genotypes, respectively (Supplementary Figure 7). In the LSL genotype, the most significant enrichment terms in BP category were carbohydrate metabolic process (GO:0005975), cellular glucan metabolic process (GO:0006073), and cellular polysaccharide metabolic process (GO:0044264), whilst in the MF category, there were nucleic acid binding transcription factor activity (GO:0001071) and transcription factor activity, sequence-specific DNA binding (GO:0003700). Transcripts from the extracellular region (GO:0005576) and the apoplast (GO:0048046) were also enriched. Accordingly, in the SSL genotype, the most significant enrichment terms were transferase activity, transferring acyl groups other than amino-acyl groups (GO:0016747) and pyridoxal phosphate binding (GO:0030170), as well as small molecule metabolic process (GO:0044281), oxoacid metabolic process (GO:0043436) and organic acid metabolic process (GO:0006082). As a further step, the DEGs were also examined against the KEGG database to identify active biological pathways between the two contrasting genotypes. However, no KEGG pathways were found to be significantly enriched in the LSL genotype, whilst in the SSL genotype, the most significant enriched pathway was phenylalanine metabolism (sly00360) that is associated with phenylpropanoid pathway.

To validate these DEGs between TRTH1620 and TRTH2510, several key genes from metabolic pathways were selected, and their expression levels were analyzed using RT-qPCR. For all the transcripts, their expression levels were in agreement with those of the RNA-Seq (R^2 = 90.3) (Supplementary Figure 8), suggesting the reliability of the RNA-seq dataset for further exploitation. In particular, it was verified that the transcript levels of ethylene biosynthetic genes such as 1-aminocyclopropane-1-carboxylate synthases (*ACS2*, *ACS4*), and 1-aminocyclopropane-1-carboxylate oxidase (*ACO1*) were induced in SSL (4.1-, 66- and 3.4-fold higher than LSL) (Supplementary Figure 9). Similarly, genes related to AsA biosynthesis (GDP-$_L$-galactose phosphorylase, *GGP*), carotenoids biosynthesis (phytoene synthase, *PSY1*), cell wall synthesis (*PG2*), phenylpropanoid pathway (1-Deoxy-D-xylulose 5-phosphate synthase, *DXS*; chalcone synthase, *CHS1*; geranylgeranyl pyrophosphate synthase, *GGPS2*), and lipid-derived volatiles (lipoxygenase, *TomloxC*) were remarkably up-regulated in SSL. These genes represent the rate-liming steps in the related pathways.

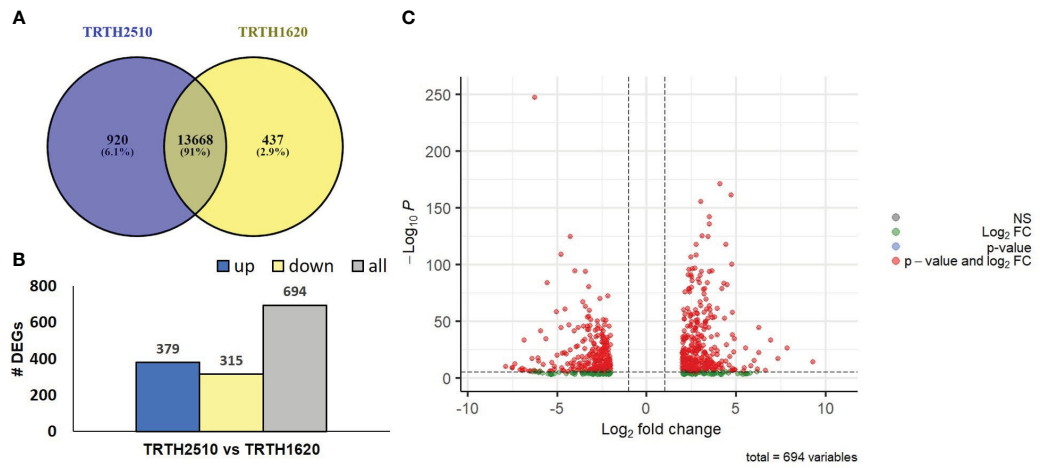

FIGURE 4
(A) Venn diagram of the expressed transcripts with FPKM>1 highlighting commonly and uniquely expressed genes in the fruits of TRTH2510 (SSL) and TRTH1620 (LSL); **(B)** The number of Differentially Expressed Genes (DEGs) representing up- and down-regulated transcripts of fruits in TRTH1620 (LSL) compared to TRTH2510 (SSL); **(C)** Volcano plot of DEGs in TRTH1620 (LSL) compared to TRTH2510 (SSL) based on p-values and log2 fold change (FC) of the transformed FPKM values. NS: non-significant.

3.4 Differentially expressed genes related to fruit quality, nutrient value and aroma

By considering DEGs as those with $p_{adj} \leq 0.01$, with no strict log2FC criterion, we ended up with a list of genes that may be able to explain the differences in the quality and metabolome reported herein between TRTH1620 (LSL) and TRTH2510 (SSL) (Supplementary Table 10). Several genes related to cell wall were differentially expressed between the two genotypes. In agreement with postharvest potential of the two contrasting genotypes, 21 cell-wall biosynthetic or expansion genes were up-regulated only in LSL, among them there were cellulose synthases (LOC101247596, LOC101249747, LOC101267858, LOC101260024), prolyl 4-hydroxylases (LOC101246711, LOC101262682), xyloglucan galactosyltransferases (LOC101245582, LOC101263331), a xyloglycan endo-transglycosylase (*tXET-B2*), xyloglucan endotransglucosylase/hydrolases (*XTH3*, LOC101255416, LOC101258345, LOC543511) and a xyloglucan 6-xylosyltransferase (LOC101263199). By contrast, 14 transcripts related to cell-wall degradation were up-regulated in SSL and suppressed in LSL, including *PG2* (LOC101246713), beta-galactosidases (*TBG1*, *TBG3*), and several pectinesterases (*PE1*, *PME2.1*, LOC101268487, LOC101254166, LOC101258356).

In addition, it was evident that the majority of key ethylene biosynthetic genes, namely *ACS2*, *ACS4*, *ACO1*, *ACO3*, *ACO4* were up-regulated in SSL, (Supplementary Table 10), a pattern reflecting the higher ethylene production in SSL (TRTH2510) (Figure 1C). It is noticeable that another *ACO* ortholog (*ACO5*) was induced in LSL. The expression of transcripts involved in S-adenosylmethionine (SAM) synthesis and degradation, such as SAM synthases (*SAMS1*, *SAMS3*, LOC101247506, LOC101245012), and one SAM decarboxylase (*SAMDC2*; LOC101260400), were remarkably higher in LSL genotype, suggesting fluxes from ethylene biosynthesis towards polyamine synthesis. The up-regulation of polyamine pathway in LSL was further supported by the higher transcript levels of two arginine decarboxylases in chromosome chr1 and chr10. Concerning the other plant hormones, two homologs of the negative regulator of fruit ripening, involved in the oxidative degradation of abscisic acid (ABA), ABA 8'-hydroxylase (*CYP707A*) were up-regulated in LSL (TRTH1620) (*CYP707A2*, *CYP707A4*), and one (*CYP707A3*) in SSL (TRTH2510). Furthermore, a type 2C protein phosphatase (*PP2C*; LOC101257069) was induced in LSL, whereas different members of ABA *Pyl* receptors were also in either SSL (*PYL3*, *PYL9*) or LSL (*PYL9*). Regarding the transcripts related to indole-3-acetic acid (IAA), gibberellins, and jasmonate were mostly up-regulated in LSL, probably directing the fluxes towards to non-ethylene dependent metabolic pathways.

Several transcripts catalyzing metabolic steps of glycolysis and TCA cycle were up-regulated in both genotypes, including isoforms of glyceraldehyde-3-phosphate dehydrogenase, pyrophosphate-fructose 6-phosphate 1-phosphotransferase, fructose-bisphosphate aldolase, malate dehydrogenase, and aconitate hydratase (Supplementary Table 10). This finding suggests that these key routes of the primary metabolism were active regardless the shelf-life potential. Nonetheless, pyruvate decarboxylases (*PCD*s, LOC101256911, LOC101247173, LOC101246495), catalyzing the conversion of pyruvate to acetaldehyde with release of carbon dioxide as part of the fermentation process that generates ethanol, were significantly up-regulated only in LSL. This is in line with the higher ethanol content found in TRTH1620 (Supplementary Table 3).

Fatty acid metabolism was mostly enhanced in SSL compared to LSL, with 15 and 8 DEGs being up-regulated, respectively (Supplementary Table 10). Among the key up-regulated transcripts in SSL, there were 3 ketoacyl-CoA synthases, 3 oxoacyl-synthases, an acetyl-CoA carboxylase, and 2 acyl-coenzyme A oxidases, whereas in LSL, there were long chain acyl-CoA synthetases, phospholipases and stearoyl-[acyl-carrier-protein] 9-desaturases (Supplementary Table 10).

Transcripts participating in isoprenoid pathway proceeding through mevalonate (MVA) or methylerythritol phosphate (MEP) pathway were also found among DEGs (Supplementary Table 10). In particular, the expression of 1-D-deoxyxylulose 5-phosphate synthase (*DXS*), *DXR*, 3-hydroxy-3-methylglutaryl-coenzyme A reductases (*HMGR3*), 4-hydroxy-3-methylbut-2-en-1-yl diphosphate synthase (*HDS*), and *GGPS2* was higher in SSL, whereas other two orthologs of *HMGR* (*HMGR1*, *HMGR2*) in LSL. This interesting finding points to the up-regulation of isoprenoid pathway through MEP in SSL.

The behavior of carotenoids and apocarotenoids pathway-related aroma genes was also differentially affected in the two contrasting genotypes, as revealed by the identification of several key transcripts among DEGs (Supplementary Table 10). However, it was clear that this pathway was transcriptionally enhanced in SSL, that exhibited higher expression of *PSYs* (*PSY1*, *PSY2*), zeta-carotene desaturase (*zds*), 15-cis-zeta-carotene isomerase (*Z-ISO*) and nine-cis-epoxycarotenoid dioxygenase (*NCED1*). Only one transcript, β-carotene hydroxylase (*CrtR-b2*), was up-regulated in LSL, that might be associated to the higher lutein level determined in TRTH1620 (Figure 3), as well could potentially contribute to the metabolic flux towards the synthesis of ABA. No carotenoid cleavage dioxygenases (*CCD*s), with the aforementioned change in *NCED1* involved in ABA production, were differentially expressed between the two genotypes that could have explained the higher accumulation of β-damascenone in SSL.

Phenylpropanoid pathway, proceeding through shikimate, as well as the following pathways generating flavonoids, anthocyanins, lignins, were exclusively up-regulated in SSL (Supplementary Table 10). In particular, phenylalanine ammonia-lyase (*PAL*; LOC101243656), trans-cinnamate 4-monooxygenases (LOC101244196, LOC101244496) from the main phenylpropanoid pathway, as well as two *CHS*s (*CHS1*, *CHS2*), isoflavone reductase (*IFR*, LOC101265488), flavonol synthase/flavanone 3-hydroxylase (LOC101249699) and flavanone 3-dioxygenase (*F3'H*) showed higher expression in SSL than in LSL. A similar pattern was also found for anthocyanins, with several anthocyanidin 3-O-glucosyltransferases being up-regulated, as well for lignins, with caffeoylshikimate esterase (*CSE*) and shikimate O-hydroxycinnamoyltransferase (*HCT*) having higher transcript levels. Therefore, the stimulation of the aforementioned secondary metabolic pathways towards flavonoid and lignin generation, is clear in the case of SSL, at least at the transcript level.

Among the structural genes of the AsA pathways, we identified one AsA biosynthetic gene and two AsA recycling genes up-regulated only in SSL (Supplementary Table 10), which also showed higher AsA content than LSL. These were *GGP* in chr6, the key rate limiting step in AsA biosynthesis (Bulley and Laing, 2016; Fenech et al., 2021; Koukounaras et al., 2022), as well as monodehydroascorbate reductase (*MDHAR*) in chr2 (LOC101253550) and glutathione reductase (*GR*) from the AsA recycling pathway. By contrast, two ascorbate oxidase (*AO*) orthologs (LOC101252344, LOC101263571) and a nucleobase-ascorbate transporter (*NAT*; LOC101264718) were induced in LSL. With regard to B6 vitamin, the key gene of its biosynthesis, pyridoxal 5'-phosphate synthase (*PDX1.2*) was also up-regulated in LSL, which also exhibited higher accumulation levels (Supplementary Table 6). On the other hand, the fact that genes strictly related to oxidative stimuli, such as peroxidases (four orthologs), were up-regulated in LSL, probably suggesting its different cellular redox state, whereas transcript levels of catalase (*cat1*) were elevated in SSL (Supplementary Table 10).

One of the most profound findings of metabolomics analysis between TRTH2510 and TRTH1620 was that the selected LSL accumulated significantly more steroidal alkaloids and glycoalkaloids than SSL (Supplementary Table 6), although these differences were not relevant for the other LSL and SSL genotypes (Table 1). Transcriptome analysis in fruits of the two cultivars revealed that these remarkable differences may be attributed to the up-regulation of four genes in LSL, including 11-β-hydroxysteroid dehydrogenase (LOC101264635), 3-β-hydroxysteroid-Delta(8), Delta(7)-isomerase (LOC101259646), squalene monooxygenase (LOC101250012), and a 2-oxoglutarate-dependent dioxygenase (LOC101246594) (Supplementary Table 10). The latter gene corresponds to *GAME31* (Solyc02g062460) that catalyzes the hydroxylation of the bitter flavor α-tomatine in tomato fruit, the first committed step toward esculeoside A (Cárdenas et al., 2016).

In line with fatty acid metabolism, that was more stimulated in SSL, genes related to lipid-derived VOCs produced through acetyl-CoA, were also up-regulated mostly in SSL. In particular, linoleate 9S-lipoxygenase (*TomloxB*) and *TomloxC* were more expressed in TRTH2510 (Supplementary Table 10), with the latter being crucial in C5 and C6 lipid-derived volatiles biosynthesis. Another lipoxygenase, linoleate 13S-lipoxygenase (*TomloxD*) was up-regulated in TRTH1620. Regarding benzenoids- and nitrogenous aroma-related VOCs, three genes were up-regulated in SSL and suppressed in LSL, including an UDP-glycosyltransferase 74F2 (LOC101247047) and two flavin-containing monooxygenases (*FMOs*; LOC101254042, LOC101254343).

Several transcription factors (TFs) were identified as DEGs between TRTH1620 and TRTH2510 (Figure 5; Supplementary Table 10). Among them, a broad number of genes related to fruit development and ripening were up-regulated in SSL and suppressed in LSL, including MADS-box TFs (*MADS-MC*) or *NAC-NOR* that regulates ethylene production, carotenoid accumulation and fruit firmness (Li et al., 2018b; Gao et al., 2020), or the floral homeotic *AGAMOUS* protein (*TAG1*), the agamous-like MADS-box protein *AGL66* and an *APETALA2*-like protein. Of particular interest is the fact that the *GRAS2* protein, a negative regulator of fruit ripening (Li et al., 2018a), was significantly induced in LSL and repressed in SSL. A broad number of ethylene-responsive TFs (*ERFs*) were also up-regulated in both genotypes, regardless of postharvest potential. In particular, *ERF1*, *ERF2*, *ERF3*, *ERF025*, *ERF027*, *ERF109* and *ERFD2* were up-regulated in LSL, whereas, *ERF5*, *ERF017*, *ERF114*, and *EIN3* were up-regulated in SSL. The same trend was evident for the

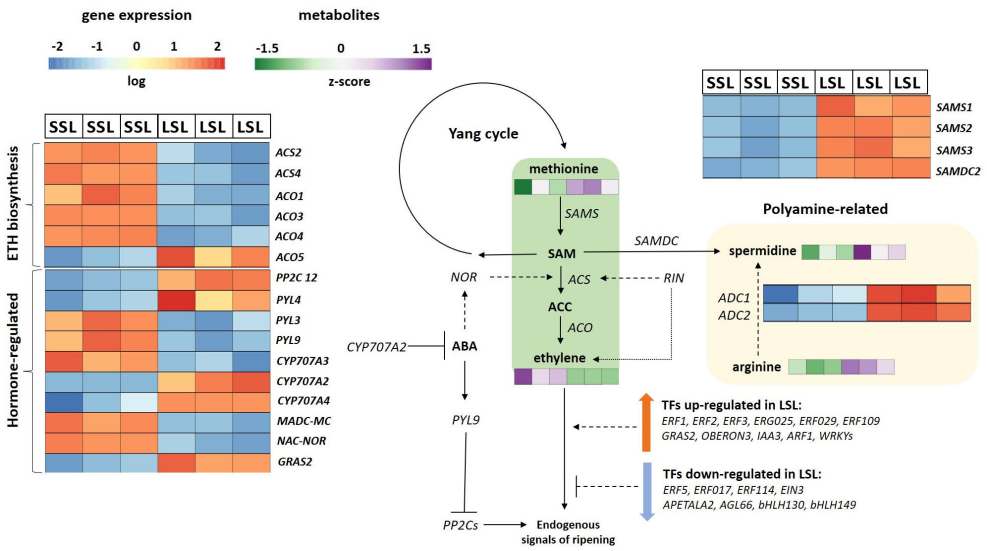

FIGURE 5
Ethylene related pathways in the SSL (TRTH2510) and LSL (TRTH1620) genotypes. The expression levels of DEGs are reported in boxes with a blue-to-red scale, while the accumulation of DAMs is in boxes green-to-purple scale. For each transcript/metabolite, the expression/abundance levels are represented by heatmaps. ABA, abscisic acid; ACC, 1-aminocyclopropane-1-carboxylate; *ACS*, ACC synthase; *ACO*, ACC oxidase; *ADC*, arginine decarboxylase; *ARF*, auxin response factor; *CYP707A*, ABA 8'-hydroxylase; *EIN3*, ethylene insensitive 3; *ERF*, ethylene-responsive transcription factor; *NOR*, non-ripening; *PP2C*, type 2C protein phosphatase; *PYL*, ABA PYL receptors; *RIN*, ripening-inhibitor; SAM, S-adenosylmethionine; *SAMS*, SAM synthase; *SAMDC*, SAM decarboxylase.

large TF families of *bZIP* and *MYBS*, with different gene orthologs being induced in either accession (Supplementary Table 10). By contrast, TFs of the wide WRKY family (*WRKY17*, *22*, *23*, *40*, *57*, *70*), as well as IAA-responsive factors (*OBERON3*, *IAA3*, *auxin response factor 1*), were exclusively induced in LSL, whereas *MYC* TFs (*MYC1*, *MYC2*) and *bHLH* TFs (*bHLH130*, *bHLH149*) were induced in SSL.

4 Discussion

4.1 Ethylene and ABA mediate transcriptome reprogramming related to improved shelf-life

Tomato ripening is a complex and dynamic process characterized by the coordinated transcriptional regulation leading to metabolic remodeling of key compounds related to fruit quality, nutritional value, taste and aroma. Over the last decades, RNA-seq approaches have been widely employed as an efficient tool to identify genes involved in metabolic pathways contributing to fruit quality (D'Esposito et al., 2017; Sacco et al., 2019) and aroma (Peng et al., 2022; Villano et al., 2023). The vast majority of the transcriptional responses during ripening are genotype-specific, highlighting the molecular events leading to metabolic clues that are biologically interesting and important from a horticultural perspective. However, modern cultivated tomatoes have narrow genetic diversity limiting their improvement potential. Due to the long-lasting emphasis of breeders on yield and postharvest potential, flavor-associated VOCs have been ignored to a great extent (Gao et al., 2019). Herein, we present a comprehensive survey of metabolome profile of a collection of tomato germplasm, consisting of underutilized traditional cultivars, differing in postharvest potential (short or long). In combination with the transcriptome profile of the best SSL *versus* the best LSL varieties, hub genes explaining the observed differences among them were also pinpointed, setting new breeding targets to develop more nutritious and flavorful tomato varieties, with enhanced shelf-life.

During tomato climacteric ripening, a burst in ethylene production occurs through the activation of an autocatalytic biosynthesis circuit, with both ethylene signaling and transcriptional regulation possessing pivotal roles in this process (Wang et al., 2020). Our 2-year experiments confirmed the classification of Greek landraces as SSL or LSL, suggesting that this trait is not under strong environmental control. Despite the fact that SSLs mostly exhibited higher ethylene production than LSLs, correlating with their poor shelf-life performance, there were some accessions like TRTH1460, TRTH0500, TRTH0550, characterized by high ethylene production rates. Although their transcriptome was not analyzed herein, this bizarre finding merits further attention to investigate what makes these accessions not overripe during postharvest, especially taking in consideration that ethylene is the end-product of the pathway.

A proposed model for the ethylene-dependent pathways differentially regulated between the two genotypes is presented in Figure 5. The increased ethylene production in SSL seems to be orchestrated by the transcription of the key ethylene biosynthetic genes (*ACS2*, *ACS4*, *ACO1*) responsible for pre- and post-climacteric ethylene biosynthesis (Van de Poel et al., 2012). *MADS-RIN*, is a crucial early regulator of fruit ripening (Vrebalov et al., 2002) binding to the promoters of *ACS2* and *ACS4*, with hundreds of gene targets controlling changes in color, flavor, texture, and taste during tomato fruit ripening. Its expression was nearly 2-fold lower in LSL compared to SSL (Supplementary Table 8), correlating with the lower ethylene production of this genotype, and probably with other important ripening-induced processes. Additionally, the *MADS-MACROCALYX* (*MADS-MC*) belonging to the *APETALA1/FRUITFULL* (*AP1/FUL*) subfamily and being part of the RIN-MC fusion protein, was also down-regulated in LSL. Down-regulation of the *RIN-MC* fusion gene has been found to accelerate the yellow ripening in *rin* mutants (Li et al., 2018b). Furthermore, it has been previously reported that the RIN-MC fusion protein is an active TF with a repressor function controlling fruit softening and color, through *PG*s, *PME*s, *PSY*s and *GGPPS2* (Li et al., 2018b; Li et al., 2020). Our findings confirmed the earlier reports, except for *PSY*s, which were down-regulated in SSL, suggesting that the exact function of this TF remains to be fully elucidated. Although *MADS-MC* alone is not considered as a master regulator of ripening (Wang et al., 2020), its down-regulation in LSL, along with the lower transcript levels of *RIN*, reveal interesting aspects of interaction with the other TFs contributing to the improved postharvest potential of TRTH1620, that merits further exploitation. Consistently, the expression of *NAC-NOR* that also plays a significant role in fruit ripening, was also up-regulated in SSL. The NAC-NOR truncated protein binds to the promoters of *ACS2*, *GGPPS2* and *PL*, stimulating ethylene biosynthesis, carotenoid accumulation and fruit softening, respectively (Gao et al., 2020). An induction of the transcript levels of these genes was also evident in this study. Several studies have shown that members of the *GRAS* TFs are widely considered as negative regulators of ripening through controlling different metabolic processes i.e. *GRAS38* (lycopene content and ethylene production) or *GRAS4* (ethylene production through binding to the promoters of *ACO*) (Liu et al., 2021). In our study, we identified another member of this family, *GRAS2*, which was significantly down-regulated in SSL. Previously, down-regulation of this TF was found to suppress the expression of down-stream genes related to fruit development, such as gibberellin (GA) biosynthesis and signal transduction pathways (Li et al., 2018a). Indeed, members of both pathways (*GA2ox2* from GA biosynthesis, and *20ox-3* from GA inactivation) were repressed in SSL, which showed significantly lower *GRAS2* transcript levels. In the same study, silencing *GRAS2* has also caused a decrease in cell size and cell expansion through regulating XTHs. However, this observation does not hold true in this study, as the up-regulation of *GRAS2* in LSL was accompanied by higher transcript levels of *XTH*s and xyloglucan galactosyltransferases (*XLT*s). This finding suggests that *GRAS2* regulation mode is more complicated and probably involves other TFs.

Apart from ethylene, ABA also functions as a significant hormone in the control of climacteric fruit ripening by triggering the expression of many ethylene-independent genes (Mou et al.,

2015). The core ABA signaling components consist of *Pyl* receptors, *PP2C*s, and sucrose nonfermenting-related protein kinases. In total, 15 members of *PYL*s have been characterized in tomato, having distinct properties (González-Guzmán et al., 2014). Herein, *PYL3* and *PYL9* were induced in SSL, whereas *PYL4* in LSL. Among them, *PYL4* has been linked to drought tolerance (Li et al., 2022b), while *PYL3* has not been characterized yet. Interestingly, silencing of *PYL9* was found to retard ripening, increase mesocarp thickness, resulting to conical/oblong and gourd-shaped fruits (Kai et al., 2019). This is presumably related to the longer shelf-life of TRTH1620, which showed lower *PYL9* transcript levels than TRTH2510, and oblong fruit shape. On the other hand, *PP2C*s are generally known to act negatively in ABA signaling regulation with additive functions. For instance, *PP2C1* retards fruit ripening, through blocking ABA and ethylene accumulation (Zhang et al., 2018), whereas *PP2C3* plays an important role in the regulation of fruit ripening and fruit glossiness in tomato (Liang et al., 2021). On the basis of these considerations, another member of this family, *PP2C12*, was induced in LSL, probably correlating with the longer storability of this genotype, although its functional role has not been determined yet. Another group of ABA regulators are the *CYP707A* genes encoding ABA 8′-hydroxylases, which catalyze the oxidative catabolism of ABA. Although different isoforms seem to have distinguished roles, it was of particular interest that the expression of *CYP707A2* was dramatically up-regulated in LSL (log2FC > 4) (Figure 5; Supplementary Table 10), suggesting that it contributes to the catabolism of ABA in fruit. Previously, silencing of *CYP707A2* significantly changed the transcripts of a broad number of ABA-responsive and ripening-related genes, including those related to lycopene-synthesis or cell wall-degrading genes (Ji et al., 2014). The key gene in ABA biosynthesis, *NCED*, was also decreased in LSL, but its role will be discussed below.

Polyamines are aliphatic amines present in all living organisms with intriguing functions in fruit development and ripening (Gao et al., 2021). In plants, polyamines and ethylene act competitively as double-edged swords in ripening and senescence processes (Mehta et al., 2002). At the same time, exogenous application of polyamines can enhance postharvest life and quality of fruits (Zahedi et al., 2019). On the basis of these considerations, LSL, the genotype producing low ethylene levels, accumulated more methionine, and had higher transcript levels of *SAMS* and *SAMDC* (Figure 5). It was therefore demonstrated that, in genotypes with long postharvest potential, the flux from Yang cycle is preferably directed towards polyamine synthesis, fueling spermidine accumulation, and not towards the ethylene synthesis. The up-regulation of polyamine pathway in LSL was further supported by the higher arginine levels, accompanied by higher transcript levels of two arginine decarboxylases genes (*ADC*s), but not of the other key genes of the pathway, i.e. ornithine decarboxylase, spermidine synthase, spermine synthases, suggesting that polyamine biosynthesis is regulated at both transcriptional and translational level during ripening. In line with our findings, overexpression of *ADC* in tomato resulted to elevated levels of polyamines accompanied by enhanced shelf-life due to the decrease in ethylene levels (Gupta et al., 2019), confirming the link between high ADC transcript levels, low ethylene accumulation and improved postharvest potential.

4.2 Isoprenoid-related genes are valuable candidates to unravel distinctive quality and postharvest properties

Through the isoprenoid-related pathways, various volatile compounds, such as monoterpenoids (C10) and sesquiterpenoids (C15) found mostly in unripe fruits, as well as carotenoids, whose synthesis, increased in ripe fruits, can be produced (Rambla et al., 2014). These compounds are synthesized from isopentenyl diphosphate (IPP) and its isomer dimethylallyl diphosphate (DMAPP), either through the cytosolic MVA or the plastid MEP pathway. Herein, the terpenoid accumulation and the transcript levels of the underlying pathway genes revealed differences between LSL and SSL, with MEP pathway being clearly stimulated in SSL, and MVA pathway more activated in LSL (Figure 6). Previously, the early transcriptional stimulation of MVA pathway that produces the building blocks for terpenoids, was correlated with reduced susceptibility of apples during postharvest storage (Roberto et al., 2022). Key up-regulated genes in the case of SSL included *DXS*, *DXR*, and *HDS* of MEP pathway, whereas in the case of LSL, two out of the three *HMGR* transcripts (MVA pathway). The accumulation of the monoterpene, 2-caren-10-al, was also enhanced in SSL, but this compound does not seem to contribute to tomato aroma. Within tomato pangenome that explored wild promoter regions, *DXR* is the only candidate gene showing a wild allele for its promoter region, whereas the cultivars possessing this wild allele have higher *DXR* expression compared to those carrying the common allele (Gao et al., 2019). This observation reinforces the hypothesis that modern breeding targets should be further explored by utilizing underutilized tomato germplasm to develop new lines with superior attributes.

Carotenoid biosynthesis takes place in plastids, starting with *PSY*, the rate-limiting enzyme, catalyzing the first committed step of the pathway by condensation of two molecules of GGPP to produce the C40 hydrocarbon 15-cis-phytoene (Zhou et al., 2022). Two are the main *PSY* genes found within tomato genomes, being expressed during fruit ripening. Although both of them were up-regulated in SSL, this increase in expression levels did not lead to high accumulation levels of 15-cis-phytoene or ζ-carotene (Figure 6). Silencing *PSY1* has been previously related to the yellow-flesh tomato phenotype (Kang et al., 2014). Up-next, *Z-ISO* and *ZDS* are responsible for the conversion of phytoene to lycopene (Ampomah-Dwamena et al., 2019). Again, although transcript levels of both genes were remarkably stimulated in SSL, the accumulation of ζ-carotene and lycopene was higher in LSL, suggesting either a feedback regulation, or a post-transcriptional regulation of the pathway. As carotenoid accumulation is tightly linked to other ripening-related signals such as ethylene biosynthesis and perception, there may be other regulators far upstream this pathway. Previously, the re-direction of fluxes from the ethylene biosynthesis towards polyamine synthesis via

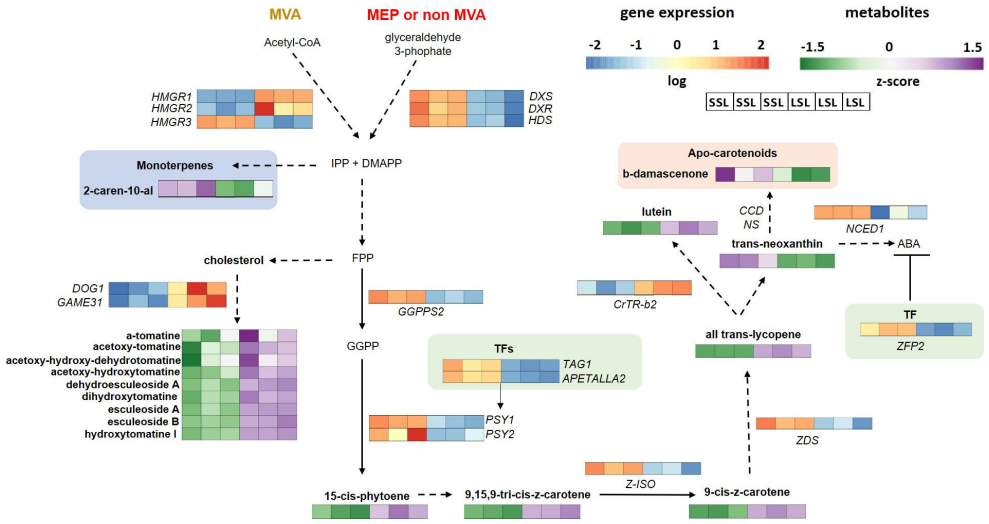

FIGURE 6
Isoprenoid, carotenoid and related biosynthetic pathways, in the cytosol (mevalonate, MVA) and in plastids (methyl-D-erythritol phosphate, MEP), of SSL (TRTH2510) and LSL (TRTH1620) genotypes, producing monoterprene-related VOCs, apocarotenoids, and steroidal alkaloids and glycoalkaloids. Only significant DEGs and DAMs are presented in the pathways. *CrtR-b2*, beta-carotene hydroxylase; CCDs, Carotenoid cleavage dioxygenase; DMAPP, dimethylallyl diphosphate; *DOG1*, DELAY OF GERMINATION 1; *DXR*, -deoxy-D-xylulose-5-phosphate reductoisomerase; *DXS*, 1-Deoxy-D-xylulose 5-phosphate synthase; FPP, farnesyl diphosphate; GGPP, geranylgeranyl pyrophosphate; *GGPPS*, geranylgeranyl pyrophosphate synthase; *HDS*, 4-hydroxy-3-methylbut-2-en-1-yl diphosphate synthase; *HMGR*, 3-hydroxy-3-methylglutaryl-coenzyme A reductase; IPP, isopentenyl diphosphate; *NCED*, nine-cis-epoxycarotenoid dioxygenase; *PSY*, phytoene synthase; *TAG1*, floral homeotic protein AGAMOUS; *ZDS*, zeta-carotene desaturase; *ZFP2*, zinc finger transcription factor; *Z-ISO*, 15-cis-zeta-carotene isomerase; NS, non-significantly different.

overexpression of a yeast *SAMDC* in tomato has led to enhanced accumulation of lycopene, accompanied by improved vine-life (Mehta et al., 2002). This regulatory mechanism through polyamines may be relevant in the case of LSL. Additionally, the MADS-box ripening regulators including Tomato *AGAMOUS-LIKE1* (*TAGL1*), *FRUITFULL1* (*FUL1*), and *FUL2*, can positively control the expression of carotenoid biosynthetic genes, and negatively the expression of genes of the downstream reactions, through binding to their promoters (Stanley and Yuan, 2019). Indeed, *TAGL1* was induced in SSL, probably leading to the induction of *PSY*s, *Z-ISO* and *ZDS*, but *FUL*s were not differentially expressed between genotypes. This is in line with another study, indicating that silencing of these genes did not alter the expression of *PSY1* in tomato (Bemer et al., 2012), questioning its role in regulating carotenoid biosynthesis. Similarly, TFs involved in hormone synthesis and signaling, such as an *APETALA2/ERF* protein, can also promote the expression of carotenoid biosynthetic genes (Karlova et al., 2011), as reported herein too.

As carotenoids are precursors of ABA, which also serves as an important trigger of fruit ripening along with ethylene, complex interactions between upstream and downstream reactions in the carotenoid pathway are rational (Mou et al., 2015). Therefore, a positive correlation between ABA and carotenoids have been widely reported (Tung et al., 2008; Mou et al., 2015). Different members of *NCED* family are up-regulated during tomato ripening (Ilahy et al., 2019), participating in the catabolism of carotenoids towards ABA generation (Sun et al., 2012), thus being important determinants of fruit coloration. Although ABA was not measured in this study, the up-regulation of *NCED1* in SSL (Figure 6) probably indicated its higher accumulation compared to LSL. However, previous reports (Diretto et al., 2020) have also shown an increased shelf-life in tomato fruits following over-expression of genes involved in carotenoid late pathway (e.g. *lycopene β-cyclase*, *LCYb*), with a simultaneous increase in total carotenoids and ABA, thus proving the existence of a complex and still not fully elucidated network of interactions within the aforementioned components and ethylene. Among the four *NCED* and the four *CYP707A* genes in the ABA metabolism pathway, *NCED1* and *CYP707A2*, respectively, are the most important in orchestrating ABA levels within fruit (Kai et al., 2019). Interestingly, *NCED1* (ABA biosynthesis) was up in SSL, while *CYP707A2* (ABA catabolism) (Figure 5) was down in SSL, further pointing to the over-accumulation of ABA in TRTH2510 (SSL). On the other hand, the zinc finger transcription factor *ZFP2* has been reported to block fruit ripening by negatively regulating ABA biosynthesis, with *ZFP2*-overexpressing containing more lycopene compared to WT (Weng et al., 2015). Its expression was stimulated in SSL, but once again, it did not correlate with carotenoid content, suggesting a different target than the carotenoid biosynthetic path.

A key group of tomato VOCs derived from the degradation of carotenoids, thus directly linked to their accumulation, is referred as apocarotenoids, that are important contributors of tomato ripe fruit aroma conferring a typical floral/fruity odor (Klee and Tieman, 2018). Most of them are directly produced by the oxidative cleavage catalyzed by carotenoid cleavage dioxygenases (CCDs), except for β-damascenone, which is highly abundant in ripe fruits (Wang et al., 2016). Previously, apocarotenoid-deficient fruits are also significantly less preferred by consumers, probably due to their correlation with sweetness as in the case of geranial (Tieman et al.,

2012). Another important apocarotenoid, the fruity-flavor β-ionone, is produced via the oxidative breakdown of β-carotene, which predominates orange-fruited genotypes, whilst geranial, neral, and citral, providing the lemon-note, mostly contributes as a background aroma odor (Distefano et al., 2022). Herein however, the only apocarotenoid compound which was found among DAMs over-accumulated in SSL was β-damascenone (Figure 6), which provides an odor of apple, rose, and honey to tomato fruit (Martina et al., 2021). Although this compound was long regarded as important for tomato aroma, mostly because of its extremely low reported odor threshold (Vogel et al., 2010), latter studies suggest that it can no longer be considered as a high-priority target for flavor enhancement as it is not associated with the intensity of tomato flavor (Tieman et al., 2012; Gao et al., 2019). Interestingly, *TomLoxC*, which is deemed to be crucial in C5 and C6 lipid-derived volatiles biosynthesis and apocarotenoid production (Chen et al., 2004), was also up-regulated in SSL. Its rare allele has been generally recovered in modern elite breeding lines, as *TomLoxC* is regarded as the key gene in flavor-associated lipid- and carotenoid-derived VOCs (Gao et al., 2019).

4.3 *GAME31* and *DOG1* are key regulators of alkaloid accumulation in ripe tomatoes

Steroidal alkaloids and steroidal glycoalkaloids are N-containing antinutritional compounds, predominantly found during the early stages of tomato fruit ripening, with α-tomatine and dehydrotomatine being mainly accumulated in green fruits (Itkin et al., 2011). Galactosyltransferase (*GAME*) genes including *GAME1*, *GAME5*, *GAME9*, *GAME17*, *GAME18*, *GAME31* have been previously reported to participate in alkaloid formation in tomato fruit, responsible for the conversion of cholesterol and tomatidine to non-bitter molecules, such as esculeoside A (Itkin et al., 2013; Cárdenas et al., 2016; Szymański et al., 2020). Among these *GAME*s, we identified a dioxygenase dependent on 2-oxoglutarate *GAME31*, which was remarkably up-regulated in LSL, and associated with enhanced levels of these alkaloid compounds (Figure 6). According to previous studies, the gene performs the conversion of α-tomatine to hydroxytomatine and has been highly conserved through domestication to ensure a less bitter and harmless tomato fruit (Cárdenas et al., 2016). Interestingly, another TF of the *bZIP* family, the *DELAY OF GERMINATION 1* (*DOG1*) that has been recently identified as a principal regulator of the pathway targeting *GAME*s transcription (Zhao et al., 2023), was also enhanced in LSL, suggesting that the pathway is activated.

4.4 *GGP*, *MDHAR* and *GR* are key determinants of AsA levels

Ascorbate (AsA) is one of the most abundant and powerful antioxidants present in plant tissues and in particular in tomato fruit (Mellidou and Kanellis, 2017). It has been well established that AsA is predominantly accumulated through the so-called $_L$-galactose pathway, with GDP-$_L$-galactose phosphorylase (GGP) that catalyzes the first committed step of the pathway, serving as the rate limiting step (Bulley et al., 2012; Mellidou et al., 2012; Koukounaras et al., 2022). Indeed, in our study, AsA levels correlated with *GGP* transcript levels, with SSL being also richer in this nutritious molecule than LSL (Figure 7). The accumulation of AsA within tomato fruit is also dependent on AsA recycling, with

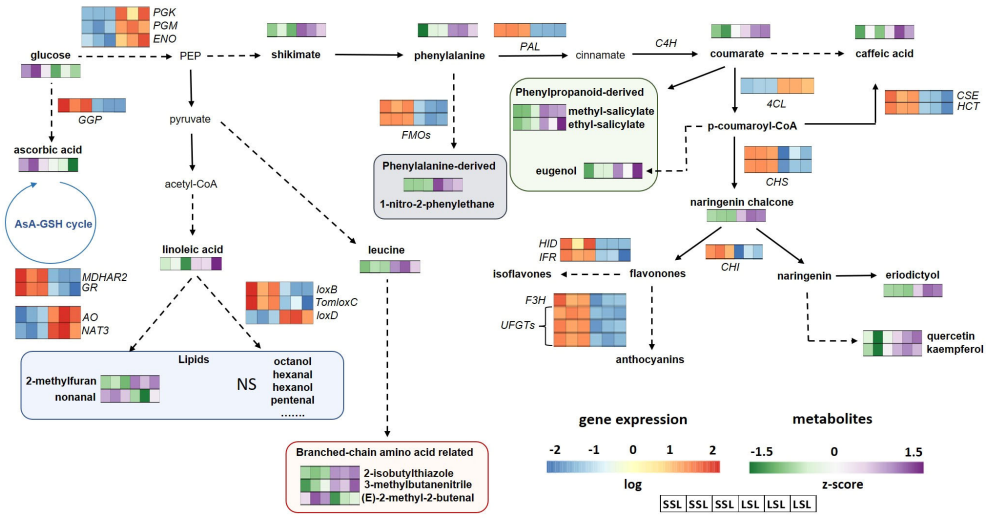

FIGURE 7
Metabolic pathways related to flavonoids, VOCs and AsA in the SSL (TRTH2510) and LSL (TRTH1620) genotypes. Only significant DEGs and DAMs are presented in the pathways. *AO*, ascorbate oxidase; AsA, ascorbic acid; *C4H*, cinnamate-4-hydroxylase; *4CL*, 4-coumarate-CoA ligase; *CHI*, chalcone-flavonone isomerase; *CHS*, chalcone synthase; *CSE*, caffeoylshikimate esterase; *ENO*, enolase; *F3H*, flavanone 3-dioxygenase; *FMO*, flavin-containing monooxygenase; *GGP*, GDP-L-galactose phosphorylase; GSH, glutathione; *GR*, glutathione reductase; *HCT*, shikimate O-hydroxycinnamoyltransferase; *HID*, hydroxyisoflavanone dehydratase; *IFR*, isoflavone reductase; *lox*, lipoxygenase; *MDHAR*, monodehydroascorbate reductase; *NAT*, nucleobase-ascorbate transporter; *PAL*, phenylalanine ammonia-lyase; *PGK*, phosphoglycerate kinase; *PGM*, phosphoglycerate mutase; *UFGT*, flavonoid 3-O-glycosyltransferase; NS, non-significantly different.

MDHAR, *DHAR* and *GR* serving as key genes in regenerating its reduced form (Noctor et al., 2016). In line with the current consensus on AsA recycling pathway, the high AsA levels determined in SSL can be attributed to the enhanced transcript levels of *MDHAR2* and *GR*. The expression of *MDHAR* has been previously related to total AsA content during tomato ripening (Mellidou et al., 2012). Additionally, AsA oxidation through an ortholog of ascorbate oxidase (*AO*) was stimulated in LSL, suggesting its involvement in cell growth and expansion to support fruit growth, as previously reported in melon (Chatzopoulou et al., 2020). Therefore, the AsA enrichment of SSL can be attributed to the enhanced expression of key AsA biosynthesis, recycling and oxidation determinants. Furthermore, in tomato, there are at least 12 nucleobase–ascorbate transporters (*NAT*s) that participate in the long-distance phloem-mediated transport of AsA. In ripe fruits of LSL, *NAT3* was significantly induced. This specific gene ortholog has been found to be widely distributed and expressed in all tomato organs, with its expression values being higher at 10 and 20 days after pollination (Cai et al., 2014), suggesting its putative role earlier in fruit development, that cannot efficiently explain AsA-related differences between LSL and SSL. None of the regulatory TFs able to "unlock" the AsA synthesis either at the transcriptional or the post-translational level (Mellidou and Kanellis, 2023) were differentially expressed between the two genotypes, suggesting that the observed differences were mostly due to the transcription of structural pathway genes.

4.5 Discrepancies in the phenylpropanoid pathway between transcript and metabolite level

Tomato fruit is a good source of polyphenolic compounds such as naringenin chalcone, rutin, quercetin, hydroxybenzoic acid, caffeic acid, naringenin and flavonones (Lu and Zhu, 2022) that contribute to tomato fruit color and volatile production during ripening (Tieman et al., 2006). As shown in Figure 7, the phenylpropanoid pathway proceeding through phenylalanine provides the precursors for the production of flavonoids and lignin, with *PAL* being the first rate-limiting step of the pathway, redirecting the flux from the primary metabolism to the synthesis of polyphenolic compounds. In the following steps, cinnamate is converted to coumarate and coumarate-CoA in reactions catalyzed by *C4H* and *4CL*, respectively. Surprisingly, KEGG enrichment analysis revealed an up-regulation of *PAL* and *4CH* transcripts in SSL, while both phenylalanine, and coumarate were most accumulated in LSL, an observation suggesting a feedback regulation of the pathway. In fact, the breakdown of glucose to PEP, shikimate and phenylalanine was also stimulated in LSL at both metabolite and transcript level (induction of *PGK*, *PGM*, *ENO*). The only gene that was positively correlated with the high phenylpropanoid levels recorded in LSL was 4-coumarate-CoA ligase (*4CL*). This gene is responsible for the esterification of coumarate to coumaroyl-CoA, that undergoes a large number of downstream reactions to generate the majority of phenylpropanoid compounds (Alberstein et al., 2012). The expression of this gene was also positively correlated with the accumulation of caffeic acid and coumarate, as well as with enhanced skin resistance and hardness in the fruits of LSL. This is in disagreement with previous studies in tomato concerning another *4CL* gene copy in chr6 (Solyc06g035960), suggesting a complex network of the different gene orthologs. Two other genes related to lignin biosynthesis caffeoylshikimate esterase (*CSE*) and shikimate O-hydroxycinnamoyltransferase (*HCT*) were also up-regulated in SSL, suggesting an up-regulation of the pathway, although no lignin was quantified in this study. High levels of lignins adversely influence consumer preferences for tomato, thereby it is an undesirable trait for the fresh market (Lu and Zhu, 2022).

The specific flavonoid pathway starts with chalcone synthase (*CHS*), which converts coumaroyl-CoA to naringenin chalcone. This reaction is further prone to isomerization, hydroxylation and oxidation to generate the primary flavonoids (Ilahy et al., 2019). Overall, mature fruits contain low level of flavonoids and even lower or zero levels of anthocyanins. Again, the two CHSs orthologs were induced in SSL, but naringenin chalcone was low in this genotype compared to LSL. Chalcone isomerase is the next limiting step in flavonoid biosynthesis that isomerize naringenin chalcone to naringenin. Similar to previous reports, *CHI* was negatively correlated with naringenin chalcone (Yang et al., 2022). The following steps proceeding towards flavonones and anthocyanins were up-regulated in SSL (at the transcript level), whereas the steps towards quercetin, kaempferol, and eriodictyol were induced in LSL (at the metabolite level), respectively, suggesting the different pathway reprogramming in the two genotypes. Rutin is considered as the major glycosylated flavonoid in ripe fruits, followed by phloretin (Ilahy et al., 2019). This observation is also confirmed herein, although no remarkable differences were identified between SSL and LSL genotypes (Supplementary Table 6).

Overall, these discrepancies between transcripts and metabolites could be due to the feedback inhibition of the flavonoid pathway, upstream the chalcone synthase and isomerase steps, as previously reported in tomato (Verhoeyen et al., 2002; Alberstein et al., 2012). Therefore, it can be hypothesized that the enhanced transcription of both *CHS* and *CHI* in SSL utilizes coumaroyl-CoA and naringenin chalcone, and that the depletion of this pool in SSL removes a point of negative feedback in flavonoid synthesis, leading to the induction of regulatory genes of the pathway. Another possible explanation is that since the entire fruit was used for both metabolomics and transcriptomics, local tissue-specific different (pericarp, septa, columella, placenta, locular gel) were not taken into consideration. This tissue-oriented differentiation holds true in the case of ethylene biosynthetic pathway during tomato fruit ripening (Van de Poel et al., 2014) that could have also affected the regulation of phenylpropanoids herein in a tissue-specific manner. In this case, the observed inconsistencies could be recovered using single-cell transcriptomics, as the bulk RNA-sequencing of a given tissue may camouflage small changes at the cell level, especially in pathways such as phenylpropanoids that produce diverse compounds with dissimilar functions. Through single-cell technologies, it will be possible to build a high-resolution expression atlas of cells that could be a key resource (Jovic et al.,

2022), especially in fruit tissues that undergo complex and uneven metabolic processes in a tissue-specific way.

4.6 Volatiles accumulation is dependent on genotype and relates to ethylene production

Fatty acids such as the polyunsaturated linoleic (c18:2) are the main precursors of fruit aroma volatiles, also known as green leaf volatiles, being synthesized either via β-oxidation or by means of lipoxygenases (LOX). Linoleic acid was remarkably higher in LSL, suggesting a stimulated flux towards the synthesis of C18 fatty acids. Among the five *LOX* genes expressed in tomato during ripening, using linoleic and linolenic acids as substrates, *TomloxC* was significantly down-regulated in LSL. This gene is widely deemed to be essential not only for the generation of fruit C6 volatiles (Chen et al., 2004), but also for synthesis of C5 volatiles, including 1-penten-3-one, (*E*)-2-pentenal, 3-pentanone, 1-pentanol, and 1-penten-3-ol (Zhu et al., 2019). Indeed, silencing *TomloxC* in tomato resulted to a 75% reduction in the levels of several C5 flavor volatiles, including pentanal (Shen et al., 2014). However, in melon, pentanal biosynthesis has been clearly related to *PCD* transcript levels, suggesting a link between fermentation and aroma production (Wang et al., 2019). Several *PCD*s were up-regulated in LSL, in line with ethanol and pentanal production (although no statistical differences in the second case), suggesting some interesting links between fermentation and volatile production. Another *LOX* gene, *TomloxD* also generating 13-hydroperoxides was up-regulated in LSL, whereas *TomloxB*, which was up-regulated in SSL, but this gene is not involved in the synthesis of C6 volatile compounds in the fruit. With regard to metabolites, the only statistically significant induced in LSL was 2-methylfuran, providing a chocolate odor (Li et al., 2019). Furthermore, (*E*)-2-heptenal, 1-hexanol, and hexanal, which are major contributors to the green/grassy aroma (Villano et al., 2023), were mostly accumulated in LSL, although the differences between genotypes were not statistically significant due to the great variability among replicates (Supplementary Table 3). On the other hand, nonanal levels, contributing to the pleasant aroma notes of ripe fruits, were higher in SSL (Ilahy et al., 2019). Additionally, (*E*)-2-hexenal (green, leafy), (*Z*)-3-hexenal (green, leafy), and 2-ethylfuran (coffee and chocolate) were also up-regulated in SSL, yet not statistically different. These results reveal interesting aspects of lipid-derived VOCs that were differentially accumulated in contrasting genotypes.

Branched-chain amino acid (BCAA) derived compounds are also major contributors to tomato aroma, including 3-methylbutanal (musty, peach), 2-methylbutanal (musty, coffee), 3-methylbutanol (musty, earthy), and 2-isobuthylthiazole (green, earthy) (Bizzio et al., 2022; Distefano et al., 2022). The majority of these compounds are derived through the reversible conversion of leucine/isoleucine into α-ketoacids, catalyzed by BCAA transferases (*BCAT*s). A chloroplastic *BCAT2* gene copy mapped in *chr12* (LOC101253875) was induced in SSL (Supplementary Table 10), whereas leucine accumulation was repressed (Figure 7). This finding implies this gene ortholog probably participates in BCAA synthesis rather than BCAA catabolism, as it is located in the chloroplast and not in mitochondria (Maloney et al., 2010). However, as there are different *BCAT*s members within the tomato genome that can mediate both synthetic and catabolic reactions of BCAA-derived VOCs, more functional characterization is required to explore the combined action of various classes of these enzymes. On the other hand, in LSL, the accumulation of both leucine as well as the nitrogen- and sulfur-containing compounds 2-isobuthylthiazole (wasabi, leafy odor) and 3-methylbutanenitrile (pungent) were induced, suggesting that the pathway is stimulated towards the production of these compounds. These leucine-derived compounds are very abundant in tomato fruit, being synthesized by the conjugation of 3-methylbutanal with cysteine (Liscombe et al., 2022; Kaur et al., 2023). However, the underlying key gene, tetrahydrothiazolidine N-hydroxylase (Wang et al., 2023), was not differentially expressed between genotypes, suggesting that other factors may also be important. All the above-mentioned BCAA-derived compounds, found in either of the two genotypes, have been associated with liking by consumers (Kaur et al., 2023).

Phenylalanine-derived VOCs originate from the catabolism of phenylalanine and include various compounds, such as phenylacetaldehyde, 2-phenylethanol, 1-nitro-2-phenylethane and 2-phenylacetonitrile, significantly contributing to consumer's liking or disliking, depending on their concentration (Martina et al., 2021). In this pathway, phenylalanine is decarboxylated by aromatic acid decarboxylases (*AADC*s) to convert it to phenethylamine, thus substrate availability is re-directed from the phenylpropanoid pathway (Tieman et al., 2006). Although phenylalanine was over-accumulated in LSL (Figure 7), no *AADC* ortholog was differentially expressed between LSL and SSL. This step has been previously demonstrated to be regulated at the transcriptional level (Li et al., 2019). In turn, phenethylamine can generate 1-nitro-2-phenylethane or benzylnitrile by the action of *FMO* using cysteine and the volatile aldehyde phenylacetaldehyde as substrates (Liscombe et al., 2022). In this study, LSL was richer in 1-nitro-2-phenylethane, presumably due to the enhanced accumulation of phenylalanine, offering a musty-earthy odor that has been associated with consumer-liking (Kaur et al., 2023) and regarded as strong umami influencer (Colantonio et al., 2022). At the same time, two *FMO*s were down-regulated in LSL, but these gene copies do not seem to have a key role in phenylalanine-derived VOCs, as previously recorded (Klee and Tieman, 2018). As ethylene can stimulate the catabolism of phenylalanine through the induction of *PAL*s (Klee and Giovannoni, 2011), it is evident that the observed low levels of these metabolites in SSL are strongly under ethylene regulation that leads to the depletion of substrate availability. Over-accumulation of phenylalanine and phenylpropanoid-derived VOCs have been previously correlated with biotic stress responses, due to the up-regulation of the antioxidant defense machinery (Distefano et al., 2022), as well as wild species such as *S. pennellii* (Zhu et al., 2019). Furthermore, phenylalanine-derived VOCs can explain a large fraction of flavor variability within tomato germplasm, largely contributing to sweetness perception (34%) and overall liking score (16%) (Colantonio et al., 2022).

Phenylpropanoid-related (or benzenoids) VOCs consist of a separate group of phenylalanine-derived VOCs, including guaiacol,

methyl salicylate, and eugenol, mostly associated from intermediates in the lignin pathway (Zhu et al., 2019). In this pathway, p-coumarate is converted to its CoA ester by *4CL*, in a key branching point of phenylpropanoid metabolism (Cheynier et al., 2013). In LSL, both coumarate content and *4CL* expression were stimulated, probably contributing to the synthesis of methyl salicylate, ethyl salicylate and eugenol (Figure 7), which are all considered as major influencers of tomato aroma, and are generally described as medicinal, green, smoky, or pungent odors (Kaur et al., 2023). Among them, eugenol is regarded as unpleasant flavor by consumers due to its pharmaceutical odor and bitter flavor, whereas the concentration of methyl salicylate may determine consumer liking or not (Tieman et al., 2012; Wang et al., 2023). Among the key genes catalyzing the methylation of salicylate, neither salicylic acid methyltransferases nor methyl esterases (Kaur et al., 2023) were differentially expressed between LSL and SSL. By contrast, some transcription factors such as *ETHYLENE INSENSITIVE3* (*EIN3*) that are negative regulators of salicylate (Li et al., 2019) were remarkably induced in SSL (Supplementary Table 10), probably accounting for the low levels of both ethyl- and methyl salicylate determined in this study. Usually, these lignin-related compounds are more abundant in unripe fruits, in heterografted plants, in off-season fruits, in biotic stresses, being unwelcomed by consumers (Distefano et al., 2022). This is probably related to their function as endogenous signal molecules to external stimuli.

5 Conclusion

This work provides for the first time a complete study of the existing diversity regarding the post-harvest potential of the Greek tomato Gene Bank collection, highlighting the dynamic interactions between ethylene and metabolic pathways that are important in determining tomato fruit quality, nutritional value and aroma. Low ethylene levels in the LSL accession (TRTH1620) were correlated with higher levels of amino acids, carotenoids and phenylpropanoids, as well as with key VOCs of tomato flavor and aroma derived from benzenoid, BCAA and phenylalanine pathways. By contrast, high ethylene levels in the SSL accession (TRTH2510) were associated with high accumulation of tocopherols, and fatty acids. Of outmost importance is the fact that in LSL, a clear shift of the ethylene biosynthetic pathway from methionine towards polyamines is evident, providing interesting clues on the mechanism that regulates fruit ripening and quality attributes in tomato. This mechanism includes the down-regulation of the key ethylene biosynthetic genes (*ACS2*, *ACS4*, *ACO1*) responsible for pre- and post-climacteric ethylene biosynthesis, accompanied by the up-regulation of various *SAMS*s and *SAMDC2*, that re-direct methionine from ethylene biosynthesis towards polyamine metabolism (spermidine). As for ABA-associated pathways, the ABA receptor, *PYL9*, was remarkably repressed in LSL, correlating with the longer shelf-life of TRTH1620. By contrast, *PP2C12*, which acts negatively in ABA signaling regulation, and *CYP707A2* related to ABA catabolism, were both induced in LSL. Although a lot of effort is still required to uncover in detail the exact role of these genes in regulating tomato shelf-life, our findings reinforce the notion that ABA has a central role in fruit postharvest dynamics that needs further exploitation. Among other interesting correlations, ethylene was positively related to cell-wall degrading genes, and AsA accumulation, but it negatively regulated steroidal alkaloids. The observed discrepancies in carotenoid and phenylpropanoid pathways between accumulated metabolites and expressed transcripts clearly points to either a feedback regulation or a post-transcriptional regulation of these routes that merits further attention. Notwithstanding these vibrant differences between genotypes, important VOCs contributing to consumer liking can be found in either of the two genotypes, indicating the complexity of the pathways related to major enhancers of tomato flavor and aroma. Lipid-derived VOCs and the apocarotenoid β-damascenone are mostly accumulated in SSL, whereas LSL was richer in phenylalanine-derived and phenylpropanoid-derived VOCs. Overall, the knowledge generated herein provides a valuable genetic tool for future functional studies that can direct breeding strategies towards the utilization of underutilized germplasm to develop the "perfect" tomato, that can appeal consumer interest on traditional varieties.

Data availability statement

The datasets presented in this study can be found in online repositories. The names of the repository/repositories and accession number(s) can be found at: https://www.ncbi.nlm.nih.gov/bioproject/PRJNA991925.

Author contributions

IM: Data curation, Investigation, Methodology, Software, Supervision, Writing – original draft, Writing – review & editing. AK: Data curation, Investigation, Methodology, Writing – original draft, Writing – review & editing. SF: Methodology, Writing – review & editing. JR: Methodology, Writing – review & editing. EP: Data curation, Methodology, Writing – review & editing. SN: Data curation, Methodology, Writing – review & editing. CP: Data curation, Methodology, Writing – review & editing. SK: Methodology, Writing – review & editing. KN: Methodology, Writing – review & editing. AG: Methodology, Writing – review & editing. GD: Methodology, Writing – review & editing. AKK: Conceptualization, Funding acquisition, Investigation, Project administration, Resources, Supervision, Writing – original draft, Writing – review & editing.

Funding

The authors declare financial support was received for the research, authorship, and/or publication of this article. AKK acknowledges the support by European Commission H2020 research and innovation program through TRADITOM project agreement No. 634561 and the co-financed by the European Union and Greek national funds through the Operational Program Competitiveness, Entrepreneurship, and Innovation, under the call RESEARCH – CREATE – INNOVATE (project code: T2EDK-01332-n-Tomatomics). For networking activities, support is acknowledged by COST Action CA18210-RoxyCost, supported

by COST (European Cooperation in Science and Technology). GD acknowledges support by the PRIMA program through PROMEDLIFE project agreement No. 2132. JR acknowledges funding by the Spanish Ministry of Science and Innovation grant (IJC2020-045612-I). AG acknowledges the support of Horizon EU program through contract 101000716.

Acknowledgments

We would like to thank Dr. F. Mylona (Hellenic Agricultural Organization – DEMETER for providing the seeds of the tomato accessions that are kept in the Greek Gene Bank.

Conflict of interest

The authors declare that the research was conducted in the absence of any commercial or financial relationships that could be construed as a potential conflict of interest.

The authors declared that they were an editorial board member of Frontiers, at the time of submission. This had no impact on the peer review process and the final decision.

Publisher's note

Supplementary material

The Supplementary Material for this article can be found online at: https://www.frontiersin.org/articles/10.3389/fpls.2023.1267340/full#supplementary-material

References

Alberstein, M., Eisenstein, M., and Abeliovich, H. (2012). Removing allosteric feedback inhibition of tomato 4-coumarate:CoA ligase by directed evolution. *Plant J.* 69, 57–69. doi: 10.1111/j.1365-313X.2011.04770.x

Alseekh, S., Aharoni, A., Brotman, Y., Contrepois, K., D'Auria, J., Ewald, J., et al. (2021). Mass spectrometry-based metabolomics: a guide for annotation, quantification and best reporting practices. *Nat. Methods* 18, 747–756. doi: 10.1038/s41592-021-01197-1

Ampomah-Dwamena, C., Thrimawithana, A. H., Dejnoprat, S., Lewis, D., Espley, R. V., and Allan, A. C. (2019). A kiwifruit (Actinidia deliciosa) R2R3-MYB transcription factor modulates chlorophyll and carotenoid accumulation. *New Phytol.* 221, 309–325. doi: 10.1111/nph.15362

Bemer, M., Karlova, R., Ballester, A. R., Tikunov, Y. M., Bovy, A. G., Wolters-Arts, M., et al. (2012). The tomato FRUITFULL homologs TDR4/FUL1 and MBP7/FUL2 regulate ethylene-independent aspects of fruit ripening. *Plant Cell* 24, 4437–4451. doi: 10.1105/tpc.112.103283

Bineau, E., Rambla, J. L., Duboscq, R., Corre, M.-N., Bitton, F., Lugan, R., et al. (2022). Inheritance of secondary metabolites and gene expression related to tomato fruit quality. *Int. J. Mol. Sci.* 23, 6163. doi: 10.3390/ijms23116163

Bizzio, L. N., Tieman, D., and Munoz, P. R. (2022). Branched-chain volatiles in fruit: A molecular perspective. *Front. Plant Sci.* 12. doi: 10.3389/fpls.2021.814138

Blanca, J., Pons, C., Montero-Pau, J., Sanchez-Matarredona, D., Ziarsolo, P., Fontanet, L., et al. (2022). European traditional tomatoes galore: a result of farmers' selection of a few diversity-rich loci. *J. Exp. Bot.* 73, 3431–3445. doi: 10.1093/jxb/erac072

Bulley, S., and Laing, W. (2016). The regulation of ascorbate biosynthesis. *Curr. Opin. Plant Biol.* 33, 15–22. doi: 10.1016/j.pbi.2016.04.010

Bulley, S., Wright, M., Rommens, C., Yan, H., Rassam, M., Lin-Wang, K., et al. (2012). Enhancing ascorbate in fruits and tubers through over-expression of the l-galactose pathway gene GDP-l-galactose phosphorylase. *Plant Biotechnol. J.* 10, 390–397. doi: 10.1111/j.1467-7652.2011.00668.x

Cai, X., Ye, J., Hu, T., Zhang, Y., Ye, Z., and Li, H. (2014). Genome-wide classification and expression analysis of nucleobase–ascorbate transporter (NAT) gene family in tomato. *Plant Growth Regul.* 73, 19–30. doi: 10.1007/s10725-013-9864-x

Cárdenas, P. D., Sonawane, P. D., Pollier, J., Vanden Bossche, R., Dewangan, V., Weithorn, E., et al. (2016). GAME9 regulates the biosynthesis of steroidal alkaloids and upstream isoprenoids in the plant mevalonate pathway. *Nat. Commun.* 7, 10654. doi: 10.1038/ncomms10654

Chatzopoulou, F., Sanmartin, M., Mellidou, I., Pateraki, I., Koukounaras, A., Tanou, G., et al. (2020). Silencing of ascorbate oxidase results in reduced growth, altered ascorbic acid levels and ripening pattern in melon fruit. *Plant Physiol. Biochem.* 156, 291–303. doi: 10.1016/j.plaphy.2020.08.040

Chen, G., Hackett, R., Walker, D., Taylor, A., Lin, Z., and Grierson, D. (2004). Identification of a specific isoform of tomato lipoxygenase (TomloxC) involved in the generation of fatty acid-derived flavor compounds. *Plant Physiol.* 136, 2641–2651. doi: 10.1104/pp.104.041608

Cheynier, V., Comte, G., Davies, K. M., Lattanzio, V., and Martens, S. (2013). Plant phenolics: Recent advances on their biosynthesis, genetics, and ecophysiology. *Plant Physiol. Biochem.* 72, 1–20. doi: 10.1016/j.plaphy.2013.05.009

Colantonio, V., Ferrão, L. F. V., Tieman, D. M., Bliznyuk, N., Sims, C., Klee, H. J., et al. (2022). Metabolomic selection for enhanced fruit flavor. *Proc. Natl. Acad. Sci. U. S. A.* 9, 119. doi: 10.1073/pnas.2115865119

Conesa, M. À., Galmés, J., Ochogavía, J. M., March, J., Jaume, J., Martorell, A., et al. (2014). The postharvest tomato fruit quality of long shelf-life Mediterranean landraces is substantially influenced by irrigation regimes. *Postharvest Biol. Technol.* 93, 114–121. doi: 10.1016/j.postharvbio.2014.02.014

Cortés-Olmos, C., Valcárcel, J. V., Roselló, J., Díez, M. J., Cebolla-Cornejo, J., Cortés-Olmos, C., et al. (2015). Traditional Eastern Spanish varieties of tomato. *Sci. Agric.* 72, 420–431. doi: 10.1590/0103-9016-2014-0322

D'Esposito, D. D., Ferriello, F., Molin, A. D., Diretto, G., Sacco, A., Minio, A., et al. (2017). Unraveling the complexity of transcriptomic, metabolomic and quality environmental response of tomato fruit. *BMC Plant Biol.* 17, 1–18. doi: 10.1186/s12870-017-1008-4

Diretto, G., Frusciante, S., Fabbri, C., Schauer, N., Busta, L., Wang, Z., et al. (2020). Manipulation of β-carotene levels in tomato fruits results in increased ABA content and extended shelf life. *Plant Biotechnol. J.* 18, 1185–1199. doi: 10.1111/pbi.13283

Distefano, M., Mauro, R. P., Page, D., Giuffrida, F., Bertin, N., and Leonardi, C. (2022). Aroma volatiles in tomato fruits: the role of genetic, preharvest and postharvest factors. *Agronomy* 12, 1–27. doi: 10.3390/agronomy12020376

Dono, G., Rambla, J. L., Frusciante, S., Fabene, E., Gómez-Cadenas, A., Granell, A., et al. (2022). Pigment-related mutations greatly affect berry metabolome in san marzano tomatoes. *Horticulturae* 8, 120. doi: 10.3390/horticulturae8020120

Fenech, M., Amorim-Silva, V., Esteban Del Valle, A., Arnaud, D., Ruiz-Lopez, N., Castillo, A. G., et al. (2021). The role of GDP-l-galactose phosphorylase in the control of ascorbate biosynthesis. *Plant Physiol.* 185, 1574–1594. doi: 10.1093/plphys/kiab010

Gao, L., Gonda, I., Sun, H., Ma, Q., Bao, K., Tieman, D. M., et al. (2019). The tomato pan-genome uncovers new genes and a rare allele regulating fruit flavor. *Nat. Genet.* 51, 1044–1051. doi: 10.1038/s41588-019-0410-2

Gao, F., Mei, X., Li, Y., Guo, J., and Shen, Y. (2021). Update on the roles of polyamines in fleshy fruit ripening, senescence, and quality. *Front. Plant Sci.* 12, 610313. doi: 10.3389/fpls.2021.610313

Gao, Y., Wei, W., Fan, Z., Zhao, X., Zhang, Y., Jing, Y., et al. (2020). Re-evaluation of the nor mutation and the role of the NAC-NOR transcription factor in tomato fruit ripening. *J. Exp. Bot.* 71, 3560–3574. doi: 10.1093/jxb/eraa131

Gonias, E. D., Ganopoulos, I., Mellidou, I., Bibi, A. C., Kalivas, A., Mylona, P. V., et al. (2019). Exploring genetic diversity of tomato (Solanum lycopersicum L.) germplasm of

genebank collection employing SSR and SCAR markers. *Genet. Resour. Crop Evol.* 66, 1295–1309. doi: 10.1007/s10722-019-00786-6

González-Guzmán, M., Rodríguez, L., Lorenzo-Orts, L., Pons, C., Sarrión-Perdigones, A., Fernández, M. A., et al. (2014). Tomato PYR/PYL/RCAR abscisic acid receptors show high expression in root, differential sensitivity to the abscisic acid agonist quinabactin, and the capability to enhance plant drought resistance. *J. Exp. Bot.* 65, 4451–4464. doi: 10.1093/jxb/eru219

Gupta, A., Pandey, R., Sinha, R., Chowdhary, A., Pal, R. K., and Rajam, M. V. (2019). Improvement of post-harvest fruit characteristics in tomato by fruit-specific over-expression of oat arginine decarboxylase gene. *Plant Growth Regul.* 88, 61–71. doi: 10.1007/s10725-019-00488-0

Hosmani, P. S., Flores-Gonzalez, M., van de Geest, H., Maumus, F., Bakker, L. V., Schijlen, E., et al. (2019). An improved *de novo* assembly and annotation of the tomato reference genome using single-molecule sequencing, Hi-C proximity ligation and optical maps. *bioRxiv*, 767764. doi: 10.1101/767764

Huang, Y., Li, G., Hong, C., Zheng, X., Yu, H., and Zhang, Y. (2021). Potential of steroidal alkaloids in cancer: perspective insight into structure–activity relationships. *Front. Oncol.* 11. doi: 10.3389/fonc.2021.733369

Ilahy, R., Tlili, I., Siddiqui, M. W., Hdider, C., and Lenucci, M. S. (2019). Inside and beyond color: Comparative overview of functional quality of tomato and watermelon fruits. Front. *Plant Sci.* 10. doi: 10.3389/fpls.2019.00769

Itkin, M., Heinig, U., Tzfadia, O., Bhide, A. J., Shinde, B., Cardenas, P. D., et al. (2013). Biosynthesis of antinutritional alkaloids in solanaceous crops is mediated by clustered genes. *Science* 341, 175–179. doi: 10.1126/science.1240230

Itkin, M., Rogachev, I., Alkan, N., Rosenberg, T., Malitsky, S., Masini, L., et al. (2011). GLYCOALKALOID METABOLISM1 is required for steroidal alkaloid glycosylation and prevention of phytotoxicity in tomato. *Plant Cell* 23, 4507–4525. doi: 10.1105/tpc.111.088732

Ji, K., Kai, W., Zhao, B., Sun, Y., Yuan, B., Dai, S., et al. (2014). SlNCED1 and SlCYP707A2: key genes involved in ABA metabolism during tomato fruit ripening. *J. Exp. Bot.* 65, 5243–5255. doi: 10.1093/jxb/eru288

Jovic, D., Liang, X., Zeng, H., Lin, L., Xu, F., and Luo, Y. (2022). Single-cell RNA sequencing technologies and applications: A brief overview. *Clin. Transl. Med.* 12, e694. doi: 10.1002/ctm2.694

Kai, W., Wang, J., Liang, B., Fu, Y., Zheng, Y., Zhang, W., et al. (2019). PYL9 is involved in the regulation of ABA signaling during tomato fruit ripening. *J Exp Bot.* 21 (70), 6305–6319. doi: 10.1093/jxb/erz396

Kang, B., Gu, Q., Tian, P., Xiao, L., Cao, H., and Yang, W. (2014). A chimeric transcript containing Psy1 and a potential mRNA is associated with yellow flesh color in tomato accession PI 114490. *Planta* 240, 1011–1021. doi: 10.1007/s00425-014-2052-z

Karlova, R., Rosin, F. M., Busscher-Lange, J., Parapunova, V., Do, P. T., Fernie, A. R., et al. (2011). Transcriptome and metabolite profiling show that APETALA2a is a major regulator of tomato fruit ripening. *Plant Cell* 23, 923–941. doi: 10.1105/tpc.110.081273

Kaur, G., Abugu, M., and Tieman, D. (2023). The dissection of tomato flavor: biochemistry, genetics, and omics. *Front. Plant Sci.* 14, 1144113. doi: 10.3389/fpls.2023.1144113

Klee, H. J. (2010). Improving the flavor of fresh fruits: genomics, biochemistry, and biotechnology. *New Phytol.* 187, 44–56. doi: 10.1111/j.1469-8137.2010.03281.x

Klee, H. J., and Giovannoni, J. J. (2011). Genetics and control of tomato fruit ripening and quality attributes. *Annu. Rev. Genet.* 45, 41–59. doi: 10.1146/annurev-genet-110410-132507

Klee, H. J., and Tieman, D. M. (2018). The genetics of fruit flavour preferences. *Nat. Rev. Genet.* 19, 347–356. doi: 10.1038/s41576-018-0002-5

Koukounaras, A., Mellidou, I., Patelou, E., and Kostas, S. (2022). Plant Physiology and Biochemistry Over-expression of GGP1 and GPP genes enhances ascorbate content and nutritional quality of tomato. *Plant Physiol. Biochem.* 193, 124–138. doi: 10.1016/j.plaphy.2022.10.023

Koutsika-Sotiriou, M., Mylonas, I., Tsivelikas, A., and Traka-Mavrona, E. (2016). Compensation studies on the tomato landrace "Tomataki Santorinis". *Sci. Hortic. (Amsterdam).* 198, 78–85. doi: 10.1016/j.scienta.2015.11.006

Li, J., Chitwood-Brown, J., Kaur, G., Labate, J. A., Vallad, G. E., Lee, T. G., et al. (2022a). Novel Sources of Resistance to Fusarium oxysporum f. sp. lycopersici Race 3 Among Solanum pennellii Accessions. *J. Am. Soc Hortic. Sci.* 147, 35–44. doi: 10.21273/JASHS05080-21

Li, J., Di, T., and Bai, J. (2019). Distribution of volatile compounds in different fruit structures in four tomato cultivars. *Molecules* 24, 2594. doi: 10.3390/molecules24142594

Li, M., Wang, X., Li, C., Li, H., Zhang, J., and Ye, Z. (2018a). Silencing GRAS2 reduces fruit weight in tomato. *J. Integr. Plant Biol.* 60, 498–513. doi: 10.1111/jipb.12636

Li, S., Xu, H., Ju, Z., Cao, D., Zhu, H., Fu, D., et al. (2018b). The RIN-MC fusion of MADS-box transcription factors has transcriptional activity and modulates expression of many ripening genes. *Plant Physiol.* 176, 891–909. doi: 10.1104/pp.17.01449

Li, Y., Zhang, X., Jiang, J., Zhao, T., Xu, X., Yang, H., et al. (2022b). Virus-induced gene silencing of SlPYL4 decreases the drought tolerance of tomato. *Hortic. Plant J.* 8, 361–368. doi: 10.1016/j.hpj.2021.06.005

Li, S., Zhu, B., Pirrello, J., Xu, C., Zhang, B., Bouzayen, M., et al. (2020). Roles of RIN and ethylene in tomato fruit ripening and ripening-associated traits. *New Phytol.* 226, 460–475. doi: 10.1111/nph.16362

Liang, B., Sun, Y., Wang, J., Zheng, Y., Zhang, W., Xu, Y., et al. (2021). Tomato protein phosphatase 2C influences the onset of fruit ripening and fruit glossiness. *J. Exp. Bot.* 72, 2403–2418. doi: 10.1093/jxb/eraa593

Liscombe, D. K., Kamiyoshihara, Y., Ghironzi, J., Kempthorne, C. J., Hooton, K., Bulot, B., et al. (2022). A flavin-dependent monooxygenase produces nitrogenous tomato aroma volatiles using cysteine as a nitrogen source. *Proc. Natl. Acad. Sci. U. S. A.* 7, 119. doi: 10.1073/pnas.2118676119

Liu, Y., Shi, Y., Su, D., Lu, W., and Li, Z. (2021). SlGRAS4 accelerates fruit ripening by regulating ethylene biosynthesis genes and SlMADS1 in tomato. *Hortic. Res.* 8, 3. doi: 10.1038/s41438-020-00431-9

Love, M. I., Huber, W., and Anders, S. (2014). Moderated estimation of fold change and dispersion for RNA-seq data with DESeq2. *Genome Biol.* 15, 550. doi: 10.1186/s13059-014-0550-8

Lu, Y., and Zhu, H. (2022). The regulation of nutrient and flavor metabolism in tomato fruit. *Veg. Res.* 2, 1–14. doi: 10.48130/vr-2022-0005

Maloney, G. S., Kochevenko, A., Tieman, D. M., Tohge, T., Krieger, U., Zamir, D., et al. (2010). Characterization of the branched-chain amino acid aminotransferase enzyme family in tomato. *Plant Physiol.* 153, 925–936. doi: 10.1104/pp.110.154922

Martina, M., Tikunov, Y., and Portis, E. (2021). The genetic basis of tomato aroma. *Genes* 12, 226. doi: 10.3390/genes12020226

Mazzucato, A., Papa, R., Bitocchi, E., Mosconi, P., Nanni, L., Negri, V., et al. (2008). Genetic diversity, structure and marker-trait associations in a collection of Italian tomato (Solanum lycopersicum L.) landraces. *Theor. Appl. Genet.* 116, 657–669. doi: 10.1007/s00122-007-0699-6

Mehta, R. A., Cassol, T., Li, N., Ali, N., Handa, A. K., and Mattoo, A. K. (2002). Engineered polyamine accumulation in tomato enhances phytonutrient content, juice quality, and vine life. *Nat. Biotechnol.* 20, 613–618. doi: 10.1038/nbt0602-613

Mellidou, I., and Kanellis, A. K. (2017). Genetic control of ascorbic acid biosynthesis and recycling in horticultural crops. *Front. Chem.* 5. doi: 10.3389/fchem.2017.00050

Mellidou, I., and Kanellis, A. K. (2023). Deep inside the genetic regulation of ascorbic acid during fruit ripening and postharvest storage. *Postharvest Biol. Technol.* 204, 112436. doi: 10.1016/j.postharvbio.2023.112436

Mellidou, I., Keulemans, J., Kanellis, A. K., and Davey, M. W. (2012). Regulation of fruit ascorbic acid concentrations during ripening in high and low vitamin C tomato cultivars. *BMC Plant Biol.* 12, 239. doi: 10.1186/1471-2229-12-239

Mellidou, I., Krommydas, K., Nianiou-Obeidat, I., Ouzounidou, G., Kalivas, A., and Ganopoulos, I. (2020). Exploring morpho-physiological profiles of a collection of tomato (*Solanum lycopersicum*) germplasm using multivariate statistics. *Plant Genet. Resour. Characterisation Util.* 18 (2), 88–97. doi: 10.1017/S1479262120000088

Metsalu, T., and Vilo, J. (2015). ClustVis: A web tool for visualizing clustering of multivariate data using Principal Component Analysis and heatmap. *Nucleic Acids Res.* 43, W566–W570. doi: 10.1093/nar/gkv468

Mou, W., Li, D., Luo, Z., Mao, L., and Ying, T. (2015). Transcriptomic analysis reveals possible influences of ABA on secondary metabolism of pigments, flavonoids and antioxidants in tomato fruit during ripening. *PLoS ONE* 10 (6), e0129598. doi: 10.1371/journal.pone.0129598

Noctor, G., Mhamdi, A., and Foyer, C. H. (2016). Oxidative stress and antioxidative systems: recipes for successful data collection and interpretation. *Plant Cell Environ.* 39, 1140–1160. doi: 10.1111/pce.12726

Nohara, T., Ono, M., Ikeda, T., Fujiwara, Y., and El-Aasr, M. (2010). The tomato saponin, esculeoside a. *J. Nat. Prod.* 73, 1734–1741. doi: 10.1021/np100311t

Parisi, M., Aversano, R., Graziani, G., Ruggieri, V., Senape, V., Sigillo, L., et al. (2016). Phenotypic and molecular diversity in a collection of 'Pomodoro di Sorrento' Italian tomato landrace. *Sci. Hortic. (Amsterdam).* 203, 143–151. doi: 10.1016/J.SCIENTA.2016.02.038

Peng, L., Gao, W., Song, M., Li, M., He, D., and Wang, Z. (2022). Integrated metabolome and transcriptome analysis of fruit flavor and carotenoids biosynthesis differences between mature-green and tree-ripe of cv. "Golden phoenix" mangoes (*Mangifera indica* L.). *Front. Plant Sci.* 13. doi: 10.3389/fpls.2022.816492

Pons, C., Casals, J., Palombieri, S., Fontanet, L., Riccini, A., Rambla, J. L., et al. (2022). Atlas of phenotypic, genotypic and geographical. *Hortic. Res.* 9. doi: 10.1093/hr/uhac112

Rambla, J. L., Medina, A., Fernández-del-Carmen, A., Barrantes, W., Grandillo, S., Cammareri, M., et al. (2017). Identification, introgression, and validation of fruit volatile QTLs from a red-fruited wild tomato species. *J. Exp. Bot.* 68, 429–442. doi: 10.1093/jxb/erw455

Rambla, J. L., Tikunov, Y. M., Monforte, A. J., Bovy, A. G., and Granell, A. (2014). The expanded tomato fruit volatile landscape. *J. Exp. Bot.* 65, 4613–4623. doi: 10.1093/jxb/eru128

Roberto, S. R., Sanzani, S. M., Naets, M., Hemelrijck, W., Gruyters, W., and Verboven, P. (2022). Time is of the essence — Early activation of the mevalonate pathway in apple challenged with gray mold correlates with reduced susceptibility during postharvest storage. *Front. Microbiol.* 13. doi: 10.3389/fmicb.2022.797234

Sacco, A., Raiola, A., Calafiore, R., Barone, A., and Rigano, M. M. (2019). New insights in the control of antioxidants accumulation in tomato by transcriptomic

analyses of genotypes exhibiting contrasting levels of fruit metabolites. *BMC Genomics* 20, 1–19. doi: 10.1186/s12864-019-5428-4

Sacco, A., Ruggieri, V., Parisi, M., Festa, G., Rigano, M. M., Picarella, M. E., et al. (2015). Exploring a tomato landraces collection for fruit-related traits by the aid of a high-throughput genomic platform. *PloS One* 10, 1–20. doi: 10.1371/journal.pone.0137139

Schmittgen, T. D., and Livak, K. J. (2008). Analyzing real-time PCR data by the comparative CT method. *Nat. Protoc.* 3, 1101–1108. doi: 10.1038/nprot.2008.73

Shen, J., Tieman, D., Jones, J. B., Taylor, M. G., Schmelz, E., Huffaker, A., et al. (2014). A 13-lipoxygenase, TomloxC, is essential for synthesis of C5 flavour volatiles in tomato. *J. Exp. Bot.* 65, 419–428. doi: 10.1093/jxb/ert382

Stanley, L., and Yuan, Y.-W. (2019). Transcriptional regulation of carotenoid biosynthesis in plants: so many regulators, so little consensus. *Front. Plant Sci.* 10. doi: 10.3389/fpls.2019.01017

Sun, L., Yuan, B., Zhang, M., Wang, L., Cui, M., Wang, Q., et al. (2012). Fruit-specific RNAi-mediated suppression of SlNCED1 increases both lycopene and β-carotene contents in tomato fruit. *J. Exp. Bot.* 63, 3097–3108. doi: 10.1093/jxb/ers026

Szymański, J., Bocobza, S., Panda, S., Sonawane, P., Cárdenas, P. D., Lashbrooke, J., et al. (2020). Analysis of wild tomato introgression lines elucidates the genetic basis of transcriptome and metabolome variation underlying fruit traits and pathogen response. *Nat. Genet.* 52, 1111–1121. doi: 10.1038/s41588-020-0690-6

Teixeira, A., Noronha, H., Frusciante, S., Diretto, G., and Gerós, H. (2023). Biosynthesis of chlorophyll and other isoprenoids in the plastid of red grape berry skins. *J. Agric. Food Chem.* 71, 1873–1885. doi: 10.1021/acs.jafc.2c07207

Tieman, D. M., Zeigler, M., Schmelz, E. A., Taylor, M. G., Bliss, P., Kirst, M., et al. (2006). Identification of loci affecting flavour volatile emissions in tomato fruits. *J. Exp. Bot.* 57, 887–896. doi: 10.1093/jxb/erj074

Tieman, D., Zhu, G., Resende, M. F. R., Lin, T., Nguyen, C., Bies, D., et al. (2017). A chemical genetic roadmap to improved tomato flavor. *Science* 80) 355, 391–394. doi: 10.1126/science.aal1556

Tieman, D., Bliss, P., Mcintyre, L. M., Blandon-ubeda, A., Bies, D., Odabasi, A. Z., et al. (2012). Report the chemical interactions underlying tomato flavor preferences 1035–1039. doi: 10.1016/j.cub.2012.04.016

Tung, S. A., Smeeton, R., White, C. A., Black, C. R., Taylor, I. B., Hilton, H. W., et al. (2008). Over-expression of LeNCED1 in tomato (Solanum lycopersicum L.) with the rbcS3C promoter allows recovery of lines that accumulate very high levels of abscisic acid and exhibit severe phenotypes. *Plant Cell Environ.* 31, 968–981. doi: 10.1111/j.1365-3040.2008.01812.x

Van de Poel, B., Bulens, I., Markoula, A., Hertog, M. L. A. T. M., Dreesen, R., Wirtz, M., et al. (2012). Targeted systems biology profiling of tomato fruit reveals coordination of the Yang cycle and a distinct regulation of ethylene biosynthesis during postclimacteric ripening. *Plant Physiol.* 160, 1498–1514. doi: 10.1104/pp.112.206086

Van de Poel, B., Vandenzavel, N., Smet, C., Nicolay, T., Bulens, I., Mellidou, I., et al. (2014). Tissue specific analysis reveals a differential organization and regulation of both ethylene biosynthesis and E8 during climacteric ripening of tomato. *BMC Plant Biol.* 14, 11. doi: 10.1186/1471-2229-14-11

Verhoeyen, M. E., Bovy, A., Collins, G., Muir, S., Robinson, S., de Vos, C. H. R., et al. (2002). Increasing antioxidant levels in tomatoes through modification of the flavonoid biosynthetic pathway. *J. Exp. Bot.* 53, 2099–2106. doi: 10.1093/jxb/erf044

Villano, C., Demurtas, O. C., Esposito, S., Granell, A., Rambla, J. L., Piombino, P., et al. (2023). Integrative analysis of metabolome and transcriptome profiles to highlight aroma determinants in Aglianico and Falanghina grape berries. *BMC Plant Biol.* 23, 241. doi: 10.1186/s12870-023-04251-6

Vogel, J. T., Tieman, D. M., Sims, C. A., Odabasi, A. Z., Clark, D. G., and Klee, H. J. (2010). Carotenoid content impacts flavor acceptability in tomato (*Solanum lycopersicum*). *J. Sci. Food Agric.* 90, 2233–2240. doi: 10.1002/jsfa.4076

Vrebalov, J., Ruezinsky, D., Padmanabhan, V., White, R., Medrano, D., Drake, R., et al. (2002). A MADS-box gene necessary for fruit ripening at the tomato ripening-inhibitor (rin) locus. *Science* 296, 343–346. doi: 10.1126/science.1068181

Wang, L., Baldwin, E. A., and Bai, J. (2016). Recent advance in aromatic volatile research in tomato fruit: The metabolisms and regulations. *Food Bioprocess Technol.* 9, 203–216. doi: 10.1007/s11947-015-1638-1

Wang, R., Angenent, G. C., Seymour, G., and De Maagd, R. A. (2020). Revisiting the role of master regulators in tomato ripening. *Trends Plant Sci.* 25, 291–301. doi: 10.1016/j.tplants.2019.11.005

Wang, S., Qiang, Q., Xiang, L., Fernie, A. R., and Yang, J. (2023). Targeted approaches to improve tomato fruit taste. *Horticult. Res.* 10 (1), uhac229. doi: 10.1093/hr/uhac229

Wang, M., Zhang, L., Boo, K. H., Park, E., Drakakaki, G., and Zakharov, F. (2019). PDC1, a pyruvate/α-ketoacid decarboxylase, is involved in acetaldehyde, propanal and pentanal biosynthesis in melon (*Cucumis melo* L.) fruit. *Plant J.* 98, 112–125. doi: 10.1111/tpj.14204

Wei, T., and Simko, V. (2017) *R Package "Corrplot": Visualization of a Correlation Matrix (Version 0.84)*. Available at: https://github.com/taiyun/corrplot.

Weng, L., Zhao, F., Li, R., Xu, C., Chen, K., and Xiao, H. (2015). The zinc finger transcription factor SlZFP2 negatively regulates abscisic acid biosynthesis and fruit ripening in tomato. *Plant Physiol.* 167, 931–949. doi: 10.1104/pp.114.255174

Yang, X., Zhao, X., Fu, D., and Zhao, Y. (2022). Integrated analysis of widely targeted metabolomics and transcriptomics reveals the effects of transcription factor NOR-like1 on alkaloids, phenolic acids, and flavonoids in tomato at different ripening stages. *Metabolites* 12, 1296. doi: 10.3390/metabo12121296

Yu, G., Wang, L. G., Han, Y., and He, Q. Y. (2012). ClusterProfiler: An R package for comparing biological themes among gene clusters. *Omi. A J. Integr. Biol.* 16, 284–287. doi: 10.1089/omi.2011.0118

Zahedi, S. M., Hosseini, M. S., Karimi, M., and Ebrahimzadeh, A. (2019). Effects of postharvest polyamine application and edible coating on maintaining quality of mango (Mangifera indica L.) cv. Langra during cold storage. *Food Sci. Nutr.* 7, 433–441. doi: 10.1002/fsn3.802

Zhang, Y., Li, Q., Jiang, L., Kai, W., Liang, B., Wang, J., et al. (2018). Suppressing type 2C protein phosphatases alters fruit ripening and the stress response in tomato. *Plant Cell Physiol.* 59, 142–154. doi: 10.1093/pcp/pcx169

Zhao, X., Zhang, Y., Lai, J., Deng, Y., Hao, Y., and Wang, S. (2023). The slDOG1 affect biosynthesis of steroidal glycoalkaloids by regulating GAME expression in tomato. *Int. J. Mol. Sci.* 24, 3360. doi: 10.3390/ijms24043360

Zhou, X., Rao, S., Wrightstone, E., and Sun, T. (2022). Phytoene synthase: the key rate-limiting enzyme of carotenoid biosynthesis in plants. *Front. Plant Sci.* 13. doi: 10.3389/fpls.2022.884720

Zhu, G., Gou, J., Klee, H., and Huang, S. (2019). Next-gen approaches to flavor-related metabolism. *Annu. Rev. Plant Biol.* 70, 187–212. doi: 10.1146/annurev-arplant-050718-100353

frontiers | Frontiers in Plant Science

TYPE Original Research
PUBLISHED 25 October 2023
DOI 10.3389/fpls.2023.1278608

OPEN ACCESS

EDITED BY
Kwanuk Lee,
Jeju National University, Republic of Korea

REVIEWED BY
Sundaravelpandian Kalaipandian,
The University of Queensland, Australia
Klára Kosová,
Crop Research Institute (CRI), Czechia

*CORRESPONDENCE
N. Bollier
norbert.bollier@inrae.fr

†PRESENT ADDRESS
R. Micol-Ponce,
Instituto de Bioingeniería, Universidad Miguel Hernández, Elche, Alicante, Spain

‡These authors have contributed equally to this work

RECEIVED 16 August 2023
ACCEPTED 06 October 2023
PUBLISHED 25 October 2023

CITATION
Bollier N, Micol-Ponce R, Dakdaki A, Maza E, Zouine M, Djari A, Bouzayen M, Chevalier C, Delmas F, Gonzalez N and Hernould M (2023) Various tomato cultivars display contrasting morphological and molecular responses to a chronic heat stress. *Front. Plant Sci.* 14:1278608. doi: 10.3389/fpls.2023.1278608

Various tomato cultivars display contrasting morphological and molecular responses to a chronic heat stress

N. Bollier[1*‡], R. Micol-Ponce[1†‡], A. Dakdaki[1], E. Maza[2], M. Zouine[2], A. Djari[2], M. Bouzayen[2], C. Chevalier[1], F. Delmas[1], N. Gonzalez[1] and M. Hernould[1]

[1]INRAE, Université de Bordeaux, BFP, Bordeaux, France, [2]Laboratoire de Recherche en Sciences Végétales, Université de Toulouse, CNRS, UPS, Toulouse INP, Toulouse, France

Climate change is one of the biggest threats that human society currently needs to face. Heat waves associated with global warming negatively affect plant growth and development and will increase in intensity and frequency in the coming years. Tomato is one of the most produced and consumed fruit in the world but remarkable yield losses occur every year due to the sensitivity of many cultivars to heat stress (HS). New insights into how tomato plants are responding to HS will contribute to the development of cultivars with high yields under harsh temperature conditions. In this study, the analysis of microsporogenesis and pollen germination rate of eleven tomato cultivars after exposure to a chronic HS revealed differences between genotypes. Pollen development was either delayed and/or desynchronized by HS depending on the cultivar considered. In addition, except for two, pollen germination was abolished by HS in all cultivars. The transcriptome of floral buds at two developmental stages (tetrad and pollen floral buds) of five cultivars revealed common and specific molecular responses implemented by tomato cultivars to cope with chronic HS. These data provide valuable insights into the diversity of the genetic response of floral buds from different cultivars to HS and may contribute to the development of future climate resilient tomato varieties.

KEYWORDS

heat stress (HS), pollen development, HS transcriptional response, tomato, flower development

1 Introduction

Population growth and global warming are two of the major issues that humanity will have to face in the next decades (IPCC, 2014). Based on current climatic models, experts commonly anticipate that rising temperatures will cause substantial yield losses in the future affecting major plant-food sources (Tripathi et al., 2016). Global warming has

already a significant impact on crop production and agricultural practices. During the past years, many regions of the world underwent extreme heat waves causing severe damages to ecosystems, human society and crop production (Stillman, 2019). The frequency and intensity of these heat waves will increase in many regions of the globe leading to major losses in agricultural yield (Lau and Nath, 2012; Molina et al., 2020).

Plant growth and development can be strongly altered by high temperatures, the most heat-susceptible phases being early seedling and reproductive phases. Heat-stress (HS) can impair essential cellular, physiological and developmental processes, including genome integrity, photosynthesis, flower development or pollen development and viability as reported for a number of plant species (Han et al., 2021; Moore et al., 2021). Detrimental effects of heat on pollen production have been described in various plant taxa, including *Arabidopsis thaliana* (Arabidopsis), *Solanum lycopersicum* (tomato) and *Oryza sativa* (rice) and for different developmental stages such as meiosis, microspore development and pollen maturation (Raja et al., 2019). Pollen development is known to be one of the most temperature-sensitive process in plant life cycle (Zinn et al., 2010), and alteration of pollen meiosis, particularly at the tetrad stage, has been reported in different species such as Arabidopsis, maize or cotton (Begcy et al., 2019; De Storme and Geelen, 2020; De Jaeger-Braet et al., 2021; Masoomi-Aladizgeh et al., 2021; Ning et al., 2021) and impaired pollen development results in poor fertilization and reduced fruit and seed yield (Giorno et al., 2013; Müller and Rieu, 2016).

The cellular responses to HS have been studied in a variety of plant species and various organ and tissues revealing both common and specific responses. HS disturbs various cellular processes, resulting, for example, in the denaturation of biological molecules, such as proteins, lipids, and nucleic acids (Bohnert et al., 2006; Kotak et al., 2007; Essemine et al., 2010) and the disintegration of subcellular structures, including membranes and cytoskeleton networks (Savchenko et al., 2002; Saidi et al., 2011). HS affects genome integrity by triggering DNA damage through nucleotide modifications and single-strand or double-strand breaks (Kantidze et al., 2016) and it also alters chromatin architecture (Pecinka and Mittelsten Scheid, 2012). To cope with HS, plants have developed highly complex intracellular signaling systems involving hormones, Ca^{2+} and reactive oxygen species (ROS) (Wahid et al., 2007). For a long time, ROS were considered as a byproduct that impairs plant growth. However, ROS recently gained attention for their function as signaling molecules involved in response to environmental stresses like HS (Medina et al., 2021). In support to this idea, it has been shown that ROS-scavenging enzymes, involved in detoxification processes, are rapidly induced by HS (Suzuki and Mittler, 2006).

HS induces rapid transcriptional changes and the elucidation of the complex transcriptional regulatory networks involved in plant responses to HS is now well advanced (Ohama et al., 2017). That is, HS rapidly activates HS-responsive transcription factors, HSFs, which regulate the transcription of a wide range of target genes involved in signaling and metabolic pathways (von Koskull-Döring et al., 2007). Among the most notable responsive proteins, the Heat Shock Proteins (HSPs) are known to play essential roles in cellular protection through their action on protein misfolding or aggregation but also in protein translocation and degradation (Vierling, 1991; Schleiff and Becker, 2011). Transcriptomic profiling has identified several molecular pathways induced under elevated temperature conditions including photosynthesis, response to light or rRNA processing (Jayakodi et al., 2019). Interestingly, in addition to the classically induced HSPs, these studies suggested potential roles for several factors involved in epigenetic, post-transcriptional and post-translational regulation as well as in hormonal regulation. Deciphering the effects of HS at the transcriptome level greatly helped defining candidate genes potentially involved in mediating plant tolerance to HS and several attempts aiming to improve thermotolerance by knocking out or overexpressing these candidate genes have been reported in different plant species including Arabidopsis, tomato, rice and *Glycine max* (soybean) (Zhu et al., 2006; Yokotani et al., 2008; Xin et al., 2010; Wu et al., 2012; Li et al., 2013; Shen et al., 2015; Xue et al., 2015; Wan et al., 2016). It is however, likely that the activation of two or more independent -but mutually complementary- pathways would improve more effectively thermotolerance in crops species. In this regard, new pathways need to be discovered in order to pave the way towards the generation of highly tolerant genotypes using the newly identified candidates for gene stacking.

HS response has been extensively investigated in plants in the past two decades. Most studies have been carried out applying very high temperatures (45°C to 50°C) for a short period of time (from 30 minutes to 3 hours) on the whole plant, or focused on specific developmental stages or organs (Qu et al., 2013; Driedonks et al., 2016; Janni et al., 2020). Strikingly so far, quite a few studies have been carried out that simulate heat wave conditions as defined by the STAtistical and Regional dynamical Downscaling of EXtremes for European regions (STARDEX) project: at least 5 consecutive days with 5 degrees anomaly with respect to mean temperature in summer (Jagadish et al., 2021). Similarly, only few studies have investigated the response of plants to chronic HS, corresponding to longer periods of heat (Sato et al., 2000). Because the effect of short-term heat treatments is unlikely to completely reproduce what happens during long term HS, studying the impact of long periods of heat on plants is essential to eventually select plant cultivars with increased heat tolerance.

Tomato is one of the most produced and consumed fruits in the world. However, tomato producers face dramatic yield losses in very warm summers, due to poor fruit setting resulting in decreased fruit number and small fruits of low quality (Adams et al., 2001). In recent years, several transcriptomic, metabolomic, proteomic or lipidomic analyses were performed to study the response of tomato plants to HS (Pressman et al., 2002; Spicher et al., 2016; Paupière et al., 2017; Almeida et al., 2021). Studies focusing on floral buds revealed that short-term HS induces the expression of *HSF* genes, *HSP* genes, ROS scavenger genes and genes involved in the control of sugar levels (Frank et al., 2009). However, most of these studies are limited to one tomato genotype and, more importantly, the short-term treatment is unlikely to completely reproduce the molecular responses to chronic stress.

Here, we aimed at identifying the common and/or specific molecular responses to a chronic HS in tomato floral buds of

various tomato cultivars. Seeds from 11 modern tomato cultivars were obtained from different seed companies, and plants were grown and subjected to a chronic HS of 3 weeks, before evaluating the pollen germination rate. Among these 11 cultivars, 2 and 3 cultivars with high and low pollen germination rate under HS respectively, were selected for subsequent genome-wide transcriptomic profiling analysis of their floral buds to identify the molecular pathways regulated during a chronic HS. These analyses highlighted the different genetic responses that tomato cultivars set-up for facing chronic HS.

2 Materials and methods

2.1 Plant material and growth

Plant material consisted of eleven different tomato cultivars: Brioso (Rijk Zwaan), Clodano (Syngenta™), Docet (Monsanto™), DRK7024 (De Ruiter™), JAG8810 (Bayer™), M82, Marbonne (Gautier Semences), Moneymaker, Rebelski (De Ruiter™), Sassari (Rijk Zwaan) and West Virginia 106 (WVA106). This set of cultivars was selected in order to cover some of the tomato diversity in terms of i) fruit morphology: small (WVA106, Sassari, Brioso, M82), medium (Docet, Moneymaker, Clodano, JAG8810), and large size (Rebelski, Marbonne, DRK7024) (Figure S2); ii) growth pattern: determinate (JAG8810, M82) *versus* indeterminate growth (DRK7024, WVA106, Brioso, Marbonne, Sassari, Moneymaker, Rebelski); and iii) market suitability: fresh market (Sassari, Brioso, M82, Clodano, Moneymaker) and processing tomatoes (JAG8810, DOCET). In non-stress (NS) conditions, plants were cultivated in a greenhouse with a photoperiod of 16h/8h with a mean temperature of 24°C during the day and a mean temperature of 18°C during the night. For HS treatments, the plants at bolting stage have been submitted during 3 weeks to a mean temperature of 35°C during the day (16h) and 25°C during the night (8h) using the main and two auxiliary heaters and the temperature has been monitored all along the HS (Figure S1A). In both conditions, the hygrometry was around 55% all day and plants had a daily watering.

2.2 Pollen developmental stage analysis

To analyze pollen development, 3-5 floral buds for each different size were dipped in Carnoy's fixative solution (60% (v/v) ethanol, 30% (v/v) chloroform, 10% (v/v) acetic acid). Then, the anthers from the flower buds were dissected in acetocarmine staining solution (1% (p/v) carmine 40, 0.5% (p/v) ferric chloride, 45% (v/v) glacial acetic acid) using gauge needles under a stereomicroscope and squashed between a slide glass and a coverslip to release the male reproductive cells as described by (Puchtler et al., 1968). Pollen developmental stages were observed using a bright field microscope (Zeiss, Axioplan) and photographed with a CCD camera (Motic 3 megapixels).

2.3 Pollen germination assays

Pollen grains from 3 to 5 tomato flowers at anthesis stage were sprayed on the top of pollen germination medium (18% sucrose, 0.01% Boric acid, 1mM $CaCl_2$, 1mM $Ca(NO_3)_2$, 1mM $MgSO_4$, 0.5% agar; pH=7). Each experiment was repeated 3 times. After 16h of incubation at 25°C in the dark, the preparation was observed using a stereomicroscope Olympus SXZ16 and photographed using a camera (Motic 10 megapixels). The pollen germination rate expressed as a percentage was determined by dividing the number of germinated pollens corresponding to those emitting a pollen tube by the total number of pollen grains.

2.4 Genome wide expression profiling

To prepare RNA samples for the subsequent RNAseq analysis, each tomato cultivar was grown under NS or HS conditions [3 weeks at 35°C during the day (16h) and 25°C during the night (8h)]. Based on the histological analysis, floral buds were harvested at the tetrad stage (tetrad floral bud, TFB) and at the pollen mature stage (pollen floral bud, PFB) based on their size (Table S1). Five to ten floral buds for each stage were sampled before and 20 days after the start of the HS from 20-25 plants per genotype for the RNAseq analysis (Figure S1B). Total RNA was isolated from 200 and 500 mg of floral buds at different developmental stages using TRIzol Reagent (Life Technologies). Total RNA extract was purified with the Qiagen RNAeasy mini kit RNA. After DNase treatment (DNA-free Kit, Life Technologies), the total RNA quantity and quality (RNA integrity number, RIN) were evaluated using an Agilent 2100 Bioanalyzer (Agilent Technologies). Only RNA extracts with a RIN of 10 were used for sequencing. The RNA libraries were constructed as described in the Illumina TruSeq Stranded mRNA guide. mRNAs were sequenced in a HiSeq 3000 sequencing system with 2 × 125 bp paired-end sequences (Illumina HiSeq SBS Kit v4) by the Genotoul bioinformatics platform, Toulouse (http://bioinfo.genotoul.fr/index.php).

Three biological replicates per plant and per stage were harvested for NS and HS conditions, resulting in 60 samples (5 cultivars × 2 conditions × 2 developmental stages × 3 biological replicates). To obtain the genome-wide expression profiling, RNA samples were subjected to next-generation sequencing.

For each RNA sample, more than 20 million of paired-end reads (10 million fragments) were generated, using an Illumina Hiseq 3000 platform. More than 95% of total clean reads were mapped against the SL3.0 version of the reference tomato genome for read mapping (ftp://ftp.solgenomics.net/genomes/Solanum_lycopersicum/Heinz1706/assembly/build_3.00/) and almost 90% of the mapped reads matched a feature on the related gene model.

2.5 Bioinformatic analyses

Statistical analyses and graphs have been performed with the R software and homemade scripts. The DE analysis has been carried

out with the DESeq2 R-package (Love et al., 2014). Some analyses, such as the PCA analysis, were carried out with functions contained in the DESeq2 package. Reads were checked using fastQC, cleaned using trimGalore, and mapped using Star, a spliced aware mapper software on the new tomato genome SLmic1.0 generated in the frame of TOMGEM project (http://tomatogenome.gbfwebtools.fr/). The mapping was guided using the gene model annotation version 1.1. FeatureCount was then used to calculate the read counts for each gene from each mapping file. A normalization step was performed in order to obtain comparable expression values between conditions and between genes. For this purpose, our pipeline takes into account the relative size of studied transcriptomes, the library sizes and the gene lengths, as described in Maza et al. (2013); Maza (2016). After data normalization using DESeq2 package, a PCA analysis has been conducted with expression data in all conditions and replicates, in order to check global sample variability.

Genome-wide expression data have been analyzed in order to identify genes differentially expressed between different conditions that have been tested. The "Relative Log Expression" normalization (RLE) implemented in the DESeq2 package has been used as normalization method. To highlight DEGs, the genes exhibiting an adjusted *p-value* < 0.05 and a log2 fold-change < -1 or > +1 have been selected. To eliminate very lowly expressed genes, the up-regulated DEGs with a count value < 10 in HS condition and the down-regulated DEGs with a count value < 10 in NS condition were filtered out.

To calculate the intersections of DEGs lists within the different conditions, Venn diagrams corresponding to textual outputs were generated by using the Venn diagram tools at http://bioinformatics.psb.ugent.be/webtools/Venn/BAR Website at http://bar.utoronto.ca/or at https://www.biovenn.nl/index.php (Hulsen et al., 2008) for area-proportional Venn diagrams. The TomExpress web site, at http://tomexpress.toulouse.inra.fr/query, was used to extract gene expression data obtained from previous genome-wide expression analyses (Zouine et al., 2017).

The GO enrichment analysis has been carried out on PLAZA 5.0 (Van Bel et al., 2022) using the Plaza workbench, with a significance threshold of 0.05 and without any data filter.

3 Results

3.1 Morphological analyses of flower development and variability in pollen germination of tomato cultivars under chronic HS

To assess phenotypic differences in response to HS of various tomato genotypes, we examined the behavior of eleven tomato cultivars corresponding to ten commercial varieties and the cherry tomato West Virginia 106 (WVA106) cultivar. Given that floral development is critical for tomato yield, we focused our analysis on the morphological and cytological changes occurring during this process under HS conditions. Under NS conditions, the 11 selected cultivars displayed variability in size and morphology of floral buds during development (Figure 1). Floral bud size distribution was not statistically different under NS and HS conditions (Figure S3), but clear morphological alterations were observed (Figure 1). In particular, only the flowers of the Sassari cultivar exhibited stigma exertion under HS compared with the complete absence of stigma exertion under NS conditions. On the other hand, HS induced the appearance of curled petals in Clodano, Docet, M82, Marbonne and Moneymaker cultivars. In addition, HS caused the sepals and petals to open at an earlier developmental stage than in NS conditions in Moneymaker, Brioso and WVA106. In this latter cultivar, sepals displayed burned extremities due to HS. In conclusion, floral development in various tomato cultivars was affected differently under HS, suggesting that the response to HS may be, at least partially, dependent on the genetic background.

Flower fertilization, and subsequent fruit set and seed production, can be impaired by poor pollen germination and pollen tube growth. We thus determined the percentage of pollen germination, used as a proxy for pollen potential for fertilization in the eleven tomato cultivars under NS and HS conditions (Figure 2). Under NS conditions, pollen germination was highly variable between the cultivars studied, with a maximum percentage of 80% for WVA106, and a minimum of 18.6% for DRK7024. Overall, the HS negatively impacted pollen germination in all cultivars, with a complete absence of germination in Clodano, DRK7024, Moneymaker, Rebelski and Sassari, indicating the extreme sensitivity to HS of the pollen in these cultivars (Figure 2). In Brioso, Docet, M82 and Marbonne cultivars, the pollen germination rate under HS was reduced respectively, by 10-, 21-, 12- and 33-fold, when compared to NS condition, indicating a high sensitivity to HS of these cultivars even though some germination capacity was maintained. Conversely, pollen germination in JAG8810 and WVA106 was only reduced by 1.4- and 3.5-fold respectively, suggesting a better tolerance to HS treatment in these cultivars. Taken together, these results indicated that pollen germination percentage is highly affected under HS conditions although the degree of sensitivity is highly genotype-dependent.

3.2 Cytological analyses of pollen development of tomato cultivars under chronic HS

To determine if the effect of the chronic HS on pollen germination was related to a perturbation of pollen development, we selected 5 cultivars showing contrasting behaviors for pollen germination under HS: namely WVA106 and JAG8810 as tolerant cultivars, and Clodano, DRK7024 and M82 as sensitive cultivars. It has been described that under NS conditions, tomato floral bud size is generally synchronized with the developmental stage of the reproductive organs (Brukhin et al., 2003). Therefore, we determined first, under our NS growth conditions, the developmental stage of the male gametophyte in relation to floral bud size, using a histological approach. Four pollen developmental stages were considered because they were easily recognizable: Microspore Mother Cell (Figure 3A), present in 4.5 mm buds in

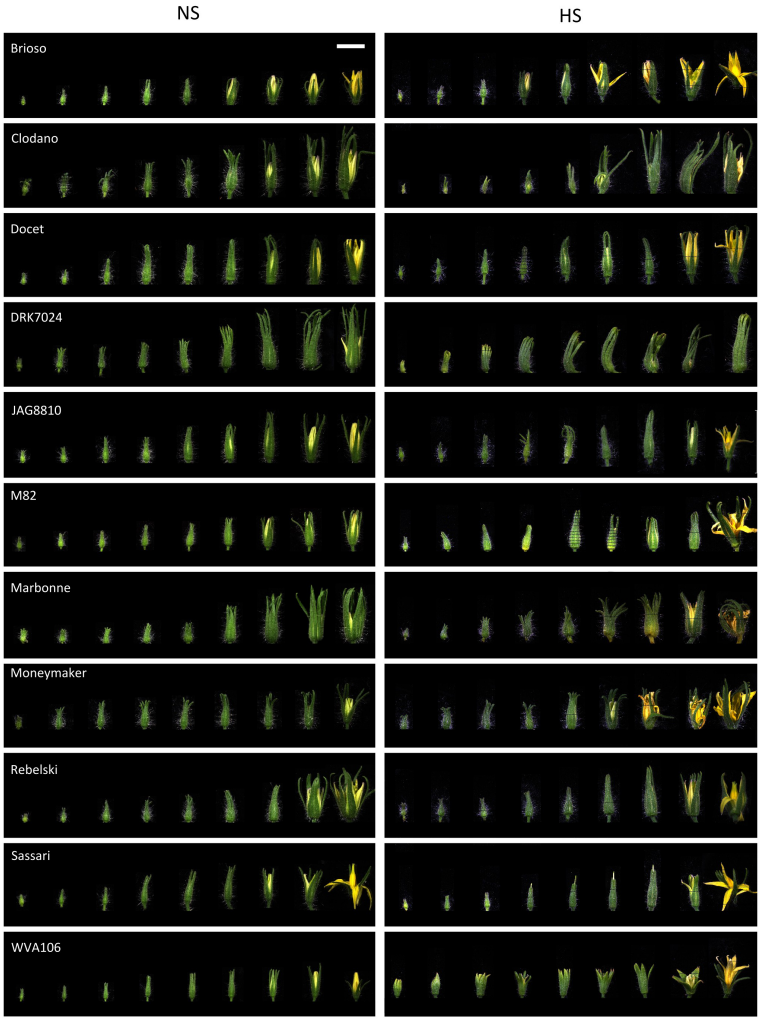

FIGURE 1
Floral bud development under heat stress (HS) and non-stress (NS) conditions in the 11 studied tomato cultivars. For each cultivar, floral buds are ordered according to their size in each condition showing the effect of the HS at different developmental stages. Bar, 1 cm (applies to all panels).

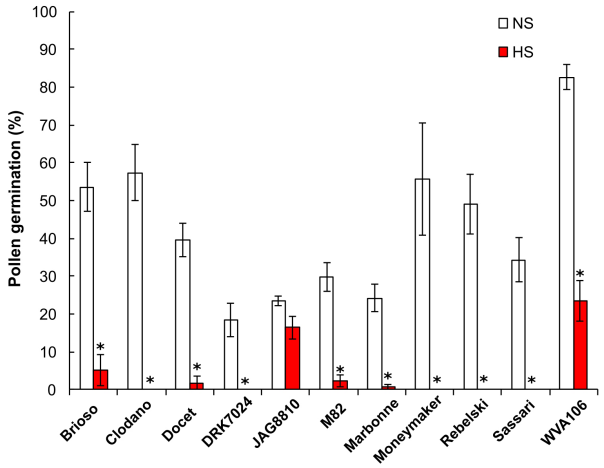

FIGURE 2
Pollen germination rate expressed as the percentage of germinating pollen grains (%) under non-stress (NS) and heat stress (HS) conditions in 11 tomato cultivars. *for ANOVA *p-value*<0.05.

WVA106; Meiosis (Figure 3B), in 5.5 mm buds in WVA106; Tetrad (Figure 3C) in 6 mm buds in WVA106 and Mature pollen grain (Figure 3D) in 7 mm buds in WVA106. Most of the time, only one pollen developmental stage was observed for a determined bud size under NS conditions, indicating the synchronization of floral bud and pollen development in the different cultivars studied. Indeed, Clodano, JAG8810, M82 and DRK7024 floral buds at 13 mm, 9 mm, 6 mm, and 18 mm respectively, only contained mature pollen grains (Figures 3E–H) and 6 mm floral buds in WVA106 only contained tetrads (Figure 3I). Under HS conditions, all cultivars, except DRK7024, showed several pollen developmental stages at these bud sizes (Figures 3J–T). For DRK7024, while only one pollen developmental stage was observed at a time, pollen development was delayed compared to NS condition as indicated by the observed microspore mother cell instead of mature pollen in 18 mm floral buds (Figures 3H, M).

These results were confirmed when reporting the size of the flower buds in relation to pollen developmental stage. In three cultivars (Clodano, DRK7024 and JAG8810), the stressed flower

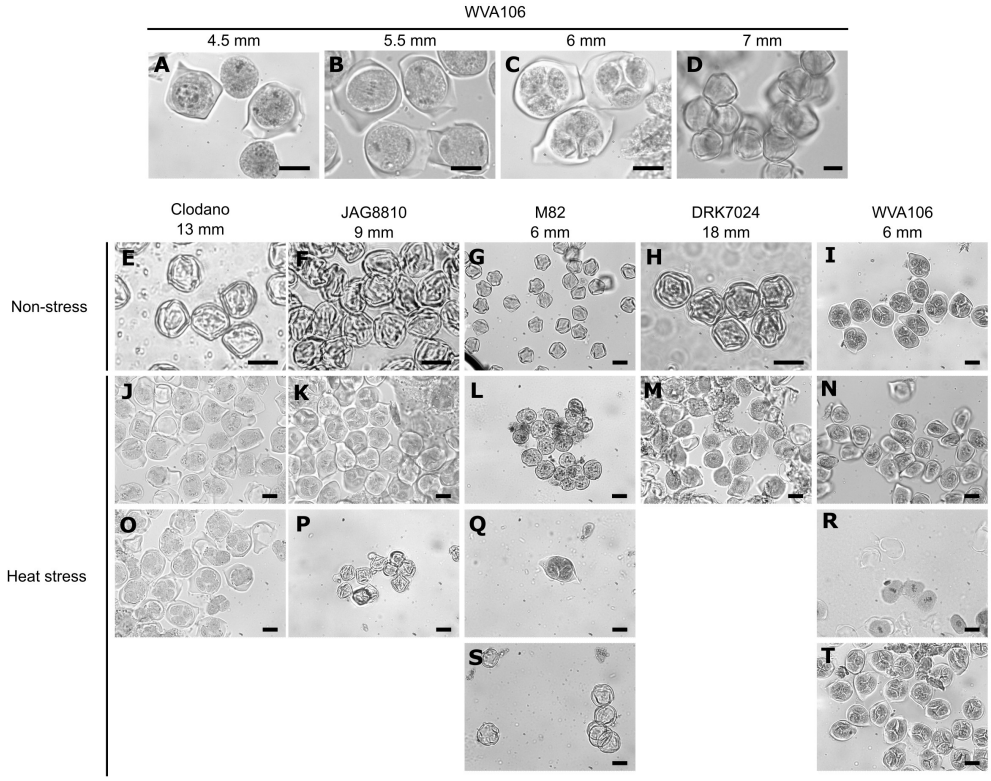

FIGURE 3
Histological analyses of pollen development in relation with bud size under non-stress (NS) and heat stress (HS) conditions in different tomato cultivars. Pollen developmental stages observed are the following: microspore mother cell **(A–M, N)**; Meiosis **(B, J, R)**; Tetrad **(C, I, K, O, Q, T)**; Mature pollen grains **(D–H, P, S)**. Bar, 20µm.

buds showed more size variability than in NS conditions for most pollen developmental stages and their length was significantly higher for Clodano and DRK7024 at the tetrad stage thus suggesting a delay in pollen development (Figure 4). Conversely, for a defined pollen developmental stage in WVA106 and M82, the floral bud size was not different between HS and NS indicating that pollen development was not delayed but rather desynchronized under HS condition in these two cultivars (Figure 4). Altogether, these results indicate that pollen development is either delayed (Clodano, DRK7024) and/or desynchronized (Clodano, JAG8810, M82, WVA106) by HS with a clear effect at the tetrad stage and regardless of the observed tolerance to the HS in terms of pollen germination capacity as determined in Figure 2.

3.3 General transcriptomic response to HS

To identify the molecular pathways differentially regulated in the floral buds of different tomato cultivars under HS, we carried out a genome-wide transcriptomic analysis by RNAseq on the five previously studied cultivars at two developmental stages: tetrad stage (tetrad floral bud, TFB) and pollen mature stage (pollen floral bud, PFB).

Following quality check and pre-processing of the sequence data, the reads were mapped against the SLmic1.0 tomato reference genome (gene model version 1.1). PCA of the RNA sequencing data showed that the samples clustered together according to both developmental stages and growth conditions factors explaining, respectively, about 60% and 10% of the whole variance (Figure S4). In TFB and PFB, the transcriptomic profiles corresponding to samples subjected to HS were clearly separated from the ones in NS conditions, indicating that the simulated chronic HS triggered a transcriptional response in all cultivars.

Differentially expressed genes (DEGs) in HS versus NS conditions were computed for each condition and for each developmental stage as described in materials and methods. The RNA-seq analysis yielded a total of 26017 expressed genes among which 3647 were significantly differentially expressed (adjusted p-value<0.05, 1<Log2FC< -1) across the five cultivars at the two stages and between the two growth conditions (Table S2). To analyze the global response to HS at each developmental stage independently of the cultivar considered, the down- or up-regulated genes from all cultivars were pooled and classified based on their GO annotation focusing on biological processes. In both PFB (1415 up and 1420 down, Table S3) and TFB (1369 up and 929 down, Table S3), most DEGs having enhanced or decreased expression in response to HS belonged to GO classes linked to response to stimulus, response to stress and response to abiotic stimulus (GO:0050896; GO:0006950 and GO:0009628 respectively) corresponding to 20 to 40% of the set of genes with an associated GO term in the studied list (Table S4).

10.3389/fpls.2023.1278608

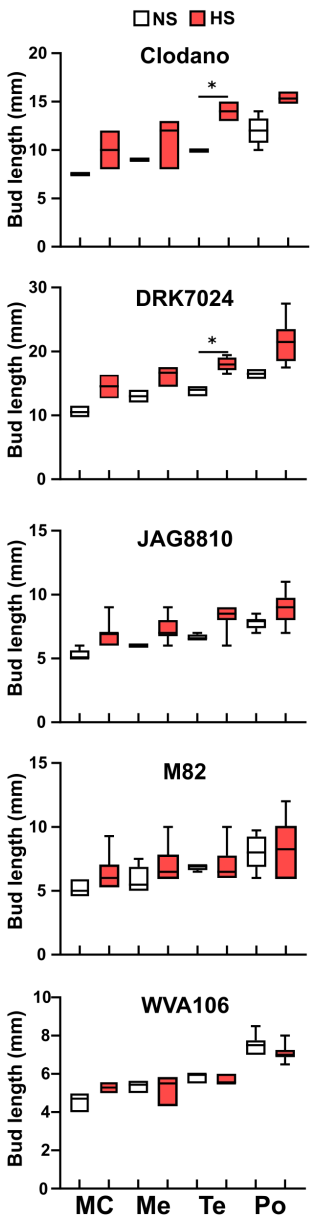

FIGURE 4
Size of floral buds for a defined pollen developmental stage in Clodano, DRK7024, JAG8810, M82, WVA106. MC, microspore mother cell; Me, Meiosis; Te, Tetrad; Po, Mature Pollen. * p-value<0.05 (Kruskal Wallis test).

As expected, the categories "response to heat" (GO:0009408) and "cellular response to heat" (GO:0034605) were found enriched in the upregulated DEGs. Additionally, "response to reactive oxygen species" (ROS, GO:0000302), "response to oxygen-containing compound" (GO:1901700) and "cellular response to oxygen-containing compound" (GO:1901701) were enriched categories, containing around 15% of the PFB and TFB up-regulated genes. Interestingly, down-regulated genes corresponding to the GO class, term or category "sporopollenin biosynthetic process" (GO:0080110) were found enriched in PFB suggesting that pollen development might be affected. This global analysis thus reveals that the floral buds at both tetrad and pollen developmental stages were severely affected by the HS resulting in an oxidative stress.

We then analyzed the DEGs commonly up- or down-regulated between PFB and TFB stages. 820 out of 1964 (42%) and 534 out of 1815 (29%) DEGs were found to be commonly up-regulated and down-regulated, respectively in PFB and TFB samples, highlighting the response similarity to HS independently of the developmental stage (Figures 5A, B). Most DEGs with enhanced expression in response to HS belonged to GO classes linked to response to stimulus such as response to heat (GO:0009408, GO:0034605) including 16 HSPs, response to ROS (GO:0000302 and GO:1901700) including ACC-oxidases, ascorbate peroxidase and catalases, and cellular processes such as protein folding (GO:0006457 and GO:0042026) (Figure 5C; Table S5). For the down-regulated DEGs, the GO enrichment analysis revealed mainly classes related to metabolic processes such as photosynthesis (GO:0009765). These results indicated that the global tomato transcriptome response at both TFB and PFB stages is largely common and suggested that both tissues undergo inhibition of photosynthetic processes.

3.4 Cultivar specific and common transcriptomic response to HS

To further evaluate the common and specific responses to HS between cultivars, we identified the DEGs in the different tomato cultivars under HS condition. At the TFB stage, we found 872 and 742 DEGs for JAG8810 and WVA106, respectively, considered as pollen tolerant cultivars *i.e.* cultivars for which the pollen germination rate was lowly affected under HS, and 1233, 1089 and 1293 DEGs for M82, DRK7024 and Clodano, respectively, considered as pollen sensitive cultivars *i.e.* cultivar for which the pollen germination rate was highly reduced under HS (Table S3). At the PFB stage 587 and 1402 DEGs were found for JAG8810 and WVA106 respectively, and 1327, 1418 and 1388 for M82, DRK7024 and Clodano respectively. We then compared the DEGs found in the five cultivars at each developmental stage. The Venn diagram of the up-regulated genes in TFB showed that 147 genes were common between all cultivars which represent between 17% (for Clodano) and 32% (for WVA106) of the up-regulated DEGs (Figure 6A; Table S6). In PFB, 57 genes were found common between the five cultivars representing between 7% (for M82) and 15% (for JAG8810) of the up-regulated DEGs (Figure 6B; Table S6). Interestingly only 13 out of 502 genes were found specifically up-regulated in JAG8810 indicating that the response at this stage in this cultivar is almost completely shared by the others. Concerning the down-regulated DEGs, 97 genes (representing between 20% for DRK7024 and 34% for WVA106) and 69 genes (representing between 9% for DRK7024 and 32% for JAG8810) were commonly down-regulated in TFB and PFB, respectively, between all cultivars (Figures 6C, D; Table S6).

The 147 commonly up-regulated DEGs identified in TFB were mainly involved in response to stimulus (GO:0050896) with 49% of the set of the genes with an associated GO term in the studied list

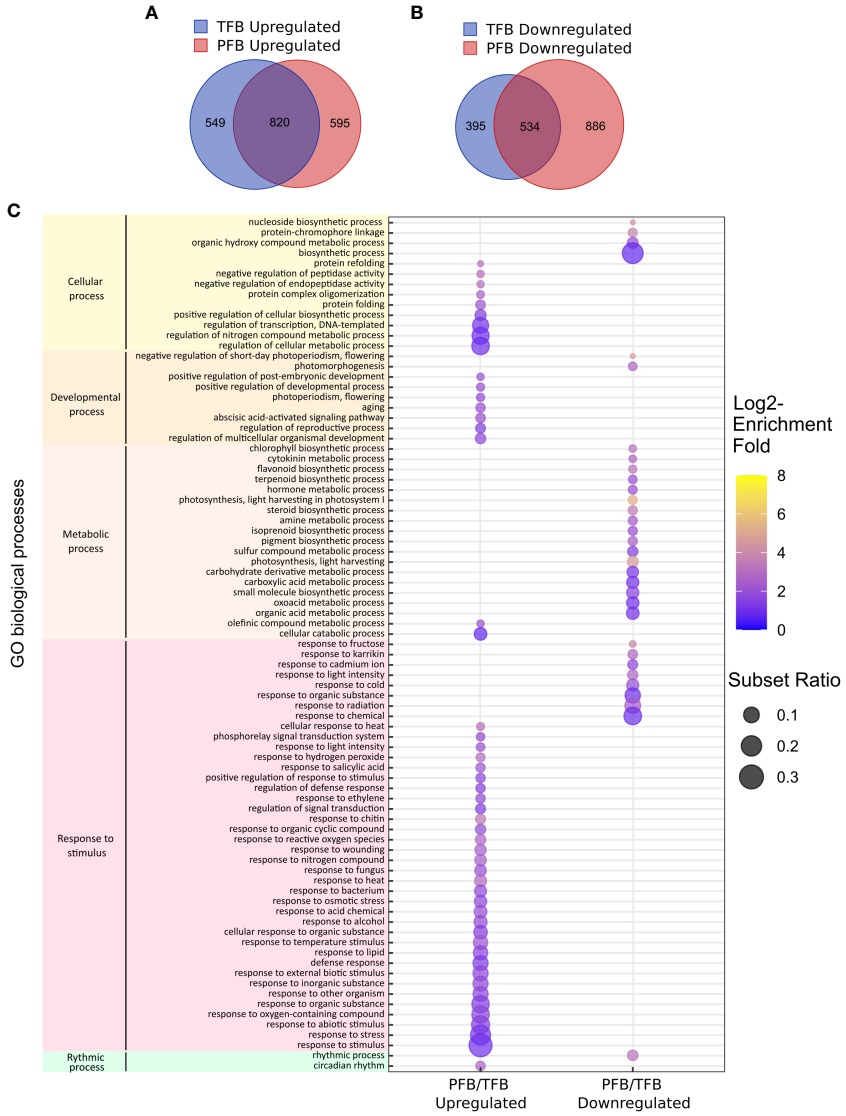

FIGURE 5
Global transcriptome response to HS in all tomato cultivars. **(A, B)** Venn diagram presenting the overlap of DEGs between upregulated **(A)** and downregulated **(B)** genes between TFB and PFB stages in all cultivars. **(C)** Gene ontology (GO) enrichment analyses of the common DEGs between PFB and TFB. The dot size is representative of the number of DEGs associated with the process and the fold enrichment is according to a heat map (dot color).

(Figure 6E; Table S7). As expected, the GO term "response to heat" (GO:0009408) and "response to oxygen-containing compound" (GO:1901700) were found enriched. Similarly, GO terms corresponding to hormonal responses including abscisic acid (GO:0009737), salicylic acid (GO:0009751) and jasmonic acid (GO:2000022) were found. In these hormone-related categories, several genes belonging to the WRKY transcription factor family such as *WRKY80* (Solyc03g095770), *WRKY81* (Solyc09g015770) and *WRKY40* (Solyc06g068460) were found up-regulated. The WRKY family proteins are important actors in the regulation of transcriptional reprogramming associated with plant stress responses (Chen et al., 2012). At PFB stage, GO terms corresponding to metabolic process (GO:0019222) were found enriched among the 57 commonly up-regulated DEGs and include genes related to the redox pathway such as glutaredoxin (Solyc01g067460) encoding a small redox enzyme known to participate to abiotic stress tolerance (Wu et al., 2017). The GO enrichment of the down-regulated DEGs at both TFB and PFB stages revealed mainly photosynthesis-related genes (GO:0009765) such as Chlorophyll a-b binding proteins and oxidoreductase activity-related genes (GO:0016491) including peroxidase, indicating that both stages are affected in photosynthesis during HS. Altogether these results suggested that the common response to HS in the five cultivars mainly corresponds to the upregulation of HS response genes,

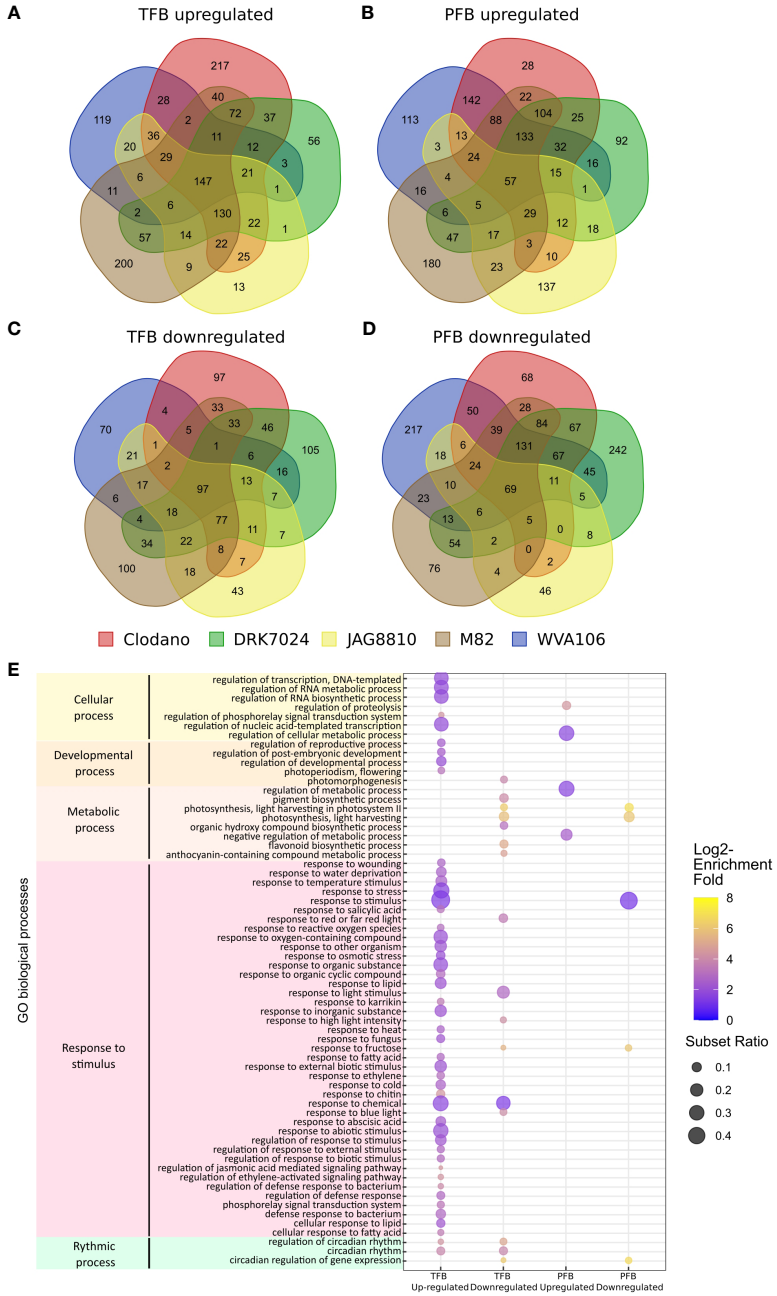

FIGURE 6
Common transcriptome response to HS between all cultivars. **(A–D)** Venn diagram presenting the overlap of DEGs between all cultivars: upregulated genes in TFB **(A)** and in PFB **(B)**; downregulated genes in TFB **(C)** and in PFB **(D)**. **(E)** Gene ontology (GO) enrichment analyses of the common DEGs between all cultivars. The dot size is representative of the number of DEGs associated with the process and the fold enrichment is according to a heat map (dot color).

oxidative stress and hormonal pathways and the down-regulation of photosynthesis related genes.

3.5 Expression of reproductive development related genes is altered under HS

The "regulation of reproductive process" (GO:2000241; 44 genes) and "developmental process involved in reproduction" (GO:000300; 130 genes) categories were found enriched in the pool of up-regulated and down-regulated DEGs, respectively, for all cultivars (Table S8) confirming that HS affected flower development. In the upregulated ones, we found genes related to flower development and inflorescence architecture such as *FRUITFULL-like MADS-box 1* (Solyc06g069430) previously described as a regulator of flowering time and inflorescence architecture in tomato (Jiang et al., 2022) but these genes were found upregulated in the pollen sensitive cultivars Clodano TFB

and DRK7024 and M82 PFB. In the downregulated ones, *SlPHD_MS1* (Solyc04g008420) a PHD-type transcription factor involved in pollen formation and tapetum development (Gökdemir et al., 2022) was found downregulated in the TFB of WVA106 and JAG8810 pollen tolerant cultivars only. Interestingly, more genes corresponding to "regulation of reproductive process" were found up-regulated in pollen sensitive (52 for Clodano; 53 for DRK7024; 44 for M82) than in pollen tolerant (29 for WVA106 and JAG8810) cultivars (Figure 7A). In addition, the mean log2-fold change between NS and HS conditions of the common DEG belonging to this category was higher for Clodano (sensitive) than WVA106 (tolerant) in TFB and for Clodano and DRK (both sensitive) than for JAG8810 and WVA106 (both tolerant) cultivars in PFB (Figure 7B). This observation suggests that the pollen sensitive cultivars might be more affected in their reproductive development than pollen tolerant cultivars.

Given the fact that the applied HS affects pollen development, we further examined the transcriptional expression of several genes expressed during tomato pollen development (Chaturvedi et al., 2013) under NS and HS conditions. We also included in our dataset genes proposed to be related to tomato pollen- and tapetum development (Jeong et al., 2014; Liu et al., 2019). Few genes specifically expressed during anther development and in the microspore were found to be down-regulated under HS in several

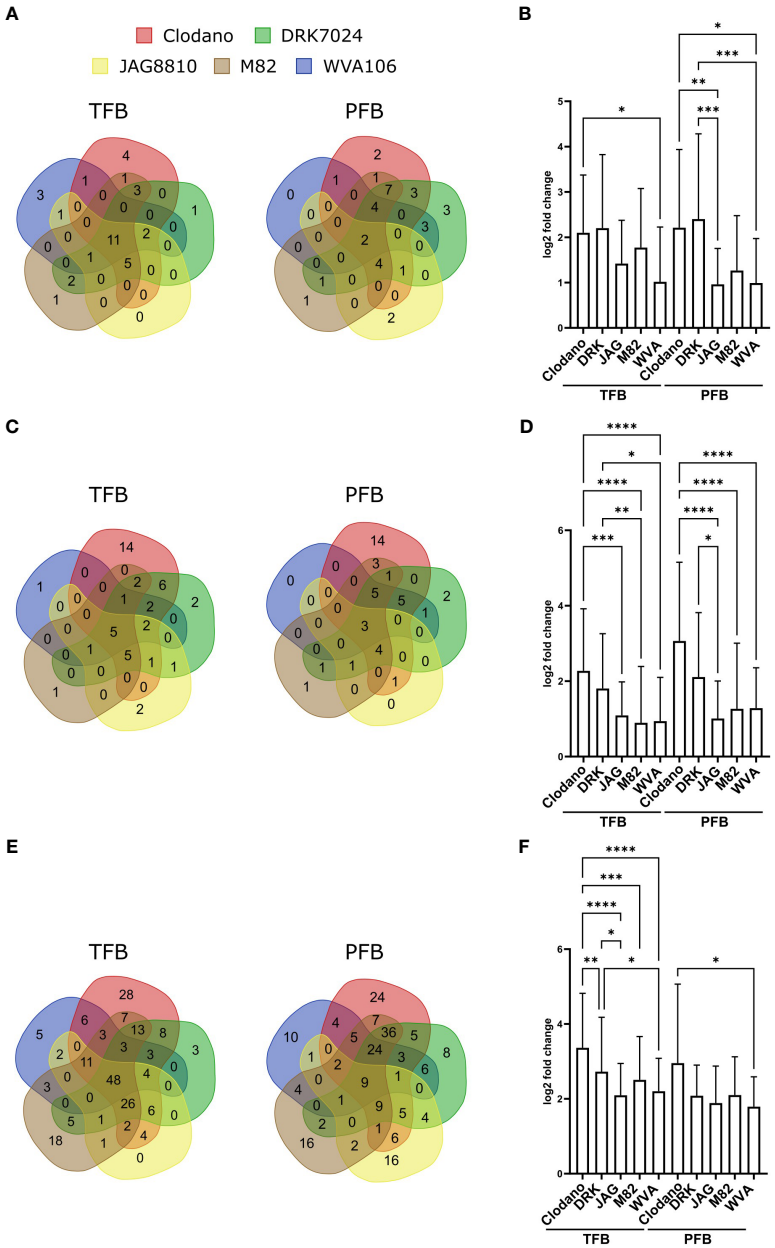

FIGURE 7
Reproductive process-, HS- and ROS-related genes response to HS between cultivars. **(A, C)** Venn diagrams presenting the overlap of up-regulated reproductive process **(A)** HS-**(C)** and ROS-**(E)** related genes between all cultivars. **(B, D, F)** Mean log2-fold change of up-regulated reproductive process-**(B)**, HS-**(D)** and ROS-**(F)** related genes between all cultivars in TFB and PFB. p-value *<0,05; **<0,01; ***<0,001; ****<0,0001 (Kruskal Wallis test).

cultivars (Table S9). However, no clear specific response could distinguish the pollen sensitive versus pollen tolerant cultivars.

3.6 Expression of *HSPs* and *HSFs* genes is altered under HS

Among the genes up- and down-regulated, we identified a high number of *HSPs* (heat shock proteins) encoding chaperone proteins and *HSFs* (heat shock factors) encoding DNA-binding proteins, known to be HS-related genes. Forty-eight and 44 out of 208 tomato HS-related genes (Keller et al., 2018) were found up-regulated in at least one cultivar in TFB and PFB, respectively, for a total number of 50 genes at both stages (Table S10). Interestingly, more HS-related genes were found upregulated in pollen sensitive (45 for Clodano; 33 for DRK7024; 22 for M82) than in pollen tolerant (20 for WVA106 and 20 for JAG8810) cultivars and only few were common between all five cultivars suggesting a specific response of each cultivar (Figure 7C). Moreover, for the up-regulated HS-related genes in all cultivars, despite a similar absolute expression level under NS conditions, the mean log2-fold change between NS and HS conditions in pollen sensitive cultivars was higher than in pollen tolerant cultivars for the two stages analyzed (Figure 7D) suggesting that the sensitive cultivars might sense the stress in a stronger manner.

3.7 Expression of ROS-related genes is altered under HS

Out of 1860 DEGs, a total of 259 genes related to the response to oxygen-containing compound GO (GO:1901700) were up-regulated at both stages in all cultivars (Table S11). Forty-eight out of 210 in TFB and only 9 out of 212 were common between all cultivars suggesting a specific response of each cultivar in terms of ROS related genes (Figure 7E). Moreover, as for HS related genes, the mean log2-fold change between NS and HS conditions in pollen sensitive cultivars was higher than in pollen tolerant cultivars for the two stages analyzed (Figure 7F). Genes encoding ROS scavenging enzymes such as the Ascorbate peroxidase (Solyc09g007270), was found upregulated in HS condition. Antioxidant enzymes such as catalases (Solyc04g082460 and Solyc12g094620) were upregulated under HS and Solyc12g094620 displayed higher expression levels under NS condition in pollen tolerant cultivars compared to pollen sensitive cultivars in both TFB and PFB stages (between 2.1- and 2.6-fold increase in TFB and between 1- and 2-fold in PFB). Moreover, enzymes involved in ROS detoxification such as the iron superoxide dismutase (Solyc06g048410) were found up-regulated.

4 Discussion

4.1 Various tomato cultivars respond unequally to HS

The effects of different types of stresses, including HS, on flower development have been studied for a long time. It is known that the optimal temperature for growing tomato plants is 25°C during the day and 20°C at night (Alsamir et al., 2017). For sensitive tomato cultivars, if the temperatures exceed 26°C during the day and 20°C during the night, floral development is altered, with, in particular, a reduction in pollen production, viability and germination capacity of pollen grains, leading to impaired fruit set and to lower number of seeds per fruit, and, therefore, reduced fruit yield (Firon et al., 2006). Because the response to stress varies widely between genotypes (Gonzalo et al., 2021), gaining deeper knowledge of the developmental and molecular response of various cultivars may provide clues for innovative breeding strategies aiming at improving commercial tomato cultivars for better adaptability to climate change. In the present work, we investigated the responses to HS in eleven tomato cultivars producing fruits of different sizes and shapes. Observation indicates that one of the most characteristic effects of HS on floral morphology is stigma exertion, which negatively impacts self-pollination due to the excessive elongation of the styles minimizing pollen access to the stigmas and reducing fertilization, and consequently decreasing fruit yield and fruit quality (Fernandez-Muñoz and Cuartero, 1991; Giorno et al., 2013). A similar response was previously described in the tomato cultivar Micro-Tom (Pan et al., 2019) and the wild species *S. pimpinellifolium*, *S. pennellii* and *S. chilense* (Alsamir et al., 2017) as a consequence of increased temperature. Interestingly, we only observed this effect in the cultivar Sassari. The absence of stigma exertion in the other cultivars could be explained by the milder stress applied in our study compared to the harsh heat condition used in previous studies 35°C/30°C and 16 h/8 h day/night for 12 days in Pan et al. (2019) and two months in a tunnel house with a maximum of 50°C and a minimum of 30°C in Alsamir et al. (2017). The pistil exertion in the Sassari cultivar could thus indicate that this cultivar is very sensitive to HS. This high sensitivity is also highlighted by the absence of pollen germination under the HS conditions we applied (Figure 2). As previously observed (Giorno et al., 2013), HS triggered additional morphological alterations including curled petals and sepals, and early opening of the sepals and petals depending on the cultivar. The morphological observations after HS thus reveal that the cultivars respond differently to the stress applied.

4.2 HS affects pollen germination in all cultivars but with different ranges

Pollen is easily damaged by exposure to HS (Bita et al., 2011; Paupière et al., 2017; Rieu et al., 2017). The exposure of tomato plants to high temperatures has three effects on pollen grains: a reduction in the number of grains and a reduction in germination and viability (Pressman et al., 2002). The impact of HS on pollen germination was described previously in many species such as in rice (Coast et al., 2016), sorghum (Sunoj et al., 2017), peanuts (Kakani et al., 2002), spring wheat (Bheemanahalli et al., 2019) and tomato (Sherzod et al., 2020). Thermotolerant tomato cultivars have been defined as plants with higher yield, high quantity of viable pollen grains, and higher germination capacity under HS conditions when compared to thermosensitive plants (Firon et al., 2006). In our study, we found

that two cultivars were possibly thermotolerant, namely WVA106 and JAG8810, since they maintain high pollen germination under HS. However, these two cultivars differ greatly with regard to their germination capacity under NS conditions (82.7% and 23.4%, respectively). Such a variability between tomato cultivars has already been reported and can be attributed to differences of pollen germination capacity between genotypes (Gentile et al., 1971; Huner and VAN Huystee, 1982; Abdul-Baki and Stommel, 1995). These variations were also observed in other studies as in spring wheat (*Triticum aestivum*) where pollen germination of 22 cultivars was compared and a germination percentages of 87% maximum and 30% minimum were observed (Bheemanahalli et al., 2019). The decrease in the capacity of pollen to germinate under HS conditions is probably due to damages in the physical structure of pollen, pollen wall composition or lower energy (sugar) status (Jiang et al., 2015; Sita et al., 2017; Sunoj et al., 2017; Djanaguiraman et al., 2018; Jagadish et al., 2021). JAG8810 might be more thermotolerant than WVA106 since the decrease of pollen germination was less important than for WVA106. In other cultivars, we found that pollen germination was lower than 10%, a very low rate probably leading to reduced seed set and yield, parameters we could not evaluate since we sampled the floral buds. These findings indicate that these 9 cultivars are sensitive to the stress applied when considering the pollen germination trait. For that trait too, it seems that the genetic background influences differently the response to HS.

4.3 HS affects pollen development in the sensitive cultivars

Pollen grains are formed inside the anthers through a series of developmental steps from microsporocyte meiosis to pollen release (Gómez et al., 2015). In general, pollen development is synchronized until microsporocyte meiosis I, and sometimes until meiosis II (Brukhin et al., 2003). Cell division synchronization is necessary for successful and coordinated pollination and fertilization (Magnard et al., 2001). Specifically, an environmental stress (extreme temperature or drought) induces asynchrony during pollen development and gives rise to meiotic abnormalities (Pécrix et al., 2011; De Storme and Geelen, 2020). When cultivated under continuous mild heat, a simultaneous reduction in pollen viability and appearance of anthers with pistil-like structures was observed in tomato indicating that HS impairs anther development (Müller et al., 2016). In our study, we show that pollen development is affected at very early stages by HS, impairing meiosis and leading to a delay or a desynchronization of pollen development depending on the cultivar considered.

4.4 Global transcriptome responses to a chronic heat stress in the five tomato cultivars

Anther and pollen development are the major flower parts being sensitive to HS (Thakur et al., 2010; Zinn et al., 2010; De Storme and Geelen, 2014), but sepals have been shown to play important roles in protecting inner floral organs from various stresses including HS (Chen et al., 2019) showing that HS affects the whole floral bud. Under the chronic heat stress we applied, not only pollen development and germination were affected in the eleven tomato cultivars, but also floral bud development and morphology were too (Figure 1). In order to further explore the gene expression changes in the floral buds of different tomato cultivars under HS, we performed a comparative RNAseq analysis on entire floral buds to reveal the differential gene expression in floral buds at tetrad stage (tetrad floral bud, TFB) and pollen mature stage (pollen floral bud, PFB) in five cultivars with contrasted pollen development tolerance to the HS. The transcriptome analysis revealed that similar stress-related processes were differentially regulated despite the phenotypic differences between the cultivars. In total, 244 and 126 genes were found differentially expressed similarly in all five cultivars under HS at TFB and PFB stages, respectively. In addition, the global transcriptome response at both TFB and PFB stages was largely common. This common response to HS mainly corresponded to the upregulation of HS responsive genes, oxidative stress and hormonal pathways and the down-regulation of photosynthesis related genes. The existence of such a robust consensus molecular response over different genetic backgrounds has already been described to mild drought stress in developing Arabidopsis leaves (Clauw et al., 2015). These results not only strongly suggest that pollen tolerance to HS is linked to the ability of the plant to mitigate the HS effects through a higher expression of heat-response factors, but also by activating a common response for short term extreme HS and chronic HS exposure to moderate high temperatures.

4.5 Reproductive development related genes under chronic HS

In our dataset, we found genes corresponding to the regulation of reproductive process being enriched in the differentially expressed genes under HS in all cultivars. These genes showed a higher level of upregulation in pollen sensitive compared to pollen tolerant cultivars suggesting that this process is more affected in the pollen sensitive cultivars. By comparing our dataset with publicly available transcriptomics data describing genes related to tomato pollen- and tapetum development (Jeong et al., 2014; Liu et al., 2019), we found a few genes specifically expressed during anther development and in the microspore, being down-regulated under HS. For example, the strictosidine synthase gene (*SlSTR1, Solyc03g053130*), a stamen-specific gene triggering male-sterility when knocked-out (Du et al., 2020), was downregulated in all cultivars at TFB stage, suggesting that the decrease in its expression under HS could be related with altered anther development. However, we could not find a clear specific response distinguishing pollen sensitive versus pollen tolerant cultivars. A possible explanation is that, since we used the entire floral bud being a highly complex structure, our RNA-seq results highlighted the global response of floral buds to the HS, hiding the

specific response of the pollen and other reproductive cell types. New technologies such as spatial transcriptomics or single-cell RNAseq could be used to reveal the specific response of the different cell types making the floral buds.

4.6 HSFs and HSPs related genes under chronic HS

Under a short HS treatment, the *HSP* and *HSF* genes are strongly induced and play important roles to protect the plant. HSPs act by maintaining the homeostasis of the plant as they have a chaperone activity to limit the misfolding of proteins, but also to protect protein complexes like photosystem II (Vierling, 1991; Tsvetkova et al., 2002; Waters, 2013). Their expression is mainly controlled by the HS transcription factors HSFs. Our global transcriptome analysis showed that all cultivars respond to a chronic HS by maintaining an increased expression of numerous *HSF* and *HSP* genes and a stronger upregulation in sensitive- compared to tolerant cultivars. Several of the commonly up-regulated genes found in our transcriptome have been already described as important factors for HS tolerance in male reproductive tissues and, particularly, at the tetrad stage such as the HsfA2 and HsfA6b (Fragkostefanakis et al., 2015). Additionally, several HSPs (Solyc02g088610, Solyc03g007890, Solyc03g113930, Solyc03g115230, Solyc11g066100, Solyc11g071830), up-regulated in one or multiple cultivars under HS, were previously identified as belonging to heat response QTLs in small-fruited tomato population suggesting that they play a general role in HS response in many tomato cultivars (Bineau et al., 2021). Therefore, our results fall in line with previous observations regarding changes in HSPs and HSFs expression under HS, and suggest that depending on the cultivar considered, the level and diversity of HS related proteins induced may vary, potentially resulting in the different responses observed.

4.7 ROS- and hormone-related genes under chronic HS

The ability of a plant organ to either prevent or repair HS-induced oxidative damage is an important component of thermotolerance. This ability is mainly mediated by the induction of ROS scavengers, such as APX, under HS conditions (Suzuki and Mittler, 2006). In the present study, we found 259 DEGs related to the response to ROS including antioxidant and ROS detoxification enzymes (ascorbate peroxidase, catalases and superoxide dismutase) induced in response to HS in floral buds of all cultivars at both developmental stages. For example, the ascorbate peroxidase gene (*Solyc09g007270*) was found up-regulated in several cultivars at both PFB and TFB stages. This gene has already been reported to be responding to HS in tomato microspores (Frank et al., 2009) and could contribute to pollen development thermotolerance in tomato.

Plant hormones signaling pathways, such as abscisic acid, ethylene, salicylic acid and jasmonic acid were proposed to play an important role in plant thermotolerance (Kotak et al., 2007). In particular, salicylic acid has previously been shown to be important for anther and pollen thermotolerance in tomato (Jansma et al., 2022). In our dataset, GO related to hormonal responses including abscisic acid, salicylic acid and jasmonic acid were found enriched indicating that these pathways are affected by the HS in tomato floral buds and the underlying genes could be interesting targets for HS tolerance. The WRKY transcription factor family is regulated by hormonal signaling and plays important roles in plant stress response including HS (Cheng et al., 2021). In pepper, *CaWRKY40* has been associated with HS tolerance and its expression is regulated by SA, JA and ethylene (Yang et al., 2022). In tomato, another member of the WRKY family, SlWRKY3 has been demonstrated to be a positive regulator of thermotolerance that activates the expression of a range of HS responsive genes involved in ROS scavenging (Wang et al., 2023). The *WRKY* genes

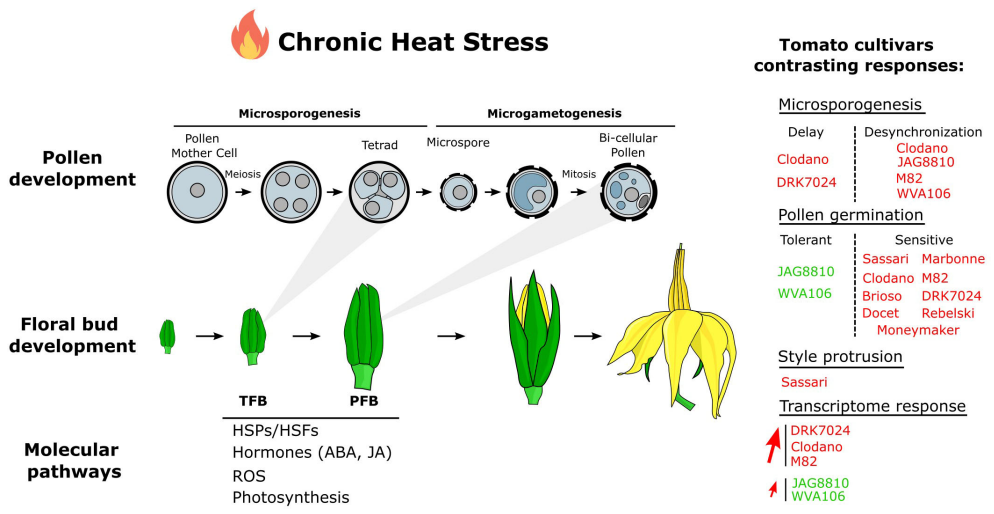

FIGURE 8
Model of tomato floral bud responses to a chronic HS.

identified as up-regulated under HS in our analysis could contribute to HS tolerance and are good candidates for future functional validation studies.

4.8 Conclusion

Our results showed that chronic HS is detrimental for pollen development in all tested tomato cultivars but the tolerance to HS widely varies between genotypes (Figure 8). The effects of global warming with the increase in heat waves magnitude and frequency on reproductive organ development thus need to be investigated using heat waves and chronic HS rather than extreme short high temperature-stress. The transcriptome dataset obtained in the present study revealed the complex response of tomato to heat and, especially the common response between five tomato cultivars. Among the up-regulated pathways, we could find a significant enrichment of GO terms related to the HS response but also to other functional categories related to photosynthesis, hormonal responses and reactive oxygen species demonstrating that tomato floral buds are commonly responding to HS through these pathways. Although the main HS response pathways were common in all cultivars studied, the number of differentially expressed genes and their expression level under HS was found highly variable depending on the genotype, suggesting that maintaining the level of transcript abundance could be important for HS tolerance. Investigating further this robust consensus response despite different phenotypic outputs under HS might be of great interest for agricultural applications.

Data availability statement

The datasets presented in this study can be found in online repositories. The names of the repository/repositories and accession number(s) can be found in the article/Supplementary Material.

Author contributions

NB: Conceptualization, Data curation, Formal Analysis, Investigation, Methodology, Writing – original draft, Writing – review & editing. RM-P: Data curation, Formal Analysis, Investigation, Writing – original draft, Writing – review & editing. ADa: Investigation, Writing – review & editing. EM: Data curation, Software, Writing – review & editing. MZ: Data curation, Software, Writing – review & editing. ADj: Data curation, Software, Writing – review & editing. MB: Conceptualization, Funding acquisition, Project administration, Resources, Supervision, Writing – review & editing. CC: Conceptualization, Funding acquisition, Project administration, Resources, Supervision, Writing – review & editing. FD: Conceptualization, Formal Analysis, Funding acquisition, Investigation, Methodology, Project administration, Supervision, Writing – review & editing. NG: Formal Analysis, Funding acquisition, Project administration, Supervision, Writing – original draft, Writing – review & editing. MH: Conceptualization, Formal Analysis, Funding acquisition, Investigation, Methodology, Project administration, Supervision, Writing – original draft, Writing – review & editing.

Funding

The author(s) declare financial support was received for the research, authorship, and/or publication of this article. Research was supported by the European Union's Horizon 2020 Research and Innovation Program through the TomGEM project under grant agreement Number 679796 and by the PRCI ANR project HEA2T (ANR-21-CE20-0028-01) coordinated by FD. R.M-P was supported by the Conselleria de Innovación, Universidades, Ciencia y Sociedad Digital de la Generalitat Valenciana under the grant APOSTD/2019/001.

Acknowledgments

We thank Isabelle Atienza for greenhouse management.

Conflict of interest

The authors declare that the research was conducted in the absence of any commercial or financial relationships that could be construed as a potential conflict of interest.

Publisher's note

Supplementary material

The Supplementary Material for this article can be found online at: https://www.frontiersin.org/articles/10.3389/fpls.2023.1278608/full#supplementary-material

References

Abdul-Baki, A. A., and Stommel, J. R. (1995). Pollen viability and fruit set of tomato genotypes under optimumand high-temperature regimes. *HortScience* 30 (1), 115–117. doi: 10.21273/HORTSCI.30.1.115

Adams, S. R., Cockshull, K. E., and Cave, C. R. J. (2001). Effect of temperature on the growth and development of tomato fruits. *Ann. Bot.* 88 (5), 869–877. doi: 10.1006/anbo.2001.1524

Almeida, J., Perez-Fons, L., and Fraser, P. D. (2021). A transcriptomic, metabolomic and cellular approach to the physiological adaptation of tomato fruit to high temperature. *Plant Cell Environ.* 44 (7), 2211–2229. doi: 10.1111/pce.13854

Alsamir, M., Ahmad, N. M., Keitel, C., Mahmood, T., and Trethowan, R. (2017). Identification of high-temperature tolerant and agronomically viable tomato (S. lycopersicum) genotypes from a diverse germplasm collection. *Adv. Crop Sci. Technol.* 05 (04). doi: 10.4172/2329-8863.1000299

Begcy, K., Nosenko, T., Zhou, L. Z., Fragner, L., Weckwerth, W., and Dresselhaus, T. (2019). Male sterility in maize after transient heat stress during the tetrad stage of pollen development. *Plant Physiol.* 181 (2), 683–700. doi: 10.1104/pp.19.00707

Bheemanahalli, R., et al. (2019). Quantifying the impact of heat stress on pollen germination, seed set, and grain filling in spring wheat. *Crop Sci.* 59 (2), 684–696. doi: 10.2135/cropsci2018.05.0292

Bineau, E., Diouf, I., Carretero, Y., Duboscq, R., Bitton, F., Djari, A., et al. (2021). Genetic diversity of tomato response to heat stress at the QTL and transcriptome levels. *Plant J.* 107 (4), 1213–1227. doi: 10.1111/tpj.15379

Bita, C. E., Zenoni, S., Vriezen, W. H., Mariani, C., Pezzotti, M., and Gerats, T. (2011). Temperature stress differentially modulates transcription in meiotic anthers of heat-tolerant and heat-sensitive tomato plants. *BMC Genomics* 12, 384. doi: 10.1186/1471-2164-12-384

Bohnert, H. J., Gong, Q., Li, P., and Ma, S. (2006). Unraveling abiotic stress tolerance mechanisms - Getting genomics going. *Curr. Opin. Plant Biol.* 9 (2), 180–188. doi: 10.1016/j.pbi.2006.01.003

Brukhin, V., Hernould, M., Gonzalez, N., Chevalier, C., and Mouras, A. (2003). Flower development schedule in tomato Lycopersicon esculentum cv Sweet Cherry. *Sex Plant Reprod.* 15 (6), 311–320. doi: 10.1007/s00497-003-0167-7

Chaturvedi, P., Ischebeck, T., Egelhofer, V., Lichtscheidl, I., and Weckwerth, W. (2013). Cell-specific analysis of the tomato pollen proteome from pollen mother cell to mature pollen provides evidence for developmental priming. *J. Proteome Res.* 12 (11), 4892–4903. doi: 10.1021/pr400197p

Chen, L., Song, Y., Li, S., Zhang, L., Zou, C., and Yu, D. (2012). The role of WRKY transcription factors in plant abiotic stresses. *Biochim. Biophys. Acta - Gene Regul. Mech.* 1819 (2), 120–128. doi: 10.1016/j.bbagrm.2011.09.002

Chen, X., Shi, L., Chen, Y., Zhu, L., Zhang, D., Xiao, S., et al. (2019). Arabidopsis HSP70-16 is required for flower opening under normal or mild heat stress temperatures. *Plant Cell Environ.* 42 (4), 1190–1204. doi: 10.1111/pce.13480

Cheng, Z., Luan, Y., Meng, J., Sun, J., Tao, J., and Zhao, D. (2021). WRKY transcription factor response to high-temperature stress. *Plants* 10 (10), 2211. doi: 10.3390/plants10102211

Clauw, P., Coppens, F., De Beuf, K., Dhondt, S., Van Daele, T., Maleux, K., et al. (2015). Leaf responses to mild drought stress in natural variants of Arabidopsis. *Plant Physiol.* 167 (3), 800–816. doi: 10.1104/pp.114.254284

Coast, O., Murdoch, A. J., Ellis, R. H., Hay, F. R., and Jagadish, K. S. V. (2016). Resilience of rice (Oryza spp.) pollen germination and tube growth to temperature stress. *Plant Cell Environ.* 39 (1), 26–37. doi: 10.1111/pce.12475

De Jaeger-Braet, J., Krause, L., Buchholz, A., and Schnittger, A. (2021). Heat stress reveals a specialized variant of the pachytene checkpoint in meiosis of Arabidopsis thaliana. *Plant Cell* 34 (1), 433–454. doi: 10.1093/plcell/koab257

De Storme, N., and Geelen, D. (2014). The impact of environmental stress on male reproductive development in plants: biological processes and molecular mechanisms. *Plant Cell Environ.* 37 (1), 1–18.

De Storme, N., and Geelen, D. (2020). High temperatures alter cross-over distribution and induce male meiotic restitution in Arabidopsis thaliana. *Commun. Biol.* 3 (1), 1–15. doi: 10.1038/s42003-020-0897-1

Djanaguiraman, M., Perumal, R., Jagadish, S. V. K., Ciampitti, I. A., Welti, R., and Prasad, P. V. V. (2018). Sensitivity of sorghum pollen and pistil to high-temperature stress. *Plant Cell Environ.* 41 (5), 1065–1082. doi: 10.1111/pce.13089

Driedonks, N., Rieu, I., and Vriezen, W. H. (2016). Breeding for plant heat tolerance at vegetative and reproductive stages. *Plant Reprod.* 29 (1–2), 67–79. doi: 10.1007/s00497-016-0275-9

Du, M., Zhou, K., Liu, Y., Deng, L., Zhang, X., Lin, L., et al. (2020). A biotechnology-based male-sterility system for hybrid seed production in tomato. *Plant J.* 102 (5), 1090–1100. doi: 10.1111/tpj.14678

Essemine, J., Ammar, S., and Bouzid, S. (2010). Impact of heat stress on germination and growth in higher plants: Physiological, biochemical and molecular repercussions and mechanisms of defence. *J. Biol. Sci.* 10 (6), 565–572. doi: 10.3923/jbs.2010.565.572

Fernandez-Muñoz, R., and Cuartero, J. (1991). Effects of temperature and irradiance on stigma exsertion, ovule viability and embryo development in tomato. *J. Hortic. Sci.* 66 (4), 395–401. doi: 10.1080/00221589.1991.11516167

Firon, N., Shaked, R., Peet, M. M., Pharr, D. M., Zamski, E., Rosenfeld, K., et al. (2006). Pollen grains of heat tolerant tomato cultivars retain higher carbohydrate concentration under heat stress conditions. *Scientia Hortic.* 109 (3), 212–217. doi: 10.1016/j.scienta.2006.03.007

Fragkostefanakis, S., Simm, S., Paul, P., Bublak, D., Scharf, K. D., and Schleiff, E. (2015). Chaperone network composition in Solanum lycopersicum explored by transcriptome profiling and microarray meta-analysis. *Plant Cell Environ.* 38 (4), 693–709. doi: 10.1111/pce.12426

Frank, G., Pressman, E., Ophir, R., Althan, L., Shaked, R., Freedman, M., et al. (2009). Transcriptional profiling of maturing tomato (Solanum lycopersicum L.) microspores reveals the involvement of heat shock proteins, ROS scavengers, hormones, and sugars in the heat stress response. *J. Exp. Bot.* 60 (13), 3891–3908. doi: 10.1093/jxb/erp234

Gentile, A. G., Gallagher, K. J., and Santner, Z. (1971). Effect of some formulated insecticides on pollen germination in tomato and petunia1. *J. Econ. Entomol.* 64 (4), 916–919. doi: 10.1093/jee/64.4.916

Giorno, F., Wolters-Arts, M., Mariani, C., and Rieu, I. (2013). Ensuring reproduction at high temperatures: The heat stress response during anther and pollen development. *Plants* 2 (3), 489–506. doi: 10.3390/plants2030489

Gökdemir, G., Seçgin, Z., Uluisik, S., and Kavas, M. (2022). CRISPR/Cas9 knock-out of SlPHD_MS1 (Solyc04g008420) gene results in complete male sterility in tomato. *Plant Growth Regul.* 98 (2), 329–341. doi: 10.1007/s10725-022-00869-y

Gómez, J. F., Talle, B., and Wilson, Z. A. (2015). Anther and pollen development: A conserved developmental pathway. *J. Integr. Plant Biol.* 57 (11), 876–891. doi: 10.1111/jipb.12425

Gonzalo, M. J., Nájera, I., Baixauli, C., Gil, D., Montoro, T., Soriano, V., et al. (2021). Identification of tomato accessions as source of new genes for improving heat tolerance: from controlled experiments to field. *BMC Plant Biol.* 21 (1), 1–28. doi: 10.1186/s12870-021-03104-4

Han, S.-H., Kim, J. Y., Lee, J.-H., and Park, C.-M. (2021). Safeguarding genome integrity under heat stress in plants. *J. Exp. Bot.* 72 (21), 7421–7435. doi: 10.1093/jxb/erab355

Hulsen, T., de Vlieg, J., and Alkema, W. (2008). BioVenn - A web application for the comparison and visualization of biological lists using area-proportional Venn diagrams. *BMC Genomics* 9, 1–6. doi: 10.1186/1471-2164-9-488

Huner, N. P. A., and VAN Huystee, R. B. (1982). Pollen germination and chilling sensitivity in two tomato cultivars of differing sensitivity to cool night temperature. *Can. J. Plant Sci.* 62 (3), 765–770. doi: 10.4141/cjps82-110

IPCC. (2014). Climate change 2014: Synthesis report. Contribution of working groups I, II and III to the fifth assessment report of the Intergovernmental Panel on Climate Change. *Core Writing Team*, Eds. R. K. Pachauri and L. A. Meyer (Geneva: IPCC). Available at: https://www.ipcc.ch/report/ar5/syr/.

Jagadish, S. V. K., Way, D. A., and Sharkey, T. D. (2021). Plant heat stress: Concepts directing future research. *Plant Cell Environ.* 44 (7), 1992–2005. doi: 10.1111/pce.14050

Janni, M., Gullì, M., Maestri, E., Marmiroli, M., Valliyodan, B., Nguyen, H. T., et al. (2020). Molecular and genetic bases of heat stress responses in crop plants and breeding for increased resilience and productivity. *J. Exp. Bot.* 71 (13), 3780–3802. doi: 10.1093/jxb/eraa034

Jansma, S. Y., Sergeeva, L. I., Tikunov, Y. M., Kohlen, W., Ligterink, W., and Rieu, I. (2022). Low salicylic acid level improves pollen development under long-term mild heat conditions in tomato. *Front. Plant Sci.* 13 (April), 1–11. doi: 10.3389/fpls.2022.828743

Jayakodi, M., Lee, S. C., and Yang, T. J. (2019). Comparative transcriptome analysis of heat stress responsiveness between two contrasting ginseng cultivars. *J. Ginseng Res.* 43 (4), 572–579. doi: 10.1016/j.jgr.2018.05.007

Jeong, H. J., Kang, J. H., Zhao, M., Kwon, J. K., Choi, H. S., Bae, J. H., et al. (2014). Tomato Male sterile 1035 is essential for pollen development and meiosis in anthers. *J. Exp. Bot.* 65 (22), 6693–6709. doi: 10.1093/jxb/eru389

Jiang, Y., Lahlali, R., Karunakaran, C., Kumar, S., Davis, A. R., and Bueckert, R. A. (2015). Seed set, pollen morphology and pollen surface composition response to heat stress in field pea. *Plant Cell Environ.* 38 (11), 2387–2397. doi: 10.1111/pce.12589

Jiang, X., Lubini, G., Hernandes-Lopes, J., Rijnsburger, K., Veltkamp, V., De Maagd, R. A., et al. (2022). FRUITFULL-like genes regulate flowering time and inflorescence architecture in tomato. *Plant Cell* 34 (3), 1002–1019. doi: 10.1093/plcell/koab298

Kakani, V. G., Prasad, P. V. V., Craufurd, P. Q., and Wheeler, T. R. (2002). Response of in *vitro* pollen germination and pollen tube growth of groundnut (Arachis hypogaea L.) genotypes to temperature. *Plant Cell Environ.* 25 (12), 1651–1661. doi: 10.1046/j.1365-3040.2002.00943.x

Kantidze, O. L., Velichko, A. K., Luzhin, A. V, and Razin, S. V. (2016). Heat stress-induced DNA damage. *Acta Naturae* 8 (29), 75–78. doi: 10.32607/20758251-2016-8-2-75-78

Keller, M., Simm, S., Bokszczanin, K. L., Bostan, H., Bovy, A., Chaturvedi, P., et al. (2018). The coupling of transcriptome and proteome adaptation during development and heat stress response of tomato pollen. *BMC Genomics* 19 (1), 1–20. doi: 10.1186/s12864-018-4824-5

Kotak, S., Larkindale, J., Lee, U., von Koskull-Döring, P., Vierling, E., and Scharf, K. D. (2007). Complexity of the heat stress response in plants. *Curr. Opin. Plant Biol.* 10 (3), 310–316. doi: 10.1016/j.pbi.2007.04.011

Lau, N. C., and Nath, M. J. (2012). A model study of heat waves over North America: Meteorological aspects and projections for the twenty-first century. *J. Climate* 25 (14), 4761–4764. doi: 10.1175/JCLI-D-11-00575.1

Li, Z., Zhang, L., Wang, A., Xu, X., and Li, J. (2013). Ectopic overexpression of slHsfA3, a heat stress transcription factor from tomato, confers increased thermotolerance and salt hypersensitivity in germination in transgenic arabidopsis. *PloS One* 8 (1). doi: 10.1371/journal.pone.0054880

Liu, X., Yang, M., Liu, X., Wei, K., Cao, X., Wang, X., et al. (2019). A putative bHLH transcription factor is a candidate gene for male sterile 32, a locus affecting pollen and tapetum development in tomato. *Horticulture Res.* 6 (1). doi: 10.1038/s41438-019-0170-2

Love, M. I., Huber, W., and Anders, S. (2014). Moderated estimation of fold change and dispersion for RNA-seq data with DESeq2. *Genome Biol.* 15, 550. doi: 10.1186/s13059-014-0550-8

Magnard, J. L., Yang, M., Chen, Y. C.S., Leary, M., and McCormick, S. (2001). The Arabidopsis gene tardy asynchronous meiosis is required for the normal pace and synchrony of cell division during male meiosis. *Plant Physiol.* 127 (3), 1157–1166. doi: 10.1104/pp.010473

Masoomi-Aladizgeh, F., Najeeb, U., Hamzelou, S., Pascovici, D., Amirkhani, A., Tan, D. K. Y., et al. (2021). Pollen development in cotton (Gossypium hirsutum) is highly sensitive to heat exposure during the tetrad stage. *Plant Cell Environ.* 44 (7), 2150–2166. doi: 10.1111/pce.13908

Maza, E. (2016). In Papyro comparison of TMM (edgeR), RLE (DESeq2), and MRN normalization methods for a simple two-conditions-without-replicates RNA-Seq experimental design. *Front. Genet.* 7, 164.

Maza, E., Frasse, P., Senin, P., Bouzayen, M., and Zouine, M. (2013). Comparison of normalization methods for differential gene expression analysis in RNA-Seq experiments: a matter of relative size of studied transcriptomes. *Commun. Integr. Biol.* 6 (6), e25849.

Medina, E., Kim, S. H., Yun, M., and Choi, W. G. (2021). Recapitulation of the function and role of ros generated in response to heat stress in plants. *Plants* 10 (2), 1–13. doi: 10.3390/plants10020371

Molina, M. O., Sánchez, E., and Gutiérrez, C. (2020). Future heat waves over the Mediterranean from an Euro-CORDEX regional climate model ensemble. *Sci. Rep.* 10 (1), 1–10. doi: 10.1038/s41598-020-65663-0

Moore, C. E., Meacham-Hensold, K., Lemonnier, P., Slattery, R. A., Benjamin, C., Bernacchi, C. J., et al. (2021). The effect of increasing temperature on crop photosynthesis: From enzymes to ecosystems. *J. Exp. Bot.* 72 (8), 2822–2844. doi: 10.1093/jxb/erab090

Müller, F., Xu, J., Kristensen, L., Wolters-Arts, M., De Groot, P. F. M., Jansma, S. Y., et al. (2016). High-temperature-induced defects in tomato (Solanum lycopersicum) anther and pollen development are associated with reduced expression of B-class floral patterning genes. *PloS One* 11 (12), 1–14. doi: 10.1371/journal.pone.0167614

Müller, F., and Rieu, I. (2016). Acclimation to high temperature during pollen development. *Plant Reprod.* 29 (1–2), 107–118. doi: 10.1007/s00497-016-0282-x

Ning, Y., Liu, Q., Wang, C., Qin, E., Wu, Z., Wang, M., et al. (2021). Heat stress interferes with formation of double-strand breaks and homolog synapsis. *Plant Physiol.* 185 (4), 1783–1797. doi: 10.1093/plphys/kiab012

Ohama, N., Sato, H., Shinozaki, K., and Yamaguchi-Shinozaki, K. (2017). Transcriptional regulatory network of plant heat stress response. *Trends Plant Sci.* 22 (1), 53–65. doi: 10.1016/j.tplants.2016.08.015

Pan, C., Yang, D., Zhao, X., Jiao, C., Yan, Y., Lamin-Samu, A. T., et al. (2019). Tomato stigma exsertion induced by high temperature is associated with the jasmonate signalling pathway. *Plant Cell Environ.* 42 (4), 1205–1221. doi: 10.1111/pce.13444

Paupière, M. J., van Haperen, P., Rieu, I., Visser, R. G., Tikunov, Y. M., and Bovy, A. G. (2017). Screening for pollen tolerance to high temperatures in tomato. *Euphytica* 213, 1–8. doi: 10.1007/s10681-017-1927-z

Pecinka, A., and Mittelsten Scheid, O. (2012). Stress-induced chromatin changes: A critical view on their heritability. *Plant Cell Physiol.* 53 (5), 801–808. doi: 10.1093/pcp/pcs044

Pécrix, Y., Rallo, G., Folzer, H., Cigna, M., Gudin, S., and Le Bris, M. (2011). Polyploidization mechanisms: Temperature environment can induce diploid gamete formation in Rosa sp. *J. Exp. Bot.* 62 (10), 3587–3597. doi: 10.1093/jxb/err052

Pressman, E., Peet, M. M., and Pharr, D. M. (2002). The effect of heat stress on tomato pollen characteristics is associated with changes in carbohydrate concentration in the developing anthers. *Ann. Bot.* 90 (5), 631–636. doi: 10.1093/aob/mcf240

Puchtler, H., Sweat Waldrop, F., Conner, H. M., and Terry, M. S. (1968). Carnoy fixation: practical and theoretical considerations. *Histochemie* 16, 361–371.

Qu, A. L., Ding, Y. F., Jiang, Q., and Zhu, C. (2013). Molecular mechanisms of the plant heat stress response. *Biochem. Biophys. Res. Commun.* 432 (2), 203–207. doi: 10.1016/j.bbrc.2013.01.104

Raja, M. M., Vijayalakshmi, G., Naik, M. L., Basha, P. O., Sergeant, K., Hausman, J. F., et al. (2019). Pollen development and function under heat stress: from effects to responses. *Acta Physiologiae Plantarum* 41 (4), 1–20. doi: 10.1007/s11738-019-2835-8

Rieu, I., Twell, D., and Firon, N. (2017). Pollen development at high temperature: From acclimation to collapse. *Plant Physiol.* 173 (4), 1967–1976. doi: 10.1104/pp.16.01644

Saidi, Y., Finka, A., and Goloubinoff, P. (2011). Heat perception and signalling in plants: A tortuous path to thermotolerance. *New Phytol.* 190 (3), 556–565. doi: 10.1111/j.1469-8137.2010.03571.x

Sato, S., Peet, M. M., and Thomas, J. F. (2000). Physiological factors limit fruit set of tomato (Lycopersicon esculentum Mill.) under chronic, mild heat stress. *Plant Cell Environ.* 23 (7), 719–726. doi: 10.1046/j.1365-3040.2000.00589.x

Savchenko, G. E., Klyuchareva, E. A., Abramchik, L. M., and Serdyuchenko, E. V. (2002). Effect of periodic heat shock on the inner membrane system of etioplasts. *Russian J. Plant Physiol.* 49 (3), 349–359. doi: 10.1023/A:1015592902659

Schleiff, E., and Becker, T. (2011). Common ground for protein translocation: Access control for mitochondria and chloroplasts. *Nat. Rev. Mol. Cell Biol.* 12 (1), 48–59. doi: 10.1038/nrm3027

Shen, H., Zhong, X., Zhao, F., Wang, Y., Yan, B., Li, Q., et al. (2015). Overexpression of receptor-like kinase ERECTA improves thermotolerance in rice and tomato. *Nat. Biotechnol.* 33 (9), 996–1003. doi: 10.1038/nbt.3321

Sherzod, R., Yang, E. Y., Cho, M. C., Chae, S. Y., and Chae, W. B. (2020). Physiological traits associated with high temperature tolerance differ by fruit types and sizes in tomato (Solanum lycopersicum L.). *Horticulture Environ. Biotechnol.* 61 (5), 837–847. doi: 10.1007/s13580-020-00280-4

Sita, K., Sehgal, A., Hanumantharao, B., Nair, R. M., Vara Prasad, P. V., Kumar, S., et al. (2017). Food legumes and rising temperatures: Effects, adaptive functional mechanisms specific to reproductive growth stage and strategies to improve heat tolerance. *Front. Plant Sci.* 8 (October), 1–30. doi: 10.3389/fpls.2017.01658

Spicher, L., Glauser, G., and Kessler, F. (2016). Lipid antioxidant and galactolipid remodeling under temperature stress in tomato plants. *Front. Plant Sci.* 7 (FEB2016). doi: 10.3389/fpls.2016.00167

Stillman, J. H. (2019). Heat waves, the new normal: Summertime temperature extremes will impact animals, ecosystems, and human communities. *Physiology* 34 (2), 86–100. doi: 10.1152/physiol.00040.2018

Sunoj, V. S. J., Somayanda, I. M., Chiluwal, A., Perumal, R., Prasad, P. V. V., and Jagadish, S. V. K. (2017). Resilience of pollen and post-flowering response in diverse sorghum genotypes exposed to heat stress under field conditions. *Crop Sci.* 57 (3), 1658–1669. doi: 10.2135/cropsci2016.08.0706

Suzuki, N., and Mittler, R. (2006). Reactive oxygen species and temperature stresses: A delicate balance between signaling and destruction. *Physiologia Plantarum* 126 (1), 45–51. doi: 10.1111/j.0031-9317.2005.00582.x

Thakur, P., Kumar, S., Malik, J. A., Berger, J. D., and Nayyar, H. (2010). Cold stress effects on reproductive development in grain crops: an overview. *Environ. Exp. Bot.* 67 (3), 429–443.

Tripathi, A., Tripathi, D. K., Chauhan, D. K., Kumar, N., and Singh, G. S. (2016). Paradigms of climate change impacts on some major food sources of the world: A review on current knowledge and future prospects. *Agriculture Ecosyst. Environ.* 216, 356–373. doi: 10.1016/j.agee.2015.09.034

Tsvetkova, N. M., Horváth, I., Török, Z., Wolkers, W. F., Balogi, Z., Shigapova, N., et al. (2002). Small heat-shock proteins regulate membrane lipid polymorphism. *Proc. Natl. Acad. Sci. U.S.A.* 99 (21), 13504–13509. doi: 10.1073/pnas.192468399

Van Bel, M., Silvestri, F., Weitz, E. M., Kreft, L., Botzki, A., Coppens, F., et al. (2022). PLAZA 5.0: Extending the scope and power of comparative and functional genomics in plants. *Nucleic Acids Res.* 50 (D1), D1468–D1474. doi: 10.1093/nar/gkab1024

Vierling, E. (1991). The roles of heat shock proteins in plants. *Annu. Rev. Plant Physiol. Plant Mol. Biol.* 42, 579–620. doi: 10.1146/annurev.pp.42.060191.003051

von Koskull-Döring, P., Scharf, K. D., and Nover, L. (2007). The diversity of plant heat stress transcription factors. *Trends Plant Sci.* 12 (10), 452–457. doi: 10.1016/j.tplants.2007.08.014

Wahid, A., Gelani, S., Ashraf, M., and Foolad, M. R. (2007). Heat tolerance in plants: An overview. *Environ. Exp. Bot.* 61 (3), 199–223. doi: 10.1016/j.envexpbot.2007.05.011

Wan, X. L., Yang, J., Li, X. B., Zhou, Q., Guo, C., Bao, M. Z., et al. (2016). Over-expression of pmHSP17.9 in transgenic arabidopsis thaliana confers thermotolerance. *Plant Mol. Biol. Rep.* 34 (5), 899–908. doi: 10.1007/s11105-016-0974-2

Wang, Y., Gai, W., Yuan, L., Shang, L., Li, F., Gong, Z., et al. (2023). Heat-inducible SlWRKY3 confers thermotolerance by activating the SlGRXS1 gene cluster in tomato. *Hortic. Plant J.* doi: 10.1016/j.hpj.2022.12.006

Waters, E. R. (2013). The evolution, function, structure, and expression of the plant sHSPs. *J. Exp. Bot.* 64 (2), 391–403. doi: 10.1093/jxb/ers355

Wu, Q., Lin, J., Liu, J. Z., Wang, X., Lim, W., Oh, M., et al. (2012). Ectopic expression of Arabidopsis glutaredoxin AtGRXS17 enhances thermotolerance in tomato. *Plant Biotechnol. J.* 10 (8), 945–955. doi: 10.1111/j.1467-7652.2012.00723.x

Wu, Q., Yang, J., Cheng, N., Hirschi, K. D., White, F. F., and Park, S. (2017). Glutaredoxins in plant development, abiotic stress response, and iron homeostasis: From model organisms to crops. *Environ. Exp. Bot.* 139 (February), 91–98. doi: 10.1016/j.envexpbot.2017.04.007

Xin, H., Zhang, H., Chen, L., Li, X., Lian, Q., Yuan, X., et al. (2010). Cloning and characterization of HsfA2 from Lily (Lilium longiflorum). *Plant Cell Rep.* 29 (8), 875–885. doi: 10.1007/s00299-010-0873-1

Xue, G. P., Drenth, J., and McIntyre, C. L. (2015). TaHsfA6f is a transcriptional activator that regulates a suite of heat stress protection genes in wheat (Triticum aestivum L.) including previously unknown Hsf targets. *J. Exp. Bot.* 66 (3), 1025–1039. doi: 10.1093/jxb/eru462

Yang, S., Cai, W., Shen, L., Cao, J., Liu, C., Hu, J., et al. (2022). A CaCDPK29–CaWRKY27b module promotes CaWRKY40-mediated thermotolerance and immunity to Ralstonia solanacearum in pepper. *New Phytol.* 233 (4), 1843–1863. doi: 10.1111/nph.17891

Yokotani, N., Ichikawa, T., Kondou, Y., Matsui, M., Hirochika, H., Iwabuchi, M., et al. (2008). Expression of rice heat stress transcription factor OsHsfA2e enhances tolerance to environmental stresses in transgenic Arabidopsis. *Planta* 227 (5), 957–967. doi: 10.1007/s00425-007-0670-4

Zhu, B., Ye, C., Lü, H., Chen, X., Chai, G., Chen, J., et al. (2006). Identification and characterization of a novel heat shock transcription factor gene, GmHsfA1, in soybeans (Glycine max). *J. Plant Res.* 119 (3), 247–256. doi: 10.1007/s10265-006-0267-1

Zinn, K. E., Tunc-Ozdemir, M., and Harper, J. F. (2010). Temperature stress and plant sexual reproduction: Uncovering the weakest links. *J. Exp. Bot.* 61 (7), 1959–1968. doi: 10.1093/jxb/erq053

Zouine, M., Maza, E., Djari, A., Lauvernier, M., Frasse, P., Smouni, A., et al. (2017). TomExpress, a unified tomato RNA-Seq platform for visualization of expression data, clustering and correlation networks. *Plant J.* 92 (4), 727–735. doi: 10.1111/tpj.13711

frontiers | Frontiers in Plant Science

TYPE Review
PUBLISHED 08 December 2023
DOI 10.3389/fpls.2023.1326689

OPEN ACCESS

EDITED BY
Antonio Granell,
Spanish National Research Council (CSIC), Spain

REVIEWED BY
José L. Rambla,
University of Jaume I, Spain
Gloria María López Casado,
Spanish National Research Council (CSIC), Spain

*CORRESPONDENCE
Muriel Quinet
muriel.quinet@uclouvain.be

RECEIVED 23 October 2023
ACCEPTED 27 November 2023
PUBLISHED 08 December 2023

CITATION
Moreels P, Bigot S, Defalque C, Correa F, Martinez J-P, Lutts S and Quinet M (2023) Intra- and inter-specific reproductive barriers in the tomato clade. *Front. Plant Sci.* 14:1326689. doi: 10.3389/fpls.2023.1326689

Intra- and inter-specific reproductive barriers in the tomato clade

Pauline Moreels[1], Servane Bigot[1], Corentin Defalque[1], Francisco Correa[2], Juan-Pablo Martinez[2], Stanley Lutts[1] and Muriel Quinet[1]*

[1]Groupe de Recherche en Physiologie végétale, Earth and Life Institute-Agronomy, Université catholique de Louvain, Louvain-la-Neuve, Belgium, [2]Instituto de Investigaciones Agropecuarias (INIA-Rayentué), Rengo, Chile

Tomato (*Solanum lycopersicum* L.) domestication and later introduction into Europe resulted in a genetic bottleneck that reduced genetic variation. Crosses with other wild tomato species from the *Lycopersicon* clade can be used to increase genetic diversity and improve important agronomic traits such as stress tolerance. However, many species in the *Lycopersicon* clade have intraspecific and interspecific incompatibility, such as gametophytic self-incompatibility and unilateral incompatibility. In this review, we provide an overview of the known incompatibility barriers in *Lycopersicon*. We begin by addressing the general mechanisms self-incompatibility, as well as more specific mechanisms in the Rosaceae, Papaveraceae, and Solanaceae. Incompatibility in the *Lycopersicon* clade is discussed, including loss of self-incompatibility, species exhibiting only self-incompatibility and species presenting both self-compatibility and self-incompatibility. We summarize unilateral incompatibility in general and specifically in *Lycopersicon*, with details on the 'self-compatible x self-incompatible' rule, implications of self-incompatibility in unilateral incompatibility and self-incompatibility-independent pathways of unilateral incompatibility. Finally, we discuss advances in the understanding of compatibility barriers and their implications for tomato breeding.

KEYWORDS

tomato, self-incompatibility, *Lycopersicon*, unilateral incompatibility, S-RNase, solanaceae

1 Introduction

Tomato (*Solanum lycopersicum* L.) is cultivated worldwide and is the second largest horticultural crop after potato (*Solanum tuberosum* L.) (Fernandes et al., 2018). Both species belong to the Solanaceae family, which also comprises other important crops such as eggplant (*Solanum melongena* L.) and pepper (*Capsicum annuum* L.). In 2021, tomato production reached approximately 189 million tons over 5.17 million ha of cultivated area (FAOSTAT, 2023). The main global tomato producers include China, India, Turkey, the

USA, Italy, and Egypt. Tomato yield differs greatly among countries, ranging from 1.47 tons per ha in Somalia to 476 tons per ha in the Netherlands (FAOSTAT, 2023). Tomatoes can be eaten raw or processed into sauces, pastes, soups, juice, or powdered concentrate (Gerszberg et al., 2015).

The tomato was first introduced into Europe and Asia from South America in the 16th century and later to Africa, and gained popularity as a crop during the 19th century (Mazzucato et al., 2010). Domestication and subsequent import of tomato led to a genetic bottleneck in the species. According to Miller and Tanksley (1990), the tomato genome contains less than 5% of the genetic diversity observed in its wild relatives. There are a total of 12 wild tomato species, which, along with *S. lycopersicum*, form the *Lycopersicon* clade (Peralta et al., 2008).

Tomato is sensitive to biotic and abiotic stresses. Since the 1930s, biotic and abiotic stress tolerance genes from wild species have been used to improve tomato stress tolerance (Verlaan et al., 2013; Zhang et al., 2017). At present, introgression of genes from wild relatives remains the most effective method to improve tomato traits through breeding (Fischer et al., 2011; Zsögön et al., 2018; Calafiore et al., 2019; Vitale et al., 2023). One of the most well-studied wild tomato species for introgression is *Solanum pennellii*, due to its resistance to various stresses and its strong capacity to hybridize with *S. lycopersicum* (Brog et al., 2019). Other wild tomato species have also been used similarly. For instance, *Solanum chilense* has been used to introgress resistance to Tomato yellow leaf curl virus (Verlaan et al., 2011; Dhaliwal et al., 2020), *Solanum pimpinellifolium* for salt tolerance and resistance to spider mite and late blight (Salinas et al., 2013; Chen et al., 2014; Rao et al., 2015; Bonarota et al., 2022), *Solanum habrochaites* for insect pest resistance as well as drought tolerance (Frelichowski and Juvik, 2001; Arms et al., 2015) and *Solanum neorickii* for powdery mildew resistance (Bai et al., 2003).

A major obstacle to using wild relatives in tomato breeding is the presence of intra- and interspecific reproductive barriers. Intraspecific barriers, known as self-incompatibility (SI), prevent self-fertilization and maintain genetic diversity in species by promoting outcrossing (Kaothien-Nakayama et al., 2010; Fujii et al., 2016; Broz and Bedinger, 2021; Chakraborty et al., 2023). SI barriers rely on self and non-self-recognition mechanisms between pollen and pistil, followed by inhibition of pollen tube development. Self and non-self-recognition is usually controlled by the *S*-locus, which has multiple S-haplotypes (Takayama and Isogai, 2005). Each S-haplotype bears specific male and female S-determinants, which enable discrimination between self and non-self (Fujii et al., 2016).

Angiosperms have two types of SI: gametophytic self-incompatibility (GSI), observed most notably in Solanaceae, and sporophytic self-incompatibility (SSI), which is present in Brassicaceae (Fujii et al., 2016). Wild tomato species can be self-compatible (as in *Solanum neorickii*), self-incompatible (as in *Solanum chilense*) or both depending on the population (as in *Solanum pennellii*), while *Solanum lycopersicum* is self-compatible (Peralta et al., 2008; Grandillo et al., 2011).

Interspecific barriers limit interspecific crosses in communities with co-flowering plants (Tovar-Méndez et al., 2017). In the *Lycopersicon* clade, interspecific barriers manifest as unilateral incompatibility, whereby pollen from one species is rejected from the pistil of another species, but the opposite cross is accepted. Specifically, it usually follows the SC x SI rule: pollen from self-compatible (SC) species will be rejected on pistils of self-incompatible (SI) species (Baek et al., 2015; Fujii et al., 2016; Tovar-Méndez et al., 2017).

In this review, we synthesize current knowledge about reproductive barriers in the tomato clade. First, we address SI: general GSI mechanisms, and more specific GSI mechanisms in Rosaceae, Papaveraceae and Solanaceae with a focus on the Collaborative Non-Self Recognition Model in Solanaceae. Then, we discuss incompatibility in tomato species, including mechanisms underlying the loss of SI and acquisition of SC. Interspecific barriers and unilateral incompatibility in general and specifically in the *Lycopersicon* clade will be addressed, with details regarding the SI x SC rule, implications of SI in unilateral incompatibility, and SI-independent pathways of unilateral incompatibility. Finally, we discuss advances in our understanding of compatibility barriers, as well as their implications for tomato breeding.

2 Self-incompatibility

2.1 Gametophytic and sporophytic self-incompatibility

Self-incompatibility (SI) is a mechanism in angiosperms that prevents self-fertilization, thereby maintaining genetic diversity (Takayama and Isogai, 2005). Specifically, SI is defined as the incapacity of a sexually capable hermaphroditic seed-plant to generate zygotes through self-pollination (Nettancourt, 2001). SI is present in roughly 40% of flowering plant species and in at least 100 families (Igic et al., 2008). The SI response depends on pollen–pistil self- or non-self-recognition, followed by inhibition of pollen tube development for self pollen. In most species exhibiting SI, pollen–pistil recognition is controlled by a single, highly polymorphic S-locus. The S-locus contains at least two transcriptional units: the male determinant and the female determinant. There are different S-alleles of the S-locus, and an incompatibility response occurs when both pistil and pollen harbor the same S-allele (Takayama and Isogai, 2005).

Angiosperms have two types of SI: sporophytic SI (SSI) and gametophytic SI (GSI) (Figure 1). The two mechanisms differ in the way the pollen SI phenotype is regulated. In GSI, the pollen SI phenotype is determined by its own haploid genome, while in SSI, the pollen SI phenotype is determined by the diploid genomes of the parental donor tissues. This means that in SSI, if the emitting pollen-producing plant has at least one S-allele in common with the receiving plant, all pollen from the emitting plant will be rejected. In contrast, in GSI, pollen will only be rejected if its haploid S-allele is the same as one of the two pistil S-alleles (Takayama and Isogai, 2005; Fujii et al., 2016). In SSI, recognition occurs in the stigma, leading to pollen hydration and germination through the style. Lack of recognition prevents pollen hydration (Fujii et al., 2016; Broz and Bedinger, 2021; Chakraborty et al., 2023; Wang and Filatov, 2023). In Rosaceae, Solanaceae and Plantaginaceae GSI, interaction between male and female SI determinants occurs in the style (Fujii et al., 2016; Broz and Bedinger, 2021; Wang and Filatov, 2023).

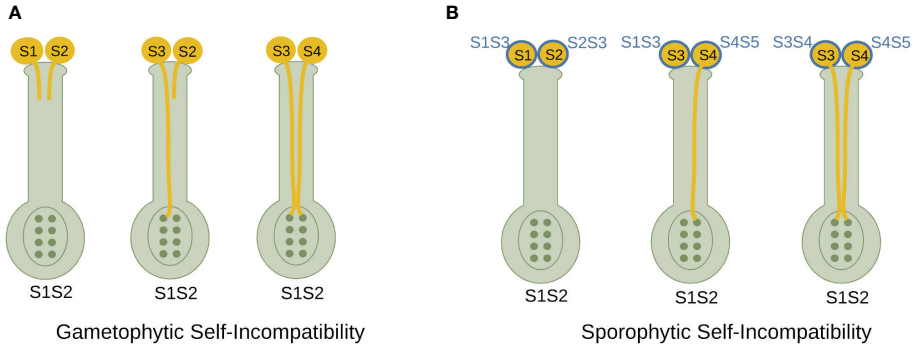

FIGURE 1
Comparative representation of self-incompatibility mechanisms.**(A)** Gametophytic self-incompatibility. The presence of identical S-alleles in the haploid pollen and diploid pistil leads to the arrest of pollen tube growth, but the presence of different S-alleles leads to fertilization. **(B)** Sporophytic self-incompatibility. Pollen grains bear the S-haplotype products of both parents, which interact with pistil S-haplotype products during the self-compatibility response. In order for fertilization to occur, the pollen S-haplotype must not share either S-allele with the pistil.

3 Genetic regulation of self-incompatibility

The genetic control of SI may differ between plant families. The genetic regulation of SSI has mainly been investigated in Brassicaceae, while GSI has mainly been investigated in Papaveraceae, Rosaceae, and Solanaceae.

In Brassicaceae, SSI is controlled by an *S*-locus comprising the female determinant *S-locus protein 11/S-locus Cys-rich* (*SP11/SCR*) and the male determinant *S-locus receptor kinase* (*SRK*) (Schopfer, 1999; Takasaki et al., 2000; Fujii et al., 2016; Chakraborty et al., 2023). The *S*-locus is highly linked to *S-locus glycoprotein* (*SLG*), and both are inherited as an S-haplotype (Nasrallah and Wallace, 1967; Nasrallah et al., 1985; Schopfer, 1999; Suzuki et al., 1999; Sehgal and Singh, 2018). The SP11 polypeptide is expressed in the anther tapetum and moves to the pollen coat; SRK localizes to the plasma membrane of stigmatic papilla cells. A specific and direct molecular interaction between SP11/SCR and SRK from the same S-haplotype triggers the incompatibility response. The response occurs in the stigma and causes self-pollen rejection (Conner et al., 1997; Stahl et al., 1998; Schopfer, 1999; Takasaki et al., 1999; Fujii et al., 2016). Thus, in SSI, the incompatibility response is a consequence of self-recognition of S-determinants (Fujii et al., 2016; Broz and Bedinger, 2021). Other factors function downstream of the self-recognition mechanism. *M* locus protein kinase (MLPK) transduces the SI signal, Armadillo repeat-containing 1 (ARC1) ubiquitinates and degrades target molecules, and thioredoxin h-like protein 1 (THL1) and kinase-associated protein phosphatase (KAPP) inhibit SRK to negatively regulate the SI response (Watanabe et al., 1994; Hatakeyama et al., 1998; Cabrillac et al., 2001; Fujii et al., 2016; Muñoz-Sanz et al., 2020; Chakraborty et al., 2023).

Papaveraceae family members exhibit GSI but also use a self-recognition mechanism, which operates at the stigmatic surface (Fujii et al., 2016; Chakraborty et al., 2023). In *Papaver rhoeas*, the *S*-locus female determinant is *Papaver rhoeas stigma S-determinant* (*PrsS*), which encodes a small protein secreted in the stigmatic papilla cells that acts as a signaling ligand (Foote et al., 1994; Wheeler et al., 2009). *Papaver rhoeas* stigma S-determinant interacts with the male determinant *Papaver rhoeas* pollen S-determinant (PrpS), generating a range of physiological responses upon self-interaction, such as Ca^{2+} and K^{+} influx and an increase in cytosolic Ca^{2+} (Wheeler et al., 2009; Wilkins, 2014). These events act on downstream targets and, in turn, lead to programmed cell death (Wilkins, 2014; Chakraborty et al., 2023).

In contrast, the GSI mechanism in the Rosaceae and Solanaceae involves a completely different mechanism, with pollen tube rejection occurring in the style. In S-RNase-based GSI, the *S*-locus contains at least two linked genes. The first gene encodes a glycoprotein with ribonuclease activity (S-RNase), which acts as a female determinant. S-RNase cytotoxic activity causes pollen rejection when the pollen S-haplotype is identical to either of the two S-haplotypes in the pistil. The second *S*-locus gene encodes an F-box protein that acts as the male determinant (Fujii et al., 2016; Broz and Bedinger, 2021; Chakraborty et al., 2023). The name of the F-box protein varies depending on the family: it is called S-locus F-box (SLF) in the Solanaceae and Rosaceae tribe Maleae, and S-haplotype-specific F-box (SFB) in the Rosaceae genus *Prunus*. F-box proteins are best known for their involvement in the Skp, Cullin, F-box-containing (SCF) complex, which recognizes target proteins for ubiquitination and degradation by the 26S proteasome. Along with other findings, this suggests a model in which non-self S-RNases are recognized by the SCF complex and degraded, while self-S-RNases would escape degradation and break down pollen RNA, terminating pollen tube growth (Fujii et al., 2016; Muñoz-Sanz et al., 2020; Broz and Bedinger, 2021; Chakraborty et al., 2023). However, mutations in *Prunus SFB* confer SC, leading to a model for *Prunus* wherein self-SFB protects self-S-RNases from a general inhibitor (Matsumoto et al., 2012).

3.1 Gametophytic self-incompatibility in the Solanaceae

Self-incompatibility of Solanaceae family members is under gametophytic control and has mainly been investigated in *Nicotiana*, *Petunia*, and *Solanum* (Fujii et al., 2016; Muñoz-Sanz et al., 2020; Chakraborty et al., 2023). In the Solanaceae family, the

10.3389/fpls.2023.1326689

S-locus contains the *S-RNase* gene encoding the female determinant, along with multiple *SLF* genes forming the male determinant. The number of *SLF* genes varies between species, ranging from 16–20 in SI *Petunia* to 23 in *Solanum pennellii*, and 19 in *Solanum lycopersicum* (Kubo et al., 2015; Li and Chetelat, 2015). Each SLF protein interacts with one or more S-RNases.

Two models have been proposed to explain GSI in Solanaceae: the Collaborative Non-Self Recognition Model (Kubo et al., 2010) and the Compartmentalization Model (Goldraij et al., 2006). In the Collaborative Non-Self Recognition Model, SLF–S-RNase recognition leads to S-RNase ubiquitination and degradation through the 26S proteasome (Figure 2) (Fujii et al., 2016). Solanaceae S-RNases possess five highly conserved regions and two hypervariable ones, while the SCF–SLF complex contains a domain fixing the S-RNase hypervariable domain in an S-specific manner, as well as a second domain fixing a conserved region. S-specific fixation leads to S-RNase polyubiquitination by the SCF complex and degradation through the 26S proteasome (Figure 2A). In contrast, lack of recognition leads to inhibition of pollen tube growth via S-RNase cytotoxic activity (Figure 2B) (Takayama and Isogai, 2005; Kubo et al., 2010; Fujii et al., 2016).

Recent studies have highlighted other factors involved in Solanaceae GSI that are independent of the *S*-locus, known as modifier genes. McClure et al. (1999) described the first modifier gene in GSI: *High Top-Band* (*HT-B*), encoding a small asparagine-rich protein involved in *Nicotiana* S-specific pollen rejection. Two *HT* genes have been identified in *Solanum* (*HT-A* and *HT-B*), although *Solanum lycopersicum* lacks functional HT proteins (Kondo et al., 2002b). The specific roles of each HT protein remain unknown. HT-B is essential for pollen rejection in *Nicotiana*, *Petunia*, and *Solanum*. However, several studies focusing on the *Lycopersicon* clade species revealed a possible overlap between HT-A and HT-B function in SI (McClure et al., 1999; Kondo et al., 2002b; O'Brien et al., 2002; Puerta et al., 2009; Covey et al., 2010; Tovar-Méndez et al., 2014). In *Nicotiana alata*, the protease inhibitor Stigma-Expressed Protein (NaStEP) participates in the SI response by protecting HT-B from degradation in the pollen tube (Jiménez-Durán et al., 2013). The exact role of NaStEP in SI has not yet been determined, but it may inhibit a subtilisin-like component (*NaSubt)* that would otherwise target HT-B during compatible crosses (Cruz-Zamora et al., 2020). A third, pollen-derived protein potentially involved in this

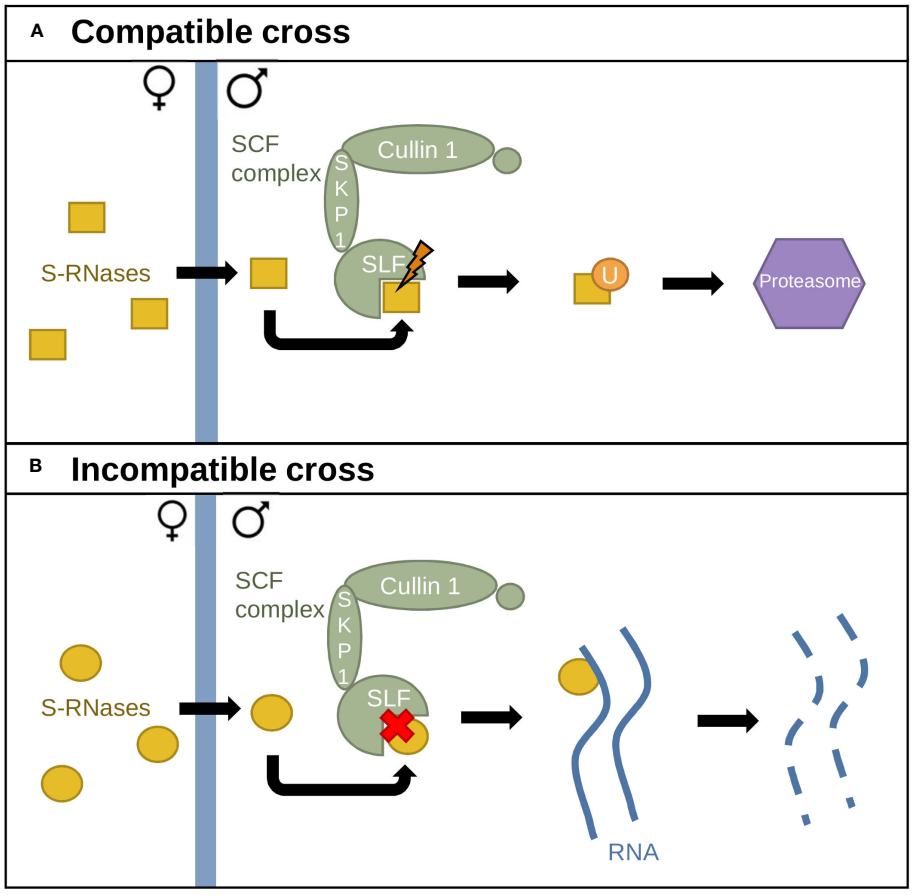

FIGURE 2
The Collaborative Non-Self Recognition Model. **(A)** Interaction between different S-alleles. S-RNases (yellow) enter the pollen tube and interact with SLF proteins, triggering recognition. S-RNases are then ubiquitinated by the SCF complex and sent to the 26S proteasome for degradation. **(B)** Interaction between identical S-alleles. Lack of recognition between SLF proteins and S-RNases leads to RNA degradation by S-RNases.

10.3389/fpls.2023.1326689

mechanism is Self-Incompatibility Pollen Protein (NaSIPP). In incompatible crosses, interaction between NaSIPP and NaStEP causes the opening of a permeability transition pore in the mitochondrial membrane, triggering an energy crisis and interruption of pollen tube growth (García-Valencia et al., 2017). Another factor in *N. alata* that participates in the SI response is a 120-kDa glycoprotein (120K) belonging to the arabinogalactan protein group. Loss of 120K leads to pollen rejection failure (Nathan Hancock et al., 2005). Moreover, a recently identified modifier gene in *N. alata* is *thioredoxin type h* (*NaTrxh*). The *NaTrxh* gene product specifically reduces a highly conserved S-RNase disulfide bond following the S-RNase–SLF interaction in incompatible crosses. This disulfide bond reduction significantly increases S-RNase ribonuclease activity, enabling pollen tube growth arrest (Torres-Rodríguez et al., 2020). How these modifier genes specifically integrate the Collaborative Non-Self Recognition Model has yet to be uncovered.

A second GSI model has been proposed in *N. alata*, which includes several modifier genes. The Compartmentalization Model (Figure 3) suggests that S-RNases are compartmentalized in vacuoles when they enter pollen tubes to contain their cytotoxic activity (Goldraij et al., 2006). A small portion of S-RNases escape this compartmentalization and interact with the SCF–SLF complex in the cytoplasm, generating the compatibility response (McClure et al., 2011). In incompatible crosses, S-specific interaction leads to NaStEP stabilization, which protects HT-B from degradation (Figure 3A). HT-B destabilizes the vacuolar membrane, releasing S-RNases. Furthermore, NaStEP–NaSIPP interaction destabilizes

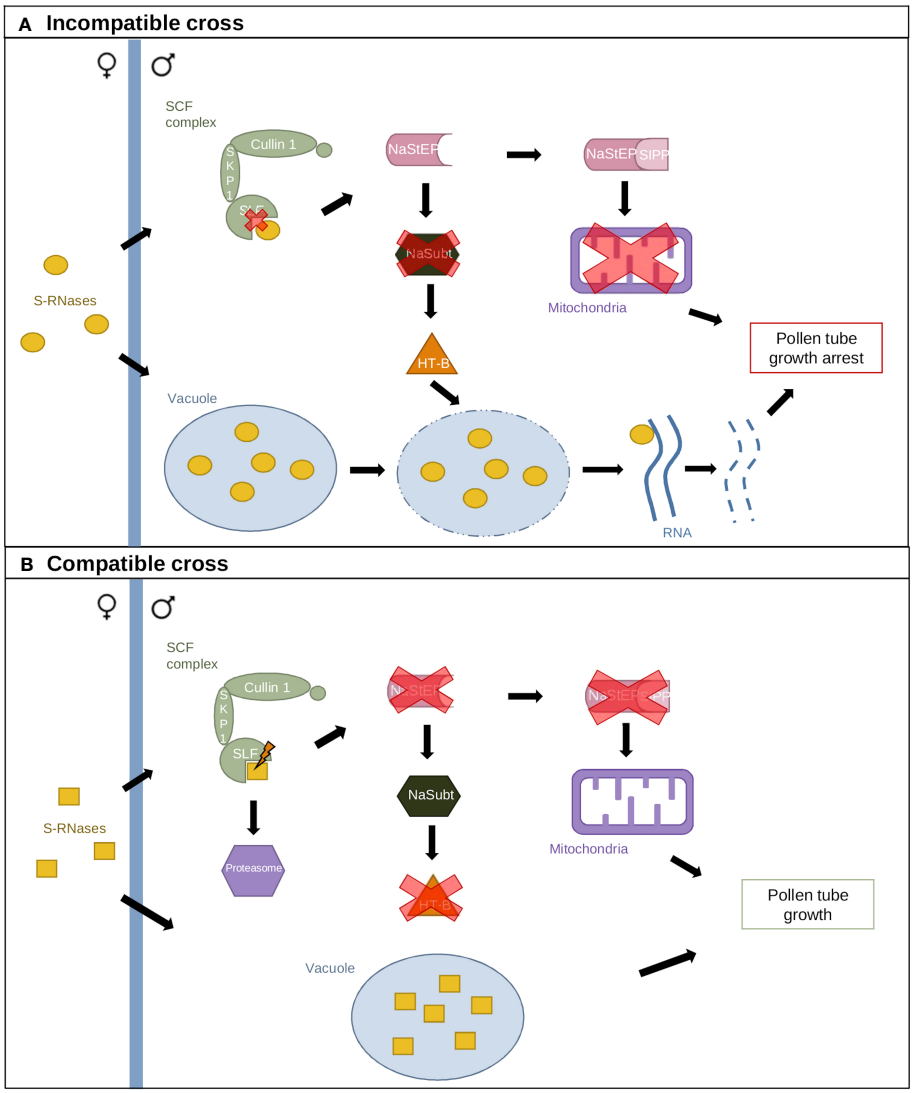

FIGURE 3
The Compartmentalization Model. **(A)** Incompatible cross resulting from identical S-allele interaction. S-RNases are sequestered in a vacuole, while a small portion interacts with the SCF complex. Lack of recognition between SLF and S-RNases leads to NaStEP maintenance, which inhibits a subtilisin-like component (NaSubt) and maintains HT-B. Interaction between the vacuole and HT-B leads to vacuolar membrane disruption and S-RNase release. NaStEP also interacts with SIPP, destabilizing mitochondria. **(B)** Compatible cross resulting from the interaction between different S-alleles. Recognition between SLF and S-RNases inhibits NaStEP, allowing NaSubt-mediated repression of HT-B. The vacuole and mitochondria remain intact, and pollen tube growth is maintained.

mitochondria. Collectively, these events arrest pollen tube growth. In compatible crosses, S-specific recognition leads to NaStEP inhibition, allowing a subtilisin-like protease to degrade HT-B (Figure 3B). HT-B loss results in intact vacuoles and S-RNase sequestration (Goldraij et al., 2006; McClure et al., 2011; Cruz-Zamora et al., 2020).

Later studies in *Petunia hybrida* showed that SLF and S-RNases interact in the cytosol, that S-RNases are polyubiquitinated and degraded by the proteasome in compatible crosses, and that the action of non-self SLF from the SCF complex mediates S-RNase degradation (Liu et al., 2014; Williams et al., 2015). Taken together, these findings support the Collaborative Non-Self Recognition Model. However, except for HT-B, no modifier genes present in *Nicotiana* have been detected in *Petunia*. Thus, compatibility response mechanisms might differ between *Nicotiana* and *Petunia* (Liu et al., 2014; Chakraborty et al., 2023). Still, the two models are not mutually exclusive; a small portion of S-RNases could be compartmentalized, whereas the majority could be degraded in the cytosol (McClure et al., 2011; Liu et al., 2014). Nevertheless, the specific roles of certain modifier genes, such as 120K, remain unknown and the incompatibility mechanisms in GSI need further exploration.

The Collaborative Non-Self Recognition Model is the most widely accepted model in *Solanum* (Li and Chetelat, 2015; Qin et al., 2018; Qin and Chetelat, 2021). Still, compared to *Nicotiana* and *Petunia*, very few studies have focused on *Solanum* SI mechanisms specifically. Additional evidence is needed to elucidate the mechanisms at play in this genus.

3.2 Self-compatible and self-incompatible species in the *Lycopersicon* clade

Cultivated tomato (*Solanum lycopersicum*) and its twelve closely related species are grouped in the so-called 'tomato' or '*Lycopersicon*' clade. This clade is divided into four sub-groups (Table 1). The first group (Esculentum) contains *S. galapagense*, *S. cheesmaniae*, *S. lycopersicum* and *S. pimpinellifolium*. The second group (Arcanum) consists of *S. neorickii*, *S. arcanum* and *S. chmielewskii*. The third group (Peruvianum) comprises *S. huaylasense*, *S. peruvianum*, *S. corneliomurelli* and *S. chilense*. The last group (Hirsutum) contains *S. habrochaites* and *S. pennellii* (Pease et al., 2016). All Esculentum group species are self-compatible. In contrast, all species in the Peruvianum group are self-incompatible except for *S. peruvianum*, which includes

TABLE 1 Groups and species in the *Lycopersicon* clade, showing their compatibility relation and S-RNase, HT-A and HT-B activities.

Group	Species	Accession	Compatibility relation	S-RNase	HT-A	HT-B
Esculentum	*S. lycopersicum*		SC	_	_	_
	S. pimpinellifolium		SC	_	_	_
	S. galapagense		SC	_	_	_
	S. cheesmaniae		SC	_	_	_
Arcanum	*S. neorickii*		SC	_	OK	_
	S. arcanum		SI/SC			
		LA2157	SC	_	OK	OK
	S. chmielewskii		SC	_	OK	_
Peruvianum	*S. huaylasense*		SI	OK	OK	OK
	S. peruvianum		SI/SC			
		LA4125	SC	?	?	?
		LA2157	SC	_	?	?
	S. corneliomulleri		SI	OK	OK	OK
	S. chilense		SI	OK	OK	OK
Hirsutum	*S. habrochaites*		SI/SC			
		LA1777	SI	OK	OK	_
		LA1223	SC	_	_	_
		LA2314	SC	_	OK	_
		LA0407	SC	_	OK	_
	S. pennellii		SI/SC			
		LA0716	SC	_	OK	OK

SC, self-compatible; SI, self-incompatible; _, no activity; OK, activity,?, unknown activity.

several facultative SC populations. The other two groups comprise species that are either SI or facultatively SC (Peralta et al., 2008; Grandillo et al., 2011).

The SI-to-SC transition can be triggered by several factors that result in loss of SI or gain of SC (Zhao et al., 2022). In the Arcanum group, *S. chmielewskii* is facultatively SC, *S. neorickii* is autogamous and *S. arcanum* is SI except for one autogamous accession, LA2157 (Grandillo et al., 2011; Markova et al., 2017). Both *S. chmielewskii* and *S. arcanum* accession LA2157 have lost pistil S-RNase activity, while *S. neorickii* has acquired a gain-of-function mutation in pollen *SLF* that allows self-recognition (Markova et al., 2017). The Esculentum clade also lost S-RNase activity, and does not possess functional *HT* genes; *HT-A* encodes a truncated peptide, while *HT-B* is not transcribed (Kondo et al., 2002a).

3.3 S-RNases in the *Lycopersicon* clade: representation and phylogeny

As the *S*-locus in Solanaceae members contains one female determinant but multiple male determinants, S-haplotype characterization is mainly based on S-RNase description (Igic et al., 2007; Kubo et al., 2010; Williams et al., 2015; Broz et al., 2021). S-RNases are 30-kDa glycoproteins secreted by the style and taken up by pollen tubes during their growth (Luu et al., 2000). Solanaceae S-RNases are part of the T2 RNase family: their sequences contain a signal peptide, five conserved regions and two hypervariable regions (Figure 4) (Silva and Goring, 2001). S-specificity could be partially attributed to the hypervariable regions. However, the precise role of sequence variation in the hypervariable regions, as well as the specific molecular interactions they mediate, remain unknown (Ioerger et al., 1991; Brisolara-Corrêa et al., 2015).

S-allele diversity in the *Lycopersicon* clade is estimated to range from 10 to 50 S-haplotypes per species, with roughly 35 S-alleles in *S. chilense* (Igic et al., 2007). Identical S-alleles from different species tend to be more closely related to each other than to S-alleles of the same species, as S-allele diversification predates speciation within the clade (Figure 5) (Brisolara-Corrêa et al., 2015). Three different scenarios may explain SC acquisition resulting from S-RNase mutation within the clade. The first involves direct gene-disrupting mutations, such as gene deletion, frameshift mutations or nonsense mutations, that generate non-functional *S-RNase* genes. The second scenario involves expressed S-alleles that are translated into proteins that harbor substitutions in crucial amino acids, rendering them non-functional. The third scenario involves S-alleles that have been transcriptionally silenced (Broz et al., 2021).

4 Unilateral incompatibility

4.1 Interspecific reproductive barriers and unilateral incompatibility

Hybridization amongst individuals from different species can lead to poorly adapted or nonviable offspring due to genetic incompatibilities arising from species divergence (Lewis and Crowe, 1958; Nettancourt, 2001; Wang and Filatov, 2023). Such interspecific reproductive barriers (IRBs) serve to limit outbreeding and can be either passive mechanisms such as differences in matching of genetic systems leading to a lack of fit between partners, referred to as incongruity, or active mechanisms such as pollen rejection, referred to as incompatibility (Lewis and Crowe, 1958; Hogenboom et al., 1997; Nettancourt, 2001; Broz and Bedinger, 2021).

Because IRBs function to prevent self-fertilization, some SI barriers play roles in interspecific incompatibility (Li and Chetelat, 2010; Broz and Bedinger, 2021; Wang and Filatov, 2023). Accordingly, SI species exhibit a stronger inclination to actively reject interspecific pollen than SC species (Lewis and Crowe, 1958). This phenomenon has been described as unilateral incompatibility (UI) (Lewis and Crowe, 1958; Nettancourt, 2001). Unilateral incompatibility is a type of interspecific incompatibility in which pollen from one species is rejected by another species'

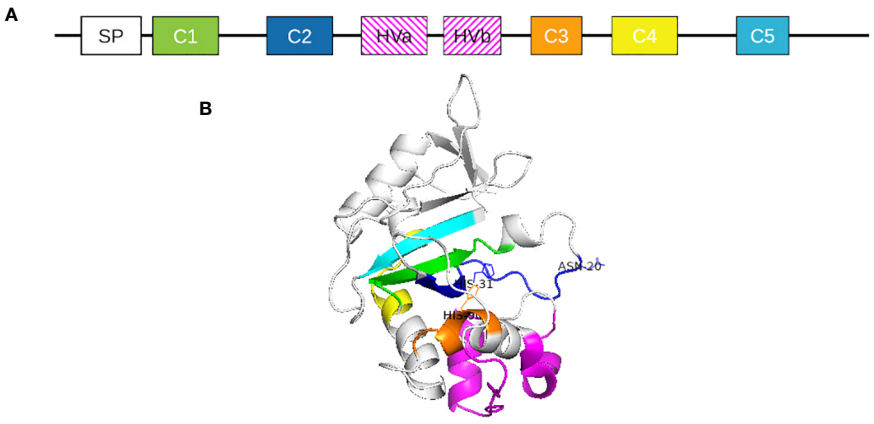

FIGURE 4
(A) Solanaceae S-RNase protein primary structure representation. SP represents the signal peptide. C1 to C5 represent highly conserved regions of the proteins and HVa and HVb represent the two hypervariable regions. **(B)** Three-dimensional structure of S. chilense S2 S-RNase. Conserved regions are indicated in color: green = C1, dark blue = C2, orange = C3, yellow = C4, cyan = C5.

10.3389/fpls.2023.1326689

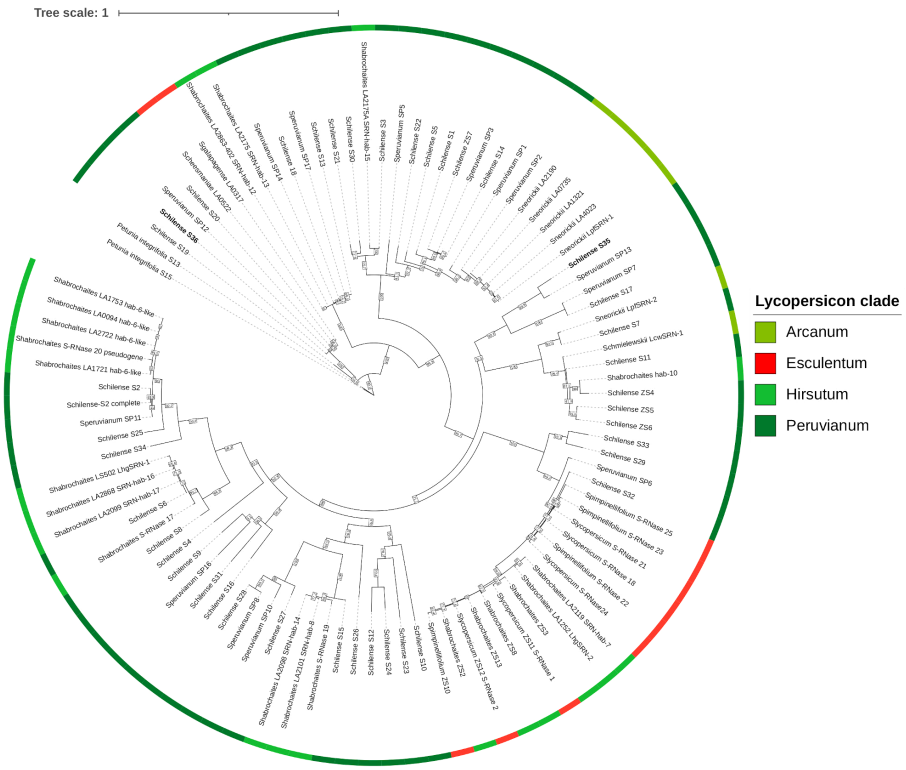

FIGURE 5
Maximum likelihood phylogram of S-alleles across the *Lycopersicon* clade. Sequences are colored by the group they belong to (See Table 1 for groups information) and color of their fruits (either green or red, see Figure 6). The NCBI accessions of the genes are detailed in Supplementary Data.

pistil, while the opposite cross is fertile (Nettancourt, 2001). Unilateral incompatibility often follows the SI x SC rule, whereby pollen from an SI species is accepted by the pistil of an SC species, while the opposite cross is rejected (Lewis and Crowe, 1958). This type of barrier has been described in families such as the Brassicaceae and Solanaceae (Lewis and Crowe, 1958; Hiscock and Dickinson, 1993; Broz and Bedinger, 2021).

4.2 Unilateral incompatibility in the *Lycopersicon* clade

Interspecific reproductive barriers have been observed within the *Lycopersicon* clade, but they may differ among species. Unilateral incompatibility has been particularly investigated in tomato species (Li and Chetelat, 2010; Tovar-Méndez et al., 2014; Tovar-Méndez et al., 2017; Qin et al., 2018; Muñoz-Sanz et al., 2021; Qin and Chetelat, 2021). In the tomato clade, the SI x SC rule often manifests as red-fruited species exhibiting SC and green-fruited species exhibiting SI (Figure 6); therefore, red-fruited species may be used as the female parent in crosses with green-fruited species, but the reverse is not true. All red-fruited species belong to the Esculentum group and lack functional S-RNases and HT proteins that prevent interspecific crosses (Grandillo et al., 2011; Tovar-Méndez et al., 2014; Baek et al., 2015). Furthermore, the tomato clade is particularly useful in studying UI since its subgroups show different levels of IRBs. In addition to the Esculentum group showing hardly any IRBs, the Arcanum group displays fewer IRBs

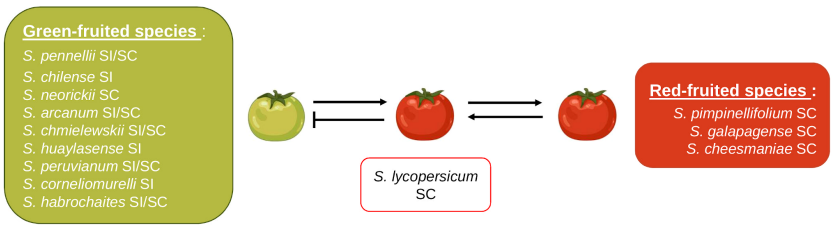

FIGURE 6
Interspecific compatibility of *S. lycopersicum* with other members of the *Lycopersicon* clade. The blunted arrow represents an incompatible cross and regular arrows represent compatible crosses.

than the Peruvianum and Hirsutum groups (Bedinger et al., 2011; Muñoz-Sanz et al., 2021).

Studies involving members of the tomato clade have shed light on SI-dependent and SI-independent mechanisms of UI. UI in tomato species has been most studied in *S. pennellii*. This species includes SI accessions as well as an accession with very low S-RNase levels, two characteristics that enable the study of S-RNase-independent UI pathways (Tovar-Méndez et al., 2014; Tovar-Méndez et al., 2017; Qin et al., 2018; Muñoz-Sanz et al., 2021; Qin and Chetelat, 2021).

Tovar-Méndez et al. (2014) showed that expression of *S-RNase* with either *HT-A* or *HT-B* could restore IRBs in *S. lycopersicum* when crossed with other red-fruited species.

In addition to S-RNases and HT proteins, other factors involved in SI also affect the UI response. Pollen-wise, a single *SLF* transgene, *SLF-23*, in combination with functional *Cullin1*, has been shown to be responsible for pollen recognition and rejection in *Solanum* sect. *Lycopersicon* UI. This finding is in agreement with the SI x SC rule, as all green-fruited species express both functional *SLF-23* and *Cullin1*, while no red-fruited species possess both functioning genes (Li and Chetelat, 2010; Li and Chetelat, 2015).

SI-independent UI pathways have also been recently described. Indeed, *S. pennellii* accession LA0716 and *S. habrochaites* accession LA1927 show very low S-RNase activity, but still reject *S. lycopersicum* pollen. Furthermore, a nonsense mutation was detected in the *S. habrochaites HT-B* gene, whereas the *HT-A* gene product was functional (Covey et al., 2010). *HT* suppression in *S. pennellii* LA0716 enabled deeper penetration of *S. lycopersicum* pollen tubes into the style, and *HT* suppression in *S. habrochaites* LA0407 and *S. arcanum* LA2157 (two S-RNase-deficient accessions) allowed ovary penetration and hybrid production (Tovar-Méndez et al., 2017). Thus, HT proteins may be involved in S-RNase-dependent and S-RNase-independent UI pathways (Table 2).

Other factors have also been linked to the S-RNase-independent way (Table 2). In *S. pennellii* LA0716, the pollen-derived protein farnesyl phosphate synthase 2 (FPS2) was shown to be involved in UI pollen rejection, with *FPS2* expression being 18-fold higher in *S. pennellii* LA0716 than in *S. lycopersicum* (Qin et al., 2018). Ornithine decarboxylase 2 (ODC2), an enzyme catalyzing the conversion of ornithine into putrescine in polyamine biosynthesis, was later identified as the pistil-derived factor that interacts with FPS2. There are four copies of *ODC2* in *S. pennellii* but only one in *S. lycopersicum*. Furthermore, *ODC2* genetically interacts with *HT* genes to strengthen pollen rejection (Qin and Chetelat, 2021). Another S-RNase-independent pistil-derived UI factor, *Defective in Induced Resistance 1-Like* (*DIR1L*), contributes to *S. lycopersicum* pollen rejection in *S. pennelli* LA0716. A deletion in the *DIR1L* coding region was identified in the Esculentum and Arcanum groups (Muñoz-Sanz et al., 2021). Transcriptomics analyses of *S. habrochaites* also highlighted other factors potentially involved in UI, such as a Kunitz-type protease inhibitor and a putative pollen arabinogalactan protein (Broz et al., 2017).

Mechanisms of UI are multiple, resulting from various pollen–pistil interactions. A complete picture of this interspecific barrier remains to be uncovered (Tovar-Méndez et al., 2017; Qin et al., 2018; Muñoz-Sanz et al., 2021; Qin and Chetelat, 2021).

5 Discussion

Understanding reproductive barriers in plants sheds light on the establishment of reproductive isolation, which is a crucial aspect of speciation (Bedinger et al., 2011). Moreover, reproductive barriers limit the use of wild relatives for crop improvement. Accordingly, overcoming such barriers would facilitate the use of wild relative germplasm in plant breeding (Bedinger et al., 2011; Muñoz-Sanz et al., 2020).

Several types of incompatibility barriers are seen in the *Lycopersicon* clade. On the one hand, gametophytic self-incompatibility prevents inbreeding on an intraspecific level, and on the other hand, unilateral incompatibility limits outbreeding. Important discoveries have expanded our comprehension of the mechanisms underlying both barrier types, especially in *Lycopersicon* clade UI. However, GSI has mainly been investigated in *Nicotiana* and *Petunia* (Solanaceae). Since GSI also plays a role in UI, additional studies in *Solanum* are needed to determine how SI mechanisms unfold in this genus, and by extension, in the *Lycopersicon* clade.

The tomato clade is an excellent model to study reproductive barriers (Bedinger et al., 2011). It comprises species with different compatibility barriers, facilitating the study of both SI and UI. Furthermore, *Solanum lycopersicum*, one of the most important agricultural crops worldwide, could directly benefit from advances

TABLE 2 Genes potentially involved in unilateral incompatibility in the *Lycopersicon* clade.

Gene	Abbreviation	S-RNase dependent?	Pollen- or pistil-side?	Literature
High Top A & High Top B	*HT-A & HT-B*	Yes and No	Pistil	(Covey et al., 2010; Tovar-Méndez et al., 2017)
Farnesyl Phosphate Synthase 2	*FPS2*	No	Pollen	(Qin et al., 2018)
Ornithine Decarboxylase 2	*ODC2*	No	Pistil	(Qin and Chetelat, 2021)
Defective in Induced Resistance 1-like	*DIR1L*	No	Pistil	(Muñoz-Sanz et al., 2021)
Kunitz-type Protease inhibitor	/	Unknown	Pistil	(Broz et al., 2017)
Putative Arabinogalactan Protein	/	Unknown	Pollen	(Broz et al., 2017)

in overcoming reproductive barriers to introgress genes of interest from wild relatives (Bedinger et al., 2011; Muñoz-Sanz et al., 2020). Moreover, insights on reproductive barriers from the *Solanum* model could be extended to other members of the Solanaceae family, as well as more distant genera. It has recently been suggested that *Prunus* could present linkages in SI and UI. (Morimoto et al., 2019). Thus, the analysis of reproductive barriers in *Prunus* could directly benefit from progress made in the *Lycopersicon* clade (Bedinger et al., 2011; Morimoto et al., 2019; Muñoz-Sanz et al., 2020).

6 Conclusion

In the last two decades, major advances have expanded our knowledge of incompatibility barriers in the *Lycopersicon* clade. Models explaining self-incompatibility mechanisms have been proposed, such as the Collaborative Non-Self Recognition Model and the Compartmentalization Model in S-RNase-based GSI. Factors participating in these SI mechanisms have been uncovered, such as HT, NaStep, NaSIPP, 120K and NaTrxh. Nevertheless, the detailed mechanisms underlying self-incompatibility and the clear roles of these factors have yet to be unraveled. So far, no model explaining unilateral incompatibility in the *Lycopersicon* clade has been proposed, although multiple factors and UI pathways have been identified. Much remains to be learned about this interspecific barrier, in the hope of using the complete array of wild tomato species for tomato breeding.

Author contributions

PM: Conceptualization, Investigation, Methodology, Visualization, Writing – original draft, Writing – review & editing. SB: Conceptualization, Supervision, Visualization, Writing – review & editing. CD: Investigation, Visualization, Writing – review & editing. FC: Investigation, Software, Visualization, Writing – review & editing. JM: Funding acquisition, Project administration, Resources, Writing – review & editing. SL: Funding acquisition, Project administration, Supervision, Writing – review & editing. MQ: Conceptualization, Funding acquisition, Project administration, Supervision, Writing – original draft, Writing – review & editing.

Funding

The author(s) declare financial support was received for the research, authorship, and/or publication of this article. This research is supported by the French-speaking Community of Belgium and the Fond National pour la Recherche Scientifique through the funding of a FRIA grant number FC 52339 and by the Wallonie-Bruxelles International (WBI/Chili) project number RI 13.

Acknowledgments

PM is grateful to the F.R.S-F.N.R.S for the FRIA research fellowship. The authors are grateful to 'Plant Editors' for English revision. This work was published with the support of the University Foundation of Belgium.

Conflict of interest

The authors declare that the research was conducted in the absence of any commercial or financial relationships that could be construed as a potential conflict of interest.

Publisher's note

Supplementary material

The Supplementary Material for this article can be found online at: https://www.frontiersin.org/articles/10.3389/fpls.2023.1326689/full#supplementary-material

SUPPLEMENTARY TABLE 1
list of the genebank accessions of the S-RNAses genes presented in .

References

Arms, E. M., Bloom, A. J., and St. Clair, D. A. (2015). High-resolution mapping of a major effect QTL from wild tomato Solanum habrochaites that influences water relations under root chilling. *Theor. Appl. Genet.* 128, 1713–1724. doi: 10.1007/s00122-015-2540-y

Baek, Y. S., Covey, P. A., Petersen, J. J., Chetelat, R. T., McClure, B., and Bedinger, P. A. (2015). Testing the SI × SC rule: Pollen–pistil interactions in interspecific crosses between members of the tomato clade (Solanum section Lycopersicon, Solanaceae). *Am. J. Bot.* 102, 302–311. doi: 10.3732/ajb.1400484

Bai, Y., Huang, C.-C., van der Hulst, R., Meijer-Dekens, F., Bonnema, G., and Lindhout, P. (2003). QTLs for Tomato Powdery Mildew Resistance (Oidium lycopersici) in Lycopersicon parviflorum G1.1601 Co-localize with Two Qualitative Powdery Mildew Resistance Genes. *Mol. Plant-Microbe Interactions®* 16, 169–176. doi: 10.1094/MPMI.2003.16.2.169

Bedinger, P. A., Chetelat, R. T., McClure, B., Moyle, L. C., Rose, J. K. C., Stack, S. M., et al. (2011). Interspecific reproductive barriers in the tomato clade: opportunities to decipher mechanisms of reproductive isolation. *Sexual Plant Reprod.* 24, 171–187. doi: 10.1007/s00497-010-0155-7

Bonarota, M.-S., Kosma, D. K., and Barrios-Masias, F. H. (2022). Salt tolerance mechanisms in the Lycopersicon clade and their trade-offs. *AoB Plants* 14. doi: 10.1093/aobpla/plab072

Brisolara-Corrêa, L., Thompson, C. E., Fernandes, C. L., and de Freitas, L. B. (2015). Diversification and distinctive structural features of S-RNase alleles in the genus Solanum. *Mol. Genet. Genomics* 290, 987–1002. doi: 10.1007/s00438-014-0969-3

Brog, Y. M., Osorio, S., Yichie, Y., Alseekh, S., Bensal, E., Kochevenko, A., et al. (2019). A Solanum neorickii introgression population providing a powerful

complement to the extensively characterized Solanum pennellii population. *Plant J.* 97, 391–403. doi: 10.1111/tpj.14095

Broz, A. K., and Bedinger, P. A. (2021). Pollen-pistil interactions as reproductive barriers. *Annu. Rev. Plant Biol.* 72, 615–639. doi: 10.1146/annurev-arplant-080620-102159

Broz, A. K., Guerrero, R. F., Randle, A. M., Baek, Y. S., Hahn, M. W., and Bedinger, P. A. (2017). Transcriptomic analysis links gene expression to unilateral pollen-pistil reproductive barriers. *BMC Plant Biol.* 17, 81. doi: 10.1186/s12870-017-1032-4

Broz, A. K., Miller, C. M., Baek, Y. S., Tovar-Méndez, A., Acosta-Quezada, P. G., Riofrío-Cuenca, T. E., et al. (2021). S-RNase alleles associated with self-compatibility in the tomato clade: structure, origins, and expression plasticity. *Front. Genet.* 12. doi: 10.3389/fgene.2021.780793

Cabrillac, D., Cock, J. M., Dumas, C., and Gaude, T. (2001). The S-locus receptor kinase is inhibited by thioredoxins and activated by pollen coat proteins. *Nature* 410, 220–223. doi: 10.1038/35065626

Calafiore, R., Aliberti, A., Ruggieri, V., Olivieri, F., Rigano, M. M., and Barone, A. (2019). Phenotypic and molecular selection of a superior solanum pennellii introgression sub-line suitable for improving quality traits of cultivated tomatoes. *Front. Plant Sci.* 10. doi: 10.3389/fpls.2019.00190

Chakraborty, S., Dutta, S., and Das, M. (2023). Genetics behind sexual incompatibility in plants: how much we know and what more to uncover? *J. Plant Growth Regulation*. 42, 7164–7188. doi: 10.1007/s00344-023-11005-z

Chen, A.-L., Liu, C.-Y., Chen, C.-H., Wang, J.-F., Liao, Y.-C., Chang, C.-H., et al. (2014). Reassessment of QTLs for late blight resistance in the tomato accession L3708 using a restriction site associated DNA (RAD) linkage map and highly aggressive isolates of phytophthora infestans. *PloS One* 9, e96417. doi: 10.1371/journal.pone.0096417

Conner, J. A., Tantikanjana, T., Stein, J. C., Kandasamy, M. k., Nasrallah, J. B., and Nasrallah, M. E. (1997). Transgene-induced silencing of S-locus genes and related genes in Brassica. *Plant J.* 11, 809–823. doi: 10.1046/j.1365-313X.1997.11040809.x

Covey, P. A., Kondo, K., Welch, L., Frank, E., Sianta, S., Kumar, A., et al. (2010). Multiple features that distinguish unilateral incongruity and self-incompatibility in the tomato clade. *Plant J.* 64, 367–378. doi: 10.1111/j.1365-313X.2010.04340.x

Cruz-Zamora, Y., Nájera-Torres, E., Noriega-Navarro, R., Torres-Rodríguez, M. D., Bernal-Gracida, L. A., García-Valdés, J., et al. (2020). NaStEP, an essential protein for self-incompatibility in Nicotiana, performs a dual activity as a proteinase inhibitor and as a voltage-dependent channel blocker. *Plant Physiol. Biochem.* 151, 352–361. doi: 10.1016/j.plaphy.2020.03.052

Dhaliwal, M. S., Jindal, S. K., Sharma, A., and Prasanna, H. C. (2020). Tomato yellow leaf curl virus disease of tomato and its management through resistance breeding: a review. *J. Hortic. Sci. Biotechnol.* 95, 425–444. doi: 10.1080/14620316.2019.1691060

FAOSTAT (2023) *Anon*. Available at: https://www.fao.org/faostat/en/#data/QCL (Accessed 9 January 2023).

Fernandes, M., de, O., Bianchi, P. A., da Silva, L. R. A., Vianna, L. S., Santos, E. A., et al. (2018). Morpho-agronomic characterization and analysis of genetic divergenceamong accessions of tomatoes (*Solanum lycopersicum* L.). *Ciec. Rural* 48. doi: 10.1590/0103-8478cr20180433

Fischer, I., Camus-Kulandaivelu, L., Allal, F., and Stephan, W. (2011). Adaptation to drought in two wild tomato species: the evolution of the Asr gene family. *New Phytol.* 190, 1032–1044. doi: 10.1111/j.1469-8137.2011.03648.x

Foote, H. C., Ride, J. P., Franklin-Tong, V. E., Walker, E. A., Lawrence, M. J., and Franklin, F. C. (1994). Cloning and expression of a distinctive class of self-incompatibility (S) gene from Papaver rhoeas L. *Proc. Natl. Acad. Sci.* 91, 2265–2269. doi: 10.1073/pnas.91.6.2265

Frelichowski, J. E. Jr., and Juvik, J. A. (2001). Sesquiterpene Carboxylic Acids from a Wild Tomato Species Affect Larval Feeding Behavior and Survival of Helicoverpa zeaand Spodoptera exigua (Lepidoptera: Noctuidae). *J. Economic Entomology* 94, 1249–1259. doi: 10.1603/0022-0493-94.5.1249

Fujii, S., Kubo, K., and Takayama, S. (2016). Non-self- and self-recognition models in plant self-incompatibility. *Nat. Plants* 2, 1–9. doi: 10.1038/nplants.2016.130

García-Valencia, L. E., Bravo-Alberto, C. E., Wu, H.-M., Rodríguez-Sotres, R., Cheung, A. Y., and Cruz-García, F. (2017). SIPP, a novel mitochondrial phosphate carrier, mediates in self-incompatibility. *Plant Physiol.* 175, 1105–1120. doi: 10.1104/pp.16.01884

Gerszberg, A., Hnatuszko-Konka, K., Kowalczyk, T., and Kononowicz, A. K. (2015). Tomato (Solanum lycopersicum L.) in the service of biotechnology. *Plant Cell Tissue Organ Culture (PCTOC)* 120, 881–902. doi: 10.1007/s11240-014-0664-4

Goldraij, A., Kondo, K., Lee, C. B., Hancock, C. N., Sivaguru, M., Vazquez-Santana, S., et al. (2006). Compartmentalization of S-RNase and HT-B degradation in self-incompatible Nicotiana. *Nature* 439, 805–810. doi: 10.1038/nature04491

Grandillo, S., Chetelat, R., Knapp, S., Spooner, D., Peralta, I., Cammareri, M., et al. (2011). "Solanum sect. Lycopersicon," in *Wild crop relatives: genomic and breeding resources: vegetables*. Ed. C. Kole (Berlin, Heidelberg: Springer), 129–215.

Hatakeyama, K., Takasaki, T., Watanabe, M., and Hinata, K. (1998). Molecular characterization of S locus genes, SLG and SRK, in a pollen-recessive self-incompatibility haplotype of brassica rapa L. *Genetics* 149, 1587–1597. doi: 10.1093/genetics/149.3.1587

Hiscock, S. J., and Dickinson, H. G. (1993). Unilateral incompatibility within the brassicaceae: further evidence for the involvement of the self-incompatibility (S)-locus. *Theor. Appl. Genet.* 86, 744–753. doi: 10.1007/BF00222665

Hogenboom, N. G., Mather, K., Heslop-Harrison, J., and Lewis, D. (1997). Incompatibility and incongruity: two different mechanisms for the non-functioning of intimate partner relationships. *Proc. R. Soc. London. Ser. B. Biol. Sci.* 188, 361–375. doi: 10.1098/rspb.1975.0025

Igic, B., Lande, R., and Kohn, J. R. (2008). Loss of self-incompatibility and its evolutionary consequences. *Int. J. Plant Sci.* 169, 93–104. doi: 10.1086/523362

Igic, B., Smith, W. A., Robertson, K. A., Schaal, B. A., and Kohn, J. R. (2007). Studies of self-incompatibility in wild tomatoes: I. S-allele diversity in Solanum Chilense Dun. (Solanaceae). *Heredity* 99, 553–561. doi: 10.1038/sj.hdy.6801035

Ioerger, T. R., Gohlke, J. R., Xu, B., and Kao, T.-H. (1991). Primary structural features of the self-incompatibility protein in solanaceae. *Sexual Plant Reprod.* 4, 81–87. doi: 10.1007/BF00196492

Jiménez-Durán, K., McClure, B., García-Campusano, F., Rodríguez-Sotres, R., Cisneros, J., Busot, G., et al. (2013). NaStEP: A proteinase inhibitor essential to self-incompatibility and a positive regulator of HT-B stability in nicotiana alata pollen tubes. *Plant Physiol.* 161, 97–107. doi: 10.1104/pp.112.198440

Kaothien-Nakayama, P., Isogai, A., and Takayama, S. (2010). "Self-incompatibility systems in flowering plants," *Plant Developmental Biology - Biotechnological Perspectives: Volume 1* (Berlin, Heidelberg: Springer).

Kondo, K., Yamamoto, M., Itahashi, R., Sato, T., Egashira, H., Hattori, T., et al. (2002a). Insights into the evolution of self-compatibility in Lycopersicon from a study of stylar factors. *Plant J.* 30, 143–153. doi: 10.1046/j.1365-313X.2002.01275.x

Kondo, K., Yamamoto, M., Matton, D. P., Sato, T., Hirai, M., Norioka, S., et al. (2002b). Cultivated tomato has defects in both S-RNase and HT genes required for stylar function of self-incompatibility. *Plant J.* 29, 627–636. doi: 10.1046/j.0960-7412.2001.01245.x

Kubo, K., Entani, T., Takara, A., Wang, N., Fields, A. M., Hua, Z., et al. (2010). Collaborative non-self recognition system in S-RNase–based self-incompatibility. *Science* 330, 796–799. doi: 10.1126/science.1195243

Kubo, K., Paape, T., Hatakeyama, M., Entani, T., Takara, A., Kajihara, K., et al. (2015). Gene duplication and genetic exchange drive the evolution of S-RNase-based self-incompatibility in Petunia. *Nat. Plants* 1, 1–9. doi: 10.1038/nplants.2014.5

Lewis, D., and Crowe, L. K. (1958). Unilateral interspecific incompatibility in flowering plants. *Heredity* 12, 233–256. doi: 10.1038/hdy.1958.26

Li, W., and Chetelat, R. T. (2010). A pollen factor linking inter- and intraspecific pollen rejection in tomato. *Science* 330, 1827–1830. doi: 10.1126/science.1197908

Li, W., and Chetelat, R. T. (2015). Unilateral incompatibility gene ui1.1 encodes an S-locus F-box protein expressed in pollen of Solanum species. *Proc. Natl. Acad. Sci.* 112, 4417–4422. doi: 10.1073/pnas.1423301112

Liu, W., Fan, J., Li, J., Song, Y., Li, Q., Zhang, Y., et al. (2014). SCFSLF-mediated cytosolic degradation of S-RNase is required for cross-pollen compatibility in S-RNase-based self-incompatibility in Petunia hybrida. *Front. Genet.* 5. doi: 10.3389/fgene.2014.00228

Luu, D.-T., Qin, X., Morse, D., and Cappadocia, M. (2000). S-RNase uptake by compatible pollen tubes in gametophytic self-incompatibility. *Nature* 407, 649–651. doi: 10.1038/35036623

Markova, D. N., Petersen, J. J., Yam, S. E., Corral, A., Valle, M. J., Li, W., et al. (2017). Evolutionary history of two pollen self-incompatibility factors reveals alternate routes to self-compatibility within Solanum. *Am. J. Bot.* 104, 1904–1919. doi: 10.3732/ajb.1700196

Matsumoto, D., Yamane, H., Abe, K., and Tao, R. (2012). Identification of a skp1-like protein interacting with SFB, the pollen S determinant of the gametophytic self-incompatibility in prunus. *Plant Physiol.* 159, 1252–1262. doi: 10.1104/pp.112.197343

Mazzucato, A., Ficcadenti, N., Caioni, M., Mosconi, P., Piccinini, E., Reddy Sanampudi, V. R., et al. (2010). Genetic diversity and distinctiveness in tomato (Solanum lycopersicum L.) landraces: The Italian case study of 'A pera Abruzzese'. *Scientia Hortic.* 125, 55–62. doi: 10.1016/j.scienta.2010.02.021

McClure, B., Cruz-García, F., and Romero, C. (2011). Compatibility and incompatibility in S-RNase-based systems. *Ann. Bot.* 108, 647–658. doi: 10.1093/aob/mcr179

McClure, B., Mou, B., Canevascini, S., and Bernatzky, R. (1999). A small asparagine-rich protein required for S-allele-specific pollen rejection in Nicotiana. *Proc. Natl. Acad. Sci.* 96, 13548–13553. doi: 10.1073/pnas.96.23.13548

Miller, J. C., and Tanksley, S. D. (1990). RFLP analysis of phylogenetic relationships and genetic variation in the genus Lycopersicon. *Theor. Appl. Genet.* 80, 437–448. doi: 10.1007/BF00226743

Morimoto, T., Kitamura, Y., Numaguchi, K., Akagi, T., and Tao, R. (2019). Characterization of post-mating interspecific cross-compatibility in Prunus (Rosaceae). *Scientia Hortic.* 246, 693–699. doi: 10.1016/j.scienta.2018.11.045

Muñoz-Sanz, J. V., Tovar-Méndez, A., Lu, L., Dai, R., and McClure, B. (2021). A cysteine-rich protein, spDIR1L, implicated in S-RNase-independent pollen rejection in the tomato (Solanum section lycopersicon) clade. *Int. J. Mol. Sci.* 22, 13067. doi: 10.3390/ijms222313067

Muñoz-Sanz, J. V., Zuriaga, E., Cruz-García, F., McClure, B., and Romero, C. (2020). Self-(In)compatibility systems: target traits for crop-production, plant breeding, and biotechnology. *Front. Plant Sci.* 11. doi: 10.3389/fpls.2020.00195

Nasrallah, J. B., Kao, T.-H., Goldberg, M. L., and Nasrallah, M. E. (1985). A cDNA clone encoding an S-locus-specific glycoprotein from Brassica oleracea. *Nature* 318, 263–267. doi: 10.1038/318263a0

Nasrallah, M. E., and Wallace, D. H. (1967). Immunogenetics of self-incompatibility in. *Heredity* 22, 519–527. doi: 10.1038/hdy.1967.67

Nathan Hancock, C., Kent, L., and McClure, B. A. (2005). The stylar 120 kDa glycoprotein is required for S-specific pollen rejection in Nicotiana. *Plant J.* 43, 716–723. doi: 10.1111/j.1365-313X.2005.02490.x

Nettancourt, D. D. (2001). *Incompatibility and incongruity in wild and cultivated plants* (Springer Science & Business Media).

O'Brien, M., Kapfer, C., Major, G., Laurin, M., Bertrand, C., Kondo, K., et al. (2002). Molecular analysis of the stylar-expressed Solanum chacoense small asparagine-rich protein family related to the HT modifier of gametophytic self-incompatibility in Nicotiana. *Plant J.* 32, 985–996. doi: 10.1046/j.1365-313X.2002.01486.x

Pease, J. B., Haak, D. C., Hahn, M. W., and Moyle, L. C. (2016). Phylogenomics reveals three sources of adaptive variation during a rapid radiation. *PloS Biol.* 14, e1002379. doi: 10.1371/journal.pbio.1002379

Peralta, I. E., Spooner, D. M., and Knapp, S. (2008). Taxonomy of wild tomatoes and their relatives (Solanum sect. Lycopersicoides, sect. Juglandifolia, sect. Lycopersicon; Solanaceae). *Systematic Bot. Monogr.* 84.

Puerta, A. R., Ushijima, K., Koba, T., and Sassa, H. (2009). Identification and functional analysis of pistil self-incompatibility factor HT-B of Petunia. *J. Exp. Bot.* 60, 1309–1318. doi: 10.1093/jxb/erp005

Qin, X., and Chetelat, R. T. (2021). Ornithine decarboxylase genes contribute to S-RNase-independent pollen rejection. *Plant Physiol.* 186, 452–468. doi: 10.1093/plphys/kiab062

Qin, X., Li, W., Liu, Y., Tan, M., Ganal, M., and Chetelat, R. T. (2018). A farnesyl pyrophosphate synthase gene expressed in pollen functions in S-RNase-independent unilateral incompatibility. *Plant J.* 93, 417–430. doi: 10.1111/tpj.13796

Rao, E. S., Kadirvel, P., Symonds, R. C., Geethanjali, S., Thontadarya, R. N., and Ebert, A. W. (2015). Variations in DREB1A and VP1.1 genes show association with salt tolerance traits in wild tomato (Solanum pimpinellifolium). *PloS One* 10, e0132535. doi: 10.1371/journal.pone.0132535

Salinas, M., Capel, C., Alba, J. M., Mora, B., Cuartero, J., Fernández-Muñoz, R., et al. (2013). Genetic mapping of two QTL from the wild tomato Solanum pimpinellifolium L. controlling resistance against two-spotted spider mite (Tetranychus urticae Koch). *Theor. Appl. Genet.* 126, 83–92. doi: 10.1007/s00122-012-1961-0

Schopfer, C. R. (1999). The male determinant of self-incompatibility in brassica. *Science* 286, 1697–1700. doi: 10.1126/science.286.5445.1697

Sehgal, N., and Singh, S. (2018). Progress on deciphering the molecular aspects of cell-to-cell communication in Brassica self-incompatibility response. *3 Biotech.* 8, 347. doi: 10.1007/s13205-018-1372-2

Silva, N. F., and Goring, D. R. (2001). Mechanisms of self-incompatibility in flowering plants. *Cell. Mol. Life Sci. CMLS* 58, 1988–2007. doi: 10.1007/PL00000832

Stahl, R. J., Arnoldo, M., Glavin, T. L., Goring, D. R., and Rothstein, S. J. (1998). The self-incompatibility phenotype in brassica is altered by the transformation of a mutant S locus receptor kinase. *Plant Cell* 10, 209–218. doi: 10.1105/tpc.10.2.209

Suzuki, G., Kai, N., Hirose, T., Fukui, K., Nishio, T., Takayama, S., et al. (1999). Genomic Organization of the S Locus: Identification and Characterization of Genes in SLG/SRK Region of S9 Haplotype of Brassica campestris (syn. rapa). *Genetics* 153, 391–400. doi: 10.1093/genetics/153.1.391

Takasaki, T., Hatakeyama, K., Suzuki, G., Watanabe, M., Isogai, A., and Hinata, K. (2000). The S receptor kinase determines self-incompatibility in Brassica stigma. *Nature* 403, 913–916. doi: 10.1038/35002628

Takasaki, T., Hatakeyama, K., Watanabe, M., Toriyama, K., Isogai, A., and Hinata, K. (1999). Introduction of SLG (S locus glycoprotein) alters the phenotype of endogenous S haplotype, but confers no new S haplotype specificity in Brassica rapa L. *Plant Mol. Biol.* 40, 659–668. doi: 10.1023/A:1006274525421

Takayama, S., and Isogai, A. (2005). Self-incompatibility in plants. *Annu. Rev. Plant Biol.* 56, 467–489. doi: 10.1146/annurev.arplant.56.032604.144249

Torres-Rodríguez, M. D., Cruz-Zamora, Y., Juárez-Díaz, J. A., Mooney, B., McClure, B. A., and Cruz-García, F. (2020). NaTrxh is an essential protein for pollen rejection in Nicotiana by increasing S-RNase activity. *Plant J.* 103, 1304–1317. doi: 10.1111/tpj.14802

Tovar-Méndez, A., Kumar, A., Kondo, K., Ashford, A., Baek, Y. S., Welch, L., et al. (2014). Restoring pistil-side self-incompatibility factors recapitulates an interspecific reproductive barrier between tomato species. *Plant J.* 77, 727–736. doi: 10.1111/tpj.12424

Tovar-Méndez, A., Lu, L., and McClure, B. (2017). HT proteins contribute to S-RNase-independent pollen rejection in Solanum. *Plant J.* 89, 718–729. doi: 10.1111/tpj.13416

Verlaan, M. G., Hutton, S. F., Ibrahem, R. M., Kormelink, R., Visser, R. G. F., Scott, J. W., et al. (2013). The tomato yellow leaf curl virus resistance genes ty-1 and ty-3 are allelic and code for DFDGD-class RNA–dependent RNA polymerases. *PloS Genet.* 9, e1003399. doi: 10.1371/journal.pgen.1003399

Verlaan, M. G., Szinay, D., Hutton, S. F., de Jong, H., Kormelink, R., Visser, R. G. F., et al. (2011). Chromosomal rearrangements between tomato and Solanum Chilense hamper mapping and breeding of the TYLCV resistance gene Ty-1. *Plant J.* 68, 1093–1103. doi: 10.1111/j.1365-313X.2011.04762.x

Vitale, L., Francesca, S., Arena, C., D'Agostino, N., Principio, L., Vitale, E., et al. (2023). Multitraits evaluation of a Solanum pennellii introgression tomato line challenged by combined abiotic stress. *Plant Biol.* 25, 518–528. doi: 10.1111/plb.13518

Wang, L., and Filatov, D. A. (2023). Mechanisms of prezygotic post-pollination reproductive barriers in plants. *Front. Plant Sci.* 14. doi: 10.3389/fpls.2023.1230278

Watanabe, M., Takasaki, T., Toriyama, K., Yamakawa, S., Isogai, A., Suzuki, A., et al. (1994). A high degree of homology exists between the protein encoded by SLG and the S receptor domain encoded by SRK in self-incompatible brassica campestris L. *Plant Cell Physiol.* 35, 1221–1229. doi: 10.1093/oxfordjournals.pcp.a078716

Wheeler, M. J., de Graaf, B. H. J., Hadjiosif, N., Perry, R. M., Poulter, N. S., Osman, K., et al. (2009). Identification of the pollen self-incompatibility determinant in Papaver rhoeas. *Nature* 459, 992–995. doi: 10.1038/nature08027

Wilkins, K. A. (2014). Taking one for the team: self-recognition and cell suicide in pollen. *J. Exp. Bot.* 65, 1331–1342. doi: 10.1093/jxb/ert468

Williams, J. S., Wu, L., Li, S., Sun, P., and Kao, T.-H. (2015). Insight into S-RNase-based self-incompatibility in Petunia: recent findings and future directions. *Front. Plant Sci.* 6, 41. doi: 10.3389/fpls.2015.00041

Zhang, H., Mittal, N., Leamy, L. J., Barazani, O., and Song, B.-H. (2017). Back into the wild—Apply untapped genetic diversity of wild relatives for crop improvement. *Evolutionary Appl.* 10, 5–24. doi: 10.1111/eva.12434

Zhao, H., Zhang, Y., Zhang, H., Song, Y., Zhao, F., Zhang, Y., et al. (2022). Origin, loss, and regain of self-incompatibility in angiosperms. *Plant Cell* 34, 579–596. doi: 10.1093/plcell/koab266

Zsögön, A., Čermák, T., Naves, E. R., Notini, M. M., Edel, K. H., Weinl, S., et al. (2018). *De novo* domestication of wild tomato using genome editing. *Nat. Biotechnol.* 36, 1211–1216. doi: 10.1038/nbt.4272

frontiers | Frontiers in Plant Science

TYPE Original Research
PUBLISHED 14 February 2024
DOI 10.3389/fpls.2024.1323665

OPEN ACCESS

EDITED BY
Anna N. Stepanova,
North Carolina State University, United States

REVIEWED BY
Athanasios Koukounaras,
Aristotle University of Thessaloniki, Greece
Fernanda Fidalgo,
University of Porto, Portugal

*CORRESPONDENCE
Noémie David-Rogeat
noemie.david-rogeat@nottingham.ac.uk

RECEIVED 18 October 2023
ACCEPTED 22 January 2024
PUBLISHED 14 February 2024

CITATION
David-Rogeat N, Broadley MR and Stavridou E (2024) Heat and salinity stress on the African eggplant F1 Djamba, a Kumba cultivar. *Front. Plant Sci.* 15:1323665. doi: 10.3389/fpls.2024.1323665

Heat and salinity stress on the African eggplant F1 Djamba, a Kumba cultivar

Noémie David-Rogeat[1,2]*, Martin R. Broadley[1,3] and Eleftheria Stavridou[2]

[1]Department of Plant Sciences, School of Biosciences, University of Nottingham, Nottingham, United Kingdom, [2]Crop Science and Production Systems, NIAB, Kent, United Kingdom, [3]Rothamsted Research, Harpenden, United Kingdom

Climate change is expected to increase soil salinity and heat-wave intensity, duration, and frequency. These stresses, often present in combination, threaten food security as most common crops do not tolerate them. The African eggplant (*Solanum aethiopicum* L.) is a nutritious traditional crop found in sub-Saharan Africa and adapted to local environments. Its wider use is, however, hindered by the lack of research on its tolerance. This project aimed to describe the effects of salinity (100 mM NaCl solution) combined with elevated temperatures (27/21°C, 37/31°C, and 42/36°C). High temperatures reduced leaf biomass while cell membrane stability was reduced by salinity. Chlorophyll levels were boosted by salinity only at the start of the stress with only the different temperatures significantly impacted the levels at the end of the experiment. Other fluorescence parameters such as maximum quantum yield and non-photochemical quenching were only affected by the temperature change. Total antioxidants were unchanged by either stress despite a decrease of phenols at the highest temperature. Leaf sodium concentration was highly increased by salinity but phosphorus and calcium were unchanged by this stress. These findings shed new light on the tolerance mechanisms of the African eggplant under salinity and heat. Further research on later developmental stages is needed to understand its potential in the field in areas affected by these abiotic stresses.

KEYWORDS

Solanum aethiopicum, salinity, heat-wave, stomatal conductance, antioxidants

1 Introduction

The last decade has been marked by increasing temperatures and longer, more intense, and more frequent heatwaves around the world, in particular in Africa (Pörtner et al., 2022). High temperatures threaten food security as most crops grown worldwide are heat-sensitive (Hassan et al., 2021). The yield reduction is due to various mechanisms triggered by heat including the reduction of leaf expansion and gas exchange to limit water loss

alongside the damages to enzymes and other key parts of the photosynthesis system due to the high leaf temperature (Hassan et al., 2021). In addition, soil salinization is increasing worldwide due to a combination of natural and man-made processes (Pörtner et al., 2022). Soil salinity also negatively impacts crop growth, leading to stunted growth and poor yields due to limited water uptake and ion imbalance (Ondrasek et al., 2022).

Under field conditions, heat and salinity often occur concurrently, especially in coastal areas. While soil salinity leads to an increase in sodium ion uptake, limiting the uptake of essential nutrients and toxic for cells, heat destroys cell membranes through the denaturation of enzymes and other compounds. These two highly damaging processes have antagonistic activity due to the key role of membranes in nutrient uptake and translocation within the plant, leading to a negative impact of the stress combination (Nadeem et al., 2022). The interaction of most processes under the combination of heat and salinity is still largely unknown. For example, heat stress might promote stomatal conductance to regulate leaf temperature but salinity stress tends to decrease it to limit water loss. It is therefore important to study their combination to understand the mechanisms in place and be able to accurately predict the impact of environmental stress on crop growth.

The introduction of tolerant and diverse crops in food production systems is crucial to enhancing food security and consumers' nutrition. Indigenous vegetables are generally more tolerant to stress than their exotic counterparts due to their selection in harsh environments and their large genetic assortment (Akinola et al., 2020). For example, wild tomatoes *Solanum cheesmaniae* L. Ridley displayed higher salinity tolerance than the commercial tomato by maintaining leaf water content, improving leaf elongation and potassium uptake, and limiting sodium ions uptake (Pailles et al., 2020). Even though indigenous vegetables have been poorly studied in the past, they have strong local importance and include all types of crops including legumes, cereals, and vegetables (Akinola et al., 2020). *Solanum aethiopicum* L., the African eggplant, is indigenous to Africa and present in multiple forms across sub-Saharan Africa, displaying a great genetic diversity and nutrition (Han et al., 2021). It is liked for its nutritional quality and is an important income stream for small-scale farmers across the African continent (Han et al., 2021). The African eggplant has been selected by the World Vegetable Center as a priority crop for breeding strategies to improve field resilience and diversity (Dinssa et al., 2016). The African eggplant's salinity tolerance was low, however, as reported by de Fatima et al. (2023) with reductions in growth and gas exchange of more than 10% observed when soil salinity was above 1.37 dS m^{-1}. Interestingly, stomatal conductance was enhanced by salinity, an increase explained by the energy re-deployment from plant growth to stomatal dynamics (de Fatima et al., 2023). In contrast, a decrease in stomatal conductance and photosynthetic parameters were noted in another African eggplant cultivar under heat (Nkansah, 2001). The vegetative growth, in this case, increased between 30°C and 40°C, suggesting contrasting impacts of heat and salinity in the African eggplant (Nkansah, 2001).

New varieties of the African eggplant are being developed industrially but lack research on their abiotic stress tolerance to ensure their relevance in the field in stress-prone areas. This is the case of the cultivar F1 Djamba developed by Novagenetic (Technisem, Longué-Jumelles, France) and promoted for its high yield. Technisem market includes tropical areas in Northern and Western Africa, which are highly likely to experience a high heat increase due to climate change alongside a constant increase in soil salinity (World Meteorological Organization, 2022). Understanding how F1 Djamba responds to the combination of stresses is thus crucial to ensure its use in every possible area. In addition, its response will be useful to get a better understanding of how the African eggplant responds to stress for future breeding.

This study aimed to understand how soil salinity and heat affect the African eggplant cv. F1 Djamba when present individually and in combination. Leaf biomass, photosynthesis parameters, and leaf biochemical analysis including proteins, antioxidants, and nutrient concentrations were assessed to clarify some stress-related mechanisms used by the African eggplant. It was hypothesized that the combination of heat and salinity would lead to specific responses not observed when the stresses were present individually. This research will be useful to understand how this plant can be used in future climates.

2 Materials and methods

2.1 Plant material and growth conditions

The combination of salinity stress and high temperatures on the African eggplant Kumba (*Solanum aethiopicum* L. cv., F1 Djamba) was investigated. F1 Djamba seeds, generously provided by Novagenetic (Technisem, Longué-Jumelles, France), were sown in modular trays in John Innes No.2 soil compost (7 loam:3 peat:2 sand) (Westland®, J Arthur Bower's) and placed in an MLR-352 growth cabinet (PHC Holdings Corporation®, Tokyo, Japan). The environmental conditions were set at 70% relative humidity, 27/21° C for a 12 h photoperiod. After four weeks, 24 homogenous seedlings were transplanted in 3 L pots (at a rate of one plant per pot) in John Innes No.2 soil and placed following a split-plot design in three growth cabinets (Plant growth chamber A1000, Conviron®, Winnipeg, Canada) fitted with Valoya LEDs lights (BX NSI spectrum 'white' LED, Valoya®, Helsinki, Finland) providing 350 μmol m^{-2} s^{-1} light intensity. The growing conditions stayed the same.

2.2 Treatment application

After 11 days of acclimation under optimal conditions, salinity stress was applied to four plants per cabinet by watering them using 100 mM NaCl solution while the other four plants, used as the control, received only water. This sodium chloride concentration corresponds to a soil electrical conductivity of around 9.8 dS m^{-1}, considered highly saline (West, 1975). As the stress was applied as irrigation for only 12 days, rather than an initial mix of the salt into the soil, this high level was selected to ensure a significant increase in soil salinity. All the plants were irrigated with the same amount of NaCl. At the same time, considered to be 1 DASH (days after salinity and heat), heat stress was applied in two of the cabinets with a maximum of 37/31°C (T37) and 42/36°C (T42) day/night

temperature when compared to 27/21°C (T27) for the control plants, a treatment also maintained for 12 days. These increased temperatures were selected based on previous research on the African eggplant (data not shown) and on temperatures sometimes reached in Northern and Western Africa during heat waves, with T42 also being higher than the average monthly temperature of most countries in Northern and Western Africa to mimic extreme conditions (Worlddata, 2023). To ensure plants were well-watered throughout the experiment, soil water content was monitored using an HH2 moisture meter attached to a WET sensor (Delta-T devices®, Burwell, UK). The daily schedules of each treatment are shown in Figure 1. The experiment was repeated once with four replicates per treatment each time.

2.3 Growth and physiological measurements

2.3.1 Leaf expansion rate

Three times a week, the length and maximum width of two labelled leaves were recorded. These leaves were originally labelled at a similar height and developmental stage and were less than 30 mm in length. The length and width leaf expansion rate (LER) were considered to be the growth difference between the repeated measurements.

2.3.2 Chlorophyll fluorescence and gas exchange

Leaf fluorescence parameter SPAD, measuring the transmittance of red and infrared through the leaf, and photosynthetic parameters photosystem II quantum yield ($\phi 2$) and quantum yields of non-photochemical exciton quenching (ϕNPQ) were measured three times a week 5 h after the start of the photoperiod from 0 to 12 DASH using a MultispeQ V2.0 device with Photosynthesis RIDES 2.0 protocol (PhotosynQ®, East Lansing, MI, United States) (Kuhlgert et al., 2016). Leaf chlorophyll, flavonoids, and nitrogen balance were measured three times a week at the same time from 0 to 12 DASH using a Dualex® device (ForceA, Montpellier, France). Stomatal conductance was recorded at 4 h after the start of the photoperiod at 0, 1, 7 and 12 DASH using a leaf porometer (Model SC-1, Decagon Devices, METER group, Pullman, WA, United States). At 12 DASH, diurnal measurements were taken at 0, 4, 8, and 12 h after the start of the photoperiod.

2.3.3 Destructive harvest

On the last day of the experiment, 12 DASH, a leaf sub-sample representing a mix of developing and developed leaves was removed from the plant, placed in liquid nitrogen straight after recording its combined weight, and stored at -80°C for biochemical analysis. Leaves and stems were weighed separately, after measuring leaf number, stem diameter and plant height, and oven-dried at 80°C until reaching a constant weight.

2.3.4 Leaf electrolyte leakage

One leaf disc (10 mm diameter) was cut out from five fully expanded leaves on each plant at the end of the treatment (12 DASH). The discs were washed three times with distilled water to remove surface contamination and placed in 20 mL of distilled water. The discs were incubated at room temperature on a shaker at 200 rpm for 24 h and the electrical conductivity of the bathing solution (EC1) was eventually recorded using a LAQUAtwin EC-33 meter (Horiba®, Kyoto, Japan). The discs were then placed in a water bath at 95°C for 60 min and a second electrical conductivity reading (EC2) was taken after cooling the solution to room temperature. The electrolyte leakage (EL), expressed as % EL, was calculated as per Equation 1:

$$EL = EC1/EC2 * 100 \quad (1)$$

2.4 Soil electrical conductivity

On the last day of the experiment, a soil sample from each pot was extracted and left to air-dry until reaching constant weight. Five grams of the dry soil was then added to 25 mL of distilled water, shaken, and left to settle for 24 h as described in He et al. (2012). The electrical conductivity of the supernatant (EC 1:5) was then measured using a LAQUAtwin EC-33 meter (Horiba®).

2.5 Biochemical analysis

2.5.1 Leaf chlorophyll content

Leaf chlorophyll content was determined following the method described in Wintermans and De Mots (1965). At 12 DASH, two

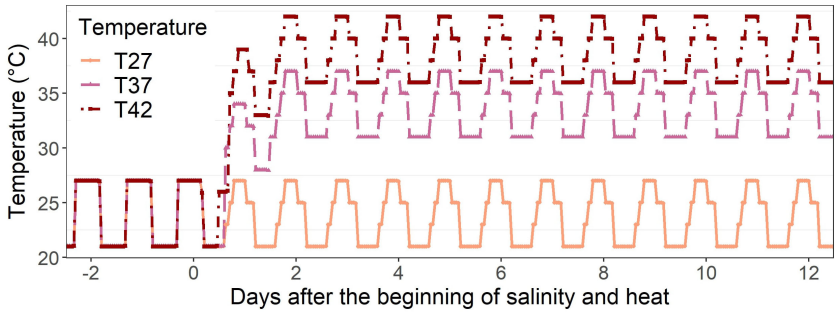

FIGURE 1
Daily temperature schedule of 27°C (T27), 37°C (T37), and 42°C (T42) treatments throughout the experimental period (from -2 DASH to 12 DASH).

leaf discs (1.54 cm^2 each) from the first two fully expanded leaves were immersed in 10 mL 95% cold ethanol (Fischer Scientific, Hampton, NH, United States) and kept at 4°C in the dark for 48 h. The absorbance of the supernatant was read at 470, 649, and 665 nm using a UV-VIS spectrophotometer (Ultrospec III, Pharmacia LKB, Stockholm, Sweden). The amount of chlorophyll a (Chl a) and b (Chl b) and carotenoids (Car) per unit area were calculated following Equations 2–4:

$$Chl\ a = (13.95 * A649)/1.54 \quad (2)$$

$$Chl\ b = (24.96 * A649 - 7.32 * A665)/1.54 \quad (3)$$

$$Car = (10^3 * A470 - 2.05 * Chl\ a - 114.8 * Chl\ b)/1.54 \quad (4)$$

2.5.2 Total carbohydrates

The amount of soluble sugars in plants at 12 DASH was quantified using the phenol-sulfuric acid colorimetric method (Dubois et al., 1956). A dry leaf sample (50 mg) was dissolved in 5 mL of 80% cold methanol (Fischer Scientific). Subsequently, 100 μL of the resulting solution was combined with 900 μL of distilled water, 2.5 mL of sulfuric acid (Fischer Scientific), and 500 μL of a 5% phenol (Fischer Scientific) solution. After incubating for 20 min at room temperature, the absorbance was measured at 490 nm using a UV-VIS spectrophotometer (Ultrospec III). Glucose (Merck, Darmstadt, Germany) served as the standard.

2.5.3 Total antioxidants

The TEAC (Trolox Equivalent Antioxidant Capacity) method was used to determine total antioxidants (Re et al., 1999). A solution of 7 mM ABTS (Merck) with 2.45 mM potassium persulfate (Merck) was made and left in darkness overnight. This solution was then diluted with ethanol (Fischer Scientific) until reaching an absorbance of 0.9 at 734 nm and warmed on a hotplate at 40°C. Fifty milligrams of dry leaf sample (extracted at 12 DASH) was diluted in 5 mL of 80% cold methanol (Fischer Scientific) and 30 μL of the sample supernatant was pipetted in 3 mL of the diluted working solution. After 15 min in a 40°C water bath, the absorbance of the samples was read at 734 nm in a UV-VIS spectrophotometer (Ultrospec III).

2.5.4 Total phenols

The Folin-Ciocalteau method described by Singleton et al. (1999) was used to measure leaf phenol content on the final day of the experiment (12 DASH). Cold methanol (80%, Fischer Scientific) was used to digest 50 mg of dry leaf sample and 300 μL of the digested sample was added to 600 μL of 10% Folin-Ciocalteau reagent (Merck) and left to stand for 2 min. Then, 2.5 mL of 700 mM sodium carbonate (Fischer Scientific) was added. The mixture was left to stand at room temperature for 1 h, after which the absorbance of each sample was read at 765 nm in a UV-VIS spectrophotometer (Ultrospec III). Gallic acid (Merck) was used as a standard.

2.5.5 Leaf nutrient concentration

Dried and milled leaf sample (300 mg), extracted at 12 DASH, was digested in 6 mL of nitric acid and placed in a digestion microwave (Multiwave PRO, Anton Paar, Graz, Austria) reaching 175°C over a 20 min period and maintained for a further 20 min followed by a 10 min cool down at 55°C. This digested extract was diluted by a factor of 36 by adding 18.2 milliQ water for multi-element analysis by ICP-MS (Inductively Couple Plasma Mass Spectrophotometry, Thermo-Fisher Scientific iCAP-Q; Thermo Fisher Scientific, Germany). Calibration standards included a multi-element solution (Claritas-PPT grade CLMS-2 from SPEX Certiprep Inc., Metuchen, NJ, United States) and a bespoke external multi-element calibration solution (PlasmaCAL, SCP Science, Quebec, Canada).

A FlashEA®1112 elemental analyzer (Thermo Fischer Scientific, Waltham, MA, United States) was used to determine leaf nitrogen concentration by burning 50 mg of dried and milled samples placed in a foil capsule. The gas mixture generated by combustion was filtrated and elemental nitrogen was detected by conversion, providing a nitrogen percentage.

2.6 Statistical analysis

Statistical studies were performed on R version 4.1.2. The data was assessed for normality and variance homogeneity of residuals. Normality was checked using a combination of the Shapiro test and visual evaluation (density plot, Q-Q plot, and histogram). Variance homogeneity was assessed using Levene's test and visual inspection of the residuals. When the requirements were met, a two-way analysis of variance (ANOVA) test was performed on continuous data using "Salinity" and "Temperature" as the main factors and including their interaction. Tukey adjustment at a 0.05 significance level was used to test for pairwise comparison among and across groups. Whenever the interaction of stresses was significant, the interaction parameter was used for posthoc tests and letters were used to show the significance throughout the manuscript for clarity. A linear mixed-effects model was also used to analyze time series of continuous data including the interaction of the parameters of interest with time and the repetitive measurement of each plant as a random factor. For count data, a generalized linear model fitted with a Poisson distribution was checked for overdispersion and used for analysis with "Salinity" and "Temperature" as interacting factors.

The log values of leaf sodium concentration were used for statistical analysis to improve residuals' normality and homogeneity due to the extreme treatment effect observed on the original dataset.

3 Results

The salinity treatment significantly increased soil EC 1:5 at every temperature (Figure 2). In addition, T37 and T42 had a significantly higher soil EC 1:5 than T27 under salinity (Figure 2).

10.3389/fpls.2024.1323665

3.1 Plant development

A linear decrease of leaf dry weight under increasing temperature was observed under both saline and non-saline conditions and salinity also decreased it (Figure 3A). Stem dry weight was maintained at T37 and reduced at T42 under 0 mM NaCl but was reduced for both T37 and T42 under 100 mM NaCl when compared to T27 (Figure 3B). Salinity did not impact stem dry weight. Plant height was only reduced by T42 under 0 mM NaCl conditions while plants under salinity were not impacted when compared to the control (Figure 3C). Salinity also impacted shoot development by reducing stem diameter while only the highest temperature reduced it in both 0 and 100 mM NaCl treatments (Figure 3D). Leaf number followed a similar pattern and was only reduced by T42 under both 0 and 100 mM NaCl conditions (Figure 3E).

Electrolyte leakage was increased by salinity but not significantly impacted by the temperatures at 0 mM NaCl and reduced by T37 when compared to T27 under 100 mM NaCl (Figure 3F).

While an increase in both length and width LER was observed from the 1st day of the treatment to the 3rd, only T27 plants continued to increase up to day 6 with T37 and T42 growth rates reducing slightly (Figure 4). From the 6th day, T42 treatment reduced length LER significantly when compared to T27 in both salinity treatments but only reduced width LER of plants under 0 mM NaCl on day 6 and 8 (Figure 4). Salinity reduced length LER on day 6 at every temperature (Figure 4). On day 8, length and width LER were only reduced for T27 and T37 plants by salinity and no further impact was noted for the rest of the experiment due to salinity (Figure 4). Both plants under saline and non-saline conditions had the same pattern of initial LER increase before slowing down and stabilizing.

3.2 Leaf chlorophyll and polyphenols

Salinity increased chlorophyll index throughout the stress (Figure 5A). Under 100 mM NaCl, chlorophyll index increased more quickly under T37 and T42 than T27 until 4 DASH and stabilized thereafter. The chlorophyll index of T27 plants, however, continued to increase until the end of the experiment and surpassed T37 and T42 levels at 8 DASH (Figure 5A). Although at no-saline conditions the chlorophyll index was not statistically different throughout the stress period between the temperature treatments, the T42 plants had lower levels than the other two temperatures at 12 DASH (Figure 5A). Salinity increased SPAD index halfway through the experiment with significant differences appearing from day 6 until day 10 (Figure 5B). The temperature stress also affected SPAD under 0 mM NaCl, with a decrease from day 8 on plants grown at T42 (Figure 5B). Under 100 mM NaCl, T42 only significantly reduced SPAD on day 10 and day 12 (Figure 5B). T42 reached its peak SPAD earlier than the other temperatures at 100 mM NaCl (Figure 5B).

Neither flavonoids nor nitrogen balance index were impacted by salinity, but they decreased and increased, respectively, under T37 and T42 from the 3rd day of stress (Figures 5C, D). Temperature decreased flavonoids from day 3 to 8, after which the T37 and T42 levels started to increase without fully recovering (Figure 5C). While the nitrogen balance index at T27 remained stable throughout the experiment, both T37 and T42 increased from day 3 to day 8 (Figure 5D). From day 8, the nitrogen balance index of T37 and T42 started to decrease and eventually reached the same level as T27 at the end of the experiment (Figure 5D). The highest nitrogen balance index was reached under the T37 treatment on day 8 while the T42 treatment effect was more moderate (Figure 5D).

Salinity did not impact final chlorophyll content (Figure 6). The highest temperature, on the other hand, decreased chlorophyll a, b, and carotenoids (Figures 6A–C). The ratio of chlorophyll a over b was increased for T42 plants compared to T37 but not T27 (Figure 6D).

3.3 Stomatal conductance and leaf fluorescence

Midday stomatal conductance increased significantly only for T37 at 100 mM NaCl when compared to the control at 1 DASH

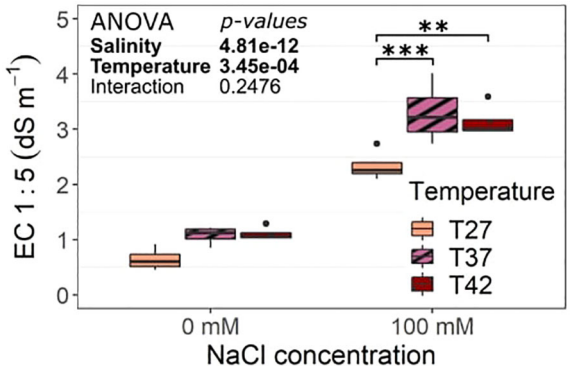

FIGURE 2
Soil electrical conductivity (EC) 1:5 at the end of the salinity treatment. The data are represented by the lower and upper whiskers, which extend to a maximum of 1.5 x Interquartile range, 25% and 75% quartiles, and median (n = 4). Stars denote the significance level based on the Tukey pairwise comparison at 95% confidence level with **p<.01 and ***p<.001. Non-significant interactions are not shown for clarity.

10.3389/fpls.2024.1323665

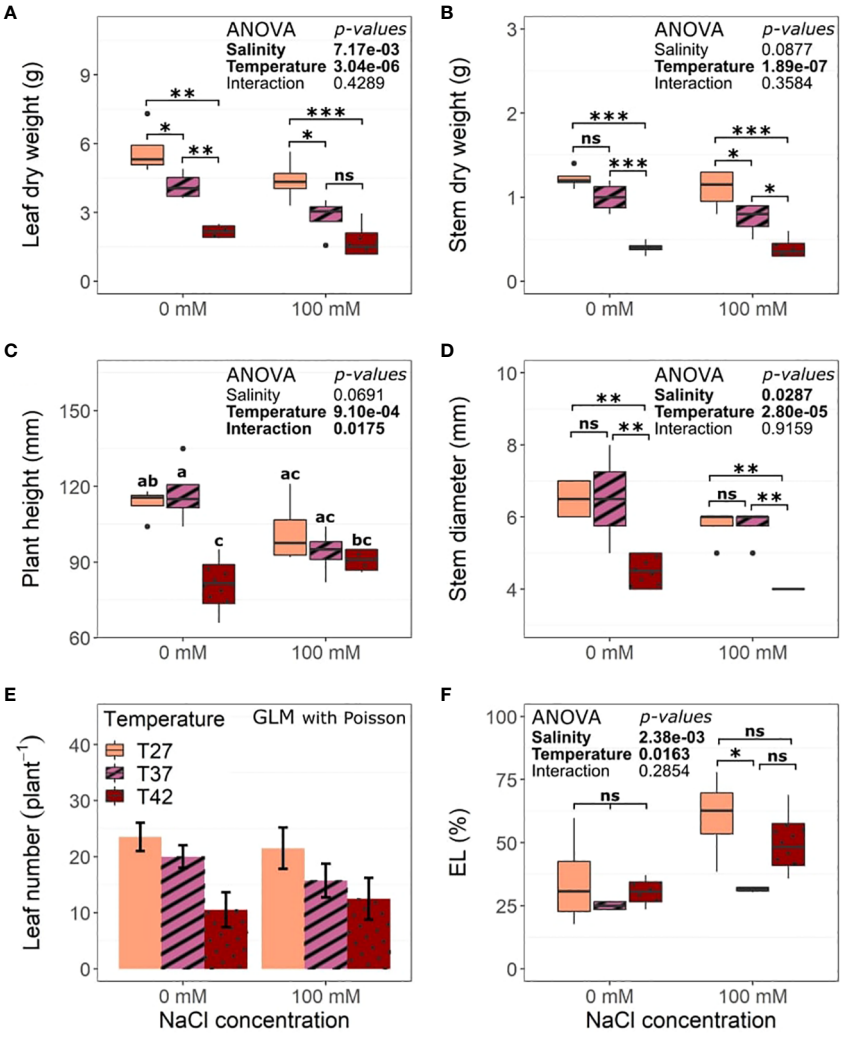

FIGURE 3
Morphological characteristics of the African eggplant at the end of the 12 days under salinity and increased temperature. Sub-plots represent **(A)** leaf dry weight, **(B)** stem dry weight, **(C)** plant height, **(D)** stem diameter, **(E)** number of leaves per plant and **(F)** electrolyte leakage (EL). The continuous datasets are represented by the lower and upper whiskers, which extend to a maximum of 1.5 x Interquartile range, 25% and 75% quartiles, and median (n = 4). Black dots represent outliers. Stars denote the significance level based on the Tukey test at 95% confidence level with * for p<.05, **p<.01, and ***p<.001. For measures where the interaction of the parameters was significant after the ANOVA, letters are used to display the difference between treatments for clarity. Boxplots not sharing any letters are significantly different in these cases. Count data are represented as the mean +/- standard deviation. ns, Non significant.

(Figure 7A). At 7 DASH, however, T42 at 0 and 100 mM NaCl was significantly higher than the control but not T37 (Figure 7A). The temperature treatment had the biggest effect on midday stomatal conductance on day 7 with both saline and non-saline T37 and T42 plants reaching their highest level then (Figure 7A). No differences between treatments were recorded on the last day of the experiment. Stomatal conductance of T42 plants dropped significantly on that day and stayed stable for T27 and T37 (Figure 7A). When looking at diurnal stomatal conductance throughout the last treatment day (12 DASH), the strongest difference was noted at the beginning of the day with a low stomatal conductance under T42 at 0 mM NaCl and under both T37 and T42 at 100 mM for the first hour of light (0 h) (Figure 7B). As the day progressed, stomatal conductance increased quickly in plants under the T42 treatment while plateaued, or even reduced, in the other temperatures (Figure 7B). The T42 treatment thus reached the same stomatal conductance as T27 and T37 eight hours after the start of the photoperiod at 0 mM NaCl (Figure 7B). T42 plants also reached their peak stomatal conductance eight hours after the beginning of the photoperiod at 100 mM NaCl (Figure 7B). At 0 mM NaCl, T37 stomatal conductance also peaked 8 h after the beginning of the photoperiod and was significantly higher than T27 (Figure 7B). The T27 plants reached their peak stomatal conductance earlier, at 4 hours after the beginning of the photoperiod. Salinity mostly affected T37 plants, which had the lowest stomatal conductance at every time point, even though only significant at the beginning and the end of the photoperiod (Figure 7B).

The T42 treatment decreased the quantum yield of photosystem II ($\phi 2$) at 1, 6, 8 and 12 DASH under both salinity and no salinity treatments (Figure 8A). This was exacerbated by salinity towards the end of the stress period (Figure 8A). The ratio of incoming light

10.3389/fpls.2024.1323665

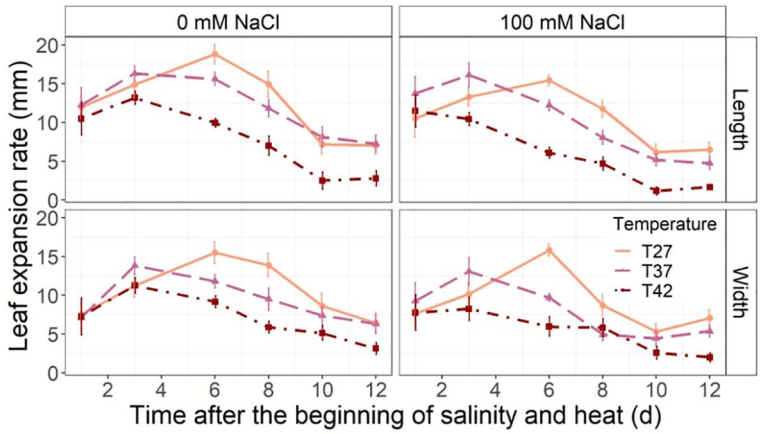

FIGURE 4
Leaf length (top row) and width (bottom row) expansion rate throughout the salinity and increased temperature. The data are shown as mean +/- standard error.

going through non-photochemical quenching (ϕNPQ) was only increased by the combination of salinity and the highest temperature at the end of the experiment at 10 and 12 DASH (Figure 8B). The ϕNPQ and ϕ2 remained constant throughout the stress period for T27 and T37 at both salinity levels (Figure 8).

3.4 Biochemical analysis

Total carbohydrates increased under T37 and T42 at 0 mM NaCl condition when compared to T27 plants, but that was not observed at 100 mM NaCl (Figure 9A). Total phenols were impacted by the temperatures with a decrease as temperature increased in both saline and non-saline treatments while salinity also decreased its levels (Figure 9B). The decrease in phenol content was noted for both T37 and T42 under 100 mM NaCl but was only significant for T42 under 0 mM NaCl treatment (Figure 9B). Total antioxidants were unchanged by either stress or their interaction (Figure 9C).

Leaf sodium concentration increased significantly for plants grown under 100 mM NaCl (Table 1). Both T37 and T42 increased the leaf sodium concentration when compared to T27 while T37 and T42 were not statistically different (Table 1). Leaf nitrogen concentration was reduced as temperature increased and when

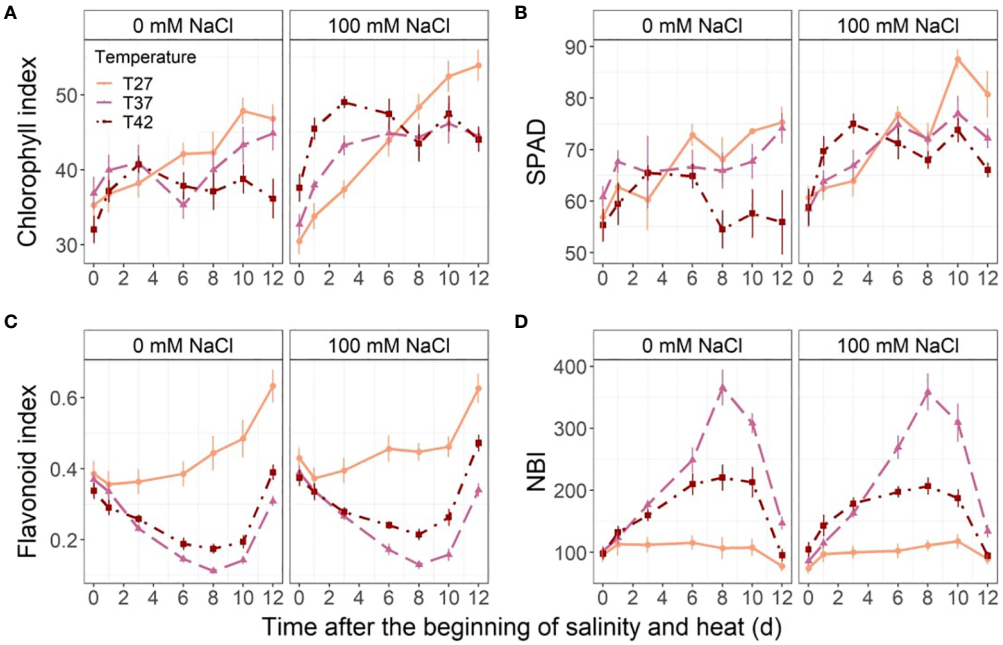

FIGURE 5
Leaf chlorophyll and polyphenols throughout the stress period. Sub-plots represent **(A)** chlorophyll index, **(B)** SPAD, **(C)** flavonoid index and **(D)** nitrogen balance index (NBI). The data are shown as mean +/- standard error.

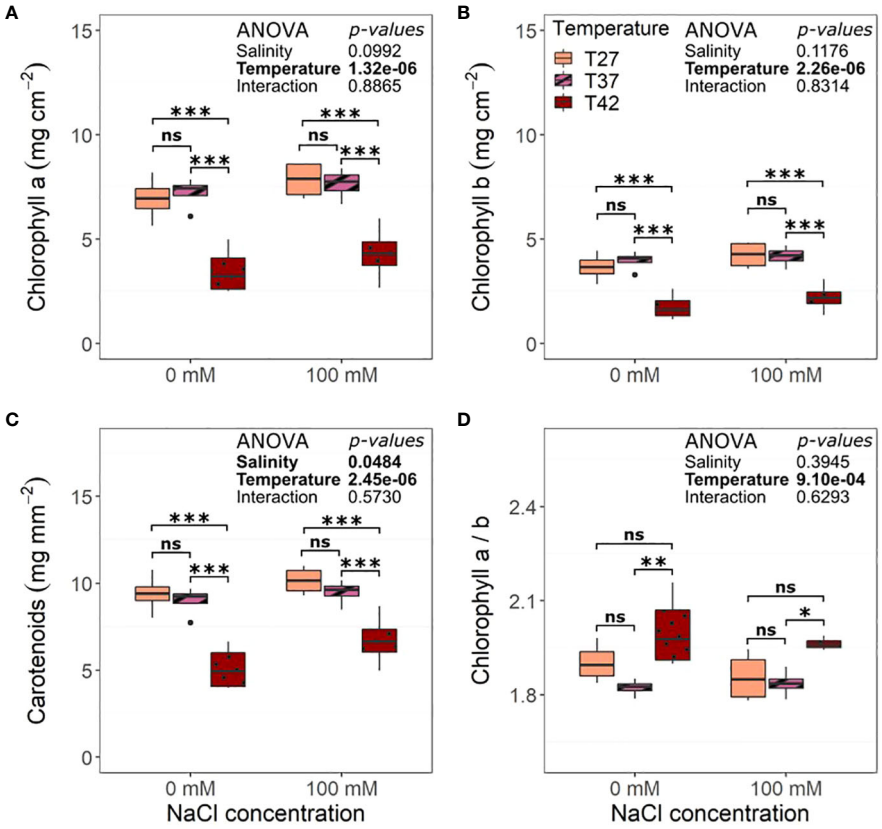

FIGURE 6
Leaf pigment content per unit area of the African eggplant after 12 days under salinity and increased temperature. Sub-plots represent **(A)** chlorophyll a, **(B)** chlorophyll b, **(C)** carotenoids, and **(D)** the ratio of chlorophyll a over chlorophyll b. The data are represented by the lower and upper whiskers, which extend to a maximum of 1.5 x Interquartile range, 25% and 75% quartiles, and median (n = 4). Black dots represent outliers. Stars denote the significance level based on the Tukey test at 95% confidence level with * for p<.05, **p<.01, and ***p<.001. ns, Non significant.

under salinity (Table 1). Leaf phosphorus concentration was unaffected by the salinity treatment but was increased by T37 and T42 when compared to T27 (Table 1). Leaf potassium concentration was reduced by salinity at both T27 and T37 but not at T42 (Table 1). Under 100 mM, T42 plants displayed the highest leaf potassium concentration while, under 0 mM NaCl, leaf potassium concentration was the highest in the T37 treatment (Table 1). Leaf calcium concentration was only affected by T42 with a significant increase when compared to T27 but was not changed by salinity (Table 1). The treatments and their interaction did not affect leaf magnesium concentration (Table 1).

Leaf manganese concentration was increased by T37 and T42 under both salinity levels (Table 1). Leaf copper concentration was increased by salinity and by T37 significantly but not by T42 when compared to T27 (Table 1). T37 was also the only treatment to increase leaf zinc concentration while T42 and salinity did not impact it significantly (Table 1). Under 0 mM NaCl, leaf iron concentration was initially increased by T37 from T27 but decreased significantly at T42 (Table 1). The initial increase was not observed under 100 mM NaCl but the decrease at T42 was also present (Table 1). Salinity also decreased leaf iron concentration for T37 plants (Table 1).

4 Discussion

The harmful or beneficial effects of salinity and heat have been reported for a range of crops but their combination is still only sparsely studied (Suzuki et al., 2014). In this study, while some plant parameters were affected by the individual stresses and not further impacted by the stress combination, such as chlorophylls and shoot dry weight, other traits responded differently to the combination of heat and salinity, in particular leaf fluorescence parameters.

Despite a slight decline in leaf expansion rate, salinity did not impact the final leaf production in the current study, which contrasts with what was previously observed in other *Solanum* species (Efimova et al., 2018; Alsafari et al., 2019; Ortega-Albero et al., 2023). Bacha et al. (2017) observed a decrease in leaf area after 14 days of stress while no differences were noted after 7 days, highlighting the role of salinity build-up and tolerance variation through time. In the current study, both high temperatures reduced leaf dry weight but leaf expansion rate and leaf number were only reduced at 42°C, suggesting another reason involved in the reduction observed at 37°C. A similar pattern was noted in a tomato (*S. lycopersicum* L.) cultivar with no reduction in leaf area and leaf number but a reduction in final shoot dry weight under heat (Zhou et al., 2017). The production of thinner leaves at high

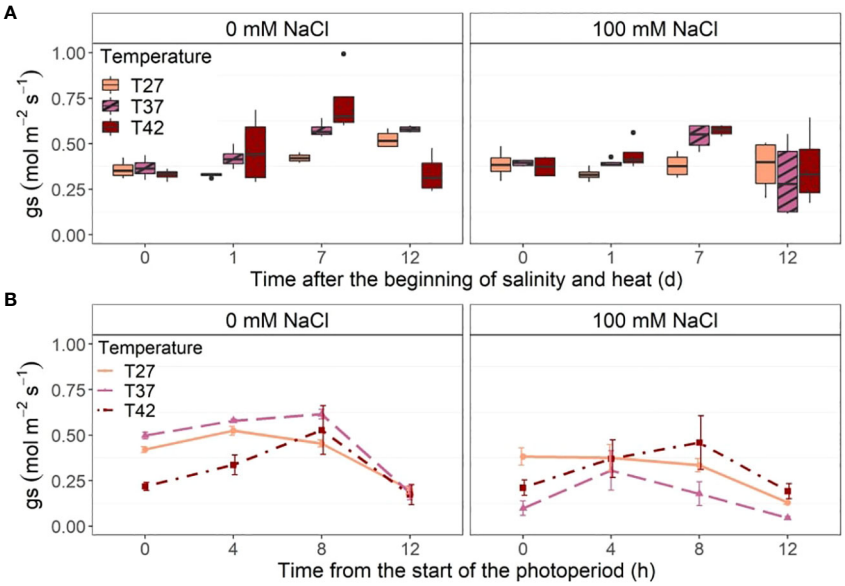

FIGURE 7
Stomatal conductance (gs) of the African eggplant. Sub-plots represent **(A)** midday stomatal conductance throughout the experiment and **(B)** diurnal stomatal conductance throughout the last day of the experiment (12 DASH). The data in **(A)** are represented by the lower and upper whiskers, which extend to a maximum of 1.5 x Interquartile range, 25% and 75% quartiles, and median (n = 4). Black dots represent outliers. The data in **(B)** are shown as mean +/- standard error.

temperatures to reduce leaf temperature, despite its impact on plant water status and membrane stability, might explain the reduction in leaf dry weight (Schiattone et al., 2017).

Salinity decreased membrane stability in the current study as in Ben Abdallah et al. (2016) study on *S. nigrum* L. Shunkao et al. (2022) reported a further decrease in membrane stability when both heat and salinity when present in wheat (*Triticum aestivum* L.), similar to what was observed in this current study at T42. However, T37 had a mitigating effect with a non-significant decrease in membrane stability which might be due to a level of protection offered by a moderate increase in temperature. Despite studies having previously shown that heat can have a protective effect against salinity on photosynthesis or sodium transport rate, similar observations in membrane stability have yet to be made (Rivero et al., 2014; Lopez-Delacalle et al., 2021). The protection effect observed in this current study might be linked to the increased leaf

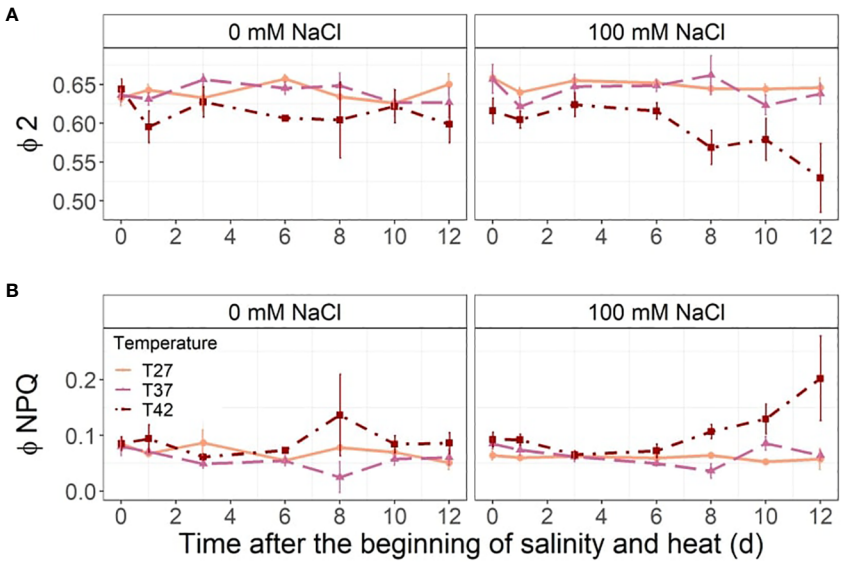

FIGURE 8
Leaf fluorescence parameters throughout the salinity and increased temperature. Sub-plots represent **(A)** quantum yield of photosystem II (ϕ 2) and **(B)** ratio of incoming light going through nonphotochemical quenching (ϕ NPQ). The data are shown as mean +/- standard error.

10.3389/fpls.2024.1323665

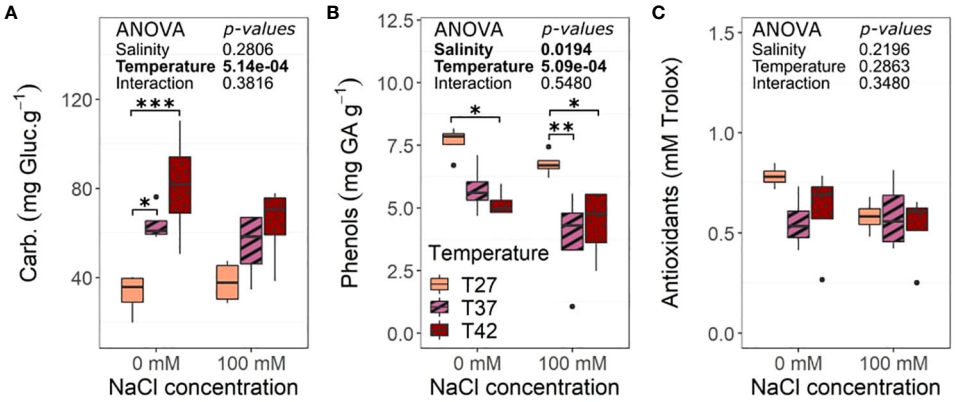

FIGURE 9
Biochemical analysis of the African eggplant dry leaves at the end of the 26 days under salinity increased temperature. Sub-plots represent **(A)** total carbohydrates, **(B)** phenols, and **(C)** total antioxidants activity. The data are represented by the lower and upper whiskers, which extend to a maximum of 1.5 x Interquartile range, 25% and 75% quartiles, and median (n = 4). Stars denote the significance level based on the Tukey test at 95% confidence level with * for p<.05, **p<.01, and ***p<.001. Non-significant interactions are not shown for clarity. Carbs, Carbohydrates; Gluc, Glucose; GA, Gallic Acid.

zinc concentration under moderate heat, a mineral element previously linked to improving membrane stability under stress (Tufail et al., 2018; Hassan et al., 2020). In accordance with the protective effects of temperature on membrane stability only appearing at T37, the increased leaf zinc concentration was not noted at T42, at which point membrane stability was reduced. Surprisingly, temperature alone did not impact membrane stability despite the negative effects of T42 on other measured characteristics being significant. Electrolyte leakage is positively correlated to the reactive oxygen species accumulation and lipid peroxidation, not

TABLE 1 Analysis of variance and mean comparisons for leaf nutrient concentrations of the African eggplants grown under different salinity and temperature levels.

Source of variance	Na	N	P	K	Ca	Mg	Mn	Cu	Zn	Fe
	g kg^{-1}						mg kg^{-1}			
Salinity (S)	***	**	ns	***	ns	ns	ns	**	ns	***
Temperature (T)	***	***	***	ns	**	ns	***	**	**	***
S x T	ns	ns	ns	*	ns	ns	**	ns	ns	*
Salinity										
0 mM NaCl	0.27^{b}	60.20^{a}	7.55	43.70	25.77	6.43	110.1	2.26^{b}	25.45	96.52
100 mM NaCl	12.27^{a}	55.08^{b}	7.43	31.70	29.40	7.17	108.3	3.01^{a}	30.02	82.35
Temperature										
T27	2.45^{b}	63.14^{a}	6.67^{b}	36.14	23.20^{b}	7.00	68.08	2.04^{b}	22.48^{b}	98.47
T37	7.31^{a}	57.72^{b}	8.03^{a}	39.42	25.24^{ab}	6.54	123.1	3.18^{a}	34.20^{a}	103.9
T42	9.04^{a}	51.81^{c}	7.78^{a}	37.55	34.31^{a}	6.87	136.4	2.69^{ab}	26.53^{b}	65.91
S x T										
0 mM + T27	0.045	66.94	6.44	41.75^{ab}	18.89	6.01	58.24^{b}	1.63	20.75	101.7^{ab}
0 mM + T37	0.23	60.80	8.26	48.39^{a}	25.27	6.68	123.2^{a}	2.76	31.35	117.9^{a}
0 mM + T42	0.55	54.84	7.94	40.94^{bc}	33.14	6.60	148.8^{a}	2.40	24.26	69.91^{c}
100 mM + T27	4.86	60.28	6.89	30.52^{d}	27.51	7.98	77.92^{b}	2.45	24.22	95.24^{b}
100 mM + T37	14.40	56.18	7.79	30.44^{d}	25.22	6.40	122.9^{a}	3.61	37.05	89.91^{b}
100 mM + T42	17.54	48.78	7.62	34.16^{cd}	35.48	7.13	124.1^{a}	2.99	28.79	61.90^{c}

Na, Sodium; N, Nitrogen; P, Phosphorus; K, Potassium; Ca, Calcium; Mg, Magnesium; Mn, Manganese; Cu, Copper; Fe, Iron; Zn, Zinc. NS, *, **, *** Non-significant or significant at P ≤ 0.05, 0.01, 0.001, respectively. Means not sharing any letters within each column are statistically different according to Tukey's test (P = 0.05).

measured in the current study, and its maintenance is generally a sign of tolerance (Demidchik et al., 2014). The negative effects of T42 observed in this current study on parameters depending on membrane stability such as chlorophylls are, however, a sign of its irrelevance regarding the overall tolerance of the African eggplant. These negative impacts might be due to other damaging processes under heat such as enzyme inhibition or transcriptional changes (Zhao et al., 2020). It has to be noted, however, that midday stomatal conductance was maintained, and even increased, under the T42 treatment. As F1 Djamba is marketed as a particularly high-yielding cultivar, mechanisms might be in place to maintain gas exchange and carbon assimilation even under stress, thus requiring sustained membrane stability. The maintenance of membrane stability might thus have been important for characteristics not measured in the current study and require further research.

Midday stomatal conductance was increased by the T42 treatment seven days after the beginning of the stress but not by the T37 treatment, suggesting different mechanisms in place to cope with high temperatures depending on their intensities. The increase in stomatal conductance, despite increasing water loss, helps regulate leaf temperature to maintain the activity of photosynthetic enzymes (Poudyal et al., 2018). This increase was noted in different tomato cultivars at lower temperatures, highlighting the high tolerance threshold of the African eggplant (Poudyal et al., 2018; Amuji et al., 2020). The increased stomatal conductance promoted by high temperatures was, however, reduced under salinity. This was previously observed in tomato plants where the lowest stomatal conductance was reached under the stress combination due to the osmotic stress created by the salinity stress, leading to mechanisms in place to limit water loss such as stomatal closure (García-Martí et al., 2019).

Plants grown under higher temperatures kept their stomata closed for longer at the start of the day in this current study. Similarly, the largest difference between drought-stressed and non-stressed *Carapa guianensis* Aubl. was observed early in the day (Carvalho et al., 2013). Stomatal conductance of sorghum (*Sorghum bicolor* L.) was reduced early as well but did not increase back to control levels during the day, unlike the observations made in the current study (Sonobe et al., 2009). The current observations may be due to adaptive mechanisms under which the plants only fully open their stomata after reaching a high level of light to balance water loss with carbon gain. However, it has to be noted that the temperature started to reduce eight hours after the start of the photoperiod as per the gradual increase and decrease temperature set-up. While still the highest temperature, T42 treatment was at 40°C at that time, reduced from 42°C which only lasted from the 2nd to the 6th hour after the start of the photoperiod. A reduction in temperature is linked to a reduction in vapor pressure deficit (VPD), allowing better gas exchange (Merilo et al., 2018). In this current study, the 2°C reduction from 42°C might be enough for the plants to recover stomatal conductance. Even if the VPD of the other treatments also decreased at this time, the change might not have improved stomatal conductance as the VPD was already within optimal levels, leading to T42 plants recovering to the levels of the other treatments.

In addition to stomatal conductance changes, the stresses in the current study impacted the photosynthesis apparatus through chlorophylls and fluorescence modifications. While SPAD and final chlorophylls were significantly reduced by T42, leaf fluorescence parameters were not drastically reduced by this treatment. This observation might be due to the relationship between chlorophyll content per area and leaf thickness (Jinwen et al., 2009). Leaf thickness is positively correlated with SPAD index but negatively correlated with $\phi 2$ due to loss of transmittance at high leaf thickness which limits the optimal utilization of each chlorophyll molecule (Knapp and Carter, 1998; Jinwen et al., 2009). In the current study, plants with a lower SPAD (under the T42 treatment) may have a higher light use efficiency, leading to the mitigated impact of the stresses on $\phi 2$ and ϕNPQ despite the noticeable loss of chlorophyll molecules.

In terms of biochemical changes, the increase in total carbohydrates under heat was also observed by Zhou et al. (2017) in tomato. In contrast, no changes in glucose and fructose were noted under heat by Botella et al. (2021) in tomato but salinity increased these compounds significantly, while the stress combination further increased them. The increase noted by other studies was attributed to the enhanced enzyme activity within the sugar biosynthesis pathways, the insufficient sink activity limiting the export of the produced sugars from leaves, and the role of sugars as osmoprotectants (Zhou et al., 2017; Botella et al., 2021). In this current study, heat might have activated one or a combination of the stated accumulating mechanisms to withstand stress but not salinity. Salinity also did not trigger a non-enzymatic antioxidative response with the absence of changes in antioxidants and a reduction in total phenols. Phenols and antioxidants are important to detoxify reactive oxygen species created under stress and are sometimes a key part of the tolerance mechanisms (Das and Roychoudhury, 2014). The observations made in this current study were in line with the results of Martínez et al. (2020) who reported no changes in antioxidants in tomato and *S. chilense* under salinity. Phenols were increased by salinity in tomato (Bacha et al., 2017) but not in brinjal eggplant (*S. melongena* L.) and only at 50 mM NaCl in *S. nigrum* (Ben Abdallah et al., 2016; Ortega-Albero et al., 2023), showing the importance of the cultivar of interest and the level of stress.

Sodium accumulation under salinity, a quick and common observation, has major negative impacts on plant development (Sousa et al., 2022). In the current study, leaf sodium concentration was highly increased under salinity, an increase further exacerbated under heat as seen previously in tomato plants (Sousa et al., 2022). The antagonist effect of plant's sodium concentration on calcium uptake was not seen in this current study despite previous reports of calcium reduction in *Solanum* under salinity (Ben Abdallah et al., 2016; Ben-Abdallah et al., 2019; Sousa et al., 2022). The decrease in leaf calcium concentration in *S. villosum* Mill. reported by Ben-Abdallah et al. (2019) was, however, only seen under 150 mM NaCl and not at 50 or 100 mM NaCl, suggesting a threshold under which its uptake is not hindered in leaves. Leaf potassium and phosphorus concentrations were reduced under heat in the study by Ali et al. (2021), which was not observed in the current study with leaf phosphorus and potassium concentrations increased and unchanged, respectively. This corroborates findings in the brinjal eggplant and potato (*S. tuberosum* L.) (Efimova et al., 2018; Ortega-Albero et al., 2023). The maintenance of these primary nutrients under stress is important

for enzyme activity, cell membrane stability, and reactive oxygen species detoxification among others and the variability of responses under stress highlights the difference in mechanisms triggered for each stress (Kumari et al., 2022). Leaf nitrogen concentration, another primary nutrient, was reduced under salinity only at T27 and T42 but not at T37. Nitrogen has key roles in various tolerance plant mechanisms and moderate temperature stress might improve its uptake or transport to enhance tolerance through improved membrane stability or photosynthetic activity (Kumari et al., 2022).

Despite the role of magnesium in enzyme activity maintenance, the abiotic stresses did not affect leaf magnesium concentration in this study as was reported previously, suggesting its non-primary role in *Solanum* stress response (Ben-Abdallah et al., 2019). Leaf zinc and copper concentrations were only increased at T37 when compared to T27, while T42 levels were similar to the T27 ones. The increase seen only at T37 might be due to the increased nutrient uptake of selected important nutrients for tolerance observed under a certain threshold in different species due to the maintained ATPase activity and increased water uptake to compensate for the higher transpiration, mechanisms potentially not in place at T42 in the current study (Klock et al., 1996; Dias and Lidon, 2009). Interestingly, the temperature experienced by the roots was not significantly different between the T37 and T42 treatments, both much higher than the T27 treatment (data not shown). The reduction in leaf zinc and copper at T42 when compared to T37 was thus not due to an increase in heat damage on the roots which commonly reduces nutrient uptake (Bravo-F and Uribe, 1981; Mishra et al., 2023). This observation might instead be due to a translocation mechanism not impacted at 37°C but hindered at 42°C. Indeed, the translocation of zinc and copper from roots to shoot and the different plant organs relies on a range of proteins which might be denatured under high temperatures (Gupta et al., 2016; Mishra et al., 2023). The promotion of nutrient uptake alongside denatured proteins might thus have led to the same leaf zinc concentration observed between T27 and T42, both lowered that in T37 where the nutrient uptake was increased without damaging effects of protein denaturation. It has to be noted that copper, zinc, and manganese play an important role in the activity of the antioxidant enzyme superoxide dismutase (Tyagi et al., 2019). The increase observed at T37 might be part of tolerance mechanisms increasing the concentrations of important nutrients to detoxify reactive oxygen species accumulated during the stress with the increase in non-photochemical quenching and other damage. Further investigation is required to better understand the role of zinc, copper and manganese in the African eggplant under heat stress and their potential impact on antioxidant enzymes.

5 Conclusion

The current study aimed to describe the effects of the stress combination on an African eggplant Kumba cultivar and showed that despite some unique responses under the combination of heat and salinity, several plant attributes followed the same trend as the individual stresses. Elevated temperatures impacted highly leaf weight, polyphenols, and chlorophyll, salinity mostly had an effect on electrolyte leakage, stomatal conductance, and sodium uptake, while the stress combination impacted $\phi 2$, ϕNPQ, and potassium. The level of heat stress was important in dictating whether the stress combination had a stronger negative effect than the individual stresses, highlighting the importance of stress intensity when multiple stresses are present. Moderate heat offered some protection against salinity stress on the African eggplant regarding cell membrane stability, leaf fluorescence, and zinc and potassium levels, highlighting some positive effects of stress combination under certain conditions. The African eggplant did not rely on non-enzymatic antioxidant mechanisms to maintain photosynthetic activity, leaf expansion or chlorophyll levels, suggesting other mechanisms triggered under stress to maintain these processes.

The current study showed that F1 Djamba supported well a 37°C air temperature on its vegetative development but not 42°C. This is an important observation for farmers to adapt their planting habits following heat wave predictions. In addition, this is relevant to breeders aiming at developing tolerant crops as some tolerance pathways have been highlighted such as polyphenols and chlorophyll adaptation. The predominance of either salinity or heat on certain characteristics is also important for breeders and researchers to understand whether a crop tolerant to one stress can be tolerant to a combination of stresses.

Data availability statement

The original contributions presented in the study are included in the article/supplementary material. Further inquiries can be directed to the corresponding author.

Author contributions

ND-R: Conceptualization, Investigation, Methodology, Writing – original draft. MB: Supervision, Validation, Writing – review & editing. ES: Supervision, Validation, Writing – review & editing.

Funding

The author(s) declare financial support was received for the research, authorship, and/or publication of this article. This research was funded primarily by the Biotechnology and Biological Sciences (BBSRC) Dotcoral Training Programme (BB/M008770/1), hosted by the University of Nottingham and the National Institute of Agricultural Botany (NIAB). Rothamsted Research received strategic funding from the BBSRC and acknowledges support from the Growing Health (BB/X010953/1) Institute Strategic Programme.

Acknowledgments

We would like to thank BBSRC and NIAB for their funding. A great thank you to the technical team at NIAB for helping with setting up the experiments and helping with the equipment used. A special thank you to the laboratory teams at the University of Nottingham, in particular Louise Williams, Lolita Wilson, Ken

Davis, and Saul Vazquez, for having performed the digestion and analysis of mineral elements and nitrogen.

Conflict of interest

The authors declare that the research was conducted in the absence of any commercial or financial relationships that could be construed as a potential conflict of interest.

Publisher's note

References

Akinola, R., Pereira, L. M., Mabhaudhi, T., De Bruin, F.-M., and Rusch, L. (2020). A review of indigenous food crops in Africa and the implications for more sustainable and healthy food systems. *Sustainability* 12, 1–30. doi: 10.3390/SU12083493

Ali, M. M., Waleed Shafique, M., Gull, S., Afzal Naveed, W., Javed, T., Yousef, A. F., et al. (2021). Alleviation of heat stress in tomato by exogenous application of sulfur. *Horticulturae* 7, 1–14. doi: 10.3390/horticulturae7020021

Alsafari, S. A., Galal, H. K., and Bafeel, S. O. (2019). Growth and anatomy of tomato (*Solanum lycopersicum* Mill.) cultivars Marmande and Oria under salinity stress. *Pakistan J. Bot.* 51, 1199–1207. doi: 10.30848/PJB2019-4(16

Amuji, C. F., Beaumont, L. J., and Rodriguez, M. E. (2020). Simulating the impact of projected West African heatwaves and water stress on the physiology and yield of three tomato varieties. *Adv. Hortic. Sci.* 34, 147–156. doi: 10.13128/ahsc-8494

Bacha, H., Tekaya, M., Drine, S., Guasmi, F., Touil, L., Enneb, H., et al. (2017). Impact of salt stress on morpho-physiological and biochemical parameters of *Solanum lycopersicum* cv. Microtom leaves. *South Afr. J. Bot.* 108, 364–369. doi: 10.1016/j.sajb.2016.08.018

Ben Abdallah, S., Aung, B., Amyot, L., Lalin, I., Lachâal, M., Karray-Bouraoui, N., et al. (2016). Salt stress (NaCl) affects plant growth and branch pathways of carotenoid and flavonoid biosyntheses in *Solanum nigrum*. *Acta Physiologiae Plantarum* 38, 1–13. doi: 10.1007/s11738-016-2096-8

Ben-Abdallah, S., Zorrig, W., Amyot, L., Renaud, J., Hannoufa, A., Lachâal, M., et al. (2019). Potential production of polyphenols, carotenoids and glycoalkaloids in *Solanum villosum* Mill. under salt stress. *Biologia* 74, 309–324. doi: 10.2478/s11756-018-00166-y

Botella, M., Hernández, V., Mestre, T., Hellín, P., García-Legaz, M. F., Rivero, R. M., et al. (2021). Bioactive compounds of tomato fruit in response to salinity, heat and their combination. *Agriculture* 11, 1–12. doi: 10.3390/agriculture11060534

Bravo-F, P., and Uribe, E. G. (1981). Temperature dependence of the concentration kinetics of absorption of phosphate and potassium in corn roots. *Plant Physiol.* 67, 815–819. doi: 10.1104/pp.67.4.815

Carvalho, K., Pinheiro, H. A., Festucci-Buselli, R. A., da Silva Júnior, D. D., de Castro, G. L. S., Cruz, F. J. R., et al. (2013). Diurnal changes in leaflet gas exchange, water status and antioxidant responses in *Carapa guianensis* plants under water-deficit conditions. *Acta Physiologiae Plantarum* 35, 13–21. doi: 10.1626/pps.8.375

Das, K., and Roychoudhury, A. (2014). Reactive oxygen species (ROS) and response of antioxidants as ROS-scavengers during environmental stress in plants. *Front. Environ. Sci.* 2. doi: 10.3389/fenvs.2014.00053

de Fatima, R. T., Nóbrega, J. S., de Lima, G. S., Soares, L. A., d., A., Pereira, M. B., et al. (2023). Seaweed extract biofertilizer modulates scarlet eggplant tolerance to salt stress. *Arid Land Res. Manage.* 38, 46–61. doi: 10.1080/15324982.2023.2224272

Demidchik, V., Straltsova, D., Medvedev, S. S., Pozhvanov, G. A., Sokolik, A., and Yurin, V. (2014). Stress-induced electrolyte leakage: The role of K^+-permeable channels and involvement in programmed cell death and metabolic adjustment. *J. Exp. Bot.* 65, 1259–1270. doi: 10.1093/jxb/eru004

Dias, A. S., and Lidon, F. C. (2009). Heat stress in triticum: kinetics of cu and zn accumulation. *Braz. J. Plant Physiol.* 21, 135–142. doi: 10.1590/S1677-04202009000200006

Dinssa, F., Hanson, P., Dubois, T., Tenkouano, A., Stoilova, T., Hughes, J., et al. (2016). Avrdc — the world vegetable center's women-oriented improvement and development strategy for traditional african vegetables in sub-saharan africa. *Eur. J. Hortic. Sci.* 81, 91–105. doi: 10.17660/eJHS.2016/81.2.3

Dubois, M., Gilles, K. A., Hamilton, J. K., Rebers, P., and Smith, F. (1956). Colorimetric method for determination of sugars and related substances. *Analytical Chem.* 28, 350–356. doi: 10.1021/ac60111a017

Efimova, M., Kolomeichuk, L., Boyko, E., Malofii, M., Vidershpan, A., Plyusnin, I., et al. (2018). Physiological mechanisms of *Solanum tuberosum* L. plants' tolerance to chloride salinity. *Russian J. Plant Physiol.* 65, 394–403. doi: 10.1134/S1021443718030020

García-Martí, M., Piñero, M. C., García-Sanchez, F., Mestre, T. C., López-Delacalle, M., Martínez, V., et al. (2019). Amelioration of the oxidative stress generated by simple or combined abiotic stress through the K^+ and Ca^{2+} supplementation in tomato plants. *Antioxidants* 8, 1–16. doi: 10.3390/antiox8040081

Gupta, N., Ram, H., and Kumar, B. (2016). Mechanism of zinc absorption in plants: Uptake, transport, translocation and accumulation. *Rev. Environ. Sci. Bio/Technology* 15, 89–109. doi: 10.1007/s11157-016-9390-1

Han, M., Opoku, K. N., Bissah, N. A., and Su, T. (2021). *Solanum aethiopicum*: The nutrient-rich vegetable crop with great economic, genetic biodiversity and pharmaceutical potential. *Horticulturae* 7, 1–17. doi: 10.3390/horticulturae7060126

Hassan, M. U., Aamer, M., Chattha, M. U., Haiying, T., Shahzad, B., Barbanti, L., et al. (2020). The critical role of zinc in plants facing the drought stress. *Agriculture* 10, 1–24. doi: 10.3390/agriculture10090396

Hassan, M. U., Chattha, M. U., Khan, I., Chattha, M. B., Barbanti, L., Aamer, M., et al. (2021). Heat stress in cultivated plants: Nature, impact, mechanisms, and mitigation strategies—a review. *Plant Biosystems-An Int. J. Dealing all Aspects Plant Biol.* 155, 211–234. doi: 10.1080/11263504.2020.1727987

He, Y., DeSutter, T., Prunty, L., Hopkins, D., Jia, X., and Wysocki, D. A. (2012). Evaluation of 1: 5 soil to water extract electrical conductivity methods. *Geoderma* 185, 12–17. doi: 10.1016/j.geoderma.2012.03.022

Jinwen, L., Jingping, Y., Pinpin, F., Junlan, S., Dongsheng, L., Changshui, G., et al. (2009). Responses of rice leaf thickness, SPAD readings and chlorophyll a/b ratios to different nitrogen supply rates in paddy field. *Field Crops Res.* 114, 426–432. doi: 10.1016/j.fcr.2009.09.009

Klock, K. A., Graves, W. R., and Taber, H. G. (1996). Growth and phosphorus, zinc, and manganese content of tomato, muskmelon, and honey locust at high root-zone temperatures. *J. Plant Nutr.* 19, 795–806. doi: 10.1080/01904169609365161

Knapp, A. K., and Carter, G. A. (1998). Variability in leaf optical properties among 26 species from a broad range of habitats. *Am. J. Bot.* 85, 940–946. doi: 10.2307/2446360

Kuhlgert, S., Austic, G., Zegarac, R., Osei-Bonsu, I., Hoh, D., Chilvers, M. I., et al. (2016). Multispeq beta: A tool for large-scale plant phenotyping connected to the open PhotosynQ network. *R. Soc. Open Sci.* 3, 1–17. doi: 10.1098/rsos.160592

Kumari, V. V., Banerjee, P., Verma, V. C., Sukumaran, S., Chandran, M. A. S., Gopinath, K. A., et al. (2022). Plant nutrition: An effective way to alleviate abiotic stress in agricultural crops. *Int. J. Mol. Sci.* 23, 1–30. doi: 10.3390/ijms23158519

Lopez-Delacalle, M., Silva, C. J., Mestre, T. C., Martinez, V., Blanco-Ulate, B., and Rivero, R. M. (2021). Synchronization of proline, ascorbate and oxidative stress pathways under the combination of salinity and heat in tomato plants. *Environ. Exp. Bot.* 183, 1–11. doi: 10.1016/j.envexpbot.2020.104351

Martínez, J. P., Fuentes, R., Farías, K., Lizana, C., Alfaro, J. F., Fuentes, L., et al. (2020). Effects of salt stress on fruit antioxidant capacity of wild (*Solanum Chilense*) and domesticated (*Solanum lycopersicum* var. cerasiforme) tomatoes. *Agronomy* 10, 1–17. doi: 10.3390/agronomy10101481

Merilo, E., Yarmolinsky, D., Jalakas, P., Parik, H., Tulva, I., Rasulov, B., et al. (2018). Stomatal VPD response: There is more to the story than ABA. *Plant Physiol.* 176, 851–864. doi: 10.1104/pp.17.00912

Mishra, S., Spaccarotella, K., Gido, J., Samanta, I., and Chowdhary, G. (2023). Effects of heat stress on plant-nutrient relations: An update on nutrient uptake, transport, and assimilation. *Int. J. Mol. Sci.* 24, 1–21. doi: 10.3390/ijms242115670

Nadeem, H., Khan, A., Gupta, R., Hashem, M., Alamri, S., Siddiqui, M. A., et al. (2022). Stress combination—when two negatives may become antagonistic, synergistic, or additive for plants: A review. *Pedosphere* 33, 287–300. doi: 10.1016/j.pedsph.2022.06.031

Nkansah, G. O. (2001). Some physiological features of the african eggplant, *Solanum aethiopicum* group 'gilo'. *Scientia Hortic.* 90, 181–186. doi: 10.1016/S0304-4238(00)00254-5

Ondrasek, G., Rathod, S., Manohara, K. K., Gireesh, C., Anantha, M. S., Sakhare, A. S., et al. (2022). Salt stress in plants and mitigation approaches. *Plants* 11, 1–21. doi: 10.3390/plants11060717

Ortega-Albero, N., González-Orenga, S., Vicente, O., Rodríguez-Burruezo, A., and Fita, A. (2023). Responses to salt stress of the interspecific hybrid *Solanum insanum*× *Solanum melongena* and its parental species. *Plants* 12, 1–26. doi: 10.3390/plants12020295

Pailles, Y., Awlia, M., Julkowska, M., Passone, L., Zemmouri, K., Negräo, S., et al. (2020). Diverse traits contribute to salinity tolerance of wild tomato seedlings from the Galapagos islands. *Plant Physiol.* 182, 534–546. doi: 10.1104/pp.19.00700

Pörtner, H.-O., Roberts, D. C., Poloczanska, E., Mintenbeck, K., Tignor, M., Alegría, A., et al. (2022). "IPCC 2022: summary for policymakers," in *Climate change 2022: Impacts, adaptation, and vulnerability. Contribution of working group II to the sixth assessment report of the Intergovernmental Panel on Climate Change*. Eds. H.-O. Pörtner, D. C. Roberts, E. Poloczanska, K. Mintenbeck, M. Tignor, A. Alegría, M. Craig, S. Langsdorf, S. Löschke, V. Möller, A. Okem and B. Rama (Cambridge, UK and New York, NY, USA: Cambridge University Press).

Poudyal, D., Rosenqvist, E., and Ottosen, C.-O. (2018). Phenotyping from lab to field–tomato lines screened for heat stress using *Fv/Fm* maintain high fruit yield during thermal stress in the field. *Funct. Plant Biol.* 46, 44–55. doi: 10.1071/FP17317

Re, R., Pellegrini, N., Proteggente, A., Pannala, A., Yang, M., and Rice-Evans, C. (1999). Antioxidant activity applying an improved ABTS radical cation decolorization assay. *Free Radical Biol. Med.* 26, 1231–1237. doi: 10.1016/s0891-5849(98)00315-3

Rivero, R. M., Mestre, T., Mittler, R., Rubio, F., García-Sanchez, F., and Martínez, V. (2014). The combined effect of salinity and heat reveals a specific physiological, biochemical and molecular response in tomato plants. *Plant Cell Environ.* 37, 1059–1073. doi: 10.1111/pce.12199

Schiattone, M., Candido, V., Cantore, V., Montesano, F., and Boari, F. (2017). Water use and crop performance of two wild rocket genotypes under salinity conditions. *Agric. Water Manage.* 194, 214–221. doi: 10.1016/j.agwat.2017.09.009

Shunkao, S., Thitisaksakul, M., Pongdontri, P., and Theerakulpisut, P. (2022). Additive effects of combined heat and salt stress is manifested in an enhanced sodium ions accumulation and increased membrane damage in wheat seedlings. *Chilean J. Agric. Res.* 82, 552–563. doi: 10.4067/S0718-58392022000400552

Singleton, V. L., Orthofer, R., and Lamuela-Raventós, R. M. (1999). Analysis of total phenols and other oxidation substrates and antioxidants by means of folin-ciocalteu reagent. *Methods enzymology* 299, 152–178. doi: 10.1016/S0076-6879(99)99017-1

Sonobe, K., Hattori, T., An, P., Tsuji, W., Eneji, E., Tanaka, K., et al. (2009). Diurnal variations in photosynthesis, stomatal conductance and leaf water relation in sorghum grown with or without silicon under water stress. *J. Plant Nutr.* 32, 433–442. doi: 10.1080/01904160802660743

Sousa, B., Rodrigues, F., Soares, C., Martins, M., Azenha, M., Lino-Neto, T., et al. (2022). Impact of combined heat and salt stresses on tomato plants—insights into nutrient uptake and redox homeostasis. *Antioxidants* 11, 1–21. doi: 10.3390/antiox11030478

Suzuki, N., Rivero, R. M., Shulaev, V., Blumwald, E., and Mittler, R. (2014). Abiotic and biotic stress combinations. *New Phytol.* 203, 32–43. doi: 10.1111/nph.12797

Tufail, A., Li, H., Naeem, A., and Li, T. (2018). Leaf cell membrane stability-based mechanisms of zinc nutrition in mitigating salinity stress in rice. *Plant Biol.* 20, 338–345. doi: 10.1111/plb.12665

Tyagi, S., Shumayla,, Singh, S. P., and Upadhyay, S. K. (2019). "Role of superoxide dismutases (SODs) in stress tolerance in plants," in *Molecular approaches in plant biology and environmental challenges. Energy, environment, and sustainability*. Eds. S. Singh, S. Upadhyay, A. Pandey and S. Kumar (Singapore: Springer), 51–77. doi: 10.1007/978-981-15-0690-13

West, R. C. (1975). *CRC handbook of chemistry and physics* Vol. 55 (Cleveland, Ohio, USA: CRC press).

Wintermans, J., and De Mots, A. (1965). Spectrophotometric characteristics of chlorophylls a and b and their phenophytins in ethanol. *Biochim. Biophys. Acta (BBA)-Biophysics including Photosynthesis* 109, 448–453. doi: 10.1016/0926-6585(65)90170-6

Worlddata (2023) *Climate comparison*. Available at: https://www.worlddata.info/climate-comparison.php (Accessed 04-11-2023).

World Meteorological Organization (2022). *State of the climate in africa 2021* (Geneva: World Meteorological Organization).

Zhao, J., Lu, Z., Wang, L., and Jin, B. (2020). Plant responses to heat stress: Physiology, transcription, noncoding RNAs, and epigenetics. *Int. J. Mol. Sci.* 22, 1–14. doi: 10.3390/ijms22010117

Zhou, R., Yu, X., Ottosen, C.-O., Rosenqvist, E., Zhao, L., Wang, Y., et al. (2017). Drought stress had a predominant effect over heat stress on three tomato cultivars subjected to combined stress. *BMC Plant Biol.* 17, 1–13. doi: 10.1186/s12870-017-0974-x

frontiers | Frontiers in Plant Science

TYPE Original Research
PUBLISHED 20 March 2024
DOI 10.3389/fpls.2024.1365490

OPEN ACCESS

EDITED BY
Daniel V. Savatin,
University of Tuscia, Italy

REVIEWED BY
Jozef Mravec,
Institute of Plant Genetics and Biotechnology (SAS), Slovakia
Juan Pablo Martinez,
Agricultural Research Institute, Chile

*CORRESPONDENCE
Agata Leszczuk
a.leszczuk@ipan.lublin.pl
Panagiotis Kalaitzis
panagiot@maich.gr

RECEIVED 04 January 2024
ACCEPTED 08 March 2024
PUBLISHED 20 March 2024

CITATION
Kutyrieva-Nowak N, Leszczuk A, Ezzat L, Kaloudas D, Zając A, Szymańska-Chargot M, Skrzypek T, Krokida A, Mekkaoui K, Lampropoulou E, Kalaitzis P and Zdunek A (2024) The modified activity of prolyl 4 hydroxylases reveals the effect of arabinogalactan proteins on changes in the cell wall during the tomato ripening process. *Front. Plant Sci.* 15:1365490. doi: 10.3389/fpls.2024.1365490

The modified activity of prolyl 4 hydroxylases reveals the effect of arabinogalactan proteins on changes in the cell wall during the tomato ripening process

Nataliia Kutyrieva-Nowak[1], Agata Leszczuk[1]*, Lamia Ezzat[2], Dimitris Kaloudas[2], Adrian Zając[3], Monika Szymańska-Chargot[1], Tomasz Skrzypek[4], Afroditi Krokida[2], Khansa Mekkaoui[2], Evangelia Lampropoulou[2], Panagiotis Kalaitzis[2]* and Artur Zdunek[1]

[1]Institute of Agrophysics, Polish Academy of Sciences, Lublin, Poland, [2]Department of Horticultural Genetics and Biotechnology, Mediterranean Agronomic Institute of Chania, Chania, Greece, [3]Department of Functional Anatomy and Cytobiology, Institute of Biological Sciences, Maria Curie-Skłodowska University, Lublin, Poland, [4]Department of Biomedicine and Environmental Research, Institute of Biological Sciences, Faculty of Medicine, John Paul II Catholic University of Lublin, Lublin, Poland

Arabinogalactan proteins (AGPs) are proteoglycans with an unusual molecular structure characterised by the presence of a protein part and carbohydrate chains. Their specific properties at different stages of the fruit ripening programme make AGPs unique markers of this process. An important function of AGPs is to co-form an amorphous extracellular matrix in the cell wall-plasma membrane continuum; thus, changes in the structure of these molecules can determine the presence and distribution of other components. The aim of the current work was to characterise the molecular structure and localisation of AGPs during the fruit ripening process in transgenic lines with silencing and overexpression of *SlP4H3* genes (prolyl 4 hydroxylase 3). The objective was accomplished through comprehensive and comparative *in situ* and *ex situ* analyses of AGPs from the fruit of transgenic lines and wild-type plants at specific stages of ripening. The experiment showed that changes in prolyl 4 hydroxylases (P4H3) activity affected the content of AGPs and the progress in their modifications in the ongoing ripening process. The analysis of the transgenic lines confirmed the presence of AGPs with high molecular weights (120–60 kDa) at all the examined stages, but a changed pattern of the molecular features of AGPs was found in the last ripening stages, compared to WT. In addition to the AGP molecular changes, morphological modifications of fruit tissue and alterations in the spatio-temporal pattern of AGP distribution at the subcellular level were detected in the transgenic lines with the progression of the ripening process. The work highlights the impact of AGPs and their alterations on the fruit cell wall and changes in AGPs associated with the progression of the ripening process.

KEYWORDS

arabinogalactan proteins, cell wall, fruit, proteoglycans, ripening, tomato, transgenic lines

1 Introduction

1.1 Arabinogalactan proteins in the fruit ripening process

The tomato (*Solanum lycopersicum* L.) is one of the most widely cultivated crops worldwide and a well-studied model for tissue-specific gene modification and fruit ripening (Feder et al., 2020). In turn, studies of fruit ripening are useful for both practical agricultural applications and improvement of the understanding of physiological programmes. The ripening process is a complex phenomenon inducing changes in fruit tissues. Alterations in fruit texture and colour are attributed to different metabolic processes in the cell wall (Orfila et al., 2002). Our previous studies have shown that there are substantial changes in the structure and distribution of arabinogalactan proteins (AGPs) correlated with the ongoing ripening process (Kalaitzis et al., 2023; Kutyrieva-Nowak et al., 2023a). As common components in the plant extracellular matrix, AGPs are attached to the plasma membrane via glycosylphosphatidylinositol (GPI) anchors (Showalter, 2001; Lopez-Hernandez et al., 2020; Zhou, 2022; Leszczuk et al., 2023). The specific and mutable distribution of AGPs in the cell wall-plasma membrane continuum allows identification of the effects of these molecules on the specific arrangement of the cell wall assembly in fruit cells (Liu et al., 2015; Leszczuk et al., 2018). Moreover, in the newest concept of the cell wall model named the APAP1 complex, AGPs are considered as cross-linkers between other cell wall components in which they are covalently attached to other polysaccharides of the cell wall, such as hemicellulose and pectins (Tan et al., 2013; Hijazi et al., 2014a, Hijazi et al., 2014b; Leszczuk et al., 2020c). Furthermore, it should also be underlined that some processes of plant growth and development, including cell expansion, somatic embryogenesis, root and stem growth, signalling during cell-cell communication, salt tolerance, and programmed cell death, require the presence of AGPs (Showalter, 2001; Borassi et al., 2020; Zhang et al., 2020; Leszczuk et al., 2023). Although the involvement of AGPs in many aspects of plant growth and development is well understood, still little is known about their function in fruit development and ripening. It is well-known that hydroxyproline-rich glycoproteins (HRGPs), i.e. the group to which AGPs are classified, are involved in fruit softening and affect the progression of the ripening process (Fragkostefanakis et al., 2012; Kalaitzis et al., 2023). Moreover, our previous investigations conducted on apple fruit after colonisation of *Penicillium spinulosum* have shown that the amount of AGPs increased in infection-associated modifications in fruit tissue. The increased amount of AGPs during the development of fungal disease is correlated with their assumed contribution in response to biotic stress, i.e. structure of the mechanical barrier against plant pathogens (Leszczuk et al., 2019c; Leszczuk et al., 2020b).

1.2 Structure and biosynthesis of AGP

AGPs are one of the most complex protein families in the plant cell wall. Notably, AGPs contain carbohydrate chains in 90-95% of their molecular mass and the protein core constitutes only 5-10%. Among others, AGPs have unique characteristics, such as the presence of arabinogalactan type II (AG) chains attached to the protein core composed of hydroxyproline (Hyp) residues and typical Ala-Pro, Pro-Ala, Thr-Pro, Ser-Pro, Val-Pro, and Gly-Pro peptide repeats (Showalter, 2001; Liu et al., 2015; Leszczuk et al., 2020b). In turn, the β-1,3-galactose chains of AGPs are modified by linking β-1,6-galactose side chains, which are further modified by the addition of arabinose (Ara), rhamnose (Rha), fucose (Fuc), xylose (Xyl), and β-glucuronic acid (GlcA) residues.

AGP synthesis is a sequence of steps, including the inter-formation of both protein moiety and carbohydrate chains accompanied by multiple enzymes. The key stages are (1) protein backbone and GPI anchor synthesis in the endoplasmic reticulum (ER), (2) AG and other sugar residues synthesis in the Golgi apparatus, and (3) formation of the AGP molecule in the cell wall-plasma membrane compartments (Ellis et al., 2010; Fragkostefanakis et al., 2012). The first stage involves the synthesis of the AGP protein core by transcription of appropriate genes onto mRNA on ribosomes and transfer of newly created peptides to the ER. In the ER, AGPs have modification and attachment GPI anchor to their hydrophobic C-terminal domain. Among the required enzymes during the AGP protein domain modification, an important function is performed by prolyl 4 hydroxylases (P4Hs). P4Hs catalyse the hydroxylation of proline residues in the polypeptide to form hydroxyproline (Vlad et al., 2007; Perrakis et al., 2019; Konkina et al., 2021). After proper hydroxylation of proline catalysed by P4Hs, AGPs undergo glycosylation, and this molecular mechanism is well known, but the effect of changes in this mechanism on AGPs as well as the mechanism of disruption of the subsequent glycosylation process by changes in the protein domain need to be elucidated. In the AGP glycosylation involved seven enzymes which are codding by 17 different genes. This step of biosynthesis is initiated by hydroxyproline galactosyltransferase affecting the attachment of the first residue of galactose onto Hyp in the protein core. The activity of β-1,3-galactosyltransferase and β-1,6-galactosyltransferase initialise the addition of galactose to the β-1,3-galactan backbone and β-1,6-galactan side chains of AGP glycans. The attachment of arabinose residues to the β-1,3-galactan backbone is activated by the arabinosyltransferase enzyme. The glucuronosyltransferases initiate the addition of glucuronic acid to the main backbone and side chains of AGPs. And finally, the fucosyltransferases add fucose residues to AGPs. In addition, during this step, other glycosyltransferases in the Golgi activate decorating AGP structure by less frequent sugar residues, such as Rha and Xyl (Ellis et al., 2010; Showalter and Basu, 2016). The heterogeneity of sugar chains, types of bonds, chains length, and abbreviations occurring during synthesis are the reasons for the structural and functional diversity of AGPs (Ellis et al., 2010; Fragkostefanakis et al., 2012).

1.3 Modification of AGP carbohydrate chains

Moreover, it is assumed that the wide functionality of AGPs is the result of their complex glycome structure (Showalter, 2001). In

more detail, it is suggested that GlcA may confer functional properties on AGPs specifically linked to β-(1→6)-galactan chains (Tan et al., 2004). One of the presumed mechanisms of the alterations in the activity and distribution of AGPs is their interaction with Ca^{2+}, which depends on the bonds with GlcA (Lamport and Várnai, 2013). In β-glucuronyltransferase mutants (*GlcAT*), a reduction of Ca^{2+} binding, which affected the cell wall and plasma membrane stabilisation and caused less intensive plant growth, was revealed. Also, the AGP's ability to release Ca^{2+} contributes to the regulation of cellular signalling (Lopez-Hernandez et al., 2020), and as a reservoir of Ca^{2+} affecting plant development (Lamport et al., 2018). Furthermore, AGs from mutant plants exhibited reduced glucuronidation, which caused binding of less Ca^{2+} *in vitro* and development deficiencies in these plants (Lopez-Hernandez et al., 2020).

Interestingly, another proposed mechanism in which the primary factor is the carbohydrate part of AGP is related to the enzymatic activity of two exo-β-1,3-galactosidases (Nibbering et al., 2020). The aforementioned investigations showed that GlcA also forms a bridging residue between pectin and AGPs, confirming the presence of the APAP1 complex (Tan et al., 2013, Tan et al., 2023). Moreover, it can be concluded that APAP1 may be the target of GH43 activity, as it affects cell wall-bound AGPs (Nibbering et al., 2020).

1.4 Modification of the protein moiety of AGPs – effect of prolyl 4 hydroxylases

As mentioned above, P4Hs catalyse proline hydroxylation, a major post-translational modification of HRGPs (Kivirikko and Myllyharju, 1998; Hieta and Myllyharju, 2002; Koski et al., 2009; Leszczuk et al., 2020c, Leszczuk et al., 2023). The impact of P4Hs on plant growth and development was demonstrated in carrot root *in vivo* (Cooper and Varner, 1983). Structural alterations in HRGPs were correlated with abnormal cell division, which influenced the loosening of the cell wall matrix and the *de novo* synthesis and rearrangement of cell wall components (Cooper et al., 1994). In other studies, mutants of *Arabidopsis* with T-DNA knockout P4Hs had shorter root hair, which was caused by destruction of extensins, and were characterised by a disrupted *O*-glycosylation process (Velasquez et al., 2015). Overall, in plants with disturbed function of P4Hs, the total hydroxyproline content is changed, leading to structural and functional changes during cell division and expansion (Vlad et al., 2007; Perrakis et al., 2019; Konkina et al., 2021). Also, alterations in tomato P4H genes caused by Virus-Induced Gene Silencing (VIGS) allowed determination of the impact on the weight and size of leaves resulting in intensified biomass production (Fragkostefanakis et al., 2014). Transient suppression of three tomato P4Hs by using Virus Induced Gene Silencing (VIGS) resulted in a decrease in the content of JIM8-bound AGPs and JIM11-bound extensins (Fragkostefanakis et al., 2014). In three stable RNAi transgenic lines of *SlP4H3*, abscission was delayed in overripe tomato fruits indicating involvement in the progression of this developmental process (Perrakis et al., 2019). Moreover, suppression and overexpression of *SlP4H3* in stable tomato transgenic lines resulted in changes in the content of AGPs-bound epitopes in flower abscission zones and/or distal and proximal tissue (Perrakis et al., 2021). In addition, *Arabidopsis* mutants of the β-linked glucuronic acid transferases resulted in lower content of glucuronic acids on AGPs leading to severe developmental phenotypes such as limited seedling growth and sterility which were associated with perturbed calcium waves indicating reduced binding of calcium due to insufficient glucuronidation of AGPs (Lopez-Hernandez et al., 2020).

Despite the well-documented importance of HRGPs, there is still insufficient information on the impact of P4H activity on AGPs. Phenotypic analyses have confirmed that overexpression and silencing of P4H genes cause changes in the *O*-glycosylation process, and the role of AGPs in the fruit ripening process may be determined via genetic manipulation of the protein backbone which changes glycan moieties. The purpose of our study was to characterise the molecular structure, content and distribution of AGPs during the ongoing fruit ripening process. The aims were accomplished through *in situ* and *ex situ* analyses of AGPs in the fruit of transgenic lines and WT at different stages of ripening. Obtaining various research results, we considered the hypothesis whether changes in the molecular parameters of AGP influence deviations in the cell wall assembly by modifying interactions with other matrix components. Taking into account the significant role of the cell wall in the ripening and softening process, we could directly analyse the fundamental factors related to the arrangement of the cell wall. The development of transgenic lines with altered *SlP4H3* expression facilitated the determination of modification in the structure and distribution of AGPs, thus contributing to the elucidation of the effect of these molecules on the whole fruit extracellular matrix.

2 Materials and methods

2.1 The SlP4H3 RNAi and overexpression transgenic lines

Homozygous T2 and T3 generation tomato (*Solanum lycopersicum* cv. 'Ailsa Craig') plants of two RNAi, RNAi#1, RNAi#7, and four overexpression, OEX#1, OEX#2, and cGFP OEX (cGFP), nGFP OEX (nGFP), lines were prepared (Perrakis et al., 2021). Plants of the T2 and T3 tomato lines were grown under hydroponic conditions in perlite sacks in one glasshouse at Chania, Greece under standard conditions of temperatures at the range of 18-27°C and relative humidity at the range of 60-80% humidity for approximately one year. Approximately 10 plants per line were grown under identical environmental conditions. Fruits were collected at the four ripening stages from more than one plant per line. Fruits of only similar size were collected. Then, the material was collected from 10 tomato fruits from each stage. Next, ten cube-shaped fruit tissue samples were taken from each examined fruit and subjected to microscopic analysis in a minimum of 50 sections (CLSM) and 5 ultrathin sections (TEM). For molecular approaches, tissue was homogenized and frozen at -80°C.

Tomato fruits were harvested at the Breaker (BR), Turning (TU), Pink (PINK), and Red Ripe (RR) previously described by Nakatsuka and coworkers (1998). The ripening stages were identified by assessment of changes in the fruit colour as proposed by Batu (2004). The first stage of the ripening process is

BR. It is the stage after development, in which tomatoes have a pale-green surface and the first signs of ripening (an orange colour) are visible. The next stage is TU, in which the first appearance of a pale-pink colour of the fruit surface is evident on 10-30% of the surface. The next stage is PINK, in which two-thirds (above 60%) of the fruit surface is red. The last stage is RR, in which the fruit is red on the entire surface (Nakatsuka et al., 1998; Kutyrieva-Nowak et al., 2023a).

2.2 RNA extraction and cDNA synthesis

Total RNA was extracted from 200 mg of pericarp tissue at the fruit ripening stages of BR, TU, PINK, and RR from the RNAi#1, RNAi#7, OEX#1, OEX#2, cGFP, nGFP lines and wild-type (WT). The samples were pulverized in liquid nitrogen and RNA was extracted using the NucleoZOL reagent (MACHEREY-NAGEL, Germany), following the manufacturer's instructions. The RNA samples were treated with DNase I (NEB, RNase-free, Ipswich, MA, USA) and approximately 1 µg of RNA was reverse transcribed using SuperScriptTM II RT (Invitrogen, Carlsbad, CA, USA) for cDNA synthesis following the manufacturer's instructions.

2.3 Real-time qRT-PCR analysis

Real-time PCR analysis was conducted using the SYBR™ Select Master Mix (Thermo Fisher Scientific, Waltham, MA, USA) in a CFX Connect™ Real-Time PCR Detection System (Bio-Rad, Hercules, CA, USA). The cDNA samples were normalized with b-actin as the reference gene using the primers SlActinF 5′-GTCCC TATTTACGAGGGTTATGCT-3′, SlActinR 5′-GTTCA GCAGTGGTGGTGAACA-3′. The primers used to determine the *SlP4H3* expression in the RNA#1, RNA#7, OEX#1, OEX#2, cGFP, nGFP lines and WT were *SlP4H3* Forward 5′-GTGA AAGGAAGGCATTCTCG-3′ and SlP4H3 Reverse 5′-CTTT CTGAGAGC CCCTGTGA-3′. The PCR conditions started at 50° C for 2 minutes and 95°C for 5 minutes, followed by 40 cycles of denaturation at 95°C for 15 seconds, annealing at 60°C for 30 seconds, and extension at 72°C for 30 seconds. A final melt-curve stage was performed, with temperatures set at 95°C for 15 seconds, followed by 60°C for 30 seconds with a 0.5°C increment at each repeat. Data analysis was carried out using the 2-ΔΔCT method (Livak and Schmittgen, 2001), and the results were presented as relative levels of gene expression with actin as the internal standard. Standard errors were calculated for all mean values. Three biological replicates were used per sample.

2.4 Molecular analyses

2.4.1 Protein extraction

Protein extraction was conducted according to Ling's protocol (Ling et al., 2021) and with modifications described in our previous work (Kutyrieva-Nowak et al., 2023a). The fruit tissue was cut into cube-shaped pieces and frozen at -80°C before the extraction procedure. The tomato fruit tissue was homogenised to a fine powder in liquid nitrogen, and then Laemmli's extraction buffer (Laemmli, 1970) was added. The modified Laemmli's buffer contained 65mM Tris-HCl pH 6.8, 2% SDS, 2mM EDTA, 1mM PMSF, 700mM β-mercaptoethanol, and a 1:10 protease inhibitor. The samples were boiled at 95°C for 5 minutes and then clarified by centrifugation at 14000 rpm at 4°C for 20 minutes. The final step was to collect the supernatant and freeze it at -80°C for the next assays. The protein content was determined by the Bradford method using ready-to-used solution of Bradford reagent (Sigma-Aldrich, USA).

2.4.2 Dot blotting with quantitative analysis

For determination of the presence of AGPs in the supernatants, an immuno-dot-blot reaction using specific antibodies against the carbohydrate epitopes of AGPs was carried out. The commercial monoclonal antibodies used to study AGPs were provided by Kerafast (USA). The experiment was conducted using primary antibodies: JIM13, which recognises the trisaccharide epitope β-D-GlcA-(1,3)-α-D-GalA(1,2)-α-L-Rha (Knox et al., 1991; Yates and Knox, 1994; Yates et al., 1996), LM2, which recognises the epitope β-linked GlcA (Yates and Knox, 1994; Smallwood et al., 1996; Yan et al., 2015), LM14, which recognises the epitope arabinogalactan type II (Moller et al., 2008), and LM1, which recognises extensin glycoprotein (Smallwood et al., 1996). The volume of dotted samples on nitrocellulose membrane (PVDF) was dependent of protein concentrations and was around 0.3 µg of protein per dot. Each sample was dotted onto a pre-prepared nitrocellulose membrane with a 0.2 µm pore size (Thermo Scientific, USA) and blocked using a 5% solution of bovine serum albumin (BSA; Sigma, USA) in phosphate-buffered saline (PBS; Sigma, USA). After washing in Tris-buffered saline (TBST, 7.6 pH) three times, the membranes were incubated for 2 h at room temperature (RT) with primary antibodies diluted 1:500 in 2.5% BSA in PBS. After washing with TBST, the membranes were incubated for 2 h at RT with secondary antibodies Anti-Rat-IgG conjugated with alkaline phosphatase (AP) (Sigma-Aldrich, USA) at a dilution of 1:1000 in 2.5% BSA in PBS. After three washing steps in TBST and AP-buffer, AGPs were finally detected using the following substrates: 4 mg of 5-bromo-4-chloro-3-indolylphosphate (BCiP; Sigma, USA) in 1 mL water and 9 mg of nitro-blue tetrazolium (NBT; Sigma, USA) in 0.3 mL water and 0.7 mL N,N-dimethylformamide (DMF; Thermo Scientific, USA) in the dark. After membrane imaging using GelDoc Go Imaging System (Bio-Rad, USA), the measurement of the colour intensity of the dots was carried out using Image Lab Software v. 6.1 (Bio-Rad, USA). The heat map was prepared using Microsoft tools in which colour intensity is proportional to a numerical value. The numerical values are rearranged to $\times 10^3$ for better representation of results. Data for each sample were obtained from three independent experiments. Each experiment presented data from the same set of samples under identical conditions. Statistic analysis was performed by Statistica v.13 tools (TIBCO Software Inc. USA) using variance (one-way ANOVA) and Tukey's Honestly Significant Difference (HSD) *post hoc* test. For all analyses, the significance level was estimated at $p<0.05$.

2.4.3 SDS-PAGE and Western blotting with quantification

Gel electrophoresis and next Western blotting were performed for identification of the molecular weight of AGPs from the fruit tissue in the different stages of ripening. After total protein extraction, quantification of the protein content was carried out using the Bradford assay. Protein separation was performed using SDS-PAGE with 12.5% resolving gel and 4% stacking gel. After SDS-PAGE electrophoresis, proteins with the gel were electroblotted onto a PVDF membrane. After Western blotting wet transfer, the membrane was washed in TBST on a shaking platform. After washing, the preincubation step was performed for 1 h at RT with 5% BSA in PBS, and the membrane was incubated for 2 h at RT with primary antibodies at a concentration of 1:500 in 2.5% BSA in PBS. After washing with TBST, the membrane was incubated for 2 h at RT with secondary antibodies conjugated with AP at a concentration of 1:1000. After washing with TBST and AP-buffer three times, visualisation of bands was performed using BCiP and NBT at a concentration described above in the GelDoc Go Imaging System (Bio-Rad, USA). For qualitative and quantitative analysis, the Pierce™ Prestained Protein MW Marker (Thermo Scientific, USA) was used. The band thickness, width, and colour depth were used for qualitative analysis (different ranges of molecular weights – 3 points: high molecular range, medium and low ones). The quantitative analysis of protein bands was performed by measurements of obtained stripes using Image Lab Software v. 6.1 (Bio-Rad, USA). Three independent analyses were carried out.

2.4.4 ELISA with quantitative analysis

Based on the number of antigen-antibody interactions produced, ELISA is a fundamental test for both qualitative and quantitative identification of AGPs in samples (Pfeifer et al., 2020; Kutyrieva-Nowak et al., 2023b). First, the samples were added to each well on a 96-well plate (Nunc MaxiSorpTM flat-bottom, Thermo Fisher Scientific, Denmark) and immobilized at 37°C for 72 h with shaking (350 rpm). Then, the coated plate was washed three times with PBS (pH 7.4), preincubated for 1 h at 37°C with 0.1% BSA in PBS, and incubated for 1 h at 37°C with primary antibodies at a concentration of 1:20 in PBS. After the washing step, the plate was incubated for 1 h at 37°C with the secondary antibody (in a dilution of 1:500 in PBS). After the incubation and washing steps, the reaction was developed by adding a freshly prepared substrate solution of p-nitrophenol phosphate (PNPP) according to Thermo Scientific instructions. The reaction was run in the dark and stopped with 2M NaOH after 20 minutes. The absorbance was measured in an ELISA reader (MPP-96 Photometer, Biosan) at 405 nm. The AGPs concentration was calculated from a calibration curve for gum Arabic with the calibration coefficient y=0.7231x, R^2=0.9871 in the case of reaction with JIM13 antibody, y=0.3417x, R^2=0.9873 in the case of reaction with LM2 antibody, y=0.6394x, R^2=0.9796 in the case of reaction with LM14 antibody and y=0.502x, R^2=0.9857 in the case of reaction with LM1 antibody. Gum Arabic was treated as a standard for AGPs. Analysis of variance (one-way ANOVA) and Tukey's Honestly Significant Difference (HSD) *post hoc* test (Statistica v.13 tools (TIBCO Software Inc. USA)) were used to compare the mean results. For all analyses, the significance level was estimated at $p<0.05$. Three independent analyses were carried out.

2.5 Biochemical–structural analyses

2.5.1 Extraction of AGPs using β-glucosyl Yariv Reagent

AGPs were isolated from tomato fruit tissue using the β-glucosyl Yariv Reagent (β-GlcY; Biosupplies, Australia) according to the extraction protocol proposed by Lamport (2013) and used in our previous studies (Leszczuk et al., 2020a, b; Kutyrieva-Nowak et al., 2023a). The liquid-nitrogen pre-frozen and homogenised fruit tissue was added to 2% $CaCl_2$ and incubated at RT. After 3 h, the homogenate was centrifuged at 10000 rpm for 30 minutes at RT. The supernatant was retained and added to 1 mg/mL β-GlcY in 2% $CaCl_2$ and left overnight at RT. The insoluble Yariv-AGP complex was centrifuged for 15 minutes at 2000 rpm, and the precipitate was resuspended in MiliQ water. Next, sodium metabisulphite (Thermo Scientific, USA) was gradually added to the precipitate and heated at 50°C to reduce the diazo linkage until the suspension was decolourised. After obtaining a clear yellow solution, the suspension was transferred to dialysis tubing with a 12-kDa MW cut-off (32 mm flat width; Sigma, USA) and stirred overnight. The dialysate was lyophilized, and then the AGPs were weighed.

2.5.2 FTIR analyses

FTIR spectra were collected on a Nicolet 6700 FTIR spectrometer (Thermo Scientific, Madison, WI, USA). The Smart iTR ATR sampling accessory was used. The spectra of the lyophilized AGP extracts were collected over the range of 4000–650 cm^{-1}. Three samples of each material were examined in the same conditions. For each sample, 200 scans were averaged with a spectral resolution of 4 cm^{-1}. Then, a final average spectrum was calculated for a given material. These spectra were baseline corrected and normalized to 1.0 at 1019 cm^{-1}. To highlight the differences between the samples, the principal component analysis (PCA) of the spectra was performed in the mid-infrared region of 4000–400 cm^{-1} using Unscrambler 10.1 (Camo Software AS., Norway). The maximum number of components taken for the analysis was five, and the NIPALS algorithm was used (Szymanska-Chargot et al., 2015; Chylińska et al., 2016). The visualisation of FTIR spectra and PCA analysis were performed using the OriginPro program (Origin Lab v. 8.5 Pro, Northampton, USA).

2.6 Microscopic analyses

2.6.1 SEM imaging

For morphological description, AGPs extracted using β-glucosyl Yariv Reagent from fruit tissue at different stages of the ripening process (the BR and RR stages) were imaged with a scanning electron microscope (SEM, Zeiss Ultra Plus, Oberkochen,

Germany) in high vacuum (5×10^{-3} Pa) using a secondary electron detector at 3 kV.

2.6.2 Preparation of material for immunocytochemistry

The microscopic analyses were carried out in accordance with our previous papers (Leszczuk et al., 2019a; Kutyrieva-Nowak et al., 2023a, Kutyrieva-Nowak et al., 2023b). For the microscopic examination, the fruit tissue was subjected to the procedure of fixation, resin embedding, and sectioning. Cube-shaped pieces of the fruit tissue were fixed in 2% paraformaldehyde (Sigma, USA) and 2.5% glutaraldehyde (Sigma, USA) in PBS and placed in vacuum (0.7 bar) seven times for 10 minutes each and then left overnight. Next, the samples were washed in PBS and distilled water and dehydrated in graded series of ethanol solutions (30%, 50%, 70%, 90%, and 96% for 15 minutes each and 99.8% twice for 30 minutes). The tissue was placed in 99.8% ethanol and LR White resin (at a ratio of 3:1, 1:1, 1:3; Sigma Aldrich, USA), and next in 100% resin LR White. The polymerisation was carried out for 48 h at 55°C. For CLSM imaging, the samples were cut into semi-thin sections (1 µm) using a glass knife-equipped ultramicrotome (PowerTome XL, RMC Boeckeler, USA). Next, the sections were placed on poly-L-lysine coated glass slides (Sigma, USA). For TEM imaging, the samples were cut into ultra-thin sections (70 nm) using a diamond knife-equipped ultramicrotome, and the sections were placed on formvar film-coated nickel square grids (EM Resolutions Ltd, UK).

2.6.3 Immunofluorescence method with confocal laser scanning microscopy (CLSM imaging)

Immunofluorescence imaging of AGP epitopes at the tissue/cellular level facilitates evaluation of changes in the distribution of AGPs in fruit at different ripening stages. The experiment was conducted using JIM13, LM2, and LM14 antibodies. Semi-thin sections on poly-L-lysine coated glass slides were circled with a liquid blocker Dako-Pen (Sigma Aldrich, USA). The samples were washed and pre-incubated for 30 minutes at RT with 2% BSA in PBS to block non-specific binding sites. After the washing step, the sections were incubated with primary antibody diluted 1:50 in 0.1% BSA in PBS overnight at 4°C. After washing with PBS three times, secondary Alexa Fluor 488 antibodies (diluted 1:200 in 0.1% BSA in PBS, goat Anti-Rat-IgM, Thermo Fisher Scientific, Denmark) were added and the sections were incubated overnight at 4°C. Then, the incubated sections were washed in PBS and MiliQ water and finally counterstained with Calcofluor White (Sigma Aldrich, USA). An Olympus BX51 CLSM microscope with corresponding software FluoView v.5.0. (Olympus Corporation, Tokyo, Japan) was used for imaging. In order to perform control reactions, the incubation with the primary antibody was omitted. All photographs, figures, and schemes were edited using the CorelDrawX6 graphics program.

2.6.4 Immunogold labelling technique with the transmission electron microscope (TEM imaging) and quantitative analysis

Immunogold labelling of AGP epitopes facilitates identification and visualization of changes in their distribution at the subcellular level. The experiment was conducted using JIM13, which recognises the most common and specific AGP epitope in fruits. Ultra-thin sections placed on grids (5 grids per sample) were washed in distilled water, and next pre-incubated for 30 minutes at RT with 1% BSA in PBS. Then, the grids were incubated for 3 h at 37°C with the primary antibody (diluted 1:10 in 0.1% BSA in PBS), washed in the blocking solution, and labelled with the secondary antibody (diluted 1:50 in 0.1% BSA in PBS, Anti-Rat-IgG – Gold antibody; Sigma, USA) for 1 h at 37°C. After washing in PBS and distilled water, the samples were stained with a 1% uracyl acetate solution (for 10 minutes) and Reynold's reagent (for 7 minutes). The observations were carried out using a transmission electron microscope (TEM Zeiss EM900) operating at 80 kV acceleration voltage (Carl Zeiss AG, Oberkochen, Germany) and equipped with a digital camera with corresponding software ImageSP v. 1.1.2.5. In the quantitative analysis of AGP labelling density, gold particles on the same size (2048 × 2048 pixels) micrographs were manually identified and counted with the software ImageJ v. 1.51. The results were expressed as the number of gold particles per 1 μm^2 area of the examined cell compartment (Corral-Martínez et al., 2016; Leszczuk et al., 2018). The statistical analysis consisted of comparing the content of AGPs in the cell wall–plasma membrane and in the cytoplasm to indicate significant differences among the transgenic lines and WT within ripening stages (according to ANOVA and Tukey's Honestly Significant Difference (HSD) *post hoc* test with the significance level $p<0.05$). All photographs, figures, and schemes were edited using the CorelDrawX6 graphics program.

3 Results

3.1 Expression of *SlP4H3* at fruit ripening stages in overexpression and silencing lines

Two *SlP4H3* RNAi independent lines, #1 and #7, and two *SlP4H3* overexpression lines, OEX#1, OEX#2 were previously produced (Perrakis et al., 2019, 2021). Moreover, two additional, independent overexpression lines were created, cGFP OEX (cGFP) and nGFP OEX (nGFP), comprising a construct in which a GFP tag was either at the C- or the N-terminus of the *SlP4H3* cDNA under the control of the 35S promoter (Perrakis et al., 2021). The expression levels of *SlP4H3* in the two silencing and the four overexpression lines were determined at the four ripening stages (Figure 1). Lower expression levels were observed by approximately 50% at the RNAi#1 and RNAi #7 fruits in all ripening stages (Figure 1). In the overexpression lines, the highest levels of expression were detected in the cGFP and nGFP lines up to approximately 92- and 20-fold, respectively (Figure 1). In the OEX#1 and OEX#2 lines, the *SlP4H3* transcript abundance was higher up to 4- and 8-fold, respectively (Figure 1).

3.2 Molecular differences between AGPs in the fruit of the transgenic lines

The molecular differences between AGPs in the fruit of the transgenic lines and WT at different stages of ripening were evaluated in several steps. Firstly, an immuno-dot-blot assay was

performed to quickly check the presence of AGP epitopes. The Western blotting method helped to determine the proportions of the molecular weights of the AGP epitopes in the fruit samples. Afterwards, selective glycome profiling of AGPs using the enzyme-linked immunosorbent assay (ELISA test) was conducted to visualise quantitative changes in the AGP content in the fruit of the examined transgenic lines during the ongoing ripening process.

3.2.1 Presence/absence of AGP epitopes during the ripening process

To validate the protein extraction and check the presence of specific AGP epitopes in the samples, an immuno-dot-blot assay was performed (Figure 2) and monoclonal antibodies against AGP epitopes (JIM13, LM2, and LM14) and against extensin (LM1) were used. The heat map obtained showed that the examined epitopes were present in different concentrations depending on the stage of the ripening process and the modification of P4H3 activity caused changes in the content of particular epitopes in the tested samples.

First of all, when analysing the ripening process itself, it is clear that the highest amount of all examined epitopes was detected at the BR stage, regardless of the line being tested. Additionally, in all cases, the number of all epitopes gradually decreased with the progression of the ripening process.

Secondly, the analysis of individual epitopes makes it possible to find differences in their content between individual lines. The assay of the fruit tissue of the RNAi#7 line with all the antibodies used indicated that silencing of the *SlP4H3* gene resulted in reduced intensity of the dots, compared to WT. In the same way, the analysis of the overexpression lines also revealed increased content of the tested epitopes in comparison to WT. The best visualisation effect of AGPs in all samples was achieved with the use of the LM2 antibody, which may indicate that modification of P4H3 activity does not significantly affect the presence of β-linked GlcA at every stage of the fruit ripening process. Despite this, the silencing of the *SlP4H3* gene in the RNAi#7 line resulted in a 5-20% reduction in the intensity of the dots, depending on the stage of ripening. The most effective demonstration of the progression of the ripening process was observed in the case of JIM13 in WT. Furthermore, an increase in the amount of the JIM13 epitope in the fruit tissue of the OEX#1 and OEX#2 lines was found. This content was 20-30% higher than in WT, even at the last stages of ripening. Also, the analysis of LM14 confirmed that the *SlP4H3* overexpression resulted in an increased number of LM14 epitopes. During the analysis of the LM1 epitopes, no significant differences in dot intensity were identified between the transgenic lines and WT and between the particular stages of ripening. It was also observed that the LM1 epitope was the least abundant and underwent the fastest degradation process, compared to the other epitopes.

3.2.2 Molecular mass disruption of AGPs during the ripening process

The Western blotting analysis also revealed the presence of all examined epitopes of AGPs, which were characterized by different molecular weights depending on the ripening stage (Figure 3). In the WT and transgenic lines, AGPs with high molecular weight (between 120 and 60 kDa) were observed as smeared bands, which are characteristic for separation of AGPs in the electric field during electrophoresis. In the analysis of Western blot membranes, special attention was paid to the bands representing low molecular weight AGPs (~30 kDa), which are markers of the finalisation of the ripening process in tomato fruit. The use of all the examined antibodies revealed the absence or trace quantities of low

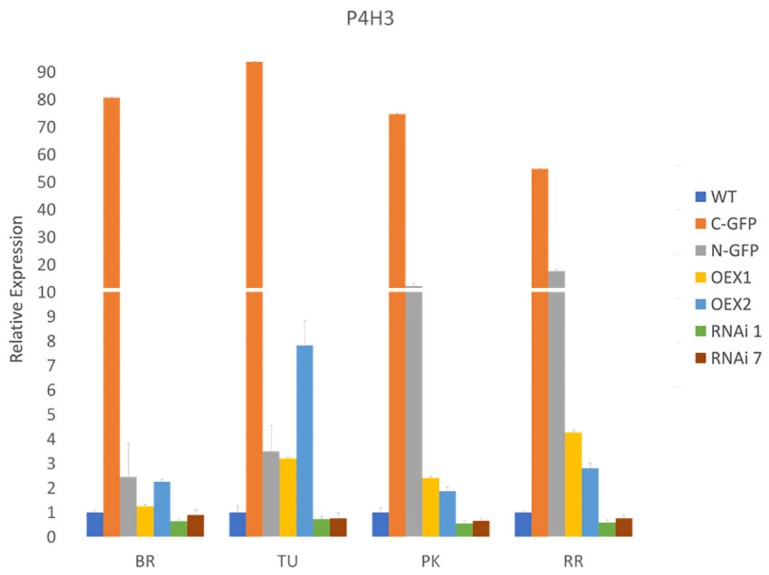

FIGURE 1
Expression of *SlP4H3* at Breaker (BR), Turning (TU), Pink (PK) and Red Ripe (RR) fruit ripening stages in cGFP, nGFP, OEX#1, OEX#2 and RNAi#1, RNAi#7 lines and WT. The relative expression was calculated based on the comparative CT method and actin was used as the internal standard. The relative fold differences for each sample were determined by normalizing the Ct value for the *SlP4H3* gene to the Ct value for actin and calculated using the formula $2^{-\Delta\Delta Ct}$. Three biological replicates were performed. Error bars represent standard error.

10.3389/fpls.2024.1365490

	BR	TU	PINK	RR	
WT	41.96 ± 1.95^{a}	35.7 ± 4.92^{ab}	33.64 ± 4.01^{ab}	28.14 ± 4.74^{bc}	JIM13
RNAi#1	27.09 ± 3.65^{b}	26.91 ± 2.82^{b}	24.64 ± 1.61^{b}	24.88 ± 1.65^{c}	
RNAi#7	38.57 ± 3.31^{a}	38.28 ± 4.65^{a}	36.88 ± 5.03^{a}	32.75 ± 3.65^{abc}	
OEX#1	42.81 ± 1.01^{a}	41.45 ± 3.74^{a}	40.98 ± 2.55^{a}	39.54 ± 5.25^{a}	
OEX#2	41.88 ± 1.31^{a}	41.51 ± 2.59^{a}	40.06 ± 1.82^{a}	36.35 ± 1.51^{ab}	
cGFP	37.67 ± 0.61^{a}	33.9 ± 3.63^{ab}	31.83 ± 5.45^{ab}	30.61 ± 5.57^{abc}	
nGFP	39.67 ± 1.01^{a}	36.34 ± 2.01^{ab}	36.23 ± 1.81^{a}	34.5 ± 1.31^{abc}	
WT	35.58 ± 2.25^{a}	33.36 ± 2.31^{a}	32.73 ± 1.51^{a}	31.7 ± 1.87^{a}	LM1
RNAi#1	32.58 ±6.25^{a}	32.41 ± 4.87^{a}	32.02 ± 6.98^{a}	32.07 ± 8.99^{a}	
RNAi#7	34.37 ± 3.23^{a}	33.15 ± 3.91^{a}	31.92 ± 1.78^{a}	31.79 ± 3.75^{a}	
OEX#1	38.72 ± 1.11^{a}	37.57 ± 0.95^{a}	36.28 ± 3.39^{a}	33.04 ± 5.56^{a}	
OEX#2	34.22 ± 1.43^{a}	33.65 ± 2.86^{a}	31.04 ± 1.62^{a}	28.08 ± 2.19^{a}	
cGFP	37.18 ± 4.04^{a}	36.91 ± 3.02^{a}	36.59 ± 3.81^{a}	35.4 ± 5.56^{a}	
nGFP	31,15 ± 2,36^{a}	28.37 ± 2.36^{a}	27.298 ± 1.22^{a}	25.397 ± 2.46^{a}	
WT	59.51 ± 0.61^{a}	49.29 ± 5.22^{a}	43.79 ± 5.08^{a}	40.58 ± 7.44^{a}	LM2
RNAi#1	48.85 ± 3.85^{ab}	48.81 ± 4.47^{a}	45.29 ± 5.43^{a}	41.62 ± 6.15^{a}	
RNAi#7	42.47 ± 7.91^{b}	40.85 ± 5.75^{a}	40.81 ± 5.12^{a}	38.94 ± 6.15^{a}	
OEX#1	48.44 ± 3.49^{ab}	45.35 ± 3.69^{a}	41.83 ± 5.31^{a}	39.88 ± 5.51^{a}	
OEX#2	47.19 ± 2.81^{ab}	43.46 ± 6.11^{a}	42.47 ± 5.58^{a}	41.63 ± 5.55^{a}	
GFP	44.24 ± 5.95^{b}	41.16 ± 6.44^{a}	39.08 ± 6.03^{a}	38.19 ± 5.95^{a}	
nGFP	41.53 ± 4.15^{b}	40.13 ± 4.64^{a}	39.23 ± 6.23^{a}	38.13 ± 6.51^{a}	
WT	36.24 ± 0.54^{a}	34.03 ± 0.43^{a}	33.85 ± 0.86^{a}	32.64 ± 1.84^{a}	LM14
RNAi#1	40.38 ± 9.15^{a}	37.61 ± 9.76^{a}	36.96 ± 8.69^{a}	36.63 ± 7.36^{a}	
RNAi#7	34.91 ± 2.04^{a}	33.04 ± 3.88^{a}	32.15 ± 3.36^{a}	31.34 ± 3.66^{a}	
OEX#1	45.25 ± 2.57^{a}	43.07 ± 2.21^{a}	41.29 ± 2.89^{a}	39.83 ± 1.29^{a}	
OEX#2	36.55 ± 1.35^{a}	36.27 ± 4.36^{a}	34.65 ± 2.28^{a}	34.54 ± 3.48^{a}	
cGFP	41.41 ± 0.95^{a}	39.41 ± 4.23^{a}	36.06 ± 3.67^{a}	34.53 ± 1.45^{a}	
nGFP	35.61 ± 3.14^{a}	34.38 ± 2.91^{a}	34.17 ± 2.47^{a}	33.17 ± 2.68^{a}	

FIGURE 2
Examination of samples using JIM13, LM1, LM2 and LM14 antibodies at different ripening stages from the fruit of wild-type plants (WT) and transgenic lines: RNAi#1, RNAi#7, OEX#1, OEX#2, cGFP, and nGFP. The numerical value in the heatmap is x10^{3}. Letters indicate differences among the transgenic lines and WT within particular ripening stages (according to ANOVA and Tukey's Honestly Significant Difference (HSD) *post hoc* test with the significance level $p<0.05$). BR, Breaker stage; TU, Turning stage; PINK, Pink stage; RR, Red Ripe stage.

molecular weight epitopes. Interestingly, the aforementioned specific bands were not present in all the transgenic lines.

The next observation was that the different epitopes with various molecular weights had impaired participation in the composition of the examined lines, in comparison to WT. Both the JIM13 and LM2 epitopes were the most abundant in the fruit of the WT and in the transgenic lines, with the highest expression level in the fruit tissue of the cGFP (JIM13 epitope) and nGFP lines (LM2 epitope). The highest LM2 expression was recorded in the nGFP transgenic line, compared to WT and the other lines. In turn, the lowest expression of the LM2 and JIM13 epitopes was observed in the fruit tissue of the RNAi#1 and RNAi#7 lines. All the transgenic lines differed from WT in the abundance of LM14 epitopes with different molecular weights. AGPs extracted from WT exhibited low expression of the LM14 epitope, while all the transgenic lines showed a significant increase in its level. The weakest participation in the sample composition in both the WT and transgenic lines was noted in the case of LM1. Only several thick bands with low molecular weight in WT (~40kDa) and with high molecular weight (~120 kDa) in the OEX#1 and cGFP lines were observed. The most significant result of the quantitative Western Blotting analysis showed that AGPs extracted from the transgenic lines were characterised by a more variable structure in comparison to AGPs extracted from WT. Generally, in the same ripening stages, a higher amount of AGPs with diverse molecular masses were noted in the transgenic lines than in WT.

3.2.3 Changes in selective glycome profiling of AGPs during ripening process

The results presented above identified molecular differences between samples representing the various transgenic lines, thus the ELISA test was performed to confirm the presence of the AGP epitopes and to achieve better visualisation of differences between the particular stages of fruit ripening in each line (Figure 4).

The results shown in Figure 4 indicate the lowest differences in the amount of the JIM13 epitope in the fruit of transgenic lines

10.3389/fpls.2024.1365490

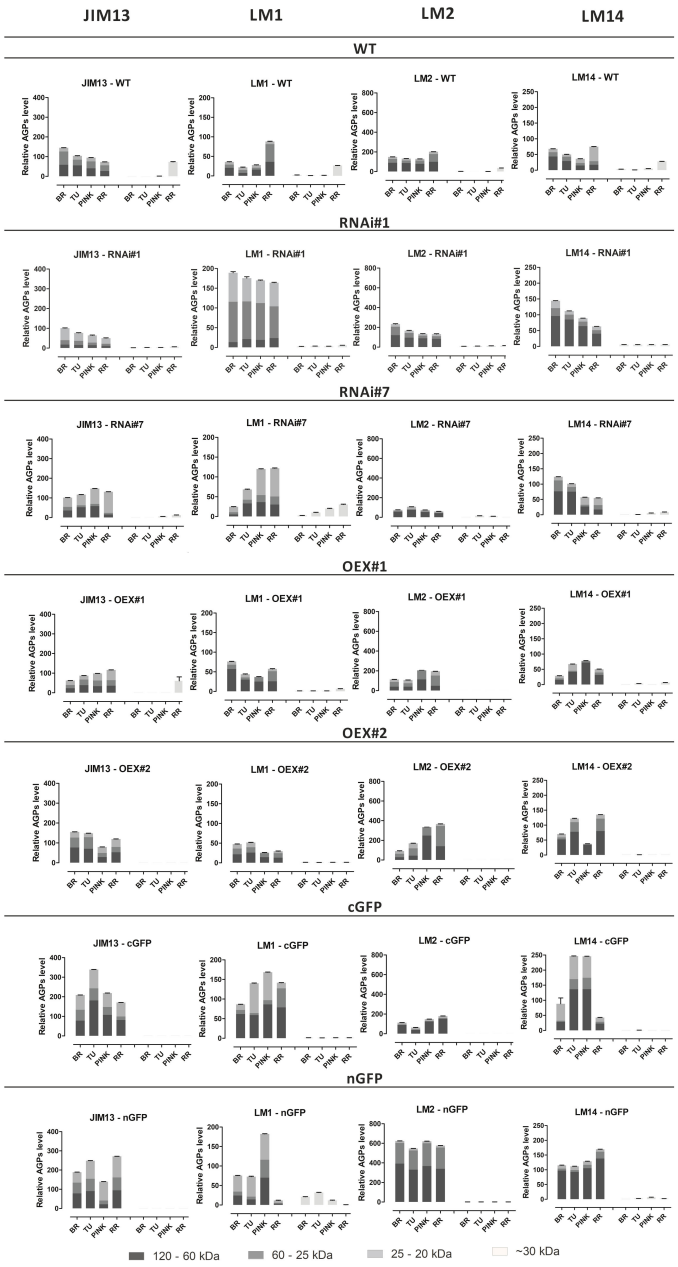

FIGURE 3
Western Blotting with quantitative analysis. Characterisation of molecular mass of AGPs from fruit at different ripening stages in wild-type plants (WT) and transgenic lines: RNAi#1, RNAi#7, OEX#1, OEX#2, cGFP, and nGFP. Western Blotting raw data (Supplementary Material). BR, Breaker stage; TU, Turning stage; PINK, Pink stage; RR, Red Ripe stage.

during the ripening process. The amount of the JIM13 epitope in the fruit tissue of the RNAi#7 line was not significantly different from that detected in WT. Besides, significant reduction of JIM13 epitope concentration in the case of RNAi#1 line. The highest concentration of the JIM13 epitope was obtained for the overexpression lines (around 55 μg/mL), and this dependence persisted to the last stages of ripening. Interesting results were obtained with the use of the LM2 antibody, as the concentration of the epitopes was significantly higher than in the analyses using the other antibodies. Only in the fruit of RNAi#1 line, the content was much lower than in other samples. Using the LM2 antibody, it was shown that the *SlP4H3* gene silencing had a significant effect on the concentration of this epitope. The AGP concentration was from approx. 700 μg/mL in WT to 1200 μg/mL for AGPs in the GFP lines, indicating that β-linked GlcA epitopes were the most abundant in the fruit AGPs. Also, the data showed that this epitope was predominant in all stages of the ongoing ripening process. In the case of overexpression of P4H3, the LM2 epitope was present in higher concentrations in comparison to native AGPs (around 20% higher for the fruit tissue of the OEX lines and around

10.3389/fpls.2024.1365490

40% for the fruit tissue of the GFP lines). The lowest absorbance value was observed after using the LM14 antibody, which correlated with the results of the dot blot analysis and Western blotting. The concentration of the LM14 epitopes had the lowest value, i.e. around 20 μg/mL in all the ripening stages and in all the tested samples. In the analyses with the LM1 antibody, significant increases in epitope concentrations were identified in the fruit tissue of the cGFP line at all the ripening stages. In turn, the fruit tissue of the RNAi#1 and RNAi#7 lines were characterised by lower LM1 epitope concentrations in comparison to WT. Also, the greatest fluctuations in the content of the LM1 epitopes were observed along with the progression of the ripening process.

3.3 Biochemical/structural differences

3.3.1 Various AGP amount in fruit at different ripening stages

For biochemical analyses, AGPs were isolated using β-glucosyl Yariv Reagent. After extraction, AGPs were lyophilised and weighed. Figure 5A shows the AGP content in tomato fruit at the BR and RR stages (mg of AGPs per g of fresh tissue). This procedure made it possible to confirm that the AGP amount decreased with the ongoing ripening process both in the WT and transgenic lines. The biochemical assay using β-GlcY determined the AGP content in the tomato fruit at the BR stage: 0.38 mg/g of WT, 0.31 mg/g of

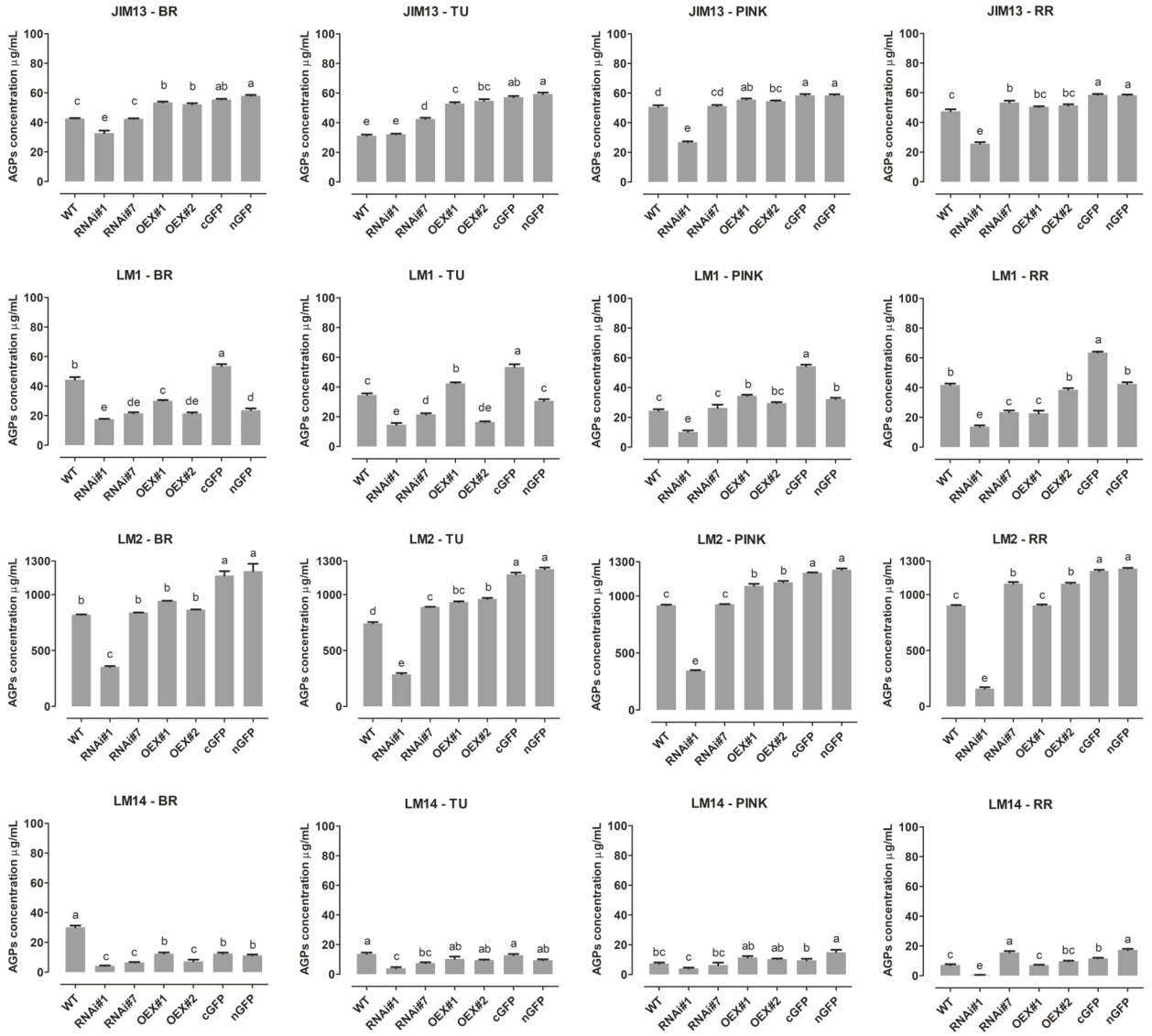

FIGURE 4
ELISA of AGPs extracted from fruit at different ripening stages from wild-type plants (WT) and transgenic lines: RNAi#1, RNAi#7, OEX#1, OEX#2, cGFP, and nGFP. Different letters indicate significant differences among the transgenic lines and WT within ripening stages (according to ANOVA and Tukey's Honestly Significant Difference (HSD) *post hoc* test with the significance level $p<0.05$). BR, Breaker stage; TU, Turning stage; PINK, Pink stage; RR, Red Ripe stage.

RNAi#7, 4.28 mg/g of OEX#1, and 0.59 mg/g of OEX#2 and at the RR stage: 0.28 mg/g of WT, 0.29 mg/g of RNAi#7, 0.75 mg/g of OEX#1, and 0.37 mg/g of OEX#2. It revealed the most intensive degradation process in the fruit tissue of the OEX#1 line, as around 82.3% of AGPs were degraded during the progression of the ripening process. In comparison, around 26.5% in WT, 7.48% in RNAi#7, and 37.5% AGPs in OEX#2 were degraded.

3.3.2 Morphological characterisation of AGPs

Figure 5B shows microphotographs of AGPs extracted from fruit at the initiation (BR) and finalisation (RR) of the ripening process. Despite the detailed observations of morphological features performed using SEM imaging, no differences between AGPs extracted from the BR and RR stages were noted. Interestingly, a high aggregation ability was visible. Thus, AGPs were imaged as compact oval aggregates composed of numerous smaller granules. The approximate diameter of the aggregates of AGPs was 1–3 µm in all the examined samples, regardless of the ripening stage.

3.3.3 Structural characterisation of AGPs

The FTIR spectra of AGPs isolated from the tomato WT and transgenic lines can be divided into several regions (Figure 6-I). The 4000–2750 region is characteristic for O-H vibrations typical for all substances and CH_2 and CH_3 stretching vibrations typical for lipids, proteins, and carbohydrates. The region from 1800 – 1400 is typical for bands assigned to C=O carbonyl stretching vibrations (1740 cm^{-1}), carboxyl ion symmetric and asymmetric vibrations (1620 and 1416 cm^{-1}, respectively), and characteristic for uronic acids. It is also typical for bands characteristic for proteins and denoted as C=O stretching in Amide I (1630 cm^{-1}), as N-H bending in Amide II (1547 cm^{-1}), and C-N stretching vibration in proteins (~1450 cm^{-1}) (Zhou et al., 2009; Szymanska-Chargot and Zdunek, 2013; Yamassaki et al., 2018). The region below 1400 cm^{-1} is called the fingerprint region and contains bands characteristic mostly for carbohydrates. The band at 1367 cm^{-1} is assigned to C-H vibrations and CH_2 bending, 1331 cm^{-1} – to bending of O-H groups in the pyranose ring of pectins, 1316 cm^{-1} – to CH_2 symmetric bending or CH_2 rocking vibration, 1230 cm^{-1} – to bending of O-H groups in the pyranose ring of pectins and proteins, 1147 cm^{-1} – to ring vibrations (C-OH) overlapped with stretching vibrations of side groups and glycosidic bond vibrations (C-O-C), 1000–1200 cm^{-1} – to skeletal vibrations of the ring or the glycoside bond, 1019 cm^{-1} – to C-O stretching and C-C stretching (Boulet et al., 2007; Szymanska-Chargot and Zdunek, 2013; Szymanska-Chargot et al., 2015; Chylińska et al., 2016). The bands at approx. 896, 835, and 776 cm^{-1} are characteristic for β-glycosidic linkages (hemicelluloses and cellulose), α-glycosidic linkages (uronic acids), 1–4 linkage of galactose, and 1–6 linkage of mannose (Bashir and Haripriya, 2016). The bands below 700 cm^{-1} are attributed to the skeletal vibrations of pyranose rings (Szymanska-Chargot et al., 2015; Bashir and Haripriya, 2016).

In the case of the AGPs isolated from the BR and RR stages of WT, the FTIR spectra did not show substantial differences (Figure 6A). Generally, in addition to arabinogalactans (β-glycosidic linkage vibrations at 776 cm^{-1}) and proteins (amide bands at 1630 cm^{-1}, 1547 cm^{-1}, and 1450 cm^{-1}), the isolates also contained uronic acids and pectins (bands at 1367 cm^{-1}, 1331 cm^{-1}, 1316 cm^{-1}, 1230 cm^{-1}, and especially 835 cm^{-1} characteristic for α-glycosidic linkages).

In the case of the RNAi#7 line, the differences in the FTIR spectra between the BR and RR stages were apparently more pronounced (Figure 6B). The spectrum for the BR stage of the RNAi#7 line was very similar to the BR stage of WT with a difference that the band at 1740 cm^{-1} for the mutant was more intense than for WT, which may evidence the presence of more esterified pectins. This band was even more intense in the spectrum for the RR stage of the RNAi#7 line. The spectrum for the RR stage of RNAi#7 line bands at 1377, 1339, 1318, 1230, 1093, 958, and 837 cm^{-1} characteristic for pectic polysaccharides, especially rhamnogalacturonans type I and II (Boulet et al., 2007), and 896 cm^{-1} characteristic for most of the hemicellulosic polysaccharides increased, while those characteristic for pure arabinogalactan glycoprotein (Arabic gum spectrum, Figure 6) at 810 and 776 cm^{-1} decreased (Szymanska-Chargot and Zdunek, 2013).

Less clear differences between spectra were obtained for the BR and RR stages in the OEX#1 line (Figure 6C). The spectra were characterized by relatively high intensity of the band at 1740 cm^{-1} assigned to esterified pectins. In turn, the bands at 1062 and 1030

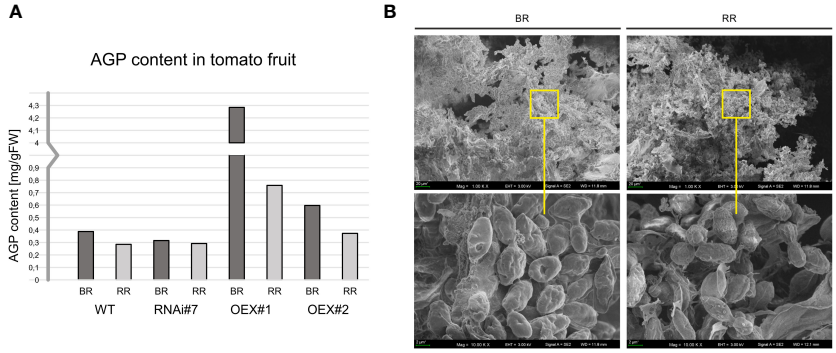

FIGURE 5
AGP content in tomato fruit at different ripening stages **(A)**. Morphological imaging using SEM with visible AGPs with high aggregation ability **(B)**. BR, Breaker stage; RR, Red Ripe stage.

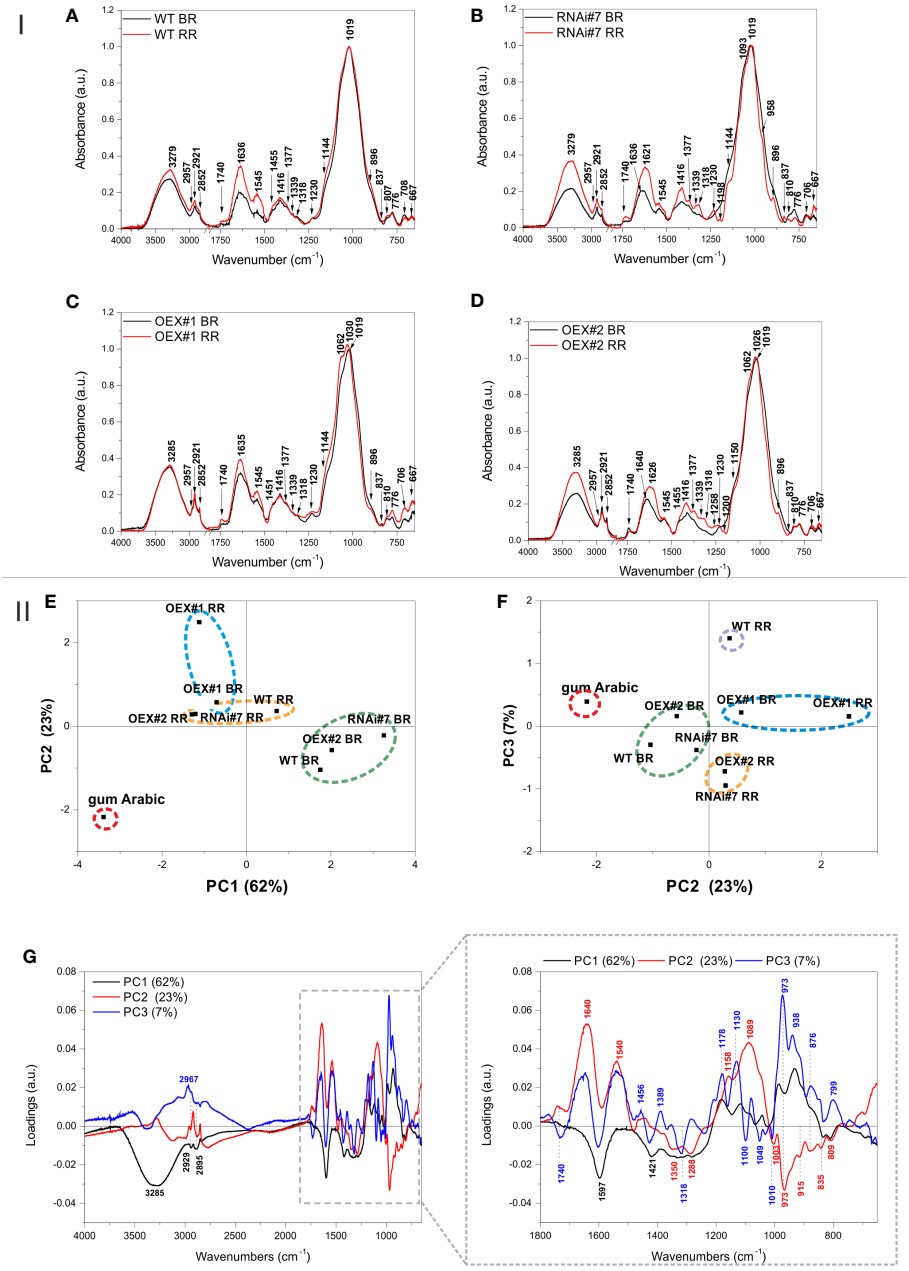

FIGURE 6
I. FTIR spectra in the range of 4000 – 650 cm^{-1} of AGP isolates obtained from tomato fruit at different ripening stages in wild-type plants (WT) **(A)** and transgenic lines: RNAi#7 **(B)**, OEX#1 **(C)**, and OEX#2 **(D)**. The 2750 – 1800 cm^{-1} region was cut out as it did not show any spectral features. The most characteristic wavenumbers are highlighted in the spectra. II. PCA of the FTIR spectra of AGP isolates from tomato fruit at different ripening stages in wild-type plants (WT) and transgenic lines: RNAi#7, OEX#1, and OEX#2. Gum Arabic was added to the analysis as the AGP standard. Scatter of PC1xPC2 **(E)** and PC2xPC3 **(F)** scores are shown together with the loading profile of components PC1, PC2, and PC3 **(G)**. The most characteristic wavenumbers are highlighted in the loadings; different colours (black, blue, and red) denote the different PC (PC1, PC2, and PC3) loadings, respectively (some of the wavenumbers are characteristic for more than one PC loading). BR, Breaker stage; RR, Red Ripe stage.

cm^{-1} that appeared in the spectrum for the RR stage of the OEX#1 line can be assigned to the vibrations of pyranose in gum Arabic and arabinogalactan polysaccharide, respectively (Wu et al., 2020). Moreover, the band at 837 cm^{-1} characteristic for pectic polysaccharides diminished and bands at 896, 810, and 776 cm^{-1} characteristic for arabinogalactans were more visible in the spectrum for the RR stage of the OEX#1 line.

Interestingly, the band at 1740 cm^{-1} declines and the band at 1640 cm^{-1} is shifted to 1626 cm^{-1} in the spectrum for the RR stage of the OEX#2 line, compared with the BR stage of the OEX#2 line (Figure 6D). This may evidence demethylation of pectic polysaccharides present in the AGP isolate from the OEX#2 line. Additionally, as in the case of the RR stage of the RNAi#7 line, the bands characteristic for pectic polysaccharides, especially

rhamnogalacturonans type I and II, also appeared in the RR stage of the OEX#2 line. However, the AGP isolate from the RR stage of the OEX#2 line was also rich in arabinogalactan polysaccharide and protein, as the bands visible at 1150, 1062, 1026, 896, 810, and 776 cm^{-1} were intense.

The PCA analysis of the obtained FTIR spectra was performed for better comparison and highlighting of the samples (Figure 6-II). Figures 6E and F present the scatter plots of the scores of the first three principal components PC1, PC2, and PC3, which together explain 92% of variability. The scores are scattered along all axes and the grouping effect of scores can be observed. The gum Arabic is separated from the other samples, which is clear evidence that the spectra of the obtained isolates differ from the AGP standard (Figure 6E, F). The samples from the BR stages of WT, RNAi#7, and OEX#2 and samples from the RR stages of WT, RNAi#7, and OEX#2 form two separate clusters in the PC1xPC2 score plot, which proves that there are spectral similarities between the samples, while the samples from the BR and RR stages of the OEX#1 line form a separate cluster (Figure 6E). In the PC2xPC3score plot, the same samples groups were obtained; however the RR stage of WT form a new separate group (Figure 6F).

Loadings that influence the differentiation of the scores are presented in Figure 6G. The wavenumbers of PC1 negative loadings that mostly influenced the sample scores lying on the negative side of PC1 (gum Arabic, the BR and RR stages of the OEX#1 line, the RR stages of the OEX#2 and RNAi#7 lines) were 3285, 2929, 2895, 1597, 1421, 1350, 1018, 1288, 835, and 810 cm^{-1}, which are mostly characteristic for esterified pectins and for AGP protein (gum Arabic spectrum), while the positive influence was associated with the following wavenumbers: 1181, 1119, 1042, 977, and 938 cm^{-1}, mostly characteristic for gum Arabic (Figure 6). On the other hand, the gum Arabic was located on the negative side of PC2, on which wavenumbers 1350, 1288, 973, 835, and 809 cm^{-1}, also characteristic for pure AGP from gum Arabic, had an influence. The other samples lying on the negative side of PC2 (but closer to PC2 = 0) were the BR stages of WT, OEX#2, and RNAi#7 lines. The wavenumbers having a positive influence on the scores of samples scattered on the positive side of PC2 were 1740, 1640, 1540, 1158, and 1089 cm^{-1}. The negative influence on the scores scattered along PC3 (the RR stages of the OEX#2 and RNAi#7 lines) had wavenumbers 1740, 1597, 1421, 1318, 1100, 1049, and 1010 cm^{-1} – characteristic mostly for pectic polysaccharides. In turn, wavenumbers 1178, 1130, 973, 938, 876, and 799 cm^{-1}, characteristic for arabinogalactans and for some phospholipids, had a positive influence.

3.4 Differences in AGP arrangement in the cell wall assembly – analyses *in situ*

3.4.1 Changed spatio-temporal localisation of AGPs at the cellular level

In planta studies were performed using the immunofluorescence technique to identify presumed changes in the spatio-temporal pattern of the AGP distribution in the fruit tissue of the examined lines. Figures 7–9 show microscopic investigations of the AGP arrangement in the tissue of WT, OEX#1, and OEX#2; RNAi#1, and RNAi#7; cGFP and nGFP lines, respectively. Our decision to focus on the two distant stages of ripening (BR and RR) was based on the fact that the differences did not appear between particular successive stages.

The microscopic observations demonstrated the anatomic changes in fruit tissues and cell walls at the cellular level. In all the fruit lines, modifications of cell walls occurred with the progression of the ripening process and were visualised as degraded cellular compartments adjacent to swollen cell walls. These modifications were correlated with typical processes of decay in fruit during the ongoing ripening process. The specific pattern of arrangement of AGPs was labelled as a line at the border between the cell wall and the plasma membrane. With the subsequent stages of ripening, the localisation of AGPs changed and the immunofluorescence intensity was lower. For WT, this correlation persisted for the samples labelled with all the antibodies.

The interpretation of microscopic results consisted in finding differences between the analysed lines after the reactions with three antibodies against AGPs. In the initial ripening stages, the fluorescence intensity in the OEX#1 fruit tissue was higher than in WT. The increased number of labelled AGP epitopes was confirmed using all antibodies. The fruit tissue of the OEX#2 line also showed an increase in the number of labelled AGP epitopes compared to WT, although the number was lower than in the fruit tissue of the OEX#1 line. The increase in the amount of AGP epitopes (mainly JIM13 and LM2) disturbed the typical pattern of localisation of AGPs, and the epitopes were visible in the whole area of the cell wall-plasma membrane continuum. Similarly, the striking typical anatomical changes in the tissue during the ripening process coincide with a decrease in the occurrence of AGP epitopes. However, the immunofluorescence signal is clearly higher compared to WT.

In samples with the silenced expression of the *SlP4H3* gene, intrusive alterations in the tissue morphology were imaged as a result of ripening progress. Significant changes in the macrostructure were found in the fruit tissue of the RNAi#1 and RNAi#7 lines. At first, compared to all lines, the tissue in the mutants mentioned above was looser even at the BR stage. In addition, at the RR stage, the tissue was disordered, the cell wall was less integrated, unevenly thickened, more undulating, and swelled. The rearrangement of epitopes was correlated with cellular dissociation. In the fruit tissue of the RNAi# lines, a decrease in all AGP epitopes was observed at both the BR and RR stages.

In the fruit tissue of the cGFP line, substantially increased fluorescence intensity was observed after the reaction performed using JIM13, LM2, and LM14, compared to WT. Moreover, AGP epitopes were present at the last stage of ripening. In the fruit tissue of the nGFP line, loosening of the cell wall was observed from the first ripening stage. With the progression of the ripening process, the cell wall became even more unevenly undulating and thickened. The number of AGP epitopes decreased, which distinguished this line from the fruit tissue of the OEX and cGFP lines.

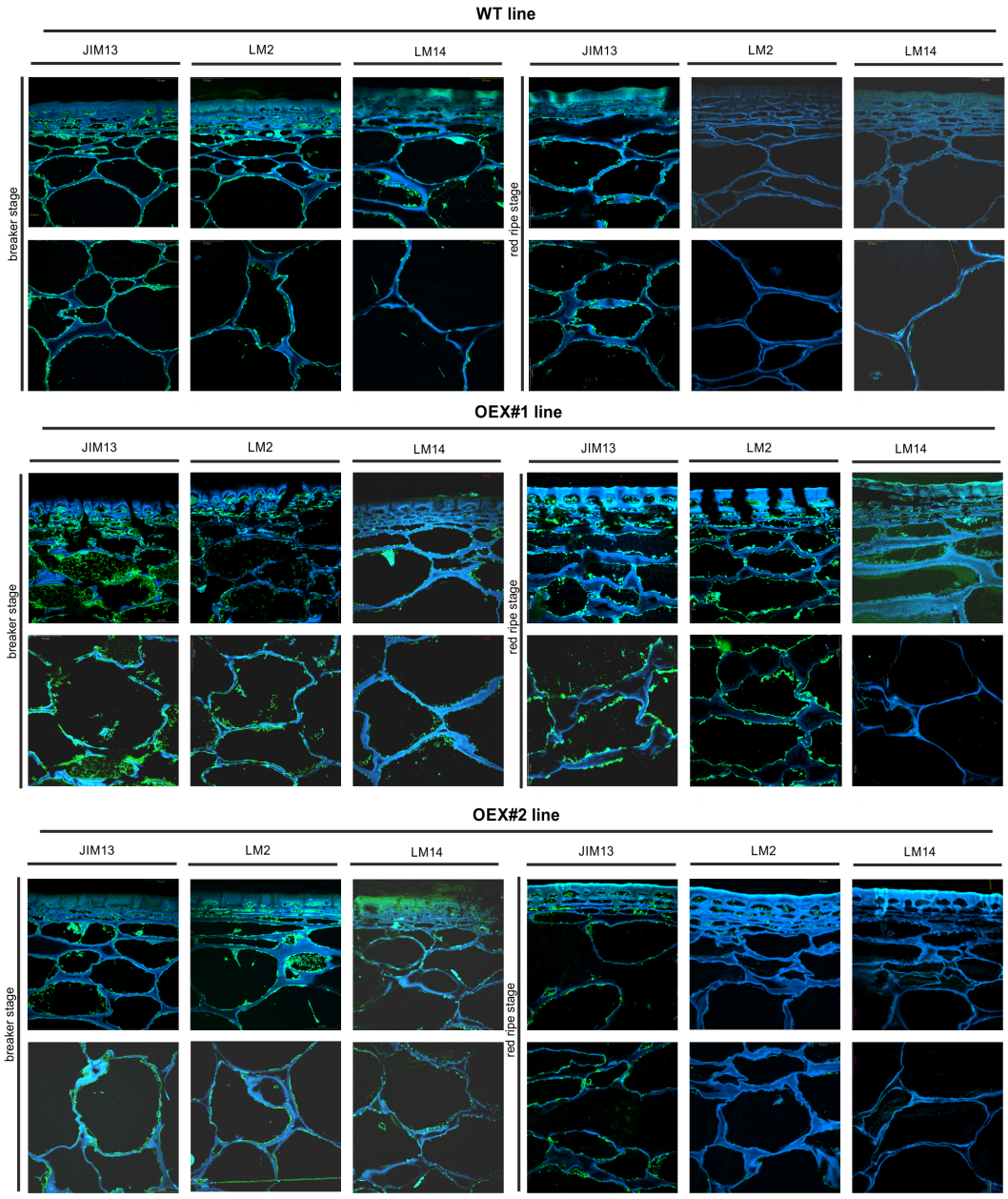

FIGURE 7
Spatio-temporal localisation of AGPs in tomato fruit tissue at different ripening stages in wild-type plants (WT) and transgenic lines OEX#1 and OEX#2. Immunofluorescence method using JIM13, LM2, and LM14 antibodies (green color) and counterstaining with Calcofluor White (blue color). Negative control for immunocytochemical reactions (Supplementary Material).

3.4.2 Disturbed localisation of AGPs at subcellular level

The immunogold labelling analysis and TEM imaging (40 kx magnification) allowed localisation of AGPs in the individual compartments of the fruit cell at the subcellular level. The analysis was carried out using the JIM13 antibody. Figure 10 shows analyses of the correlation between the localisation of AGPs in the cellular compartments and the stages of the ripening process. JIM13 epitopes, visible as dark points marked with red circles (Figure 10A), were observed in the entire cell, and labelling mainly occurred in the cell wall-plasma membrane continuum and the cytoplasm. For consistency, we analysed two cell compartments (cell wall-plasma membrane and cytoplasm) in all cases. Since there were no significant differences between all the subsequent stages of the ripening process noted by CLSM imaging at the cellular level, the analysis at the subcellular level was carried out in two distant stages of ripening. Generally, AGP epitopes were detected less frequently in the RR stage of ripening than in the BR stage. In almost every case, the cell wall-plasma membrane continuum exhibited the largest amounts of AGP epitopes, with the exception of the RR stage in the fruit tissue of the cGFP and nGFP lines.

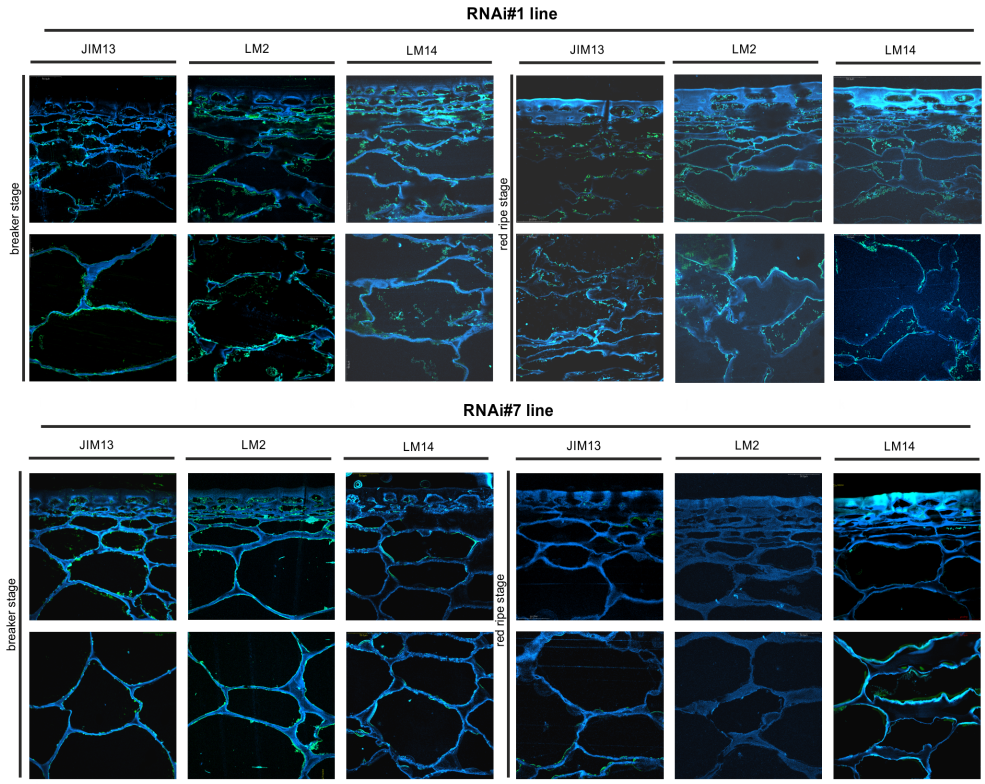

FIGURE 8
Spatio-temporal localisation of AGPs in tomato fruit tissue at different ripening stages in transgenic lines RNAi#1 and RNAi#7. Immunofluorescence method using JIM13, LM2, and LM14 antibodies (green color) and counterstaining with Calcofluor White (blue color).

The quantitative analysis of immunogold labelling confirmed the specific spatio-temporal pattern of distribution of AGPs and indicated changes in the amount of AGPs in the cell wall and cytoplasm in the transgenic lines during the ripening process (Figure 10B). Once again, the most characteristic distribution of AGPs was obtained in the WT fruit tissue. At the BR stage, the AGP epitopes were more organized and localised mainly in the cell wall-plasma membrane continuum. Only 10% of gold particles were localised in the cytoplasm. However, during the ripening process, the number of gold particles increased in the cytoplasm and accounted for nearly 40% at the RR stage. This may evidence the process of degradation of the cell wall and release of residues of cell wall compartments into the cytoplasm.

The AGP distribution pattern was disrupted in the fruit of the transgenic lines, where AGPs were dispersed in the whole area of the extracellular matrix. It was shown that modifications of *SlP4H3* gene activity caused changes in the number of gold particles in particular cell parts. Moreover, different proportions of gold particles in the cell wall-plasma membrane and in the cytoplasm were found in the examined samples, compared to WT. In lines with the overexpression of the *SlP4H3* gene, an increased amount of AGPs in the cytoplasm was found. Furthermore, the subcellular localisation of the AGP epitope in the fruit tissue of the cGFP and nGFP lines at the BR stage showed the presence of half of the amount of gold particles in the continuum cell wall-plasma membrane (0.38 and 0.14 particles per μm^2, respectively), and the rest was distributed in the cytoplasm (0.29 and 0.15 particles per μm^2, respectively). On the other hand, a significant reduction in the number of gold particles in the cell wall-plasma membrane (almost 80%) was observed in the lines with silenced *SlP4H3* gene expression (RNAi#1 and RNAi#7) at the BR stage. Similarly, at the RR stage, the AGP assembly disorder was assessed, and a higher amount of gold particles was noted in the cytoplasm than in the cell wall-plasma membrane.

5 Discussion

The ripening process is the subject of extensive research, but the role of AGPs in this process is still poorly known (Seymour et al., 2013). In our research, the genetic modification in the AGP biosynthesis process by changes in the activity of the P4H enzyme allowed identification of AGP alterations during the ripening process. First of all, the disruption in hydroxylation and subsequent AGP glycosylation processes most probably induce a sequence of modifications in the arrangement of cell walls. In the current work, we did the work step by step to investigate how changes in the process of forming the protein moiety may influence the subsequent phase of the AGP molecule synthesis pathway, such as the attachment of carbohydrate chains. The analyses performed using molecular, structural, and microscopic tools in *ex situ* and then *in situ* studies revealed crucial changes in AGP features in the

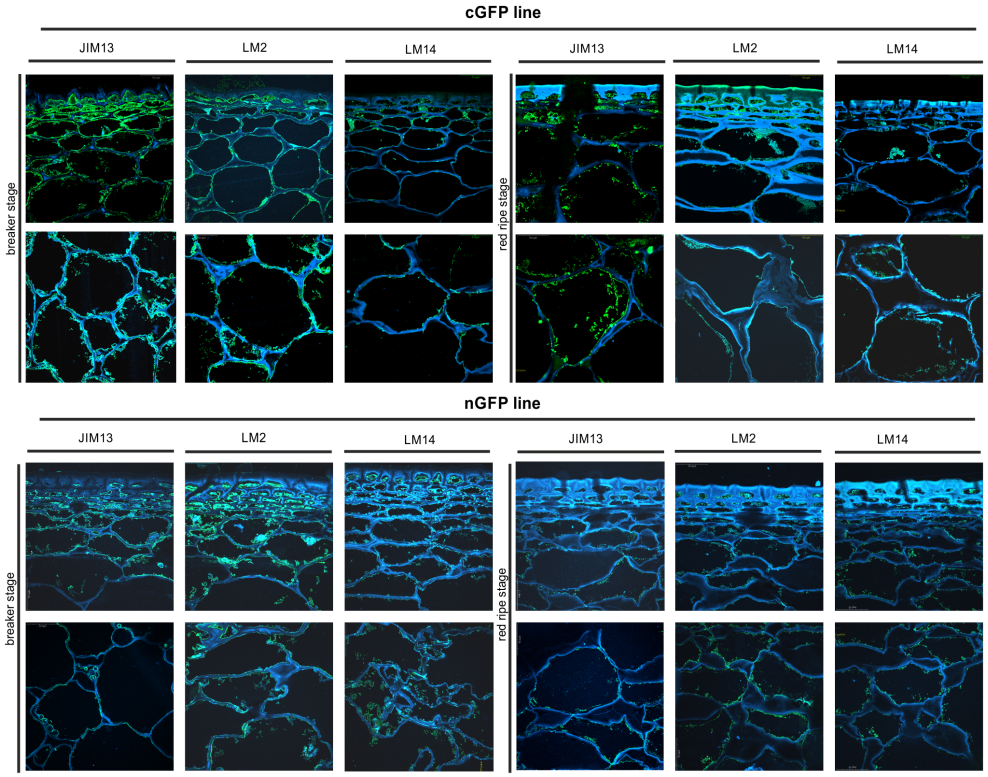

FIGURE 9
Spatio-temporal localisation of AGPs in tomato fruit tissue at different ripening stages in transgenic lines cGFP and nGFP. Immunofluorescence method using JIM13, LM2, and LM14 antibodies (green color) and counterstaining with Calcofluor White (blue color).

fruit of the transgenic lines in comparison to the wild-type plants. Based on the results obtained, a meticulous pattern of consecutive events in fruit cells that is associated with P4H3 was developed.

The development of the overexpressing and silenced P4H3 tomato lines facilitated the determination of alterations in the AGP carbohydrate design that induced changes in their localisation in the cell wall, allowing identification of AGP structural functions in the fruit tissue. So far, it has been demonstrated that hydroxyproline-rich glycoproteins are involved in fruit ripening (Moore et al., 2014; Kalaitzis et al., 2023). One of the major findings of a study conducted by Moore and coworkers on the anti-extensin LM1 antibody showed an increasing amount of extensin epitopes in ripe grapes as a response to the ripening process (Moore et al., 2014). These observations were consistent with the results of the analysis carried out by Nunan and coworkers that protein components rich in arginine and hydroxyproline also accumulate in grapes at the last stages of ripening (Nunan et al., 1997; Nunan et al., 1998). Similarly, our previous studies on apple and tomato fruit have shown that the amount of AGPs during the fruit ripening process changed with a significant concentration increase at the particular stages of the ripening programme (Leszczuk et al., 2020c; Kutyrieva-Nowak et al., 2023a). The analysis carried out with the use of β-glucosyl Yariv Reagent, whose reactivity is one of the most important criteria in the identification of AGPs (Seifert and Roberts, 2007; Kitazawa et al., 2013; Tsumuraya et al., 2019), also confirmed the differences in the AGP content between the specific stages of ripening. The confirmation was found also in the present work, as the content of AGPs decreased with the ongoing ripening process both in WT and in all the examined transgenic lines. Interestingly, an increased amount of AGPs in the overexpression lines was observed, indicating the influence of P4Hs in the AGP biosynthetic pathway.

The next research step involved comprehensive structural analyses on extracted AGPs aimed at revising changes that may have appeared as a result of the P4H3 modifications. The FTIR technique used for this purpose provided information about carbohydrate chains in AGPs during the fruit ripening process. Previous single FTIR reports of monosaccharide compositional analysis of AGPs isolated from *Lycium ruthenicum* Murr fruit revealed that arabinose and galactose represented by absorbance regions at 1060-1040, 975 cm^{-1}, and 945 cm^{-1}, respectively, were the major AGP sugars (Coimbra et al., 1998). The results obtained in the current work also confirm the occurrence of these carbohydrates in the isolated AGPs. The FTIR spectra showed that the AGP isolates from tomato fruit contained pure arabinogalactan proteins and a trace of pectic polysaccharides (uronic acids, rhamnogalacturonan) and hemicelluloses. The PCA analysis in the current work identified three PC groups with different polysaccharide compositions. The result obtained for the analysis of AGPs from the OEX#1 line seems interesting, as samples collected at different ripening stages formed a common group, compared to the two separate groups of the BR and RR stages.

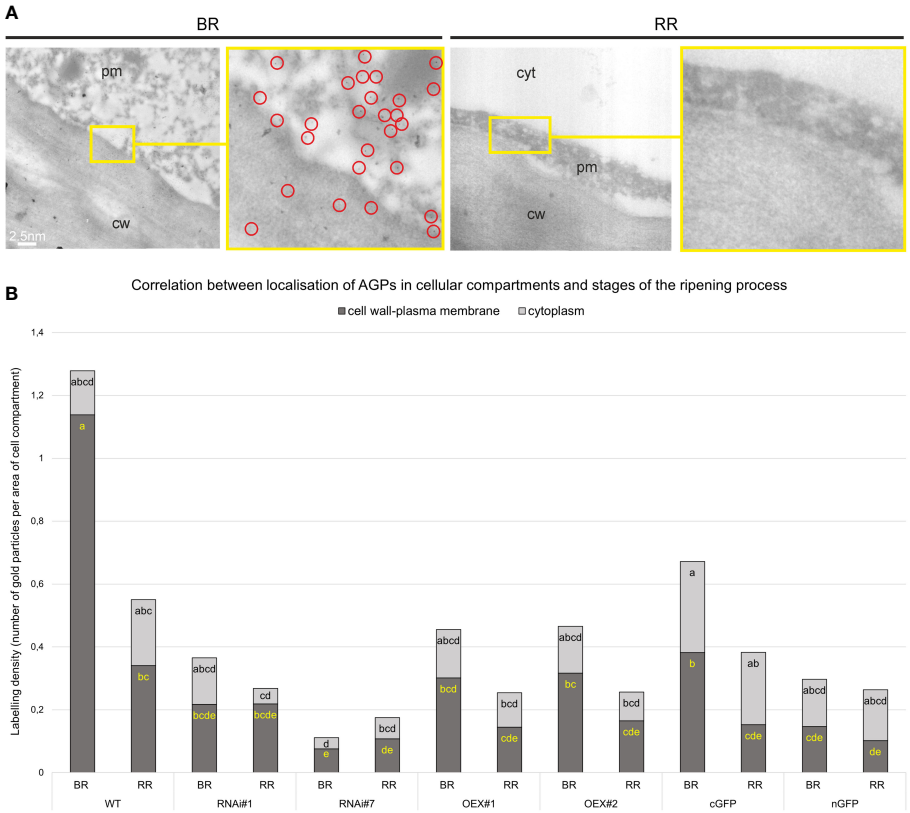

FIGURE 10
Ultrastructural TEM imaging of immunogold labeling of AGPs in tomato fruit at different ripening stages. Gold particles marked with red circles **(A)**. Quantitative data derived from analyses of the density of gold particles **(B)**. Different letters (yellow letters for cell wall – plasma membrane and black letters for cytoplasm) indicate significant differences among the transgenic lines and WT within ripening stages (according to ANOVA and Tukey's Honestly Significant Difference (HSD) *post hoc* test with the significance level $p<0.05$). cw, cell wall; pm, plasma membrane; cyt, cytoplasm; BR, Breaker stage; RR, Red Ripe stage.

Besides, the PC2xPC3 analysis identified a disruption of the 'native' ripening pattern of the transgenic lines, as they did not form a common group with the WT RR. In both PCA analyses, samples at the BR stage from the OEX#2 and RNAi#7 lines formed one group with WT. We conclude that the modification of *SlP4H3* significantly affects the progression of the ripening process, causing changes in the profiles of the AGPs structure.

Molecular studies were performed for the verification of the differences between the tomato lines in detail. In contrast to the β-glucosyl Yariv Reagent assays, anti-AGP antibodies recognizing specific carbohydrate epitopes used in these methods constitute a differentiating factor (Gao et al., 1999). Firstly, the immunoprinting on the nitrocellulose membrane confirmed the presence of AGP epitopes in tomato extracts and highlighted that the overexpression lines were characterised by a general trend towards increased content of the tested AGP epitopes. Secondly, a detailed analysis of the composition of individual epitopes showed further differences indicating disturbance in the carbohydrate chains of AGPs as a result of the modifications in P4H3 activities. In the study conducted by Fragkostefanakis and coworkers on tomato pericarp tissue with a ripening process without disorders, changes in the amount of AGP epitopes and a significantly higher number of the JIM13 epitope were noted (Fragkostefanakis et al., 2012). Western blotting analyses of the JIM13 epitopes revealed a slight decrease in high molecular weight epitopes in the last ripening stages. In the case of the JIM8 antibody, a gradually decrease in the presence of AGPs was also observed after the turning stage (Fragkostefanakis et al., 2012). On the other hand, in the study carried out by Sun and coworkers, only one fraction contained AGPs with a molecular weight of 48 kDa was collected using the LeAGP-1 antibody (Sun et al., 2004). In the first report on the molecular mass of AGPs extracted from fruit, AGP epitopes recognised by JIM8 and JIM13 epitopes in tomato pericarp tissue were in the range of 210-55 kDa and 300-45 kDa, respectively (Fragkostefanakis et al., 2012). In our previous papers, the molecular mass of AGPs was about 250-70 kDa from apple fruit (Leszczuk et al., 2020c) and 120-20 kDa from tomato fruit (Kutyrieva-Nowak et al., 2023a), which may indicate a variable pattern of AGPs in different fruits. In addition, in the case of the JIM13 epitope in WT at the beginning ripening stages, AGPs with 120–60 kDa and 60–25 kDa molecular weight predominated, and at the last stages contained 30–20 kDa AGPs, which were considered a marker of the finalisation of the ripening process (Kutyrieva-Nowak et al., 2023a). In the current work, AGPs from the transgenic lines were characterised by an altered molecular mass in comparison to WT. The molecular differences and the absence of single low molecular weight bands in the last stages of ripening

indicate an effect of the P4H3 activity disruption on AGP structural modifications. The changes observed also pointed to the disturbed process of degradation of 'native' carbohydrate chains with the ripening progress.

Selective glycome profiling of AGPs using an enzyme-linked immunosorbent assay allows rapid analysis of carbohydrate epitopes (Pattathil et al., 2010). Data from previous papers provided information about the relative absorbance of AGP epitopes for the JIM13 antibody. The strength of ELISA signals was characterised by absorbance at 0.05-0.08 in the case of banana fruit and at 0.71-1.18 in the case of mango fruit (Rongkaumpan et al., 2019). Research on tomato fruit from wild-type plants showed an average absorbance level of 0.5-3.5, with significant changes correlated with the ongoing ripening process (Kutyrieva-Nowak et al., 2023a). The present data showed that the absorbance level dependent on the tested lines was different from that of AGPs extracted from fruit in previous studies. This mainly involved the use of JIM13 and LM2 antibodies, where we noted absorbance levels at 2.5-4 and 2.9-4.2, respectively. The results obtained with the LM14 antibody seemed interesting as the absorbance of the transgenic lines was 0.5-0.9 compared to the absorbance of around 2.0 for WT. The glycome profiling with the LM1 antibody did not allow definite determination of the dependence of absorbance changes during the ripening process, as it was quite variable at the different stages of ripening. The changes found were related to disruptions in the concentration of specific epitopes caused by modifications in *SlP4H3* gene expression. Interestingly, the increase in the AGP concentration in the overexpression lines and the decrease in the AGP concentration in the lines with silenced P4H3 expression were confirmed by this method as well. All structural and molecular approaches used in this part of the work clearly indicate a linkage between P4H3 activity and the AGP carbohydrate moiety structure.

Ex situ studies showed that AGPs extracted from the examined transgenic lines were characterised by different molecular structures of carbohydrate chains, which is also connected with particular alterations linked with the stages of ripening. Thus, our next goal was to investigate how the structural changes affected the AGP localisation in the cell wall area. This issue is even more interesting and necessary to analyse, as previous studies have identified the characteristic spatio-temporal pattern of AGP distribution in the cell wall-plasma membrane continuum at the cellular and subcellular levels (Leszczuk et al., 2018; Kutyrieva-Nowak et al., 2023a). Next, subcellular studies of fruit proved that AGP epitopes changed their location and demonstrated a decrease in the number of AGP epitopes with the progression of the fruit senescence process, which is linked to degradative processes in the cell wall and the release of its cellular compartments (Leszczuk et al., 2018). Research conducted by Szymanska-Chargot and coworkers provided information on changes in polysaccharide distribution during post-harvest apple storage (Szymanska-Chargot et al., 2016). Also, comprehensive microarray polymer profiling demonstrated an increase in JIM13 and LM2 epitopes during the ripening process of grapes (Moore et al., 2014). Moreover, the ripening-associated changes had an impact on not only the localisation and distribution of AGPs and other cell wall components but also the fruit texture, causing differences in the anatomical features in the fruit tissue (Winisdorffer et al., 2015; Leszczuk et al., 2019b). This confirms that the correct glycosylation is essential for proper cell wall assembly and extracellular matrix functioning (Velasquez et al., 2011). Also, the analyses conducted in the present work revealed a decrease in the total number of epitopes during the ripening process with a concomitant increase in AGPs in the cytoplasm, compared to the cell wall-membrane continuum. Nevertheless, the significant disruption of the specific and well-documented AGP localisation pattern in all the examined transgenic lines must be underlined. In addition, the disorder of the proportion of AGPs attached to the cell wall and placed in other cellular compartments was also observed for all the transgenic lines. Numerous observations at the tissue level allow concluding that the overall appearance and structure of fruit tissue are also modified. The visible different localisation of AGPs related to the structural and molecular disruption caused by the change in the P4H3 activity is connected with modifications of fruit tissue morphology.

All analyses performed in the present study create complementary evidence that the effect of modifications of *SlP4H3* gene expression is supported by changes in the AGP amount, structure, and compositional properties, and thus impaired distribution of AGPs in fruit cells.

6 Conclusions

To sum up, the study demonstrated the disturbance i.e. changes in the AGP content, disruption of AGP molecular mass, alterations in the molecular composition, changes in the amount of AGPs bound by Yariv Reagent, structural differences indicating various degrees of ripening progress, and the disordered distribution pattern in the cell wall, plasma membrane, and cellular compartments.

Based on the obtained results, we focused on presenting the sequence of events that may take place in the fruit cells in response to changed P4H3 activity:

1) Disturbance of the 'native' AGP structure. The changed content of hydroxyproline residues affects the protein moiety of AGPs, which is associated with altered attachment of carbohydrate chains;
2) Disruption of the AGP molecular structure (mainly carbohydrate chains) causes changes in their localisation at the subcellular level;
3) Changes in the spatio-temporal AGP distribution may be related to the formation of a stable network between AGPs with other cell wall components (APAP1).
4) The lack of properly formulated carbohydrate chains affects the interlinking in the APAP1 network. In turn, the modified stability of the cell wall assembly has an influence on anatomical changes visible at the cellular level.
5) Changes in the continuity and durability of the cell wall affect the entire fruit tissue and the sequence of tissue transformation during the progression of the ripening process.

We conclude that the impaired P4H3 activity has an effect on the AGP molecular and structural features and, consequently, affects the degradation of AGPs during the ongoing ripening process. We may suppose that the 'native' structure of AGPs, mainly their carbohydrate moieties, is important for the strictly scheduled extracellular matrix arrangement and is essential for the correct course of the fruit ripening process. An interesting result is that the modifications caused changes in the anatomical image of the entire fruit tissue. In subsequent studies, it is necessary to focus on other components of the cell wall as part of the APAP1 complex that may be changed as a result of disturbed P4H activity.

Data availability statement

The raw data supporting the conclusions of this article will be made available by the authors, without undue reservation.

Author contributions

NK-N: Data curation, Investigation, Methodology, Software, Visualization, Writing – original draft, Writing – review & editing. AL: Conceptualization, Data curation, Formal analysis, Funding acquisition, Investigation, Methodology, Project administration, Resources, Software, Supervision, Validation, Visualization, Writing – original draft, Writing – review & editing. LE: Investigation, Writing – review & editing. DK: Investigation, Writing – review & editing. AZa: Data curation, Investigation, Writing – original draft. MS-C: Investigation, Writing – review & editing. TS: Investigation, Writing – review & editing. AK: Investigation, Writing – review & editing. KM: Writing – review & editing. EL: Writing – review & editing. PK: Conceptualization, Investigation, Writing – review & editing. AZd: Writing – review & editing.

Funding

The author(s) declare that financial support was received for the research, authorship, and/or publication of this article. The authors gratefully acknowledge the financial support by the National Science Center Poland (Sonata16, no 2020/39/D/NZ9/00232). Also, this work has been financed by the European Regional Development Fund of the European Union and Greek national funds through the Operational Competitiveness, Entrepreneurship and Innovation, under the call RESEARCH-CREATE-INNOVATE (T2EDK-01332: n-Tomatomics - Development of new tomato cultivars by using -omics technologies).

Acknowledgments

We would like to thank Mr Emil Zięba for his excellent technical assistance.

Conflict of interest

The authors declare that the research was conducted in the absence of any commercial or financial relationships that could be construed as a potential conflict of interest.

The author(s) declared that they were an editorial board member of Frontiers, at the time of submission. This had no impact on the peer review process and the final decision.

Publisher's note

Supplementary material

The Supplementary Material for this article can be found online at: https://www.frontiersin.org/articles/10.3389/fpls.2024.1365490/full#supplementary-material

References

Bashir, M., and Haripriya, S. (2016). Assessment of physical and structural characteristics of almond gum. *Int. J. Biol. Macromol* 93, 476–482. doi: 10.1016/j.ijbiomac.2016.09.009

Batu, A. (2004). Determination of acceptable firmness and colour values of tomatoes. *J. Food Eng.* 61, 471–475. doi: 10.1016/S0260-8774(03)00141-9

Borassi, C., Gloazzo Dorosz, J., Ricardi, M. M., Carignani Sardoy, M., Pol Fachin, L., Marzol, E., et al. (2020). A cell surface arabinogalactan-peptide influences root hair cell fate. *New Phytol.* 227, 732–743. doi: 10.1111/nph.16487

Boulet, J. C., Williams, P., and Doco, T. (2007). A Fourier transform infrared spectroscopy study of wine polysaccharides. *Carbohydr Polym* 69, 79–85. doi: 10.1016/j.carbpol.2006.09.003

Chylińska, M., Szymanska-Chargot, M., and Zdunek, A. (2016). FT-IR and FT-Raman characterization of non-cellulosic polysaccharides fractions isolated from plant cell wall. *Carbohydr Polym* 154, 48–54. doi: 10.1016/j.carbpol.2016.07.121

Coimbra, M. A., Barros, A., Barros, M., Rutledge, D. N., and Delgadillo, I. (1998). Multivariate analysis of uronic acid and neutral sugars in whole pectic samples by FT-IR spectroscopy. *Carbohydr Polym* 37, 241–248. doi: 10.1016/S0144-8617(98)00066-6

Cooper, J. B., Heuser, J. E., and Varner, J. E. (1994). 3,4-Dehydroproline inhibits cell wall assembly and cell division in tobacco protoplasts. *Plant Physiol.* 104, 747–752. doi: 10.1104/pp.104.2.747

Cooper, J. B., and Varner, J. E. (1983). Insolubilization of hydroxyproline-rich cell wall glycoprotein in aerated carrot root slices. *Biochem. Biophys. Res. Commun.* 112, 161–167. doi: 10.1016/0006-291X(83)91811-9

Corral-Martínez, P., García-Fortea, E., Bernard, S., Driouich, A., and Seguí-Simarro, J. M. (2016). Ultrastructural immunolocalization of arabinogalactan protein, pectin and hemicellulose epitopes through anther development in *Brassica napus*. *Plant Cell Physiol.* 57, 2161–2174. doi: 10.1093/pcp/pcw133

Ellis, M., Egelund, J., Schultz, C. J., and Bacic, A. (2010). Arabinogalactan-proteins: Key regulators at the cell surface? *Plant Physiol.* 153, 403–419. doi: 10.1104/pp.110.156000

Feder, A., Jensen, S., Wang, A., Courtney, L., Middleton, L., Eck, J. V., et al. (2020). Tomato fruit as a model for tissue-specific gene silencing in crop plants. *Hortic. Res.* 7, 142–148. doi: 10.1038/s41438-020-00363-4

Fragkostefanakis, S., Dandachi, F., and Kalaitzis, P. (2012). Expression of arabinogalactan proteins during tomato fruit ripening and in response to mechanical wounding, hypoxia and anoxia. *Plant Physiol. Biochem.* 52, 112–118. doi: 10.1016/j.plaphy.2011.12.001

Fragkostefanakis, S., Sedeek, K. E. M., Raad, M., Zaki, M. S., and Kalaitzis, P. (2014). Virus induced gene silencing of three putative prolyl 4-hydroxylases enhances plant growth in tomato (*Solanum lycopersicum*). *Plant Mol. Biol.* 85, 459–471. doi: 10.1007/s11103-014-0197-6

Gao, M., Kieliszewski, M. J., Lamport, D. T. A., and Showalter, A. (1999). Isolation, characterization and immunolocalization of a novel, modular tomato arabinogalactan-protein corresponding to the LeAGP-1 gene. *Plant J.* 18, 43–55. doi: 10.1046/j.1365-313X.1999.00428.x

Hieta, R., and Myllyharju, J. (2002). Cloning and characterization of a low molecular weight prolyl 4-hydroxylase from *Arabidopsis thaliana*. Effective hydroxylation of proline-rich, collagen-like, and hypoxia-inducible transcription factor alpha-like peptides. *J. Biol. Chem.* 277, 23965–23971. doi: 10.1074/jbc.M201865200

Hijazi, M., Roujol, D., Nguyen-Kim, H., Del Rocio Cisneros Castillo, L., Saland, E., Jamet, E., et al. (2014a). Arabinogalactan protein 31 (AGP31), a putative network-forming protein in *Arabidopsis thaliana* cell walls? *Ann. Bot.* 114, 1087–1097. doi: 10.1093/aob/mcu038

Hijazi, M., Velasquez, S. M., Jamet, E., Estevez, J. M., and Albenne, C. (2014b). An update on post-translational modifications of hydroxyproline-rich glycoproteins: Toward a model highlighting their contribution to plant cell wall architecture. *Front. Plant Sci.* 5, 1–10. doi: 10.3389/fpls.2014.00395

Kalaitzis, P., Giannoutsou, E., and Konkina, A. (2023). "Role of the cell wall in the regulation of fruit ripening," in *Plant Cell Walls: Research Milestones and Conceptual Insights* (Boca Raton: CRC Press), 147–161.

Kitazawa, K., Tryfona, T., Yoshimi, Y., Hayashi, Y., Kawauchi, S., Antonov, L., et al. (2013). β-galactosyl Yariv reagent binds to the β-1,3-galactan of arabinogalactan proteins. *Plant Physiol.* 161, 1117–1126. doi: 10.1104/pp.112.211722

Kivirikko, K. I., and Myllyharju, J. (1998). Prolyl 4-hydroxylases and their protein disulfide isomerase subunit. *Matrix Biol.* 16, 357–368. doi: 10.1016/S0945-053X(98)90009-9

Knox, J. P., Linstead, P. J., Peart, J., Cooper, C., and Roberts, K. (1991). Developmentally regulated epitopes of cell surface arabinogalactan proteins and their relation to root tissue pattern formation. *Plant J.* 1, 317–326. doi: 10.1046/j.1365-313X.1991.t01-9-00999.x

Konkina, A., Klepadlo, M., Lakehal, A., Zein, Z. E., Krokida, A., Botros, M., et al. (2021). An *Arabidopsis* prolyl 4-hydroxylase is involved in the low oxygen response. *Front. Plant Sci.* 12, 1–12. doi: 10.3389/fpls.2021.637352

Koski, M. K., Hieta, R., Hirsilä, M., Rönkä, A., Myllyharju, J., and Wierenga, R. K. (2009). The crystal structure of an algal prolyl 4-hydroxylase complexed with a proline-rich peptide reveals a novel buried tripeptide binding motif. *J. Biol. Chem.* 284, 25290–25301. doi: 10.1074/jbc.M109.014050

Kutyrieva-Nowak, N., Leszczuk, A., Zając, A., Kalaitzis, P., and Zdunek, A. (2023a). Arabinogalactan protein is a molecular and cytological marker of particular stages of the tomato fruit ripening process. *Sci. Hortic.* 310, 1–10. doi: 10.1016/j.scienta.2022.111718

Kutyrieva-Nowak, N., Leszczuk, A., and Zdunek, A. (2023b). A practical guide to in *situ* and *ex situ* characterisation of arabinogalactan proteins (AGPs) in fruits. *Plant Methods* 19, 1–18. doi: 10.1186/s13007-023-01100-3

Laemmli, U. K. (1970). Cleavage of structural proteins during the assembly of the head of bacteriophage T4. *Nature* 227, 680–685. doi: 10.1038/227680a0

Lamport, D. T. A. (2013). Preparation of arabinogalactan glycoproteins from plant tissue. *Bio Protoc.* 3. doi: 10.21769/BioProtoc.918

Lamport, D. T. A., Tan, L., Held, M., and Kieliszewski, M. J. (2018). Pollen tube growth and guidance: Occam's razor sharpened on a molecular arabinogalactan glycoprotein Rosetta Stone. *New Phytol.* 217, 491–500. doi: 10.1111/nph.14845

Lamport, D. T. A., and Várnai, P. (2013). Periplasmic arabinogalactan glycoproteins act as a calcium capacitor that regulates plant growth and development. *New Phytol.* 197, 58–64. doi: 10.1111/nph.12005

Leszczuk, A., Chylinska, M., and Zdunek, A. (2019a). Distribution of arabinogalactan proteins and pectins in the cells of apple (*Malus* × *domestica*) fruit during post-harvest storage. *Ann. Bot.* 123, 47–55. doi: 10.1093/aob/mcy133

Leszczuk, A., Chylińska, M., and Zdunek, A. (2019b). Enzymes and vitamin C as factors influencing the presence of arabinogalactan proteins (AGPs) in *Solanum lycopersicum* fruit. *Plant Physiol. Biochem.* 139, 681–690. doi: 10.1016/j.plaphy.2019.04.035

Leszczuk, A., Chylińska, M., Zięba, E., Skrzypek, T., Szczuka, E., and Zdunek, A. (2018). Structural network of arabinogalactan proteins (AGPs) and pectins in apple fruit during ripening and senescence processes. *Plant Sci.* 275, 36–48. doi: 10.1016/j.plantsci.2018.07.019

Leszczuk, A., Cybulska, J., Skrzypek, T., and Zdunek, A. (2020a). Properties of arabinogalactan proteins (AGPs) in apple (*Malus* × *domestica*) fruit at different stages of ripening. *Biology* 9, 1–12. doi: 10.3390/biology9080225

Leszczuk, A., Kalaitzis, P., Blazakis, K. N., and Zdunek, A. (2020b). The role of arabinogalactan proteins (AGPs) in fruit ripening – a review. *Hortic. Res.* 7, 1–12. doi: 10.1038/s41438-020-00397-8

Leszczuk, A., Kalaitzis, P., Kulik, J., and Zdunek, A. (2023). Review: structure and modifications of arabinogalactan proteins (AGPs). *BMC Plant Biol.* 23, 45. doi: 10.1186/s12870-023-04066-5

Leszczuk, A., Pieczywek, P. M., Gryta, A., Frąc, M., and Zdunek, A. (2019c). Immunocytochemical studies on the distribution of arabinogalactan proteins (AGPs) as a response to fungal infection in *Malus* × *domestica* fruit. *Sci. Rep.* 9, 1–14. doi: 10.1038/s41598-019-54022-3

Leszczuk, A., Zając, A., Kurzyna-Szklarek, M., Cybulska, J., and Zdunek, A. (2020c). Investigations of changes in the arabinogalactan proteins (AGPs) structure, size and composition during the fruit ripening process. *Sci. Rep.* 10, 1–14. doi: 10.1038/s41598-020-77749-w

Ling, Q., Mohd. Sadali, N., Soufi, Z., Zhou, Y., Huang, B., Zeng, Y., et al. (2021). The chloroplast-associated protein degradation pathway controls chromoplast development and fruit ripening in tomato. *Nat. Plants* 7, 655–666. doi: 10.1038/s41477-021-00916-y

Liu, Z., Persson, S., and Sánchez-Rodríguez, C. (2015). At the border: the plasma membrane-cell wall continuum. *J. Exp. Bot.* 66, 1553–1563. doi: 10.1093/jxb/erv019

Livak, K. J., and Schmittgen, T. D. (2001). Analysis of relative gene expression data using real-time quantitative PCR and the 2-ΔΔCT method. *Methods* 25, 402–408. doi: 10.1006/meth.2001.1262

Lopez-Hernandez, F., Tryfona, T., Rizza, A., Yu, X. L., Harris, M. O. B., Webb, A. A. R., et al. (2020). Calcium binding by arabinogalactan polysaccharides is important for normal plant development. *Plant Cell* 32, 3346–3369. doi: 10.1105/tpc.20.00027

Moller, I., Marcus, S. E., Haeger, A., Verhertbruggen, Y., Verhoef, R., Schols, H., et al. (2008). High-throughput screening of monoclonal antibodies against plant cell wall glycans by hierarchical clustering of their carbohydrate microarray binding profiles. *Glycoconj J.* 25, 37–48. doi: 10.1007/s10719-007-9059-7

Moore, J. P., Fangel, J. U., Willats, W. G. T., and Vivier, M. A. (2014). Pectic-b(1,4)-galactan, extensin and arabinogalactan-protein epitopes differentiate ripening stages in wine and table grape cell walls. *Ann. Bot.* 114, 1279–1294. doi: 10.1093/aob/mcu053

Nakatsuka, A., Murachi, S., Okunishi, H., Shiomi, S., Nakano, R., Kubo, Y., et al. (1998). Differential expression and internal feedback regulation of 1-aminocyclopropane-1-carboxylate synthase, 1-aminocyclopropane-1-carboxylate oxidase, and ethylene receptor genes in tomato fruit during development and ripening. *Plant Physiol.* 118, 1295–1305. doi: 10.1104/pp.118.4.1295

Nibbering, P., Petersen, B. L., Motawia, M. S., Jørgensen, B., Ulvskov, P., and Niittylä, T. (2020). Golgi-localized exo-β1,3-galactosidases involved in cell expansion and root growth in *Arabidopsis*. *J. Biol. Chem.* 295, 10581–10592. doi: 10.1074/jbc.RA120.013878

Nunan, K. J., Sims, I. M., Bacic, A., Robinson, S. P., and Fincher, G. B. (1997). Isolation and characterization of cell walls from the mesocarp of mature grape berries (*Vitis vinifera*). *Planta* 203, 93–100. doi: 10.1007/s00050169

Nunan, K. J., Sims, I. M., Bacic, A., Robinson, S. P., and Fincher, G. B. (1998). Changes in cell wall composition during ripening of grape berries. *Plant Physiol.* 118, 783–792. doi: 10.1104/pp.118.3.783

Orfila, C., Huisman, M. M. H., Willats, W. G. T., van Alebeek, G.-J. W. M., Schols, H. A., Seymour, G. B., et al. (2002). Altered cell wall disassembly during ripening of Cnr tomato fruit: implications for cell adhesion and fruit softening. *Planta* 215, 440–447. doi: 10.1007/s00425-002-0753-1

Pattathil, S., Avci, U., Baldwin, D., Swennes, A. G., Mcgill, J. A., Popper, Z., et al. (2010). A comprehensive toolkit of plant cell wall glycan-directed monoclonal antibodies. *Plant Physiol.* 153, 514–525. doi: 10.1104/pp.109.151985

Perrakis, A., Bita, C. E., Arhondakis, S., Krokida, A., Mekkaoui, K., Denic, D., et al. (2019). Suppression of a prolyl 4 hydroxylase results in delayed abscission of overripe tomato fruits. *Front. Plant Sci.* 10, 1–11. doi: 10.3389/fpls.2019.00348

Perrakis, A., Denic, D., Blazakis, K. N., Giannoutsou, E., Kaloudas, D., Bita, C. E., et al. (2021). A tomato prolyl-4-hydroxylase causes relocation of abscission zone and alters abscission kinetics. *bioRxiv*, 1–36. doi: 10.1101/2021.04.20.440677

Pfeifer, L., Shafee, T., Johnson, K. L., Bacic, A., and Classen, B. (2020). Arabinogalactan-proteins of *Zostera marina* L. contain unique glycan structures and provide insight into adaption processes to saline environments. *Sci. Rep.* 10, 1–10. doi: 10.1038/s41598-020-65135-5

Rongkaumpan, G., Amsbury, S., Andablo-Reyes, E., Linford, H., Connell, S., Knox, J. P., et al. (2019). Cell wall polymer composition and spatial distribution in ripe banana and mango fruit: implications for cell adhesion and texture perception. *Front. Plant Sci.* 10, 1–11. doi: 10.3389/fpls.2019.00858

Seifert, G. J., and Roberts, K. (2007). The biology of arabinogalactan proteins. *Annu. Rev. Plant Biol.* 58, 137–161. doi: 10.1146/annurev.arplant.58.032806.103801

Seymour, G. B., Chapman, N. H., Chew, B. L., and Rose, J. K. C. (2013). Regulation of ripening and opportunities for control in tomato and other fruits. *Plant Biotechnol. J.* 11, 269–278. doi: 10.1111/j.1467-7652.2012.00738.x

Showalter, A. (2001). Arabinogalactan – proteins: Structure, expression and function. *Cell Mol. Life Sci.* 58, 1399–1417. doi: 10.1007/PL00000784

Showalter, A. M., and Basu, D. (2016). Extensin and arabinogalactan-protein biosynthesis: Glycosyltransferases, research challenges, and biosensors. *Front. Plant Sci.* 7, 814. doi: 10.3389/fpls.2016.00814

Smallwood, M., Yates, E. A., Willats, W. G. T., Martin, H., and Knox, J. P. (1996). Immunochemical comparison of membrane-associated and secreted arabinogalactan-proteins in rice and carrot. *Planta* 198, 452–459. doi: 10.1007/BF00620063

Sun, W., Zhao, Z. D., Hare, M. C., Kieliszewski, M. J., and Showalter, A. M. (2004). Tomato LeAGP-1 is a plasma membrane-bound, glycosylphosphatidylinositol-anchored arabinogalactan-protein. *Physiol. Plant* 120, 319–327. doi: 10.1111/j.0031-9317.2004.0236.x

Szymanska-Chargot, M., Chylinska, M., Kruk, B., and Zdunek, A. (2015). Combining FT-IR spectroscopy and multivariate analysis for qualitative and quantitative analysis of the cell wall composition changes during apples development. *Carbohydr Polym* 115, 93–103. doi: 10.1016/j.carbpol.2014.08.039

Szymanska-Chargot, M., Chylińska, M., Pieczywek, P. M., Rösch, P., Schmitt, M., Jürgen, P., et al. (2016). Raman imaging of changes in the polysaccharides distribution in the cell wall during apple fruit development and senescence. *Planta* 243, 935–945. doi: 10.1007/s00425-015-2456-4

Szymanska-Chargot, M., and Zdunek, A. (2013). Use of FT-IR spectra and PCA to the bulk characterization of cell wall residues of fruits and vegetables along a fraction process. *Food Biophys.* 8, 29–42. doi: 10.1007/s11483-012-9279-7

Tan, L., Eberhard, S., Pattathil, S., Warder, C., Glushka, J., Yuan, C., et al. (2013). An *Arabidopsis* cell wall proteoglycan consists of pectin and arabinoxylan covalently linked to an arabinogalactan protein. *Plant Cell* 25, 270–287. doi: 10.1105/tpc.112.107334

Tan, L., Qiu, F., Lamport, D. T. A., and Kieliszewski, M. J. (2004). Structure of a hydroxyproline (Hyp)-arabinogalactan polysaccharide from repetitive Ala-Hyp expressed in transgenic *Nicotiana tabacum*. *J. Biol. Chem.* 279, 13156–13165. doi: 10.1074/jbc.M311864200

Tan, L., Zhang, L., Black, I., Glushka, J., Urbanowicz, B., Heiss, C., et al. (2023). Most of the rhamnogalacturonan-I from cultured *Arabidopsis* cell walls is covalently linked to arabinogalactan-protein. *Carbohydr Polym* 301, 1–12. doi: 10.1016/j.carbpol.2022.120340

Tsumuraya, Y., Ozeki, E., Ooki, Y., Yoshimi, Y., Hashizume, K., and Kotake, T. (2019). Properties of arabinogalactan-proteins in European pear (*Pyrus communis* L.) fruits. *Carbohydr Res.* 485, 1–9. doi: 10.1016/j.carres.2019.107816

Velasquez, S. M., Ricardi, M. M., Dorosz, J. G., Fernandez, P. V., Nadra, A. D., Pol-Fachin, L., et al. (2011). O-glycosylated cell wall proteins are essential in root hair growth. *Sci. (1979)* 332, 1401–1403. doi: 10.1126/science.1206657

Velasquez, S. M., Ricardi, M. M., Poulsen, C. P., Oikawa, A., Dilokpimol, A., Halim, A., et al. (2015). Complex regulation of prolyl-4-hydroxylases impacts root hair expansion. *Mol. Plant* 8, 734–746. doi: 10.1016/j.molp.2014.11.017

Vlad, F., Spano, T., Vlad, D., Daher, B., Ouelhadj, A., and Kalaitzis, P. (2007). Arabidopsis prolyl 4-hydroxylases are differentially expressed in response to hypoxia, anoxia and mechanical wounding. *Physiol. Plant* 130, 471–483. doi: 10.1111/j.1399-3054.2007.00915.x

Winisdorffer, G., Musse, M., Quellec, S., Barbacci, A., Gall, S. L., Mariette, F., et al. (2015). Analysis of the dynamic mechanical properties of apple tissue and relationships with the intracellular water status, gas distribution, histological properties and chemical composition. *Postharvest Biol. Technol.* 104, 1–16. doi: 10.1016/j.postharvbio.2015.02.010

Wu, J., Xu, Y., Zhu, B., Liu, K., Wang, S., Sheng, Y., et al. (2020). Characterization of an arabinogalactan from the fruit hulls of *Ficus pumila* Linn. and its immunomodulatory effect. *J. Funct. Foods* 73(104091), 1–11. doi: 10.1016/j.jff.2020.104091

Yamassaki, F. T., Campestrini, L. H., Zawadzki-Baggio, S. F., and Maurer, J. B. B. (2018). Chemical characterization and complement modulating activities of an arabinogalactan-protein-rich fraction from an aqueous extract of avocado leaves. *Int. J. Biol. Macromol* 120, 513–521. doi: 10.1016/j.ijbiomac.2018.08.072

Yan, Y., Takáč, T., Li, X., Chen, H., Wang, Y., Xu, E., et al. (2015). Variable content and distribution of arabinogalactan proteins in banana (*Musa* spp.) under low temperature stress. *Front. Plant Sci.* 6, 1–14. doi: 10.3389/fpls.2015.00353

Yates, E. A., and Knox, J. P. (1994). Investigations into the occurrence of plant cell surface epitopes in exudate gums. *Carbohydr Polym* 24, 281–286. doi: 10.1016/0144-8617(94)90072-8

Yates, E. A., Valdor, J.-F., Haslam, S. M., Morris, H. R., Dell, A., Mackie, W., et al. (1996). Characterization of carbohydrate structural features recognized by anti-arabinogalactan-protein monoclonal antibodies. *Glycobiology* 6, 131–139. doi: 10.1093/glycob/6.2.131

Zhang, Y., Held, M. A., and Showalter, A. M. (2020). Elucidating the roles of three β-glucuronosyltransferases (GLCATs) acting on arabinogalactan-proteins using a CRISPR-Cas9 multiplexing approach in *Arabidopsis*. *BMC Plant Biol.* 20, 1–20. doi: 10.1186/s12870-020-02420-5

Zhou, K. (2022). The regulation of the cell wall by glycosylphosphatidylinositol-anchored proteins in *Arabidopsis*. *Front. Cell Dev. Biol.* 10, 1–8. doi: 10.3389/fcell.2022.904714

Zhou, X.-L., Sun, P.-N., Bucheli, P., Huang, T.-H., and Wang, D. (2009). FT-IR methodology for quality control of arabinogalactan protein (AGP) extracted from green tea (*Camellia sinensis*). *J. Agric. Food Chem.* 57, 5121–5128. doi: 10.1021/jf803707a

frontiers | Frontiers in Plant Science

TYPE Original Research
PUBLISHED 11 June 2024
DOI 10.3389/fpls.2024.1352253

OPEN ACCESS

EDITED BY
Hiroshi Ezura,
University of Tsukuba, Japan

REVIEWED BY
Ya-Ping Lin,
World Vegetable Center, Taiwan
Weihua Pan,
Chinese Academy of Agricultural Sciences, China

*CORRESPONDENCE
Marko Petek
marko.petek@nib.si

†These authors have contributed equally to this work and share first authorship

RECEIVED 07 December 2023
ACCEPTED 20 May 2024
PUBLISHED 11 June 2024

CITATION
Zagorščak M, Zrimec J, Bleker C, Nolte N, Juteršek M, Ramšak Ž, Gruden K and Petek M (2024) Evidence-based unification of potato gene models with the UniTato collaborative genome browser.
Front. Plant Sci. 15:1352253.
doi: 10.3389/fpls.2024.1352253

Evidence-based unification of potato gene models with the UniTato collaborative genome browser

Maja Zagorščak†, Jan Zrimec†, Carissa Bleker, Nadja Nolte, Mojca Juteršek, Živa Ramšak, Kristina Gruden and Marko Petek*

Department of Biotechnology and Systems Biology, National Institute of Biology, Ljubljana, Slovenia

Potato (*Solanum tuberosum*) is the most popular tuber crop and a model organism. A variety of gene models for potato exist, and despite frequent updates, they are not unified. This hinders the comparison of gene models across versions, limits the ability to reuse experimental data without significant re-analysis, and leads to missing or wrongly annotated genes. Here, we unify the recent potato double monoploid v4 and v6 gene models by developing an automated merging protocol, resulting in a Unified poTato genome model (UniTato). We subsequently established an Apollo genome browser (unitato.nib.si) that enables public access to UniTato and further community-based curation. We demonstrate how the UniTato resource can help resolve problems with missing or misplaced genes and can be used to update or consolidate a wider set of gene models or genome information. The automated protocol, genome annotation files, and a comprehensive translation table are provided at github.com/NIB-SI/unitato.

KEYWORDS

***Solanum tuberosum*, bioinformatics analysis, plant genome annotation, Solanaceae, gene model annotations, Phureja group, GFF files**

1 Introduction

Solanum tuberosum (potato) is among the most important food crops and a model tuber species. The crop is highly useful as an organism for studying plant responses to environmental stress factors (Lukan et al., 2022; Bleker et al., 2024), such as herbivory (Petek et al., 2020a), viral diseases (Baebler et al., 2020), transcriptional (Tomaž et al., 2023) and small RNA regulation (Križnik et al., 2020), single and combined abiotic stress responses (Demirel et al., 2020), and growth-defense trade-offs (Huot et al., 2014). Potato also serves as an excellent platform for transferring and testing vast amounts of knowledge garnered in *Arabidopsis* with an agriculturally relevant crop (Ramšak et al.,

2018; Zagorščak et al., 2018; Schwacke et al., 2019), aiding toward solving present-day food security issues (Cole et al., 2018).

Apart from novel wild potato (Tang et al., 2022) and pan-genome assemblies (Hoopes et al., 2022; Bozan et al., 2023), the double monoploid (DM) clone of group Phureja DM1–3 516 R44 was until recently the standard variety on which gene models were defined. DM genome assemblies and gene models have been introduced by multiple consortia, including the Potato Genome Sequencing Consortium (PGSC), International Tomato Genome Consortium (ITAG), and Buell Lab (University of Georgia). These sequenced and assembled (Yandell and Ence, 2012) up to 88% of the potato genome that included between 35,004 (ITAG) (Tomato Genome Consortium, 2012) and 39,428 (PGSCv4.04) (Potato Genome Sequencing Consortium et al., 2011) gene models, with the recent nanopore long read assembly DMv6.1 (Pham et al., 2020) annotating 40,652 genes (in the working version). Moreover, we previously unified the PGSC v4 and ITAG gene models into a merged DMv4n version containing 49,322 genes (Petek et al., 2020b).

In contrast to *Arabidopsis* gene models, where version control and gene model tracking have been utilized for over a decade and gene annotations are optimized (Rhee et al., 2003; Lamesch et al., 2012), this is not the case with potato and similar less matured crop assemblies. Here, sequencing assemblies and gene models are only slowly advancing, and while each subsequent version improves sequencing depth, coverage, and assembly statistics, the gene models are reformulated. Frequently, previous gene model versions are not accounted for, and mapping and translation tables are not provided (e.g., Pham et al., 2020; Hoopes et al., 2022). This unfortunately limits potato research in multiple ways: i) hindering comparison of gene models across versions and experiments, ii) limiting the reuse and integration of experimental data based on older model versions (e.g., v4) with the latest version (v6) without extensive reprocessing of the RNA-Seq data, and iii) impeding the use of certain popular comparative genomics resources, such as Plaza and Ensembl plants (Valentin et al., 2021; Van Bel et al., 2022; Yates et al., 2022), which, as of writing this paper, have not been updated to the latest gene model versions (v6). Plaza is a platform for comparative, evolutionary, and functional plant genomics, which even in its latest version (5.0) uses v4 potato gene models (Van Bel et al., 2022). On the other hand, Ensembl plants (Yates et al., 2022), a plant genome analysis platform, is based on even older PGSC v3 potato gene models (Visser et al., 2009), yet is a source for other derived ontology (Schwacke et al., 2019) and transcription factor databases (Tian et al., 2020).

In addition to the previously mentioned issues, inadequate consideration of previous gene model information has resulted in the omission of a number of known genes (Visser et al., 2009; Potato Genome Sequencing Consortium et al., 2011; Tomato Genome Consortium, 2012; Petek et al., 2020b). In the case of the recent v6 gene models, we observed that they do not include certain well-known genes with important molecular functions, as they do not account for previous gene model information (Pham et al., 2020). An example is the transcription factor TGA2, an essential regulator of hormonal signaling (Tomaž et al., 2023). Aside from such missing genes, some are also moved, merged, or split (as presented in the sections below). These deviations can lead to differences in interpretation in downstream analyses (e.g., gene family expansion, differential expression, marker selection, gene set enrichment analysis) (Yandell and Ence, 2012). In addition to these imperfect annotations negatively affecting future experiments, existing published results using previous gene models, including, e.g., AlphaFold structure predictions (Tomaž et al., 2023), have become outdated, making it essential to update and consolidate gene predictions.

To help resolve these issues, here, we expand the ITAG and PGSC v4 annotations with v6 annotations (Pham et al., 2020), unifying the different gene models. In addition, we include experiment-based evidence from our pan-transcriptome (Petek et al., 2020b), short- and long-read sequencing data (Lukan et al., 2020; Hoopes et al., 2022), and Solanaceae proteomes (Hosmani et al., 2019; Wang et al., 2024), thereby creating an improved and more accurate potato gene annotation model for downstream analyses. To ensure the transparency and accuracy of future gene models, we present the Unified poTato genome annotation resource (UniTato). UniTato is provided through an Apollo web interface (Dunn et al., 2019), enabling a community-driven effort for real-time revision and enhancement of gene models by experts. This will increase the interpretational power of experimental datasets and facilitate the reuse of experimental analyses conducted on v4, thus expediting progress in potato research.

2 Results

2.1 A unified v4 and v6 potato genome annotation

To compare the potato gene model versions, we mapped gene annotations of older PGSCv4.04 (Potato Genome Sequencing Consortium et al., 2011) and ITAG assemblies (Tomato Genome Consortium, 2012) to the recent potato DMv6.1 assembly (Pham et al., 2020) using Liftoff (Shumate and Salzberg, 2020) and used Bedtools *intersect* (Quinlan and Hall, 2010) to find intersecting genes (Figure 1, see Methods 2.2). Briefly, Liftoff is a tool that accurately maps annotations between assemblies of the same or closely related species. We used it to transfer the gene model annotations from v4 to the v6 assembly. Two genome assemblies (either ITAG or PGSC v4 and DMv6.1) and a v4 annotation file (ITAG or PGSC v4, respectively) were provided as input. The v4 gene models were aligned chromosome by chromosome to the v6 genome assembly. Bedtools *intersect* (Quinlan and Hall, 2010) was then used to check for overlap (intersection) between the sets of v4 and v6 gene models.

We first explored the Liftoff *flank* parameter, which controls the amount of flanking sequence upstream and downstream of a gene, by using a setting of either none or 500 nt. In order to include the gene neighborhood, the upstream and downstream expansion of each v4 gene sequence (combined PGSC/ITAG v4 dataset) before mapping can improve mapping precision. This is especially important for the ITAG annotation which contains only CDS

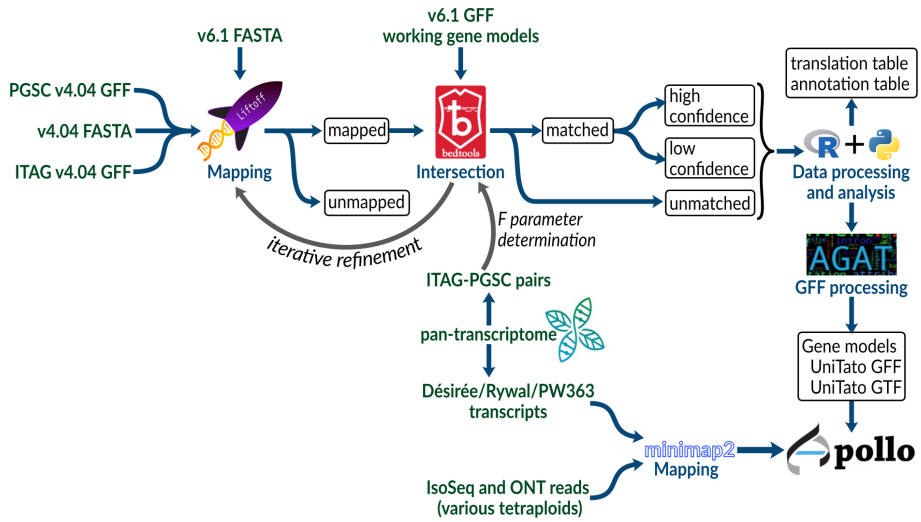

FIGURE 1
Schematic overview of the procedure used to create a unified DM v4 and v6 potato genome annotation resource.

regions, as opposed to the PGSC annotation, where complete mRNA sequences are provided. Without a flanking sequence (0 nt), we mapped 72,143 v4 gene models, whereas when using a flanking sequence of 500 nt length, we mapped 73,820 v4 gene models. Using either of the *flank* parameter settings, 316 PGSC and 211 ITAG gene models could not be mapped to the v6 genome assembly (Table 1; Supplementary Table S1).

Next, to identify the overlap between the sets of v4 and v6 gene models, we explored the Bedtools *F* parameter, which allows for control over the minimum overlap required as a fraction of the length of v4 gene models. By ranging *F* from 0.0001 to 1, we found that 0.30 was the optimum value (Supplementary Figure S1; Table 2). With the Liftoff *flank* parameter of 500 nt, we achieved a mapping coverage (*F* >= 0.3, high identity) with 56,776 v4 gene models mapping to 31,594 v6 models [of these, 92% belong to v6 high confidence gene models as defined by Pham et al. (2020), Supplementary Table S1]. Since *flank* can also capture v4 assembly gaps (N runs) or misassemblies that were corrected in the v6 assembly, using it may not always be the optimal choice. For example, we found that no flanking sequence (0 nt) achieved a better mapping coverage *F* with 387 v4 gene models mapping to 458 v6 models. We thus decided to keep the Liftoff result with the better mapping coverage per gene (either 0 or 500 nt *flank*), as reported above. For gene models with a Bedtools coverage *F* above or equal to 0.30, we kept the v6 gene models and added 17,272 v4 models with low coverage ($F < 0.30$). This merge resulted in the final genome annotation model, termed UniTato (Figures 2A, B). Note that the v6 genome assembly has many inversions compared to the v4 assembly, most evidently in chromosome 12 (Figure 2C).

Of the observed 17,272 v4 gene models with low coverage ($F < 0.30$), 11,832 were from the PGSC dataset and 5,440 from ITAG. These sequences are present in the v6 assembly but were not identified as genes (Pham et al., 2020). We decided to retain all such "rescued" genes and assigned them with the identifier from v4. Of these, 16,117 mapped to the intergenic regions in v6 ($F < 0.0001$). On the other hand, 8,888 v6 working version gene models were not supported by v4 annotations (of these, 5,979 with v6 annotation "hypothetical protein"), of which 3,742 were high-confidence v6 gene models. Finally, we further analyzed the genome-mapped and unmapped v4 genes, searching for evidence of their expression within our published pan-transcriptome dataset (Petek et al., 2020b). The v4 gene models that do not match any v6 gene models ($F < 0.0001$) but do match tetraploid transcriptomes (3,596 out of 15,590 gene models) were considered to be valid genes. On the other hand, some of the 11,924 gene models that match neither the v6 models nor the pan-transcriptome are likely unreliable gene model predictions. Note that 292 out of 559 v4 gene models did not map to the v6 genome yet match tetraploid Désirée,

TABLE 1 Overview of total gene counts and Liftoff results at different flank parameter values for v4 and v6 gene models.

	Total gene count	No *flank*, unmapped	*Flank* 500 nt, unmapped	No *flank*, mapped	*Flank* 500 nt, mapped
PGSC (v4)	39,428 (100.00%)	492 (1.25%)	363 (0.92%)	38,936 (98.75%)	39,065 (99.08%)
ITAG (v4)	35,004 (100.00%)	1,797 (5.13%)	249 (0.71%)	33,207 (94.87%)	34,755 (99.29%)
DMV6.1 working	40,652 (32,917 hc)	/	/	/	/

Three hundred sixteen PGSC and 211 ITAG gene models could not be mapped to the v6 genome assembly (unmapped) with either flank parameter value.
hc, gene models defined as "high confidence" in v6 (Pham et al., 2020).

10.3389/fpls.2024.1352253

TABLE 2 Coverage of v4 to v6 gene models by the number of models and % of all v6 models, at different Bedtools *intersect* sequence coverage (*F*) parameter values.

	Version	*F* = 1	*F* >= 0.30	*F* >= 0.0001
PGSC/ITAG no *flank*, working version	v4	40,252 (54.08%)	56,512 (75.92%)	57,663 (77.47%)
	v6	27,103 (66.67%)	31,481 (77.44%)	32,263 (79.36%)
PGSC/ITAG no *flank*, high confidence	v4	38,095 (51.18%)	53,360 (71.69%)	54,199 (72.81%)
	v6	25,331 (76.95%)	28,986 (88.06%)	29,470 (89.53%)
PGSC/ITAG *flank* 500 nt, working version	v4	40,586 (54.53%)	57,040 (76.63%)	58,209 (78.20%)
	v6	27,261 (67.06%)	31,669 (77.90%)	32,452 (79.83%)
PGSC/ITAG *flank* 500 nt, high confidence	v4	38,373 (51.55%)	53,793 (72.27%)	54,637 (73.40%)
	v6	25,443 (77.29%)	29,113 (88.44%)	29,586 (89.88%)

Genes that mapped with the same F value with and without flank are counted twice.

Rywal, or PW363 transcripts. These genes were lost with the reassembly of the DM scaffold in v6 (Pham et al., 2020). Moreover, we obtained additional evidence about the reliability of the transcriptome-unsupported rescued genes, by mapping to the genome RNA-Seq reads of DM Phureja and tetraploid cultivars (Lukan et al., 2020; Petek et al., 2020b; Hoopes et al., 2022) as well as protein sequences of *Arabidopsis* (Cheng et al., 2017; Pasha et al., 2020) and three *Solanaceae* species (Hosmani et al., 2019; Wang

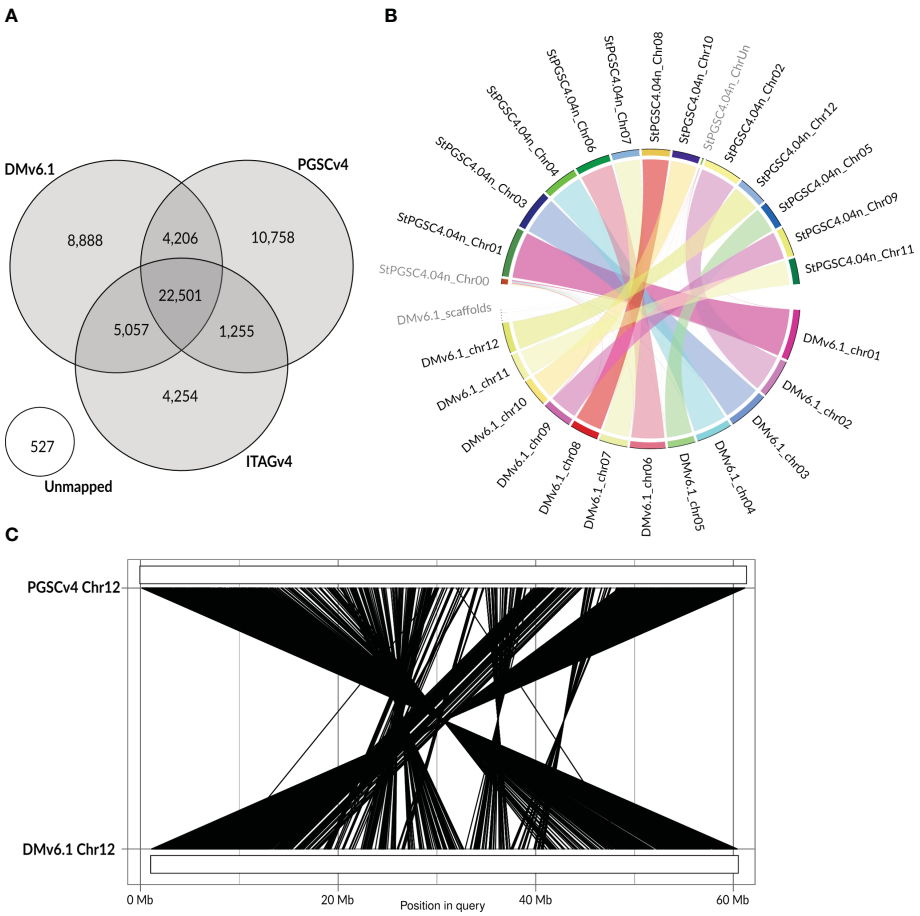

FIGURE 2
Mapping v4 to v6 gene models. **(A)** Venn diagram of overlaps between the v4 and v6 gene models obtained using Liftoff and Bedtools *intersect* (*F* > 0.30). In the intersected areas, note that the number of v6 IDs is shown. **(B)** Chord diagram of the synteny between v4 and v6 gene models. The diagram shows that most chromosomes are almost completely syntenic across models; however, some scaffolds remain unanchored. **(C)** Rearrangements of chromosome 12 in v6 genome assembly vs. the v4 genome assembly. The lines represent synteny between gene model coding regions. Other chromosomes' pairwise synteny graphs can be found on the Unitato GitHub page (https://github.com/NIB-SI/unitato).

et al., 2024) (see Results ch. 2.2). Finally, the newly generated GFF3 file and a table linking identifiers of ITAG and PGSC v4 gene models with v6 gene models are available at GitHub (https://github.com/NIB-SI/unitato).

2.2 UniTato database access and user interface

The UniTato database (accessible at http://unitato.nib.si/) is hosted in a deployment of the community-focused genome annotation editor Apollo (Dunn et al., 2019) (Figure 3). Based on the popular JBrowse genome viewer (Buels et al., 2016), Apollo allows visitors to browse, compare, and interpret the available evidence-based gene models. The annotator panel in the Apollo interface provides several tabs, allowing easy navigation through the genome and the ability to view or hide tracks as well as to locate and view annotation details. For further information, we refer the reader to the Apollo documentation (https://genomearchitect.readthedocs.io/).

The Apollo interface currently contains a number of tracks (see Table 3, Supplementary Table S2), which include various gene models (v4, v6, unified v4 and v6) as well as different subsets of high-confidence matching and rescued genes. To aid in interpreting and evaluating the gene models, a number of evidence tracks are also available, including long read and short paired-end Illumina mappings from DM Phureja and tetraploid cultivars (Lukan et al., 2020; Petek et al., 2020b; Hoopes et al., 2022), reference proteomes of Arabidopsis (*Arabidopsis thaliana*) (Cheng et al., 2017; Pasha et al., 2020), tomato (*Solanum lycopersicum*) (Hosmani et al., 2019), tobacco (*Nicotiana tabacum*) and *Nicotiana benthamiana* (Wang et al., 2024), and reference transcriptomes of potato cultivars Désirée, PW363, and Rywal (Petek et al., 2020b). These tracks are publicly viewable by all UniTato web page visitors. On the other hand, potential contributors are encouraged to use the contact details on the web page to request edit access through a user account. Upon login, these users have access to the curator tools, providing the ability to collaboratively add, remove, and modify potato gene models. The improvements can then be exported as an updated version of the genome annotation file (GFF, VCF, or FASTA).

2.3 UniTato improves the coverage and accuracy of gene models

Merging of v4 and v6 genome annotations improves the coverage and accuracy of the computationally predicted gene models (Supplementary Table S3), whereas manual annotation by experts will provide the necessary quality control. The improved coverage is most evident by adding the rescued v4 genes showing experimental evidence for expression. These include important genes, such as a gene encoding a cysteine protease inhibitor (PGSC0003DMG400010139/Sotub03g015980) and the salicylic acid-binding protein 2 (PGSC0003DMG400028777/Sotub06g025780; for details see Phureja_v4-v6.1_translations.xlsx on GitHub). Apart from the missing genes, several v6 genome models have been wrongly predicted. One such case is the TGA2 transcription factor gene encoded by two v6 gene models and correctly annotated as a single gene model by ITAG v4 (Tomaž et al., 2023). The Iso-Seq read mapping suggests that the gene's 5′-untranslated region extends into another exon (Figure 3). Such mis-annotations can be easily manually curated in the UniTato Apollo instance. Here, tracks of mapped transcripts can additionally help curators build more accurate gene models (see Supplementary Tables S3–S5).

We further decided to identify genomic loci where the v4 and v6 gene models were predicted very differently and/or overlap in a "many-to-many" fashion. Thus, without additional evidence, for these loci, it is very challenging to decide which gene models are more probable. A full list of such complex cases of gene models is available in "overlaps.xlsx" on the UniTato GitHub repository (Supplementary Figure S2). We showcase here two such genomic loci. The first is the v6 model Soltu.DM.02G032590 on chromosome 2 encoding a transferase gene (Figure 4A). The mapped Iso-Seq

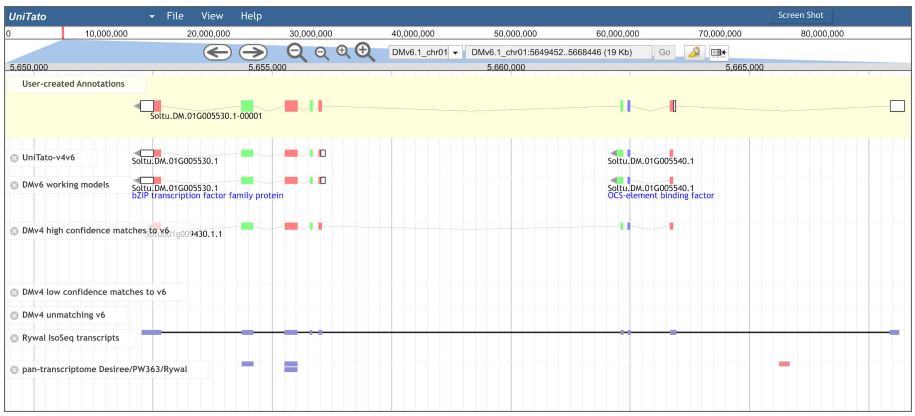

FIGURE 3
Overview of the UniTato user interface and TGA2 use case. Screenshot of the Apollo server web interface for the *Solanum tuberosum* DM gene model manual annotation, showing the manual annotation of a TGA2 transcription factor gene model which was split into two gene models in v6 (track "DMv6 working models"). The gene model's manual annotation with nine exons (track "User-created Annotations") was based on the correctly predicted ITAG v4 CDS and the Rywal Iso-Seq transcript mapping.

reads and the tomato ortholog sequence architecture with 18 exons fit better the v4 model PGSCG0003DMT400001369 than the v6 gene model. The second is the v6 gene model Soltu.DM.04G024440, a chimeric model of the laccase gene and the adjacent ribosomal protein S15A gene (Figure 4B). Based on the Iso-Seq data and the presence of only five exons in the tomato laccase ortholog, the v4 Sotub04g025130 gene model is more accurate.

3 Discussion

The advancement and maturation of high-throughput and long-read sequencing has led to several different potato genome assemblies, gene annotations, and transcriptomic datasets. Sequencing the group Phureja DM (Potato Genome Sequencing Consortium et al., 2011) still enables functional studies of polyploid potato cultivars using RNA-Seq technologies, although with the limitation of not covering cultivar-specific gene expression (Petek et al., 2020b; Hoopes et al., 2022). For practical reasons, most potato researchers use only one genome annotation, either PGSC (Potato Genome Sequencing Consortium et al., 2011) or ITAG (Tomato Genome Consortium, 2012), especially when conducting high-throughput analyses. However, using an incomplete gene set can lead to false outcomes regarding gene presence or gene family diversity, severely affecting downstream results (Yandell and Ence, 2012; Petek et al., 2020b). It is well known that incorrect or incomplete annotations corrupt all subsequent experiments that rely on them, making it essential to have the ability to share accurate and up-to-date annotations (Yandell and Ence, 2012; Bolger et al., 2018).

Our motivation here was thus two-fold: first, to transfer both gene model sets from the older PGSC assembly (Potato Genome Sequencing Consortium et al., 2011; Tomato Genome Consortium, 2012) to the new DMv6.1 assembly (Pham et al., 2020) and, at the same time, to merge the gene models (Figure 2), allowing for data interoperability of previous experimental results (e.g., from RNA-Seq) (Petek et al., 2020b) with the unified gene model set, UniTato. Annotation merging was performed using an in-house-developed bioinformatics pipeline that utilizes open-source software and complementing it with evidence from published tetraploid transcriptomes (Petek et al., 2020b) (Figure 1). The resulting annotation files were incorporated into an Apollo web server (Dunn et al., 2019), which enables the potato community to curate and refine potato gene models collaboratively and in real time, facilitating the establishment of a single standardized potato genome annotation (Figure 3). Moreover, by comparing v4 and v6 annotations with UniTato, we observed multiple complex cases of gene models that cannot be straightforwardly resolved and will need to be manually curated (see "overlaps.xlsx" on the UniTato GitHub for a list of gene identifiers for these complicated cases). We thus show how UniTato can be used to identify gene models that are either missing or were moved, merged, or split (see Figures 3, 4; Supplementary Figure S2).

This showcases the usefulness of the established resource for resolving genome assembly and annotation issues. Bioinformatics users can thus i) compare gene models visually across versions and tracks, pinpointing and resolving errors and ensuring that the most accurate gene models are constructed and applied; ii) compare experimental results obtained on v4 to those obtained on the new v6 assembly or higher, such as for instance with RNA-Seq, where results with old identifiers can be incorporated with new results using v6 identifiers (via the translation table), without requiring repeated read mapping and computations; iii) curate potato gene models in problematic regions, such as determining gene structures in tandemly repeated gene regions, which cause problems with most annotation pipelines (multiple long-read and short-read tracks available in UniTato, see Table 3); and iv) use current data with popular genome analysis resources that still rely on older annotations (Van Bel et al., 2022; Yates et al., 2022), facilitating, e.g., translation of gene descriptions and ontologies via orthology from model plants. Furthermore, with the provided v4–v6 mapping and available evidence tracks (Table 3), UniTato also aids wet lab research. This includes i) guiding experiment design and interpretation, enabling users to check for off-target effects across different gene models; ii) defining and cloning functional orthologs based on experimental results and not merely partial sequence similarity, by revealing if orthologs from another plant map to the v6 assembly (see RNA-Seq and proteome tracks, Table 3); and iii) primer design, since the unified gene models are an improvement over the initial v4 and v6 models, enhancing gene coverage and accuracy (e.g., the user can visually determine if the amplicon is covering variations in the RNA-Seq tracks, Table 3).

In conclusion, we believe that building upon existing gene models to improve and unify them in a community-wise manner is a reasonable and transparent way to improve potato gene model annotations. The repeated creation of new genome model versions, without interlinking, is not contributing to the FAIR data paradigm (Wilkinson et al., 2016; Petek et al., 2022) and thus hinders agricultural research, including precision agriculture and food safety (Cole et al., 2018). The requirements of periodic annotation curation and incorporating experimental data and novel findings into the annotation process are inherent also to other plant species (Yandell and Ence, 2012; Kersey, 2019). Even in model plants, up to 40% of protein-coding genes can still be of unknown function, suggesting that much work is still required to fully resolve, annotate, and understand most plant genomes (Horan et al., 2008; Wang et al., 2023). We propose that a similar approach for evidence- and community-based revision as the one presented here can be utilized for any other insufficiently annotated species, for which genome models of closely related species are available. Apart from updating our database with new assemblies as they become available (Yang et al., 2023), future developments include the addition of novel experimental omics datasets and expansion to related genomes.

4 Methods

4.1 Data sources

To develop UniTato, we used the publicly available potato group Phureja DM gene models: DMv6.1 (Pham et al., 2020), ITAG (Tomato Genome Consortium, 2012), and PGSCv4.04 (Potato Genome Sequencing Consortium et al., 2011), as well as

TABLE 3 Overview of the evidence tracks available in the UniTato v1.0 web server.

	Track name	Track description
Gene models and gene model subsets	UniTato-v4v6	DM Phureja potato unified (merged) v4 and v6 gene models (GFF)
	DMv4 unmatching v6	DM Phureja potato v4 gene models not matching v6 gene models (GFF), added to UniTato GFF
	DMv4 low-confidence matches to v6	DM Phureja potato v4 gene models matching v6 gene models with low confidence (GFF), added to UniTato GFF
	DMv4 high-confidence matches to v6	DM Phureja potato v4 gene models matching v6 gene models with high confidence (GFF), included in the translation table
Pan-transcriptome	Pan-transcriptome Desiree/PW363/Rywal	Representative *de-novo* assembled transcripts of potato cv. Desiree, cv. Rywal, and breeding clone PW363 (BAM)
Long-read transcriptomes	Rywal Iso-Seq transcripts	cv. Rywal potato Iso-Seq reads (BAM)
	Altus Iso-Seq transcripts	cv. Altus potato Iso-Seq reads (BAM)
	Avenger Iso-Seq transcripts	cv. Avenger potato Iso-Seq reads (BAM)
	Colomba Iso-Seq transcripts	cv. Colomba potato Iso-Seq reads (BAM)
	Spunta Iso-Seq transcripts	cv. Spunta potato Iso-Seq reads (BAM)
	PRJNA612026 ONT transcripts	Potato ONT reads from SRA project PRJNA612026 (BAM)
Short paired-end read transcriptomes	Phureja tuber Illumina PE	*Solanum tuberosum* L. Phureja Illumina NovaSeq 6000 reads (bw)
	Potato seed-tubers Illumina PE	*Solanum tuberosum* tuber-seeds from northern Antioquia/Cundinamarca/Boyaca (bw)
	Phureja DM1–3 516 R44 Illumina PE	*Solanum tuberosum* strain: DM1–3 516 R44 genome sequencing and assembly (bw)
	Phureja pistil Illumina PE	C065 pistil transcriptome sequencing (bw)
	Phureja Illumina PE	*Solanum phureja* lines contrasting by resistance to nematode (bw)
	Potato landraces young leaves Illumina PE	Transcriptomes of *in-vitro* young leaves in 11 potato landraces (bw)
	Phureja seed-tuber sprouts Illumina PE	RNA-Seq of certified and informal potato seed tubers in the province of Antioquia (bw)
Reference proteomes	Arabidopsis proteome Araport11	*Arabidopsis thaliana* proteome (v. Araport11) aligned to UniTato genome using miniprot
	Tomato proteome ITAG4.1	*Solanum lycopersicum* proteome (v. ITAG 4.1) aligned to UniTato genome using miniprot
	Tobacco proteome NtaSR1	*Nicotiana tabacum* proteome (v. SR1) aligned to UniTato genome using miniprot
	Benthi proteome NbeHZ1	*Nicotiana benthamiana* proteome (v. HZ1) aligned to UniTato genome using miniprot

reference transcriptomes of Désirée, Rywal, and PW363 tetraploid genotypes, and an ITAG/PGSC translation table (Petek et al., 2020b). The latter consolidated the two publicly available PGSC and ITAG gene models into a single unified one.

4.2 Data processing

To map gene annotations across potato genome assemblies (Figure 1), GFF files were sorted using the *sort* function from Bedtools v2.25.0 (Quinlan and Hall, 2010). Liftoff v.1.6.3 (Shumate and Salzberg, 2020) uses Minimap2 (Li, 2018) to map annotations between assemblies of the same or closely related species. We modified it to accept the number of nucleotides for the *flank* parameter (https://github.com/NIB-SI/Liftoff), instead of the ratio of sequence size, and used with the following parameters: i) coverage of 0.90%, ii) sequence identity of 90%, iii) flanking sequence length *flank* of either 0 or 500 nucleotides, and iv) Minimap2 v.2.24-r1122 "asm5" option for long assembly to reference mapping. In addition, Minimap2 was used with the same set of parameters as for Liftoff (–end-bonus 5 –eqx -N 50 -p 0.8 -ax asm5) to map the reference CDSome and transcriptome (Petek et al., 2020b) of three potato genotypes: Désirée, PW363, and Rywal. FASTQ files of long-read transcriptomics datasets were downloaded from SRA. The Iso-Seq reads were mapped to the v6 genome assembly using Minimap2 with parameters "-ax splice:hq -G 10000 -uf".

Next, to compare the mapped annotation across the assemblies, as well as overlaps within the DMv6.1, the *intersect* function from

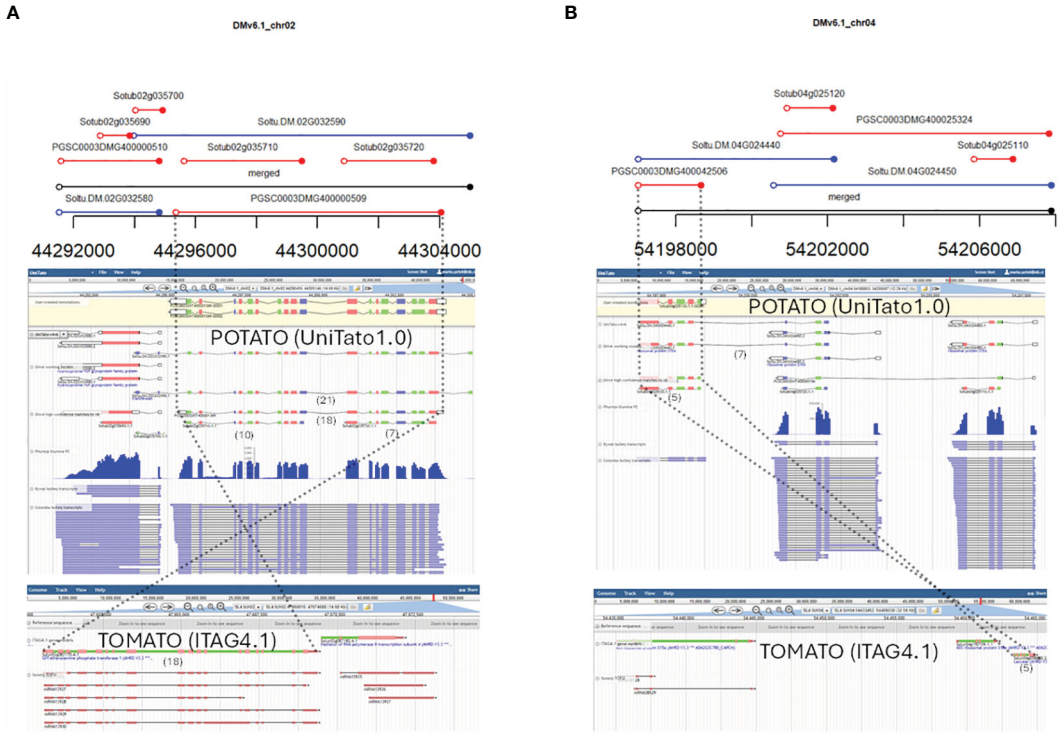

FIGURE 4
Examples of overlapping v4 and v6 gene models that require RNA-Seq read mapping and ortholog evidence for manual curation. From top to bottom: graphical representation of v4 and v6 gene model overlaps from "04_intervals_many-to-many.html" file on the UniTato GitHub repository, UniTato Apollo representation of these gene models with RNA-Seq Illumina PE and Iso-Seq tracks, and representation of tomato synthetic genomic region from the SolGenomics genome browser showing tomato ITAG4.1 annotation and Iso-Seq tracks. The numbers in brackets below the gene models show the exon count. Dotted lines follow the curated gene models through the three representations. **(A)** Manual curation of a v6 transferase gene model Soltu.DM.02G032590 for which the v4 model PGSCG0003DMT400001369 better fits the transcriptome data and the tomato ortholog evidence. **(B)** Manual curation of a chimeric v6 gene model Soltu.DM.04G024440 for which the v4 Sotub04g025130 model better fits the transcriptome and ortholog evidence.

Bedtools (Quinlan and Hall, 2010) was used with the following minimum overlap as a fraction (*F*) ranging incrementally from 0.0001 to 1. Pairs from our existing merged v4 genome model (Petek et al., 2020b) were used to determine the optimal *F* threshold value of 0.30 (Supplementary Figure S1). All reported v6 values below refer to working model versions unless stated otherwise. To obtain additional evidence about the reliability of the transcriptome-unsupported rescued genes, we mapped i) short paired-end Illumina RNA-Seq reads of DM Phureja (Pham et al., 2020) using STAR (Dobin et al., 2013) and of cv. Rywal (Lukan et al., 2020) using Salmon (Patro et al., 2017); ii) long reads of tetraploid cultivars (Della Bartola et al., 2020; Lukan et al., 2020; Hoopes et al., 2022) using Minimap2 (Li, 2018); and iii) protein sequences of the model plant *Arabidopsis* (Cheng et al., 2017; Pasha et al., 2020) and three Solanaceae species (Hosmani et al., 2019; Wang et al., 2024) using miniprot v.0.13-r24 (-G 100 -O 10 -J 34 -F 30 -j1 -M0 –gff-only -ut64) (Li, 2023).

For visualization, packages circlize v0.4.15 (Gu et al., 2014) and intervals v0.15.4 (github.com/edzer/intervals) were used with default settings. For topological sorting of unified GFF features, AGAT v0.6.2 (Dainat et al., 2023) was used with default settings.

4.3 Database implementation

A web server hosting the Apollo genomic annotation editor (Dunn et al., 2019) for real-time collaborative analysis and curation was deployed at https://unitato.nib.si. The reference DM genome assembly (DMv6.1) was uploaded as the base organism. Several evidence tracks corresponding to the different gene models are available for exploration and curation. The database instance is running Apollo 2.7.0, deployed with docker, with default parameters. Data upload was carried out using JBrowse utility scripts (Buels et al., 2016).

4.4 Software and code

The programming environments R v.4.3 (https://www.r-project.org/) and Python v3.8 (https://www.python.org/) were used. Code to reproduce the analysis and results including scripts used for constructing the mapping table between v4 and v6 gene IDs, as well as merging v4 and v6 models are available at the GitHub repository (https://github.com/NIB-SI/unitato).

Data availability statement

Data and code to reproduce the analysis are available at the GitHub repository https://github.com/NIB-SI/unitato/. The GFF and GTF files and the identifier translation table are also available from https://unitato.nib.si/downloads/. Publicly available RNA-Seq datasets were used in the study. The data can be found under the following SRA accession numbers: SRR8281993-SRR8282008 (Rywal IsoSeq reads; SRA study SRP172523), SRR14298411-SRR14298459 (Altus, Avenger, Colomba and Spunta IsoSeq reads; SRA study SRP315827), SRR11431596-SRR11431617 (PRJNA612026 ONT reads; SRA study SRP254248), SRR10690850, SRR10690852, SRR10690854, SRR10690856, SRR10690857, SRR10690858 (Rywal Illumina reads; SRA study SRP237525; GEO accession GSE142002), SRR122108, SRR122109, SRR122113, SRR122122, SRR122124, SRR122129, SRR122139 (Phureja Illumina reads; SRA study SRP005965), SRR7047512 (Phureja Illumina reads; SRA study SRP141363), SRR8457030-SRR8457059 (Phureja Illumina reads; SRA study SRP180310), SRR14627804-SRR14627805 (Phureja Illumina reads; SRA study SRP321011), SRR17202512-SRR17202515 (Phureja Illumina reads; SRA study SRP350333), SRR17244262-SRR17244298 (Phureja Illumina reads; SRA study SRP350981), and SRR10153126 (Phureja Illumina reads; SRA study SRP222783).

Author contributions

MZ: Conceptualization, Data curation, Formal analysis, Investigation, Methodology, Software, Validation, Visualization, Writing – original draft, Writing – review & editing. JZ: Formal analysis, Funding acquisition, Investigation, Methodology, Writing – original draft, Writing – review & editing. CB: Formal analysis, Funding acquisition, Investigation, Methodology, Software, Visualization, Writing – review & editing. NN: Formal analysis, Investigation, Validation, Writing – review & editing. MJ: Formal analysis, Investigation, Validation, Writing - review and editing. ŽR: Investigation, Writing – review & editing. KG: Conceptualization, Investigation, Project administration, Supervision, Writing – review & editing, Funding acquisition, Resources. MP: Conceptualization, Data curation, Formal analysis, Funding acquisition, Investigation, Methodology, Project administration, Resources, Supervision, Validation, Visualization, Writing – original draft, Writing – review & editing.

Funding

The author(s) declare that financial support was received for the research, authorship, and/or publication of this article. The study was supported by the EU Horizon 2020 Research and Innovation Programme under grant agreement no. 862858 (ADAPT); the Marie Skłodowska-Curie Actions (MSCA) Doctoral Network "LongTREC" under grant agreement no. 101072892; the Public Scholarship, Development, Disability and Maintenance Fund of the Republic of Slovenia grant no. 11013–9/2021–2; and the Slovenian Research and Innovation Agency under grant agreements no. P4–0165, P4–0431, J2–3060, and Z4–50146.

Conflict of interest

The authors declare that the research was conducted in the absence of any commercial or financial relationships that could be construed as a potential conflict of interest.

Publisher's note

Supplementary material

The Supplementary Material for this article can be found online at: https://www.frontiersin.org/articles/10.3389/fpls.2024.1352253/full#supplementary-material

References

Baebler, Š, Coll, A., and Gruden, K. (2020). Plant molecular responses to potato virus Y: A continuum of outcomes from sensitivity and tolerance to resistance. *Viruses* 12. doi: 10.3390/v12020217

Bleker, C., Ramšak, Ž, Bittner, A., Podpečan, V., Zagorščak, M., Wurzinger, B., et al. (2024). Stress Knowledge Map: A knowledge graph resource for systems biology analysis of plant stress responses. *Plant communications*, 100920. doi: 10.1016/j.xplc.2024.100920

Bolger, M. E., Arsova, B., and Usadel, B. (2018). Plant genome and transcriptome annotations: from misconceptions to simple solutions. *Briefings Bioinf.* 19, 437–495. doi: 10.1093/bib/bbw135

Bozan, I., Achakkagari, S. R., Anglin, N. L., Ellis, D., Tai, H. H., and Strömvik, M. V. (2023). Pangenome analyses reveal impact of transposable elements and ploidy on the evolution of potato species. *Proc. Natl. Acad. Sci. United States America* 120, e22111171205. doi: 10.1073/pnas.2211117120

Buels, R., Yao, E., Diesh, C. M., Hayes, R. D., Munoz-Torres, M., Helt, G., et al. (2016). JBrowse: A dynamic web platform for genome visualization and analysis. *Genome Biol.* 17, 66. doi: 10.1186/s13059-016-0924-1

Cheng, C.-Y., Krishnakumar, V., Chan, A. P., Thibaud-Nissen, F., Schobel, S., and Town, C. D. (2017). Araport11: A complete reannotation of the arabidopsis thaliana reference genome. *Plant Journal: For Cell Mol. Biol.* 89, 789–8045. doi: 10.1111/tpj.13415

Cole, M. B., Augustin, M. A., Robertson, M. J., and Manners, J. M. (2018). The science of food security. *NPJ Sci. Food* 2, 14. doi: 10.1038/s41538-018-0021-9

Dainat, J., Hereñú, D., Murray, D. K. D., Davis, E., Crouch, K., Lucile, S., et al. (2023). NBISweden/AGAT: AGAT: Another Gff Analysis Toolkit to handle annotations in any GTF/GFF format (Version v1.2.0). doi: 10.5281/zenodo.8178877

Della Bartola, M., Byrne, S., and Mullins, E. (2020). Characterization of potato virus Y isolates and assessment of nanopore sequencing to detect and genotype potato viruses. *Viruses* 12. doi: 10.3390/v12040478

Demirel, U., Morris, W. L., Ducreux, L. J.M., Yavuz, C., Asim, A., Tindas, I., et al. (2020). Physiological, biochemical, and transcriptional responses to single and combined abiotic stress in stress-tolerant and stress-sensitive potato genotypes. *Front. Plant Sci.* 11, 169. doi: 10.3389/fpls.2020.00169

Dobin, A., Davis, C. A., Schlesinger, F., Drenkow, J., Zaleski, C., Jha, S., et al. (2013). STAR: ultrafast universal RNA-seq aligner. *Bioinformatics* 29, 15–215. doi: 10.1093/bioinformatics/bts635

Dunn, N. A., Unni, D. R., Diesh, C., Munoz-Torres, M., Harris, N. L., Yao, E., et al. (2019). Apollo: democratizing genome annotation. *PloS Comput. Biol.* 15, e10067905. doi: 10.1371/journal.pcbi.1006790

Gu, Z., Gu, L., Eils, R., Schlesner, M., and Brors, B. (2014). Circlize implements and enhances circular visualization in R. *Bioinformatics* 30, 2811–2125. doi: 10.1093/bioinformatics/btu393

Hoopes, G., Meng, X., Hamilton, J. P., Achakkagari, S. R., Guesdes, F. d. A. F., Bolger, M. E., et al. (2022). Phased, chromosome-scale genome assemblies of tetraploid potato reveal a complex genome, transcriptome, and predicted proteome landscape underpinning genetic diversity. *Mol. Plant* 15, 520–536. doi: 10.1016/j.molp.2022.01.003

Horan, K., Jang, C., Bailey-Serres, J., Mittler, R., Shelton, C., Harper, J. F., et al. (2008). Annotating genes of known and unknown function by large-scale coexpression analysis. *Plant Physiol.* 147, 41–575. doi: 10.1104/pp.108.117366

Hosmani, P. S., Flores-Gonzalez, M., Geest, H. v. d., Maumus, F., Bakker, L. V., Schijlen, E., et al. (2019). An improved de novo assembly and annotation of the tomato reference genome using single-molecule sequencing, hi-C proximity ligation and optical maps. *bioRxiv*. doi: 10.1101/767764

Huot, B., Yao, J., Montgomery, B. L., and He, S. Y. (2014). Growth-defense tradeoffs in plants: A balancing act to optimize fitness. *Mol. Plant* 7, 1267–1875. doi: 10.1093/mp/ssu049

Kersey, P. J. (2019). Plant genome sequences: past, present, future. *Curr. Opin. Plant Biol.* 48, 1–8. doi: 10.1016/j.pbi.2018.11.001

Križnik, M., Baebler, Š, and Gruden, K. (2020). Roles of small RNAs in the establishment of tolerant interaction between plants and viruses. *Curr. Opin. Virol.* 42, 25–31. doi: 10.1016/j.coviro.2020.04.006

Lamesch, P., Berardini, T. Z., Li, D., Swarbreck, D., Wilks, C., Sasidharan, R., et al. (2012). The arabidopsis information resource (TAIR): improved gene annotation and new tools. *Nucleic Acids Res.* 40, D1202–D1210. doi: 10.1093/nar/gkr1090

Li, H. (2018). Minimap2: pairwise alignment for nucleotide sequences. *Bioinformatics* 34, 3094–3100. doi: 10.1093/bioinformatics/bty191

Li, H. (2023). Protein-to-genome alignment with miniprot. *Bioinformatics* 39. doi: 10.1093/bioinformatics/btad014

Lukan, T., Pompe-Novak, M., Baebler, Š., Tušek-Žnidarič, M., Kladnik, A, Križnik, M., et al. (2020). Precision transcriptomics of viral foci reveals the spatial regulation of immune-signaling genes and identifies RBOHD as an important player in the incompatible interaction between potato virus Y and potato. *Plant Journal: For Cell Mol. Biol.* 104, 645–661. doi: 10.1111/tpj.14953

Lukan, T., Veillet, F., Križnik, M., Coll, A., Povalej, T. M., Pogačar, K., et al. (2022). CRISPR/cas9-mediated fine-tuning of miRNA expression in tetraploid potato. *Horticulture Res.* 9, uhac147. doi: 10.1093/hr/uhac147

Pasha, A., Subramaniam, S., Cleary, A., Chen, X., Berardini, T., Farmer, A., et al. (2020). Araport lives: an updated framework for arabidopsis bioinformatics. *Plant Cell* 32, 2683–2865. doi: 10.1105/tpc.20.00358

Patro, R., Duggal, G., Love, M. I., Irizarry, R. A., and Kingsford, C. (2017). Salmon provides fast and bias-aware quantification of transcript expression. *Nat. Methods* 14, 417–195. doi: 10.1038/nmeth.4197

Petek, M., Coll, A., Ferenc, R., Razinger, J., and Gruden, K. (2020a). Validating the potential of double-stranded RNA targeting colorado potato beetle mesh gene in laboratory and field trials. *Front. Plant Sci.* 11, 1250. doi: 10.3389/fpls.2020.01250

Petek, M., Zagorščak, M., Blejec, A., Ramšak, Ž., Coll, A., Baebler, Š., et al. (2022). pISA-tree - a data management framework for life science research projects using a standardised directory tree. *Sci. Data* 9, 6855. doi: 10.1038/s41597-022-01805-5

Petek, M., Zagorščak, M., Ramšak, Ž., Sanders, S., Tomaž, Š., Tseng, E., et al. (2020b). Cultivar-specific transcriptome and pan-transcriptome reconstruction of tetraploid potato. *Sci. Data* 7, 2495. doi: 10.1038/s41597-020-00581-4

Pham, G. M., Hamilton, J. P., Wood, J. C., Burke, J. T., Zhao, H., Vaillancourt, B., et al. (2020). Construction of a chromosome-scale long-read reference genome assembly for potato. *GigaScience* 9. doi: 10.1093/gigascience/giaa100

Potato Genome Sequencing Consortium, Xu, X., Pan, S., Cheng, S., Zhang, B., Mu, D., et al. (2011). Genome sequence and analysis of the tuber crop potato. *Nature* 475, 189–195. doi: 10.1038/nature10158

Quinlan, A. R., and Hall, I. M. (2010). BEDTools: A flexible suite of utilities for comparing genomic features. *Bioinformatics* 26, 841–425. doi: 10.1093/bioinformatics/btq033

Ramšak, Ž., Coll, A., Stare, T., Tzfadia, O., Baebler, Š., Peer, Y. V. d., et al. (2018). Network modeling unravels mechanisms of crosstalk between ethylene and salicylate signaling in potato. *Plant Physiol.* 178, 488–499. doi: 10.1104/pp.18.00450

Rhee, S. Y., Beavis, W., Berardini, T. Z., Chen, G., Dixon, D., Doyle, A., et al. (2003). The arabidopsis information resource (TAIR): A model organism database providing a centralized, curated gateway to arabidopsis biology, research materials and community. *Nucleic Acids Res.* 31, 224–228. doi: 10.1093/nar/gkg076

Schwacke, R., Ponce-Soto, G. Y., Krause, K., Bolger, A. M., Arsova, B., Hallab, A., et al. (2019). MapMan4: A refined protein classification and annotation framework applicable to multi-omics data analysis. *Mol. Plant* 12, 879–925. doi: 10.1016/j.molp.2019.01.003

Shumate, A., and Salzberg, S. L. (2020). Liftoff: accurate mapping of gene annotations. *Bioinformatics*. doi: 10.1093/bioinformatics/btaa1016

Tang, D., Jia, Y., Zhang, J., Li, H., Cheng, L., Wang, P., et al. (2022). Genome evolution and diversity of wild and cultivated potatoes. *Nature* 606, 535–541. doi: 10.1038/s41586-022-04822-x

Tian, F., Yang, D.-C., Meng, Y.-Q., Jin, J., and Gao, G. (2020). PlantRegMap: charting functional regulatory maps in plants. *Nucleic Acids Res.* 48, D1104–D1113. doi: 10.1093/nar/gkz1020

Tomato Genome Consortium (2012). The tomato genome sequence provides insights into fleshy fruit evolution. *Nature* 485, 635–641. doi: 10.1038/nature11119

Tomaž, Š., Petek, M., Lukan, T., Pogačar, K., Stare, K., Prates, E. T., et al. (2023). A mini-TGA protein modulates gene expression through heterogeneous association with transcription factors. *Plant Physiol.* 191, 1934–1952. doi: 10.1093/plphys/kiac579

Valentin, G., Abdel, T., Gaëtan, D., Jean-François, D., Matthieu, C., and Mathieu, R. (2021). GreenPhylDB v5: A comparative pangenomic database for plant genomes. *Nucleic Acids Res.* 49, D1464–D1471. doi: 10.1093/nar/gkaa1068

Van Bel, M., Silvestri, F., Weitz, E. M., Kreft, L., Botzki, A., Coppens, F., et al. (2022). PLAZA 5.0: extending the scope and power of comparative and functional genomics in plants. *Nucleic Acids Res.* 50, D1468–D1474. doi: 10.1093/nar/gkab1024

Visser, R. G.F., Bachem, C. W.B., de Boer, J. M., Bryan, G. J., Chakrabati, S. K., Feingold, S., et al. (2009). Sequencing the potato genome: outline and first results to come from the elucidation of the sequence of the world's third most important food crop. *Am. J. Potato Research: Off. Publ. Potato Assoc. America* 86, 417–429. doi: 10.1007/s12230-009-9097-8

Wang, J., Zhang, Q., Tung, J., Zhang, X., Liu, D., Deng, Y., et al. (2024). High-quality assembled and annotated genomes of nicotiana tabacum and nicotiana benthamiana reveal chromosome evolution and changes in defense arsenals. *Mol. Plant* 17, 423–437. doi: 10.1016/j.molp.2024.01.008

Wang, X., Wang, B., and Yuan, F. (2023). Deciphering the roles of unknown/uncharacterized genes in plant development and stress responses. *Front. Plant Sci.* 14, 1276559. doi: 10.3389/fpls.2023.1276559

Wilkinson, M. D., Dumontier, M., Aalbersberg, I.J. J., Appleton, G., Axton, M., Baak, A., et al. (2016). The FAIR guiding principles for scientific data management and stewardship. *Sci. Data* 3, 160018. doi: 10.1038/sdata.2016.18

Yandell, M., and Ence, D. (2012). A beginner's guide to eukaryotic genome annotation. *Nat. Rev. Genet.* 13, 329–425. doi: 10.1038/nrg3174

Yang, X., Zhang, L., Guo, X., Xu, J., Zhang, K., Yang, Y., et al. (2023). The gap-free potato genome assembly reveals large tandem gene clusters of agronomical importance in highly repeated genomic regions. *Mol. Plant* 16, 314–317. doi: 10.1016/j.molp.2022.12.010

Yates, A. D., Allen, J., Amode, R. M., Azov, A. G., Barba, M., Becerra, A., et al. (2022). Ensembl genomes 2022: an expanding genome resource for non-vertebrates. *Nucleic Acids Res.* 50, D996–1003. doi: 10.1093/nar/gkab1007

Zagorščak, M., Blejec, A., Ramšak, Ž., Petek, M., Stare, T., and Gruden, K. (2018). DiNAR: revealing hidden patterns of plant signalling dynamics using differential network analysis in R. *Plant Methods* 14, 78. doi: 10.1186/s13007-018-0345-0

frontiers | Frontiers in Plant Science

TYPE Original Research
PUBLISHED 01 July 2024
DOI 10.3389/fpls.2024.1386824

OPEN ACCESS

EDITED BY
Hiroshi Ezura,
University of Tsukuba, Japan

REVIEWED BY
Wim H. Vriezen,
Maastricht University, Netherlands
Andrea Mazzucato,
University of Tuscia, Italy

*CORRESPONDENCE
Michal Lieberman-Lazarovich
michall@volcani.agri.gov.il

RECEIVED 16 February 2024
ACCEPTED 10 June 2024
PUBLISHED 01 July 2024

CITATION
Bashary N, Miller G, Doitsch-Movshovits T, Beery A, Ouyang B and Lieberman-Lazarovich M (2024) New population of *Solanum pimpinellifolium* backcross inbred lines as a resource for heat stress tolerance in tomato. *Front. Plant Sci.* 15:1386824. doi: 10.3389/fpls.2024.1386824

New population of *Solanum pimpinellifolium* backcross inbred lines as a resource for heat stress tolerance in tomato

Neta Bashary[1], Golan Miller[1], Tzion Doitsch-Movshovits[1], Avital Beery[1], Bo Ouyang[2] and Michal Lieberman-Lazarovich[1*]

[1]Department of Vegetables and Field Crops Sciences, Institute of Plant Sciences, Agricultural Research Organization - Volcani Center, Rishon LeZion, Israel, [2]National Key Laboratory for Germplasm Innovation and Utilization of Horticultural Crops, College of Horticulture and Forestry Sciences, Huazhong Agricultural University, Wuhan, Hubei, China

The occurring temperature increase in crop production areas worldwide is generating conditions of heat stress that negatively affect crop productivity. Tomato (*Solanum lycopersicum*), a major vegetable crop, is highly susceptible to elevated temperatures. Under such conditions, fruit set is dramatically reduced, leading to significant yield losses. *Solanum pimpinellifolium*, a wild species closely related to the cultivated tomato, was shown to have beneficial attributes under various abiotic stress growth conditions. We have utilized a new population of backcross inbred lines originated from a cross between *S. pimpinellifolium* and *S. lycopersicum*, in order to evaluate its potential as a new genetic resource for improvement of reproductive performance of cultivated tomato under heat stress conditions. This population was screened for various heat stress-related traits, under controlled heat stress and non-stress conditions. Our results show that significant variation exists for all the heat stress related traits that were examined and point at individual lines with better reproductive performance under heat stress conditions that share a common introgression from the wild *S. pimpinellifolium* parent, suggesting several candidate genes as potential drivers of thermotolerance. Thus, our results place this population as a valuable new resource for the discovery of heat stress related genetic loci for the future development of heat stress tolerant tomato cultivars.

KEYWORDS

tomato, moderate chronic heat stress, fruit-set, pollen viability, *Cpn60*

1 Introduction

Tomato (*Solanum lycopersicum*) is one of the most important vegetable crops worldwide. Similarly to other plant species, tomato is very sensitive to high ambient temperatures, a globally increasing phenomenon due to climatic changes. For tomato plants, temperatures exceeding 32°C during the day, and 21°C during the night create

conditions of heat stress, leading to various physiological and developmental effects that drive dramatic reduction in fruit set and total yield, thus necessitating the identification of novel resources for tomato breeding (Hazra et al., 2007; Liu et al., 2023). The negative effect of heat stress on yield is the consequence of multiple molecular, physiological and developmental processes that are hindered by elevated temperatures, underlining tomato thermotolerance a highly complex trait.

The reproductive phase of development is more thermosensitive compared with the vegetative phase. Starting at early stages of flowering, the number of flowers produced under high temperature conditions may be reduced (Charles and Harris, 1972; Abdul-Baki, 1991; Xu et al., 2017). Additionally, flower abnormalities are very abundant under heat stress conditions, therefore these traits are indicative of heat stress sensing and damage. High temperatures may also lead to protrusion of the style over the anther cone thus hindering self-pollination (Rick and Dempsey, 1969; Lohar and Peat, 1998). Excessive heat stress may also result in anther deformations, as the cone-shaped anthers burst open, hindering pollination as well (Bita and Gerats, 2013; Müller et al., 2016; Ayenan et al., 2019). The most dramatic effect of heat stress on tomato flowers is bud abscission (Sato et al., 2001). Nevertheless, the most sensitive tissue to elevated temperatures is the male gametophyte in the period of 8–13 days prior to anthesis (Sato et al., 2002). High temperatures lead to reduced pollen viability and germination, vital functions for successful fertilization (Charles and Harris, 1972; Peet et al., 1998; Pressman et al., 2002). Consequently, fruit set is severely damaged. For example, under mean daily temperature of 29°C compared with control conditions at 25°C, tomato fruit set was reduced by 77% (Peet et al., 1997). Later studies presented similar results under different heat stress regimes (Sato et al., 2000; Firon et al., 2006; Sato et al., 2006). Due to the reduced ability of the pollen grains to initiate fertilization under heat stress conditions, the number of seeds per fruit is significantly reduced, occasionally accompanied by a reduction in fruit size (Sato et al., 2001).

For most crop species, the largest reservoir of genetic variation exists not within modern cultivars, but in their undomesticated wild relatives. In tomato, it was estimated that less than 5% of the available genetic variation exists in cultivars and the other 95% is found in wild relatives (Miller and Tanksley, 1990). For this reason, interrogating wild relatives for abiotic stress resistance traits is of great value. To-date, 17 species of wild tomato relatives are recognized, originating from various environments, from high mountains to dry coastal regions, and they exhibit great differences in morphological characters, disease susceptibility, and stress resistance traits (Kimura and Sinha, 2008; Peralta et al., 2008; Conesa et al., 2017). The use of wild relatives may be sometimes hindered due to cross incompatibility, F1 hybrid sterility, infertility of the segregating generations, reduced recombination between the chromosomes of the two species, or linkage-drag (genes of negative effect being tightly linked to the trait of interest) (Zamir, 2001). Despite these obstacles, backcross breeding was successfully used in tomato to improve quantitative traits by the introgression of genes from wild germplasm into elite cultivars while maintaining the favorable horticultural characteristics of the elite materials (Hartman and St Clair, 1999; Doganlar et al., 2002; Kabelka et al., 2004).

The wild species *Solanum pimpinellifolium*, considered as the ancestor of the cultivated tomato, is originated in the coastal deserts of Peru and Ecuador (Peralta and Spooner, 2000; Pease et al., 2016). The *S. lycopersicum* and *S. pimpinellifolium* species are both self-compatible, red-fruited and they are known to hybridize naturally (Rick, 1958). Despite their close relationship, the two species differ in many morphological aspects, especially in fruit size and growth habits and several other economically important traits, many of which are polygenic. For this reason, *S. pimpinellifolium* is considered an attractive source for tomato breeding. Several studies have already utilized *S. pimpinellifolium* for the identification of important quantitative trait loci (QTLs). Among these are QTLs for increased yield, soluble solids content, and improved fruit color (Grandillo and Tanksley, 1996). *S. pimpinellifolium* was shown to be a suitable source for improving nitrogen use efficiency. A collection of 29 Introgression Lines (ILs) resulting from a cross between the To-937 accession of *S. pimpinellifolium* and the *S. lycopersicum* cv Moneymaker (MM) was used to identify specific regions in the *S. pimpinellifolium* genome involved in the responses to N inputs of fruit production and fruit quality. Interestingly, the identified region contains genes involved in C and N metabolism (Renau-Morata et al., 2024).

In terms of abiotic stress tolerance, it was reported that seeds of *S. pimpinellifolium* exhibit better germination under drought stress compared with cultivated tomato (Lin et al., 2002; Villalta et al., 2008; Rao et al., 2013), while five QTLs were found to be linked with salt tolerance during vegetative growth (Foolad et al., 2001). Additionally, several *S. pimpinellifolium* accessions were characterized as having high salinity tolerance (Lin et al., 2002; Villalta et al., 2008; Rao et al., 2013). In regard to heat stress, pollen number, pollen viability and style protrusion, representing key reproductive heat stress-related traits, were evaluated in various wild species, among them eight accessions of *S. pimpinellifolium* (LA1670, LA1630, LA1645, LA1629, LA0114, LA1579, LA1237 and LA1547). Although no overall thermotolerant species was identified, several *S. pimpinellifolium* individuals of the LA1630 accession outperformed the best performing cultivars in terms of pollen viability under heat stress conditions (Driedonks et al., 2018). In another study, 22 QTLs involved in reproductive traits at different temperatures were identified, using an *S. pimpinellifolium* recombinant inbred lines (RIL) population. All 168 lines were subjected to increased temperature conditions and individual lines presented improved performance under these conditions (Gonzalo et al., 2020), demonstrating the high value and potential of *S. pimpinellifolium* as a genetic source for heat stress tolerance in tomato.

Climatic models in tomato-growing locations around the globe predict that temperatures will continue to rise and the severity and frequency of above-optimal temperature episodes will increase (Bell et al., 2000). These conditions strongly and negatively affect reproductive success and thus yield, implying that breeding for thermotolerant cultivars is critical for food security. The sub-optimal growth conditions in which *S. pimpinellifolium* was evolved in, its proven resistance to various abiotic stresses and its

genetic relatedness to the cultivated species *S. lycopersicum*, place it as a good source for the identification of heat stress tolerance traits. Here we present a detailed phenotypic characterization of heat stress related traits of a new population based on *S. pimpinellifolium*. Using this new BILs (Backcross Introgression Lines) population originated from a cross between *S. pimpinellifolium* and *S. lycopersicum*, we found high variation in heat stress related traits, and identified specific lines with better performance under heat stress conditions, making this BILs population an additional and highly relevant source for thermotolerance QTL identification and breeding of thermotolerant tomato cultivars.

2 Materials and methods

2.1 Plant material

The BILs population was obtained from the laboratory of Prof. Dani Zamir (The Robert H. Smith Faculty of Agriculture, Food and Environment at the Hebrew University of Jerusalem). This population was constructed by crossing *S. lycopersicum* cv. M82 and the wild specie *S. pimpinellifolium* accession LA1589. Two backcross cycles to *S. lycopersicum* TA209 and nine generations of self-fertilization resulted in a set of 166 homozygous BC2S9 lines (M82 and TA209 being Israeli and US adapted open-pollinated varieties, respectively, and are almost identical at the genome sequence level).

2.2 Growth conditions

All three experiments were carried out at the Agricultural Research Organization (ARO) Volcani Center greenhouses. The plants were planted in 10 L pots filled with a soil mixture (GREEN, EvenAri LTD, Israel) and fertilized with Gat fertilizer (Deshen Gat LTD, Israel) containing M6% + Ca1.5% + Mg0.9%. In the non-controlled experiment, the entire BILs population (166 lines) along with the M82 and *S. pimpinellifolium* LA1589 parental lines were grown in a greenhouse between June and December 2018, therefore experiencing high ambient temperatures. Temperature was monitored every ten minutes using HOBO data loggers (U-Series Data Logger, Onset Computer Corporation, USA). The average daily temperature was 30/24°C day/night. The average maximum temperature during the day was 36°C and the minimum at night was 21°C, creating Moderate Chronic Heat Stress (MCHS) conditions. Under these conditions, plants were scored for various developmental and heat stress related traits. Next, in the controlled experiment (repeated twice), due to space limitations, 14 lines that represent the phenotypic variation in this population and include 90.12%of the *S. pimpinellifolium* genome (Supplementary Figure S2) were grown together with the parental lines. The experiment was carried out in two controlled greenhouses and included four plants per line in each greenhouse, in a randomized set up, identical between the greenhouses. First, both greenhouses were set at the same, non-stress temperatures (26°C/20°C day/night – control conditions). At the onset of flowering, MCHS was initiated in one of the greenhouses, by setting day/night temperatures to 32°C/22°C. The other greenhouse was kept at control conditions (26°C/20°C day/night). Temperature was recorded every 15 minutes using HOBO data loggers (U-Series Data Logger, Onset Computer Corporation, USA). Two weeks after the initiation of MCHS, three inflorescences per plant were marked and scored for the different traits.

2.3 Phenotypic analyses

2.3.1 Flower types

Three inflorescences were marked per plant, and flowers were scored as: normal, style elongated, anthers deformed, the appearance of anther browning, or aborted. Percentage per type per inflorescence was calculated and averaged per line.

2.3.2 Number of fruits and fruit set

The number of fruits from three to four inflorescences per plant were counted and averaged. Per inflorescence, the percentage of fruits out of total flowers was calculated to obtain the percentage of fruit set.

2.3.3 Fruit weight

All fruits from the marked inflorescences were collected at the red-ripe stage and weighted. Single fruit weight was calculated by dividing the total weight in the number of fruits, per plant.

2.3.4 Pollen viability

Three flowers at anthesis per plant were collected (at early morning) and anthers separated. Each anther was divided in two and inserted into a tube containing germination solution (Sato et al., 2000), followed by adding 20 µL of Alexander dye (Alexander, 1980). Samples were analyzed using a Leica DMLB epi-fluorescence microscope (Leica, Germany). Three fields containing representative pollen patterns were captured with a DS-Fi1 digital camera using NIS-Elements BR3.0 software (Nikon, Japan). Viable (purple) and non-viable (blue/green) pollen grains were counted with the ImageJ software version 1.43 using the 'Cell counter' plugin (Schneider et al., 2012).

2.3.5 Pollen germination

Three flowers at anthesis from each plant were collected and dried for 1 h. Dried anthers were transferred to 0.5 mL of liquid germination media (20 mg H_3BO_3, 60 mg $CaNO_3$, 40 mg $MgSO_4$, 20 mg KNO_3, 10 g sucrose, 100 mL double distilled water) and vortexed vigorously for 10 s. SeaKem® LE Agarose (LONZA Company) was added to the liquid media (to a final concentration of 2%), dissolved and poured onto a microscope slide, flatted with a Parafilm® tape and another slide on top. After solidification, slides were transferred to a dark closed chamber to maintain humidity. Then, the pollen containing solution was transferred to the solid media and incubated for 1.5 h. Slides were analyzed using a DM500 Leica microscope (Leica, Germany).

Pollen germination was scored and counted using the ImageJ software version 1.43 (Schneider et al., 2012).

2.3.6 Number of seeds

Tomato red ripe fruits were cut horizontally and all seeds were extracted and incubated with Sulfuric acid (2%) for 3 h. Then, the seeds were washed well in tap water and sterilized with a 10% TSP (Tri Sodium Phosphate) solution for 30 minutes while shaking. Seeds were washed, dried, and counted by picture analysis using ImageJ (Schneider et al., 2012).

2.4 Statistical analyses

The Students' t-test was employed to identify significant differences between lines ($p < 0.05$). All statistical analyses were performed using JMP Version 3.2.2 (SAS Institute, Inc., Cary, NC, USA).

2.5 RNA isolation and quantitative-real-time PCR analysis

Young leaves from three plants per line were collected and frozen immediately in liquid nitrogen. Total RNA was isolated using RiboEx™ (GeneAll; Seoul, South Korea) according to the manufacturer's protocol. RNA was treated with DNaseI (Thermo Fischer Scientific, CA, USA) and cDNA was synthesized from 0.5 µg of DNaseI-treated total RNA using the qPCRBIO cDNA Synthesis Kit (PCR Biosystems, London, UK) according to the manufacturer's instructions. Relative expression of *Hsp17.6* (NM_001246984.3) was determined using quantitative real-time PCR (qRT-PCR) on an Applied Biosystems StepOnePlus Real-Time PCR System (Thermo Fischer Scientific, CA, USA). *Ubiquitin* (*Solyc07g064130*) and *EF1α* (*Solyc06g009970*) were used as reference genes. Each 10 µl qRT-PCR reaction consisted of qPCRBIO SyGreen Blue Mix Hi-ROX (PCR Biosystems, London, UK), gene-specific primers, and 1:5 diluted cDNA template. Thermocycling conditions were performed according to the manufacturer's instructions. Data were analyzed using the Applied Biosystems StepOne™ software v 2.3 (Thermo Fischer Scientific, CA, USA). Primer sequences are as follows (all 5' to 3'); *Hsp17.6* (*Solyc08g062450*) forward: GGAAGAGGGAAGAA GAGAAAGAA, reverse: ACCACAAACCATCAAAACAGAGT. Ubiquitin reference gene (*Solyc07g064130*) forward: GGACGGAC GTACTCTAGCTGAT, reverse: AGCTTTCGACCTCAAGGGTA. For *eEF1α* (*Solyc06g009970*), forward: AGTCAACTACCACTGG TCAC, reverse: GTGCAGTAGTACTTAGTGGTC.

3 Results

3.1 Developmental variation in the *S. pimpinellifolium* BILs population

All 166 lines of the BIL population and the parental lines M82 and S. *pimpinellifolium* (accession LA1589) were grown in a greenhouse. In order to evaluate developmental variation in this population, plants were qualitatively scored during the vegetative stage for the following traits: plant stature (normal, high or stunted), branching (normal or compound), stem pubescence (normal or high), and the occurrence of necrotic lesions (none or apparent) which are naturally more abundant in *S. pimpinellifolium*. During the reproductive stage of plant development, plants were scored for time to flowering (normal or delayed. None were found to flower earlier than normal), flowers color (yellow or pale) and size (normal size, smaller or bigger), length of inflorescences (normal or long) and sepals (normal or big). During fruit development and ripening, the following traits were evaluated; fruit color (normal, lighter or darker), fruit size (normal – medium, small or large), fruit shoulders at the green stage (apparent or not), appearance of the peel (shiny or not), and weather the fruits become dehydrated on the plant (normal or raisin). We found that for all these traits, the vast majority of lines (72–97%) presented a normal phenotype, i.e., similar to the parental M82 cultivar (Figure 1). The trait that showed the highest non-M82 rate was sepal size, with 28% of all lines presenting over-sized sepals. The most infrequent phenotypes were late flowering and raisin-like fruits, each found in 3% of all lines. In ten out of 13 traits examined, we found a non-parental phenotype. These are, stunted stature (7% of all lines), big flowers (2%), pale flower color (4%), the appearance of fruit shoulders (11%), and shiny fruit peel (13%) (Figure 1).

3.2 Heat stress-related phenotypic variation in the BILs population

In order to evaluate the adequacy of the *S. pimpinellifolium* BILs population for the identification of genetic elements linked with heat tolerance traits, all lines were grown in a greenhouse during the summer. Throughout the reproductive phase of the plants, day temperatures did not go below 32°C, and night temperatures were usually above 20°C, creating conditions of moderate chronic heat stress (MCHS, Figure 2A). Under these conditions, we monitored inflorescences for the occurrence of heat stress related phenotype, i.e., anther deformation, anther browning, style elongation and seeds production (Figure 2B; Supplementary Figure S1). We found that the anther structural deformations appeared in 9% of the lines. For anthers browning and style elongation we used a 5-levels scale, from "none" to "extreme" according to the severity of the phenotype. In approximately half of the lines (56% and 54% for anther browning and style elongation, respectively), flowers were normal, with no stress-related impairments. However, 11% of the lines presented high or extreme occurrence of anther browning, and style elongation was intensely observed in 16% of the lines. The most drastic effect of the high temperatures was observed in seed production. Almost all lines (91%) produced seedless fruits. Few lines (4%) did not produce fruits at all, and only 5% of all lines were able to produce seeds under these growth conditions (Figure 2; Supplementary Figure S1).

Additionally, we measured several quantitative traits and examined their distribution across the lines. Among these are the number of flowers per inflorescence, number of fruits per inflorescence, and single fruit weight (Figure 3). Traits known to

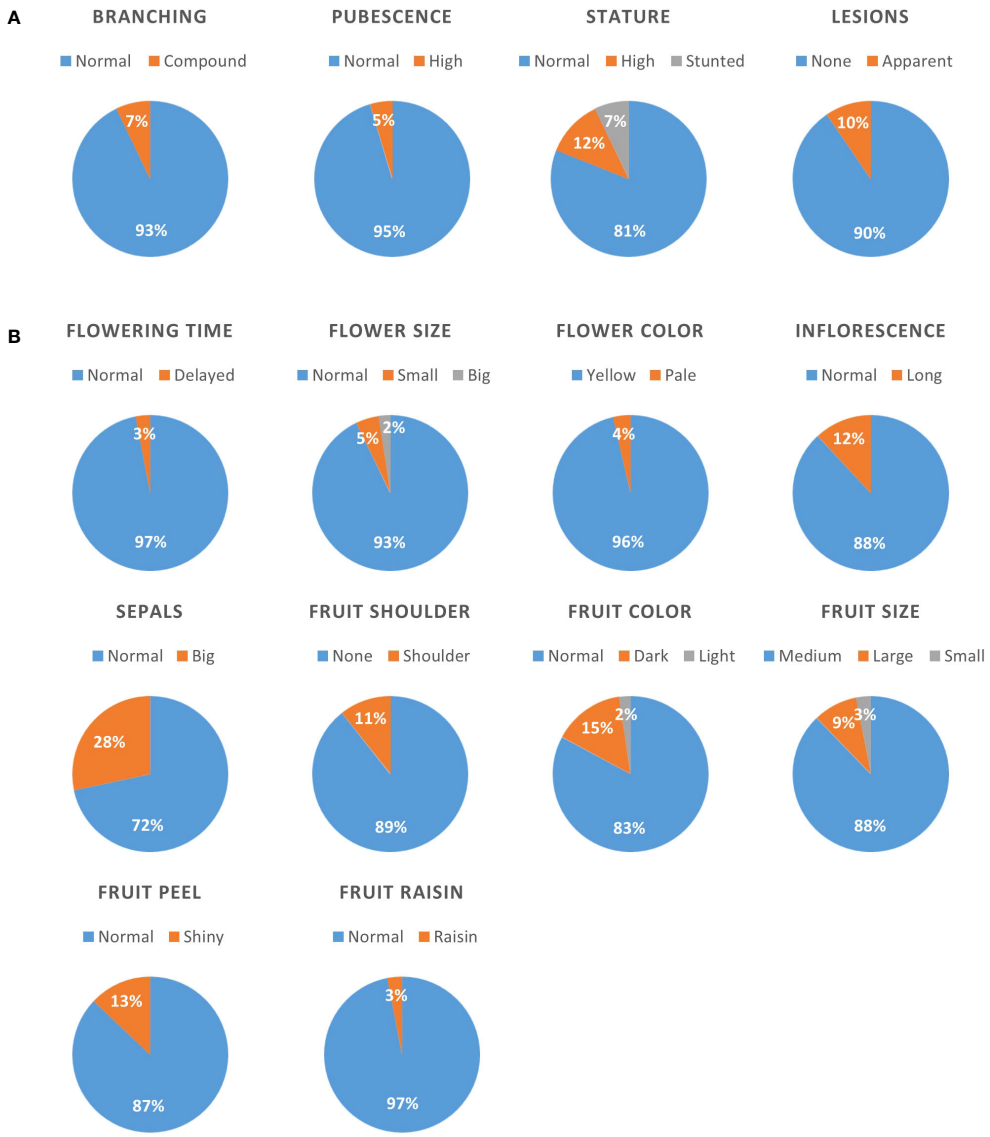

FIGURE 1
Qualitative characterization of the BILs population for developmental traits. All lines were scored for various traits, and the distribution is presented as pie charts for vegetative **(A)** and reproductive **(B)** traits. Numbers within the charts denote the percentage of lines presenting the specific phenotype. The phenotype of the M82 and TA209 parental lines is denoted "normal".

be related to heat stress response include the rate of normal flowers, flowers with elongated style, flowers with browning of anthers, flowers with anther deformations, aborted buds or flowers, and the rate of fruit set - all scored per inflorescence (Figure 3). We found a wide distribution for all traits examined. However, only a small proportion of the population presented heat stress sensitivity in terms of anther deformation and aborted buds/flowers. On the contrary, fruit set rate, which is an important yield trait strongly affected by heat stress, presented a very wide distribution (Figure 3; Table 1). Out of the 160 lines scored for this trait, we found all levels of fruit set, from zero to 100%, with an average of 74.8% (Table 1). Considering the M82 value, which is 68.6% under these conditions, our results suggest that there are several lines with improved fruit set under heat stress conditions.

3.3 Individual lines present improved heat stress tolerance attributes

The phenotypic screen that was performed on the entire collection of *S. pimpinellifolium* BILs under heat stress conditions revealed that indeed, phenotypic variation for heat stress related traits exists in this population. In order to directly link these phenotypes to elevated temperatures and to identify specific lines with heat stress tolerance traits, we conducted an environmentally controlled experiment in which selected lines were grown in parallel under MCHS (32°C/22°C day/night) and control (26°C/20°C day/night) conditions (Figures 4A, B). The lines were selected based on their genetic maps to maximize genome coverage of LA1589, considering space limitation in the controlled setup

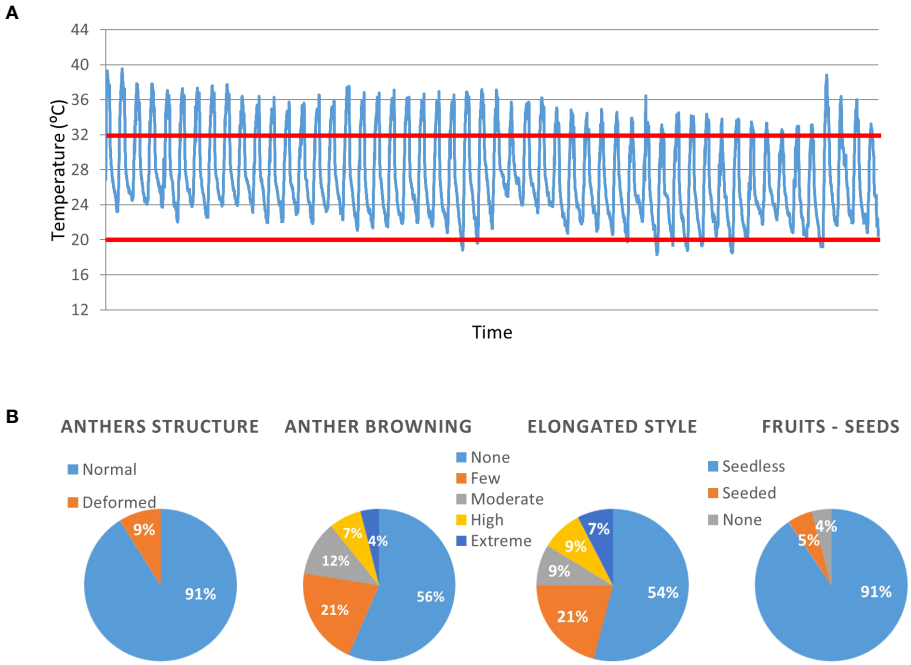

FIGURE 2
Qualitative characterization of the BILs population for heat stress related traits. All lines were grown under non-controlled, moderate chronic heat stress (MCHS) conditions **(A)** and scored for reproductive traits **(B)**. The heat-stress day and night temperature thresholds are denoted by red lines. Numbers within the charts denote the percentage of lines presenting the specific phenotype. The phenotype of the M82 and TA209 parental lines is denoted "normal".

(Supplementary Figure S2). The stress conditions were initiated at the beginning of flowering and the response of plants to the stress was confirmed on the molecular level, by validating the increased transcription of the heat stress responsive gene *Hsp17.6* exclusively in plants under MCHS conditions. This gene was almost undetectable in plants grown under control, non-stress conditions (Figure 4C). When plants reached full flowering and fruit development stages, the effect of MCHS was highly apparent. The number of fruits per inflorescence and the rate of fruit set were dramatically reduced in MCHS relative to control conditions, for all lines tested (Figures 5A, B). However, when comparing the lines under MCHS conditions only, two lines were able to produce a higher number of fruits per inflorescence. Similarly, two lines (one in common) presented a significantly higher level of fruit set (Figure 5B). The number of flowers and single fruit weight are not always affected by heat stress and indeed, we did not detect a significant reduction in MCHS compared with control for any of the lines (Figures 5C, D). In addition to the traits measured in the whole-population screen experiment (Figure 3), in the controlled experiment we included measurements of pollen germination, and number of seeds per fruit, which are well known to be strongly affected by heat stress. Our results show an intense reduction in these traits for all lines under MCHS conditions, compared to control (Figures 5E, F). Pollen germination (the fraction of germinated pollen) was highly variable already under control conditions, differing between the parental lines (63.5% and 28.2% in *S. pimpinellifolium* and M82, respectively), and ranging between lines from 16.8% to 74.3%. Nonetheless, under MCHS conditions, all lines presented a sharp decrease in pollen germination, from a complete lack of germination (0%) and up to an exceptional line presenting 36.2% of pollen germination (Figure 5E). The most variable trait under control conditions was the number of seeds per fruit, which is linked with fruit size, where high variation is expected considering the big difference in fruit size between the parental lines. Whereas fruits from *S. pimpinellifolium* and M82 produced on average 19 and 64 seeds per fruit, respectively, under control conditions, in the BILs seeds production ranged between 17 and 64 seeds per fruit on average. Under MCHS conditions, both parental lines did not produce seeds at all, whereas two lines were able to produce a small amount of seeds (6.2 and 6.5 per fruit on average, Figure 5F), although the increase was not significant. Overall, we observed a significant reduction in all lines in MCHS compared with control, for all heat stress related traits (i.e. number of fruits, fruit set, pollen germination and seeds per fruit). For some traits, we could detect one or two lines that performed better than the sensitive M82 parental cultivar under MCHS conditions, further reinforcing our claim that this BIL population is suitable for mining for heat stress tolerance related lines and the future identification of heat stress QTL, given further research.

3.4 Three heat stress tolerant lines share a common genetic introgression

In the course of the controlled heat stress experiment, we identified several lines that were performing better than parental

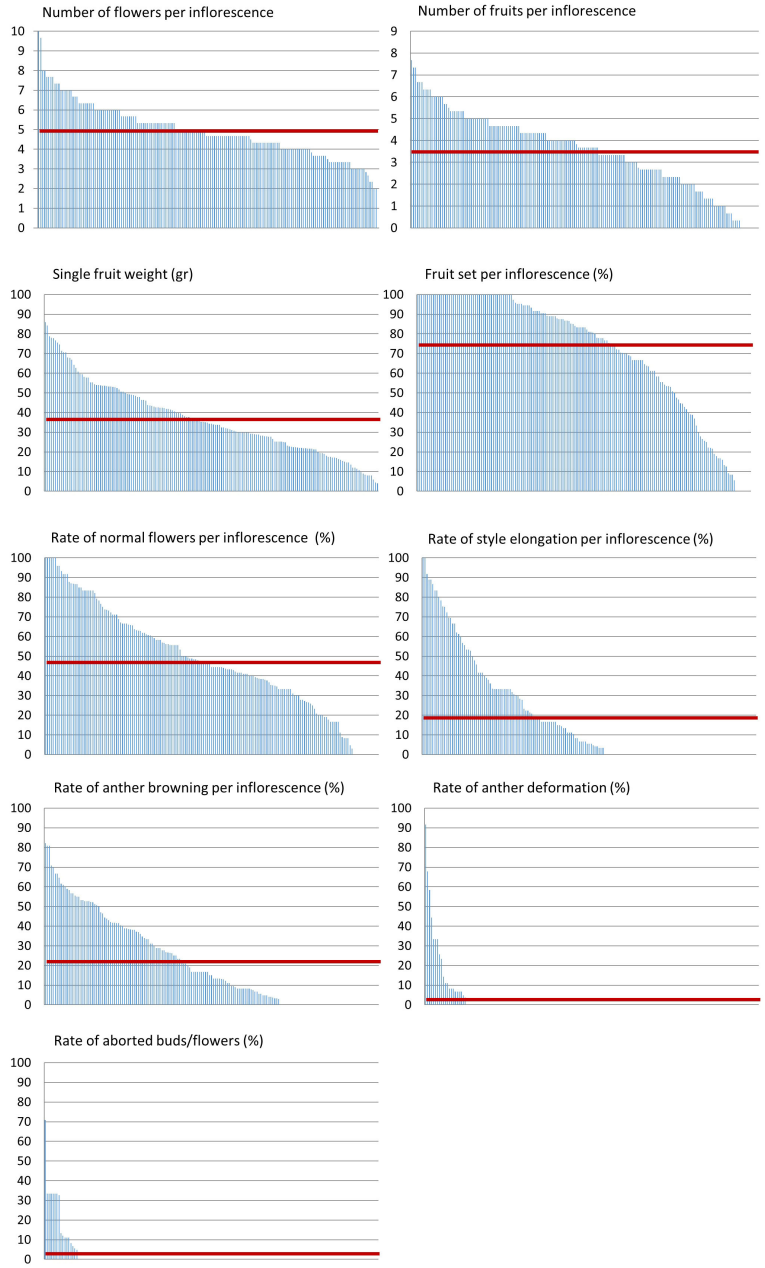

FIGURE 3
Phenotypic distribution of developmental and stress-related traits. All lines (X axis) were grown under non-controlled heat stress conditions and scored for developmental and heat stress related traits depicted in the charts' titles. The average value per trait is marked by a red line.

lines under MCHS conditions, for several traits. These lines, named pi-058, pi-117 and pi-147, presented normal vegetative development and leaf shape (Figure 6), but were among the only lines that were able to produce seeds under MCHS conditions (Figure 6). In order to validate this observation, we carried out controlled heat stress experiments including the TA209 line that was used for a backcross step during the construction of the BILs population, hence is considered another cultivated parental line, in addition to M82. Using the same set-up and conditions, MCHS was initiated at flowering (Figure 4) and we scored the plants for number of fruits per inflorescence, fruit weight, fruit-set, and pollen viability. We found that fruit weight of pi-058 and pi-117 was much less affected by the stress compared with parental lines – presenting an average reduction of 32% and 39%, respectively, while M82 reached 86% reduction in fruit weight and TA209 88% reduction. LA1589 did not produce fruits in these conditions (Figure 7A). Pi-147 was more similar to the M82 and TA209 parental lines in terms of single fruit weight, however, it did perform significantly better in terms of number of fruits per inflorescence, while pi-058 and pi-117 did not produce more fruits compared to either M82 or TA209 (Figure 7B). Importantly, all three lines, i.e. pi-058, pi-117 and pi-147 reached higher fruit-set rates under MCHS conditions. While the parental lines did not go beyond 11.38% (TA209), fruit set rates in pi-058, pi-

10.3389/fpls.2024.1386824

TABLE 1 Phenotypic characterization of the BILs population - quantitative traits statistics.

Trait	MCHS - related	Min	Max	Avg	Med	CV (%)	M82	SP
Number of flowers	No	0	10	4.9	4.7	2.2	5.3	8.0
Normal flowers (%)	Yes	0	100	47.8	46.1	4.3	86.7	74.4
Anther browning (%)	Yes	0	82.2	21.7	15.0	7.9	0	0
Elongated style (%)	Yes	0	100	19.4	5.6	10.5	13.3	47.8*
Anther deformation (%)	Yes	0	91.7	3.0	0	29.4	0	0
Aborted buds (%)	Yes	0	70.8	2.3	0	29.2	0	11.1
Fruit number	No	0	7.7	3.5	3.7	3.9	3.7	0**
Fruit set (%)	Yes	0	100	74.8	83.7	2.9	68.6	0**
Single fruit weight (gr)	No	4	85.9	36.8	34.3	3.9	30.4	na

All traits were scored per inflorescence, except single fruit weight. M82 – the cultivated parent, SP – the *S. pimpinellifolium* parent (LA1589), MCHS – moderate chronic heat stress. *elongated style is a naturally occurring phenomenon in wild species, denoting self-incompatibility. **under normal greenhouse watering, reproduction of wild species is hindered.

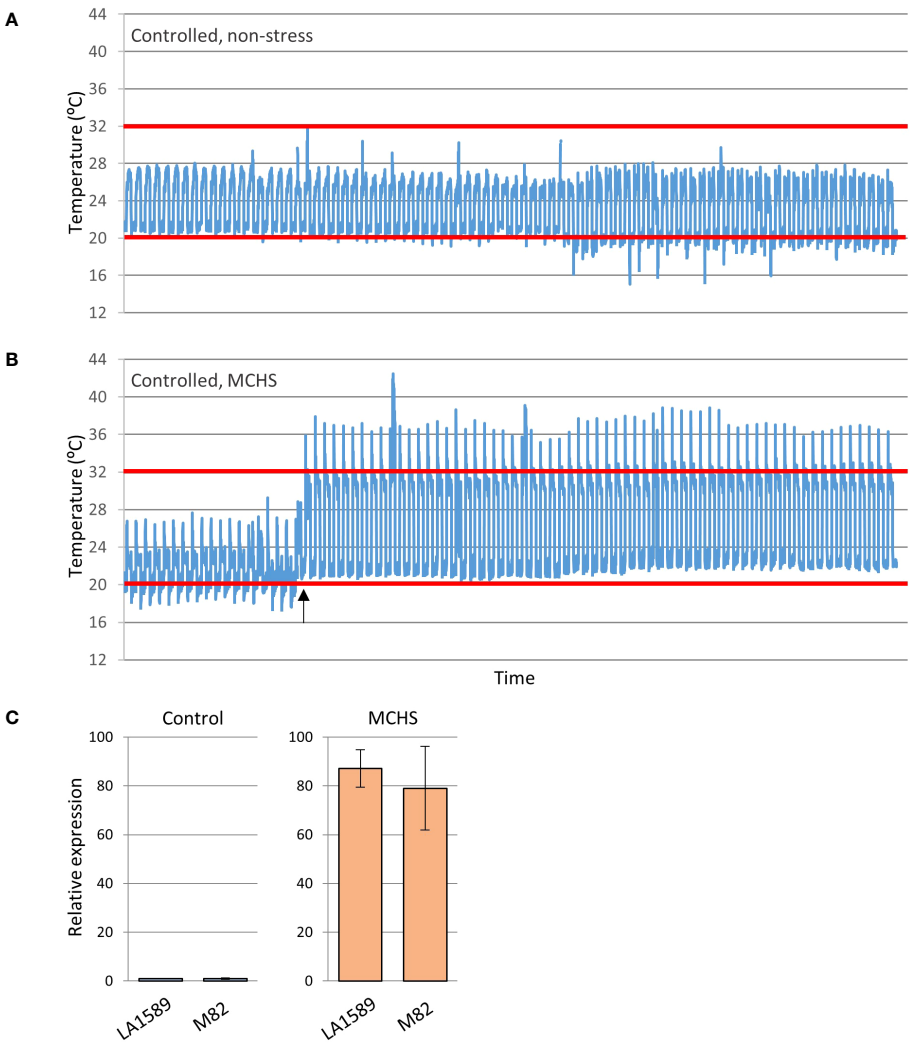

FIGURE 4
Conditions of the controlled heat stress experiment. Selected lines were grown under controlled non-stress **(A)** and moderate chronic heat stress (MCHS) **(B)** conditions. Expression of the heat-stress responsive gene Hsp17.6 was tested to validate the occurrence of heat stress in the two parental lines, M82 and LA1589 (*S. pimpinellifolium*) **(C)**. The heat-stress day and night temperature thresholds are denoted by red lines. Black arrow marks the initiation of heat stress.

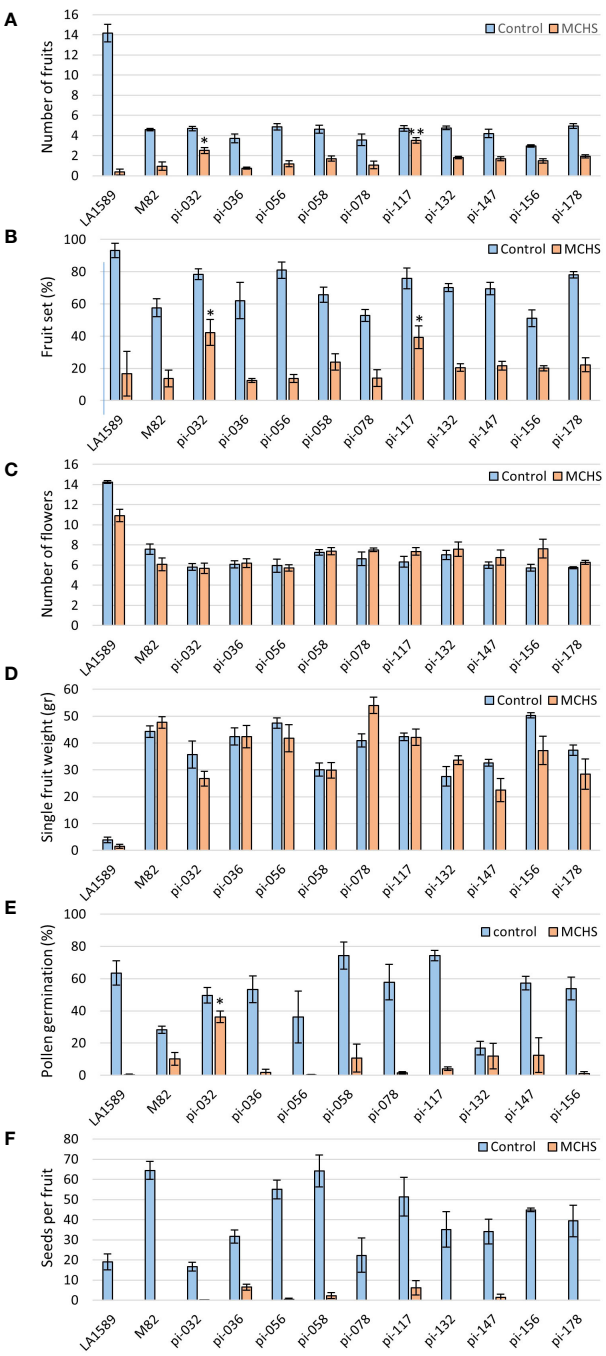

FIGURE 5
The effect of moderate chronic heat stress (MCHS) on the number of fruits **(A)**, fruit-set rate **(B)**, number of flowers **(C)**, single fruit weight **(D)**, pollen germination **(E)**, and number of seeds per fruit **(F)**. Selected lines were grown in parallel under control (26°C/20°C day/night) and MCHS (32°C/22°C day/night) conditions, and scored for reproductive performance. Each bar represents an average value of four plants per line. Statistical significance was tested using TTEST for each line compared with the heat stress sensitive M82 in MCHS conditions. (*) - p-value < 0.05, (**) - p-value < 0.01.

117 and pi-147 were 23.95%, 39.29% and 21.6%, respectively (Figure 7C), confirming their heat-stress tolerance. The levels of pollen viability were as well adversely affected by the stress treatment, being reduced to 3–11.3% in the parental lines. However, pi-117 maintained a very high rate of viable pollen (63.75%) under these conditions, as well as pi-058 that reached 31.66%. The line pi-147 reached 14.67%, which was not significantly higher than either M82 or TA209 (Figure 8).

Although heat stress tolerance is a highly complex trait, it is controlled by a finite number of regulators, which activate the heat stress response. Therefore, it is possible that common factors are controlling the tolerance effect of pi-058, pi-117 and pi-147, mainly observed by the high fruit-set rate under MCHS conditions (Figure 7C). Utilizing the genetic maps of these lines, we identified a single common introgression of the LA1589 genome at the end of chromosome 9, located between 65.5 and 66.3Mbp (Figure 9; Table 2). This 0.8Mbp region contains 128 annotated genes (Supplementary Table 1). GO term enrichment analysis (https://amigo.geneontology.org/) revealed that GO:0009408 - response to heat – was highly enriched in this group of genes (p-value = 1.37E-06, corrected p-value = 1.41E-04), including the *Cpn60* Chaperonin (*Solyc09g091180*, Table 3), which is known to contribute to heat stress tolerance.

Overall, our results demonstrate the suitability of the presented BIL population derived from *S. pimpinellifolium* wild-species accession LA1589 and the tomato cultivars M82 and TA209 for heat stress related research and possible future identification of QTL for heat tolerance in tomato as a mean to mitigate the negative impact of increased temperatures on tomato development and productivity.

4 Discussion

The increased ambient temperatures in many agricultural regions around the world have detrimental influence on crop yield, therefore the development of heat stress resistant cultivars is of upmost importance. Utilizing the broad genetic variation that exists in wild species is a prevalent approach for the identification of genes and alleles that improve crops' performance under harsh environmental conditions, including heat stress (Zamir, 2001). In order to evaluate a new BILs population generated from a cross between M82 (*S. lycopersicum*) and the *S. pimpinellifolium* LA1589 accession for its relevance as a source for the identification of heat stress tolerance genes, we screened the population under non-controlled heat stress and under controlled, moderate chronic heat stress (MCHS) conditions. Since thermotolerance is a highly complex trait, we examined several vegetative and reproductive parameters that include plant stature and flowering time, inflorescence length, flower size and color, anther structure and apparent damage, fruit color, size and seeds content. Additionally, we analyzed the number of flowers and fruits, the rate of fruit set, single fruit weight, pollen germination rate, and the number of seeds per fruit. We observed a wide range of responses for all traits tested (Figure 3).

Owing to the controlled experimental set up, which allowed the comparison between MCHS and control conditions, we could identify the traits that are directly affected by MCHS. These include number of fruits and fruit set rate, pollen germination rate, and the number of seeds per fruit, all are well known heat stress

10.3389/fpls.2024.1386824

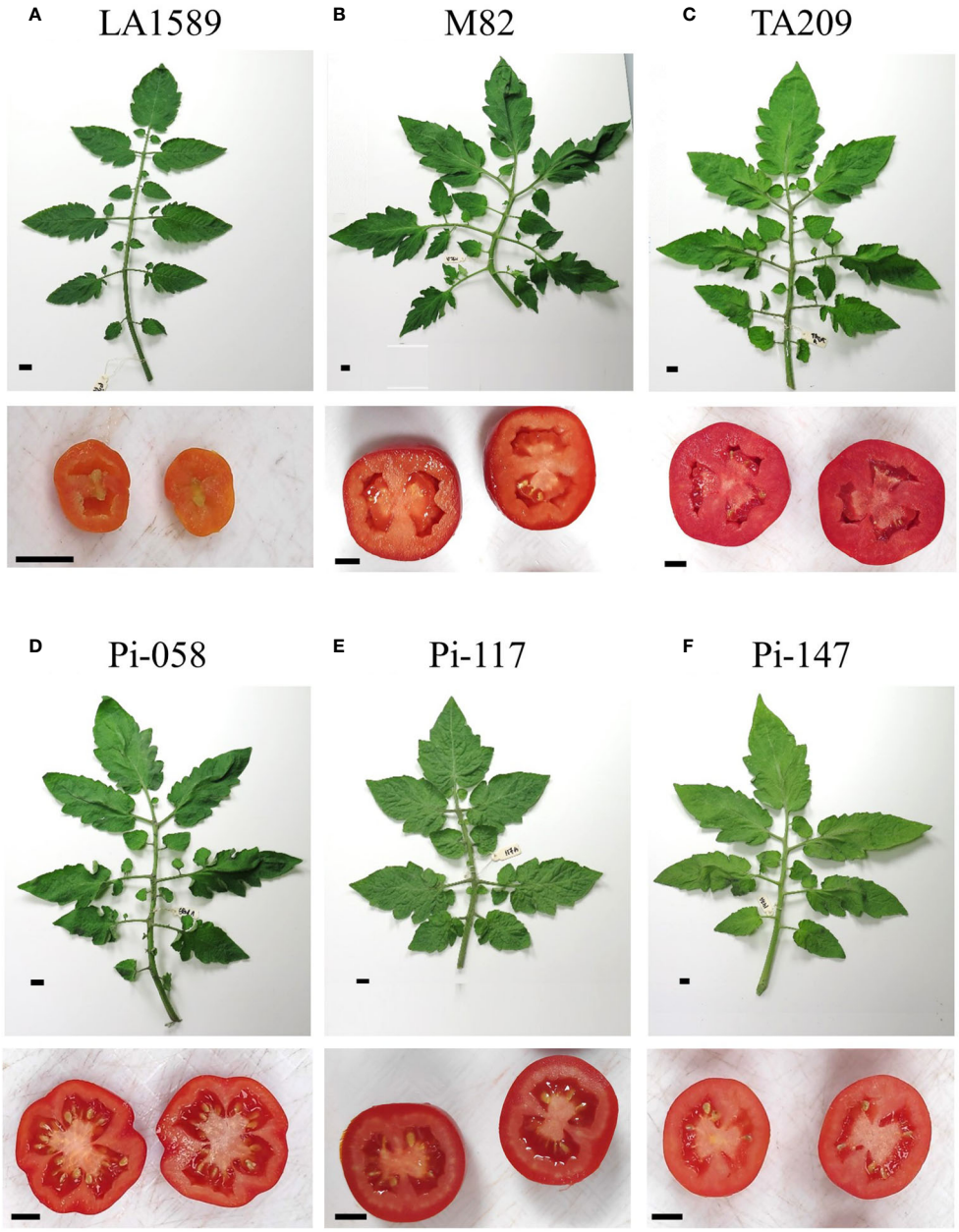

FIGURE 6
Leaf and seeds set of parental lines LA1589 **(A)**, M82 **(B)**, TA209 **(C)** and tolerant BILs pi-058 **(D)**, pi-117 **(E)** and pi-147 **(F)** under MCHS conditions. The black bar indicates 1 cm.

related traits (Peet et al., 1998; Pressman et al., 2007), thus supporting our hypothesis that this BIL population is a relevant germplasm for exploring heat stress response in tomato.

In the controlled experiments, the number of flowers and single fruit weight were generally not affected by the MCHS conditions employed. Several studies reported a reduction in flower production under high temperature conditions, but under moderate heat stress conditions, flower number seemed to be unaffected (Abdul-Baki, 1991; Xu et al., 2017). Others show that there is no significant decrease in the number of flowers under heat treatment compared to the control (Peet et al., 1997; Sato et al., 2006; Gonzalo et al., 2020). Fruit weight was also reported to be reduced up to 83% under heat stress conditions (Peet et al., 1998). These differences may be attributed to the heat stress conditions employed, i.e., acute stress versus moderate chronic stress. Moreover, the response to the different stress regimes is genotype-dependent. Style protrusion is highly variable between lines and cultivars as the frequency of this trait may range from 12.5% to 80% (Levy et al., 1978). Notably, this phenomenon is naturally occurring in wild relatives of tomato (Chen et al., 2007) and therefore cannot be considered as a pure heat stress related trait in the *S. pimpinellifolium* population. Nevertheless, our phenotypic screen revealed that about half of the lines (54%) did not present style protrusion at all, and 25% of the lines presented moderate (9%), high (9%), or extreme (7%) level

10.3389/fpls.2024.1386824

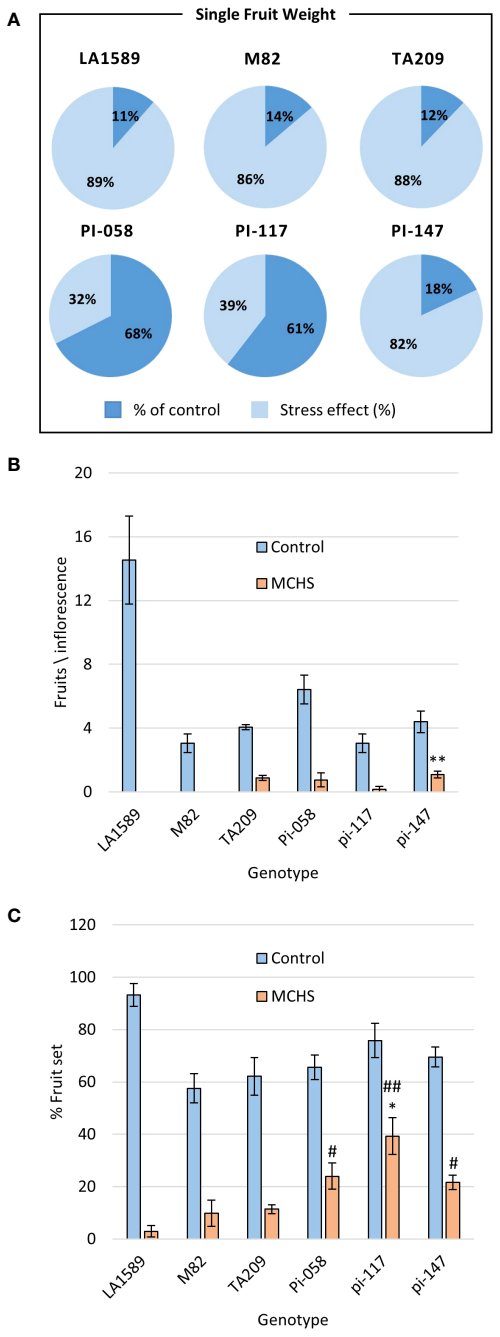

FIGURE 7
The lines pi-058, pi-117, and pi-147 present heat stress tolerance in fruit-related phenotypes. The effect of MCHS was tested for single fruit weight as a ratio of fruit weight in MCHS relative to fruit weight in control conditions **(A)**, number of fruits per inflorescence **(B)**, and fruit-set rate **(C)** Using Student's TTEST compared with M82 and TA209 separately. (*), p-value < 0.05 compared to M82. (**), p-value < 0.01 compared to M82. (#), p-value < 0.05 compared to TA209. (##), p-value < 0.01 compared to TA209.

of style protrusion. Levy et al. (1978) reported up to 66% flower buds drop rate in a tomato heat sensitive cultivar. Our population screen results show that although most lines did not present buds or flowers abortion, 16 BILs presented varying abortion rates, ranging between 5% and 70%. Since pollen grain is the most thermosensitive organ (Zinn et al., 2010), special attention is given to pollen quality and performance under heat stress conditions. Pressman et al. (2002) reported a reduction of 62% and 92%, in pollen viability and germination, respectively. Similarly, Firon et al. (2006) showed a 29–78% decrease in pollen viability and 80–90% decrease in pollen germination as a result of heat stress. Our results indicate as well a very strong reduction in pollen viability and germination under MCHS conditions. While some BILs completely lost germination capability, the best performing lines presented a decrease of 32% in pollen germination compared with reductions of 80% in the M82 parental line.

It was very clear throughout our experiments, that LA1589, the parental *S. pimpinellifolium* wild-species itself, was not more tolerant than the cultivated tomato lines, in any of the traits tested. In fact, it was the most sensitive. This can partially explained by the unnatural environment in the greenhouse which includes detached soil growth media, and consistent watering and fertilization for homogenous treatment to all plants across all experiments, but are actually stressful for the wild-adapted *S. pimpinellifolium*. Nonetheless, the hypersensitivity of LA1589 to heat stress in our hands, together with the wide variation in heat-stress related traits among the BILs, and the identification of three tolerant lines, suggest that epistatic effects contribute to the observed heat stress tolerance.

Overall, our results highlight the relevance and importance of this BIL population as a new resource for the identification of heat stress related tolerance genes and QTLs. This population was never tested for heat stress related traits. Specifically, the genetic structure of this population may facilitate the identification of candidate genes or QTLs by aligning genetic maps of phenotypically similar lines, as demonstrated by the phenotypic and genetic comparison of pi-058, pi-117 and pi-147 (Figures 7–9; Supplementary Figure S3). In the analysis presented here, we identified a 0.8 Mbp region on chromosome 9 found exclusively in lines pi-058, pi-117 and pi-147 and absent in the other, non-tolerant lines (Supplementary Figure S3), which was enriched for genes related to heat stress response, thus these may be involved in the observed heat stress tolerance of pi-058, pi-117 and pi-147. This introgression includes seven genes related to heat stress response (Table 3), some of them are known to contribute to tolerance under heat stress conditions. For example, the chaperonin 60 (*Cpn60*, *Solyc09g091180*) was found to be overexpressed in thermotolerant tomato that presents high pollen viability under heat stress (Mazzeo et al., 2018) and to support photosystem II under conditions of heat stress (Preczewski et al., 2000). Two additional genes found in the common introgression, *Solyc09g091660* and *Solyc09g091670*, encode ABC transporters responsible for heat stress tolerance by maintaining cell membrane integrity under heat stress conditions. These genes also regulate the transport, distribution and accumulation of ABA and secondary metabolites in different organs of the plant, which in turn modulate thermotolerance (Dahuja et al., 2021). *Solyc09g090870* and *Solyc09g090890* are involved in DNA mismatch repair which plays an important role in DNA repair following heat stress (Kantidze et al., 2016). Therefore, although *Cpn60* is an immediate candidate for supporting the heat stress tolerance of pi-058, pi-117 and pi-147, it is possible that a joint

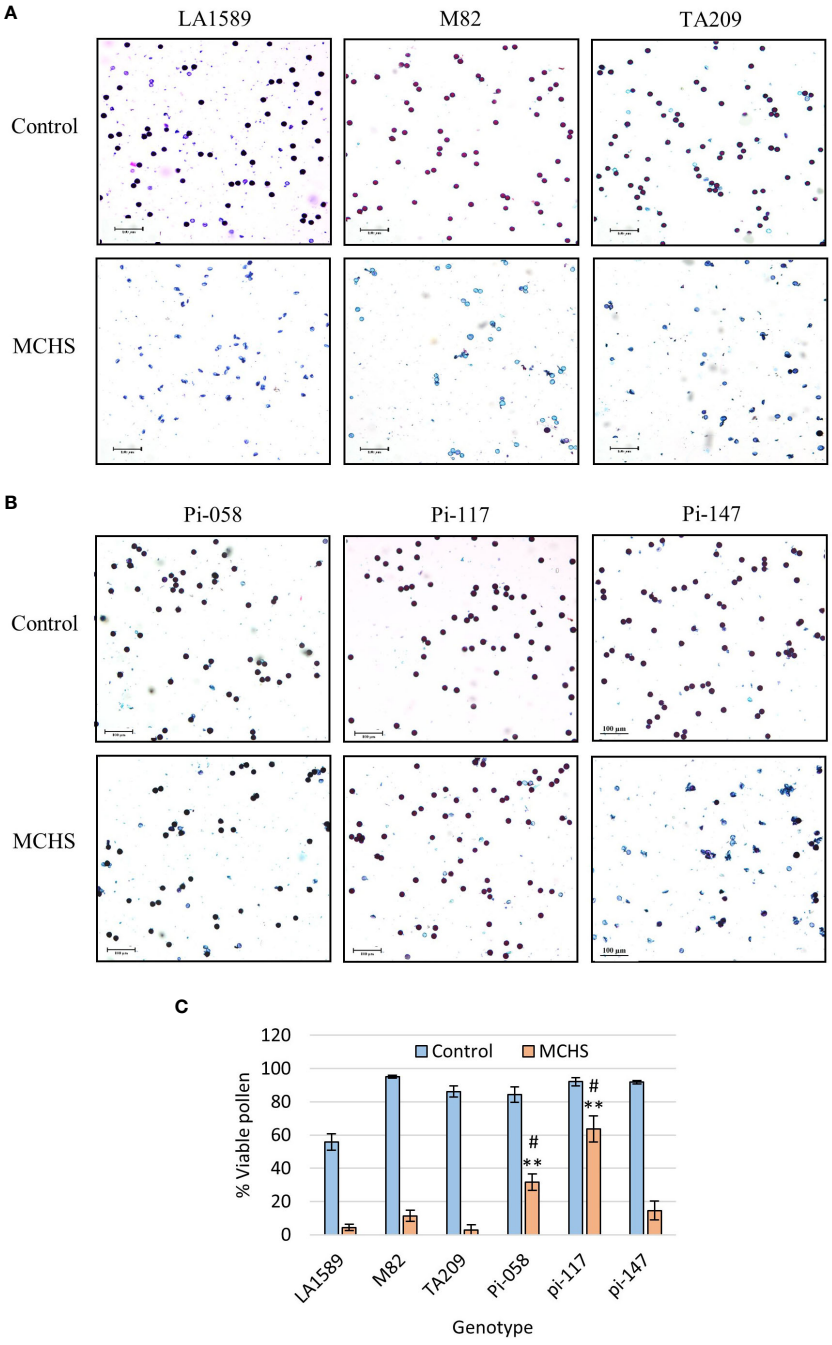

FIGURE 8
Pollen viability in lines pi-058, pi-117, and pi-147. Differential Alexander staining was performed on pollen from flowers sampled from plants grown under control or MCHS conditions. Viable pollen is round and stained purple, while unviable pollen is light blue and frequently mis-shaped. The frequency of viable pollen is reduced in MCHS conditions in all lines, as shown in representative figures presenting the LA1589, M82 and TA209 parental lines **(A)**, the pi-058, pi-117, pi-147 lines **(B)**, and quantification of the results for all lines **(C)**. (**), p-value < 0.01 compared to M82. (#), p-value < 0.05 compared to TA209.

activity of all or some of these seven genes (Table 3) are responsible for the observed effect. Moreover, this introgression may not be the sole effector that promotes thermotolerance, as epistatic effects may also take place, as mentioned here before.

It is interesting to note that among the three thermotolerant lines identified in this study, pi-147 is, for some traits, not performing as well as pi-058 and pi-117 which are highly similar (Figures 7A, 8). Since pi-058 and pi-117 contain another common introgression on chromosome 9 which is absent in pi-147 (Figure 9), genes found in this region may be driving this difference, an hypothesis that requires further studies. Since in our experimental setup, LA1589 was not performing well under MCHS conditions, having evolved in harsh conditions, it is unlikely that the heat stress tolerance of specific BILs will be attributed to a single introgression. It is possible though, that a specific interaction between a single introgression and the cultivated genome will generate a causal network for tolerance. This should be

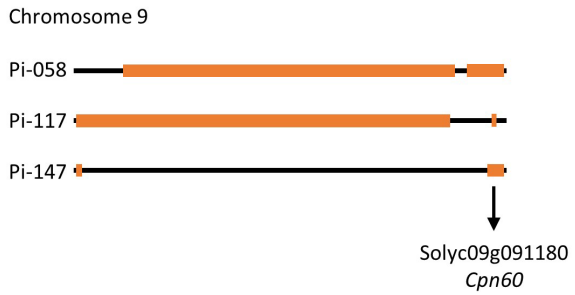

FIGURE 9
Schematic representation of chromosome 9 in lines pi-058, pi-117 and pi-147. Orange boxes mark the LA1589 *S. pimpinellifolium* introgressions. The black arrow indicated the common introgression containing the Cpn60 chaperonin gene.

further studied considering the common introgression on chromosome 9 (Figure 9).

Taking into consideration other publications demonstrating a beneficial contribution of *S. pimpinellifolium* accessions to heat stress tolerance, we suggest that this BIL population may be useful for the identification of heat stress related QTLs. Introgression Lines (IL) population originated from a cross between a cultivated tomato and the *S. pimpinellifolium* TO-937 accession was used in a study that successfully identified 22 QTLs involved in reproductive traits under high temperatures. For example, fruit-set was reduced by less than 50% in several RILs while in the Moneymaker background, reduction was up to 87% (Gonzalo et al., 2020). Moreover, the specific *S. pimpinellifolium* accession LA1589 was also suggested to contribute to heat stress tolerance as two clusters of QTLs involved in the responses of reproductive traits to heat stress were identified in a LA1589-derived population (Gonzalo et al., 2022). For each of the heat stress related traits that were tested, we could identify specific lines that were performing significantly better than other lines, and of both parental lines. These lines will serve as a starting genetic material in future studies aiming to identify QTLs and causal genes for each of the tolerance traits. Moreover, since the controlled MCHS experiments were performed on selected lines, not including the entire population (due to space limitations), our results suggest that additional tolerant lines may be identified in future studies that will complement the MCHS controlled screen for the entire population, in a future perspective of developing heat stress tolerant tomato cultivars.

TABLE 2 Physical location of LA1589 introgressions in chromosome 9 of the pi-058, pi-117 and pi-147 lines.

Line	Introgression no.	Length Mbp, (SL2.4)	Start End Mbp, (SL2.4)
pi-058	1	52.20	7.80
			60.00
	2	5.90	61.80
			67.70
pi-117	1	58.65	0.35
			59.00
	2	**0.80**	**65.50**
			66.30
pi-147	1	0.85	0.05
			0.90
	2	2.60	65.10
			67.70

The second introgression in pi-117 (Bold) is common between all three lines.

TABLE 3 Genes with the GO term 'response to heat' that are found in the common 0.8Mbp introgression.

Locus name	Description
Solyc09g090700	Aldehyde dehydrogenase
Solyc09g090870	DNA mismatch repair
Solyc09g091180	Chaperonin (Cpn60)
Solyc09g090890	DNA mismatch repair protein
Solyc09g091660	ABC transporter
Solyc09g091670	ATP-binding cassette transporter
Solyc09g091830	Peptidoglycan binding domain containing protein

Data availability statement

The original contributions presented in the study are included in the article/Supplementary Material. Further inquiries can be directed to the corresponding author.

Author contributions

NB: Conceptualization, Formal analysis, Investigation, Writing – original draft, Writing – review & editing. GM: Formal analysis, Investigation, Methodology, Project administration, Supervision, Writing – review & editing. TD-M: Formal analysis, Investigation, Writing – review & editing. AB: Formal analysis, Investigation, Writing – review & editing. BO: Writing – review & editing, Funding acquisition. DZ: Writing – review & editing, Resources. ML-L: Conceptualization, Data curation, Formal analysis, Funding acquisition, Investigation, Methodology, Supervision, Validation, Visualization, Writing – original draft, Writing – review & editing.

Funding

The author(s) declare financial support was received for the research, authorship, and/or publication of this article. This research was supported by the Ministry of Science & Technology, Israel, grant no. 001877, & The National Key R&D Program of China, grant no. 2022YFE0100900.

Acknowledgments

We would like to thank Prof. Dani Zamir and Dr. Yaacov Micha Brog, from the Robert H. Smith Faculty of Agriculture, Food and Environment, Hebrew University of Jerusalem, Rehovot, Israel, for providing the *S. pimpinellifolium* BILs population. We also wish to thank Dr. Adi Faigenboim, ARO – Volcani center for bioinformatic analysis and to Dr. Hillary Voet, ARO, for statistical support.

Conflict of interest

The authors declare that the research was conducted in the absence of any commercial or financial relationships that could be construed as a potential conflict of interest.

Publisher's note

Supplementary material

The Supplementary Material for this article can be found online at: https://www.frontiersin.org/articles/10.3389/fpls.2024.1386824/full#supplementary-material

References

Abdul-Baki, A. A. (1991). Tolerance **of** tomato cultivars and selected germplasm to heat stress. *J. Am. Soc. Hortic. Sci.* 116, 1113–1116. doi: 10.21273/JASHS.116.6.1113

Alexander, M. P. (1980). A versatile stain for pollen fungi, yeast and bacteria. *Stain Technol.* 55, 13–18. doi: 10.3109/10520298009067890

Ayenan, M. A. T., Danquah, A., Hanson, P., Ampomah-Dwamena, C., Sodedji, F. A. K., Asante, I. K., et al. (2019). Accelerating Breeding for Heat Tolerance in Tomato (*Solanum lycopersicum L.*): An integrated approach. *Agronomy* 9, 720. doi: 10.3390/agronomy9110720

Bell, J., Duffy, P., Covey, C., and Sloan, L. (2000). Comparison of temperature variability in observations and sixteen climate model simulations. *Geophys. Res. Lett.* 27, 261–264. doi: 10.1029/1999GL006080

Bita, C. E., and Gerats, T. (2013). Plant tolerance to high temperature in a changing environment: scientific fundamentals and production of heat stress-tolerant crops. *Front. Plant Sci.* 4. doi: 10.3389/fpls.2013.00273

Charles, W. B., and Harris, R. E. (1972). Tomato fruit-set at high and low temperatures. *Plant Sci.* 52, 497–506. doi: 10.4141/cjps72-080

Chen, K.-Y., Cong, B., Wing, R., Vrebalov, J., and Tanksley, S. D. (2007). Changes in regulation of a transcription factor lead to autogamy in cultivated tomatoes. *Science* 318, 643–645. doi: 10.1126/science.1148428

Conesa, M.À., Muir, C. D., Roldán, E. J., Molins, A., Perdomo, J. A., and Galmés, J. (2017). Growth capacity in wild tomatoes and relatives correlates with original climate in arid and semi-arid species. *Environ. Exp. Bot.* 141, 181–190. doi: 10.1016/j.envexpbot.2017.04.009

Dahuja, A., Kumar, R. R., Sakhare, A., Watts, A., Singh, B., Goswami, S., et al. (2021). Role of ATP-binding cassette transporters in maintaining plant homeostasis under abiotic and biotic stresses. *Physiologia Plantarum* 171, 785–801. doi: 10.1111/ppl.13302

Doganlar, S., Frary, A., Ku, H.-M., and Tanksley, S. D. (2002). Mapping quantitative trait loci in inbred backcross lines of *Lycopersicon pimpinellifolium* (LA1589). *Genome* 45, 1189–1202. doi: 10.1139/g02-091

Driedonks, N., Wolters-Arts, M., Huber, H., de Boer, G.-J., Vriezen, W., Mariani, C., et al. (2018). Exploring the natural variation for reproductive thermotolerance in wild tomato species. *Euphytica* 214, 1–12. doi: 10.1007/s10681-018-2150-2

Firon, N., Shaked, R., Peet, M. M., Pharr, D. M., Zamski, E., Rosenfeld, K., et al. (2006). Pollen grains of heat tolerant tomato cultivars retain higher carbohydrate concentration under heat stress conditions. *Scientia Hortic.* 109, 212–217. doi: 10.1016/j.scienta.2006.03.007

Foolad, M. R., Zhang, L. P., and Lin, G. Y. (2001). Identification and validation of QTLs for salt tolerance during vegetative growth in tomato by selective genotyping. *Genome* 44, 444–454. doi: 10.1139/g01-030

Gonzalo, M. J., Li, Y. C., Chen, K. Y., Gil, D., Montoro, T., Nájera, I., et al. (2020). Genetic control of reproductive traits in tomatoes under high temperature. *Front. Plant Sci.* 11. doi: 10.3389/fpls.2020.00326

Gonzalo, M. J., da Maia, L. C., Nájera, I., Baixauli, C., Giuliano, G., Ferrante, P., et al. (2022). Genetic control of reproductive traits under different temperature regimes in inbred line populations derived from crosses between *s. Pimpinellifolium* and *s. Lycopersicum* accessions. *Plants 2022* 11, 1069. doi: 10.3390/PLANTS11081069

Grandillo, S., and Tanksley, S. D. (1996). QTL analysis of horticultural traits differentiating the cultivated tomato from the closely related species *Lycopersicon pimpinellifolium*. Theor. *Appl. Genet.* 92, 935–951. doi: 10.1007/BF00224033

Hartman, J. B., and St Clair, D. A. (1999). Combining ability for beet armyworm, *Spodoptera exigua*, resistance and horticultural traits of selected *Lycopersicon pennellii*-derived inbred backcross lines of tomato. *Plant Breed.* 118, 523–530. doi: 10.1046/j.1439-0523.1999.00437.x

Hazra, P., Samsul, A., Sikder, D., and Peter, K. V. (2007). Breeding tomato (*lycopersicon esculentum* mill.) Resistant to high temperature stress. *Int. J. Plant Breed.* 1, 31–40.

Kabelka, E., Yang, W., and Francis, D. M. (2004). Improved tomato fruit color within an inbred backcross line derived from *Lycopersicon esculentum* and L. hirsutum involves the interaction of loci. *J. AMER. Soc Hortic. Sci.* 129, 250–257. doi: 10.21273/JASHS.129.2.0250

Kantidze, O. L., Velichko, A. K., Luzhin, A. V., and Razin, S. V. (2016). Heat stress-induced dna damage. *Acta Naturae* 8, 75. doi: 10.32607/20758251-2016-8-2-75-78

Kimura, S., and Sinha, N. (2008). Tomato (*Solanum lycopersicum*): a model fruit-bearing crop. *Cold Spring Harbor Protoc.* 3, 1–9. doi: 10.1101/pdb.emo105

Levy, A., Rabinowitch, H. D., and Kedar, N. (1978). Morphological and physiological characters affecting flower drop and fruit set of tomatoes at high temperatures. *Euphytica* 27, 211–218. doi: 10.1007/BF00039137

Lin, G. Y., Foolad, M. R., and Zhang, L. P. (2002). "QTL comparison of salt tolerance during seed germination and vegetative stage in a Lycopersicon esculentum x L. pimpinellifolium RIL population," in *XXVI International Horticultural Congress: Environmental Stress and Horticulture Crops*, vol. 618, 59–67. doi: 10.17660/ActaHortic.2003.618.5

Liu, B., Song, L., Deng, X., Lu, Y., Lieberman-Lazarovich, M., Shabala, S., et al. (2023). Tomato heat tolerance: progress and prospects. *Scientia Hortic.* 322, 112435. doi: 10.1016/j.scienta.2023.112435

Lohar, D. P., and Peat, W. E. (1998). Floral characteristics of heat-tolerant and heat-sensitive tomato (*Lycopersicon esculentum* Mill.) cultivars at high temperature. *Scientia Hortic.* 73, 53–60. doi: 10.1016/S0304-4238(97)00056-3

Mazzeo, M. F., Cacace, G., Iovieno, P., Massarelli, I., Grillo, S., and Siciliano, R. A. (2018). Response mechanisms induced by exposure to high temperature in anthers from thermo-tolerant and thermo-sensitive tomato plants: A proteomic perspective. *PloS One* 13, e0201027. doi: 10.1371/journal.pone.0201027

Miller, J. C., and Tanksley, S. D. (1990). RFLP analysis of phylogenetic relationships and genetic variation in the genus Lycopersicon. *Theor. Appl. Genet.* 80, 437–448. doi: 10.1007/BF00226743

Müller, F., Xu, J., Kristensen, L., Wolters-arts, M., de Groot, P. F. M., Jansma, S. Y., et al. (2016). High-temperature-induced defects in tomato (*Solanum lycopersicum*) anther and pollen development are associated with reduced expression of B-Class floral patterning genes. *PloS One* 11, e0167614. doi: 10.1371/journal.pone.0167614

Pease, J. B., Haak, D. C., Hahn, M. W., and Moyle, L. C. (2016). Phylogenomics reveals three sources of adaptive variation during A rapid radiation. *PloS Biol.* 14, 1–24. doi: 10.1371/journal.pbio.1002379

Peet, M. M., Sato, S., and Gardner, R. G. (1998). Comparing heat stress effects on male-fertile and male-sterile tomatoes. *Plant Cell Environ.* 21, 225–231. doi: 10.1046/j.1365-3040.1998.00281.x

Peet, M. M., Willits, D. H., and Gardner, R. (1997). Response of ovule development and post-pollen production processes in male-sterile tomatoes to chronic, sub-acute high temperature stress. *J. Exp. Bot.* 48, 101–111. doi: 10.1093/jxb/48.1.101

Peralta, I. E., and Spooner, D. M. (2000). Classification of wild tomatoes: a review. *Tomo* 28, 45–54. Available at: http://hdl.handle.net/11336/152176.

Peralta, I. E., Spooner, D. M., and Knapp, S. (2008). Taxonomy of wild tomatoes and their relatives (Solanum sect. Lycopersicoides, sect. Juglandifolia, sect. Lycopersicon; Solanaceae). *Syst. Bot. Monogr.* 84.

Preczewski, P. J., Heckathorn, S. A., Downs, C. A., and Coleman, J. S. (2000). Photosynthetic thermotolerance is quantitatively and positively correlated with production of specific heat-shock proteins among nine genotypes of Lycopersicon (tomato). *Photosynthetica* 38, 127–134. doi: 10.1023/A:1026760311255/METRICS

Pressman, E., Peet, M. M., and Pharr, D. M. (2002). The effect of heat stress on tomato pollen characteristics is associated with changes in carbohydrate concentration in the developing anthers. *Ann. Bot.* 90, 631–636. doi: 10.1093/aob/mcf240

Pressman, E., Shaked, R., and Firon, N. (2007). Tomato response to heat stress: focus on pollen grains. *Plant Stress* 1, 216–227.

Rao, E. S., Kadirvel, P., Symonds, R. C., and Ebert, A. W. (2013). Relationship between survival and yield related traits in Solanum pimpinellifolium under salt stress. *Euphytica* 190, 215–228. doi: 10.1007/s10681-012-0801-2

Renau-Morata, B., Cebolla-Cornejo, J., Carrillo, L., Gil-Villar, D., Martí, R., María Jiménez-Gómez, J., et al. (2024). Identification of *Solanum pimpinellifolium* genome regions for increased resilience to nitrogen deficiency in cultivated tomato. *Scientia Hortic.* 323, 112497. doi: 10.1016/j.scienta.2023.112497

Rick, C. M. (1958). The role of natural hybridization in the derivation of cultivated tomatoes of western South America. *Econ. Bot.* 12, 346–367. doi: 10.1007/BF02860023

Rick, C. M., and Dempsey, W. H. (1969). Position of the stigma in relation to fruit setting of the tomato. *Bot. GAZ.* 130, 180–186. doi: 10.1086/336488

Sato, S., Kamiyama, M., Iwata, T., Makita, N., Furukawa, H., and Ikeda, H. (2006). Moderate increase of mean daily temperature adversely affects fruit set of *Lycopersicon esculentum* by disrupting specific physiological processes in male reproductive development. *Ann. Bot.* 97, 731–738. doi: 10.1093/aob/mcl037

Sato, S., Peet, M. M., and Gardner, R. G. (2001). Formation of parthenocarpic fruit, undeveloped flowers and aborted flowers in tomato under moderately elevated temperatures. *Scientia Hortic.* 90, 243–254. doi: 10.1016/S0304-4238(00)00262-4

Sato, S., Peet, M. M., and Thomas, J. F. (2000). Physiological factors limit fruit set of tomato (Lycopersicon esculentum Mill.) under chronic, mild heat stress. *Plant Cell Environ.* 23, 719–726. doi: 10.1046/j.1365-3040.2000.00589.x

Sato, S., Peet, M. M., and Thomas, J. F. (2002). Determining critical pre- and post-anthesis periods and physiological processes in *Lycopersicon esculentum* Mill. exposed to moderately elevated temperatures. *J. Exp. Bot.* 53, 1187–1195. doi: 10.1093/jexbot/53.371.1187

Schneider, C., Rasband, W., and Eliceiri, K. (2012). NIH Image to ImageJ: 25 years of image analysis. *Nat. Methods* 9 (7), 671–675. doi: 10.1038/nmeth.2089

Villalta, I., Reina-Sanchez, A., Bolarin, M. C., Cuartero, J., Belver, A., Venema, K., et al. (2008). Genetic analysis of Na+ and K+ concentrations in leaf and stem as physiological components of salt tolerance in Tomato. *Theor. Appl. Genet.* 116, 869–880. doi: 10.1007/s00122-008-0720-8

Xu, J., Wolters-Arts, M., Mariani, C., Huber, H., and Rieu, I. (2017). Heat stress affects vegetative and reproductive performance and trait correlations in tomato (*Solanum lycopersicum*). *Euphytica* 213, 156. doi: 10.1007/s10681-017-1949-6

Zamir, D. (2001). Improving plant breeding with exotic genetic libraries. *Nat. Rev. Genet.* 2, 983–989. doi: 10.1038/35103590

Zinn, K. E., Tunc-Ozdemir, M., and Harper, J. F. (2010). Temperature stress and plant sexual reproduction: uncovering the weakest links. *J. Exp. Bot.* 61, 1959–1968. doi: 10.1093/jxb/erq053

frontiers | Frontiers in Plant Science

TYPE Original Research
PUBLISHED 11 February 2025
DOI 10.3389/fpls.2025.1495494

OPEN ACCESS

EDITED BY
Ujjwal Layek,
Rampurhat College, India

REVIEWED BY
Ruirui Huang,
University of San Francisco, United States
Norbert Bollier,
INRAE Nouvelle-Aquitaine Bordeaux, France

*CORRESPONDENCE
Mondher Bouzayen
mondher.bouzayen@toulouse-inp.fr
Guojian Hu
guojian.hu@zju.edu.cn

†These authors have contributed equally to this work

RECEIVED 12 September 2024
ACCEPTED 08 January 2025
PUBLISHED 11 February 2025

CITATION
Li X, He B, Djari A, Frasse P, Maza E, Regad F, Pirrello J, Hu G and Bouzayen M (2025) Transcriptomic reprogramming and epigenetic regulation underlying pollination-dependent and auxin-induced fruit set in tomato.
Front. Plant Sci. 16:1495494.
doi: 10.3389/fpls.2025.1495494

Transcriptomic reprogramming and epigenetic regulation underlying pollination-dependent and auxin-induced fruit set in tomato

Xiaohan Li[1,2,3†], Bing He[4†], Anis Djari[5], Pierre Frasse[5], Elie Maza[5], Farid Regad[5], Julien Pirrello[5], Guojian Hu[1,2,3,5*] and Mondher Bouzayen[5*]

[1]College of Agriculture and Biotechnology, Zhejiang University, Hangzhou, China, [2]Zhejiang Provincial Key Laboratory of Horticultural Plant Integrative Biology, Zhejiang University, Hangzhou, China, [3]The State Agriculture Ministry Laboratory of Horticultural Plant Growth, Development and Quality Improvement, Zhejiang University, Hangzhou, China, [4]College of Horticulture, China Agricultural University, Beijing, China, [5]Laboratoire de Recherche en Sciences Végétales—Génomique et Biotechnologie des Fruits—UMR5546, Université de Toulouse, Centre national de la recherche scientifique (CNRS), Université de Toulouse 3 - Paul Sabatier (UPS), Toulouse-Institut National Polytechnique (INP), Toulouse, France

The transition from flower to fruit, naturally triggered by flower pollination and known as fruit set, is instrumental for plant reproduction, seed formation, and crop yield. Notably, this developmental process can also proceed in the absence of flower fertilization, although it remains unclear whether pollination-dependent and pollination-independent fruit sets undergo similar transcriptomic reprogramming. Genome-wide transcriptomic profiling of the flower-to-fruit transition, either pollination-induced or triggered by auxin treatment, shows that both types of triggers modulate the expression of a common large set of genes primarily expressed in maternal tissues. These include genes related to auxin, gibberellin, brassinosteroid, and ethylene signaling. Furthermore, analysis of changes in histone marking during this transition phase indicated that gene reprogramming underlying both types of fruit set primarily correlated with dynamic changes in H3K9ac and H3K4me3 histone marks. Notably, *MCM1, AG, DEFA and SRF (MADS)-box* and *NAM, ATAF1/2, and CUC2 (NAC)* genes were extensively downregulated during the transition from flower to fruit, suggesting their negative roles in fruit initiation. In contrast, *Teosinte branched1/Cincinnata/proliferating cell factor (TCP), SQUAMOSA -promoter binding proteins (SBP), Sucrose nonfermenting 2 (SNF2), Growth-regulating factor (GRF), and Su (var)3-9, Enhancer-of-zeste and Trithorax (SET)* family genes were significantly upregulated in both pollinated and auxin-treated young developing fruits, suggesting their active roles in promoting fruit sets. Despite these similarities, a comparative analysis of the effects of natural pollination and auxin treatment revealed several differences, primarily related to seed development and hormone signaling. Taken together, the data support the idea that auxin serves as the central hormone orchestrating the extensive gene reprogramming associated with fruit initiation in tomato.

KEYWORDS

fruit set, auxin, pollination, transcriptomic reprogramming, epigenetic regulation, tomato

Introduction

Fruit set, an essential transition from flower opening to young fruit development, is naturally triggered by ovule fertilization, which coordinately activates developmental programs, including seed development and the growth of various peripheral structures that protect the developing seeds (Pandolfini et al., 2007). During the anthesis stage, the unpollinated ovary enters a temporary growth arrest until flower fertilization occurs, triggering a developmental switch that forms the arrested ovary into a rapidly growing fruit. Underpinning this developmental transition, cell division is rapidly initiated in the placenta and pericarp tissues following successful ovule fertilization. While it is generally accepted that fertilized ovules, now developing into young seeds, are the primary structures releasing signals that trigger cell division and fruit growth in various plant species, the molecular nature of these signal(s) and their diffusion into the surrounding tissues remain poorly understood.

Phytohormones play a pivotal role in transitioning an arrested ovary into a growing fruit. Several lines of evidence single-out auxin and gibberellins (GA) as prominent positive regulators of fruit set, as the application of these hormone substrates to unpollinated ovaries stimulates parthenocarpic fruit formation in various plant species (Gustafson, 1936; Bünger-Kibler and Bangerth, 1982; Pandolfini et al., 2007; Serrani et al., 2008; de Jong et al., 2009a). Direct evidence that auxin triggers fruit set has been explored across physiological, biochemical, and molecular levels, encompassing auxin biosynthesis, metabolism, polar transport, perception, signal transduction, and responses. For instance, increasing levels of auxin through the expression of the *Pseudomonas* pv. *savastanoi iaaM* gene in the ovule or the *Agrobacterium rhizogenes rolB* gene in the ovary has been shown to promote parthenocarpic fruit formation in several horticultural crops (Rotino et al., 1997, 2005; Donzella et al., 2000; Pandolfini et al., 2002; Carmi et al., 2003; Mezzetti et al., 2004). Similarly, knocking down the expression of the auxin efflux carrier *SlPIN4* gene results in parthenocarpic fruit setting (Mounet et al., 2012), and altering auxin perception through the overexpression of *TRANSPORT INHIBITOR 1* (*SlTIR1*) also induces parthenocarpy (Ren et al., 2011). More recently, impairing the expression of several components of the auxin signaling pathway, including *IAA9*, *SlARF7*, and *ARF8A/B* has been reported to result in seedless fruit setting (Wang et al., 2005; Goetz et al., 2007; de Jong et al., 2009b; Hu et al., 2023). Altogether these data clearly emphasize the primary role of auxin during the flower-to-fruit transition. GAs are another factor controlling fruit set and subsequent fruit development. High levels of GA have been reported in parthenocarpic tomato lines *pat-2* and *pat-3/pat-4* (Fos et al., 2000, 2001), and inactivation of *GA 2-oxidase* genes leads to the formation of parthenocarpic fruits in *Arabidopsis* (Rieu et al., 2008). Similarly, the alternation of the active GA form by overexpression of the citrus *CcGA20ox1* gene in tomato triggers fruit growth in the absence of pollination (Garcia-Hurtado et al., 2012). Activation of the GA signaling pathway relies on the presence of GA3, which stimulates the ubiquitin-dependent proteolytic degradation of the nuclear repressor DELLA by the 26S proteasome, thereby releasing the repression of GA response genes by DELLA (Davière and Achard, 2013). Along the same line, downregulation of the *SlDELLA* gene expression, which encodes a negative regulator of GA signaling, induces parthenocarpic fruit formation and reduced fruit size in tomato (Martí et al., 2007). Taken together, these data support the notion that active GA signaling promotes fruit set and ovary growth. Furthermore, auxin has been reported to positively regulate the expression of GA biosynthesis genes in the ovules, leading to GA accumulation, suggesting that auxin acts prior to GA in promoting fruit initiation. Accordingly, transcripts corresponding to the copalyldiphosphate synthase (*SlCPS*), *SlGA20ox1*, *SlGA20ox2*, *SlGA20ox3*, and *SlGA3ox1* genes accumulate to higher levels in 2,4-D-treated ovaries, while transcript levels of GA-inactivating enzyme *SlGA2ox2* are decreased (Dorcey et al., 2009). In addition, the gaseous hormone ethylene also appears to influence fruit set, as ethylene production decreases in pollination-induced and in pollination-independent fruit set in the auxin hypersensitive tomato mutant *iaa9-3* (Shinozaki et al., 2015). Accordingly, mutation of the ethylene perception gene *Sletr1-1* in tomato leads to elevated levels of bioactive GAs the formation of elongated parthenocarpic fruit, suggesting that ethylene plays a role in maintaining ovary growth arrest prior to pollination by suppressing GA metabolism. Altogether, this reveals the complexity of the hormonal regulatory network underlying the fruit-set process.

In addition to the central role of hormones, the flower-to-fruit transition involves the intervention of several developmental factors, most of which are transcription factors (TFs). For instance, loss-of-function of the *PI* MADS-box gene in apples produces *apetalous* flowers and seedless fruits (Yao et al., 2001). Silencing of the *SEPALLATA* (*SEP*) MADS-box gene *TM29* leads to parthenocarpic fruit formation in tomato (Ampomah-Dwamena et al., 2002). Two other MADS-box genes, *Tomato Agamous1* (*TAG1*) and *Tomato Agamous6* (*TAGL6*), were suggested to play negative roles in fruit setting, based on the observation that their transcript levels dramatically decrease during both pollination-induced and pollination-independent fruit set in wild-type and in *IAA9* tomato mutants, respectively (Wang et al., 2009). In addition, miR156 and its target SQUAMOSA promoter-binding protein-like (SPL or SBP-box) genes were found to be differentially expressed in pre- and postanthesis ovaries. Overexpression of *AtMIR156* resulted in partial seedless fruit formation, defining miR156 and SPL transcription factors as a regulatory module controlling the early stages of fruit development (Silva et al., 2014). Moreover, the transcript levels of *GROWTH REGULATING FACTOR 2* (*GRF2*), a member of the transcription activator gene family, were shown by cDNA-amplified fragment length polymorphism (AFLP) to increase in pollinated ovaries (Vriezen et al., 2007). Although our understanding of the central roles of hormones and transcription factors in fruit setting has progressed tremendously in recent decades, the similarities and differences between the molecular mechanisms of the hormonal signaling and transcriptomic reprogramming involved in pollination-dependent and pollination-independent fruit setting have largely been overlooked.

Epigenetic marking, including DNA methylation of 5′ cytosine residues and posttranslational modification of histones (Henderson

and Jacobsen, 2007), appears to be the main mechanism regulating gene expression during developmental transitions underlying organ and tissue differentiation, as well as plant reproduction in living organisms (Pu and Sung, 2015; Gehring, 2019). In plants, histone modifications are a major factor in controlling transitions across various developmental stages, including the circadian clock, stress response (Berr et al., 2011; Malapeira et al., 2012), and fruit set induced by pollination (Hu et al., 2021). Extensive research has demonstrated that the biosynthesis, transport, and signaling of phytohormones are regulated by histone modifications (Rudolf et al., 2024). For instance, H3K27me3 acts as a repressive mark across large genomic regions for genes involved in auxin metabolism and transport, such as *YUCCA* (*YUC*), *CYTOCHROME P450* (*CYP*), and *TRYPTOPHAN AMINOTRANSFERASE 1/ TRYPTOPHAN AMINOTRANSFERASE-RELATED* (*TAA1/TAR*) and *PIN-FORMED* (*PINs*) genes (Lafos et al., 2011; He et al., 2012). Importantly, the POLYCOMB REPRESSIVE COMPLEX2 (PRC2)-mediated FERTILIZATION INDEPENDENT (FIS-PRC2) complex has been shown to block the expression of auxin biosynthesis and gibberellin-related genes in unfertilized ovules through H3K27me3 deposition. This repression is lifted upon fertilization, leading to paternal expression of auxin biosynthesis genes, which promotes endosperm formation and seed set in *Arabidopsis* (Figueiredo et al., 2015, 2016). Furthermore, transcription factors can reshape the epigenetic state of the chromatin regions they bind to, either by facilitating the binding of other transcription factors or by directly recruiting histone modifiers (Soufi et al., 2012). For instance, *TCP5* regulates the transition from cell division to postmitotic expansion of petal primordia in *Arabidopsis* (Huang and Irish, 2015). The RABBIT EARS (RBE) transcriptional repressor maintains the downregulation of its direct target, *TCP5*, by recruiting the TOPLESS (TPL)-HDA19 corepressor complex to inhibit *TCP5* transcription (Huang and Irish, 2024). The reduced transcription of *TCP5* is associated with a decrease in H3K9ac and an increase in H3K27me3 histone marks. It is noteworthy that silencing the corepressor *SlTPL1* induces facultative parthenocarpic fruit formation in tomato (He et al., 2021), a phenotype similar to that observed in the antisense line of its partner, *IAA9*. Altogether, these studies reveal the interplay among hormones, TFs, and epigenetic mechanisms, underscoring their critical role in driving developmental transitions in plants.

Using combined genome-wide transcriptomic profiling and Chromatin immunoprecipitation followed by sequencing (ChIP-seq) strategies, we previously showed that histone marking, rather than DNA methylation, is strongly correlated with the transcriptomic reprogramming underpinning fruit set in tomato, with H3K9ac and H3K4me3 permissive marks being the primary players in this control mechanism (Hu et al., 2021). Considering that auxin can trigger fruit set independently of pollination, we sought to comparatively investigate whether histone marking plays a role in both auxin-mediated natural pollination-induced fruit setting. The outcome of the study supports the notion that both auxin-induced and pollination-triggered fruit sets rely on the expression of a common large set of genes, primarily expressed in maternal tissues and that the two types of fruit set correlate primarily with the dynamic changes of H3K9ac and H3K4me3 histone marks.

Materials and methods

Plant materials and sampling

All plants used in this study were *Solanum lycopersicum* L. cv MicroTom. The seeds were directly sown in soil and grown under standard culture chamber conditions as follows: 14-h-day/10-h-night cycle, 25/20°C day/night temperature, 80% relative humidity, 250 mol m^{-2} s^{-1} light intensity.

Ovary samples at 0 days postpollination (0 DPA) correspond to the anthesis stage when the stamens were loosely enclosed by petals. Fruits at 4 days postpollination (4 DPA) correspond to 4 days postanthesis. For the 4 days after auxin treatment (4 IAA) fruit samples, the flowers were first emasculated 1 day before anthesis (to avoid accidental self-pollination). From anthesis and for the next 4 days, the ovaries were treated daily with 10 µL of 500 µM indole-3-acetic acid (IAA; Sigma Aldrich, US). This treatment is considered appropriate because both pollination- and IAA-treated fruits ultimately reach similar fruit sizes at 4 and 9 days after anthesis (Hu et al., 2021). Each biological replicate corresponds to a pool of at least 50 ovaries (fruits) from 25 plants.

RNA sample preparation and sequencing

Total RNA was extracted from ~ 200 mg of tissue for each sample using the TRIzol RNA Isolation Kit (Thermo Fisher Scientific, US). After DNA removal (DNA-free™ DNA Removal Kit, Ambion, US), RNA was purified, and its quality was checked using an Agilent 2100 analyzer. Only samples with an RIN > 8.6 were used for Illumina sequencing. Eight biological replicates were performed for each sampling stage. Paired-end RNA sequencing (2 nt × 125 nt) was performed using a Truseq Illumina SBS Kit V4 and a Hiseq2500 platform.

RNA-seq data processing

Raw paired-end RNA-seq sequences in FASTQ format were analyzed. Low-quality reads were removed using the FASTQ quality filter from the FASTX Toolkit version 0.0.13 (http://hannonlab.cshl.edu/fastx_toolkit/). Trimmed reads were then mapped to the *S. lycopersicum* reference genome and gene annotation (ITAG4.1 Tomato_Genome_Consortium, 2012, https://solgenomics.net/) using TopHat-2.0.14 (Trapnell et al., 2009), which calls Bowtie 2.1.0 (Langmead and Salzberg, 2012). To perform differential gene analysis, HTSeq (Anders et al., 2015) was used to calculate raw counts. Raw counts of 34,727 tomato genes were normalized, and mean counts per kilobase of the transcript were used as gene expression. Differentially expressed genes between 4 DPA and 0 DPA tissues or 4 IAA and 0 DPA tissues were identified using DEseq2 (Love et al., 2014). Raw *p*-values were adjusted as "*padj*" by multiple tests using the methods of Benjamini and Hochberg (1995). Genes with |log2Fold| > 1 and *padj* < 0.01 were defined as significantly differentially expressed genes.

Chromatin immunoprecipitation and sequencing

The experiment was performed as previously described (Hu et al., 2021). Tissues at 0 DPA, 4 DPA, and 4 IAA were cross-linked by vacuum infiltration (760 mmHg) for 15 min in 1% formaldehyde fresh 1 × PBS solution (with 0.015% Triton X-100). To ensure efficient crosslinking, 4 DPA or 4 IAA fruits were cut in half prior to crosslinking. Crosslinking was stopped by adding glycine (0.125 M final concentration) and incubating under vacuum infiltration for an additional 5 min. After washing twice with cold 1 × PBS solution, samples were thoroughly dried between paper towels, snap-frozen in liquid nitrogen, and stored at − 80°C. ChIP assays were performed as described previously (Gendrel et al., 2005) with minor modifications. Briefly, ~1 g of crosslinked tissue was ground to a fine powder in liquid nitrogen. Shearing of the chromatin was achieved through Diagenode Bioruptor sonication (5 runs of 10 cycles: 30 s "ON" and 30 s "OFF"). The size of the sonicated chromatin was checked to ensure that it was within the range of 100–500 bp. Subsequently, 10 µL of sonicated supernatant was kept aside as input. For each sample (120 µL supernatant), a dilution buffer was added to bring the final volume to 1.5 mL. Depending on the histone mark, either 5 µL of H3K9ac rabbit polyclonal antibody (Millipore, US; Cat. No. 07-352; Lot No. 2586454), 5 µL of H3K4me3 rabbit polyclonal antibody (Millipore; Cat. No. 07-473; Lot No. 2430389), or 8 µL of H3K27me3 rabbit polyclonal antibody (Millipore; Cat. No. 07-449; Lot No. 2475696) were added prior to incubation overnight (4°C at 10 rpm). For the control experiment without histone mark antibodies, 5 µL of nonimmunized rabbit IgG antibody (Millipore; Cat. No. 12-370; Lot No. 2426484) was added. For the empty control (Mock), no antibody was added. Afterward, 50 µL of protein A/G agarose beads (Pierce™ Protein A/G UltraLink™ Resin; Thermo Scientific; Cat. No. 53133) was added, and the samples were incubated for 3 h at 4°C. Beads were then sequentially washed with low salt wash buffer, high salt wash buffer, LiCl wash buffer, and finally with TE buffer. Elution was performed as previously described (Gendrel et al., 2005). Eluates of immunoprecipitated samples (IP) and input samples not subjected to immunoprecipitation were first reverse-crosslinked at 65°C overnight and then treated with 20 mg proteinase K (Invitrogen, US) for 3 h, followed by phenol/chloroform extraction, and ethanol precipitation in the presence of NaCl (3 M: pH 5.2) and glycogen. The precipitated DNA was resuspended in 10 µL of nuclease-free water and quantified by Qubit Fluorometer (Qubit dsDNA HS Assay Kit Cat. No. Q32851, Molecular Probes, US). For each sample, 10 ng of immunoprecipitated DNA was used for library construction and sequencing.

ChIP-seq data processing

ChIP-seq read alignment was performed using Bowtie2 with default parameters, and only uniquely aligned reads were retained. Enriched regions in the nonredundant mapped reads were identified by MACS2 v1.4.2 (Zhang et al., 2008) (effective genome size = 770 Mb, *p*-value cutoff = 1.00*e*−05). Heatmap representations of signal intensity (computeMatrix scale-regions followed by plotHeatmap) were generated using the deepTools suite (Ramírez et al., 2014). The BEDtools package (Quinlan and Hall, 2010) was used to detect the tomato genes (ITAG4.1) overlapping with the detected peaks. A matrix of genes intersecting with peaks for each sample was created for downstream analyses using R software (www.r-project.org/). Differentially associated peaks were normalized and identified using the "MAnorm" method (Shao et al., 2012). For this method, the normalized *M*-value (*M* = log2 [read density in 4 IAA samples/read density in 0 DPA sample]) represents log2-transformed fold changes in enrichment intensities at each peak region. Only regions with *p*-value < 0.01 were defined as differentially associated regions (DA) (Supplementary Table S4).

Gene ontology analysis

Gene ontology (GO) analysis of differentially expressed genes (DEGs) (*padj* < 0.05) was performed using PANTHER GO. Significantly enriched GO categories were selected with a false discovery rate (FDR) < 0.05.

Quantitative RT-PCR

Total RNA extraction, genomic DNA removal, cDNA generation, and qRT-PCR were performed as previously described (Hao et al., 2015). The comparative threshold cycle method (ΔΔCt) was used for quantitative PCR (LightCycler ® 480 II system, Roche, US). Tomato Actin (*Solyc11g005330*) was used as an internal reference. Primers for qRT-PCR analysis are listed in Supplementary Table S5. Three independent biological replicates were performed.

Accession numbers

The datasets supporting the conclusions of this article are available (study PRJEB19602) from the European Nucleotide Archive (http://www.ebi.ac.uk/ena/data/view/PRJEB19602) with the following accession numbers: ERS1572545, ERS1572546, ERS1572547, ERS1572553, ERS1572554, ERS1572555, ERS1572556, ERS1572557, and ERS1572558 for RNA-seq analysis; ERS1572559, ERS1572560, ERS1572561, ERS1572562, ERS1572563, ERS1572564, ERS1572565, ERS1572566, ERS1572567, ERS1572568, ERS1572569, and ERS1572570 for ChIP-seq analysis.

Results

Global transcriptomic changes associated with auxin-induced and pollination-dependent fruit set

Fruit set is naturally triggered upon flower pollination and fertilization, and this genetically programmed process involves the

complex coordination of multiple signaling pathways. This developmental transition is associated with dramatic physiological and structural changes, including hormone regulation, cell division, cell proliferation, and tissue differentiation. Auxin is well known for its ability to trigger fruit initiation and subsequent fruit growth independently from pollination. Exogenous IAA treatment of tomato ovary (cv. MicroTom) induces fruit set and early growth in a manner similar to that triggered by flower pollination. To investigate the extent to which the two types of fruit setting involve the same gene regulatory networks, we implemented a genome-wide transcriptomic profiling of the flower-to-fruit transition through deep sequencing. To prevent accidental self-pollination, tomato flowers were emasculated 1 day before anthesis and were either manually pollinated or treated with IAA, then sampled simultaneously at 4 DPA or 4 IAA (Hu et al., 2021).

Deep sequencing generated reads ranging from 23 to 33 million, depending on the sample, with 87%~89% of the reads being uniquely mapped to the *S. lycopersicum* genome (ITAG4.1). Gene expression values are provided as mean normalized counts per kilobase of transcript. Overall, the transcripts detected in 0 DPA, 4DPA, or 4 IAA tissues correspond to a total of 25,037 genes, representing 72% of the 34,688 tomato genes. Among these, 21,516 (62.0%) were expressed in all samples (Supplementary Table S1). Out of the 22,762 (65.6% of total tomato genes) expressed in 4 IAA samples, only 310 genes are specifically expressed in this tissue, while the expression of 905 genes (3.8%) is specific to 0 DPA samples, and 727 (3.1%) to 4 DPA fruits. Together, 1,548 genes were specifically expressed in young fruits (either in 4 DPA or 4 IAA fruits).

DEGs were identified using DESeq2 for raw count normalization. Considering a fold change ≥ 2 and an adjusted *p*-value < 0.01, a total of 6,710 and 4,749 genes were assigned as DEGs upon pollination and auxin treatment, respectively. Notably, a high proportion of DEGs (4,271 genes) were shared between pollination- and auxin-induced fruit (Figure 1A), and most of these DEGs showed the same trend of expression changes during the switch from flower to fruit (R = 0.94, Figure 1B), suggesting a largely similar transcriptomic reprogramming of the fruit set triggered by both auxin and pollination signals. In addition, qRT-PCR performed to validate the DEGs in both pollination- and auxin-induced fruit sets indicated that, among 16 randomly selected from DEGs, all exhibited a similar trend of expression changes for both pollination- and auxin-induced fruit sets (Supplementary Table S2; Figure 1C). Notably, this was further validated in a nondwarf cherry tomato cultivar, WVA106, which showed that 81% (13 genes) of the DEGs were consistently regulated during the two types of fruit set. These data indicated that the DEGs identified in our study are reliable for further analysis. GO analysis of the DEGs indicated that 41 GO terms were significantly enriched in both 4 DPA and 4 IAA samples. Among these, one-third of the biological processes are

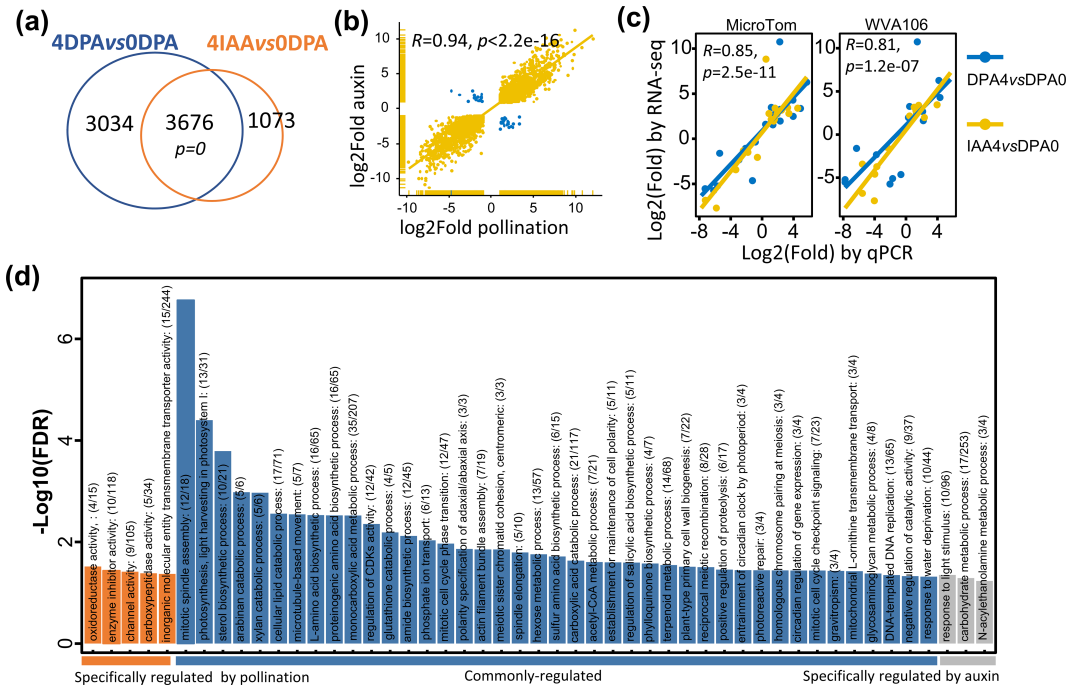

FIGURE 1
Genome-wide transcriptomic profiling of tomato genes during the fruit-set process induced by natural pollination and auxin induction. **(A)** Comparison of the number of differentially expressed genes during pollination- and auxin-induced fruit sets. Fold change > 2 and *padj* < 0.01. **(B)** Correlation of expression changes in common DEGs between pollination-induced and auxin-treated fruit sets. Statistical significance between the two gene datasets was evaluated using a hypergeometric test, with all expressed genes considered total size. **(C)** Correlation levels between RNA-seq and qRT-PCR expression data were assessed in two distinct tomato cultivars (MicroTom and Wva106). The statistical significance of the correlation between RNA-seq expression and qRT-PCR data was determined by a two-sided Pearson's correlation test. **(D)** GO enrichment analysis for DEGs regulated by pollination or auxin during fruit set. Selected significantly enriched biological processes (BH-adjusted overrepresented *p*-value < 0.05) were annotated in the figure.

related to cell division and differentiation processes. Out of 44 DEGs related to cell division identified in the tomato genome, 55% (27 genes) are commonly induced by pollination and auxin, including cell cycle genes, cell division protein kinases (CDKs), and other regulators controlling cell division, consistent with the active cell division occurring at early stages of fruit development. Genes related to photosynthesis and carbohydrate metabolic processes were also differentially expressed in pollination- and auxin-induced fruits (Figure 1D), further supporting the idea that photosynthesis starts at a very early stage of fruit development in tomato. Importantly, a large number of common DEGs belong to the hormone signaling pathway, highlighting the critical role of hormones in regulating fruit set. Interestingly, several lipid-related processes, such as lipid oxidation, lipid catabolic processes, and cellular responses to lipids, were also significantly enriched. In summary, these data indicate that the common set of DEGs between auxin-induced and pollination-triggered fruit defines the fundamental processes required for fruit initiation in tomato.

Notably, a large proportion (45%, 3,034 genes) of DEGs are specific to pollination-dependent fruit sets, compared to only 22% that are specific to auxin-induced fruit set. GO analysis of pollination-specific DEGs further indicated that oxidoreductase, carboxypeptidase, and enzyme inhibitor activities were among the top-enriched biological processes, suggesting that more enzyme activity characterizes the pollination-triggered fruit set. On the other hand, GO terms enriched in 4 IAA DEGs are related to carbohydrate and *N*-acylethanolamine metabolic processes, suggesting that auxin treatment likely triggers more active sugar and lipid metabolism to support the fast growth of the fruit. Further examination of the DEGs at the tissue levels, based on previously reported LCM RNA-seq data (Pattison et al., 2015), showed a higher representation of embryo- and endosperm-preferentially expressed genes in pollination-induced fruit than in auxin-induced DEGs (Table 1). These data reflect the contrasted situation with regard to seed development in pollination-triggered fruit and auxin-treated fruit. Interestingly, individual investigation of these DEGs in embryo and endosperm tissues showed that their expression is promoted by pollination while repressed by auxin (Supplementary Figures S1A, B). By contrast, both auxin treatment and pollination lead to a relatively high proportion (from 21.30% to 30.43%, Table 1) of common DEGs observed in maternal tissues of the two types of young fruits, compared to embryo and endosperm tissues. These data indicate that in maternal tissues, the transcriptomic reprogramming relies on a set of genes largely common to pollination-induced and auxin-triggered fruits, whereas a highly contrasted situation prevails in embryo and endosperm tissues.

Both pollination and auxin induce massive changes in the expression of hormone-related genes

Auxin and gibberellin are two critical hormones for fruit sets, but whether other hormones are also actively involved in this transition remains unclear. The large number of biological processes related to hormone regulation that are enriched in pollination- or auxin-induced fruit (Figure 1D) prompted us to investigate the expression changes of individual genes involved in hormone metabolism and signaling. We first generated the most comprehensive list of genes for each hormone category by performing a BLAST search with *Arabidopsis* orthologs (TAIR10) along with publicly available genes. Out of 120 auxin-related genes identified in the tomato genome, nearly half (52) were differentially expressed during either pollination- or auxin-induced fruit set. Genes involved in all aspects of auxin metabolism and responses (Figure 2A) were affected by these changes, including auxin synthesis (tryptophan aminotransferases and flavin monooxygenases), transport (SlPINs, SlLAXs, and SlPILSs), and signaling (Aux/IAAs and Auxin Response Factors). Among these DEGs, 50% were similarly regulated by both pollination and auxin induction, and their expression changes were significantly higher than those DEGs specific to auxin-treated or pollination-induced samples (Figure 2B). IAA is mainly synthesized from the amino acid tryptophan (Trp) in a two-step pathway by Tryptophan Aminotransferase of *Arabidopsis*

TABLE 1 Number of DEGs in different tissue-preferential gene sets.

Preferential tissues[a]	Gene Nb	Pollination-DEG		Auxin-DEG		Common-DEG[b]		Diff-DEG[c]	
		Nb	%	Nb	%	Nb	%	Nb	%
Embryo	1,535	204	13.29%	124	8.08%	93	6.06%	3	0.20%
Endosperm	591	121	20.47%	82	13.87%	53	8.97%	4	0.68%
Seed coat	457	224	49.02%	148	32.39%	125	27.35%	2	0.44%
Funiculus	385	132	34.29%	105	27.27%	82	21.30%	0	0.00%
Pericarp	731	261	35.70%	217	29.69%	166	22.71%	2	0.27%
Septum	966	426	44.10%	348	36.02%	294	30.43%	2	0.21%
Placenta	1,096	384	35.04%	295	26.92%	234	21.35%	1	0.09%

[a]Preferential tissues refer to tissue-preferentially expressed gene clusters adapted from previous tissue-specific transcriptomic data (Pattison et al., 2015): embryo, cluster 12; endosperm, cluster 19; seed coat, cluster 14; funiculus, cluster 21; pericarp, clusters 8 and 28; septum, clusters 27 and 29; and placenta, clusters 20 and 26.
[b]DEGs that exhibit common trends in changes induced by both pollination and auxin treatment.
[c]DEGs exhibit opposite changes between pollination and auxin treatments.

10.3389/fpls.2025.1495494

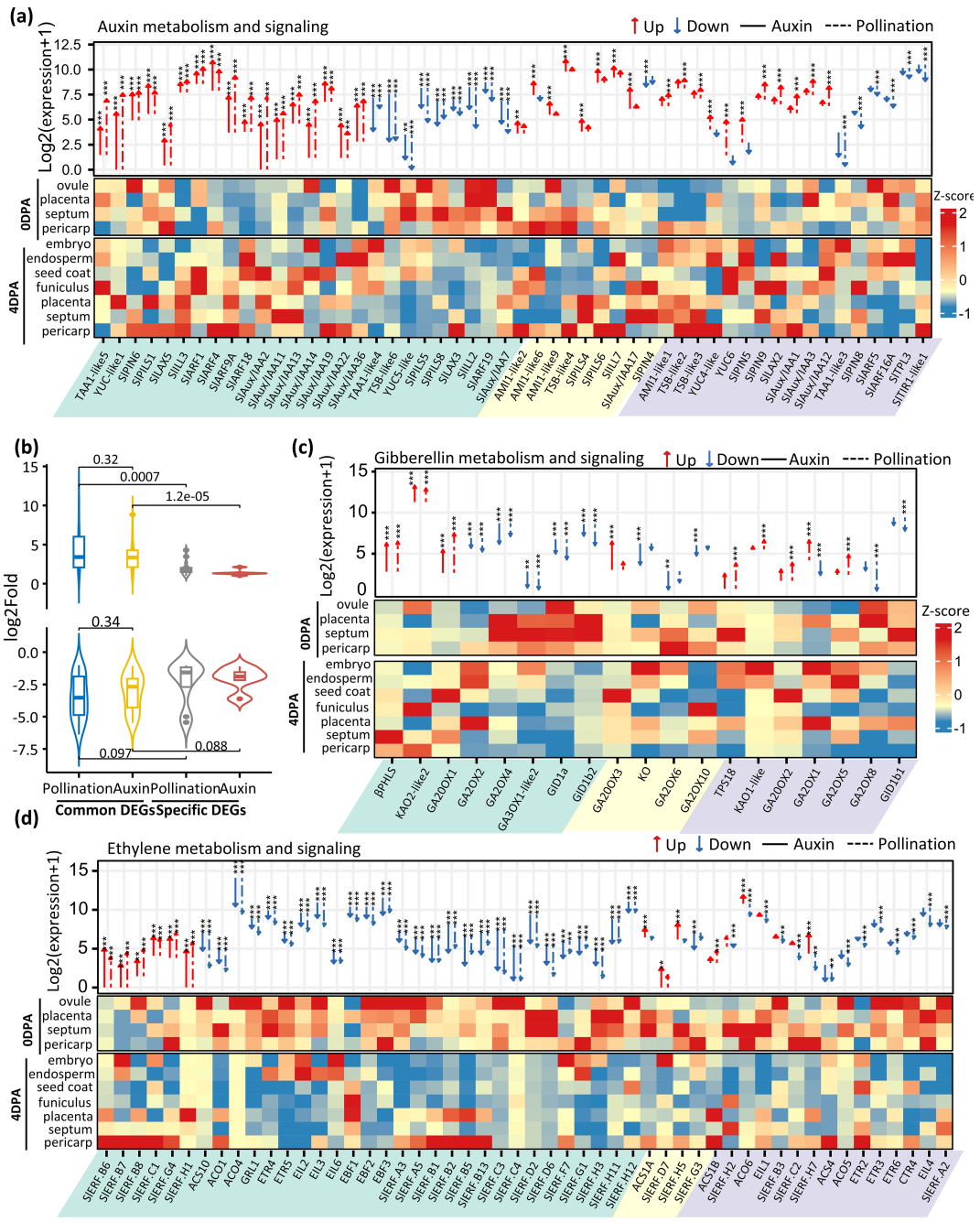

FIGURE 2
Differential expression of hormone-related genes during fruit set. DEGs associated with auxin **(A)**, gibberellin **(C)**, and ethylene **(D)** metabolism and signaling are shown. Gene expression is indicated as Log2 of mean normalized counts per kilobase +1. Common-, auxin-specific-, and pollination-specific DEGs are shaded in green, yellow, and purple, respectively. Dashed lines represent natural pollination, while solid lines indicate auxin treatment. Genes with significant differential expression were marked by asterisks. Gene expression (z-score) in selected tissue types from the ovary and pollination-induced young fruit is adapted from a previous study (Pattison et al., 2015) and displayed in the lower panel. **(B)** Average gene expression of common or type-specific DEGs associated with auxin metabolism and signaling. Genes with significant differential expression were marked by asterisks (** Fold > 2 and 0.001< *p*-value < 0.01; *** Fold > 2 and *p*-value < 0.001).

(TAAs) and flavin monooxygenases (YUCCAs) or in an IAM-dependent pathway by indole-3-acetamide hydrolase (AMI) family. Consistently, *TAA1-like5* and *YUC-like1* were significantly upregulated in both pollination- and auxin-induced fruit, while *YUC4-like* and *YUC6* were only induced by pollination, in line with their specific expression in seed tissues. It is noteworthy that *YUC-like1* is highly and preferentially induced in the septum, suggesting that the septum is one of the main tissues contributing to overall auxin synthesis required for both pollination-dependent and pollination-independent fruit initiation in tomato. Although several TAAs, Trp synthases (TSBs), and YUCs were downregulated, these changes might be due to a sample dilution effect, considering that the upregulation of their expression occurs specifically in the embryo tissue of pollination-induced fruit. Alternatively, given that

the embryo and endosperm tissues are absent in auxin-induced fruit, it might simply reflect a decreased expression of these genes in maternal tissues, since both pollination and auxin induction lead similarly to the downregulation of these genes (Figure 2A). On the other hand, a high number of ARFs and Aux/IAAs genes were activated during the fruit set process, including the previously reported ARF4 (Jones et al., 2002) and ARF9A (de Jong et al., 2015), which are involved in cell division. Consistently, the majority of these auxin signaling genes were expressed in maternal tissues, with *Aux/IAA2* being highly induced in the seed coat and septum, and *Aux/IAA 11* and *Aux/IAA 13* in the placenta. Altogether, these data indicate that high auxin activity is promoted in maternal tissues during both pollination-dependent and pollination-independent fruit set in tomato.

Nine out of the 19 GA-related DEGs were upregulated upon auxin or pollination, among which eight are involved in GA synthesis (Figure 2C), including two kaurene synthases (*TPS18* and beta-phellandrene synthase [*βPHLS*]), three kaurenoic acid oxidases (*KAO2-like2*, *KO* and *KAO1-like*), and three GA20 oxidases (*GA20ox1*, *GA20ox2*, *GA20ox3*). Among the 11 downregulated genes, six encode GA2 oxidases involved in reducing endogenous bioactive GA levels and three encode gibberellin receptors. Notably, all three GA20 oxidase genes were highly expressed in the funiculus of pollination-induced fruit, while most GA2OXs were depleted in the same tissue, consistent with highly active GA levels in the funiculus during fruit initiation. Altogether, the data support the idea that both pollination-dependent and pollination-independent fruit setting require active GA synthesis and signaling, and that exogenous auxin treatment promotes GA synthesis through a similar set of GA-related genes as the pollination-dependent fruit set.

Notably, out of 11 DEGs related to brassinosteroids, 10 showed significantly increased transcription in auxin-induced or natural pollination-induced fruit. Among these, eight brassinosteroid synthesis genes showed remarkably high expression, including *DET2*, *SMT1-like*, *SMT2-like3*, *delta14-sterol reductase*, *DWARF1-like*, *DWARF5-like2*, *HYD1-like*, and *STE1-like2* (Supplementary Figure S2). In particular, the steroid synthesis gene *DWARF1-like*, involved in the early C-22 hydroxylation pathway, displayed very high transcript levels in both 4 DPA and 4 IAA fruits. These data suggest that BR input also plays an important role in the control of fruit setting.

Strikingly, the downregulation of ethylene-related genes emerges as a major trend of the flower-to-fruit transition, with up to 41 genes (79%) of the 52 DEGs in this category showing significant downregulation (Figure 2D). Among these, 27 genes were downregulated by both pollination and auxin treatment, including six ethylene biosynthesis genes (1-Aminocyclopropane 1-Carboxylic Acid (ACC) *synthase* and three *ACC oxidases*), three ethylene perception genes (two *ETRs* and *GRL1*), three *EIN-like* genes, three *EBF* genes, and 15 ethylene response factor (*ERF*) genes. These data clearly emphasize the need for drastic repression of ethylene activity to allow the initiation of the fruit set process in tomato.

Genes involved in cytokinin synthesis are downregulated in both pollination and auxin-induced fruit. Among 20 DEGs in this category, 15 show a significant decrease in transcript levels, including adenosine phosphate-isopentenyl transferase genes (IPTs) (*IPT3-like* and *IPT5*), the rate-limiting enzymes for isopentenyladenine (iP) nucleotide synthesis. Consistently, cytokinin signaling and response genes also showed downregulation in pollination- or auxin-induced fruit, with 16 DEGs involved in cytokinin signal transduction and response. This indicates that cytokinin activity is also tuned down during the fruit initiation process (Supplementary Figure S2).

Moreover, genes related to abscisic acid, jasmonates, and salicylic acid undergo significant changes in their expression levels (Supplementary Figure S2). Several genes related to ABA (31 DEGs out of 85), JA (19 DEGs out of 45), and SA (17 DEGs out of 80) were also identified as differentially expressed. Overall, the data clearly support the idea that the fruit set process is under complex multihormonal control, with genes related to auxin, GAs, and BRs being mostly upregulated, whereas those related to ethylene are strongly downregulated, and those related to CK, JA, and ABA are rather tuned down.

Auxin induces significant changes in histone marking similar to pollination-induced fruit set

We previously showed that a high proportion of DEGs in auxin-induced fruit set underwent similar changes in histone marking as those in pollination-dependent fruit set. To further explore the similarities and differences in histone marking between pollination-dependent and pollination-independent fruit sets, we separately profiled the association with three histone marks, including acetylation of lysine residue 9 (H3K9ac) and trimethylation of lysine residues 4 (H3K4me3) and 27 (H3K27me3), based on their changes in gene expression (Figure 3). The data showed a higher correlation between gene expression and association with the two permissive histone marks H3K4me3 and H3K9ac than the repressive mark H3K27me3. Notably, most of the common DEGs showed a clear correlation between changes in gene expression and changes in histone mark association.

Given that a large number of genes related to hormone regulation underwent changes in histone marks during pollination-induced fruit setting, we investigated whether auxin induces similar histone modifications. To address this issue, all DEGs related to the metabolism and signaling of auxin, gibberellin, ethylene, cytokinin, ABA, brassinosteroids, jasmonates, and salicylic acid were investigated for changes in their association with H3K9ac, H3K4me3, and H3K27me3.

Out of 52 DEGs associated with auxin metabolism and signaling identified in both types of fruit initiation, 48 showed differential association in at least one of the three histone marks (Figure 4A). Moreover, of the 16 DEGs common to pollination and auxin-induced fruit set, 26 displayed similar trends of changes in either H3K9ac or H3K4me3 histone marks. Notably, gaining either of these two histone marks correlated with increased gene expression, as exemplified by those involved in auxin synthesis, auxin transport, and auxin response. For instance, transcript accumulation of *SlAux/*

10.3389/fpls.2025.1495494

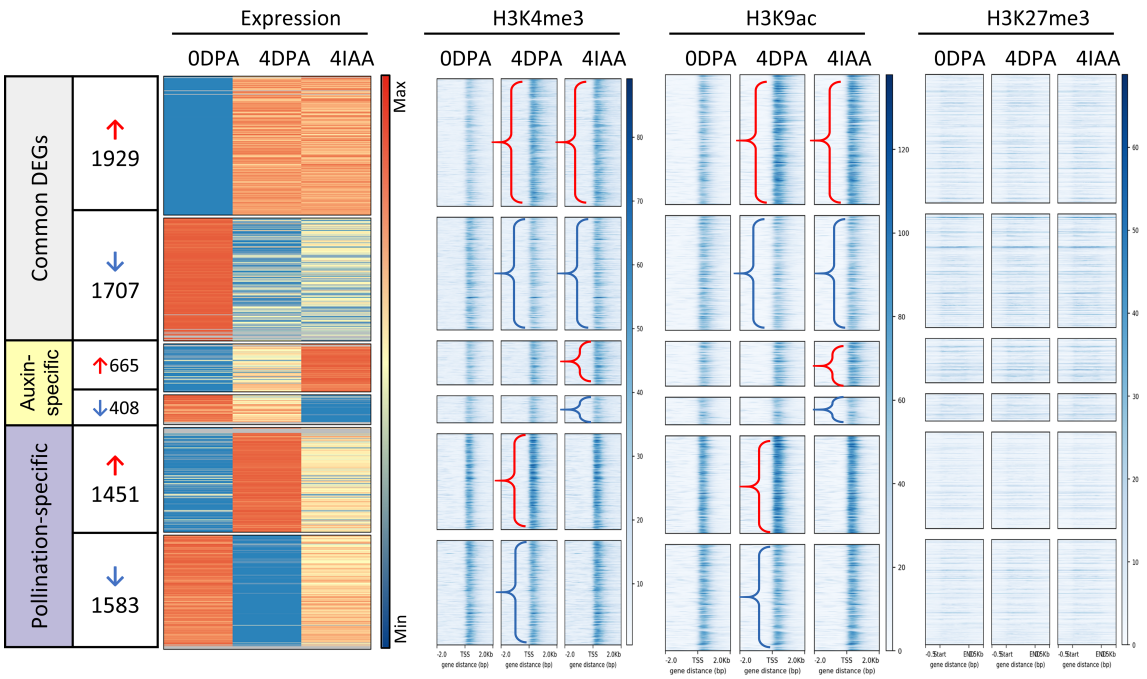

FIGURE 3
Profiles of gene expression and histone mark association for DEGs during fruit set. The density profile of gene expression (DE fold change > 2 and *p*-value < 0.01, first panel) is shown alongside changes in histone mark association from 0 to 4 DPA and 4 IAA tissues. Genes are ordered by the fold change of 4 DPA/0 DPA from high to low. Arrows indicate cases with differential histone mark association: red represents histone mark from 0 DPA to 4 DPA or 4 IAA, and blue represents the loss of histone marks.

IAA2 was significantly increased in both auxin and pollination, along with their enrichment in H3K9ac and H3K4me3 marks and loss of H3K27me3 (Figure 4B). Along the same line, genes showing downregulation by both auxin- and pollination-induced fruit set display a clear decrease in active histone marks, as exemplified by *SlPILS5* (Figure 4B). Interestingly, it is remarkable that pollination dramatically enhanced (16 times) the expression of the *YUC6* gene (Figure 4B), with significant enrichment in H3K9ac and H3K4me3 marks. In contrast, auxin did not induce such a change in expression, suggesting that the induced expression of *YUC6* by natural pollination might occur specifically in the developing seeds, which are missing in auxin-treated fruits. *SlPIN5* also showed a distinct change in gene expression with pollination and auxin treatment (Figure 4B), indicating that these two inputs promote internal auxin transport in different ways. In keeping with the idea that H3K9ac and H3K4me3 histone marks are the major histone marks driving the changes in gene expression, these data indicate that pollination and auxin mostly trigger the same core set of auxin-related genes undergoing histone modifications during fruit set.

Most DEGs (17 out of 19) involved in gibberellin signaling, regulated by both pollination and auxin, displayed similar changes in at least one histone mark (Figures 4C, D). For example, pollination induced a gain in permissive H3K9ac and H3K4me3 marks on *GA20 oxidase 1* (*GA20OX1*; Figure 4D), resulting in significantly increased gene transcription. By contrast, auxin-induced enrichment in H3K4me3 but not in H3K9ac mark association. This indicates that pollination and auxin mark histone tails in slightly different ways, although H3K4me3 is the main driver modulating gene expression by both treatments. Moreover, compared to pollination, auxin specifically represses the association with H3K9ac and H3K4me3, accompanying the decreased transcription of *ent-kaurene oxidase* gene (Figure 4C), which encodes the enzyme catalyzing the early three-step oxidation required for gibberellin biosynthesis. This supports the idea that gibberellin is synthesized following the pollination-induced accumulation of auxin, which may promote GA biosynthesis in a later step, as evidenced by the significant increase in transcript levels of *KAO2-like2* and *GA20OX1* after pollination or auxin treatment.

Strikingly, almost all the DEGs (nine out of 11) related to brassinosteroid metabolism and signaling displayed a similar trend of increased H3K9ac and H3K4me3 histone marks in both pollination- and auxin-induced fruit initiation processes (Supplementary Figure S3). Notably, all these genes, with the exception of *BEH4-like2*, failed to show a change in H3K27me3-association during the fruit set, suggesting that their expressions are not hampered by the H3K27me3 repressive mark in the diverse tissues of young developing fruit. The data indicate that promoting brassinosteroid synthesis and signaling may make an important contribution to the control of the fruit set.

In accordance with the ethylene-related DEGs exhibiting mainly a downregulation trend during both auxin- and pollination-induced fruit set, their association with H3K9ac or H3K4me3 also mostly decreases during this developmental transition (Figure 5A). In total, out of 27 downregulated DEGs common to both pollination and auxin

10.3389/fpls.2025.1495494

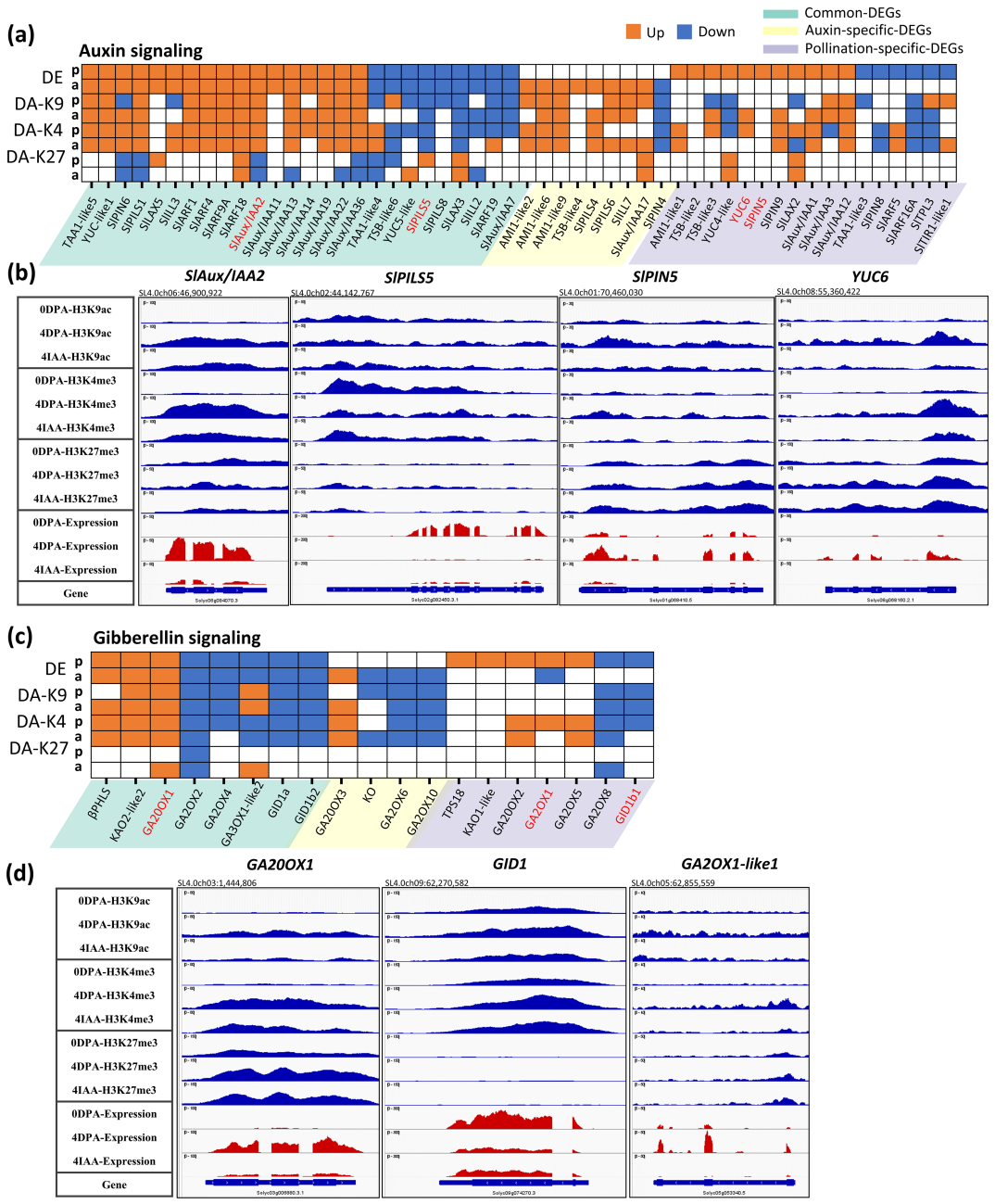

FIGURE 4
Differential expression and differential histone mark associations of auxin-related genes during fruit set. **(A, C)** Heatmap of DE and DAs (DA-K9, DA-K4, and DA-K27). Orange blocks indicate an increase in gene expression (fold > 2 and *p*-value < 0.01) or histone mark association (*p*-value < 0.01), while blue blocks indicate a decrease in gene expression or histone mark association. *p*, pollination-induced fruit set; *a*, auxin-induced fruit set. **(B, D)** Examples of differential mark association and gene expression of auxin- **(B)** and gibberellin-related **(D)** genes, visualized in IGV. Histone mark associations are marked in blue (top) and gene expression is marked in red (bottom).

treatment, 18 show a similar trend of changes in either H3K9ac or H3K4me3 histone marks in the two types of fruit initiation processes. For example, *ACO4*, the main ACC oxidase gene expressed in ovules, displayed a net decrease in gene expression from 0 DPA to 4 DPA or 4 IAA stages, along with a dramatic loss of H3K9ac and H3K4me3 histone marks during this process (Figure 5B). The data reveal that both auxin and pollination similarly promote the flower-to-fruit transition by extensively lowering ethylene synthesis and perception. It is striking that all of the commonly upregulated DEGs are members of the *ERF* gene family, including *SlERF.B6-B8*, *SlERF.C1*, *SlERF.G4*, and *SlERF.H1*, which all show a significant increase in gene expression and H3K9ac or (and) H3K4me3 association after ovary fertilization and auxin treatment. This indicates that specific *SlERFs* might be activated during fruit set, but since ethylene biosynthesis genes are strongly downregulated, it can be assumed that the upregulation of these ERFs is not under direct regulation of ethylene. It is important to mention that although the expression of some genes is specifically regulated by auxin treatment or by pollination, their expression

10.3389/fpls.2025.1495494

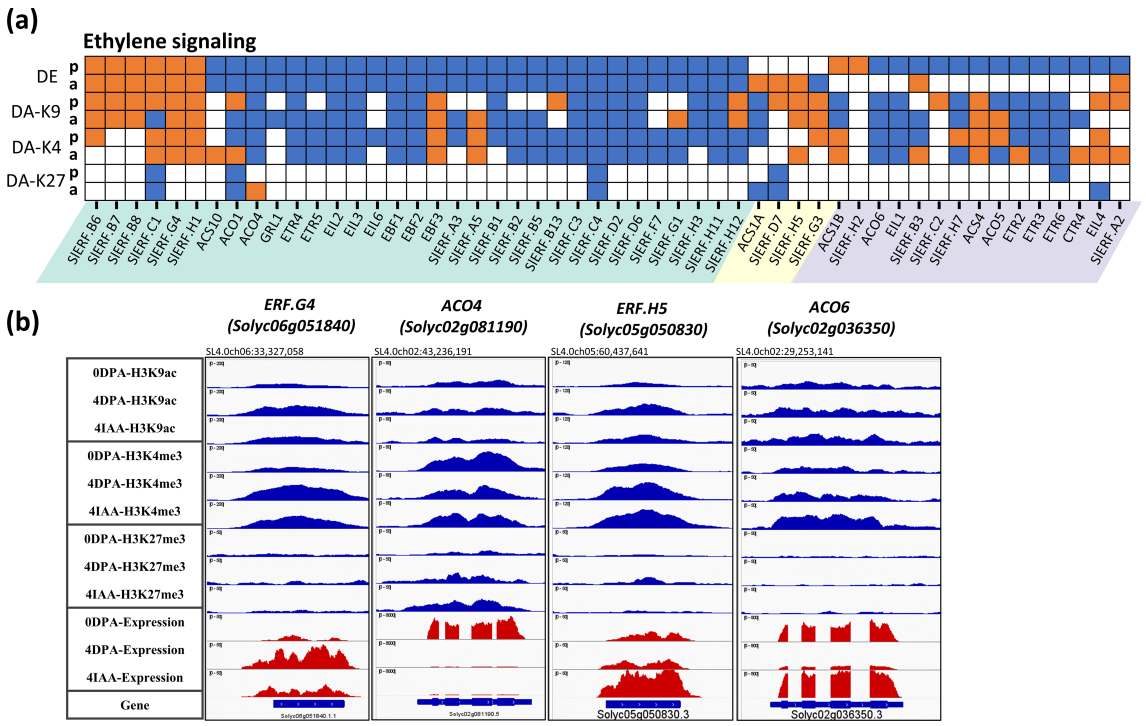

FIGURE 5
Differential expression and differential histone mark associations of ethylene-related genes during fruit set. **(A)** Heatmap of DE and DAs (DA-K9, DA-K4, and DA-K27). Orange blocks indicate an increase in gene expression (fold > 2 and *p*-value < 0.01) or histone mark association (*p*-value < 0.01), while blue blocks indicate a decrease in gene expression or histone mark association. *p*, pollination-induced fruit set; *a*, auxin-induced fruit set. **(B)** Examples of differential mark association and gene expression of ethylene-related genes, visualized in IGV. Histone mark associations are marked in blue (top), and gene expression is marked in red (bottom).

generally showed low fold changes and relatively low changes in histone mark association, supporting the hypothesis that auxin and pollination control flower-to-fruit transition mostly through the same subset of genes. The large number of genes related to cytokine, ABA, SA, and JA that display significant changes in histone marking and in their expression levels during pollination- and auxin-induced fruit setting (Supplementary Figure S3) clearly indicate that successful fruit initiation relies on a complex multihormonal control of the subordinated gene expression network.

A large panel of transcription factor genes undergo changes in expression and epigenetic marks during the flower-to-fruit transition

The large number (642 in total) of transcription factors displaying differential expression reflects the magnitude of transcriptomic reprogramming underlying the fruit-set process (Figure 6A). Remarkably, half (324) of these DEGs encoding TFs are commonly regulated by both pollination and auxin, while a smaller number are specifically regulated by auxin (41 upregulated and 60 downregulated) or pollination (with 77 upregulated and 140 downregulated).

To further understand the differences between auxin- and pollination-induced fruit setting we investigated the changes in gene expression and histone marking of individual TF genes in response to these two types of inputs. A similar proportion (93.9% by auxin induction and 92.8% by pollination induction) of TF DEGs showed differential association with at least one histone mark (Figure 6B). Notably, most of these TF genes were differentially associated with H3K9ac (71.1% of auxin-induced and 76.0% of pollination-induced) and H3K4me3 (77.8% and 80.4%) marks, while a lower proportion (32.2% and23.8%) displayed simultaneous changes in both active marks during fruit set. This is consistent with the critical role of active H3K9ac and H3K4me3 histone marks in driving gene transcription. Moreover, it is interesting to note that, in addition to the increased expression of *Aux/IAA* and *ARF* genes related to auxin activity, several other TF families displayed significant transcript elevation during fruit setting (Supplementary Table S3). These include *TCP* (six upregulated and two downregulated), *SBP* (four upregulated and two downregulated), *SNF2* (six upregulated and two downregulated), *GRF* (seven upregulated and one downregulated), *SET* (six upregulated), and *PhD* (three upregulated) family genes. Among these, several TFs showed a strong link with the fertilization and fruit development process. For example, two TCPs (*Solyc07g062680* and *Solyc03g116320*), whose homologs in *Arabidopsis* (TCP4 and TCP14) are required for endosperm development and activation of embryonic growth in seeds (Sarvepalli and Nath, 2011; Zhang et al., 2019), displayed increased transcript levels after pollination (by sevenfold) and auxin treatment (by four- to fivefold) (Supplementary Table S3). In addition, three *SBPs* (*Solyc01g090730*, *Solyc10g018780*, and

10.3389/fpls.2025.1495494

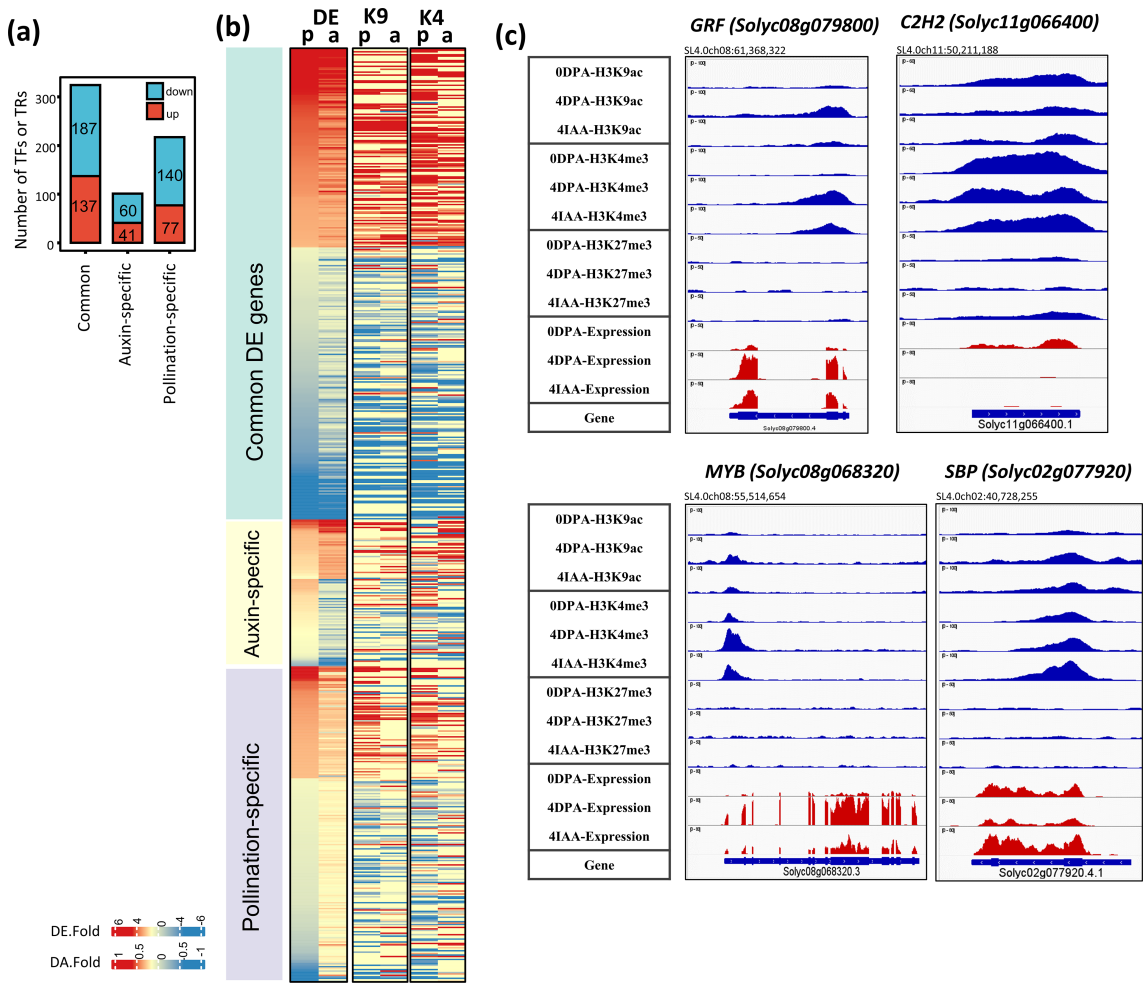

FIGURE 6
Differential expression and differential histone mark associations of TF genes regulated by both auxin and pollination. **(A)** Number of TF DEGs. **(B)** The heatmap of TF genes shows changes in gene expression and association with histone marks (DA-K9 and DA-K4). Red blocks indicate an increase in gene expression (fold > 2) or histone mark association by H3K9ac or H3K4me3 (p-value < 0.01); blue blocks indicate a decrease in gene expression or histone mark association. *p*, pollination-induced fruit set; *a*, auxin-induced fruit set. **(C)** Examples of differential mark association and gene expression of selected TFs, visualized in IGV. Histone mark associations are marked in blue (top), and gene expression is marked in red (bottom).

Solyc10g078700) are significantly upregulated by both pollination and auxin treatment. Their strong expression levels in tomato carpels have been reported to play critical roles in early fruit development (Silva et al., 2014). Additionally, seven *GRF* TFs, involved in cell proliferation and cell expansion (Omidbakhshfard et al., 2015), were preferentially upregulated in 4 DPA or 4 IAA fruit. Among them, one (*Solyc08g079800*) showed a significant increase in H3K9ac (by pollination) and oH3K4me3 (by both pollination and auxin treatment) (Figure 6B).

The transcriptional increases of epigenetic regulation genes related to chromatin remodeling (SNF2 family) and histone methyltransferase (SET family) further emphasize the significance of the epigenetic modifications in this developmental transition. For instance, homologs of CHROMATIN REMODELING 1 (CHR1), which are involved in gene silencing and maintenance of DNA and histone methylation (*DDM1-like1* and *DDM1-like2*) (Osakabe et al., 2021), as well as *SDG30*, homologous to trithorax group proteins involved in H3K4me3 methylation in *Arabidopsis* (Alvarez-Venegas et al., 2003; Schuettengruber et al., 2011), displayed increase in their transcript levels during the fruit initiation process.

By contrast, genes belonging to several TF families exhibited a significant decrease in their transcript levels during both pollination-dependent and pollination-independent fruit initiation, such as those encoding C2H2 (10 upregulated and 24 downregulated), NAC (four upregulated and 20 downregulated), MADS-MIKC/M-type (18 downregulated), and PLATZ (four downregulated). These genes also displayed a significant loss of H3K9ac and/or H3K4me3 histone marks during fruit setting. For example, the C2C2 gene, *Solyc11g066400*, displayed a loss of histone marks during fruit setting (Figure 6C). Additionally, the expression of a NAC member (*Solyc07g045030*), whose ortholog in *Arabidopsis* encodes JUNGBRUNNEN1, a repressor of GA and BR biosynthesis (Shahnejat-Bushehri et al., 2017), was significantly reduced by both pollination (17 times) and auxin treatment (12

times) (Supplementary Table S3), further supporting the active role of GA and BR in fruit set. Furthermore, MIKC- and M-type MADS-box genes, including *SlDEF*, *AP3/PI*, and homologs of AGL62 (*Solyc01g10630*), AGL6 (*Solyc01g090960*), and AGL22 (*Solyc11g010570*) in *Arabidopsis*, also show significantly decreased transcript levels at 4 DPA and 4 IAA fruits. Notably, *SlAGL6*, one of the key regulators for parthenocarpic fruit formation in tomato (Klap et al., 2017), exhibited significant downregulation and a gain of H3K27me3 marks in both pollination-dependent and pollination-independent fruit setting. Given their expression pattern, these NAC and MADS-box TFs may function primarily as transcriptional repressors, acting as negative regulators of the onset of fruit formation.

The present study reveals that a majority (196 out of 217, 90.3%) of TF DEGs specifically induced by pollination were differentially associated with changes in at least one histone mark. Auxin treatment induced a similar proportion of TF DEGs, albeit a distinct subset displayed differential histone marking. Notably, while auxin modulates most TFs in the same way as pollination, the two types of fruit set can also diverge in their regulation of gene expression and histone marking. For instance, CNR, a critical regulator of fruit ripening that is repressed during the fruit development stages by DNA methylation, is specifically promoted by auxin, exhibiting a 2.5-fold increase in transcript levels and a gain in H3K4me3 mark. These data reveal that auxin uses a different pathway than natural pollination to promote gene transcription during fruit setting.

Compared to the 23.8% of TF DEGs differentially associated with H3K27me3 in pollination-induced fruit set, a higher proportion (32.2%) of TF genes underwent differential association with H3K27me3 in auxin-induced fruit formation (Supplementary Table S3). Of the TFs specifically induced by auxin, 38.6% were differentially marked by H3K27me3, whereas a lower proportion (19.8%) were found in pollination-specific regulated DEGs (Supplementary Table S3).

TF DEGs displaying changes in all three histone marks are regarded as specific regulators of the fruit set. The data indicate that 35 TF DEGs showed consistent changes in all three histone marks (Figure 7A), with a gain of H3K9ac or H3K4me3 active marks and a loss of H3K27me3 repressive mark, or a loss of active marks associated with a gain of the repressive mark. This is exemplified by the changes in transcript levels of *C3H* (*Solyc12g008660*), *ERF1a-like* (*Solyc05g051180*), *Tify* (*Solyc08g036660*), and *C2C2-Dof* (*Solyc04g070960*), in which the three histone marks undergo significant modifications (Figure 7B).

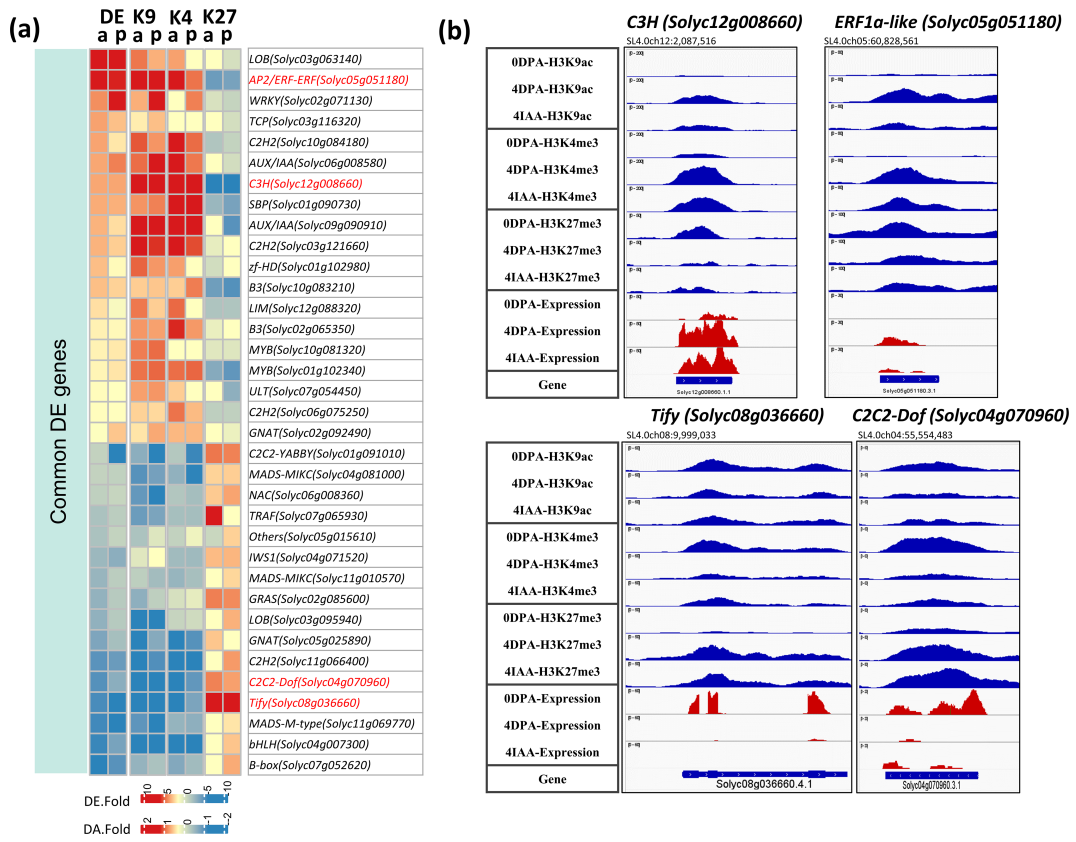

FIGURE 7
Differential expression and differential histone mark associations of TF genes regulated by both auxin and pollination. **(A)** Heatmap of commonly regulated DE TFs and their association changes with histone marks (DA-K9, DA-K4, and DA-K27). The red blocks indicate an increase in gene expression (fold > 2 and *p*-value < 0.01) or histone mark association by H3K9ac or H3K4me3 (*p*-value < 0.01); the blue blocks indicate a decrease in gene expression or histone mark association. *p*, pollination-induced fruit set; *a*, auxin-induced fruit set. **(B)** Examples of differential mark association and gene expression of selected TFs, visualized in IGV. Histone mark associations are marked in blue (top), and gene expression is marked in red (bottom).

10.3389/fpls.2025.1495494

Discussion

Fruit set is a genetically programmed process, governed by the interaction between multiple hormonal signaling pathways and diverse transcriptional regulators, which coordinate a series of subordinate programs, including cell division, embryo development, photosynthesis, and epigenetic regulation. In the last decade, a large number of genes involved in fruit setting have been identified using diverse approaches, including cDNA-amplified fragment length polymorphism (AFLP), microarray, next-generation RNA sequencing, and studies in various mutants or hormone-treated fruits. However, the gene regulatory networks underlying this developmental shift, which is essential in determining crop yield, are still far from being fully understood. Our present study combining genome-wide transcriptomic profiling and ChIP-seq analysis, provides a comprehensive list of potential candidate genes associated with pollination-dependent and pollination-independent fruit sets. These findings may serve as novel resources for further deciphering the functional roles and contributions of these genes to fruit set. The data also revealed the role of auxin in triggering the transcriptomic reprogramming leading to the fruit set and showed that auxin operates in a manner largely similar to natural pollination in triggering the fruit initiation process in tomato (Figure 8). Common processes of cell division, including "DNA replication", "cytokinesis", "G2/M transition", and "spindle assembly", as well as of developmental processes, including "photosynthesis", "flower development", and "ovule development", are enriched by both pollination and auxin treatment. Consistent with this, several transcription factor families involved in cell division or cell proliferation, such as *TCP* and *GRF* families, were significantly activated. Specifically, six out of eight *TCP* DEGs were significantly upregulated, in line with their conserved role in modulating cell cycle progression across various tissues and organs in diverse species (Huang and Irish, 2015; Resentini et al., 2015; Zhao et al., 2018, 2021; Ferrero et al., 2021; Gao et al., 2024). These findings suggest that TCPs contribute to fruit set and early fruit growth in both pollination- and auxin-induced fruit sets. It is noteworthy that in *Arabidopsis*, TCP homologs are also actively involved in hormone regulation. For instance, the *tcp14tcp15* double mutant has been shown to enhance gibberellin activity associated with cell division in the root apex (Resentini et al., 2015) and to regulate auxin activity in cell elongation (Ferrero et al., 2021). However, the precise functional roles of these TCPs in fruit set and fruit growth remain to be fully elucidated.

Ethylene and ABA have been proposed to play antagonistic roles to auxin and gibberellin during fruit set, keeping the ovary in a temporally protected and dormant state (Vriezen et al., 2007). Recent studies support the notion that ethylene suppresses tomato fruit set through the modification of gibberellin metabolism (Shinozaki et al., 2015). In addition, the knockout of EIN2, a key regulator of ethylene signaling, also leads to parthenocarpic fruit formation (Huang et al., 2022). In line with this view, the comprehensive exploration described in our present study indicates that the ethylene signaling pathway is significantly repressed in developmental ovaries and that the lower expression of genes involved in ethylene biosynthesis and activity is critical for early fruit initiation. This sharply contrasts with the increased ethylene levels in the abscission zone of flowers when fertilization fails. Altogether, these data open new possibilities for uncoupling hormone signaling pathways, beyond auxin and gibberellin, through cutting-edge genome editing strategies aimed at improving crop yield in fruit. For instance, manipulating the expression of ACC or ethylene biosynthesis genes prior to pollination could offer the potential to develop breeding lines with enhanced fruit set and reduced flower abscission.

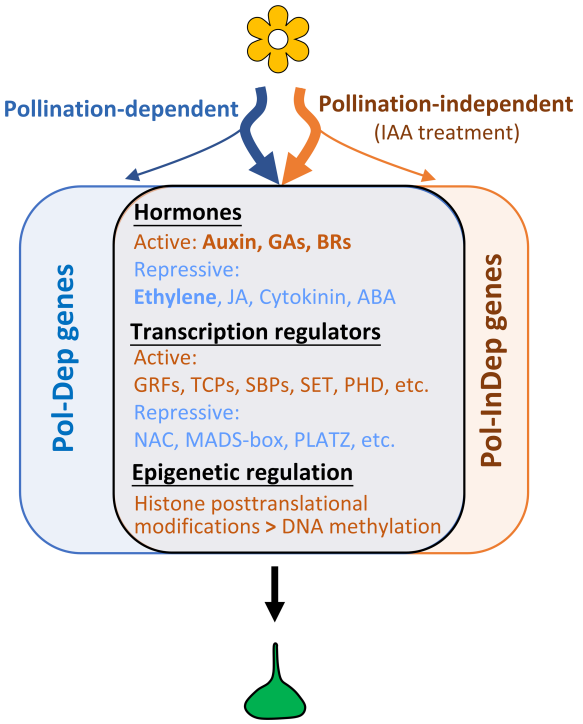

FIGURE 8
A schematic diagram of gene regulations underlying pollination-dependent and pollination-independent fruit set in tomato. A large number of genes related to hormones and transcription regulators exhibited similar trends in gene expression and histone marking in both pollination- and auxin-induced fruit sets, indicating largely similar genetic and epigenetic reprogramming of fruit set triggered by both auxin and pollination signals. Nevertheless, a significant number of genes are specifically triggered or repressed by auxin or pollination, suggesting that distinct pathways might also be involved in initiating the switch from flower to fruit in tomato. Among these, the genes related to seed development are specific to pollination-dependent fruit set, as this process is absent in auxin-induced fruit set.

Auxin and gibberellin are two central hormones for fruit initiation, and our data show that auxin synthesis (*YUCCAs*), transport (*PIN4*), signal transduction (*SlARF4*, *SlARF9*, and *SlARF18*), and response (AUX/IAA, GH3, and SAUR families) genes undergo change in their expression, associated with changes in H3K9ac or H3K4me3 histone marks. Consistently, *SlPIN4* and *SlARF9* have been reported to regulate fruit set in tomato, suggesting that modifications in histone marking on these auxin signaling genes are required for triggering the appropriate process of fruit development. Moreover, gibberellin synthesis genes were primarily upregulated and enriched in H3K9ac and H3K4me3 marks. This is clearly exemplified by the genes encoding *ent*-kaurenoic acid oxidase (*KAO2*) and GA 20-oxidase biosynthetic enzymes (*SlGA20ox1*,

SlGA20ox2, and *SlGA20ox3*), which are significantly upregulated, while *SlGA2ox1* and *SlGA2ox2*, which encode GA-inactivating enzymes, were downregulated in ovaries at 4 days after pollination. This supports the idea that auxin-induced fruit set is partially mediated by gibberellin metabolism in tomato (Serrani et al., 2008). Similar to what is observed for the auxin signaling pathway, a large number of GA biosynthesis genes show changes in H3K27me3 marks. Unexpectedly, we did not detect a significant change in transcript levels of *SlIAA9*, *SlARF7*, *SlARF8*, and *DELLA*, all of which are known to be critical for fruit set (Wang et al., 2005, 2009; Goetz et al., 2007; Martí et al., 2007; de Jong et al., 2009b). This might be explained by the selected ovary stages and the use of whole ovary tissues for transcriptomic profiling. It has been shown previously that at the anthesis stage, *IAA9* expression localizes in the ovule, placenta, and funiculus, but is weak in the ovary wall and columella, gradually decreasing following pollination and spreading across the developing tissues (Wang et al., 2005). In summary, our data highlight the importance of chromatin modifications (H3K9ac and H3K4me3) and coordinated changes in transcript levels during the fruit set, whether induced by natural pollination or by auxin treatment. Nevertheless, it is anticipated that fast-developing spatial transcriptomic or single-cell resolution transcriptomic studies will provide, in the near future, a more precise picture of the genetic reprogramming underlying the transition from flower to fruit.

Data availability statement

The datasets presented in this study can be found in online repositories. The names of the repository/repositories and accession number(s) can be found in the article/Supplementary Material.

Author contributions

XL: Formal analysis, Investigation, Methodology, Resources, Writing – review & editing. BH: Formal analysis, Methodology, Visualization, Writing – original draft. AD: Data curation, Methodology, Writing – review & editing. PF: Investigation, Methodology, Writing – review & editing. EM: Methodology, Writing – review & editing. FR: Methodology, Writing – review & editing. JP: Methodology, Writing – review & editing. GH: Conceptualization, Investigation, Data curation, Writing – original draft, Writing – review & editing. MB: Funding acquisition, Validation, Writing – review & editing.

Funding

The author(s) declare financial support was received for the research, authorship, and/or publication of this article. The research was supported by the European Union grants H2020 TomGEM 679796 and HARNESSTOM 101000716.

Conflict of interest

The authors declare that the research was conducted in the absence of any commercial or financial relationships that could be construed as a potential conflict of interest.

The reviewer NB declared a past co-authorship with the author EM to the handling editor.

Publisher's note

Supplementary material

The Supplementary Material for this article can be found online at: https://www.frontiersin.org/articles/10.3389/fpls.2025.1495494/full#supplementary-material

References

Alvarez-Venegas, R., Pien, S., Sadder, M., Witmer, X., Grossniklaus, U., and Avramova, Z. (2003). ATX-1, an Arabidopsis homolog of trithorax, activates flower homeotic genes. *Curr. Biol.* 13, 627–637. doi: 10.1016/S0960-9822(03)00243-4

Ampomah-Dwamena, C., Morris, B. A., Sutherland, P., Veit, B., and Yao, J.-L. L. (2002). Down-regulation of TM29, a tomato SEPALLATA homolog, causes parthenocarpic fruit development and floral reversion. *Plant Physiol.* 130, 605–617. doi: 10.1104/Pp.005223

Anders, S., Pyl, P. T., and Huber, W. (2015). HTSeq–a Python framework to work with high-throughput sequencing data. *Bioinformatics* 31, 166–169. doi: 10.1093/bioinformatics/btu638

Benjamini, Y., and Hochberg, Y. (1995). Controlling the false discovery rate - a practical and powerful approach to multiple testing. *J.R.Stat.Soc.Ser.B Stat.Methodol.* 57, 289–300. doi: 10.1111/j.2517-6161.1995.tb02031.x

Berr, A., Shafiq, S., and Shen, W.-H. (2011). Histone modifications in transcriptional activation during plant development. *Biochim. Biophys. Acta* 1809, 567–576. doi: 10.1016/j.bbagrm.2011.07.001

Bünger-Kibler, S., and Bangerth, F. (1982). Relationship between cell number, cell size and fruit size of seeded fruits of tomato (Lycopersicon esculentum Mill.), and those induced parthenocarpically by the application of plant growth regulators. *Plant Growth Regul.* 1, 143–154. doi: 10.1007/BF00036994

Carmi, N., Salts, Y., Dedicova, B., Shabtai, S., and Barg, R. (2003). Induction of parthenocarpy in tomato via specific expression of the rolB gene in the ovary. *Planta* 217, 726–735. doi: 10.1007/s00425-003-1052-1

Davière, J.-M., and Achard, P. (2013). Gibberellin signaling in plants. *Dev. (Cambridge England)* 140, 1147–1151. doi: 10.1242/dev.087650

de Jong, M., Mariani, C., and Vriezen, W. H. (2009a). The role of auxin and gibberellin in tomato fruit set. *J. Exp. Bot.* 60, 1523–1532. doi: 10.1093/jxb/erp094

de Jong, M., Wolters-Arts, M., Feron, R., Mariani, C., and Vriezen, W. H. (2009b). The Solanum lycopersicum auxin response factor 7 (SlARF7) regulates auxin signaling during tomato fruit set and development. *Plant journal : Cell Mol. Biol.* 57, 160–170. doi: 10.1111/j.1365-313X.2008.03671.x

de Jong, M., Wolters-Arts, M., Schimmel, B. C. J., Stultiens, C. L. M., de Groot, P. F. M., Powers, S. J., et al. (2015). Solanum lycopersicum AUXIN RESPONSE FACTOR 9 regulates cell division activity during early tomato fruit development. *J. Exp. Bot.* 66, 3405–3416. doi: 10.1093/jxb/erv152

Donzella, G., Spena, A., and Rotino, G. L. (2000). Transgenic parthenocarpic eggplants: superior germplasm for increased winter production. *Mol. Breed.* 6, 79–86. doi: 10.1023/A:1009613529099

Dorcey, E., Urbez, C., Blázquez, M., and Carbonell, J. (2009).Fertilization-dependent auxin response in ovules triggers fruit development through the modulation of gibberellin metabolism in Arabidopsis. Available online at: http://onlinelibrary.wiley.com/doi/10.1111/j.1365-313X.2008.03781.x/full (Accessed October 25, 2016).

Ferrero, L. V., Gastaldi, V., Ariel, F. D., Viola, I. L., and Gonzalez, D. H. (2021). Class I TCP proteins TCP14 and TCP15 are required for elongation and gene expression responses to auxin. *Plant Mol. Biol.* 105, 147–159. doi: 10.1007/s11103-020-01075-y

Figueiredo, D. D., Batista, R. A., Roszak, P. J., Hennig, L., and Köhler, C. (2016). Auxin production in the endosperm drives seed coat development in Arabidopsis. *eLife* 5, 1–23. doi: 10.7554/eLife.20542

Figueiredo, D. D., Batista, R. A., Roszak, P. J., and Köhler, C. (2015). Auxin production couples endosperm development to fertilization. *Nat. Plants* 1, 15184. doi: 10.1038/nplants.2015.184

Fos, M., Nuez, F., and García-Martínez, J. L. (2000). The gene pat-2, which induces natural parthenocarpy, alters the gibberellin content in unpollinated tomato ovaries. *Plant Physiol.* 122, 471–480. doi: 10.1104/pp.122.2.471

Fos, M., Proano, K., Nuez, F., and Garcia-Martinez, J. L. (2001). Role of gibberellins in parthenocarpic fruit development induced by the genetic system pat-3/pat-4 in tomato. *Physiologia Plantarum* 111, 545–550. doi: 10.1034/j.1399-3054.2001.1110416.x

Gao, Y., Regad, F., Li, Z., Pirrello, J., Bouzayen, M., and van der Rest, B. (2024). Class I TCP in fruit development: much more than growth. *Front. Plant Sci.* 15. doi: 10.3389/fpls.2024.1411341

Garcia-Hurtado, N., Carrera, E., Ruiz-Rivero, O., Lopez-Gresa, M. P., Hedden, P., Gong, F., et al. (2012). The characterization of transgenic tomato overexpressing gibberellin 20-oxidase reveals induction of parthenocarpic fruit growth, higher yield, and alteration of the gibberellin biosynthetic pathway. *J. Exp. Bot.* 63, 5803–5813. doi: 10.1093/jxb/ers229

Gehring, M. (2019). Epigenetic dynamics during flowering plant reproduction: evidence for reprogramming? *New Phytol.* 224, 91–96. doi: 10.1111/nph.15856

Gendrel, A.-V., Lippman, Z., Martienssen, R., and Colot, V. (2005). Profiling histone modification patterns in plants using genomic tiling microarrays. *Nat. Methods* 2, 213–218. doi: 10.1038/nmeth0305-213

Goetz, M., Hooper, L. C. L. C., Johnson, S. S. D., Rodrigues, J. C. M., Vivian-Smith, A., and Koltunow, A. M. (2007). Expression of aberrant forms of AUXIN RESPONSE FACTOR8 stimulates parthenocarpy in Arabidopsis and tomato. *Plant Physiol.* 145, 351–366. doi: 10.1104/pp.107.104174

Gustafson, F. G. (1936). Inducement of fruit development by growth-promoting chemicals. *Proc. Natl. Acad. Sci.* 22, 628–636. doi: 10.1073/pnas.22.11.628

Hao, Y., Hu, G., Breitel, D., Liu, M., Mila, I., Frasse, P., et al. (2015). Auxin response factor SlARF2 is an essential component of the regulatory mechanism controlling fruit ripening in tomato. *PLoS Genet.* 11, e1005649. doi: 10.1371/journal.pgen.1005649

He, C., Chen, X., Huang, H., and Xu, L. (2012). Reprogramming of H3K27me3 is critical for acquisition of pluripotency from cultured Arabidopsis tissues. *PLoS Genet.* 8, e1002911. doi: 10.1371/journal.pgen.1002911

He, M., Song, S., Zhu, X., Lin, Y., Pan, Z., Chen, L., et al. (2021). SlTPL1 silencing induces facultative parthenocarpy in tomato. *Front. Plant Sci.* 12, 672232. doi: 10.3389/fpls.2021.672232

Henderson, I. R., and Jacobsen, S. E. (2007). Epigenetic inheritance in plants. *Nature* 447, 418–424. doi: 10.1038/nature05917

Hu, G., Huang, B., Wang, K., Frasse, P., Maza, E., Djari, A., et al. (2021). Histone posttranslational modifications rather than DNA methylation underlie gene reprogramming in pollination-dependent and pollination-independent fruit set in tomato. *New Phytol.* 229, 902–919. doi: 10.1111/nph.16902

Hu, J., Li, X., and Sun, T. (2023). Four class A AUXIN RESPONSE FACTORs promote tomato fruit growth despite suppressing fruit set. *Nat. Plants* 9, 706–719. doi: 10.1038/s41477-023-01396-y

Huang, W., Hu, N., Xiao, Z., Qiu, Y., Yang, Y., Yang, J., et al. (2022). A molecular framework of ethylene-mediated fruit growth and ripening processes in tomato. *Plant Cell* 34, 3280–3300. doi: 10.1093/plcell/koac146

Huang, T., and Irish, V. F. (2015). Temporal control of plant organ growth by TCP transcription factors. *Curr. Biol.* 25, 1765–1770. doi: 10.1016/j.cub.2015.05.024

Huang, R., and Irish, V. F. (2024). An epigenetic timer regulates the transition from cell division to cell expansion during Arabidopsis petal organogenesis. *PLoS Genet.* 20, e1011203. doi: 10.1371/journal.pgen.1011203

Jones, B., Frasse, P., Olmos, E., Zegzouti, H., Li, Z. G., Latché, A., et al. (2002). Down-regulation of DR12, an auxin-response-factor homolog, in the tomato results in a pleiotropic phenotype including dark green and blotchy ripening fruit. *Plant J.* 32, 603–613. doi: 10.1046/j.1365-313X.2002.01450.x

Klap, C., Yeshayahou, E., Bolger, A. M., Arazi, T., Gupta, S. K., Shabtai, S., et al. (2017). Tomato facultative parthenocarpy results from Sl AGAMOUS-LIKE 6 loss of function. *Plant Biotechnol. J.* 15, 634–647. doi: 10.1111/pbi.12662

Lafos, M., Kroll, P., Hohenstatt, M. L., Thorpe, F. L., Clarenz, O., and Schubert, D. (2011). Dynamic regulation of H3K27 trimethylation during Arabidopsis differentiation. *PLoS Genet.* 7, e1002040. doi: 10.1371/journal.pgen.1002040

Langmead, B., and Salzberg, S. L. (2012). Fast gapped-read alignment with Bowtie 2. *Nat. Methods* 9, 357–359. doi: 10.1038/nmeth.1923

Love, M. I., Huber, W., and Anders, S. (2014). Moderated estimation of fold change and dispersion for RNA-seq data with DESeq2. *Genome Biol.* 15, 550. doi: 10.1186/s13059-014-0550-8

Malapeira, J., Khaitova, L. C., and Mas, P. (2012). Ordered changes in histone modifications at the core of the Arabidopsis circadian clock. *Proc. Natl. Acad. Sci. U.S.A* 109, 21540–21545. doi: 10.1073/pnas.1217022110

Martí, C., Orzáez, D., Ellul, P., Moreno, V., Carbonell, J., and Granell, A. (2007). Silencing of DELLA induces facultative parthenocarpy in tomato fruits. *Plant* 52, 865–876. doi: 10.1111/j.1365-313X.2007.03282.x

Mezzetti, B., Landi, L., Pandolfini, T., and Spena, A. (2004). The defH9-iaaM auxin-synthesizing gene increases plant fecundity and fruit production in strawberry and raspberry. *BMC Biotechnol.* 4, 4. doi: 10.1186/1472-6750-4-4

Mounet, F., Moing, A., Kowalczyk, M., Rohrmann, J., Petit, J., Garcia, V., et al. (2012). Down-regulation of a single auxin efflux transport protein in tomato induces precocious fruit development. *J. Exp. Bot.* 63, 4901–4917. doi: 10.1093/jxb/ers167

Omidbakhshfard, M. A., Proost, S., Fujikura, U., and Mueller-Roeber, B. (2015). Growth-regulating factors (GRFs): A small transcription factor family with important functions in plant biology. *Mol. Plant* 8, 998–1010. doi: 10.1016/j.molp.2015.01.013

Osakabe, A., Jamge, B., Axelsson, E., Montgomery, S. A., Akimcheva, S., Kuehn, A. L., et al. (2021). The chromatin remodeler DDM1 prevents transposon mobility through deposition of histone variant H2A.W. *Nat. Cell Biol.* 23, 391–400. doi: 10.1038/s41556-021-00658-1

Pandolfini, T., Molesini, B., and Spena, A. (2007). Molecular dissection of the role of auxin in fruit initiation. *Trends Plant Sci.* 12, 327–329. doi: 10.1016/j.tplants.2007.06.011

Pandolfini, T., Rotino, G. L., Camerini, S., Defez, R., and Spena, A. (2002). Optimisation of transgene action at the post-transcriptional level: high quality parthenocarpic fruits in industrial tomatoes. *BMC Biotechnol.* 2, 1. doi: 10.1186/1472-6750-2-1

Pattison, R. J., Csukasi, F., Zheng, Y., Fei, Z., van der Knaap, E., and Catalá, C. (2015). Comprehensive tissue-specific transcriptome analysis reveals distinct regulatory programs during early tomato fruit development. *Plant Physiol.* 168, 1684–1701. doi: 10.1104/pp.15.00287

Pu, L., and Sung, Z. R. (2015). PcG and trxG in plants - friends or foes. *Trends Genet.* 31, 252–262. doi: 10.1016/j.tig.2015.03.004

Quinlan, A. R., and Hall, I. M. (2010). BEDTools: A flexible suite of utilities for comparing genomic features. *Bioinformatics* 26, 841–842. doi: 10.1093/bioinformatics/btq033

Ramírez, F., Dündar, F., Diehl, S., Grüning, B. A., and M., T. (2014). DeepTools: A flexible platform for exploring deep-sequencing data. *Nucleic Acids Res.* 42, W187–W191. doi: 10.1093/nar/gku365

Ren, Z., Li, Z., Miao, Q., Yang, Y., Deng, W., and Hao, Y. (2011). The auxin receptor homologue in Solanum lycopersicum stimulates tomato fruit set and leaf morphogenesis. *J. Exp.* 62, 2815–2826. doi: 10.1093/jxb/erq455

Resentini, F., Felipo-Benavent, A., Colombo, L., Blázquez, M. A., Alabadí, D., and Masiero, S. (2015). TCP14 and TCP15 mediate the promotion of seed germination by gibberellins in Arabidopsis thaliana. *Mol. Plant* 8, 482–485. doi: 10.1016/j.molp.2014.11.018

Rieu, I., Eriksson, S., Powers, S. J., Gong, F., Griffiths, J., Woolley, L., et al. (2008). Genetic analysis reveals that C19-GA 2-oxidation is a major gibberellin inactivation pathway in Arabidopsis. *Plant Cell* 20, 2420–2436. doi: 10.1105/tpc.108.058818

Rotino, G. L., Acciarri, N., Sabatini, E., Mennella, G., Lo Scalzo, R., Maestrelli, A., et al. (2005). Open field trial of genetically modified parthenocarpic tomato: seedlessness and fruit quality. *BMC Biotechnol.* 5, 32. doi: 10.1186/1472-6750-5-32

Rotino, G. L., Perri, E., Zottini, M., Sommer, H., and Spena, A. (1997). Genetic engineering of parthenocarpic plants. *Nat. Biotechnol.* 15, 1398–1401. doi: 10.1038/nbt1297-1398

Rudolf, J., Tomovicova, L., Panzarova, K., Fajkus, J., Hejatko, J., and Skalak, J. (2024). Epigenetics and plant hormone dynamics: a functional and methodological perspective. *J. Exp. Bot.* 75, 5267–5294. doi: 10.1093/jxb/erae054

Sarvepalli, K., and Nath, U. (2011). Hyper-activation of the TCP4 transcription factor in *Arabidopsis thaliana* accelerates multiple aspects of plant maturation. *Plant J.* 67, 595–607. doi: 10.1111/j.1365-313X.2011.04616.x

Schuettengruber, B., Martinez, A.-M., Iovino, N., and Cavalli, G. (2011). Trithorax group proteins: switching genes on and keeping them active. *Nat. Rev. Mol. Cell Biol.* 12, 799–814. doi: 10.1038/nrm3230

Serrani, J. C., Ruiz-Rivero, O., Fos, M., and García-Martínez, J. L. (2008). Auxin-induced fruit-set in tomato is mediated in part by gibberellins. *Plant J.* 56, 922–934. doi: 10.1111/j.1365-313X.2008.03654.x

Shahnejat-Bushehri, S., Allu, A. D., Mehterov, N., Thirumalaikumar, V. P., Alseekh, S., Fernie, A. R., et al. (2017). Arabidopsis NAC transcription factor JUNGBRUNNEN1 exerts conserved control over gibberellin and brassinosteroid metabolism and signaling genes in tomato. *Front. Plant Sci.* 8. doi: 10.3389/fpls.2017.00214

Shao, Z., Zhang, Y., Yuan, G.-C., Orkin, S. H., and Waxman, D. J. (2012). MAnorm: a robust model for quantitative comparison of ChIP-Seq data sets. *Genome Biol.* 13, R16. doi: 10.1186/gb-2012-13-3-r16

Shinozaki, Y., Hao, S., Kojima, M., Sakakibara, H., Ozeki-Iida, Y., Zheng, Y., et al. (2015). Ethylene suppresses tomato (Solanum lycopersicum) fruit set through modification of gibberellin metabolism. *Plant J.* 83, 237–251. doi: 10.1111/tpj.12882

Silva, G. F. F., Silva, E. M., da Silva Azevedo, M., Guivin, M. A. C., Ramiro, D. A., Figueiredo, C. R., et al. (2014). microRNA156-targeted SPL/SBP box transcription factors regulate tomato ovary and fruit development. *Plant J.* 78, 604–618. doi: 10.1111/tpj.12493

Soufi, A., Donahue, G., and Zaret, K. S. (2012). Facilitators and impediments of the pluripotency reprogramming factors' initial engagement with the genome. *Cell* 151, 994–1004. doi: 10.1016/j.cell.2012.09.045

Tomato_Genome_Consortium (2012). The tomato genome sequence provides insights into fleshy fruit evolution. *Nature* 485, 635–641. doi: 10.1038/nature11119

Trapnell, C., Pachter, L., and Salzberg, S. L. (2009). TopHat: discovering splice junctions with RNA-Seq. *Bioinformatics* 25 (9), 1105–1111. doi: 10.1093/bioinformatics/btp120

Vriezen, W. H., Feron, R., Maretto, F., Keijman, J., and Mariani, C. (2007). Changes in tomato ovary transcriptome demonstrate complex hormonal regulation of fruit set. *New Phytol.* 177, 60–76. doi: 10.1111/j.1469-8137.2007.02254.x

Wang, H., Jones, B., Li, Z. G., Frasse, P., Delalande, C., Regad, F., et al. (2005). The tomato Aux/IAA transcription factor IAA9 is involved in fruit development and leaf morphogenesis. *Plant Cell* 17, 2676–2692. doi: 10.1105/tpc.105.033415

Wang, H., Schauer, N., Usadel, B., Frasse, P., Zouine, M., Hernould, M., et al. (2009). Regulatory features underlying pollination-dependent and -independent tomato fruit set revealed by transcript and primary metabolite profiling. *Plant Cell* 21, 1428–1452. doi: 10.1105/tpc.108.060830

Yao, J., Dong, Y., and Morris, B. (2001). Parthenocarpic apple fruit production conferred by transposon insertion mutations in a MADS-box transcription factor. *Proc. Natl. Acad. Sci. U.S.A* 98, 1306–1311. doi: 10.1073/pnas.98.3.1306

Zhang, W., Cochet, F., Ponnaiah, M., Lebreton, S., Matheron, L., Pionneau, C., et al. (2019). The MPK 8- TCP 14 pathway promotes seed germination in Arabidopsis. *Plant J.* 100, 677–692. doi: 10.1111/tpj.14461

Zhang, Y., Liu, T., Meyer, C. A., Eeckhoute, J., Johnson, D. S., Bernstein, B. E., et al. (2008). Model-based analysis of chIP-seq (MACS). *Genome Biol.* 9, R137. doi: 10.1186/gb-2008-9-9-r137

Zhao, Y., Su, X., Wang, X., Wang, M., Chi, X., Aamir Manzoor, M., et al. (2021). Comparative genomic analysis of TCP genes in six rosaceae species and expression pattern analysis in Pyrus bretschneideri. *Front. Genet.* 12. doi: 10.3389/fgene.2021.669959

Zhao, J., Zhai, Z., Li, Y., Geng, S., Song, G., Guan, J., et al. (2018). Genome-wide identification and expression profiling of the TCP family genes in spike and grain development of wheat (Triticum aestivum L.). *Front. Plant Sci.* 9. doi: 10.3389/fpls.2018.01282

Frontiers in
Plant Science

Cultivates the science of plant biology and its applications

The most cited plant science journal, which advances our understanding of plant biology for sustainable food security, functional ecosystems and human health.

Discover the latest Research Topics

See more →

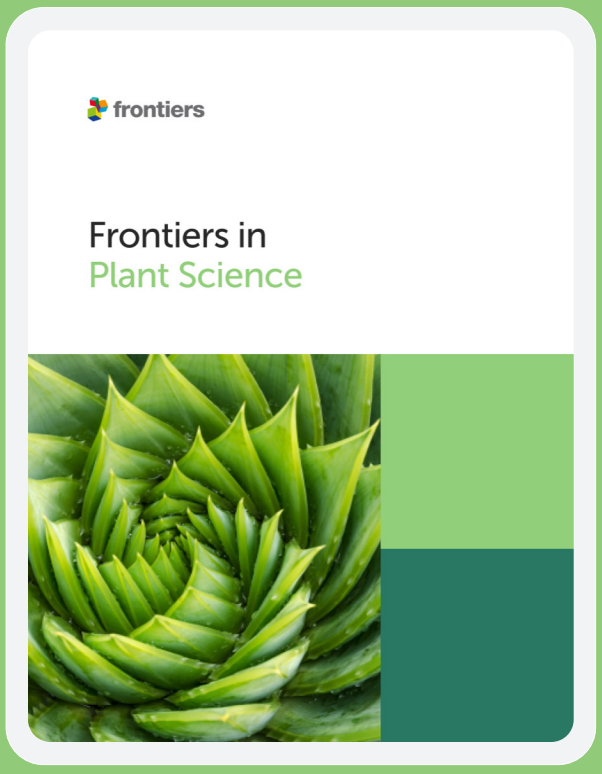

Frontiers

Avenue du Tribunal-Fédéral 34
1005 Lausanne, Switzerland
frontiersin.org

Contact us

+41 (0)21 510 17 00
frontiersin.org/about/contact